

December 11, 2010 | <http://pubs.acs.org>
Publication Date: March 30, 1998 | doi: 10.1021/bk-1998-0689.fw001

Organic Coatings for Corrosion Control

December 11, 2010 | <http://pubs.acs.org>
Publication Date: March 30, 1998 | doi: 10.1021/bk-1998-0689.fw001

ACS SYMPOSIUM SERIES

689

Organic Coatings for Corrosion Control

Gordon P. Bierwagen, EDITOR
North Dakota State University



American Chemical Society, Washington, DC

In Organic Coatings for Corrosion Control; Bierwagen, G.;
ACS Symposium Series; American Chemical Society: Washington, DC, 1998.



Organic coatings for corrosion control

This book is printed on acid-free, recycled paper.



Copyright © 1998 American Chemical Society

Distributed by Oxford University Press

ISBN 0-8412-3549-X

ISSN 0097-6156

All Rights Reserved. Reprographic copying beyond that permitted by Sections 107 or 108 of the U.S. Copyright Act is allowed for internal use only, provided that a per-chapter fee of \$20.00 plus \$0.25 per page is paid to the Copyright Clearance Center, Inc., 222 Rosewood Drive, Danvers, MA 01923, USA. Republication or reproduction for sale of pages in this book is permitted only under license from ACS. Direct these and other permissions requests to ACS Copyright Office, Publications Division, 1155 16th Street, N.W., Washington, DC 20036.

The citation of trade names and/or names of manufacturers in this publication is not to be construed as an endorsement or as approval by ACS of the commercial products or services referenced herein; nor should the mere reference herein to any drawing, specification, chemical process, or other data be regarded as a license or as a conveyance of any right or permission to the holder, reader, or any other person or corporation, to manufacture, reproduce, use, or sell any patented invention or copyrighted work that may in any way be related thereto. Registered names, trademarks, etc., used in this publication, even without specific indication thereof, are not to be considered unprotected by law.

PRINTED IN THE UNITED STATES OF AMERICA

**American Chemical Society
Library**

1155 16th St., N.W.

In Organic Coatings for Corrosion Control; Bierwagen, G.;
ACS Symposium Series; American Chemical Society: Washington, DC, 1998.

Advisory Board

ACS Symposium Series

Mary E. Castellion
ChemEdit Company

Arthur B. Ellis
University of Wisconsin at Madison

Jeffrey S. Gaffney
Argonne National Laboratory

Gunda I. Georg
University of Kansas

Lawrence P. Klemann
Nabisco Foods Group

Richard N. Loeppky
University of Missouri

Cynthia A. Maryanoff
R. W. Johnson Pharmaceutical
Research Institute

Roger A. Minear
University of Illinois
at Urbana-Champaign

Omkaram Nalamasu
AT&T Bell Laboratories

Kinam Park
Purdue University

Katherine R. Porter
Duke University

Douglas A. Smith
The DAS Group, Inc.

Martin R. Tant
Eastman Chemical Co.

Michael D. Taylor
Parke-Davis Pharmaceutical
Research

Leroy B. Townsend
University of Michigan

William C. Walker
DuPont Company

Foreword

THE ACS SYMPOSIUM SERIES was first published in 1974 to provide a mechanism for publishing symposia quickly in book form. The purpose of the series is to publish timely, comprehensive books developed from ACS sponsored symposia based on current scientific research. Occasionally, books are developed from symposia sponsored by other organizations when the topic is of keen interest to the chemistry audience.

Before agreeing to publish a book, the proposed table of contents is reviewed for appropriate and comprehensive coverage and for interest to the audience. Some papers may be excluded in order to better focus the book; others may be added to provide comprehensiveness. When appropriate, overview or introductory chapters are added. Drafts of chapters are peer-reviewed prior to final acceptance or rejection, and manuscripts are prepared in camera-ready format.

As a rule, only original research papers and original review papers are included in the volumes. Verbatim reproductions of previously published papers are not accepted.

ACS BOOKS DEPARTMENT

Preface

THIS BOOK RESULTED from a request from Dr. George Pilcher, then Program Chair of the Polymeric Materials: Science and Engineering (PMSE) division, that I organize a symposium on coatings and corrosion for the Spring 1996 ACS National Meeting in New Orleans. PMSE had not held a symposium on this topic for several years, and George thought it appropriate to again hold such a symposium. When I sent our announcements and contacted workers seeking papers in this area of research and development, we received many positive replies. At this time, I contacted ACS Books concerning the possibility of publishing the papers of this symposium, and received encouragement to plan for publication. This book is the result of much hard work by the authors, reviewers, and secretaries, plus the help of the ACS Books staff.

Research on organic coatings for corrosion control has always been important to the area of coatings science, but is receiving renewed interest in university, government, and corporate laboratories. Several driving forces are causing this renewal. The first is imminent legislation that will require removal of chromates from coating formulae and the coating production workplace, due to toxicity and hazardous materials handling issues. No longer can corrosion-control coatings systems be based on chromate metal treatments and chromate pigments. This removal has been impending for quite a few years, but is now required. Further, all government agencies, including the Department of Defence (DOD), are under this removal mandate. Why chromates act in such a unique manner is not yet fully understood, and much work is in progress to achieve such an understanding.

The second driving force is the bevy of new experimental methods and instrumentation for numerically characterizing organic coatings in their corrosion protective mode. Far too much emphasis has been placed on qualitative, subjective test methods for the corrosion-control properties of organic coatings. Combining new and old techniques with new computer hardware and software has led to many easy-to-use methods that are being rapidly incorporated into laboratory practice. Examples are new electrochemical methods, new microscopic probes (scanning probe microscopies, et al.), and new application of the tools of materials science, such as thermal, spectroscopic and acoustic methods.

The third driving force is the design of new materials and systems for corrosion control coatings. Conductive polymers offer an ecologically viable op-

tion for corrosion protection, with a potential increase in efficiency over chromate replacement systems. Microscopic engineering of the metal–pretreatment–coating interfaces is under extensive examination, as all corrosion failures occur at these loci.

These driving forces, and the renewed understanding that false economic judgments of the value and need for long-term, effective protection of objects with high capital value (e.g. aircraft, bridges, automobiles), have resulted in renewed R&D that will lead to the better design and testing of organic coatings for corrosion protection. No longer is the development of a new alloy the solution to a corrosion problem. There is a large investment in objects and structures already in place, and it is cost effective to lower their maintenance costs and extend their lifetimes. The proper use of organic coatings, pretreatments, and coating application methods of high performance and high quality that provide predictable, consistent corrosion control is still the most cost effective way of protecting our infrastructure, and the objects and systems that are integral parts of our lives.

This book includes papers coauthored by some of the leaders in the field described by the book title. The reader will find extensive coverage of electrochemical methods, especially electrochemical impedance spectroscopy and electrochemical noise methods of assessing the quality and lifetime of corrosion protection provided by organic coatings. The reader will also learn about corrosion protection under various environmental exposure conditions, ranging from underground pipelines to microbial-induced corrosion, and substrates ranging from steel to aerospace Al alloys. Two papers offer insight into the corrosion protection provided by polyaniline as a coating material. Several papers cover new pigments and pretreatment materials as substitutes for chromates. The book is truly an international endeavor, with contributing authors from Sweden, Germany, England, South Africa, Italy, the Netherlands, Japan, Ukraine, and the Czech Republic.

This book was developed from a symposium sponsored by the Division of Polymeric Materials: Science and Engineering at the 211th National Meeting of the American Chemical Society, New Orleans, Louisiana, March 24–28, 1996.

Acknowledgments

I wish to thank the authors of the papers presented below, as well as their institutions, for providing the time and support that is involved in their preparation. I wish to also thank all the agencies and corporations that have provided support to the research efforts in corrosion/coatings here at NDSU, including the Office of Naval Research (ONR), The American Gas Association–Pipeline Research Committee, Xerxes, Inc., AKZO-Nobel America, EXXON, the Air Force Materials Laboratory at WPAFB, the Air Force Office of Scientific Research (AFOSR) and the National Science Foundation—Coatings Research Center (IUCRC). I wish to give a special thanks to Dr. John Sedriks of ONR for all of

the advice and encouragement that he has provided me since I began studying corrosion protection by coatings. Finally, I wish to thank Ms. Carol Johnson, who was instrumental in handling all of the administrative and clerical efforts that brought this book into publishable form.

GORDON P. BIERWAGEN
Professor, Polymers & Coatings
North Dakota State University
Fargo, ND 58105

Chapter 1

Corrosion and Its Control by Coatings

Gordon P. Bierwagen

Department of Polymers and Coatings, North Dakota State University,
Fargo, ND 58105

Corrosion protection of metallic substrates has long been one of the key roles performed by organic coatings. Such coatings remain one of the most cost-effective means of providing practical protection from corrosion to easily corrodible metallic (and sometimes non-metallic) structures and objects. This choice of a coating by (material + application cost) only has created a mentality so widespread that little basic research has been done in recent years towards significantly improving the performance of corrosion control coatings or developing new measurement methods for their assessment. There are several technical organizations besides the ACS to which the corrosion control by organic coatings is very important. The National Association of Corrosion Engineers (NACE), Steel Structures Painting Council (SSPC), the Electrochemical Society (ECS), and the Federation of Societies for Coatings Technology (FSCT) are all very much interested in this topic and hold regular symposia on this topic. But, this book based on a Symposium held by the ACS-Polymeric Materials: Science & Engineering (PMSE) Division is unique in the quality and insight into the chemistry of how and why coatings control corrosion, and illustrates the need for more PMSE Symposia in this area. During the sessions at which most of the chapters published in this book were presented orally, the attendance was quite high, indicating, even in oral presentation, these papers elicited a considerable interest with large attendance at the Symposium.

From the user's point of view, corrosion control by coatings is very important, especially for those objects and items that are subject to environments that cause corrosion. Many users would like to have to paint/coat an object only once for corrosion protection, and then assume appearance and function will maintain. This, of course, does not occur, but when failure in corrosion protection of a coating occurs, the function of the coated object can be threatened. The main goal of users of corrosion protective coatings is to provide protection of the coated object as long as possible. Often this desire and need for corrosion protection by a coating extends beyond just the intact coating, as the user wishes the coating to protect areas of the coated object that have undergone minor damage in handling or use. Thus, the coating is not just a barrier layer between the object and its environment, but should

also act to protect small, local areas of substrate exposed by damage, as well as stop the spread of the damage.

A major difficulty for coating users is to assess the present state of protection against corrosion in a coated system after it has been exposed to its environment. Visual observation is very difficult for many parts of objects, and certain items, such as underground pipelines and storage tanks, are impossible to view without much special effort. A user would like to know a specific time to carefully check the performance of his corrosion protective system, either by a known lifetime of performance of the coating or by a measurement that can be made on an intact coating system that will predict remaining lifetime. Most coating users also desire a coating that generates no hazardous waste in application and removal.

Developers/designers of corrosion protective coatings need new materials to replace hazardous materials in coatings and new test methods for evaluating new coatings and new materials. Many of the more efficient materials used in the past for corrosion control are considered to be toxic or hazardous. There is a considerable list, but recently the elimination of these materials makes it difficult to use past coating formulation practice as any guide to new developments. Working with totally new materials also makes lifetime prediction for new coatings very difficult, as there is no past history of performance to use as a guide for such predictions. Further, salt fog testing according to ASTM B117 has been shown to be a poor predictor of performance(1), but until very recently, no substitute has been put forth, and many coating specifications still require a certain performance in this test.

Fundamental research on corrosion control by coatings has been addressing both the issues of new test methods and new materials. This has been difficult in an era where there has been decreasing support for long-term research. Within many companies, long-term research has been severely curtailed, especially among metal makers and coatings manufacturers. Support for fundamental research on corrosion control by coatings has been limited, but the focus both in government labs and academia has been to find better methods of predicting protective lifetimes. Coupling electrochemical methods and cyclic exposure methods has shown promise(2). Also, several questions remain unanswered: such as why and how do chromate pigments and pretreatments work, what can replace chromates - especially for protection of Al alloys, what gives true wet adhesion to metals in coatings, and what measurement(s) give the best predictions of in-field performance of coatings.

However, the situation concerning corrosion control coatings is now rapidly changing. The long pending imposition of rules and regulations severely limiting or eliminating chromate-based metal pretreatments and chromate pigments in coatings is coming to pass. Restrictions on the handling of hazardous materials is making manufacture, application, and removal of coatings containing hexavalent chromium in either the coating pigmentation or in the metal pretreatment very difficult, soon to be almost impossible. For example, the US Air Force (USAF) has a goal of Cr-free (pretreatment + coating) systems by the year 2000. Current USAF aircraft coatings are based on SrCrO₄ pigmented primers and chromate-based anodizing as the aerospace aluminum alloy pretreatment. A new pretreatment and pigmentation paradigm is needed to replace the current Cr-based systems, especially for structural aerospace Al alloys.

Further, the ubiquitous continuous salt fog test for corrosion control performance by coatings is acknowledged by most workers in corrosion control assessment to be of little value for the prediction of the performance of environmentally compliant coating systems. Yet, most government and many commercial specifications for coatings have historically required passing up to 2000 hours of this test. Why such a test method, apparently designed for the assessment of lead and chromate based pigmentation of solvent-borne alkyd coatings, remains so widely incorporated into specifications in place today is a mystery to many and a problem for many users and suppliers of corrosion control coatings. Most of the newer environmentally compliant coating technologies such as powder coatings, high solids and water-borne systems perform worse in regular salt-spray testing than their equivalent solvent-borne coatings, but under use conditions, they perform better. This is being acknowledged in the move within users and manufacturers of corrosion control coatings in the shift to cyclic testing such as Prohesion™ and the objective predictive electrochemical methods of electrochemical impedance spectroscopy (EIS) and electrochemical noise methods (ENM).

Corrosion Control by Coatings

Corrosion of metal objects occurs by electrochemical reactions at the surface involving the oxidation of the metal in the presence of water, electrolyte and oxygen. Most metals, except for the so-called noble metals, are most stable as oxides under most ambient conditions. Coatings are often used as a protective layer over the metal substrate to prevent the substrate from oxidizing in a manner deleterious to the function and appearance of an object. They do so in several ways (3). First, they act as a barrier limiting the passage of current necessary to connect the areas of anodic and cathodic activity on the substrate. This occurs especially if the coating wets the substrate surface very well and has good adhesion in the presence of water and electrolyte. Coatings do not really stop oxygen sufficiently to make its concentration at the surface rate limiting, and they do not completely stop water ingress into coatings. However, a good barrier coating slows water and electrolyte penetration and is not displaced by water at the substrate/coating interface. Barrier properties can come mainly from the polymer or from pigment volume concentration effects. As pigments block diffusion of water and oxygen below the critical pigment volume concentration (CPVC), increasing the pigment volume concentrations improves the barrier property of coatings. If the CPVC is exceeded, even locally, voids allow easy passage of water to the substrate surface and the barrier properties are lost. Coatings that act as barriers usually give better protection as their film thickness increases (without imperfections) or they are applied in multiple layers.

Second, coatings can act to release inhibitor materials that passivate the substrate or block the corrosion reactions. These are usually primer coatings that contain inhibitive pigments such as chromates, phosphates or molybdates. Coatings such as this will protect damaged areas of coatings by stopping corrosion reactions on local areas of the surface exposed by physical damage. Some coatings use soluble organic inhibitors, but these often leach out the film too rapidly to give long term protection.

Third, coatings can provide cathodic protection to a substrate if they are formulated with a metal pigment that is more electroactive than the substrate. This is most commonly done with zinc powder used over steel or iron. Other metal powders that might provide cathodic protection are too reactive in particulate form (Mg) or form oxide films that prevent electrical contact between particles. The metal pigment volume concentration must exceed the CPVC to have all of the particles touching and also in contact with the metal surface. These are the so-called Zn-rich coatings often used as primers for steel objects where galvanizing cannot be used. This type of coating provides protection for damaged areas, but must be overcoated by a topcoat to keep the metal pigments from being directly oxidized by atmospheric exposure.

Coatings Used for Corrosion Control

There are many coatings on the market today that offer some form of corrosion protection to metal substrates. Major use areas where corrosion protective properties of coatings are a preeminent requirement for so-called Original Equipment Manufacture (OEM) or factory-applied coatings are: automotive coatings systems; appliance coatings; metal coil coatings; powder coatings for heavy duty use, especially pipeline coatings (usually identified as a class as fusion-bonded epoxy coatings); farm and construction equipment coatings; and general use coatings for objects used in exterior exposure, such as lawn furniture, metal window frames, etc. This list is not all-inclusive, but identifies major OEM areas where corrosion protection by coatings is important. Field applied coatings where corrosion protection is of primary concern are aircraft coatings, pipeline coatings in the field, marine coatings, railroad car coatings, the general area called industrial maintenance coatings - general purpose coatings for exterior protection- bridges, decks, industrial plants, storage tanks, exterior metal structures, etc. These coatings are often multiple layer systems with the primer coatings (first layer next to the metal substrate and its pretreatment) usually designed to provide the corrosion protection in damaged areas and the overcoat(s) providing barrier and UV protection to underlying layers.

Polymers that are most successfully used for corrosion protective coatings are epoxy-based materials; polyurethane based polymers, urethane topcoats over epoxy primers, some cross-linked polyester materials, and some melamine cross-linked polymers. One thing in common among these polymers is their ability to wet and adhere to metal oxides, plus their stability in the presence of water and basic conditions. Coatings that can be cross-linked at relatively high temperatures in thin films give relatively good performance. One other characteristic of successful corrosion protective coatings is that they can be applied in relatively defect free films. Film thickness uniformity is very important for corrosion protection (4). There is much information from suppliers and trade publications about the relative merits of various coating systems, and it is suggested that the reader see these sources for details.

Coating systems work successfully only when the metal surface is well cleaned. In factory use, when the metal often receives a pretreatment to form a protective oxide or related material. This is often done using chromate baths for Al alloys and phosphate-based pretreatment for steels. These baths are often acidic to remove prior surface oxides and leave a controlled oxide surface with chromate or phosphate incorporated. Again, this is a field with much information on field use available from

suppliers and trade literature. One issue that users of these pretreatments must face is environmental legislation, especially on waste material from these systems, which can be toxic, especially chromate baths. Dry pretreatments or environmentally benign systems that put down thin adherent protective layers are now being examined to replace earlier systems. Plasma cleaning and deposition as well as sol-gel chemistry are being examined, especially in systems with high maintenance and refinishing costs. In production, $\frac{3}{4}$ ths of the coating line space and cost is often devoted to cleaning and pretreatment. Also, galvanizing is being used on many sheet steel systems, especially for automobile, siding and appliance use. This often provides a more uniform surface for coating than untreated steel, as well as providing cathodic protection to the steel.

Measurement of Corrosion Protection by Coatings

The area of corrosion protection by coatings is that is currently undergoing the most change is the area of testing of performance. It is safe to stick with proven tests, and many specifications have existing tests included. However, the single most used test method, the continuous salt spray test has significant weaknesses. It is in the process of being replaced by other tests, which have been shown to be better predictors of performance. As new technologies have developed to provide coatings that protect against corrosion while reducing VOC and the use of toxic pigments and inhibitors, older test methods have not been always able to identify correctly those new coatings, which provide improved protection. There is a new generation of test methods that have been developed that provide objective, numerical characterization of coating performance, or improved ranking types of tests that while still subjective, provide better prediction of new coating performance. The numerical test methods are based on electrochemical methods, and they include Electrochemical Impedance Spectroscopy (EIS) (5), and Electrochemical Noise Methods (ENM) (6), among others. Many of the chapters of this book include work based on these methods, and how they are being used for the study of organic coatings over metals.

Other developments in test protocols for determining coating performance against corrosion have included cyclic testing methods (7) such as the Prohesion™ cabinet test, alternating wet-dry cycling of coatings, and using UV exposure in the cyclic exposure of coatings. These exposures are now being coupled to some of the electrochemical methods just mentioned for more realistic studies of coating performance.

Lifetime and Cost Issues in Coatings for Corrosion Protection

As stated above, coatings remain one of the most cost-effective means of providing practical protection from corrosion to easily corrodible metallic (and sometimes non-metallic) structures and objects. But often they are chose by initial investment cost only. The use of organic coatings for corrosion control (the term control is used because, in a thermodynamic sense, corrosion can never be eliminated, only controlled to a low enough rate as to be ignored) is so pervasive in our society that is too often taken for granted. Quality and effectiveness of corrosion control by coatings is assumed by many users to be low cost and easy to achieve. For these and

other reasons, users of corrosion control coatings often choose coatings only by (material + application) cost and appearance, not by cost effectiveness as measured by their true performance and lifetime of that performance. However, with high labor costs and difficulties in recoating large, buried, difficult to reach or complex objects, more sophisticated coatings users are focusing on the total costs of corrosion prevention and control. This leads to a realization that a coating system that provides long use life but is somewhat more expensive initially for initial application will pay for itself in reduced maintenance costs and reduced need for expensive recoating. The more this reasoning is followed in analyzing the cost of corrosion protection by coatings, the more the research into measuring and predicting the protective properties of coatings will be performed. Analyzing the coating by its initial cost alone makes a coating that significantly increases the lifetime of protection at a somewhat higher cost not well accepted in the marketplace. The payoff on developing systems based on true lifetime costs has been shown in the automobile industry, where the use of two sided galvanized steel + enhanced corrosion protective ED primers has raised the average lifetime until noticeable rust damage on cars to about 10 years.

New Technologies

New technologies and materials for corrosion protection by coatings are coming into the coatings science from other areas. The possibility of providing corrosion protection by incorporating the use of conductive polymers, such as doped polyaniline, is being actively pursued by researchers. The extension of the thin film technologies developed for the semi-conductor electronics industry to surface preparation of substrates for protective coatings is being pursued. Plasma cleaning and plasma deposition of thin films for subsequent coatings is being examined, as well as the use of sol-gel thin films for surface pretreatment. Both of these latter may replace Chromate-based pretreatments for metals. The in-situ sensing of the state of corrosion protection in a system by implanted electrodes, and some other non-destructive testing method is being considered by large users of coated metals as another way of doing maintenance on a need basis, not only on a regular cycle. Because of the cost of the objects that they protect and the large costs of maintenance and repainting, the corrosion protective properties of organic coatings are more important than ever. Any added lifetime of use of objects and materials that coatings can add is in actuality a significant contribution to the economy and the environment.

Summary

Corrosion protection is a key property of organic coatings, and their use for this purpose is a key contribution that coatings make to the world economy. If coatings continue to receive the minimal attention from the many users and developers of coatings that treat coatings for corrosion protection as almost commodities, the continued investment of coatings suppliers and research agencies will significantly slow. This will increase the burden that corrosion already has on our economy and also increase the need for maintenance and repair. If we continue and increase our investment in understanding and preventing corrosion by well designed new coatings,

everyone will benefit. One can see this effect already in the drastically increased lifetimes against corrosion of cars and household appliances vs. 10-15 years ago, effects due to a combination of improved substrates and coatings.

The symposium contains a good number of papers examining these newer test methods, showing the value of electrochemical testing in combination of cyclic exposure testing, and also, showing how environmentally compliant coatings are rapidly displacing regular coatings in corrosion control use. Many of the chapters of this symposium book are devoted to the electrochemical testing of coatings, and the examination of the test methods with respect to predicting coating lifetimes, or at least ranking coatings within a cohort of candidate coatings. These papers are Chapters 1-8, 11-12, 14, 34. The emphasis within these papers is to improve numerical ranking of corrosion performance; to develop measurement tools that provide insight into what is happening at the metal/coating interface, as well as within the coating during exposure; and to provide insight into the mechanisms that lead to the failure of the protection the coating affords to the metal. Some of the issues addressed in these papers are what is the proper exposure for the testing, what should the composition of the immersion electrolyte be for electrochemical testing, and what accelerating factors are valid to give failure within a laboratory test procedure in a manner that properly emulates field service failure. The statistics of sampling to predict coating failure is also considered (Ch. 18).

Localized measurement methods for examination of defect areas in coatings are also described, including scanning acoustic microscopy (Ch. 10), localized electrochemical impedance spectroscopy (Ch. 2.), and SEM. These are all utilized to give insight into local failures in the coatings. There is also a paper discussing the relationship between defects, local fluctuations in film thicknesses and other coating properties, and corrosion protection (Ch. 16). Another paper gives predictive modeling for the formation of a common local defect noted in corrosion failure of coatings, blister formation (Ch. 17). Several papers address the important issue of water uptake and diffusion in protective coatings, and how water transport in coatings and its effects on coating properties is a key issue that requires attention *vis a vis* corrosion control (Ch 12-13).

Several papers consider new thin-film technologies for corrosion protection. One paper (Ch. 21) considers self-assembled monolayers and multi-layers as films for the protection of copper. Two papers address the formation of thin plasma-polymer protective layers for improvement of the subsequent adhesion of thicker, standard corrosion protective films (Ch. 19-20). Another examines the properties of electro-polymerized thin films (Ch. 23). There were also two papers addressing the still yet unresolved issues about the potential corrosion protection afforded by poly(aniline) films to metals (Ch. 30-31). This latter is an area of extreme interest, because there have been indications that chemically doped conductive poly(aniline) can provide corrosion protection without the need for pigmentation, but solely due to electrochemical effects. Two papers address the issues of microbial induced corrosion and its assessment in coated systems (Ch. 25-26)

The other papers consider a diverse range of problems in the use of corrosion protective coatings. There are two papers that consider the specific problems of aircraft protective coatings (Ch. 23 & 24), and one paper focusing on the protection of concrete (Ch. 27), a topic closely allied to the protection of metals. Also examined

are coatings for use in oil fields (Ch. 15) and marine anti-corrosion coatings (Ch. 28). There are also papers that address issues of the development of substitutes for chromates in pigmentation (Ch. 32 & 33) and metal pretreatment (Schulman paper), new polymer matrices for corrosion protective coatings (Ch. 29), environmentally compliant coatings from natural products (34), and a chapter on MoS₂ in protective poly(ethylene) films.

Organizing and participating in this symposium has been a very satisfying experience for me, and I wish to take this opportunity to thank all of the presenters of papers at the symposium and those that prepared the papers that make up the chapters of this book for their contributions. I wish to thank ACS Books for the opportunity to organize and publish this symposium and the help that they have provided in making this book possible.

Literature Cited

- (1) Skerry, B.S & Simpson, C.H. "Accelerated Test Method for Assessing Corrosion and Weathering of Paints for Atmospheric Corrosion," *Corrosion* **1993**, 49B 663674.
- (2) ASTM D5894, *Annual Book of ASTM Standards*; Amer. Soc. Testing & Materials, West Conshohaken, PA, 1997.
- (3) Bierwagen, G.P. "Reflections on Corrosion Control by Coatings," *Prog. Organic Coatings* **1996**, 28, 43-48.
- (4) Bierwagen, G P. "Defects & Heterogeneities in Corrosion Protective Organic Coatings Films and Their Effects on Performance" ACS Symposium Book, *Corrosion and Its Control By Coatings*, G.P. Bierwagen, ed.
- (5) Fredrizzi, L.; Deflorian, F.; Boni, G.; Bonora, P.L. and Pasini, E. "EIS Study of Environmentally Friendly Coil Coating Performances," *Prog. Org. Coatings* **1996**, 29, 89-96.
- (6) Mills, D. J.; Bierwagen, G. P.; Tallman, D.E. and Skerry, B.S. "Investigation of Anticorrosive Coatings by the Electrochemical Noise Method," *Material Perf.*, **1995**, 34, 33.
- (7) Appleman, B.R. "Cyclic Accelerated Testing: The Prospects for Improved Coating Performance Evaluation" *J. Protective Coatings & Linings* **Nov. 1989**, 71-79. And Appleman, B.R., "Survey of Accelerated Test Methods for Anti-Corrosive Coating Performance" *J. Coatings Tech.* **1990**, 62, (#787), 57-67.

Chapter 2

Long-Term Electrochemical Impedance Spectroscopy and Electrochemical Evaluations of Five Distinct Types of Navy Coatings

J. N. Murray

Naval Surface Warfare Center, Carderock Division, Code 613, Corrosion Branch,
Building 60, 9500 MacArthur Boulevard, West Bethesda, MD 20817-5700

Electrochemical Impedance Spectroscopy (EIS) has been successfully utilized to characterize and monitor three types of polyamide cured epoxy barrier coatings applied to clean or tightly rusted, conventional low carbon steel sheets. The coatings which satisfy MIL-P-24441 Type I or Type IV preparations on clean steel have exhibited reasonably consistent EIS parameters for up to 6 years continuous exposure to ASTM-D-1141 substitute ocean water. Experiments with the Type IV coatings over rusted steel during the first year's exposure have demonstrated the ability to monitor the onset and continuation of the corrosion process at the rust/steel interface. Dielectric constants from the essentially anhydrous coatings, near saturation water absorption values as well as water absorption diffusion coefficients have also been determined.

Barrier coatings such as polyamide cured epoxies satisfying MIL-P-24441, "Military Specification; Paint, Epoxy-Polyamide; General Specification For", have been utilized for protecting steel and other metallic substrates in immersion applications for over 20 years. Although electrochemical testing has been involved in characterizations of these coating systems, there are few experiments reported where data are presented for more than a 12-month exposure period. Many tests are being limited to evaluation of the paint condition after from 3000 to 5000 hours exposure to salt fog testing per ASTM-B-117 or an equivalent test modification. This paper briefly summarizes electrochemical test data obtained for up to six years, from epoxy coatings exposed to aerated ASTM-D-1141 substitute ocean water. The test methods included electrochemical impedance spectroscopy (EIS) and potential measurements to characterize five distinct types of epoxy/steel substrate systems.

Experimental

Four of the coating systems were sprayed or dip-applied onto clean 1010 carbon steel panels either precleaned or prerusted in the local Maryland environment and wire brushed prior to coating. The four coating systems included a three layer MIL-P-24441 Type I (600 g/l volatile organic compounds (VOC)) F-150, F-151, F-154 system; 2, 3 and 4 layer transparent (fillerless and pigmentless) Type I coatings; a MIL-C-85285 urethane topcoated Type I, F-150 epoxy primed system; and a two layer Type IV (350 g/l VOC) F-150, F-151 coating. The majority of the samples were prepared at the Naval Surface Warfare Center, Carderock Division (NSWCCD), Annapolis site. One set of Type I coatings and the urethane topcoated samples were prepared by the Mare Island Naval Shipyard (MINSY) .int Shop as part of a NSWCCD/NCEL (Navel Civil Engineering Laboratory), EIS/coating evaluation project. The Type I coatings were applied at Annapolis over as-received panels supplied by Q-Panels, Inc., acetone washed and room temperature dried just prior to coating. The Type IV coatings were applied to grit blasted Q-Panels, one set being epoxy paint sprayed onto "white metal" surfaces. The other Type IV set was sprayed onto "tight rust". Grit blasted steel panels were exposed to Maryland weather for 30 days to allow formation of a "natural" rust, then water rinsed and wire brushed to remove any easily loosened corrosion product just prior to applying the coating(s). In accord with MIL-P-24441, between 12 and 16 hours of cure/drying time was allowed between coating layer applications.

Following application of the last layer of the Type I coating systems, the normal process was to dry the coatings at ambient temperature for approximately 1 week. Then the samples were confined in a "dry" box containing freshly regenerated molecular sieves for a minimum of 30 days. Previous testing with 1 mm thick thermoplastic polymers such as polysulfone established that the polymer could be dehydrated to less than 4% of the water saturation level in approximately 30 days. This dehydration approach was elected to preclude any high temperature T_g transformations and therefore test the coating systems in the dehydrated, but as-prepared condition. The Type IV coatings were only cured for 7 days with no attempt to dehydrate the cured polymer system.

Clamp-on, O-ring seal, glass cells with either 13 or 31 cm² wetted area were permanently attached to the majority of the coated panels. This approach eliminated any possibility of electrolyte penetration to the coating/steel interface via edge leakage. A minimum of 5 samples of each type of coating were evaluated monthly for up to 6 years exposure (to date) using EIS as the primary characterization tool. The Type IV epoxy coating samples have only been evaluated for the first year's exposure (to date). The EIS data were collected from 100 kHz to 5 mHz using a 5 mV AC input signal. The EG&G, PAR Model 388 software, driving the PAR model number (M/N) 273 Potentiostat coupled with the EG&G M/N 5206 Lock-In Analyzer, was utilized for the EIS experiments. Potentials of the coated steel panels were independently obtained using a basket style Ag/AgCl reference electrode in conjunction with a high ($10^{14} \Omega$) impedance digital electrometer.

All experiments were performed at ambient laboratory temperature, which ranged from 20 to 26°C. The test electrolytes were exposed to the laboratory air and are

considered as air saturated. Water lost by evaporation was resupplied with 16 M Ω deionized water roughly every 3 months.

The EIS data were analyzed using the conventional nested RC pair model(1) (Figure 1). The conventional parameters of coating capacitance (C_{coat}), the maximum impedance at low frequency (Z_{max}), the coating pore impedance (Z_{pore}) when evident, and the break-point frequencies as discussed by Haruyama (2) or Hack/Scully (3) were utilized.

Results and Discussion

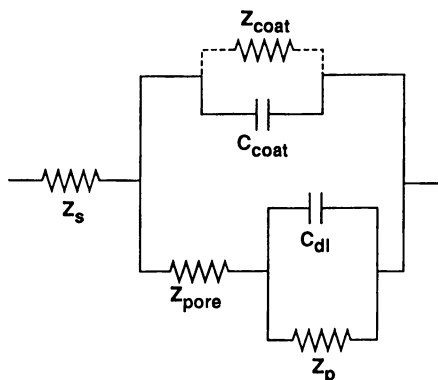
Physical Appearance. Negligible blistering has been observed with the transparent and Type I epoxy systems after 6+ years exposure. The blistering of the urethane topcoated system has occurred starting at the fourth year with two of the five test panels having blisters on the major surface. No blistering of the Type IV epoxy samples has been observed in the 1 year exposure accumulated to date.

Potentials. With highly effective barrier coatings applied over clean steel surfaces, the potentials of the substrate relative to the Ag/AgCl reference electrode tend to be positive and decrease to the -0.2 V level as H₂O absorbs within the polymer film during the first day of exposure. Typical results from the Type IV panels are presented as Figure 2. If the coating contains pores or defects which extend through the coating exposing the metal substrate to the test electrolyte, the observed potentials tend to approach the -0.6 to -0.7 V range, the normally observed E_{corr} range for steel in neutral pH, aqueous electrolytes. For 5 of the 6 Type IV epoxy coatings applied over tightly rusted steel, the potential shifts during the initial influx of H₂O were more pronounced, decreasing to the -0.3 V range within the first 2 weeks of exposure. The time dependent E_{corr} data are summarized in Figure 3 and as can be seen, the potentials of the rusted steel interface have slowly decreased to the -0.55 V range.

EIS Data. The EIS data evaluated using the Bode magnitude and Bode phase formats were essentially those expected from a capacitive film with a few, extremely small defects, traversing the coating system to the substrate steel.

Capacitance Data. The coating capacitance data as determined in the 10⁴ to 10⁵ Hz range have been utilized to determine the dry film dielectric constants as well as the water absorption quantities and water diffusion rates. The unfilled polymer dielectric constant as determined at 1 hour electrolyte exposure averaged 3.8. The constants for both Type I and Type IV coating systems which contain approximately 26 volume percent (v/o) TiO₂/magnesium silicate filler and pigment(s) were measured at 7.6, this average consistent with the value of 7.3 calculated from theoretical considerations. Typical capacitance-reciprocal thickness data are presented in Figure 4 for the Type I epoxy system.

The transparent and Type I coating systems (Figure 5) required a considerable period to approach water saturation. The data from the Type IV system are shown in Figure 6, and this coating system seemed to saturate more rapidly. The only inflection point at approximately 250 hours exposure did not correlate with the inflection seen in the potential-time data (Fig. 2). Water content values were calculated from the capacitance data using the Brasher-Kingsbury equation (4) and



Where:

- Z_s ≡ Bulk Solution Impedance
- Z_{coat} ≡ Coating Electronic Impedance (normally $>10^{12} \Omega$)
- C_{coat} ≡ Coating Capacitance
- Z_{pore} ≡ Solution Impedance Within Coating Pores
- C_{dl} ≡ Double Layer Capacitance of Exposed Substrate
- Z_p ≡ Polarization Impedance of Exposed Substrate

Figure 1. Conventional Nested-Pair, Equivalent Circuit Model for Organic Coated Metal Substrate.

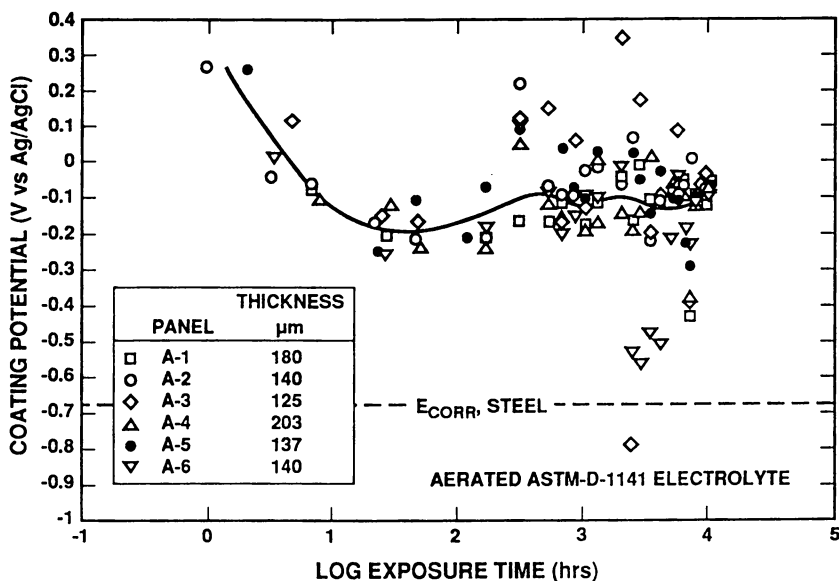


Figure 2. Typical E_{corr} vs (log) Exposure Time Data; Type IV Epoxy Applied Over Clean Steel. 31 cm^2 Sample Area. First Year Exposure.

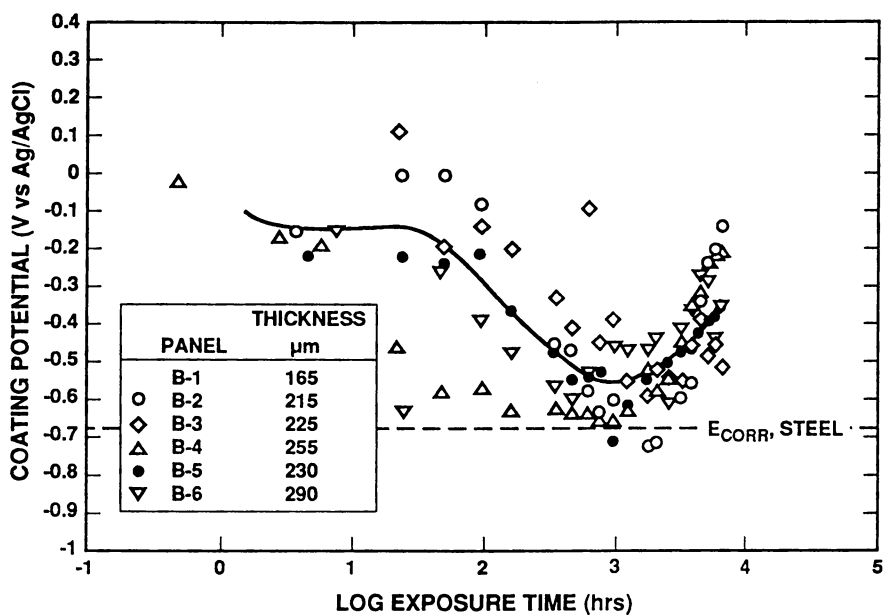


Figure 3. E_{corr} vs (log) Exposure Time Data; Type IV Epoxy Applied Over Tight Rust on Steel. 31 cm^2 Sample Area. First Year Exposure.

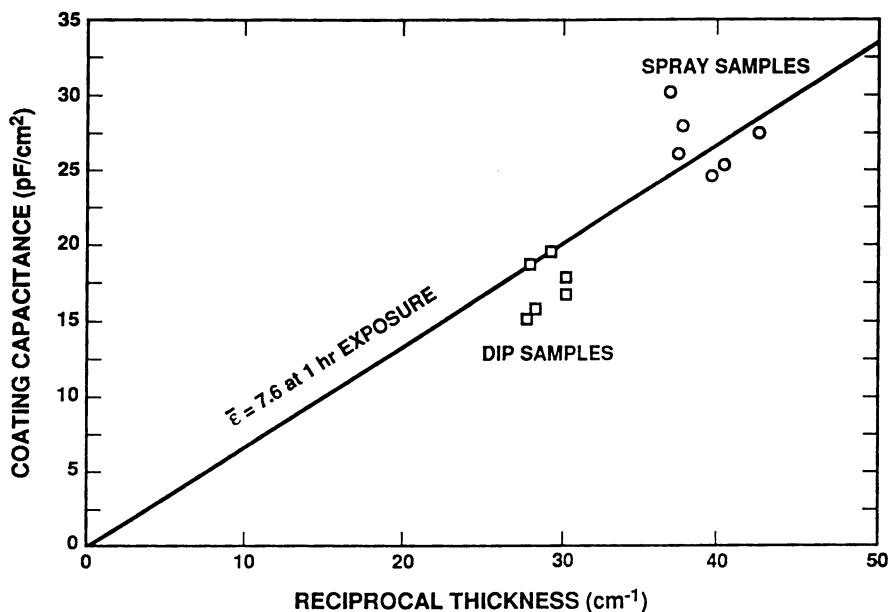


Figure 4. Dipped MIL-P-24441, Type I Epoxy Coatings. Coating Capacitance vs Reciprocal Thickness. 13 cm^2 Sample Area.

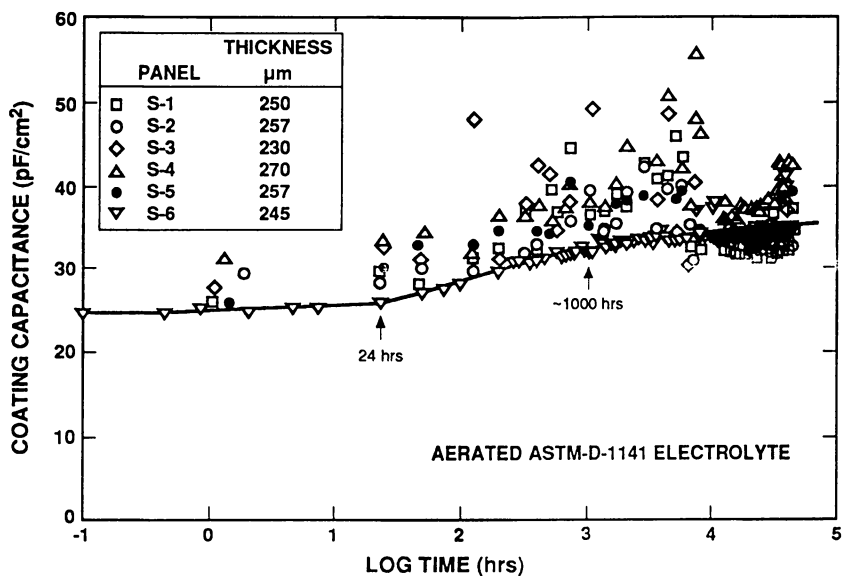


Figure 5. Coating Capacitance vs (log) Exposure Time; MIL-P-24441, Type I, Sprayed F-150, F-151, F-154 Epoxy Coating System, >30 Day Cure. 13 cm^2 Sample Area.

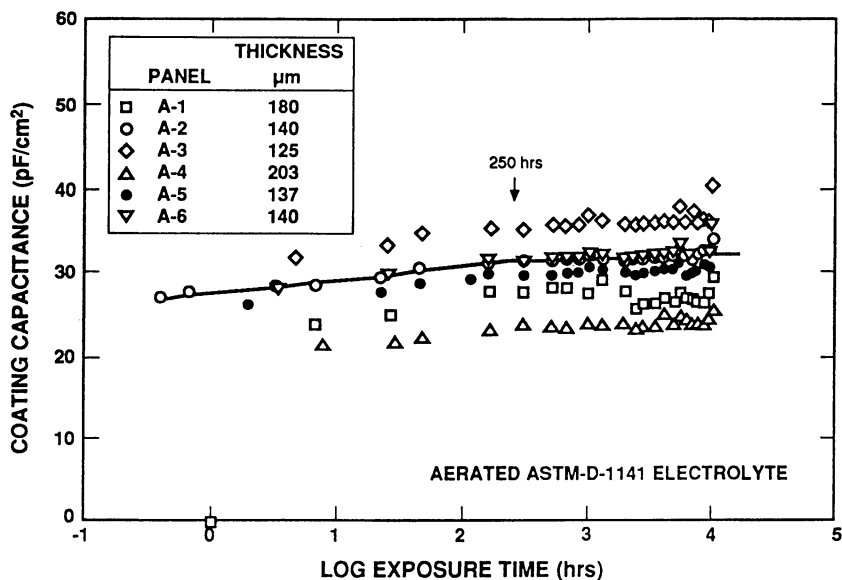


Figure 6. Coating Capacitance vs (log) Exposure Time; MIL-P-24441, Type IV, Sprayed F-150, F-151 Epoxy Coating System, 7 Day Cure. 31 cm^2 Sample Area.

diffusion coefficients were calculated from the 50% water saturation value (5). Whereas the water diffusion coefficients for the sieve dried and longer cured Type I systems were calculated to be between 10^{-9} and 10^{-10} cm^2/sec range, the water diffusion coefficients for the Type IV samples were calculated to be in the 4×10^{-8} cm^2/sec range. The Type IV values are in reasonable agreement with the value of 1×10^{-8} cm^2/sec obtained by Scully (6) from MIL-P-24441, Type II coatings. Additional studies are required to determine if the different diffusion rates are due to material differences or the different drying/curing approaches that were undertaken.

Z_{max} . In general, all coatings exhibited a high initial impedance in the 10^{10} to 10^{11} $\Omega \cdot \text{cm}^2$ range when measured in the low frequency range of ≤ 0.01 Hz. As reported by Bacon (7) in 1948, this value usually decreases to the 10^9 to 10^{10} $\Omega \cdot \text{cm}^2$ range during the 30 days exposure. For excellent coatings the values then return to the high initial ranges, the increase assumed to be the result of corrosion products precipitating within the coating pores reestablishing the higher ionic resistance paths. Typical data from the 4.6 years of exposure for the sprayed Type I coatings are summarized in Figure 7. The spread of the Z_{max} values is due in part to a deliberate preparation of slightly different coating thicknesses. The data for the panels prepared by MINSY in Figure 8 are seen to follow the same general trends for up to 6 years. The data from the first year exposure of the Type IV samples are presented as Figure 9. Although there were differences between Types I and IV coatings in the calculated capacitances, the Z_{max} data are essentially the same. The arrest in the decrease of Z_{max} at approximately 65 hours exposure did not correspond with the shift in the capacitance data (Fig. 6) which occurred at approximately 250 hours.

The maximum impedance values from three of the five Type IV coating samples applied over tight rust decreased significantly within the first 21 days exposure. The Z_{max} data summarized in Figure 10 follow the potential shifts shown in Figure 3. The other two samples have maintained high Z_{max} values throughout the exposure period. A comparison of the Bode plots from a "good" and a "poorer" Type IV sample is presented in Figure 11.

The polyurethane topcoated system has slowly decreasing Z_{max} values starting at about 3.5 years and is now in the 2×10^7 $\Omega \cdot \text{cm}^2$ range. The Z_{max} data are summarized in Figure 12. Three of the five samples have no blistering on the primary surface after 5.7 to 6.3 years) exposure. The first panel (2516B) showed blistering at an area outside the EIS cell location at approximately 4.3 years exposure and the other sample (2517C) at 5.6 years exposure.

Break-point Frequencies, f_{lo} and f_{hi} . All the stable coatings having one RC time constant have exhibited break-point frequency (f_{lo}) range from 0.1 to 1 Hz throughout the 6 years exposure. Based on the Hack/Scully (3) analysis of the nested pair model, this range represents an exposed pore (defect) area of approximately 0.00001%. The f_{lo} value for the urethane topcoated system has increased to the 40 to 650 Hz range during the same timeframe. Based on the Hack/Scully (3) analysis of the nested pair model, this increase represents approximately 0.01% of the coating area as through-coating defects.

The case of the Type IV coatings applied over tight rust is another matter. As indicated earlier, two of the samples have maintained high Z_{max} values with f_{lo} values

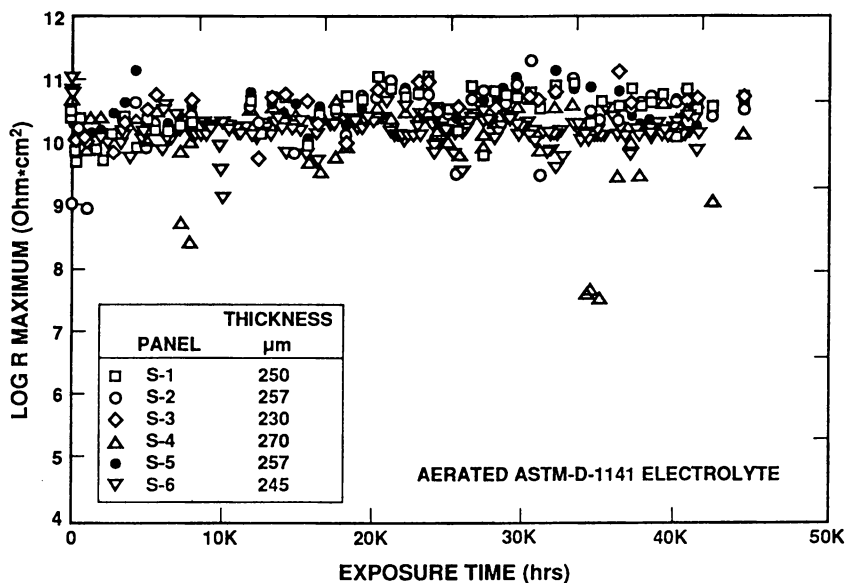


Figure 7. Log Maximum Impedance vs Exposure Time; MIL-P-24441, Type I, Annapolis Sprayed F-150, F-151, F-154 Epoxy Coating System, >30 Day Cure. 13 cm² Sample Area.

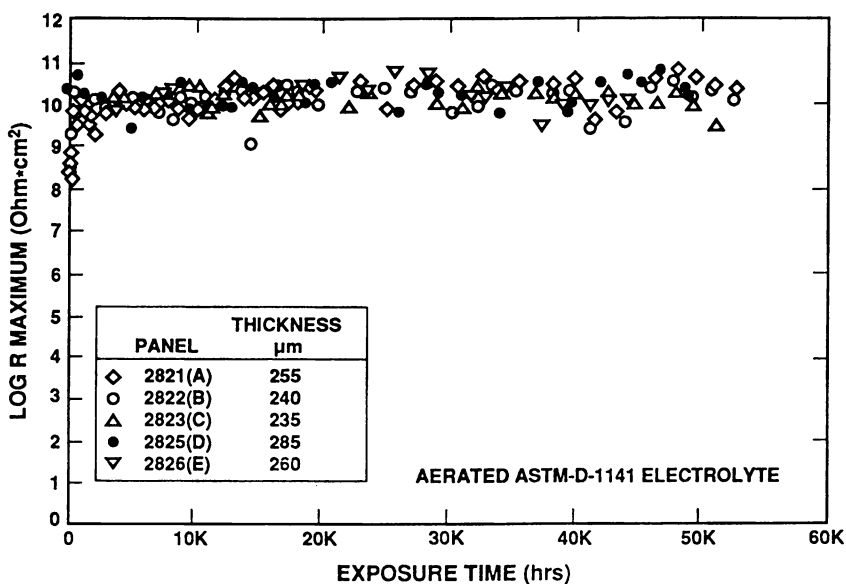


Figure 8. Log Maximum Impedance vs Exposure Time; MIL-P-24441, Type I, MINSY Sprayed F-150, F-151, F-154 Epoxy Coating System, >30 Day Cure. 13 cm² Sample Area.

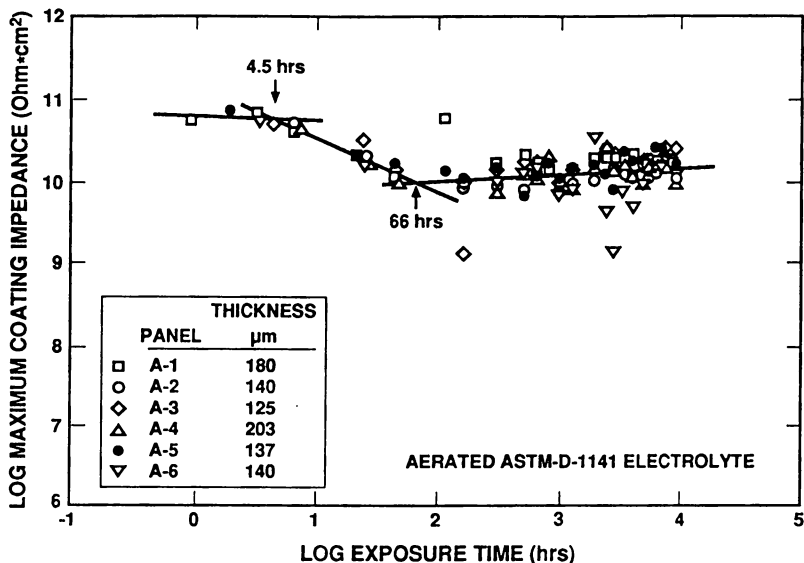


Figure 9. Log Maximum Impedance vs Exposure Time; MIL-P-24441, Type IV, Sprayed F-150, F-151 Epoxy Coating System, 7 Day Cure. 31 cm^2 Sample Area.

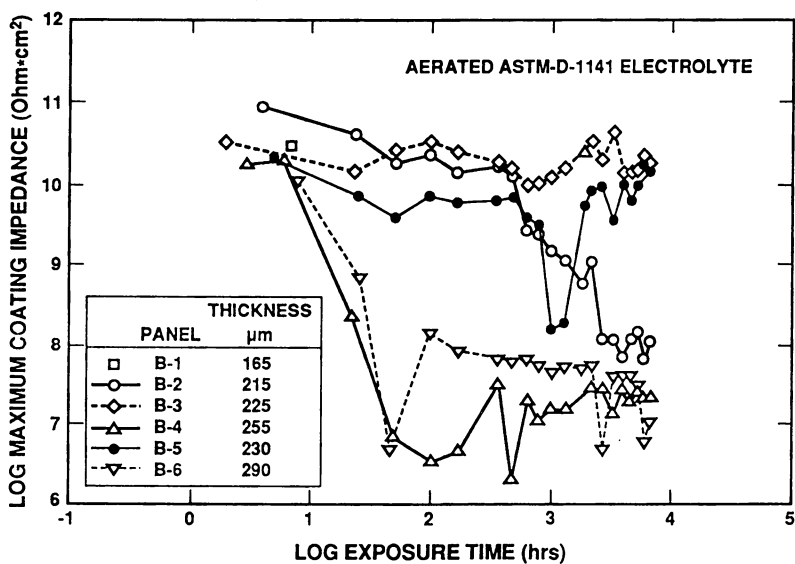


Figure 10. Log Maximum Impedance vs Exposure Time; MIL-P-24441, Type IV, F-150, F-151 Epoxy Sprayed Over Tight Rust, 7 Day Cure. 31 cm^2 Sample Area.

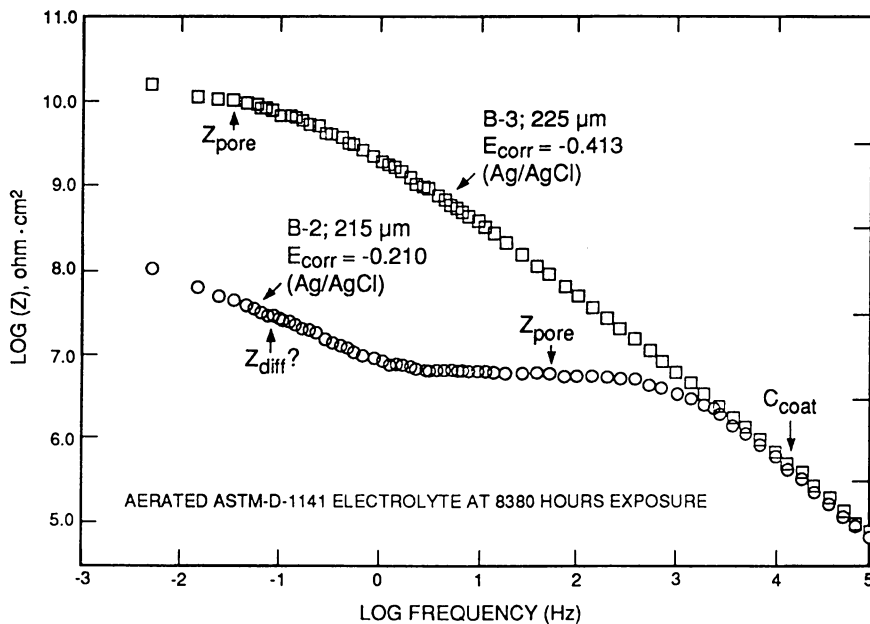


Figure 11a. Bode Magnitude Plots; MIL-P-24441, Type IV, F-150, F-151 Epoxy Sprayed Over Tight Rust, 7 Day Cure. 31 cm^2 Sample Area.

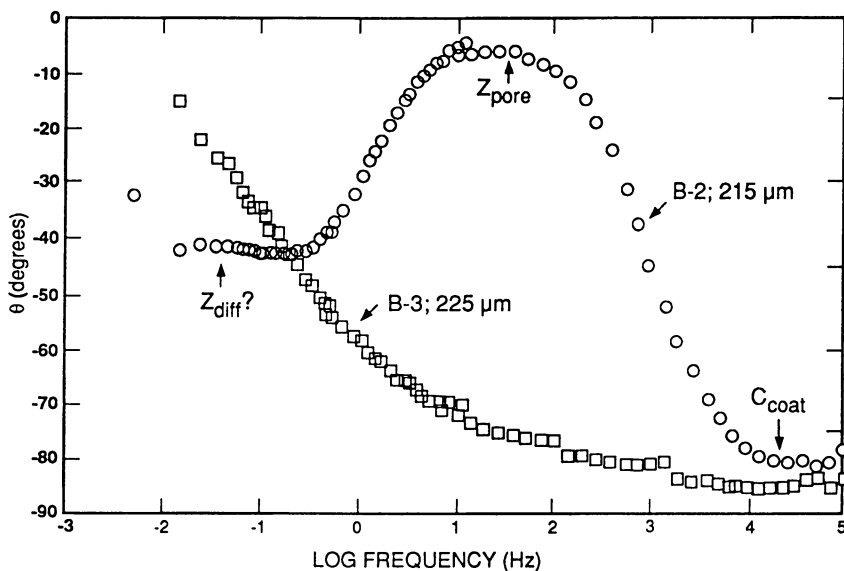


Figure 11b. Bode Phase Shift Plots; MIL-P-24441, Type IV, F-150, F-151 Epoxy Sprayed Over Tight Rust, 7 Day Cure. 31 cm^2 Sample Area.

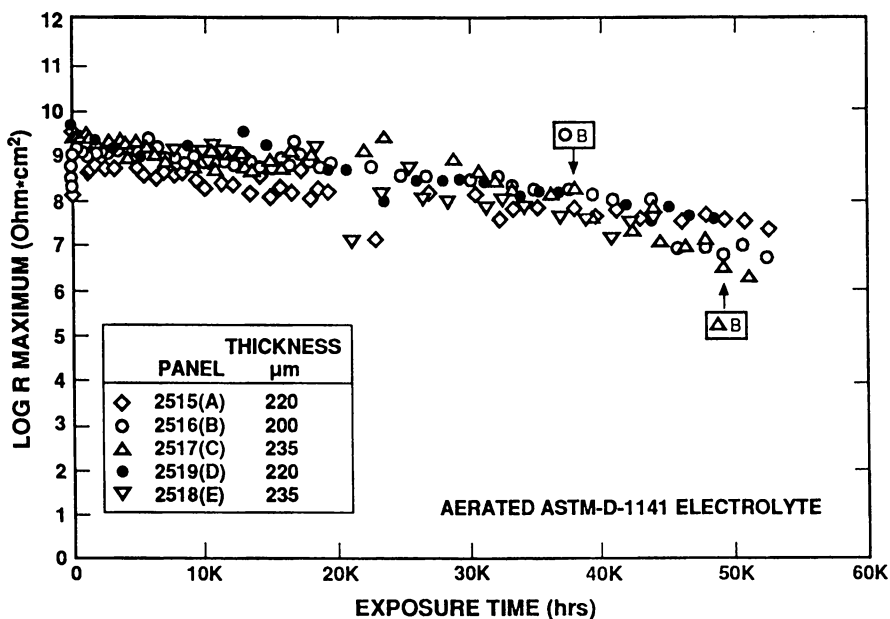


Figure 12. Log Maximum Impedance vs Exposure Time; MIL-C-85285, Urethane Topcoated Over MIL-P-24441, Type I, F-150 Epoxy Primer (MINSY), >30 Day Cure. 13 cm² Sample Area. B Indicates Initial Blister Observation.

in the ≤ 1 Hz range, suggesting $< 0.00001\%$ exposed defect area. The other three samples exhibited 2 RC time constant behavior within 21 days with no visual sign of blistering or rusting even at one year exposure. As indicated in Figure 11, the data from Sample B-3 is better fit with the addition of a Warburg (diffusion) element placed in series with the R_p element (shown in Fig. 2). The f_{hi} break-point of approximately 1000 Hz (Fig. 11) would suggest a defect area of 0.00025% based on the Hack/Scully analysis (3).

The break-point frequency method initially presented by Haruyama (2) for quantifying coating disbondment or uncovered area and reanalyzed by Hack/Scully for pore/defect areas (3) has been shown to be applicable to very thin epoxies (2,3,8), latex coatings (9) and typical automotive finishes (10). However, serious questions have been raised (11) regarding the applicability of the break-point analysis to the disbonding of thick, barrier-type coatings (like epoxies) with Z_{max} values exceeding $10^8 \Omega \cdot \text{cm}^2$. Here, with the Type IV epoxy coating applied over tight rust, one might assume the coating to be considerably less bonded to the substrate than the coating applied to clean steel. The general shape of the Bode formatted EIS data from three of the samples would suggest much more electrochemical activity at the Type IV/rusted steel interface than exhibited by the coatings applied to bare steel. It does remain as more than a curiosity as to the relationship between the assumed loss of adhesion without blistering and the appearance of the additional EIS characteristics.

Summary

EIS has been successfully utilized to characterize a variety of MIL-P-24441 epoxy coating systems. The three-layer, Type I, all-epoxy-coating system has been shown to be electrochemically and physically stable in substitute ocean water for over 6 years continuous exposure. Although the EIS evaluations are limited to only a 1 year exposure period, the data suggest the stability of the Type IV epoxy coating system is inferior to the Type I system. Experiments with the Type IV epoxy coatings applied over tightly rusted steel have reconfirmed that electrochemical techniques do allow monitoring of the processes at the coating substrate interface although the significance of the data with respect to coating disbondment remains to be established.

Acknowledgments

This project has been supported and promoted by Mr. I.L. Caplan, Code 0115, NSWCCD, as part of the Seaborne Coatings and Corrosion Control Projects now under the sponsorship of ONR, Dr. A. John Sedriks, Code 332. The MINSY samples and initial support from NCEL were provided under the supervision of Mr. Daniel Zarati. The Type I sample preparation at NSWCCD was provided by Ms. Angela Ross (Code 641), the Type IV samples and evaluation funding supplied by Ms. Karen Poole (Code 641). All evaluation work has been performed within the Corrosion Branch (Code 613), Mr. Robert J. Ferrara, Branch Head.

Literature Cited

1. Walter, G.W. *A Review of Impedance Plot Methods Used for Corrosion Performance Analysis of Painted Metals* *Corr. Sci* **1986**, 26, No. 9, pp 681-703.
2. Haruyama, S.; Asari, M. and Tsuru, T. *Impedance Characteristics During Degradation of Coated Steel* in *Proc. Corrosion Protection by Organic Coatings*; The Electrochemical Soc.: Pennington, NJ, 1987, Vol. 87-2, pp 197-207.
3. Hack, H.P. and Scully, J.R. *Defect Area Determination of Organic Coated Steels in Seawater Using the Breakpoint Frequency Method* *J. Electrochem. Soc.* **1991**, Jan., 138, No. 1, pp 33-40.
4. Brasher, D.M. and Kingsbury, A.H. *Electrical Measurements in the Study of Immersed Paint Coatings on Metal. I. Comparison Between Capacitance and Gravimetric Methods of Estimating Water-Uptake* *J. Appl. Chem* **Feb. 1954** 4, pp 62-72.
5. Li, S.Z.; Pak, Y.S.; Adamic, K.; Greenbaum, S.G.; Lim, B.S.; Xu, G. and Nowick, A.S. *Diffusion and Deuteron Nuclear Magnetic Resonance Study of the Distribution of Water Molecules in Polyimide Films* *J. Electrochem. Soc.* **Mar. 1992**, 139, No. 3, pp 662-667.
6. Scully, J.R. *Electrochemical Impedance of Organic-Coated Steel: Correlation of Impedance Parameters with Long-Term Coating Deterioration* *J. Electrochem. Soc.* **Apr. 1989**, 136, No. 4, pp 979-989.
7. Bacon, R.C., Smith, J.J. and Rugg, F.M. *Electrolytic Resistance in Evaluating Protective Merit of Coatings on Metals* *I&EC* **Jan. 1948**, 40, No. 1, pp 161-167.
8. McCluney, S.A.; Popova, S.N.; Popov, B.N.; White, R.E. and Griffin, R.B. *Comparing Electrochemical Impedance Spectroscopy Methods for Estimating the Degree of Delamination of Organic Coatings on Steel* *J. Electrochem. Soc.* **June 1992**, 139, No. 6, pp 1556-1560.
9. Murray, J.N. and Hack, H.P. *Use of the Haruyama Break-Point Frequency to Evaluate Coatings*; P/N 92230, CORROSION/92; NACE: Houston, TX, March 1992.
10. Simpson, T.C. and Hoffman, J.D. *Effects of Substrate and Phosphate Type on the Painted Corrosion Performance of Galvanneal Coated Sheet*; P/N 950379, 1995 Int. Congress and Expos. Soc. Auto. Eng.; Soc. Auto. Eng.: Warrendale, PA, 1995.
11. Kendig, M.W. *Discussion on the Relationship of Break-Point Frequencies to Delamination* *Corrosion* **47 Dec. 1991**, No. 12, pp. 964-965.

Chapter 3

Application of Localized Electrochemical Impedance Spectroscopy to the Study of the Degradation of Organic Coatings

F. Zou and D. Thierry

Swedish Corrosion Institute, Roslagsvägen 101, Hus 25, 10405 Stockholm, Sweden

A high resolution probe that allows localized Electrochemical Impedance Spectroscopy (LEIS) has been developed. In this paper some possible applications of the use of LEIS in the study of the degradation of organic coating on metal surfaces are presented. It is shown that LEIS can be successfully applied to locate micro-blisters on painted metal surfaces. It is also shown that the technique can be useful in order to obtain mechanistic information on the kinetics of activation and passivation of metals in the vicinity of a defect in an organic coating.

During the last decades, Electrochemical Impedance Spectroscopy (EIS) has been extensively used to study the degradation of coated metals exposed to various environments ^{1,2}. However, the interpretation of the EIS data is generally difficult due to the complexity of the systems studied and to the fact that the impedance are averaged over the whole exposed area while the degradation generally occurs locally. Several attempts to develop a scanning impedance technique has been reported in the literature ³. However, the spatial resolution of these techniques was limited by the size of the probe and the mass transport process may be influenced by the cell geometry.

A novel method of measuring local impedance spectra has been reported by Lillard et al.⁴. In this method, local impedance spectroscopy (LEIS) was performed by determining the local AC solution current density using a two-electrode microprobe. The probe consists in two platinum electrodes mounted in glass capillaries. The AC potential difference associated with the AC current flow in the solution was measured between the two electrodes. The local AC solution current density is then calculated using Ohm's law according to:

$$i(\omega) = \Delta V(\omega)_{\text{probe}} \frac{\kappa}{d} \quad [1]$$

where $i(\omega)$ is the local AC solution current density, $\Delta V(\omega)_{\text{probe}}$ is the AC potential difference at the probe, κ is the conductivity of the electrolyte, and d the distance between the two tips of the capillaries.

The local impedance was thereafter calculated according to :

$$Z(\omega)_{\text{local}} = \frac{V(\omega)_{\text{applied}}}{i(\omega)} \quad [2]$$

The technique has been applied to study galvanic corrosion on an Al/Mo electrode⁴ and to study coating failure for thin coated mild steel cans⁵.

In a more recent paper, Wittmann and Taylor⁶ used Ag/AgCl micro-reference electrodes instead of Pt. The resolution of the system was 125 μm and the impedance limit was $10^6 \Omega \cdot \text{cm}^2$ which limits the frequency range over which impedance data can be collected. The authors applied the impedance probe to locate heterogeneities such as pinhole defects in organic coatings.

In this paper, a newly designed high resolution probe⁷⁻⁹ (i.e. 30-40 μm in lateral resolution) that allows localized impedance measurements has been applied to the study of the degradation of organic coatings on metal surfaces. The main objective of this work was to determine the feasibility of using a local electrochemical impedance technique to detect the formation of blisters on painted metals. The technique has also been applied to study the mechanisms of activation and passivation of iron in the vicinity of a defect in an epoxy primer.

Experimental

Probe and Experimental Setup

The experimental setup used to measure localized EIS data has been described in details elsewhere⁷⁻⁹. The probe consists in a pair of microelectrodes (Pt-Ir with a tip of 10 μm). The microelectrodes were plated in a PtCl_2 solution in order to decrease the interfacial impedance at the tip. The relative position of the two tips were adjusted so that a straight line passing through the two tips was perpendicular to the surface of the specimen. The local AC IR drop in solution was measured as the AC potential difference between the two microelectrodes. The applied voltage was 30 mV. The signal was first preamplified using a preamplifier (PAR model 5113 with an input impedance of 100 M Ω and a gain of 25). Both the in-phase and the quadrature of the signal associated with the AC current flow in the solution were measured using either a lock-in amplifier or a multichannel frequency response analyzer (Solartron 1254). The local AC solution current density and the local impedance were thereafter calculated using equations [1] and [2]. The scanning of the probe was accomplished by using three stepper motors (spatial resolution 0.4 μm).

The EIS spectra were interpreted using the software "Equivalent Circuit" written by Boukamp¹⁰. This software obtains from the Nyquist plots the approximate values of the passive elements in the equivalent circuit which are then fitted using a Non-Linear Least Squares (NLLS) method.

Specimens

Carbon steel and hot-dip galvanized steel (zinc thickness 20 μm) were used as substrates in this work.

The pretreatment for the hot-dip galvanized steel panels consisted of alkaline cleaning, alkaline oxidation and a chromic acid after rinse. The panels were

thereafter painted with an epoxy primer and a top-coat of polyester to a total thickness of 35 μm . The sample was thereafter exposed to a 0.3 M HCl solution as this procedure has shown to produce fast blistering on these samples ¹¹.

The surface of carbon steel was partially contaminated by dropping approximately 10 μl of a 3% NaCl on the substrate and then forced drying prior to paint with an epoxy primer at a thickness of 25 μm . This procedure was used in order to obtain fast blistering at the paint/metal interface. The impedance measurements were performed in a 10 mM NaCl solution.

Results and Discussion

Detection of Micro-blister

Figure 1 shows the local AC solution current density over painted electrogalvanized steel exposed for different times to 0.3 M HCl. The measurements were performed at a frequency of 890 Hz. Figure 1b shows a slight increase in the AC IR drop at

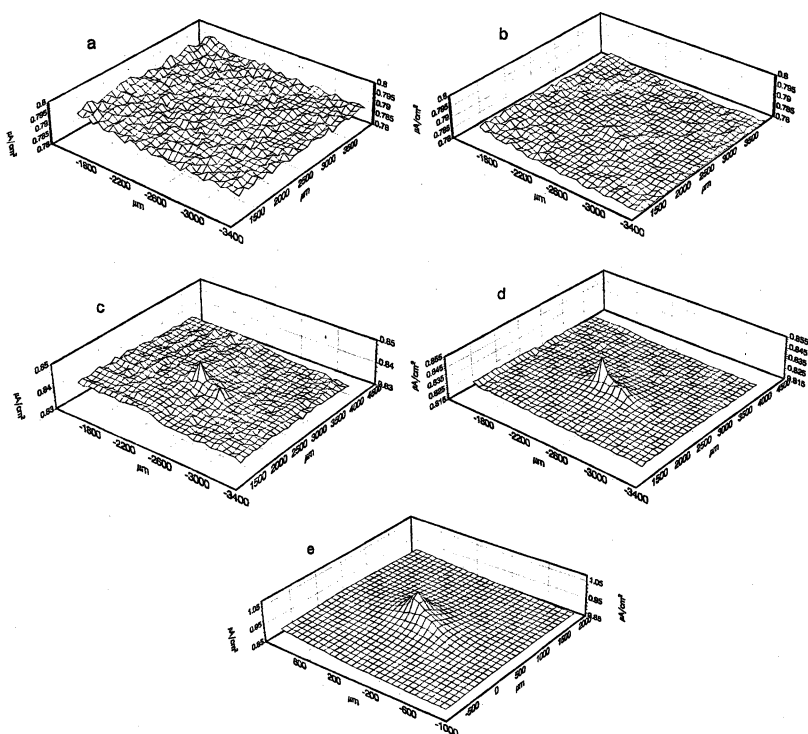


Figure 1: Current density maps for electrogalvanized steel exposed to 0.3 M HCl. a) 1 hour, b) 3 hours, c) 5 hours, d) 7 hours and e) 20 hours.

one location near the center of the sample (-2368,2457). The increase of the local current density is due to the creation of a low impedance site at this location (see equations [1] and [2]). At this stage the surface of the organic coating shows no visible changes using a microscope (magnification x100). Figure 1c, 1d and 1e show a clear peak at this location, and in this case a small micro-blister was also visible under a microscope (magnification X 100). It is well known that in the case of intact paint films the impedance response in the high frequency region will be dominated by the contribution of the capacitance of the paint layer. Hence, the results shown in Figure 1 c and 1 d seems to indicate that the increase in the local current density over the blistered region may be related to an increase in the capacitance of the organic coating in this region (i.e. as the capacitance is directly proportional to the AC current measured by the probe in the case of a pure capacitor). This is in agreement with the results of Van der Weijde and al. showing using traditional EIS measurements that the curve of the capacitance of the organic coating against time for a barrier type coating shows a small step indicating the onset of delamination¹². However, one cannot exclude the possibility that micro-cracks were formed during the blistering process which may lead to a decrease of the local impedance at these locations.

After 20 hours of exposure (Figure 1e) in 0.3 M HCl the paint layer over the micro-blister was visually ruptured resulting in the formation of a macroscopic defect down to the metal substrate.

As noted in the experimental section, a traditional EIS measurement was performed immediately following each LEIS map. Figures 2 shows the evolution of Bode plots obtained using traditional EIS measurements on painted electrogalvanized steel exposed for different time in 0.3 M HCl. The impedance spectra change rapidly to the behavior typical of intact coatings (Figure 2a) to that of deteriorated coated with spectra exhibiting two time constants after 20 hours of exposure (Figure 2e). It should be noted that for "intact" blisters (i.e. Figure 1a-d), the EIS spectra only show one visible time constant. A comparison of Figure 1 and 2 indicates that the visual rupture of the micro-blister corresponds to a large decrease in the impedance of the system.

The EIS data shown in Figure 2a-d were interpreted using the simple equivalent circuit shown in Figure 3 whereas the EIS data displayed in Figure 2e were interpreted using the general equivalent circuit given for painted metals¹. Cpf was modeled as constant phase elements (i.e. CPE for which the impedance may be

expressed as $Z(\omega) = \frac{1}{Y_o(j\omega)^n}$) representing the non-ideal dielectric behavior of this

element. The variation of C_{pf} with the time of exposure is shown in Table 1 together with an estimation of the size of the micro-blister obtained from the current density maps shown in Figure 1. The coating capacitance increases largely during the first stage of exposure (i.e. in connection with the development of the micro-blister at the metal/paint interface), and then remains almost constant until the rupture of the blister. It should also be noted that the n value of the CPE associated with the organic coating decreases largely due to the formation of the blister. This may be related to an increase distribution of this passive element due to blister formation.

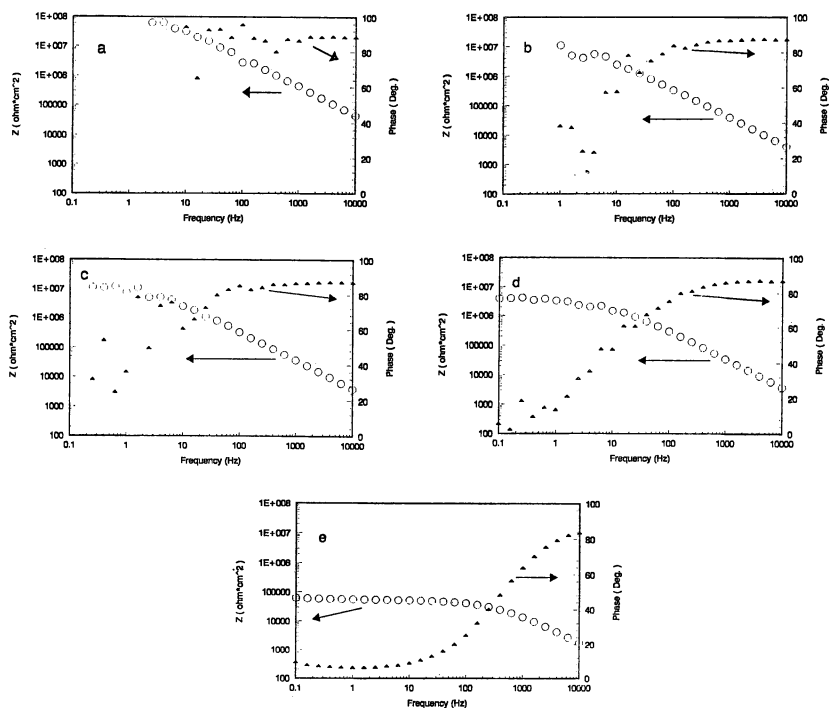


Figure 2: Bode plots obtained by traditional impedance measurements on electrogalvanized steel exposed to 0.3 M HCl. a) 1 hour, b) 3 hours, c) 5 hours, d) 7 hours and e) 20 hours.

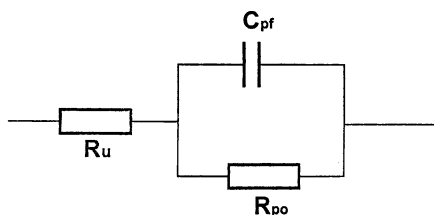


Figure 3: Simple electrical equivalent circuit. R_u is the electrolyte resistance, C_{pf} the capacitance of the organic coating and R_{po} the pore resistance (see reference 2 for more details).

Table 1: Variation of Cpf and the size of the blister with the time of exposure to 0.3 M HCl.

Time of exposure, hours	Cpf, F.cm ⁻²	n of CPE	Blistered area, μm ²
1	2.10 ⁻¹⁰	0,98	-
3	610 ⁻⁹	0,96	60
5	5,810 ⁻⁹	0,96	80
7	710 ⁻⁹	0,955	900
20	2.510 ⁻⁸	0,89	Open blister 1200

LEIS Spectra of Defected Painted Steel Samples

Figure 4 shows the local AC solution current density over painted steel exposed for different times to 10 mM NaCl. The steel surface was contaminated by dropping NaCl on the surface prior to painting. This results in a very fast blistering and in the perforation of the organic coating. Figure 4a clearly shows that such defects in the organic coating can be monitored using LEIS. The size of the defect was estimated from the half height of the peak to be 0.06 mm². The frequency of the applied signal was 890 Hz. As further shown in Figure 4 the current density decreases largely over the defect when increasing the exposure time in the NaCl solution. This corresponds to an increase of the impedance at the defect due to the formation of corrosion products that limits the diffusion of oxygen to the metal surface.

Traditional and LEIS data have been recorded for defected painted steel after different time of exposure to 10 mM NaCl (i.e. corresponding to the AC IR drop maps shown in Figure 4). In this case, the localized impedance data were recorded at the defect located by scanning impedance measurements shown in Figure 4, whereas traditional impedance data represent an averaged impedance including the defected area and the intact coating. Figure 5 shows Nyquist plots generated by traditional (Figures 5a and 5c) and from LEIS (Figures 5b and 5d) after different times of exposure to 10 mM NaCl. The traditional EIS spectra show a feature that has been reported previously for painted metals with defects. The contribution of the "intact" organic coating is found in the high frequency region, whereas the contribution of the corrosion processes in the defected area is found in the intermediate and low frequency regions. The Nyquist plots generated by LEIS show are very different from that obtained by traditional EIS. At early stage of exposure, three time constants are visible (a high frequency capacitive loop, an intermediate frequency capacitive loop and a low frequency capacitive loop). The high frequency loop defined with a characteristic frequency of 30-40 Hz is probably due to charge transfer while the low frequency loops probably corresponds to the kinetic of intermediate species in the dissolution path of iron in the vicinity of the defect. From figure 5d, it is obvious that the low frequency region transforms in a negative resistance loop characteristic of the passivation after 5 hours of exposure in 10 mM NaCl. The present results are in good agreement to previous work performed with traditional EIS on iron in neutral and basic media¹³.

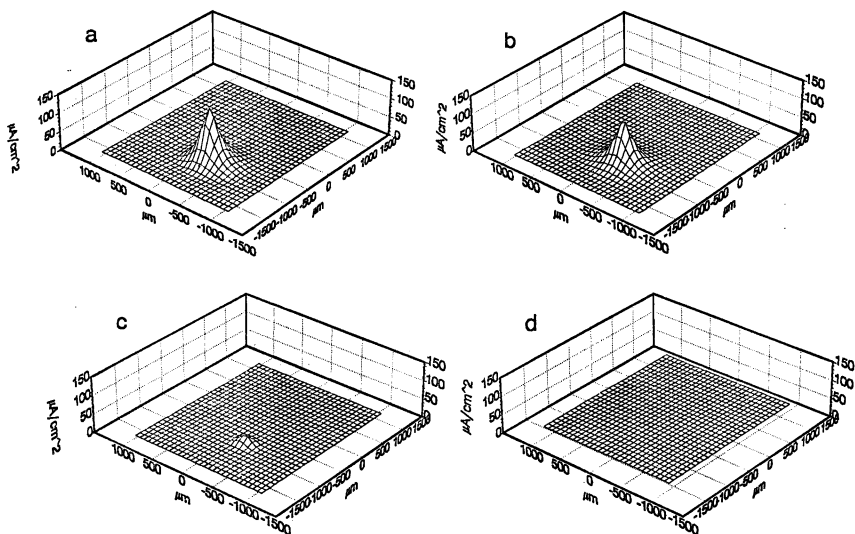


Figure 4: Current density maps for contaminated and painted carbon steel exposed to 10 mM NaCl. a) 30 min, b) 150 min, c) 270 min and d) 470 min

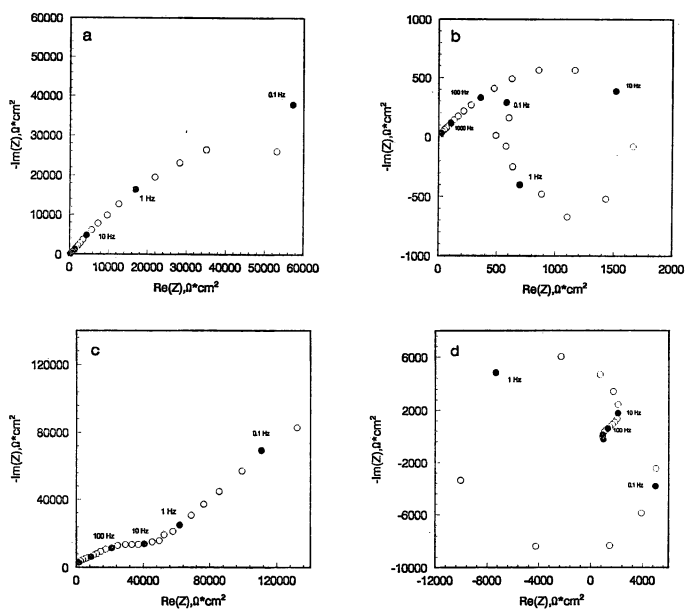


Figure 5: Nyquist plots for contaminated and painted carbon steel exposed to 10 mM NaCl. a) Traditional EIS (30 min) b) LEIS (30 min), c) Traditional EIS (300 min) and d) LEIS (300 min).

Hence from the data presented in Figure 5 to obtain an estimate of the local corrosion rate in the vicinity of the defect. However, local changes in conductivity of the electrolyte in the defect area due to the metal dissolution should be taken into consideration. This is the subject for further research in our laboratory.

Conclusions

-LEIS is sensitive to follow localized variations in the dielectric properties of organic coatings due to blistering.

-LEIS can be used to obtain qualitative information on the mechanisms of dissolution and passivation of iron in the vicinity of a defect in an organic coating.

References

- 1- A. Amirudin, Doctoral Thesis, Stockholm (Sweden), 1994.
- 2- A. Amirudin and D. Thierry, *Prog. in Org. coatings*, 26, p 1, 1995.
- 3- H.S. Isaacs and M.W. Kendig, *Corrosion* 36(6), p 269, 1980.
- 4- R.S. Lillard, P.J. Moran and H.S. Isaacs, *J. Electrochemical Soc.* 139(4), p 1007, 1992.
- 5- R.S. Lillard, J. Kruger, W.S. Tait and P.J. Moran, *Corrosion* Vol 51, No4 p 251, 1995.
- 6- M.W. Wittman and S.R. Taylor, in *Advance in Corrosion Protection by Organic Coatings II*, ECS proceedings, PV 95-13: 158, 1995.
- 7- H.S. Isaacs, A.J. Aldykiewicz Jr., D. Thierry and T.C. Simpson: *Corrosion* 95, NACE International, 1995.
- 8- F. Zou, D. Thierry, A. Annergren and H.S. Isaacs, submitted to *J. of Electrochem. Soc.*, 1996
- 9- A. Annergren, D. Thierry and F. Zou, submitted to *J. of Electrochem. Soc.*, 1996
- 10- B. Boukamp, *Proc. 9th Eur. Corr. Cong.*, Utrech, FU-252, 1989
- 11- A. Iversen, internal report, Swedish Corrosion Institute, 1996.
- 12- D.H. Van der Weijde, E.P.M. van Westing and J.H.W. De Wit, *Corrosion Science*, Vol 36, No 4, p 643, 1994.
- 13- I. Epelboin, C. Gabrielli, M. Keddam and H. Takenouti, in *Comprehensive Treatise on Electrochemistry*, Ed J.O'M Bockris, B.E. Conway and E.B. Yeager, Plenum Press (New York) Vol 4, p 151, 1981

Chapter 4

Electrochemical Impedance Analysis of Anticorrosive Latex Paint Films

Carleton J. Barbour

Analytical Research, Rohm and Haas Company, Spring House, PA 19477

Short term Electrochemical Impedance Spectroscopic evaluation and ranking of experimental styrene - acrylic co-polymer showed good correlation with long term performance in the field. The formulations containing a reactive pigment had superior EIS behavior to those without reactive pigment. EIS also differentiated between two reactive pigments and predicted their relative performance. These experiments correlated EIS data with exterior exposure and applications data and may lead to EIS data's use as a predictor for coating performance in the field. Film formation studies on paints showed strong correlations between repair performance properties and EIS data. EIS showed correlations between water acceptance, as measured by coating capacitance, and reparability. Near Infrared Spectroscopy, during the film formation process, confirmed the correlation between water concentration, the coating capacitance and performance properties.

Inconsistent data from salt spray and other conventional applications tests for industrial coatings has led to the increased use of Electrochemical Impedance Spectroscopy (EIS) as a coating evaluation tool. (1) Much of this work has concentrated on solution epoxy, urethane, and alkyd coatings which contain high levels of volatile organic compounds. (2-8) Concern for the environmental impact of volatile organics has accelerated need to use and understand the properties of water borne coatings. (9) Unfortunately, there are few literature examples of EIS work on water - borne acrylic coatings. Our initial experiments describe EIS data collected during the immersion of metal panels coated with an experimental latex primer in 3 % aqueous sodium chloride solution. The relative rankings predicted by short term EIS data predicted long term exposure behavior of the experimental latex maintenance

primer. The magnitudes of the coating resistances and capacitances changed over the six month experiment but the relative ranking remained consistent with exposure results.

In the past ten years, high gloss latex paints have made a significant impact on the marketplace even though their applications properties are not ideal. Most high gloss latex paints have good sag resistance but have limited repair properties. We have invented a technology that retains the sag resistance properties of most high gloss latex paints while approaching the repair properties of solvent based paints. Open time is defined as the time a coating remains open (or wet) enough to work and make repairs without damaging the final film appearance. To fully exploit this technology, we have developed methods to quantitatively assess the repair properties and understand the basic mechanisms in operation. EIS experiments in conjunction with Near Infrared Spectroscopy (NIR) confirmed the role of water loss and acceptance in determining the performance properties of latex systems.

In an EIS experiment, a variable frequency AC potential is applied to a system and current is measured. The response follows Ohm's Law, ($E = IZ$) where the current (I) and impedance (Z) are complex numbers. The frequency-independent impedance is related to resistance (R) and the frequency-dependent impedance is related to capacitance (C). When the data is computer modeled a modified Randles Circuit (Figure 1) adequately describes the sample's behavior (I). The model accounts for the double layer capacitance (C_{DL}), charge-transfer resistance (R_{ct}) and diffusional impedance (CPE) at the electrode interface as well as the resistance and capacitance associated with the coating (R_c and C_c). While the values of R_{ct} , C_{DL} and CPE are significant when monitoring redox reactions, our analysis concentrates on the characteristics of the polymer film and R_c and C_c . The model easily alerts us to changes in the electrode interface while concentrating on the polymer film. Changes in R_c are related to changes in the coating's ionic conductivity,

$$R_c = \rho d/A = (\sigma)^{-1} = (\mu e n z)^{-1} \quad (1)$$

where ρ is resistivity, d is electrode separation distance, A is the electrode area, μ is mobility, e is the charge on an electron, and the other parameters have their usual meanings. Since under normal experimental conditions the number of charge carriers and their charge are constants, changes in R_c will reflect changes in the mobilities of ions in the polymer films. Changes in C_c reflect changes in the dielectric constant of the coating,

$$C_c = (\epsilon \epsilon_0 / d) A \quad (2)$$

where ϵ is the dielectric constant, ϵ_0 is the permittivity of free space, and A is the electrode area. Typically, the dielectric constants of polyacrylates lie in the 3-6 range whereas that for water is approximately 80. The contribution of water to the dielectric constant of the polymer system dominates its value. Therefore, changes in water content are reflected in the dielectric constant and the capacitance. (I) The

comparisons between coating resistance and ionic mobilities and coating capacitance and dielectric constants allow us to observe the chemical properties the electronic components represent.

Experimental

Electrochemical Impedance Spectroscopy.

Equipment. The impedance spectra ($1 \times 10^6 - 5 \times 10^{-1}$ Hz, 50 mV amplitude) were recorded continuously, with a 1260 Gain/Phase Analyzer (Schlumberger) running through a PC with Z60 Impedance Software (Scribner Associates) or with a 1255 Frequency Response Analyzer (Schlumberger), 273A Potentiostat \ Galvanostat (EG&G Princeton Applied Research) and Zplot Impedance Software (Scribner Associates), at pre - defined time intervals. Individual data files were fit to the modified Randles circuit [Zsim Impedance Software (Scribner Associates)], their impedance parameter plotted as a function of time, and compared. The Zsim Impedance Software uses a Complex Non-Linear Least Squares (Levenberg - Marquardt) routine (12) to determine the function of the data, find its absolute minimum and provide values for the model circuit.

Anti Corrosive Latex Film Exposure. Hot rolled steel panels coated with a medium particle size latex film (Styrene acrylic co-polymer, 35 PVC, 47 % solids) were immersed in a 3% (w/w) aqueous sodium chloride solution while impedance spectra were collected continuously. An example coating cell is shown in Figure 2. It consists of the coated aluminum or steel working electrode, Ag/Ag⁺ reference electrode and carbon rod counter electrode with the 3% aqueous sodium chloride supporting electrolyte solution. Two sets of panels were used in the study, each set contained one formulation without reactive pigment (NRP) and two others with different reactive pigments (RP1, RP2). The first set (exposure) was placed on the test fences while the second set (lab) was kept in the laboratory. Impedance data sets were collected periodically over the six month test.

Latex Film Formation Properties. To mimic application test methods, samples of the conventional and experimental high gloss paints were drawn down (3 mil wet) onto novel 5 mm dual gold band electrodes. The dual band electrodes were prepared by sputtering gold onto microscope slides where a center line had been masked (Figure 3). A non-conducting strip of bare glass was uncovered when the mask was removed and this area was used for draw downs. A second coat (5 mil) was applied after drying for four, six, eight, ten, twelve or fourteen minutes. The impedance spectra were recorded continuously until the paints formed films.

Near Infrared Spectroscopy. A FT-NIR (Analect Diamond 20) spectrometer with a DTGS detector coupled to fiber optic cables was used to measure the NIR spectra (4000 to 8000 cm^{-1}) of latex films as they were drying. Films were drawn down on microscope slides just prior to placing the slides in the sample path between the two fiber optic cables. The fiber optics brought the light to the film and returned the

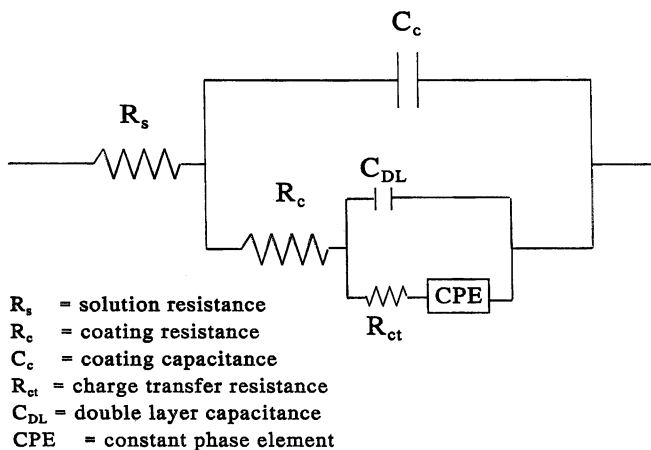


Figure 1. Modified Randles Circuit describing the properties of the coating and the metal substrate. R_s represents the system or solution resistance, R_c represents the coating resistance, C_c represents the coating capacitance, and C_{DL} represents the double layer capacitance, R_{ct} resistance to charge-transfer and CPE is a constant phase element.

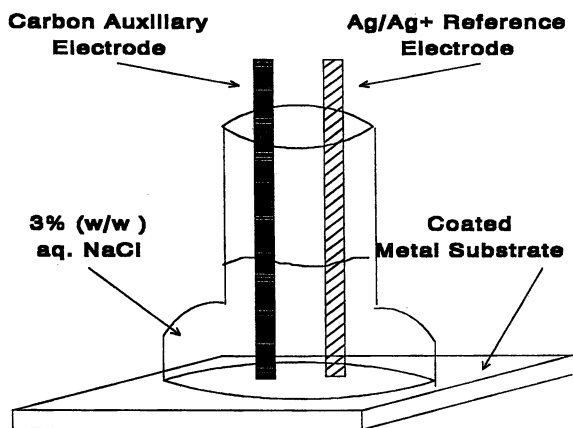


Figure 2. Impedance exposure cell for 3% aqueous sodium chloride immersions of coated metal panels. The cell consists of a coated steel working electrode, a silver / silver chloride reference electrode and a carbon rod counter electrode.

transmitted light back to the detector. The sampling area of the fiber optic on the film is around 3 mm in diameter which equals only a few percent of the total film area. Sampling is done in the middle of the film. The percent transmission is converted to absorbance values. The NIR spectral region is useful for this because water gives strong bands at 5180 cm^{-1} (OH combination band) and 6870 cm^{-1} (OH overtone band). Even in the final latex film with pigment enough light is transmitted below 8000 cm^{-1} to provide useable water absorption bands.

Results and Discussion

Anti Corrosive Latex Film Exposure. The slewing rates and frequency limits of the potentiostat and frequency response analyzer prevent direct electrical observation of phenomena like polymer chain motion but does allow us to see how the impedance (ionic conductivity and capacitance) is affected by those motions. As described above, changes in the coating resistance are dominated by changes in ion mobility since the number of charge carriers and / or their charges are constant. The mobility can be described by a free volume argument where polymer chain segmental motions allow ion mass transport. (13-15) Factors, such as plasticizer content and crystallinity, which affect segmental motions also affect the resistance. Practically, the mobility represents the film porosity where films with more free volume are more porous and more conductive. As the amount of water in the film begins to decrease, the ion mobility decreases as seen by the rising resistance.

The capacitance is directly proportional to the dielectric constant which is a complex quantity with contributions from each component in a system. Typically, the dielectric constants of polyacrylates lie in the 3-6 range whereas that for water is approximately 80. The water's contribution to the dielectric constant dominates the contributions from the latex, the surfactant and other components in the polymer film. Therefore, changes in water content are reflected in the dielectric constant and the capacitance. Bellucci used the Brasher - Kingsbury equation to describe the water content of Poly(ethylene terephthalate) films with capacitance data. (16-18) The model assumes uniform and random distribution of water through the film and assumes the concentration of water is small. The following equation describes this relationship through the volume fraction of water (ϕ);

$$\phi = \frac{\text{Log}(C_t / C_o)}{\text{Log } \epsilon_{H_2O}} \quad (3)$$

where C_t is the capacitance at time t , C_o is the capacitance of the dry film, determined independently, and ϵ is the dielectric constant of water. The data, as the volume fraction of water, may make more intuitive chemical sense than capacitance.

A goal of the present study is to determine whether the relative performance ranking predicted by short term EIS data could predict the relative ranking of coatings based on exterior exposure. To address this goal, panels exposed on the test fences were periodically brought into the laboratory for impedance testing. A second set of panels were prepared concurrently and stored in the laboratory for testing at the same time as

the exterior exposure panels. The second set determined whether EIS on laboratory samples gave ranking consistence with exterior exposure. Comparisons between formulations in each set and the two sets of panels were made with the impedance spectra collected after an hour of immersion in the sodium chloride solution. Figure 4 shows the change in the logarithm of the coating capacitance with time for the exposure panels of the three formulations drawn down on hot rolled steel. The data points are the results from the Complex Non-Linear Least Squares fits. The film without reactive pigment (NRP) shows a decreasing capacitance, representing the continuing curing process in the film. The two films with reactive pigments, RP1 and RP2, show little change in capacitance during the six month experiment. The data also shows that the large differences in film capacitance and water sensitivity between formulations, seen at early film formation times, disappear as the films cure. The convergence of the capacitance values is within experimental error and does not permit the determination of the relative ranking between formulations. The convergence also implies that water sensitivity may be factor in determining corrosion protection, for this system, but does not appear to be the dominant factor. The discontinuity in the data at thirty days of exposure is attributed to data sampling. Data collection on the panels was limited to one spot on each panel during each testing period. The random choice of testing area and exposure placement, may have affect the film formation and panel degradation before the thirty day experiments.

The coating resistance for the NRP sample (Figure 5), determined from the same fit, shows an increasing trend in coating resistance during the experiment. This increasing trend in resistance, decreases ionic conductivity, is further evidence of film curing. The reactive pigment samples, however, show little change in coating resistance during the experiment. Since the differences in coating resistance are greater than experimental error, a relative ranking of the formulations is allowable. The relative ranking the films from least to most resistive, NRP, RP2, RP1. This relative ranking predicts that the least resistive film should be more susceptible to degradation through water sorption, ion motion and environmental effects and is consistence with exterior exposure ranking.

Experiments on similar panels stored under laboratory conditions, 70 °F, 50 % relative humidity, were performed to determine whether laboratory results would correlate with exterior exposure data. Figures 6 and 7 show the coating capacitance and resistance data, respectively, for the laboratory panels. Figure 6 shows behavior similar to Figure 4, where the NRP film showed a decreasing coating capacitance and water sensitivity. As seen previously, the small differences in coating capacitance, though significant in this experiment, make it difficult to differentiate between samples. The coating resistance plot (Figure 7) for the laboratory samples is similar to that seen for the exposed panels. The plots shows that the coating resistance increases with times as the films continually cure. As seen previously, in Figure 5, the relative performance ranking predicted by EIS are consistent with exposure data, though the difference in film formation conditions leads to different magnitudes for the coating resistance.

The value of the experiments is that EIS data predicted the same relative ranking for the films after seven days of curing that six months exterior testing provided. The implications for shortening the coating development process are enormous. This

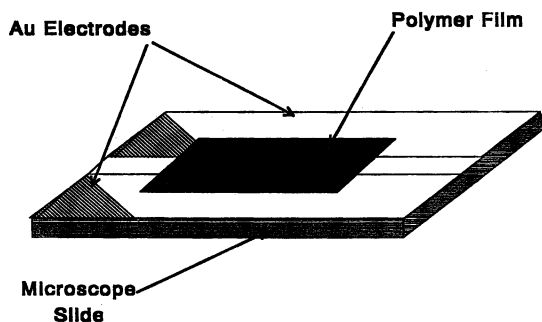


Figure 3. Gold dual band electrodes for polymer film formation and humidity exposure experiments. The electrode consists of two sputter deposited gold strips on a microscope slide.

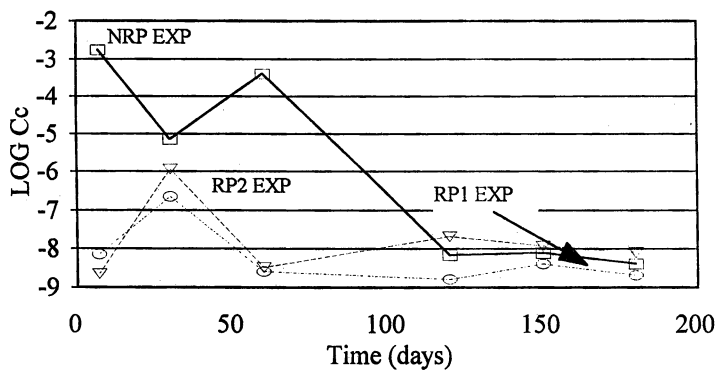


Figure 4. Plot of the logarithm of the coating capacitance against time for the sample series on hot - rolled steel exposed on the test fences. NRP (\square) is the sample without reactive pigment, RP1 (\circ) is the sample with reactive pigment one, and RP2 (∇) is the sample with reactive pigment two.

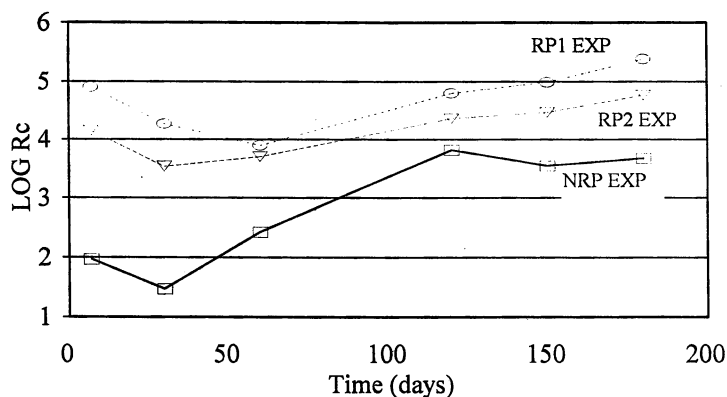


Figure 5. Plot of the logarithm of the coating resistance against time for the sample series on hot - rolled steel exposed on the test fences. NRP (\square) is the sample without reactive pigment, RP1 (\circ) is the sample with reactive pigment one, and RP2 (∇) is the sample with reactive pigment two.

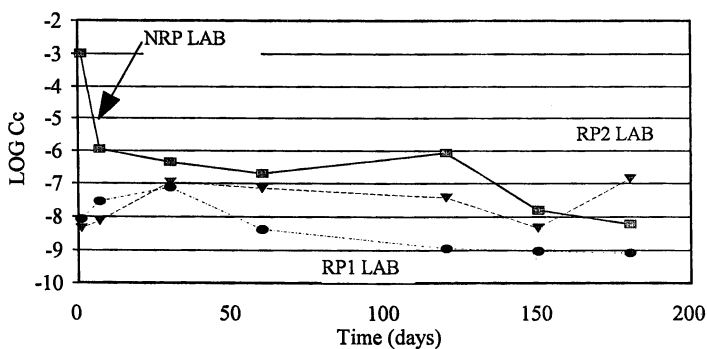


Figure 6. Plot of the logarithm of the coating capacitance against time for the sample series on hot rolled steel stored in the laboratory. NRP (\blacksquare) is the sample without reactive pigment, RP1 (\bullet) is the sample with reactive pigment one, and RP2 (\blacktriangledown) is the sample with reactive pigment two.

potential ability to predict long term exposure with short term data could substantially improve the time-line for developing new formulations.

To support the EIS experiments additional work was performed using NIR spectroscopy. In the experiment, polymer films were drawn down on a dual band electrode and the NIR spectra and EIS spectra were monitored simultaneously. NIR data was collected, in reflectance mode, by placing a mirror below the electrode and directing the NIR light onto the non-conductive strip between the electrodes. Figure 8 shows a plot of the 5180 cm^{-1} NIR water combination band and the logarithm of the coating capacitance versus time for a traffic paint film. The plot shows that the time-scale for the intensity change in the NIR spectra agrees reasonably well with the time-scale for the capacitance change. This agreement implies that water loss, as measured by NIR, correlates with the capacitance change. Therefore, changes in capacitance can be used to predict changes in water content. Similarly, Figure 9 shows a plot of the 5180 cm^{-1} NIR water combination band and the logarithm of the coating resistance versus time for the same traffic paint sample. The plots demonstrates a similar time-scale for the increase in coating resistance and decrease in band intensity further relating ion mobility water content.

Latex Film Formation Properties. Performance properties of lattices and their comparison to traditional solvent - based paints are a primary focus of applications research. Though lattices enjoy an advantage in their potential environmental impact, some application properties still lag behind solvent - based systems. One application property of particular significance in the architectural coating market is open time or reparability. Open time is defined as the time a coating remains open (or wet) enough to work and make repairs without damaging the final film appearance. Conventional thought attributes open time to stabilization of latex particles during polymer film formation. The stabilization is thought to occur through van der Waals forces by either electrostatics, or steric stabilization between latex particles. Water stabilizes particles through electrostatics by shielding particle- particle charge. Disadvantages to stabilizing latex emulsions electrostatically include, sensitivity to shear, sensitivity of electrolytes in aqueous phase, potential for corrosion, and poor freeze / thaw stability. We have developed new technology which uses steric stabilization as the primary latex stabilization mechanism and overcomes the disadvantages associated with electrostatic stabilization while improving the open time of an architectural coating formulation. Conventional methods for achieving steric stabilization involves a system that relies on stabilization provided by graft copolymer stabilizers. This new technology uses a latex polymer and steric stabilizer each containing reactable group. The reaction between the two functional groups provides ionic or covalent binding of the steric stabilizer to the latex particle. In the current experiments, EIS and Near Infrared Spectroscopy were used to quantitatively assess the repair properties and understand the basic mechanisms in operation. The two experiments confirmed the role of water loss and acceptance in determining the performance properties of this latex system. To investigate the stabilization mechanism and the role of water in polymer film formation EIS film formation experiments were performed. In the experiment, the impedance spectra of an emulsion or paint drawn down on a gold dual band electrode were monitored as the polymer films formed. Figure 10 shows the coating

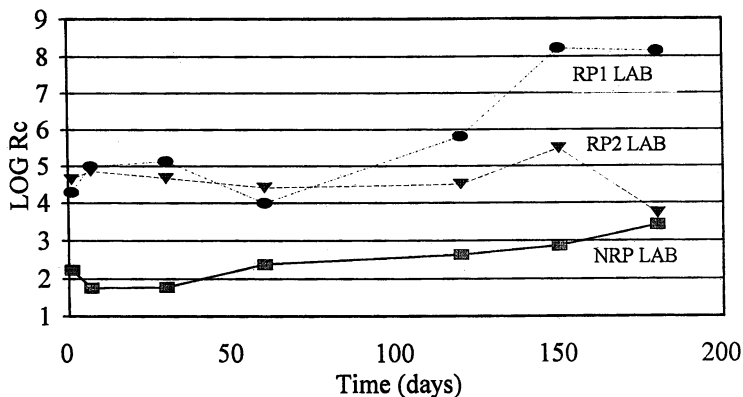


Figure 7. Plot of the logarithm of the coating resistance against time for the sample series on hot rolled steel stored in the laboratory. NRP (■) is the sample without reactive pigment, RP1 (●) is the sample with reactive pigment one, and RP2 (▼) is the sample with reactive pigment two.

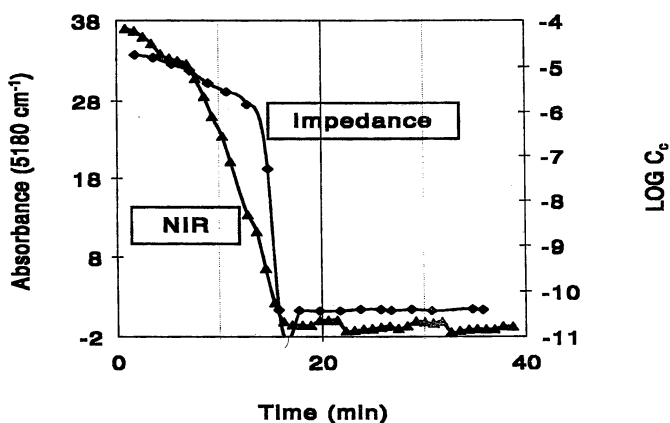


Figure 8 Plot of the intensity of NIR OH combination band (▲) (5180 cm^{-1}) and logarithm of the coating capacitance (◆) against time for an experimental quick drying traffic paint.

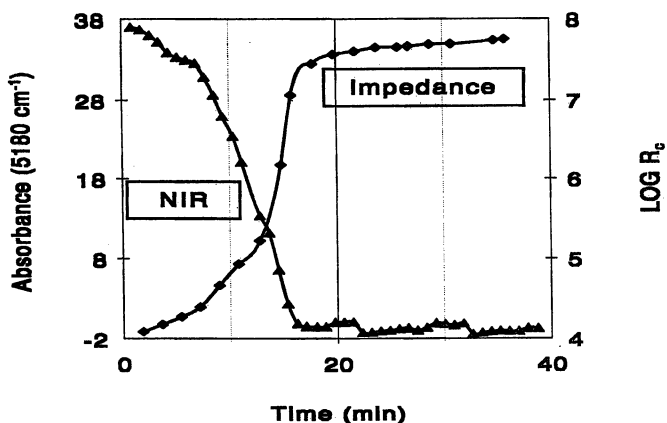


Figure 9 Plot of the intensity of NIR OH combination band (\blacktriangle) (5180 cm^{-1}) and logarithm of the coating resistance (\blacklozenge) against time for an experimental quick drying traffic paint.

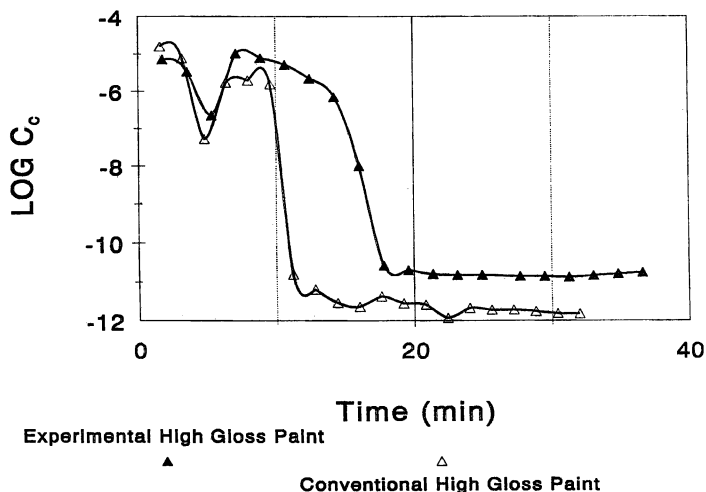


Figure 10. Plot of the logarithm of the coating capacitance against time for the experimental (\blacktriangle) and conventional (\triangle) high gloss paints drawn down on gold dual band electrodes. A second 5 mil wet thick film was applied six minutes after the first was applied.

capacitance as a function of time for the conventional and experimental high gloss paints during an experiment where second coats was applied over the initial ones after six minutes of curing. The experimental paint was designed to use steric effects as a mechanism for latex particle - particle stabilization whereas the conventional paint was not. In both paints, the capacitances initially decrease as water leaves the forming films and its concentration decreases. Upon recoat, the capacitance rises due to the reintroduction of water to the film. The capacitance then begins to decrease again as water leaves the film. Incidentally, the electrodes in the experiment are at the bottom of the film so that changes in capacitance, as measured by the electrode response, are due to sorption of water through the entire film. The figure shows little difference in behavior upon re-coating between the conventional and experimental paints. Both paints appear to accept the water from the new paint film and then begin to lose water again. The difference in time-scale for the final curing of the film may play a role in their film formation characteristics.

The capacitance as a function of time for films recoated after eight minutes is shown in Figure 11. Similar to the six minute experiment, the capacitance initially decreases as water leaves the forming film. Upon recoat, however, the experimental paint shows an increase in capacitance not seen for the conventional paint. The increase in capacitance indicates that at eight minutes the experimental paint still accepts water into the entire film whereas the conventional paint does not. The conventional film appears to have cured to a point that water sorption is severely inhibited. The ability to accept water by the experimental paint, as opposed to the actual water concentration upon recoat, may support steric stabilization as a possible mechanism for increased open time. Since the concentrations of water at the time of the re-coat

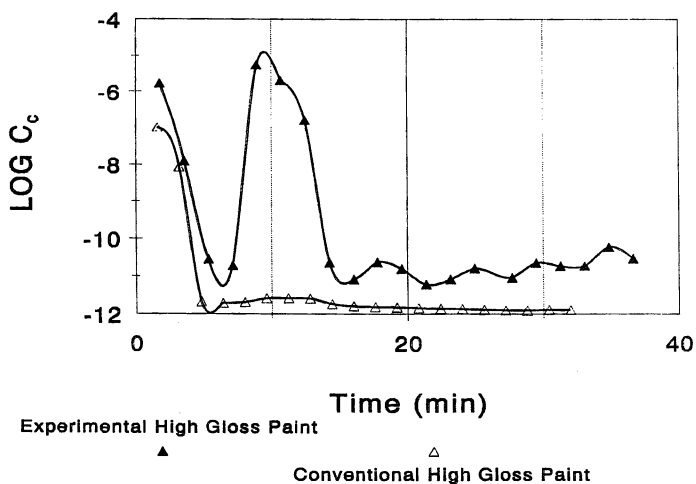


Figure 11. Plot of the logarithm of the coating capacitance against time for the experimental (\blacktriangle) and conventional (\triangle) high gloss paints drawn down on gold dual band electrodes. A second 5 mil wet thick film was applied eight minutes after the first was applied.

are similar, and the experimental paint is "open" and the conventional one is not, water holding and its effect on the van der Waals and electrostatic forces between particles does not appear to govern open time. These observations support steric stabilization as a possible mechanism for particle - particle stabilization.

Extending the time scale for recoat to twelve minutes (Figure 12) supports the above interpretation. Upon recoat, the experimental paint is still open and accepts the water from the previous film while the conventional film is not open and does not accept more water.

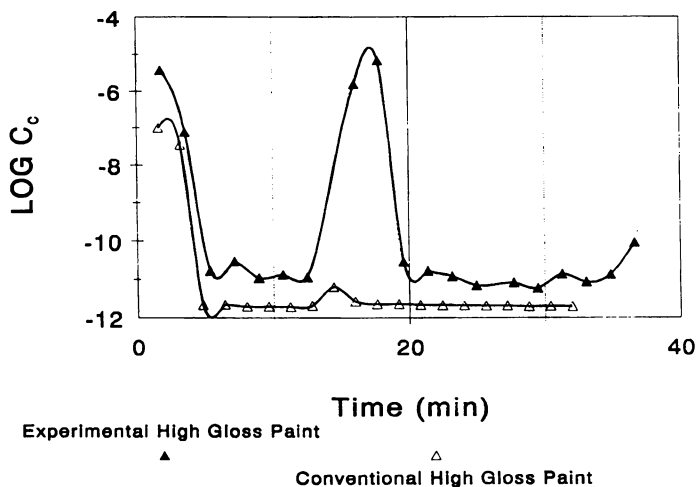


Figure 12. Plot of the logarithm of the coating capacitance against time for the experimental (\blacktriangle) and conventional (\triangle) high gloss paints drawn down on gold dual band electrodes. A second 5 mil wet thick film was applied twelve minutes after the first was applied.

Acknowledgments. This work was supported by S. Bush, R. Flynn, B. Frechem and F. Hirsekorn of the Rohm and Haas Company. I thank H.L. M^cPeters for the NIR data, M. Lightcap for the anti-corrosive latex film samples and L. Adamson for the open time samples.

Literature Cited

1. Mansfeld, F.; Kendig, M. W. In **Laboratory Corrosion Tests and Standards**, ASTM STP 886; Haynes, G. S.; Baboian, R. Eds.; American Society for Testing and Materials: Philadelphia, PA, 1985, 122-142.
2. Murray, J. N.; Hack, H. P. *Corrosion* 91, 1991, 131.
3. Scully, J. R. *J. Electrochem. Soc.*, 1989, 136(4), 979-989.
4. Compère C.; Fréchette É.; Ghali E. *Corrosion Science*, 1993, 34 (8), 1259-1274.

5. Mansfield, F.; Tsai, C. H. *Corrosion*, **1991**, 47(12), 958-963.
6. Tsai, C. H.; Mansfield F. *Corrosion*, **1993**, 49(9), 726-737.
7. Hack, H. P.; Scully, J. R. *J. Electrochem. Soc.*, **1991**, 138(1), 33-40.
8. Hirayama, R.; Haruyama, S. *Corrosion*, **1991**, 47(12), 952-958.
9. Guruviah, S. A.; Krishnan, S. M. *Bull. Electrochem.*, **1990**, 6(6), 588-589.
10. Agarwal, P.; Orazem, M. E.; Garcia-Rubio, L. H. *J. Electrochem. Soc.*, **1992**, 139(7), 1917-1927.
11. Hill, R. M.; Dissado, L. A.; Strivens, T. A. *Adv. Org. Coat. Sci. Technol. Ser.* **1991**, 13, 71-89.
12. Press, W. H.; Flannery, B. P.; Teukolsky, S. A.; Vetterling, W. T. *Numerical Methods: The Art of Scientific Computing*, Cambridge University Press, 1986.
13. Angell, C. A. *Solid St. Ionics* **1983**, 9/10,3-16.
14. Miyamoto T.; Shibayama K. *J. Appl. Phys.* **1973**, 44(12), 5372 - 5376.
15. Ratner, M. A.; Shriver, D. F. *Chem. Rev.* **1988**, 88, 109-124.
16. Brasher, D. M.; Kingsbury, A. H. *J. Appl. Chem.* **1954**, 4, 62.
17. Bellucci F.; Nicodemo L. *Corrosion*, **1993**, 49(3), 235-247.
18. Bellucci, F.; Nicodemo, L.; Nicolais L. *Polymer News*, **1992**, 17, 272-277.

Chapter 5

Application of Impedance Spectroscopy During the Lifetime of Organic Coatings

D. H. van der Weijde¹, E. P. M. van Westing², G. M. Ferrari², and J. H. W. de Wit¹

¹Laboratory for Materials Science and Engineering, Delft University of Technology, Rotterdamseweg 137, 2628 AL Delft, Netherlands

²TNO Centre for Coatings Research, P.O. Box 57, 1780 AB Den Helder, Netherlands

In this paper the use of Electrochemical Impedance Spectroscopy is evaluated for three situations during the lifetime of organic barrier coating. These situations are:

- Defect free coatings
- Delaminated, but intact coatings
- Coatings with defects combined with cathodic delamination

It is shown that in the first case EIS is reduced to a dielectric study of the coating polymer. This study gives information on the technical lifetime of an intact coating. In the second case only a qualitative indication of the onset of delamination can be obtained. In the last case contributions of the pore and the corrosion product within the pore are measured. It is not possible to measure a delaminated area.

Electrochemical Impedance Spectroscopy (EIS) has been used for several years now to evaluate the performance of different organic coatings. In literature there is, however, no general approach to both measuring and interpretation of EIS-data measured on coatings. Partly this is caused by the differences in interest of research groups (coating or corrosion oriented, practical or fundamental research) and partly by the nature of the coating itself (active corrosion protection or barrier properties). Due to these different approaches it is difficult to compare the possibilities of the different methods and to choose which one is most suitable in a given situation. The research described in this paper is performed to get more knowledge on the possibilities of EIS for lifetime prediction of barrier coatings that are used in industrial, marine or off-shore applications. In general, the EIS experiments presented can be divided into two groups:

- Measurements on intact coatings
- Measurements on defect coatings

Intact Coatings. Experiments on intact barrier coatings are often designed to measure the breakdown of the barrier properties of the coating that becomes visible in a change of specific parameters like the break-point frequency (1,2) or the pore or coating resistance (3). In case of heavy-duty coatings for industrial and marine applications the time to reach such measurable degradation however is far too long since the DC resistance of these coatings exceeds $200\text{G}\Omega$, even after corrosion has started underneath. This paper describes experiments that show clearly the inability of EIS to get mechanistic or kinetic information from corrosion processes in blisters underneath these coatings. It is however possible to get some valuable information for heavy-duty coatings because the dielectric properties of the coating-polymer will change a little when they degrade. If enough information on the system is known, these dielectric studies may lead to an estimation of the technical "age" of the coating or in the ideal case to a predictions about remaining lifetime.

Coatings with Defects. Experiments on coatings with defects are mainly performed to monitor the growth of the delaminated area of a defect as a function of time in order to predict a remaining service lifetime. In the case of a barrier coating on grit blasted steel it is most likely that this proceeding de-adherence is caused by cathodic delamination. This paper describes experiments that show the possibilities and impossibilities of EIS on barrier coatings on steel that are mechanically perforated.

Experimental

EIS measurements were performed in 3% NaCl and in concentrated synthetic Dutch coastal rainwater. In case of the delaminated coating only a 3% NaCl solution was used. The measurements were performed using a Solartron 1286 ECI in combination with a Solartron 1255 FRA and the ISIS (4) software developed in our laboratory. The frequency range was for the intact coating 100 Hz to 100 kHz. Fitting of the data was performed between 1 kHz and 10 kHz. In case of the measurements on defects the frequency range was extended to lower frequencies (typically 10 mHz)

Intact Coatings. For the study of the intact coatings two different sets of experiments were designed. The first experiments were designed to examine intact coatings and possible ways to use EIS for lifetime estimation or prediction of these coatings. The second group of experiments was performed to analyse the influence of a local delamination underneath these intact coatings. To make a comparison between the two groups possible in both cases the same types of coatings were used. These were a commercially available two-layer alkyd and a commercially available two-layer epoxy. If applied according to the prescription both do have a total layer thickness of around $150\mu\text{m}$. The coatings were applied with an airless spray to hot rolled steel that was grit blasted and to cold rolled steel that was phosphatised. Since no influence of the pre-treatment was observed (5) in the behaviour of the intact coating these different substrates will not be dealt with separately.

As is well known these systems can under normal conditions be represented by the simple equivalent circuit given in Figure 1.

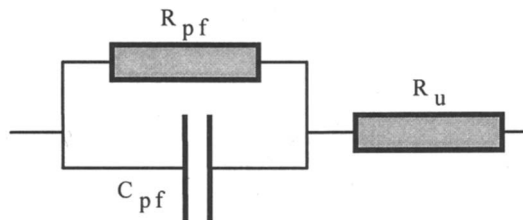


Figure 1. Simple equivalent circuit.

Normal values for the parameters are: Coating capacitance (C_{pf}) < 1nF; coating resistance (R_{pf}) > 200G Ω ; External resistance (R_u) \approx 100 Ω . In many cases the C_{pf} should be replaced by a Constant Phase Element (CPE) to describe small deviations from the ideal capacitive behaviour. The CPE is characterised by two parameters: Y_0 and n . Y_0 is comparable to C_{pf} if $n \approx 1$ while n represents the deviation from ideal behaviour. In terms of equations for the impedance (Z) both look very much the same if n is close to one:

$$Z_{CPE} = \frac{1}{Y_0(j\omega)^n} \quad Z_C = \frac{1}{C(j\omega)^1} \quad [\text{eq.1}]$$

For this paper the behaviour of intact coatings with and without blisters underneath was analysed using the CPE.

Intact without Blisters. On the previously mentioned coatings EIS measurements were taken as a function of immersion time. As long as the coatings were not damaged the behaviour of the CPE parameters in time was similar to that shown in Figure 2. The coating resistance was too high to be determined accurately from the measurements.

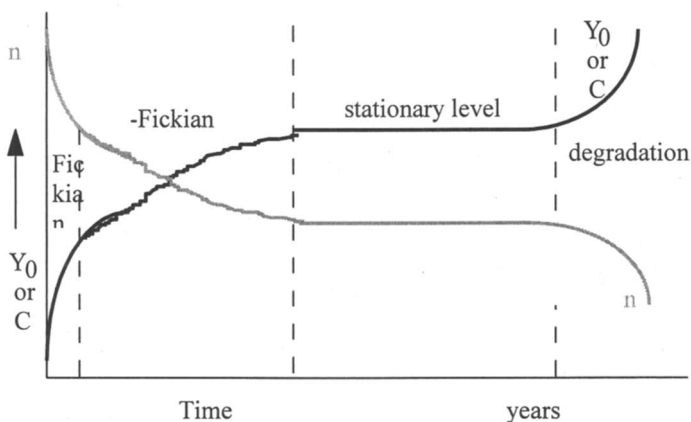


Figure 2. The behaviour of the CPE parameters of a coating during prolonged immersion in an electrolyte.

General Behaviour

In the beginning an almost Fickian water absorption can be seen, followed by a region of non-Fickian behaviour due to secondary effects like curing, relaxation, swelling etc. After a long period, typically some months, a stable situation is reached. When the degradation starts the stationary values change again.

Water absorption. The first period in the presented "life-time curve" is initially dominated by Fickian water absorption. Numerous references in literature (5,6) have been using this behaviour to calculate the diffusion coefficient and solubility of water in coatings. However, if the C_{pf} or CPE behaviour is studied during prolonged immersion it appears that no real saturation is reached after this initial Fickian period (7). The capacitance of the coating is increasing at a low rate for periods of several months. This behaviour can be due to a combination of several effects like post-curing, swelling and relaxation. The influence of post curing is rather well known but relaxation is less studied. Polymers may however show some relaxation and physical ageing (8) in their structure and may even crystallise to some extent.

To show the influence of relaxation on the water uptake some experiments were performed on a free film of high-density polyethylene (HDPE). This polymer is partly crystalline and partly rubbery. Because both the epoxy and the alkyd used in the other studies are fully amorphous and in a glassy state the results on these HDPE films cannot directly be translated to the coatings that are used for the other experiments. The measurements are however illustrative for the effects that relaxation or physical ageing may have on coating properties.

Two samples were cut out of the same sheet. Both samples were heated to 125°C for several hours. At this temperature the polymer is just above the melting temperature of the crystalline phase. One sample was then rapidly quenched in liquid nitrogen (-196°C) while the other was cooled to room temperature in about three hours (annealed). This difference in cooling rate will give a difference in the internal polymer structure. The slowly cooled sample will be more crystalline than the other.

If water enters the amorphous phase it will act as a plasticiser and some additional relaxation may occur. According to Willems (9) this is a secondary crystallisation or relaxation of the interaction between crystalline and amorphous phase. This because the amorphous phase of the HDPE is far above the T_g and differences in normal relaxation between the two samples will therefore not exist. Because of the difference in crystallinity this secondary crystallisation or relaxation will be different for both samples. Because the crystalline phase will take up almost no water the quenched sample is also supposed to take up more water than the annealed.

Since HDPE does not contain OH groups or other reactive groups the differences in internal structure or molecular arrangement are the only possible differences between the two samples. If differences in water uptake are measured they must be caused by the differences mentioned above.

On both samples EIS measurements were performed during water uptake in a free-film cell. From this long series of relatively short measurements the change in capacitance was calculated using the data between 10kHz and 1kHz. The results of the measurements are plotted in Figure 3 as graphs of both Y_0 and n (Q_{foil}) as a function of immersion time.

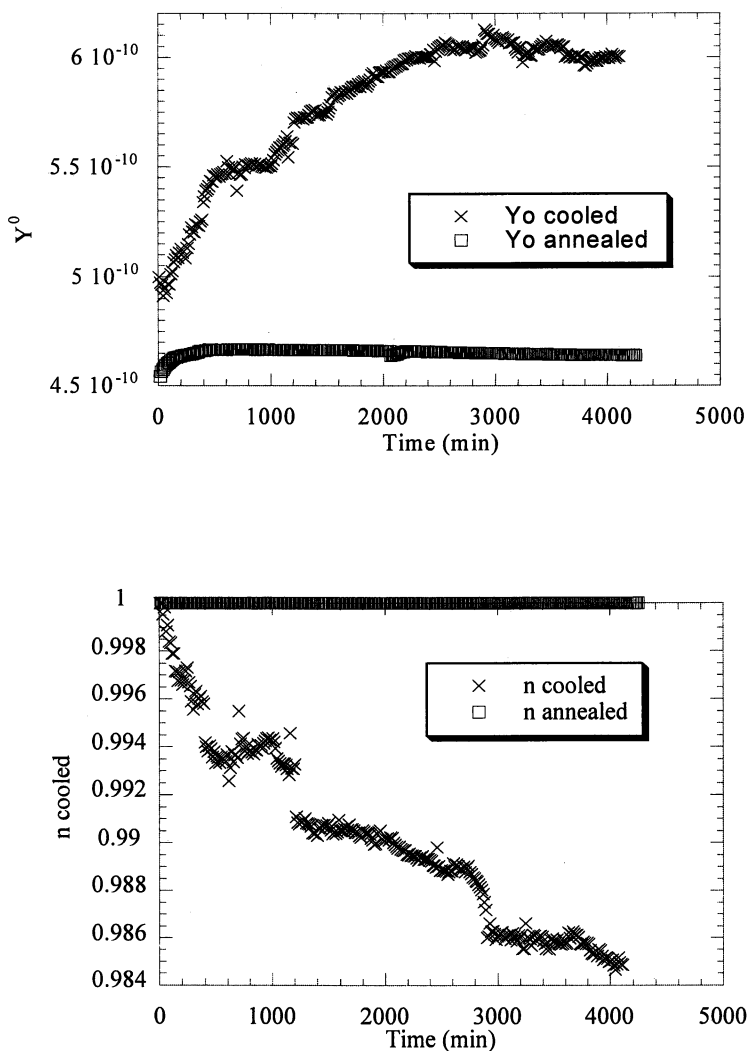


Figure 3. Y_0 and n (Q_{foil}) of two identical HDPE samples during water uptake. The differences are caused by a different heat pre-treatment.

From these figures one can clearly see the large influence of the differences in pre-treatment of the polymers. Not only the initial capacitance is changed, also the change in capacitance which is directly related to the water uptake is much larger for the fast-cooled sample. This indicates a more open structure, which is not unexpected, since amorphous polymers are less dense than crystalline polymers.

The changes in “n” are also much larger for the fast cooled sample. In case of the annealed sample the n is almost 1 for the total immersion time which indicates a true capacitive behaviour. The less ordered structure of the fast cooled sample shows a less ideal behaviour indicated by an “n” that differs slightly from one. This deviation from unity grows with increasing water uptake.

Although the observed behaviour may be different for the epoxy and alkyd coatings these experiments show that not only the chemical composition and structure of the polymer is important. Also the “physical arrangement” of the molecules has a large influence on the water uptake and the dielectric behaviour. For other (dry) polymers like PET the influence of the “thermal history” and crystallinity on the dielectric properties (that are related to the internal polymerstructure) was studied already in detail by Willems (9).

Stationary Region

(It is beyond the scope of this paper to give a full presentation of the measurements results. More information can be found in the contribution of van Westing (10) and in ref. 5) The second period in the lifetime curve is a more or less stationary period. The resistance of the coatings in this stationary region still exceeds 200GΩ (measured with a Keithley electrometer in DC conditions) which makes it impossible to get a correct and accurate value for this resistance using our equipment. The values of the CPE parameters ($Y_0 \approx C$ and $n \approx$ deviation from ideal capacitive behaviour) in this stationary situation are representative for the coating system. They contain information on the type of coating and the thickness of the individual layers. If the stationary parameters of the individual layers (e.g. primer and topcoat) are known from measurements the stationary values of a complete system (with known thickness) can be calculated using equation 2 and can be compared with measured values.

$$n_t = \frac{n_1 d_1 + n_2 d_2}{d_t} \quad E_t = \frac{d_t(E_1 E_2)}{d_2 E_1 + d_1 E_2} \quad Y_0 = \frac{E_0 E_t A}{d} \quad [\text{eq.2}]$$

with n and Y_0 the parameters of the CPE, E the dielectric constant when the Y_0 is treated like a capacitance, d the thickness and the indices t,1 and 2 apply to either the total system, layer 1 and layer 2 respectively.

For the epoxy systems, very good correlations were achieved between calculated and measured values for a complete matrix of various coatings thicknesses using these equations. Also for a polyester coil-coat system the correlation was high. In the 4 by 4 matrix a systematic variation in the thickness of the primer and topcoat of the coating-system was investigated. Until now the alkyd

system has a different response which is probably caused by the continuous post curing of this system.

Using this method of calculating the stationary levels of a given coating system, a simple measurement of the stationary values can give information about the "state" of the coating: before saturation, at the stationary level or beyond the stationary level. This indicates the onset of larger changes in the polymer structure due to stresses (blisters), chemicals (high pH due to cathodic delamination) etc. This method does, however, require knowledge of the behaviour of the individual layers.

Degradation

In general the deviation from the stationary values indicates the onset of degradation. The stationary values can also be used in combination with cyclic exposition test (10).

Several processes can cause the changes in Y_0 and n (Q_{pf}) that indicate the degradation: swelling, porosity, corrosion underneath the coating and chemical attack. As an example: in the case of cathodic delamination, high concentrations of OH^- (pH values around 12-14) can be formed underneath the coating. To simulate this the impedance of coatings was measured during a normal water uptake. At a certain point the pH of the electrolyte was changed from neutral to 12. This caused a sharp increase in Y_0 (see Figure 4) and a decrease in n (Q_{pf}).

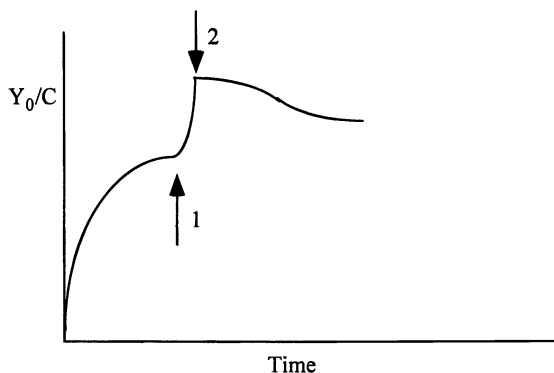


Figure 4. Schematic picture of a water uptake of an epoxy coating. At the first arrow OH^- is added to the water, at the second arrow it is removed again.

After some time, the electrolyte was replaced again by a neutral solution. The Y_0 decreased and n increased, but neither got back to the original values. Apparently the OH^- , which can be formed during corrosion processes, created chemical changes within the coating polymer that can be measured with EIS.

Intact Coatings with Defects (11)

When blisters occur underneath intact barrier coatings the simple equivalent circuit from Figure 1 does not describe the complete system of coating and corrosion

underneath. In literature, several equivalent circuits have been proposed for this system. In general, all these circuits have a sub-circuit inserted in series with the coating resistance representing the double layer and charge transfer reactions. The values for the components of this sub-circuit are, in general, in the order of some μF 's and several hundred or thousand Ω 's.

However, when the impedance parameters of the intact coating polymer above a blister do not change in orders of magnitude, it can be shown that the contribution of the corrosion processes will have the same order of magnitude as the (small) noise that is always present in measurements (typical $<1\%$). This is because the contribution of the corrosion processes is not in parallel, but in series with the impedance of (part of) the coating. So, direct information of the corrosion processes cannot be measured. However, small changes in the capacitance or CPE-parameters of the coating will be visible as is shown in Figure 5. This figure shows the change of capacitance due to water uptake of an alkyd coating. Prior to the application of the coating the panel was pre-contaminated with a drop of $5\mu\text{l}$ of a 3% NaCl solution. Since blister formation is in this case forced by an amount of salt underneath the coating it is very visible and the capacitance can be used to visualise the results. For smaller blisters the CPE parameters will give better information.

The arrow in Figure 5 indicates where the behaviour is starting to deviate from the expected Fickian behaviour.

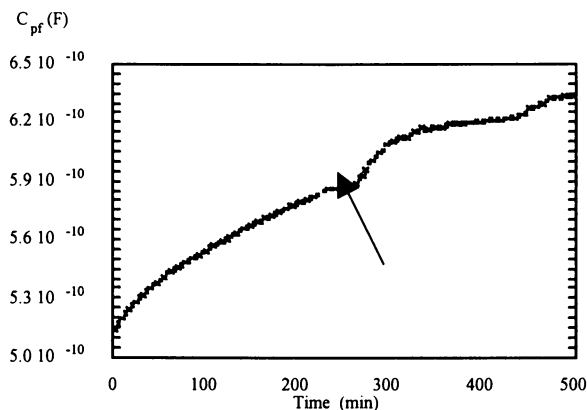


Figure 5. Capacitance of the coating as a function of time. After 300 minutes the formation of a blister starts (see arrow).

This deviation is caused by the formation of a blister (12) which initiated at a pre-contaminated site. Some time after it became visible in the measurement it was also visible for the eye. A Nyquist plot from an EIS measurement on this coating when the blister was already visible is given in Figure 6.

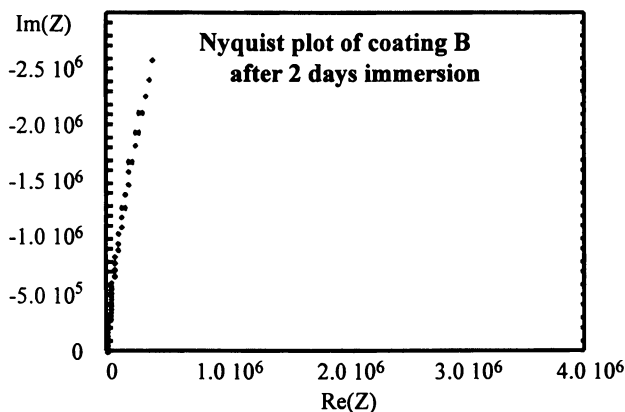


Figure 6. Nyquist plot of the coating two days after immersion and the initiation of the blister have started. The insert is the same coating after perforation of the blister.

When the blister is perforated mechanically with a needle the response immediately changes to that of the insert in Figure 6. In this case the contribution of the coating shifts to higher frequencies whilst the contribution of the corrosion processes become visible in the impedance as a second “half-circle” at moderate frequencies.

From the series of experiments it became clear that the contribution of corrosion processes cannot be measured directly if the barrier properties of the coating are undamaged.

Mechanically Damaged Coatings

In Figure 6 in the preceding paragraph, it was shown that the response of a mechanically damaged coating contains information from the corrosion processes in the defect and underneath the coating, combined with diffusion processes that may occur. It is, however, questionable if the complete system of coating and corrosion can be characterised using only EIS, and if not fully, what can be concluded from the measurements. For the case of cathodic delamination on steel some model experiment were performed to characterise the system. These results were compared with measurements on panels showing cathodic delamination.

The model describing cathodic delamination (13) assumes that anode and cathode become separated due to an oxygen concentration gradient: Above the exposed metal oxygen is consumed (Fe^{2+} to Fe^{3+} oxidation) and a membrane of corrosion product is formed (this membrane of corrosion products is also reported to be semi-permeable for oxygen). As a result of this the oxygen concentration at

the anode surface is low and the cathodic oxygen reduction reaction mainly takes place at the edges of the blister where oxygen permeates through the coating. This cathodic reaction results in a high pH in the cathodic region, which causes a local loss of adhesion. On this fresh surface the oxygen reduction can proceed. In an earlier publication (14) we did already show that the membrane of corrosion products is not only present above the anodic area, but is also present between the anodic and cathodic area as a separating membrane between the acidic centre and the basic periphery. Together with the membrane on top a closed cap of corrosion products is formed. Figure 7 gives an impression of this.

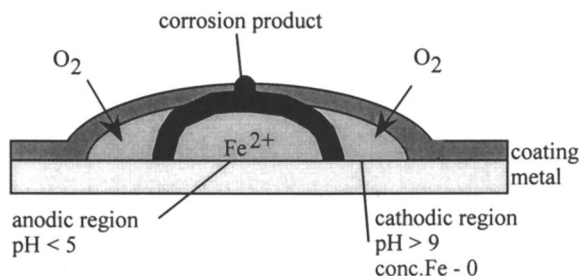


Figure 7. Schematic view of a blister during cathodic delamination.

Figure 8 shows an example of the metal underneath a cathodic blister. For this sample an iron plate was polished and coated. After the blister had grown the coating, that had delaminated fully, was removed and the photograph was taken (magnification 50 times).

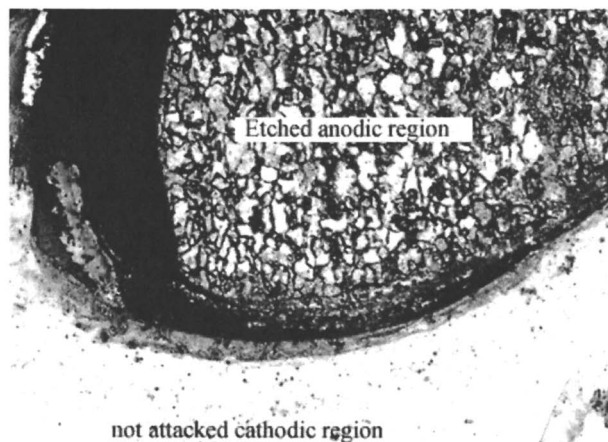


Figure 8. Photograph of the metal underneath a cathodic blister. Clearly visible are the etched anodic area and the non-attacked cathodic areas.

As was shown in the preceding paragraphs, the direct contributions of the corrosion processes can hardly be measured through barrier coating since the impedance of the intact coating above the delaminated areas remains very high ($G\Omega$, nF). This implies that the impedance of the cathodic regions can only be measured through two layers of semi-permeable corrosion product: first from the outside through the corrosion product in the pore and secondly, through the membrane between anodic and cathodic area. In the second membrane, the ionic conduction through the solutions changes from the acidic anodic (Fe^{n+} , H^+ and Cl^- ions) to the alkaline cathodic solution (OH^- and Na^+ ions).

This second membrane that is present between anodic and cathodic areas can also be prepared in a test tube by carefully filling it with representative electrolytes for both the anodic and cathodic areas. For the cathodic area, this is an NaOH solution of around pH 12 and for the anode a HCl solution of pH 3. The acidic solution also contains Fe^{2+} and Fe^{3+} ions. When these solutions are carefully brought into the test-tube (NaOH first, below that the HCl) this produces the situation of Figure 9.

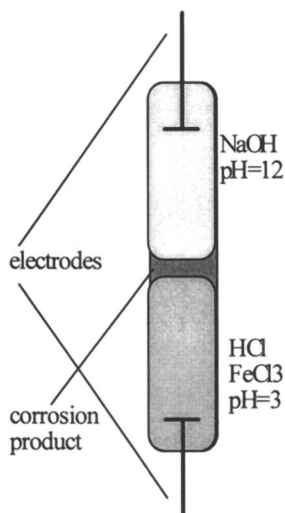


Figure 9. Artificial blister in a test-tube.

Between the electrodes in the test-tube EIS measurements can be performed. An example of such a measurement is given in Figure 10. In this figure a result of a measurement in a test-tube with iron ions is compared with the result measured in a test-tube that only contained HCl and NaOH solution. So the first has a layer of corrosion products in between the two electrodes while the second is soon mixed up by diffusion and convection to produce a NaCl solution.

From these results it is clear that the impedance of the membrane of corrosion products is rather high compared to that of a normal corroding surface. The consequence of this high impedance is that the contribution to the total impedance of the cathodic area is more or less shielded and cannot be determined

accurately. As a result the delaminated area cannot be determined in the case of the cathodic delamination of a coating on steel. Instead, the corrosion product in the defect is characterised, and some contribution of the anodic area will be measured

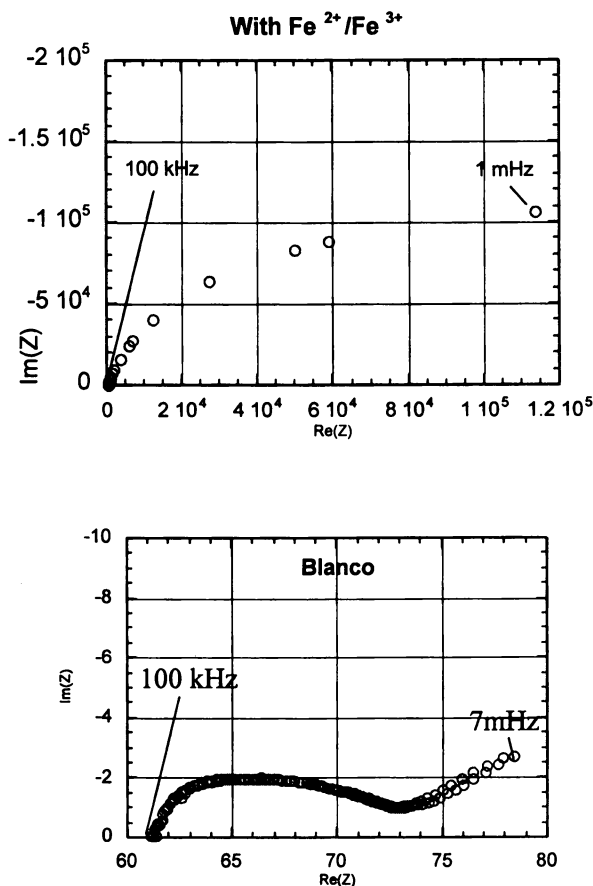


Figure 10. Nyquist plot of an EIS measurement on the corrosion product in the test-tube with Fe-ions (top) and of the solution in the test-tube without Fe-ions (bottom).

Conclusions and Discussion

(Service) Lifetime of organic coatings is a complex quantity. In some cases EIS can be used to obtain more knowledge about the degradation of coatings. In case of the heavy-duty barrier coatings discussed in this paper there are several possibilities:

- In the case of an undamaged coating the dielectric properties of the coating during immersion, expressed in capacitance or, more sensitive, in the CPE-parameters, give information on the state of the coating.

- In the case blisters are formed underneath an intact coating, a qualitative indication of the start of the blister can be derived from EIS measurements. Mechanistic or quantitative data cannot be derived. This is caused by the high resistance and low capacitance of the coating polymer above the delaminated area.
- In case of damaged coatings, EIS measurements may easily be misinterpreted. If cathodic delamination occurs, the corrosion product blocking the pore will dominate the EIS response. This can probably be used to evaluate active anti-corrosive pigmentations.

Overall, the conclusion should be that EIS-measurements on these heavy-duty coatings should mainly be used to monitor the small changes in dielectric properties during water absorption and degradation. Together with chemical information on the binder EIS can be an accurate monitor to evaluate the influence of different treatments or small variations in formulation on the lifetime of the coatings.

For the investigation of defects in coatings EIS can only be used to study the onset of delamination and the formation of corrosion product in the defects and pores. Other techniques should be used to monitor and quantify delamination.

Literature Cited

- 1 Hirayama, R.; Haruyama, S. *Corrosion* **1991**, 42, pp. 952.
- 2 Mansfeld, F.; Tsai, C.H. *Corrosion* **1991**, 42, pp. 958.
- 3 Deflorian, F.; Fedrizzi, L.; Bonora, P.L. *Corrosion* **1994**, 50, pp. 113.
- 4 Lenderink, H.J.W.; Dinx, M.M. and van der Weijde, D.H. *Interactive Software for Impedance Spectroscopy (ISIS)*, Delft University 1991.
- 5 van der Weijde, D.H. Thesis Delft University of Technology, 1996.
- 6 Crank, J. *The Mathematics of Diffusion* Clarendon Press: Oxford, 1975.
- 7 Elsner, C.I.; DiSarli, A.R.; Braz, J. *Chem.Soc* **1994**, Vol. 5, No. 1, 15-18.
- 8 Struik, L.C.E. *Physical aging in amorphous polymers*, Elsevier: Amsterdam, 1978.
- 9 Willems, C.R.J., Thesis Delft University of Technology, 1995.
- 10 van Westing, E.P.M.; van der Weijde, D.H.; Vreijling, M.P.W.; Ferrari, G.M.; de Wit, J.H.W. this conferencebook.
- 11 van der Weijde, D.H.; van Westing, E.P.M.; deWit, J.H.W. *Corrosion Science* **1994**, 36, pp. 643.
- 12 van Westing, E.P.M.; Ferrari, G.M.; deWit, J.H.W.; *Corrosion Science* **1994**, 36, pp. 979.
- 13 Funke, W. *Progr.in.Org.Coatings* **1981**, 9, pp. 29.
- 14 van der Weijde, D. H.; van Westing, E.P.M.; de Wit, J.H.W. *Electroch.Acta* **1996**, Vol. 41, No. 7/8.

Chapter 6

Using Reliability Statistics To Estimate Metal-Container Failure Levels from Censored Tests

W. Stephen Tait

S. C. Johnson and Son, Inc., 1525 Howe Street, Racine, WI 53403

Tests terminated prior to failure of all test samples are referred to as censored tests, and the samples in a censored test are referred to as censored samples. Failure times for censored samples can be estimated if the pit depth and pitting rate are known, or if the pitting rate can be reasonably estimated from pit depth and exposure time. Reliability statistics are used to estimate failure levels from censored data so that censored tests can be used to estimate population failure levels. Cumulative failure levels are estimated by calculating median rank for each estimated failure time, and failure levels are plotted versus corresponding times on a Weibull probability plot. The Weibull plot typically yields a linear graph that can be extrapolated to find failure levels outside the data set.

The objective of corrosion testing is usually to determine metal service lifetime: that is, when will a metal, exposed to a given environment, fail from corrosion. Failure is a subjective term that is usually defined by the type of service for which the metal is being used. Failure is defined here as when a pit perforates a metal container wall and causes the container to leak.

It is also often the objective of a corrosion test to determine what level of failures to expect after a specified amount of time. Failure level is defined here as the total number of metal containers failing by a given time. Failure levels are obvious when a test is allowed to run until all samples (containers) fail. Unfortunately, one does not always have the luxury of waiting long times for results (e.g., years). Time constraints often force one to either prematurely remove all samples from a test prior to failure, and (destructively) inspect them for corrosion, or prematurely remove a

fraction of the samples from test at several intermediate times and (destructively) inspect for corrosion.

Tests whose samples are removed before test completion (i.e., before all samples fail) are referred to as censored tests, and samples removed from test prior to failure are referred to as censored or suspended samples.¹ Data from censored samples are often used to estimate the percentage of a population that will fail by a specified time: for example, ten percent of all metal containers are expected to fail one year after filling.

It will be shown that: 1) expected failure time (EFT) can be estimated when a censored sample is pitted, 2) failure levels can be estimated from expected failure times (EFTs) using statistical median ranking,² and 3) a Weibull probability plot³ of failure levels (median ranks) versus corresponding EFTs can be used to determine failure levels outside of the data set.

Experimental

A previous publication contains descriptions of both uncoated and internally coated metal containers.⁴ Filled metal containers were stored in a 21°C (70°F) constant temperature room, and sets of samples were periodically removed and inspected for corrosion inside the containers. Test length was one year. Containers that were inspected for corrosion were not returned to test because they were emptied and cut open in order to locate pits and measure their depths. Pit depths were measured by taking the difference between the point of focus at the pit mouth and the point of focus at the pit bottom. The coefficient of variation⁵ for this type of depth measurement is approximately ten percent.

Pitting corrosion

Pitting corrosion occurs in small localized areas and proceeds through several stages: 1) nucleation, 2) growth to a critical size, and 3) steady state growth.⁶⁻¹²

Pit nucleation. It is not unusual to have samples, in a set of censored samples, with different pit depths. Pits nucleate at different times,¹³⁻¹⁵ thus different pit depths among censored samples are most likely due to different pit nucleation times and not different pitting rates. It is reasonable to hypothesize that the deepest pit found at any given exposure time has been growing for the longest time, and has the smallest times for nucleation and growth to critical size.

Pit growth to critical size. Only pits reaching a critical size¹⁶⁻¹⁸ continue growing until their aspect ratio decreases below a critical level,¹⁹ or the pit perforates the metal.²⁰⁻²² Pits on censored samples (containers) that are visible to the unaided eye are most likely larger than critical size, because most critical sizes reported in the literature are on the order of 50 μm (human hair is approximately 25 μm thick).^{17,18}

Mature pit steady state growth. Figure 1 contains a typical graph of maximum pit depths observed in metal containers after different exposure times. It can be seen in Figure 1 that maximum pit depth increases with time, supporting the hypothesis that mature pits grow at a steady state rate, whose magnitude is determined by a given environment. Other researchers observed the same pit growth trend for

different metals and environments.²³⁻²⁵ A filled metal container is a closed static system, thus a visible pit is most likely larger than critical size and will continue growing until it perforates a container, providing the container is not prematurely removed from test.

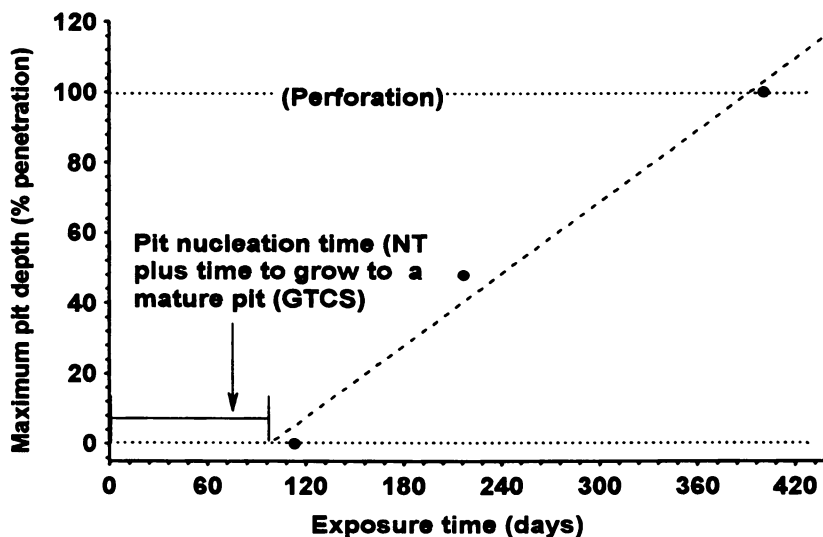


Figure 1. Maximum pit depth increases with time.

Steady state growth rate of mature pits can be mathematically expressed in terms of the three stages of pitting corrosion:

$$\text{Pitting Rate (PR)} = \frac{\text{Pit depth}}{\text{ET} - (\text{GTCS} + \text{NT})} \quad (1)$$

Nucleation time (NT) is the time it takes for a pit to nucleate after initial exposure of a metal to a corrosive environment (stage 1); growth to critical size (GTCS) is the time it takes after nucleation for a pit to grow to critical size (stage 2); and exposure time (ET) is the total time a metal is exposed to a corrosive environment (stages 1-3). Pit depth in Equation (1) is the total depth measured when the sample is opened for inspection.

Failure times (FT) for pitted censored samples can be calculated when pit depths, NT, GTCS, and PR are known:

$$\text{FT} = \frac{(\text{Original thickness} - \text{Pit depth})}{\text{PR}} + \text{ET} \quad (2)$$

Unfortunately, PR is difficult to determine for metal containers because the magnitudes of NT and GTCS are rarely known. A good estimate for pitting rate can be obtained by applying linear regression to data like that in Figure 1. The slope of the regression line in Figure 1 is the pitting rate. NT plus GTCS can also be estimated from the intersection of the line with the time axis as illustrated in Figure 1. However,

it takes a long time (e.g., one year) to generate data like that in Figure 1, and more than three data points are needed to obtain a proper regression line.

Figure 1 suggests there is a unique pitting rate for a given metal-environment system. Unfortunately this unique rate must be estimated because there is currently no way to determine NT and GTCS. We found it useful to estimate the system pitting rate as follows: a) set NT and GTCS equal to zero, b) use Equation (1) to calculate pitting rates for all pitted censored samples, c) use the highest rate among all samples as an estimate for the system rate. The highest rate is substituted for PR in Equation (1) to yield:

$$EFT = \frac{(\text{Original thickness} - \text{pit depth})}{PR_{\max}} + ET \quad (3)$$

PR_{\max} in Equation (3) is the highest pitting rate observed among all censored test samples, and Equation (3) is used to calculate the expected failure time (EFT) for each censored pitted sample. It will be shown that Equation (3) yields expected failure levels (EFLs) that are the same order of magnitude as observed failure levels.

Reliability Statistics

The procedure for calculating EFLs includes: 1) ranking all samples, and 2) calculating cumulative probabilities according to rank.

Table 1 contains a raw data set from a test that was prematurely terminated after 364 days. The table consists of containers (samples) that are: a) perforated (10, 12, 15, 19, and 20), b) pitted censored samples (5-7, 14, 16-18), c) non-pitted censored samples (1-4, 8, 9, 11, and 13), and d) unopened censored containers (21-24).

Table 1. Example failure data

Sample	Exposure	EFT (days)	Sample	Exposure	EFT (days)
1	200 days		13	308 days	
2	200 days		14	347 days	521
3	214 days		15	347 days	347
4	217 days		16	349 days	549
5	234 days	421	17	349 days	522
6	234 days	401	18	357 days	454
7	234 days	401	19	357 days	357
8	234 days		20	364 days	364
9	234 days		21	unopened	
10	302 days	302	22	unopened	
11	302 days		23	unopened	
12	308 days	308	24	unopened	

Non-pitted and unopened censored samples are temporarily assigned an EFT equal to their ET, because it is not possible to calculate an EFT when no pits are present. Temporary EFTs in Table 2 are in parentheses. For example, container

numbers 1 and 2 are temporarily assigned an EFT equal to their 200 day exposure time, and unopened containers 21-24 are temporarily assigned a 364 day EFT, which is the total length of the test.

Table 2. Failure data with temporary EFT values

Sample	Exposure	EFT (days)	Sample	Exposure	EFT (days)
1	200 days	(200)	13	308 days	(308)
2	200 days	(200)	14	347 days	521
3	214 days	(214)	15	347 days	347
4	217 days	(217)	16	349 days	549
5	234 days	421	17	349 days	522
6	234 days	401	18	357 days	454
7	234 days	401	19	357 days	357
8	234 days	(234)	20	364 days	364
9	234 days	(234)	21	unopened	(364)
10	302 days	302	22	unopened	(364)
11	302 days	(302)	23	unopened	(364)
12	308 days	308	24	unopened	(364)

EFT data are arranged in ascending order as illustrated in Table 3. Non-pitted and unopened samples precede pitted samples when their EFTs are equal. For example, no pits were found on sample 11 when it was opened at 302 days and sample 10 perforated at 302 days. Both samples have 302 day EFTs, but sample 11 is a censored sample (with a temporary EFT) so it precedes sample 10.

Table 3. EFT data in ascending order

Sample	Exposure	EFT (days)	Sample	Exposure	EFT (days)
1	200 days	(200)	21	364 days	(364)
2	200 days	(200)	22	364 days	(364)
3	214 days	(214)	23	364 days	(364)
4	217 days	(217)	24	364 days	(364)
8	234 days	(234)	20	364 days	364
9	234 days	(234)	6	234 days	401
11	302 days	(302)	7	234 days	401
10	302 days	302	5	234 days	421
13	308 days	(308)	18	357 days	454
12	308 days	308	14	347 days	521
15	347 days	347	17	349 days	522
19	357 days	357	16	349 days	549

EFLs are calculated only for pitted containers (samples), so temporary EFTs are removed from the table, after arranging in ascending order, to give a table like that in Table 4.

Table 4. Ranked EFT data without temporary EFTs

Sample	Exposure	EFT (days)	Sample	Exposure	EFT (days)
1	200 days		21	364 days	
2	200 days		22	364 days	
3	214 days		23	364 days	
4	217 days		24	364 days	
8	234 days		20	364 days	364
9	234 days		6	234 days	401
11	302 days		7	234 days	401
10	302 days	302	5	234 days	421
13	308 days		18	357 days	454
12	308 days	308	14	347 days	521
15	347 days	347	17	349 days	522
19	357 days	357	16	349 days	549

Median statistical ranks are calculated for EFTs like those in Table 4, and these ranks are used to calculate cumulative probabilities (EFLs) for each EFT.²⁶ There are other statistical ranking methods,²⁷ but they all give approximately the same probability (EFL) as illustrated in Figure 2. Statistical medians are at the center of a data set, thus more than one EFT is needed to use median ranking because a single EFT will always have a 50% EFL.

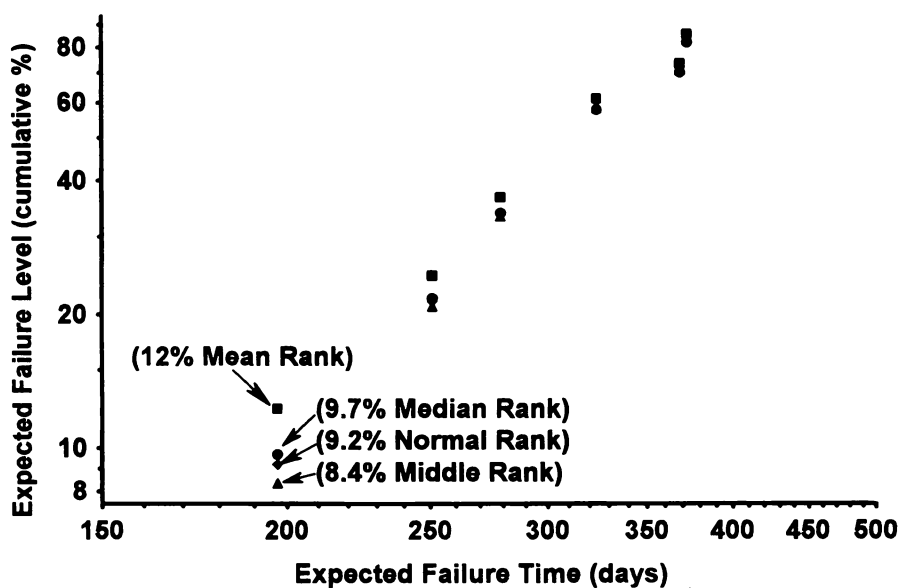


Figure 2. Different statistical ranking methods yield approximately the same estimates for cumulative failure at a given expected failure time.

Failure data are typically not a continuous function of time as can be seen in Figure 3. A continuous linear function is needed to extrapolate data outside of a data set. Fortunately cumulative failures are a continuous function of time as seen in Figure 4. Cumulative failure curves typically have an S-shape like that in Figure 4,²⁸⁻³⁰ and can be made linear by plotting the data on probability paper.

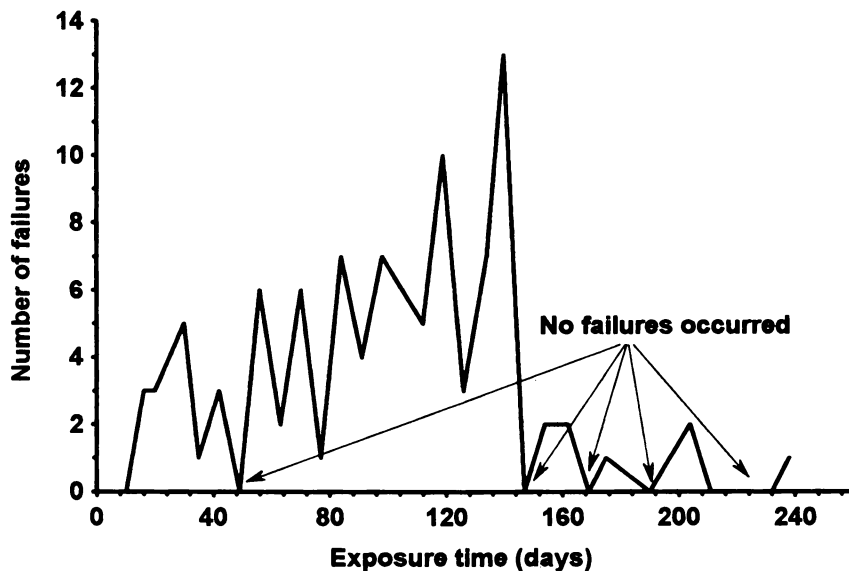


Figure 3. Number of failures is not a continuous function of time.

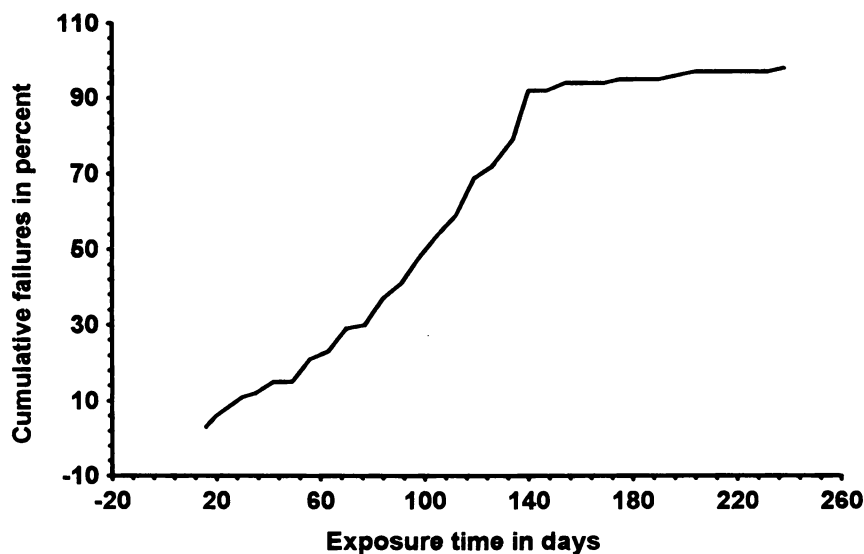


Figure 4. Cumulative number of failures are a continuous function of time.

Weibull probability plots were used for EFL and EFT data like that in Table 4 (or Figure 4) because the Weibull function can be transformed into a linear form. The cumulative Weibull equation is:

$$F(t) = 1 - e^{-(t/\theta)^\beta} \quad (4)$$

$F(t)$ is the cumulative number of failures at a given time, t , and θ is the point on a Weibull curve that divides the curve area into 63.2% and 36.8% (θ is analogous to the mean for a normal distribution curve), and β is the shape parameter for the Weibull probability density function.

The cumulative expected failure level (EFL) can be substituted for $F(t)$ and EFT for t in Equation (4) to yield:

$$\text{EFL} = 1 - e^{-(\text{EFT}/\theta)^\beta} \quad (5)$$

Rearranging Equation (5) and taking the natural log twice yields an equation that has the linear form shown in Equation (6):

$$\text{Ln}(\text{EFT}) = (1/\beta)\text{Ln} \left[\frac{1}{(1 - \text{EFL})} \right] + \text{Ln}\theta \quad (6)$$

Figure 5 contains a Weibull plot of EFL and EFT data like that in Table 4. The resulting linear plot is continuous and can be extrapolated (within reason) outside the data set as shown in Figure 5, where a two percent failure level is expected to occur by 124 days (or 100% failures at 509 days). Using Weibull probability paper allows EFT and EFL data to be plotted without having to mathematically transform the data in order to obtain a linear graph.³¹

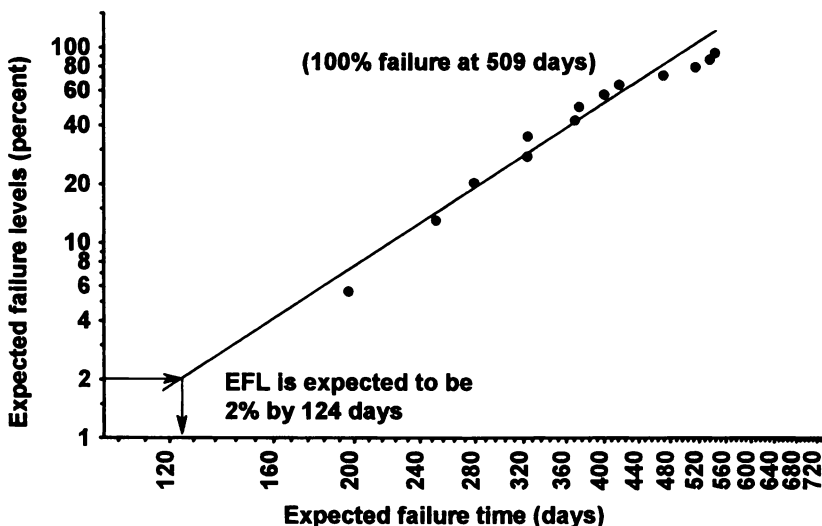


Figure 5. A Weibull probability plot of EFLs versus EFTs.

Results and Discussion

Several comparisons between EFLs obtained from Weibull probability plots and observed failure levels are contained in Table 5. It can be seen from Table 5 that EFLs are typically the same order of magnitude as observed failure levels. It can also be seen in Table 5 that approximately half of the EFLs are lower than observed levels.

Table 5. Comparisons between estimated and observed failure levels

Percent EFL	Observed cumulative % failures
5	11.5
18.5	16.7
17.7	33.3
9.2	22.2
8.1	8.3
36.8	30
55.9	55.6
64.4	63.6
5.6	8.3
12.6	8.3
13.5	16.7
8.3	12.5
6.7	10
41.3	41.7
23.8	25
23	14.3
29.8	33.3

Underestimation of failure levels arises from underestimating pitting rates. Rate underestimation comes from assuming NT and GTCS are zero, as was done when total exposure time (ET) was used to calculate censored sample pitting rates to find the maximum pitting rate. However, the comparative data in Table 5 show that the error in pit rate estimation is small enough to yield EFLs that are within the same order of magnitude as actual failure levels.

The accuracy of EFTs (and thus EFLs) could be improved with a method that measures (without having to destroy samples) either: a) actual pitting rate (PR), or b) GTCS and NT. Equations (1) and (2) can be used to calculate failure times when PR, NT and GTCS magnitudes are known. However, without these quantities the method discussed here provides a reasonable approximation of failure times and levels.

Conclusions

The three stages of pit growth were used to develop an algorithm for estimating when pitting corrosion will perforate metal containers. The highest pitting rate observed in all censored test containers is used to calculate expected failure times (EFTs) for all censored pitted samples. Expected failure levels (EFLs) obtained from these EFTs are

the same order of magnitude as actual failure levels. More accurate EFLs could be obtained if the actual pitting rate could be measured without having to destroy the sample to locate and measure pit depth.

The method described in this paper can be used for both internally coated and uncoated metal containers, and for other metal-environment systems where failure is defined as metal thinning or perforation. The algorithm described here can also be used for any coating system where failure can be defined quantitatively, and failure time can be estimated for censored samples. Failure time and level data like that in Figure 5 can be used to estimate when a given level of failure will occur, and whether or not a given product meets product warranty or lifetime expectations.

References

1. W. Nelson, *Journal of Quality Technol.*, **1970**, 2(3), p. 126
2. K. C. Kapur and L. R. Lamberson, *Reliability in Engineering Design*, John Wiley and Sons, NY, **1977**, Chapter 11, p.297,
3. K. C. Kapur and L. R. Lamberson, *Op. Cit.*, p. 303
4. W. S. Tait, *Corrosion Protection by Organic Coatings*, The Electrochemical Society, Pennington, NJ, **1987**, 87-2, p. 229
5. I. Miller and J. E. Freund, *Probability and Statistics for Engineers*, third edition, Prentice-Hall, Englewood Cliffs, NJ, **1977**, Chapter 5, p. 156
6. W. S. Tait, *An Introduction to Electrochemical Corrosion Testing for Practicing Engineers and Scientists*, PairODocs Publications, Racine WI, **1994**, Chapter 3, pp. 37-42
7. N. D. Greene and M. G. Fontana, *Corrosion*, **1959**, 15, p. 25t
8. P. M. Aziz and H. P. Godard, *Ind. Eng. Chem.*, **1952**,44, p. 1791
9. P. M. Aziz, *Corrosion*, **1953**, 9, p. 85t
10. R. May, *J. Inst. Metals*, **1953**, 32, p. 65
11. M. A. Streicher, *J. Electrochem. Soc.*, **1956**, 103, p. 375
12. W. S. Tait, *Corrosion*, **1979**, 35(7), p. 296
13. J. R. Scully, S. T. Pride, H. S. Scully, and J. L. Hudson, **1995** (October 8-13), abstract number 105, *Electrochemical Society Fall meeting, Chicago IL*
14. D. E. Williams, C. Westcott, and M. Fleischmann, HAREWELL publication AERE-M3371, United Kingdom Atomic Energy Authority, **1984**
15. P. M. Aziz, *Corrosion*, **1956**, 12, p. 495t
16. G. T. Burstein and S. P. Mattin, **1995** (October 8-13), abstract number 104, *Electrochemical Society Fall meeting, Chicago IL*
17. M. Kowaka, *Introduction to Life Prediction of Industrial Plant Materials*, Allerton Press, N.Y., **1994**, Chapter 3, p. 22
18. Y. Hisamatsu, *Corrosion Engineering*, **1983**, 32, p. 9
19. M. Wang and H. W. Pickering, *J. Electrochem. Soc.*, **1995**, 142 (9), pp. 2986 - 2995
20. C. C. Nathan and J. R. Schieber, **1977** (March 14-18), paper number 177, *CORROSION/77*, San Francisco, CA
21. Z. Szklarska-Smialowska, *Pitting Corrosion of Metals*, National Association of Corrosion Engineers, Houston, TX, **1986**, Chapter 6, pp. 121-125
22. M. Janik-Czachor, *Br. Corr. Journ.*, **1971**, 6, p. 57
23. J. E. Strutt, J. R. Nichols, and B. Barbier, *Corrosion Science*, **1985**, 25(5), pp. 305-315
24. J. W. Provan and E. S. Rodriguez III, *Corrosion*, **1989**, 45(3), pp. 178-192

25. D. L. Crews, *Galvanic and Pitting Corrosion - Field and Laboratory Studies*, ASTM STP 576, American Society for Testing and Materials, Philadelphia, PA, 1976, pp. 217-230,
26. K. C. Kapur and L. R. Lamberson, *Op. Cit.*, pp. 314-322
27. B. F. Kimball, *J. American Statistical Assoc.*, 1960, 55, p. 546
28. I. Miller and J. E. Freund, *Op. Cit.*, p. 143,
29. W. S. Tait, *Corrosion*, 1994, 50(5), pp. 373-377
30. J. E. Strutt, J. R. Nicholls, and B. Barbier, *Corrosion Science*, 1985, 25(5), p. 305
31. W. Nelson, *Accelerated Testing*, John Wiley and Sons, NY, 1990, Chapter 3, p. 129

Chapter 7

Quantification of Coating Aging Using Impedance Measurements

E. P. M. van Westing¹, D. H. van der Weijde², M. P. W. Vreijling¹, G. M. Ferrari¹,
and J. H. W. de Wit²

¹Department for Corrosion Prevention, TNO Centre for Coatings Research, P.O. Box 57, 1780 AB Den Helder, Netherlands

²Laboratory for Materials Science, Division for Corrosion Technology and Electrochemistry, Delft University of Technology, P.O. Box 5025, 2600 GA Delft, Netherlands

This chapter shows the application results of a novel approach to quantify the ageing of organic coatings using impedance measurements. The ageing quantification is based on the typical impedance behaviour of barrier coatings in immersion. This immersion behaviour is used to determine the limiting case for the interpretation of results on coatings exposed to artificial and outdoor weathering.

Impedance studies on organic coatings, performed for many years already (1-9) are mostly aimed to estimate the quality and performance of the coating and anti corrosion pigments and the remaining service life. The majority of these studies are based on the determination of the DC-resistance (8) or on the amount of blistering (9). The results of these studies are often poor as both a low DC resistance and the growth rate of blisters only yield information on a coating that has already failed. The time before failure is more important than the corrosion rate after failure as the first period will and should be significantly longer. It could be argued that the study of corrosion rate after failure is important, for instance when the performance of anti corrosion agents on the occurrence of blistering is evaluated. However, this still requires a detailed study of the coating impedance (10), as results presented in the preceding chapter by van der Weijde (11) show the pitfalls in the estimate of the corroding surface area underneath a coating.

It has been shown in former studies that coatings can retain a very high DC-resistance while water and ions (12,13) are taken up followed by loss of adhesion and the start of the corrosion process (14,15). This high resistance makes the DC-signal unreliable as a detection method for this event. However, detection of delamination is possible from the changing dielectrical properties of the coating polymer, leading to the onset of corrosion. Even so, these changes are not reflected by the "ordinary" coating capacitance. Only analysis of the coating impedance using a Constant Phase

Element (denoted by Q_{pf} , pf = paint film) enables the accurate detection of the onset of the coating delamination, leading up to the start of the corrosion process. The changes in the dielectric properties of the coating polymer that indicate the onset of corrosion are the result of the swelling (13-15) that occurs with the delamination of the coating.

The previous chapter (11) showed that the life cycle of barrier coatings (without any sign of defect) in immersion can be divided in three stages: Stage 1) The pre saturation stage: in the beginning of the immersion where water and ions are taken up; Stage 2) Stationary phase: where values of Y_0 and n (Q_{pf}) are determined by the type of coating and the thickness of the individual coatings layers; Stage 3) Degradation stage: In this stage the degradation of the coating starts by the formation of blisters and the start of the corrosion process. During this period the coating maintains its barrier properties -high DC-resistance- and there are no visual signs of the presence of defects.

Experimental Method

Materials. Two types of coatings for maritime applications were used in the investigations: one epoxy and one alkyd based. The primers of both coating systems contain zinc phosphate. The coatings were applied to the steel panel by air spraying. The steel substrate for these coatings consisted of standardised test panels.¹ The mill surface on one side of these panels was completely removed by abrasive grinding. The coatings were applied to this side of the panels.

Part of the experiment was carried out on polyester coil coated material. This is a pre-coated material consisting of a hot dip galvanised cold rolled steel substrate with a chromate surface pre-treatment, a polyester primer and a polyester topcoat. This coated material was selected for its uniform properties. Different sections of the same sheet only have small differences in layer thickness and dielectric properties, so effects of a cyclic immersion test can be accurately monitored with this material.

Equipment and data analysis. The electrochemical impedance measurements were carried out using the following Solartron instruments: 1286 Electrochemical Interface and 1250/1255 Frequency Response Analysers. This equipment was controlled by a PC. Further information on the instrumental set-up and the electrochemical cell can be found elsewhere (16).

Impedance measurements were performed in the range between 100 kHz and 100 Hz when coatings are immersed only for short periods (< 60h) and the coating impedance changes rapidly. This set-up allows for a highly accurate impedance measurement every 7 minutes. For longer immersion periods coating impedance is measured between 500 kHz and 0.1 Hz. The results were normally analysed between 10 kHz and 1 kHz as it is impossible to measure the DC-resistance at low frequencies with the barrier coatings used here. Low frequencies were measured only to be sure of the possibility to detect failure of the barrier properties.

The results of the impedance measurements were analysed using Boukamp's EQUIVCRT (17,18). For the analysis of the impedance of barrier coatings an

Q-panel Company, Cleveland, Ohio USA, type S

equivalent circuit consisting of a resistor (electrolyte resistance) in series with a Constant Phase Element (CPE, denoted by a Q) (17,18) is used. The CPE represents the response of the coating. The instrumental set-up (19) allows for very accurate results of the impedance measurements. The variation in the results can be derived from the scatter in the plots of Y_0 and n , as no data reduction was carried out.

Electrolytes. All coatings tested in the laboratory only were immersed in a 3% NaCl solution. The coatings from the accelerated weathering and the outdoor exposure were immersed in artificial rainwater based on coastal rainwater composition in The Netherlands. The concentrations were increased 50 times. This electrolyte was chosen to measure the impedance of coatings of coatings in outdoor exposure from time to time. An electrolyte for this purpose should not be more aggressive than rainwater. The composition of this electrolyte is listed in table 1. Both the salts from which the electrolyte is composed and the resulting ionic composition are given.

Table I. The composition of the artificial rainwater. The salts from which the electrolyte is composed as well as the ionic composition are given. (pH = 4.06)

Salts	Contents ($\mu\text{mol/l}$)	Contents ($\mu\text{mg/l}$)	Ions	Contents ($\mu\text{mol/l}$)
$\text{CuSO}_4 \cdot 5\text{H}_2\text{O}$	0.2	0.0499	NH_4^+	375
$\text{FeCl}_2 \cdot 4\text{H}_2\text{O}$	5.0	0.9941	Na^+	760
$\text{NiCl}_2 \cdot 6\text{H}_2\text{O}$	0.1	0.0238	K^+	30
$\text{MgCl}_2 \cdot 6\text{H}_2\text{O}$	62.5	12.7069	Ca^{2+}	6.5
NH_4Cl	135.2	7.2318	Mg^{2+}	62.5
Na_2SO_4	135.2	19.2038	F^-	7.5
NaCl	479.6	28.0278	Cl^-	750
$(\text{NH}_4)\text{SO}_4$	114.6	15.1432	NO_3^-	250
NH_4NO_3	10.6	0.8484	SO_4^{2-}	250
$\text{Ca}(\text{NO}_3)_2 \cdot 4\text{H}_2\text{O}$	75.0	17.7113	Cu^{2+}	0.2
KNO_3	30.0	3.0333	Fe^{2+}	5.0
NaF	7.5	0.3149	Ni^{2+}	0.1
HNO_3	59.4	3.7428		
NaHCO_3	2.0	0.1680		

Experimental Results and Discussion

Results of experiments on the dielectrical behaviour of organic coatings during long-term immersion are presented in the preceding chapter (11). This behaviour can be used as a basis for the interpretation of impedance results for the determination of coating performance in alternating environments as outdoor exposure and artificial weathering.

When a dried coating that had already reached Stage 2 once, the stationary situation, is reimmersed, the impedance of the stationary situation will be re-established rapidly (20). This is illustrated in Figures 1a, b, and c, by impedance

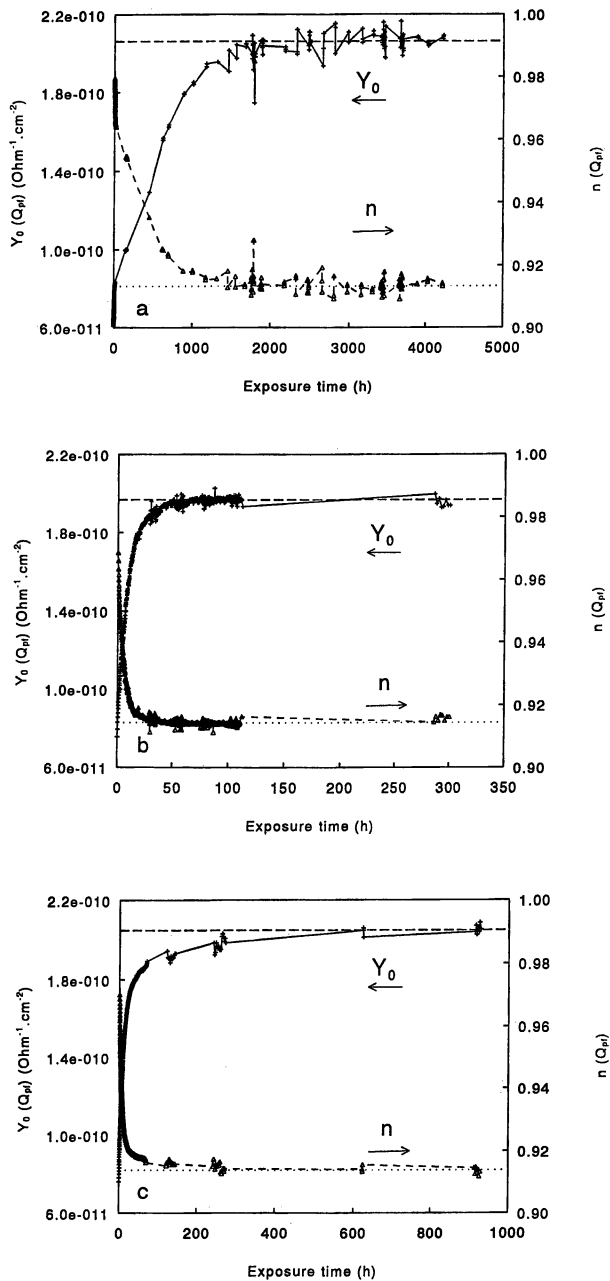


Figure 1: Curves of Y_0 and n (Q_{pf}) of an epoxy coating system (105 :m) as function of time during immersion in a 3% NaCl solution. a) first immersion, b) second immersion after 30 days of drying and c) third immersion after 53 days of drying.

curves of an intact barrier epoxy coating system ($\approx 105\mu\text{m}$) during the first, second and third immersion. The stationary levels of the coating impedance parameters Y_0 and $n(Q_{pf})$ are represented by dashed lines. In Figure 1a, it can be observed that the time to reach the stationary situation (Stage 2) for the first time was about 2000 h. In the second (Figure 1b) and third (Figure 1c) immersion this level was reached in much less time. The physical differences between these situations indicate the irreversible changes resulting from ageing of the coating polymer.

From a similar experiment on a barrier epoxy coating that had reached Stage 3 (with a defect, but high DC-resistance, probably loss of adhesion due to localised excessive swelling, no visual sign of any defect) similar behaviour can be observed. This is illustrated with the impedance curves in Figure 2a and b. From this figure, the values of Y_0 and $n(Q_{pf})$ at the end of the first and the second immersion are the same. However, these values are reached in a much shorter time in the second immersion. From experience it is known that a stationary level for $n(Q_{pf})$ for this type of coating would be around 0.92. Due to the poor performance of the coating, it does not show any stationary behaviour (Stage 2).

From these results one can deduce that the curves of the coating impedance parameters contain relevant information for the determination of the ageing of coatings in alternating exposure. This is further shown by the behaviour of a polyester coil coating system in an immersion cycle in the laboratory. This cycle consisted of 24h immersion in a 3% NaCl solution and 72 h drying at 35 °C. Before drying, the cell was partly emptied, leaving behind a small layer of the electrolyte that dried out during the drying stage. The curves of Y_0 and $n(Q_{pf})$ as a function of time during successive immersions are plotted in Figure 3a and b. In this figure it can be observed that Y_0 and $n(Q_{pf})$ change systematically with successive immersions. The changes can be further pointed out by curves of Y_0 and $n(Q_{pf})$ from the 10th immersion, given in Figure 4a and b respectively. In these figures Y_0 and $n(Q_{pf})$ change rapidly in the first five hours of the immersion. Then, the changes of Y_0 and $n(Q_{pf})$ become approximately linear with time. In this stage the values of Y_0 and $n(Q_{pf})$ change as if the coating is immersed continuously. A linear interpolation of the curves between 10 and 15 h of immersion and extrapolation to $t=0$ -see Figures 4a and b- yields values of Y_0 and $n(Q_{pf})$ ($t=0$) that can be related to the amount of ageing that had occurred prior to this measurement.

To compare these extrapolated values with the impedance of a coating of the same type during continuous immersion, some transformations should be made for (small) differences in layer thickness and initial curing stage (reflected in the dielectric properties) of the polyester coil coating. Both parameters affect the value of $Y_0(Q_{pf})$ at $t=0$ of the first immersion of the coating in both the wet/dry cycle and in continuous immersion. The transformation can be carried out using Formula 1 (the subscript 0 of $Y_0(Q_{pf})$ is omitted for ease of use). In this formula $Y_0(Q_{pf})$ is treated as a capacitance:

$$Y_{2C} = (Y_{2E} - Y_{2(t=0)}) * \frac{l_2}{l_1} + Y_{1(t=0)}$$

Where: Subscript 1 denotes the continuously immersed coating, and subscript 2 indicates the coating in alternating wet/dry exposure. Y_{2C} is the corrected value $Y_0(Q_{pf})$ extrapolated to ($t=0$) of the alternating wet/dry exposed coating (subscript 2) to

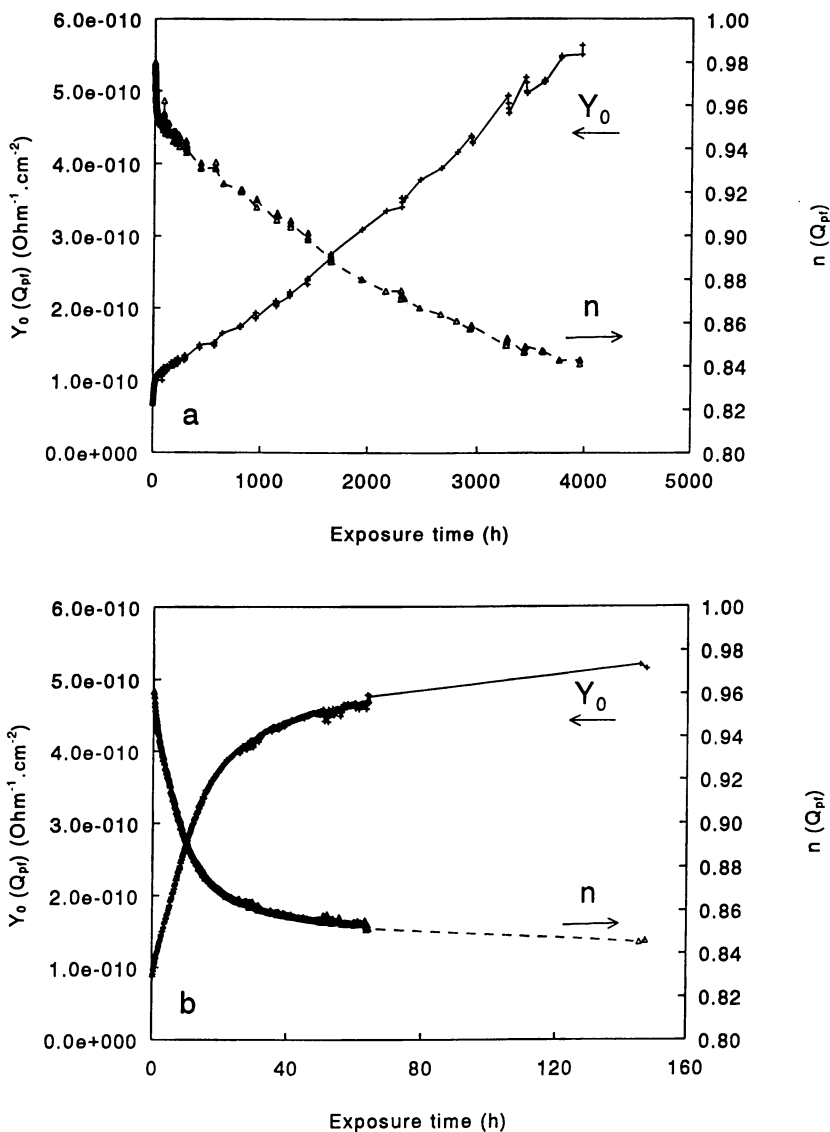


Figure 2: Curves of Y_0 and $n(Q_{pf})$ of an epoxy coating system (97 :m) that already reached stage 3 as function of time during immersion in a 3% NaCl solution. a) first immersion, b) second immersion after 30 days drying.

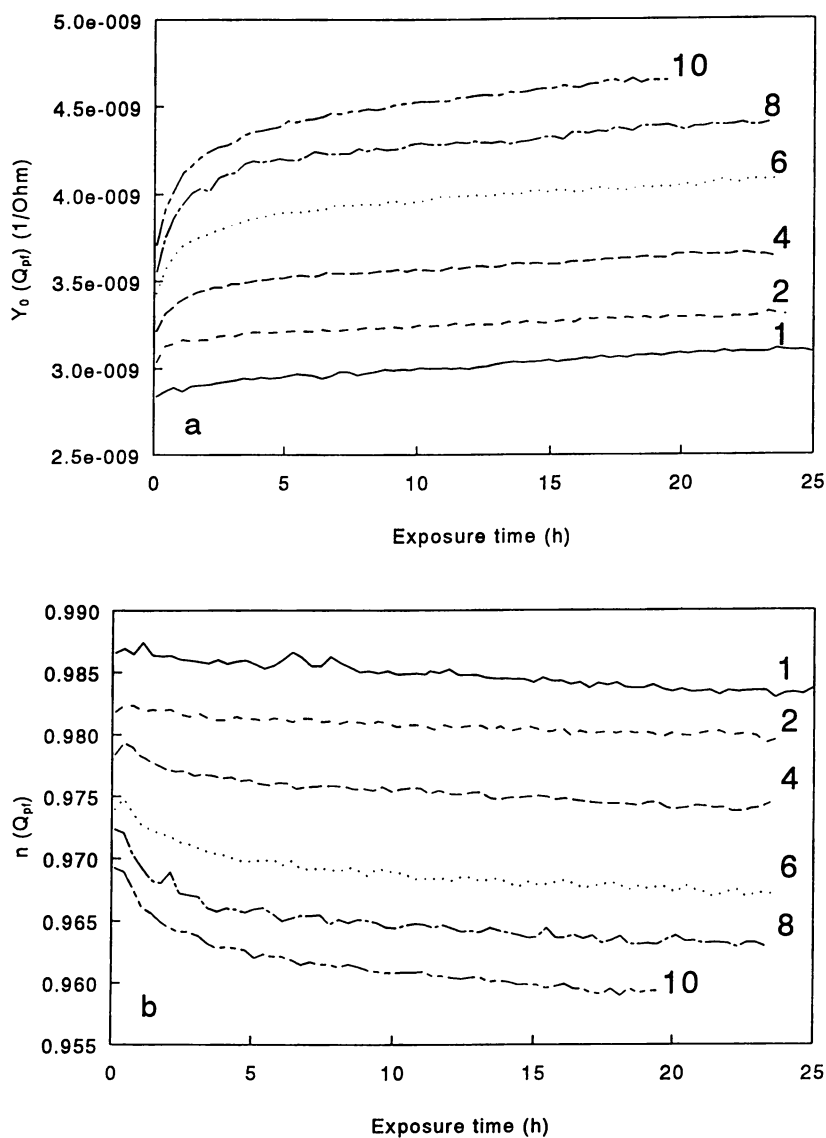


Figure 3: Curves of Y_0 (a) and n (b) (Q_{pf}) as function of time of a polyester coil coating (about 30:μm) during successive immersion cycles in a 3% NaCl solution.

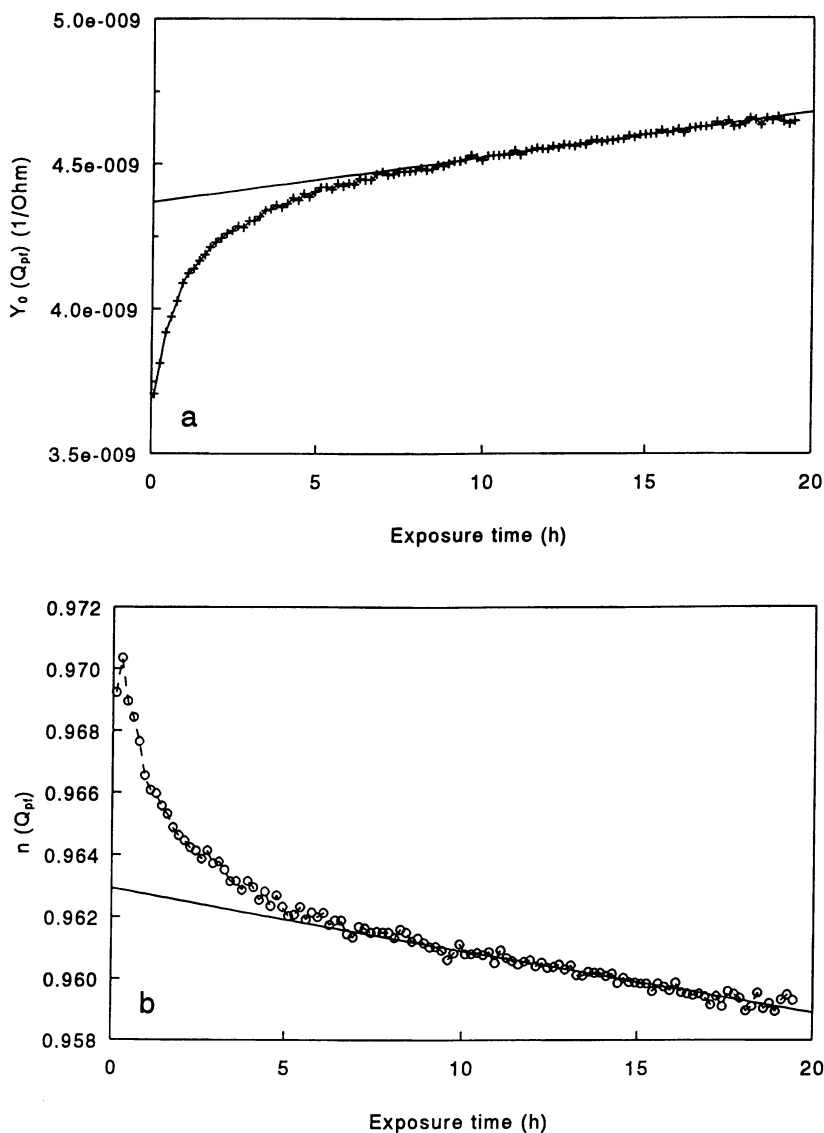


Figure 4: Curves of Y_0 (a) and n (b) (Q_{pf}) as function of time of a polyester coil coating (about 30:μm) during the 10th immersion cycle in a 3% NaCl solution.

be plotted on the curve of $Y_0(Q_{pf})$ as a function of exposure time of the continuously immersed coating (subscript 1). Y_{2E} is the value of $Y_0(Q_{pf})$ extrapolated to $(t=0)$ measured during the wet period of coating 2. $Y_{2(t=0)}$ is the value of $Y_0(Q_{pf})$ at $t=0$ of coating 2 measured in the beginning of the first wet period. $Y_{1(t=0)}$ is the value of $Y_0(Q_{pf})$ at $t=0$ of coating 1 measured in the beginning of the continuous immersion. l_1 and l_2 are the thickness of coatings 1 and 2 respectively.

The values of Y_0 and $n(Q_{pf})(t=0)$ obtained by linear extrapolation and corrected with formula 1 are plotted on the impedance curve of a similar coating in immersion in Figure 5. In this figure, it can be observed that the values of Y_0 and $n(Q_{pf})(t=0)$ determined independently for successive immersion cycles correspond to approximately the same immersion time.

From these results it can be derived that, using this method of interpretation, impedance measurements can be used to quantify the ageing of coatings in alternating wet/dry exposures. The power of this method is further illustrated by the fact that a parallel investigation of the water transport parameters: diffusion coefficient D and solubility S could not establish any systematic change with increasing immersion cycle number and increasing ageing.

In the following sections examples will be given of the application of the method described above.

Industrial Epoxy-based Coating on Phosphated Mild Steel. In Figure 6a and b the curves of Y_0 and $n(Q_{pf})$ are given of two similar industrial epoxy-based coatings on phosphated mild steel as function of time during immersion in artificial rainwater (Figure 6a: average coating thickness $\approx 98.6\mu\text{m}$, Figure 6b: average coating thickness $\approx 103.3\mu\text{m}$). In spite of the small difference in coating thickness, impedance values will be compared without corrections, as these data show more scatter than the results obtained with the polyester coil coating. In this figure the three stages are clearly visible. In Figure 6a stage 2 ends around 2000h, in Figure 6b stage 2 ends around 4000h. In stage 3 defects are formed, resulting in loss of barrier properties around 14000h and blistering around 15000h for the coating of Figure 6a. The coating of Figure 6b showed barrier properties and no visible defects up to 13000h of immersion. From stage 2 values of Y_0^S and $n^S(Q_{pf})$ for maximum saturation can be derived: $Y_0^S(Q_{pf}) = 8.7e-10$ (1/Ohm), $n^S(Q_{pf}) = 0.982$. These values are necessary for the interpretation of the impedance measurements on coatings from the cyclic tests and outdoor exposure. Here no corrections for (small) differences in layer thickness could be made since one parameter for equation 1 (the coating impedance in the beginning of the ageing) is not available for the coatings from outdoor exposure and accelerated weathering.

A similar coating (type and layer thickness) was aged in the Hoogovens Corrosion Test (HCT) (21). The impedance of the coating was measured after three different amounts of weathering cycles. The panels were temporarily removed from the test cabinet and immersed in artificial rainwater for the duration of the measurement. In Figure 7a, measured after 1 cycle HCT, normal behaviour can be observed (comparable to the polyester coil coating of Figure 5). In this stage the epoxy coating acts as a barrier, and the values of Y_0 and $n(Q_{pf})(t=0)$ show minor degradation when compared to the values of Y_0^S and $n^S(Q_{pf})$ from the immersion curves in Figure 6. In Figure 7b, measured after 2 cycli HCT, anomalous behaviour can be observed: In the beginning of the immersion $Y_0(Q_{pf})$ increases, but after about

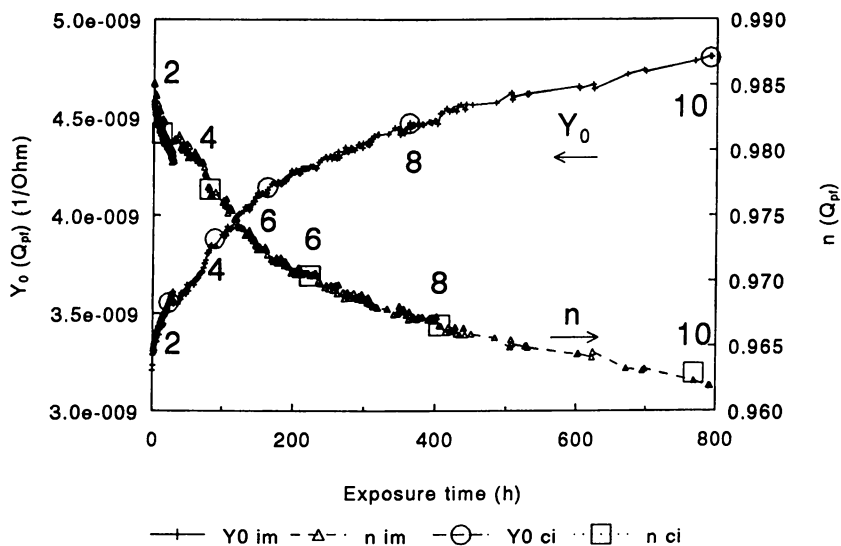


Figure 5: Values of Y_0 and n (Q_{pf}) ($t=0$) -determined with cyclic immersion (ci)- plotted on the curve Y_0 and n (Q_{pf}) as a function of time during continuous immersion (im) of a polyester coil coat system in a 3% NaCl solution. Values are corrected for small differences in layer thickness. Y_0 (Q_{pf}) is plotted on the left axis, n (Q_{pf}) on the right axis.

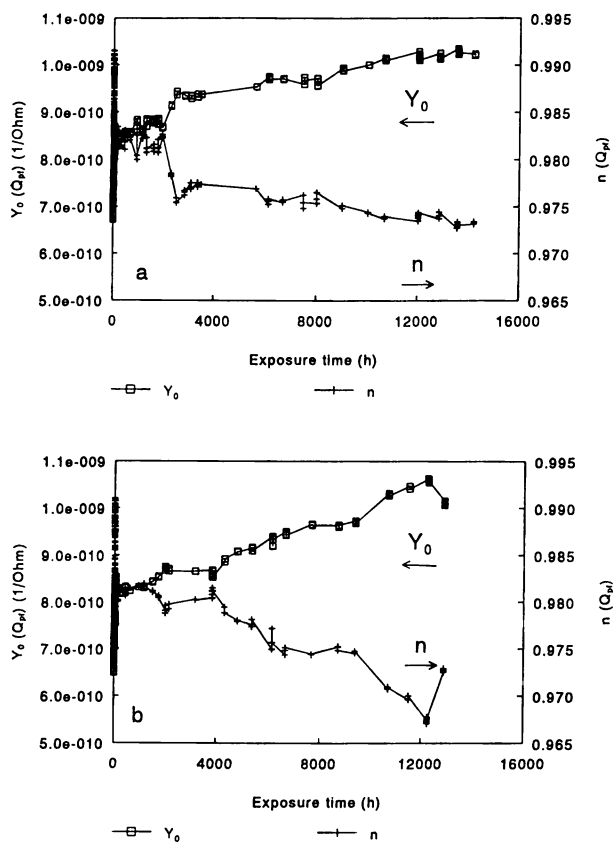


Figure 6: Curves of Y_0 and n (Q_{pr}) of two similar epoxy-based industrial coating systems as a function of time during immersion in artificial rainwater.

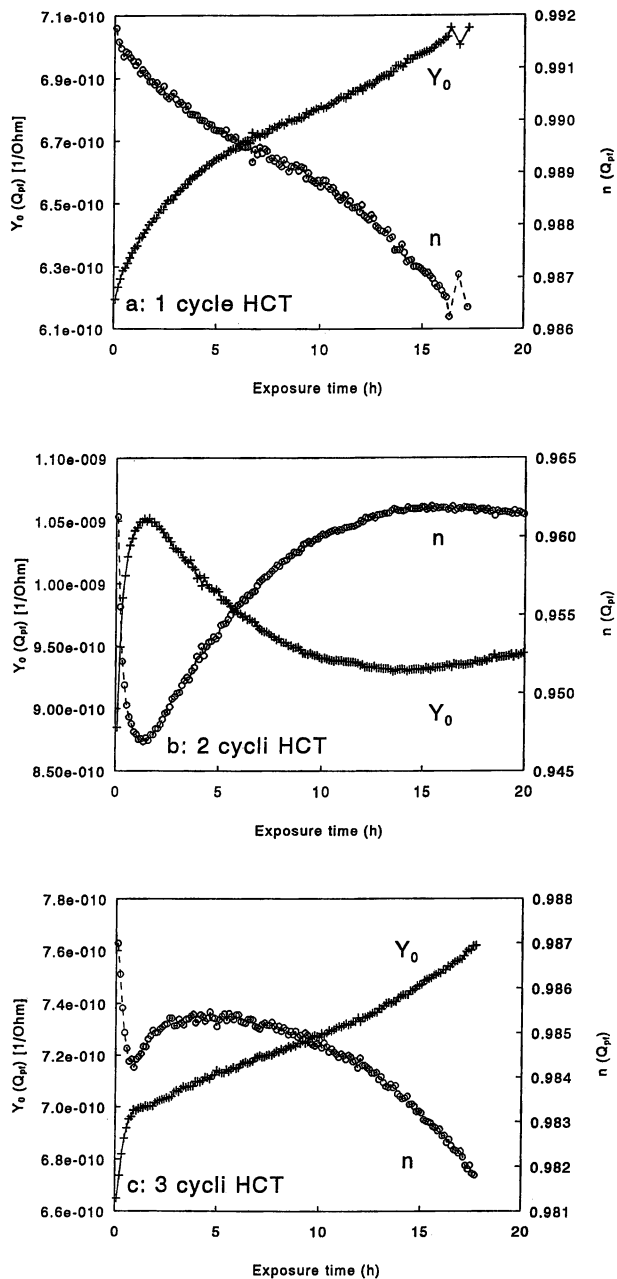


Figure 7: Examples of the curves of Y_0 and n (Q_{pf}) of the epoxy-based industrial coating during immersion in artificial rainwater after different weathering periods in the HCT. a) 1 cycle HCT, b) 2 cycli HCT and c) 3 cycli HCT.

2.5 h the curve starts to decline. The curve of $n(Q_{pf})$ as a function of time shows opposite behaviour (Note that both these values of Y_0 and $n(Q_{pf})$ are both beyond the stationary levels of stage 2 for this type of coating). This phenomenon is the result of (erroneously) fitting one time constant over the impedance of two overlapping time constants. A corrosion-related process causes this second time constant. With the measurement set-up chosen, which cannot be adapted due to the rapidly changing system (rapid water uptake), only a small frequency range is measured (100 kHz - 100 Hz), and fitting of data is carried out between 10 kHz and 1 kHz. This set-up has been optimised for rapidly changing systems, and does not allow distinguishing between the two time constants. When $Y_0(Q_{pf})$ reaches a maximum, the corrosion reaction at the interface starts. This is further illustrated by the curve of the electrode potential during this measurement, see Figure 8. During the first measurement (after 1 cycle) the electrode potential could not be measured, as the DC-resistance of the coating was too high.

With the third measurement after 3 cycli HCT lower values of $Y_0(Q_{pf})$ and higher values of $n(Q_{pf})$ are observed than after 2 cycli HCT (see Figure 7b and c). Both the values of Y_0 and $n(Q_{pf})$ are beyond the stationary levels of stage 2 and the electrode potential of the coating could not be measured anymore as the DC-resistance was too high during this measurement. From this can be derived that the defects observed in the second measurement were 'repaired' by the anti corrosion pigments in the coating and/or the phosphate pretreatment at the interface.² This is also reflected by the decreasing value of E_c after 10 h of immersion, during the previous measurement (after 2 cycli HCT, see Figure 8). Corrosion products, assisted by the pigments and/or phosphate layer block the defects. It should be noted that in this stage (after 3 cycli HCT) the curves of Y_0 and $n(Q_{pf})$ do not have the shape that is normally observed with Fick-like uptake of water where some kind of saturation takes place in a short time (see also Figure 3, 4 and 7a). This yields the conclusion that the corrosion protection is not as adequate as it was when the weathering started, due to the more 'open' character of the repaired defects.

According to these results the method for interpretation of coating impedance of weathered coatings to quantify ageing can be summarised as follows:

- 1) When the impedance of the weathered coating, reflected by the curves of Y_0 and $n(Q_{pf})$, shows normal Fick-like behaviour during the beginning of immersion, ageing can be quantified by determining the values of Y_0 and $n(Q_{pf})$. These should be extrapolated to $t=0$ after which the resulting values can be compared with the curves of these parameters of a similar coating during continuous immersion. Attention should be paid to the barrier properties of the coating. The DC resistance should remain very high (no measurable electrode potential should be present).

² The phenomenon of Y_0 and $n(Q_{pf})$, that have reached values beyond stage 2, dropping to values around the stationary levels of stage 2 when a pore is formed in the coating, was observed earlier with epoxy primers immersed in seawater (10,19).

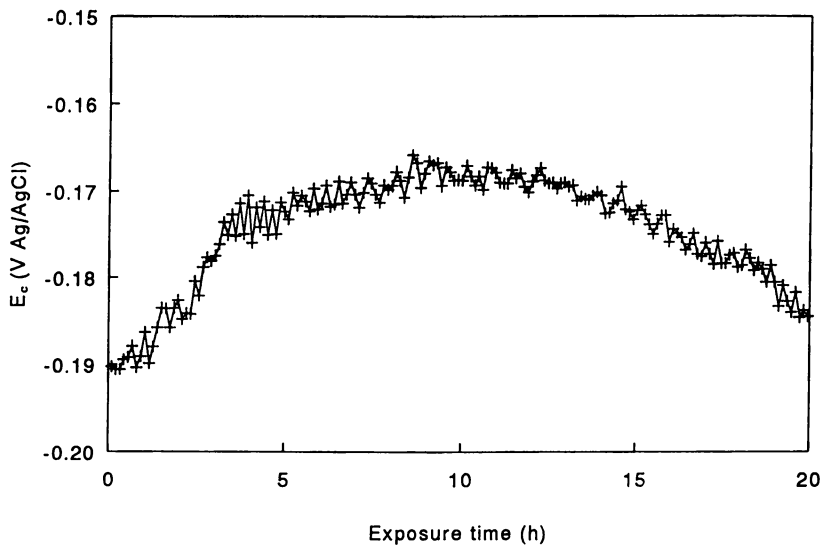


Figure 8: The electrode potential of the epoxy-based industrial coating as a function of time during immersion in artificial rainwater after 2 cycli HCT.

- 2) When anomalous behaviour is observed, the values of Y_0 and $n(Q_{pf})$ as a function of time usually show the weathering stage of the coating qualitatively. The presence of defects will result in a measurable electrode potential. Some coatings show barrier properties but have an anomalous curve of the parameters Y_0 and $n(Q_{pf})$ as a function of time. This is an indication of the presence of defects -rapid diffusion paths- in the coating that are 'repaired'/passivated/plugged by the inhibitive action of the anti corrosion pigments and/or the pre-treatment layer and/or corrosion products. The performance of this coating is worse in the latter case, but for both systems long-term corrosion protection cannot be expected anymore.

Figure 9 presents the curves of Y_0 and $n(Q_{pf})$ of three outdoor exposed, industrial epoxy-based coatings as a function of immersion time in artificial rainwater. One coating (9a) was exposed for 18 months at a severe marine exposure site, the second for 18 months at a less severe industrial/rural site (9b), and the third for 15 months at the same less severe industrial/rural site (9c). From these figures it can be derived that the coatings from Figure 9a and b (still exhibiting barrier properties) are suffering severe ageing beyond maximum saturation (Stage 2). This conclusion can be observed from the values of $n(Q_{pf})$ as a function of time when n is compared to the curve of $n(Q_{pf})$ of the similar coating during immersion, see Figure 6a and b. The coating from the marine site is aged the most (lowest value of $n(Q_{pf})$). From this it must be concluded that both coatings will fail soon, which was also reflected by the delamination from scratch and failure of other coated panels (same coating, different substrates and pretreatments) from these exposure sites after the same duration. The coating exposed for 15 months at the industrial rural site shows ageing up to Stage 2 when the curve of $n(Q_{pf})$ (Figure 9c) is compared to the curves in Figure 6a and b.

In this case the curves of $n(Q_{pf})$ indicate the ageing of the coatings, the values of $Y_0(Q_{pf})$ in these curves are relatively low. The reason for this is as yet unknown.

Alkyd and epoxy coatings for marine applications in laboratory test cycle and outdoor exposure. In the following section the investigation using impedance measurements to determine the performance of alkyd and epoxy coating systems for marine applications will be described.

Before the results after weathering can be discussed the curves of the impedance of the coatings in immersion will be given. The curves of E_R and $n(Q_{pf})$ of the epoxy and the alkyd coating system are given in Figure 10a and b respectively. From these graphs the following limiting values can be derived: Epoxy coating system ($\approx 260\mu\text{m}$) $E_R^S(Q_{pf}) = 20$, $n^S(Q_{pf}) = 0.93$, and alkyd coating system ($\approx 193\mu\text{m}$) $E_R^S(Q_{pf}) = 27$, $n^S(Q_{pf}) = 0.975$ (approx.). E_R (the relative dielectric constant) is calculated from $Y_0(Q_{pf})(t=0)$, using the relation for an ideal parallel plate capacitor. The value of $n^S(Q_{pf})$ for the alkyd coating shows some scatter and is estimated by interpolation.

In Figure 11 the curves of E_R and $n(Q_{pf})(t=0)$ are given of an epoxy coating system ($\approx 245\mu\text{m}$) from outdoor exposure in a marine environment. These values are

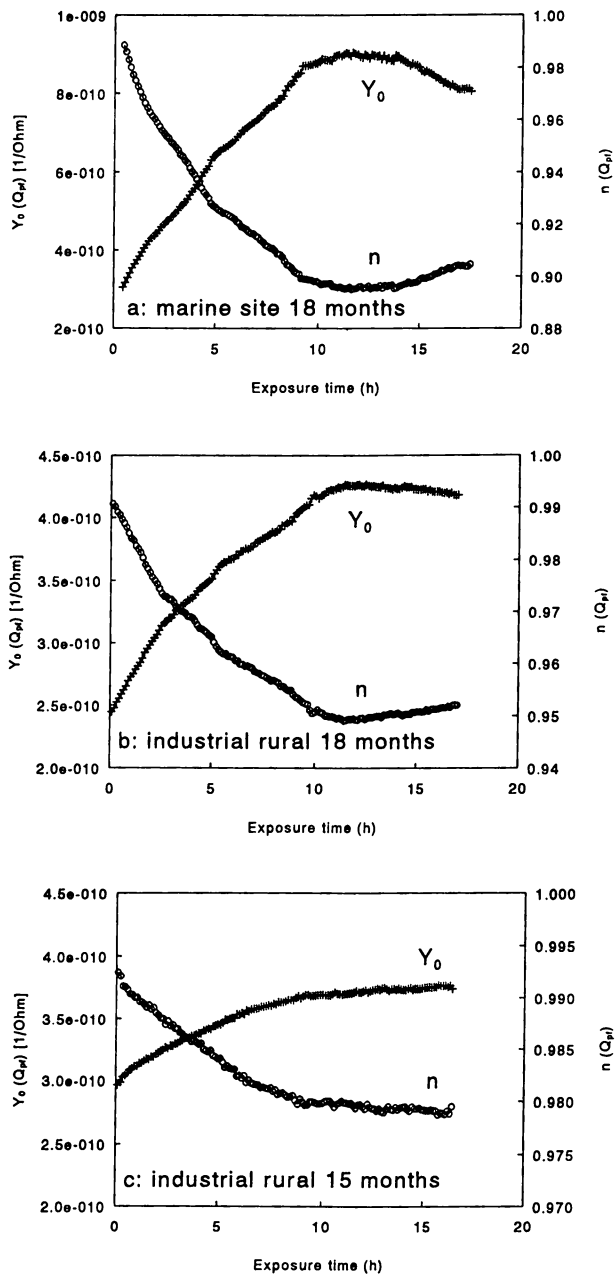


Figure 9: The curves of Y_0 and n (Q_{pf}) as a function of time during immersion in artificial rainwater of three similar epoxy-based industrial coatings after outdoor exposure: a) 18 months at a severe marine site, b) 18 months at a industrial/rural site, and c) 15 months at a industrial/rural site.

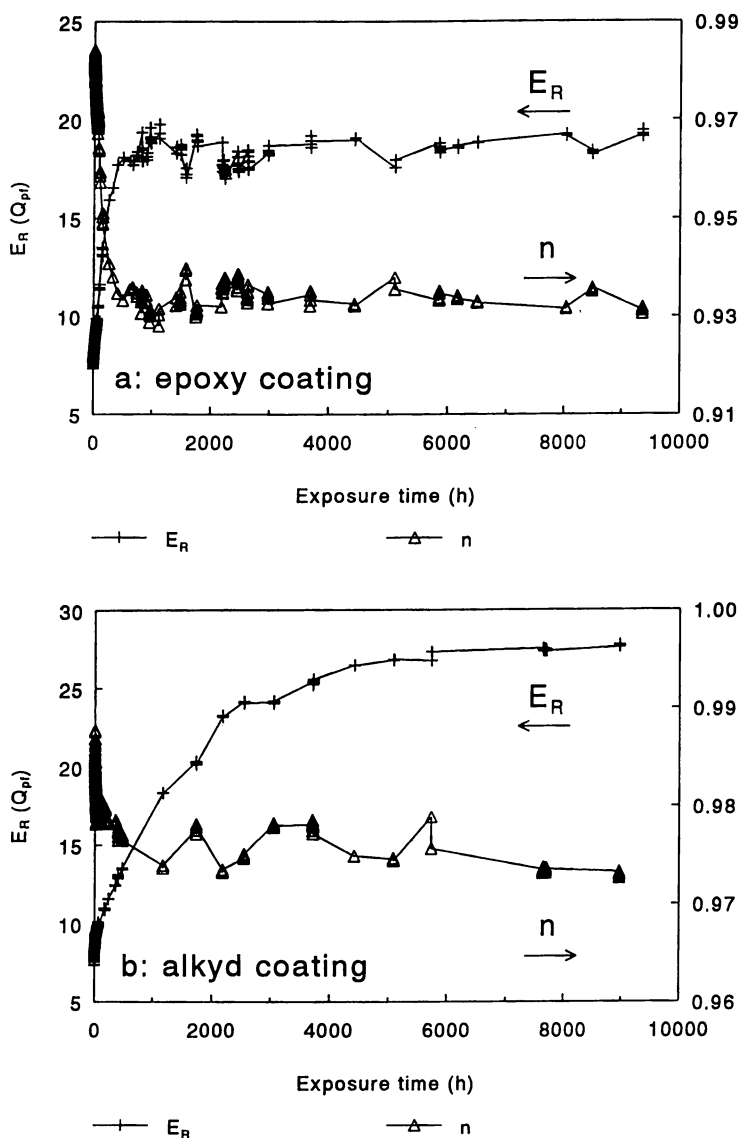


Figure 10: Curves of Y_0 and n (Q_{pf}) of two marine coatings (a: epoxy coating . 260:m and b: alkyd coating . 193:m) as a function of time during immersion in a 3% NaCl solution.

determined by linear interpolation of the coating impedance parameters between 20 and 40 h immersion in artificial rainwater. These results do not show any systematic variation, however the weather seems to influence the results of impedance measurements on the panels from outdoor exposure. The exposure was started in summer, and the first measurement was performed during a rainy period in autumn. With this measurement, relatively high values of E_R and relatively low values of $n(Q_{pf})(t=0)$ are found. These values are close to the stationary values of these parameters in Stage 2, see Figure 10a. Later the weather became better and the fourth measurement around 370 days of outdoor exposure was carried out in a dry and hot summer resulting in a lower value of E_R and a higher value of $n(Q_{pf})(t=0)$. The same cycle was repeated the next year, yielding relatively high values of E_R and relatively low values of $n(Q_{pf})(t=0)$ in autumn (around 500 days), and lower values of E_R and high values of $n(Q_{pf})(t=0)$ in the following summer (around 680 days). From these typical results it was concluded that the water content in the coating (strongly related to the humidity) determined the results of the measurements. Increasing water content in the coating yields an increasing rate of water uptake and this results in a higher value of $E_R(Y_0)$ and a lower value of $n(Q_{pf})$. To deal with these varying outdoor conditions the measurement procedure has to be adapted. The coated panels coming from outdoor exposure are dried for 48 h at 35° C., followed by 24 h at 20° C. and 50% RH. The measurements in the following period after 700 days show that the extreme effect of the season is damped. Never the less, still no systematic increase of ageing is visible, but since this system is a high performance coating for marine applications this could be expected.

A similar seasonal effect can be observed with an alkyd coating ($\approx 173\mu\text{m}$) together with the epoxy coating exposed outdoors. The graphs of E_R and $n(Q_{pf})(t=0)$ of this alkyd coating are given in Figure 12. The seasonal effect is damped out after about two years (with the new procedure) and only a minor amount of ageing could be derived from these graphs, which is reflected by the condition of the coating.

Ageing experiments were also carried out in the laboratory. Epoxy and alkyd coatings were aged in the laboratory in a weekly cycle consisting of four days immersion in a 3% NaCl solution, followed by drying at 35° C. for two days and stabilising at 20° C with 50% RH for one day. Before drying, the electrochemical cell was emptied; leaving behind a small layer of the electrolyte that dried out during the drying period. Results from impedance measurements are presented in Figures 13 and 14, where E_R and $n(Q_{pf})(t=0)$ are plotted for an alkyd and an epoxy coating respectively. These values were determined by linear interpolation of the coating impedance parameters between 20 and 40 h immersion and extrapolation to $t=0$.

From the curves in Figure 13 (alkyd coating, $\approx 180\mu\text{m}$) it can be derived that in the beginning of the cyclic test there is an increased amount of ageing, reflected by an increasing $E_R(Q_{pf})(t=0)$. The value of $n(Q_{pf})(t=0)$ increases with increasing cycle number, which does not reflect increasing ageing. The reason for this is unknown, but it is probably related to a post-curing effect of the coating (20). This post-curing is frequently observed with coatings, especially with alkyd and epoxy coatings. It results in a decrease of Y_0 or $E_R(Q_{pf})$ and an increase of $n(Q_{pf})$ during exposure. The changes in E_R and $n(t=0)(Q_{pf})$ are small however, but after about 40 cycles these parameters start to change systematically. $E_R(t=0)(Q_{pf})$ increases and $n(t=0)(Q_{pf})$ decreases, both indicating an increasing ageing of the coating. When compared to the

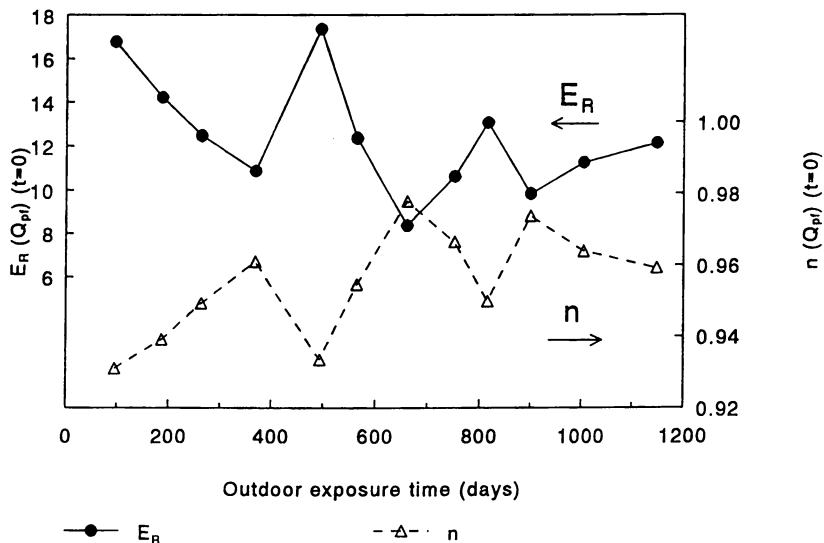


Figure 11: Values of E_R (a) and n (b) (Q_{pf}) ($t=0$) of an epoxy coating (245:m) for marine applications during outdoor exposure.

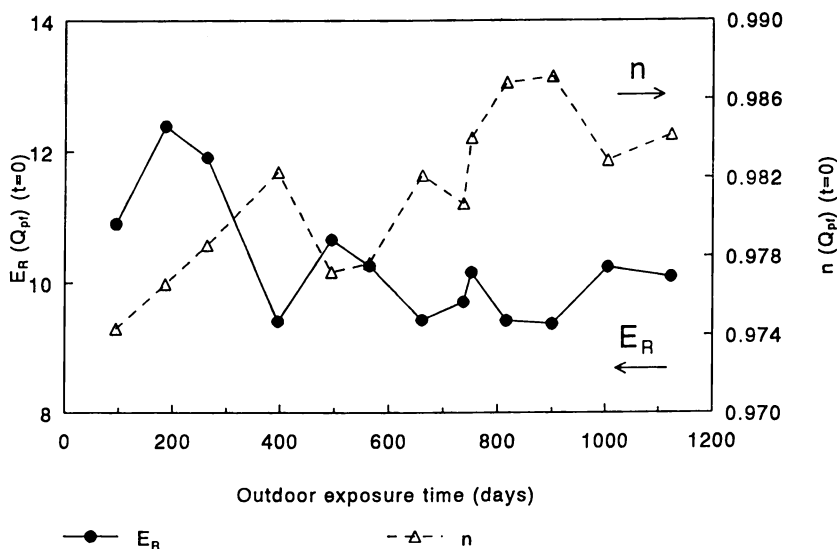


Figure 12: Values of E_R (a) and n (b) (Q_{pf}) ($t=0$) of an alkyd coating (173:m) for marine applications during outdoor exposure.

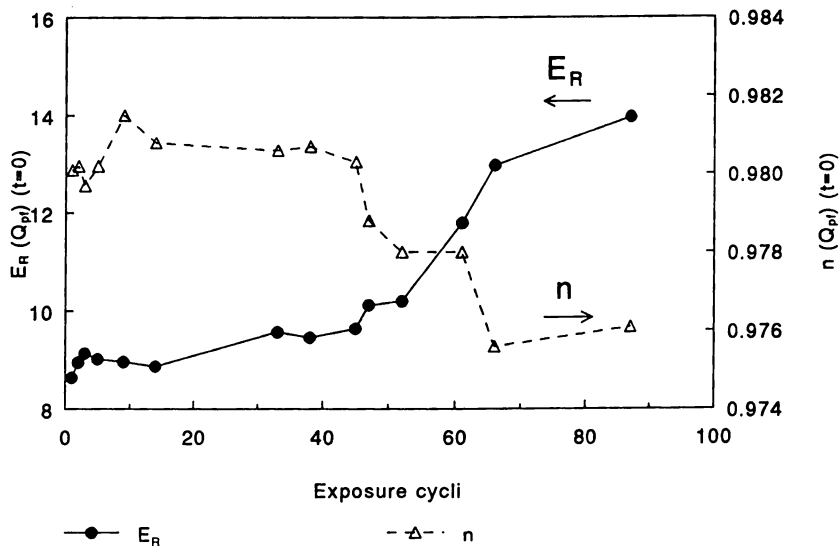


Figure 13: Values of E_R and $n (Q_{pf}) (t=0)$ of an alkyd coating (180:m) for marine applications during weathering in the laboratory.

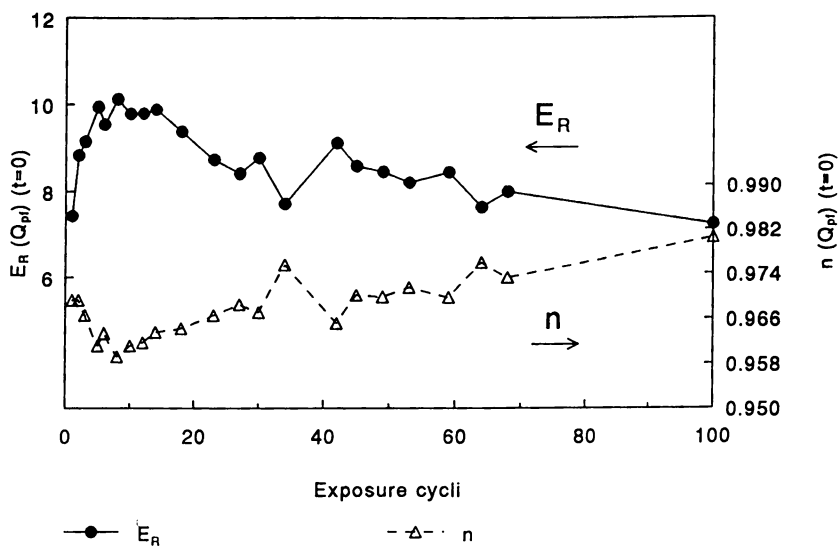


Figure 14: Values of E_R (a) and $n (Q_{pf}) (t=0)$ (b) of an epoxy coating (258:m) for marine applications during weathering in the laboratory.

impedance of a similar coating in immersion -see Figure 10b- it can be derived that the amount of ageing is still small.

The epoxy coating ($\approx 258\mu\text{m}$) shows similar behaviour in this laboratory exposure cycle. Curves of E_R and $n(Q_{pf})$ ($t=0$) are given in Figure 14. It can be observed that, after an initial increase of the amount of ageing, some kind of recovery occurs. This may originate from post-curing, but also other processes may be involved.

This work on the application of EIS for the determination of ageing of coatings is still in progress. Other ageing tests like the Hoogovens Corrosion Test, cyclic UV and corrosion tests, and outdoor exposure are carried out. These results will further illustrate the effects of, among others, UV and the applicability of EIS in this field.

Conclusion

From the results presented in this chapter the following main conclusion can be drawn:

The impedance of organic coatings in immersion shows typical behaviour. In this typical behaviour three stages can be distinguished, which can be related to stages in the service life of the coatings. This approach is not only valid for coatings in immersion, but also for coatings from artificial and natural weathering.

The method for the analysis of impedance measurements on weathered coatings enables the determination of ageing. With the relation to the typical behaviour of coatings in immersion, where the three stages in the coating impedance can be identified, it is possible to quantify the amount of ageing and estimate the remaining service life of the coating. The validity of this approach is shown for coatings from artificial weathering. For outdoor weathering more investigations are needed.

Literature Cited

1. Walter, G. W. *J. Electroanal. Chem.* **1981**, *118*, pp. 259-273.
2. Walter, G.W. *Corr Sci.* **1986**, *26* (9), pp. 681-703.
3. Walter, G.W. *Corr Sci.* **1990**, *30*, pp. 617-629.
4. Eden, D. A.; Hoffmann, M.; and Skerry, B. S. In *Polymeric Materials for Corrosion Control*; Dickie, R. A. and Floyd, F. L., Editors; ACS Symposium Series 322; American Chemical Society: Washington DC, 1986, pp. 36-47.
5. Pereira, D.; Scantlebury, J.D.; Ferreira, M.G.S.; and Almeida, M.E., *Corr Sci.* **1990**, *30* (11), pp. 1135-1147.
6. Kendig, M. and Scully, J., *Corrosion-Nace* **1990**, *46* (1), p. 22.
7. Mansfeld, F. and Kendig, M. *Proc. Int. Congr. Metallic Corrosion, Toronto, Canada* **1984**, *3* (1), pp. 74-84.
8. Morcillo, M. et. al., In *Polymeric Materials for Corrosion Control*; Dickie, R.A. and Floyd, F.L., Editors; ACS Symposium Series 322; American Chemical Society: Washington DC, 1986, p. 86.
9. Mansfeld, F. & Tsai, C.H. *Corrosion* **1991**, *42*, p. 958.
10. van Westing, E. P. M., Ferrari, G. M. and de Wit, J. H. W. *Corros. Sci.* **1994**, *36*, p. 1323.

11. van der Weijde, D. H.; van Westing, E. P. M.; Ferrari, G. M. and de Wit, J.H.W. In *ACS Symposium Series on Corrosion Control by Coatings*; Bierwagen, G. P., Editor; ACS Books; Washington DC, 1997, Chapter 4.
12. Brasher, D. M. and Kinsbury, A. H. *J. Appl. Chem.* **1954**, *4*, p. 62.
13. van Westing, E. P. M.; Ferrari, G. M. and de Wit, J. H. W. *Corros. Sci.* **1994**, *36*, p. 957.
14. van Westing, E. P. M.; Ferrari, G. M. and de Wit, J. H. W. *Corros. Sci.* **1994**, *36*, p. 979.
15. van Westing, E. P. M.; Ferrari, G. M. and de Wit, J. H. W. *Electrochim. Acta* **1994**, *39*, p.899.
16. van Westing, E. P. M.; Ferrari, G. M.; Geenen, F. M. and de Wit, J. H. W. *Prog. Org. Coat.* **1993**, *23*, p. 89.
17. Boukamp, B. A. *Solid State Ionics* **1986**, *20*, p. 31.
18. Boukamp, B.A. *Manual AC-immittance Data Analysis System 'Equivalent Circuit'*, Twente University of Technology, Enschede, The Netherlands, 1989.
19. (van Westing, E. P. M. Determination of coating performance, Thesis, Technical University-Delft, The Netherlands, 1992.)
20. Vreijling, M. P. W.; van Westing, E. P. M.; Ferrari, G. M.; van der Weijde, D. H. and de Wit, J. H. W. In *Procedures of the Symposium on Advances in Corrosion Protection by Organic Coatings II*; Scantlebury, D. and Kendig, M., Editors; The Electrochemical Soc.; Pennington, 1995, Proceedings Volume 95-13; p. 193.
21. Blekkenhorst, F. and Nagel Soepenbergh, E. *Proceedings in Corrosion '88 St. Louis (USA)*, **1988**, NACE Conference Proceedings, Paper no. 354.

Chapter 8

Study of the Water Barrier Properties of Paints After Natural and Accelerated Photooxidative Degradation

E. Deflorian, L. Fedrizzi, and P. L. Bonora

Department of Materials Engineering, University of Trento, Trento, Italy

The evaluation of the corrosion protection properties of organic coatings is often obtained by the exposure of coated samples to natural environment (for example, marine or industrial atmosphere) and by accelerated weathering tests (salt spray fog, UV irradiation, cycles, etc.). At the end of the test, however, the visual observation of the tested samples, comparing the coating appearance with defined standards, is currently the only checking system.

Such procedures generally take a long time and the results are influenced by operator judgment; therefore, they are not completely objective. For this reason, the use of quantitative analysis, for example, EIS (electrochemical impedance spectroscopy) or FTIR can provide information on physical and chemical properties of the coating and on the corrosion process, allowing an early evaluation of the degradation phenomena.

In this work the effects of natural UV degradation after exposure for several years in the atmosphere are compared with the consequences of artificial weathering in an UV chamber (ASTM G53) using electrochemical, infrared and calorimetric techniques.

The comparison shows the remarkable differences in the two degradation mechanisms giving information on future developments for new testing procedures.

The possibility of a reliable life time prediction for an organic coating, in particular concerning the maintenance of the corrosion protection properties, is extremely important for the paint industry. The reduction of the testing time for a new product is proportional to the availability of reliable and accurate testing procedures. For this reason, many different accelerated tests are generally employed for simulating the actual field environment (1). At the same time, however, there are many criticisms about the realistic effectiveness of accelerated degradation (2). Moreover, the evaluation techniques usually involve visual observation of the samples, so the accuracy, and hence, reproducibility are limited.

The study of the deterioration of organic coatings in the presence of the combined action of UV radiation and water is demanded by the wide use of paints in external environments that are exposed to both solar radiation and humidity.

This paper deals with the degradation of both chemical and barrier properties of samples irradiated with artificial and solar UV sources in order to compare the effects of accelerated testing on the degradation mechanisms of organic coatings. The UV-polymer interaction can induce microstructural and chemical changes due to photo-oxidative processes, which, in the presence of water, reduce the corrosion protection properties of paint.

Photo-oxidative phenomena may cause important changes in the paint, not only aesthetic (change of color or gloss), but also functional (bonds breakdown and consequent loss of elasticity, reduction of the barrier properties etc.) (3).

A simple approach to the study of corrosion protection properties of UV-treated organic coatings has been that of separating in time the two phenomena. First, having the painted products undergo different UV radiation times. Then, immersing them in an aqueous solution and studying the absorption phenomena.

The photooxidation in organic coatings causes permanent modification in the polymeric chains through mechanisms of initiation, propagation and termination (4). Under the effect of the energy related to the ultra-violet (UV) irradiation, the polymer can produce free radicals by chemical bond breakdown (initiation). These free radicals can react either with oxygen, producing unstable peroxides, or with other polymeric chains (chain propagation). The final chemical products are obtained from the reaction of free radical recombination (generally ketones or alcohols).

The chemical bond breakdown of the polymeric chains with the formation of oxidized compounds causes the production of small molecules, which are not adherent to the coating and are easily removed in an aggressive environment. After this modification, the polymeric coating becomes more brittle (therefore, some cracks can be produced, e.g. by thermal cycles) and possibly thinner. In the case of pigmented coatings, the loss of polymeric mass leads to a superficial pigment concentration higher than the critical level. This causes a further embrittlement (5-6).

The chemical bond modification can be usefully studied by means of infrared spectroscopy in reflectance (FTIR). Measuring the change in intensity (reflectance) and position of the peaks (wavenumber), it is possible to characterize the relative changes in chemical bonds (7).

In order to study the reduction protection properties of an organic coating (without active pigments) as a consequence of the weathering, it is important to know the barrier properties of the paint with regard to water and ions.

The evaluation of the water absorption process in an organic coating immersed in a solution is a very important phenomenon. Normally, it precludes paint-metal interface loss of adhesion. Also, it is a presupposition for the electrochemical reaction and the reduction of the resistance to the passage of ions through the coating itself. This process can be studied with accuracy by means of electrochemical impedance spectroscopy (EIS) (8-9).

With the same technique, it is also possible to quantify the barrier properties of the coating regarding aggressive ions. The higher the ionic resistance of the paint, the higher the corrosion protection performance. In fact, the presence of defects, as well as incorrect surface preparation, can decrease the ionic resistance and increase the corrosion rate (10-11). The ionic resistance is the effective mechanism in the corrosion protection properties of barrier paints.

Materials and Experimental Procedure

The studied system consists of sand blasted mild steel (Sa 2 1/2) coated with an epoxy polyamide primer (10 μm) followed by an alkydic topcoat cured with isocyanates (150 μm). The product comes from industrial production.

Two different classes of weathered samples are considered: the first group contains samples exposed to an industrial atmosphere (Turin, Italy) for 2, 10, 14 and 19 years. The second group consists of just prepared specimens artificially weathered in a UV chamber.

The samples were irradiated with UV radiation according to the ASTM G53 standards. This fixes the UV source spectrum (270-290 nm, peak 313 nm), in addition to the radiation geometry. After some preliminary measurements, four different radiation times were chosen: 24, 48, 96 and 400 hours (the reference sample was not irradiated). The studied samples and the weathering procedure are reported in Table 1.

For each of these materials (4 test samples for each radiation time) an electrochemical impedance spectroscopy (EIS) characterization was carried out in order to assess the phenomena of water absorption and underpaint corrosion. The measuring cell consisted of a work electrode (coated metal) of about 30 cm^2 of area immersed in a 3.5% solution, a platinum counter-electrode, and a reference electrode (saturated potassium sulphate SSE, +642mV vs SHE). A potentiostat EG&G PAR 273 and a Solartron 1255 frequency response analyzer were used for the electrochemical measurements. The frequency range for the measurements ranges from 10,000 Hz to 0.001 Hz with a signal amplitude of 20 mV.

The samples were also characterized by using differential scanning calorimetry (DSC) for measuring the glass transition temperature (T_g). The temperature range was -60, +100°C and the equipment used a Mettler TC 10A.

In order to identify the chemical changes in the polymer structure due to the UV interaction, some FTIR (Nicolet DXL in reflectance) measurements were carried out.

Results and Discussion

The effects of artificial and solar UV radiation were compared using infrared spectroscopy (FTIR) to verify if differences in the chemical structure can be found before and after UV treatment. Also, if it is possible to chemically distinguish the effects of the two different types of UV degradation.

Comparing the new samples, some differences (both in shape and intensity) of peaks are evident in all the UV treated samples (Figure 1). The most important peaks are reported in Table 2 with the relevant wave numbers. These changes are mainly related to the degradation of the functional group biuret (part of the esamethylendiisocyanate), and only marginally, to the urethane group. The comparison between the FTIR measurements obtained on samples exposed to the natural atmosphere and the samples after artificial UV weathering show that these two types of degradation are substantially chemically equivalent. In both cases it is possible to note a sharp reduction of the peak intensity for the wave number related to the biuret group. However, there are a few important differences concerning the mechanisms of chemical degradation. With attention to Figure 1 and Table 2, it is possible to observe a different effect of the weathering procedure on the urethane group. In

Table 1: Materials and treatments

SYMBOL	TREATMENT
new	-
UV48	48 hours ASTM G53
UV96	96 hours ASTM G53
UV400	400 hours ASTM G53
S2	2 years of solar exposure
S10	10 years of solar exposure
S14	14 years of solar exposure
S19	19 years of solar exposure

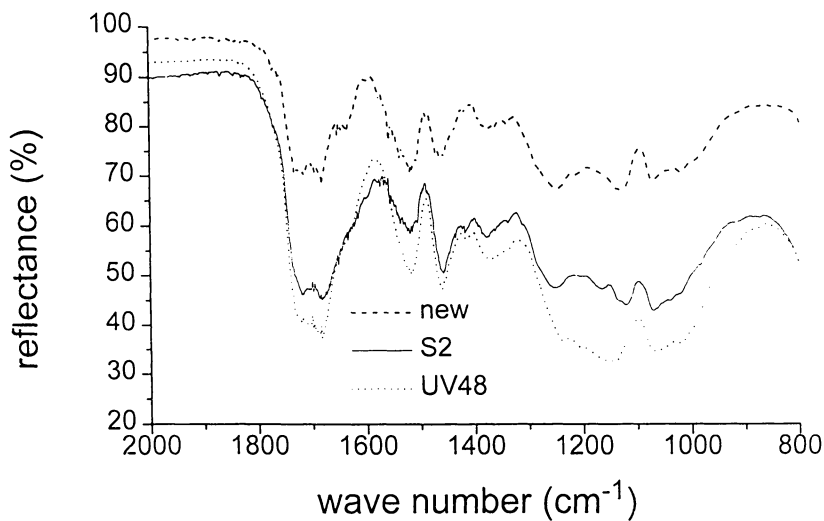


Figure 1: FTIR spectrum for new samples (new), samples exposed in the Turin atmosphere for 2 years (S2) and samples treated with UV radiation for 48 hours (UV48).

particular, the laboratory-accelerated test induces a higher breakdown of the urethane group than the solar irradiation. This difference is particularly clear considering the stretching of the C-O bond in the urethane group at 1250 cm^{-1} : only the artificial irradiation induces a significant intensity reduction of this peak, while the change in the peak intensity for the naturally weathered samples is very small. This is also true for long term exposure.

The main difference distinguishing the natural and artificial UV-treated samples is the thickness of degradation. In Figure 2, the spectra of new samples are compared with the spectra of two weathered samples obtained 40-50 μm under the surface (the external layer was previously removed). It is possible to note that the chemical degradation of artificially UV treated samples (UV48) involves only the surface layer of the coating, having the spectrum similar to the one obtained on untreated samples. This behavior is also confirmed for very long (400 hours) time of exposure. The case of naturally exposed samples (even after only two years) in which the chemical modification (biuret degradation) is maintained along the whole thickness is different. The reasons for such differences can be found in different aspects. First, it is important to remember that artificial UV weathering, unlike solar exposure, causes the production of a significant amount of ozone, changing the oxidative behavior of the atmosphere. Moreover, the higher UV concentration in the accelerated radiation chamber induces the formation of many free radicals in the external layer of paint.

The photo-oxidative degradation can be divided into different principal steps: initiation, i.e. the molecular excitation forming free radicals; propagation, i.e. the interaction between the free radical and other molecules; and termination, i.e. the reaction between two free radicals.

Under artificially accelerated UV conditions the superficial free radical concentration is very high. Comparing the UV radiation energy described in ASTM G53 and the values of UV solar radiation energy experimentally determined in Turin, the first value is more than two orders of magnitude higher than the second. The competition in the propagation and termination reactions is a function of the free radical concentration. In fact, the propagation rate is proportional, as a first approximation, to the free radical concentration (assuming constant molecular polymer concentration). On the contrary, the termination rate is proportional to the square of the free radical concentration and, therefore, it is more efficient than the propagation reaction in increasing the free radical concentration.

These considerations can explain the reason for the thinner modified paint layer for accelerated UV treated samples because, in this case, the termination reaction reduces the interaction layer maintaining the presence of free radicals in the upper layers of the coating.

This conclusion is also confirmed by the glass transition temperature (T_g) measurements, which show that all the artificial UV treated samples, have the same T_g as the new ones (about 30°C). This proves that the chemical and microstructural modification of the paint involves only a small superficial part of the mass of the coating. On the contrary, the samples exposed to the Turin atmosphere show a T_g that is higher ($35\text{-}38^\circ\text{C}$) by increasing the time of exposure, in agreement with a degradation mechanism acting in most of the thickness of the coating.

Further, to determine the chemical modification due to the natural and artificial UV radiation, the influence of weathering on the actual corrosion protection properties of the studied samples was studied. To this purpose the samples were

Table 2: Wavenumber, chemical bonds and position in the polymer structure of the principal peaks measured in the FTIR spectra.

WEVENUMBER (CM ⁻¹)	CHEMICAL BONDS	POSITION OF THE BOND IN THE POLYMER STRUCTURE
1720	C=O stretching	urethane
1680	C=O stretching	ester
1635	C=O stretching	biuret
1520	N-H bend	urethane and biuret
1375	C-H bend	
1460	O-H, C-H bend	
1250	C-O stretching	urethane
1210	C-H, C-C stretching	
1120	C-O stretching	ester
1070	C-C stretching	ester

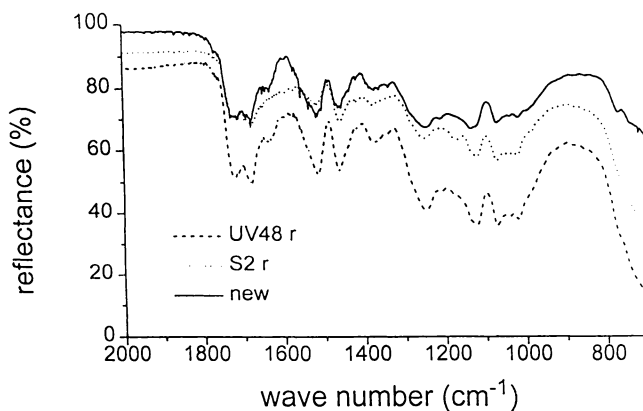


Figure 2: FTIR spectrum for new samples (new), samples exposed in the Turin atmosphere for 2 years (S2r) and samples treated with UV radiation for 48 hours (UV48r) both after 50 μm of thickness removal.

characterized by using electrochemical impedance spectroscopy (EIS). By analyzing the experimental results of this technique it is possible to quantify the barrier properties of the coating and the electrochemical corrosion process occurring on the metal surface. The typical Nyquist impedance plot for natural and artificial weathered samples after some days of immersion in the sodium chloride solution is shown in Figure 3. The shape of the diagram seems to indicate the presence of a single depressed loop related to a single time constant. With a more accurate analysis of the electrochemical data, by fitting the results with specific software, it is possible to define a more complex behavior with more time constants. However, the goal of this study is the coating degradation. Therefore, we have isolated (in the high frequency range) the electrical and dielectrical behavior due exclusively to the organic coating, neglecting in this step of the research, the corrosion process, which is very limited due to the quality of the coating. For frequencies higher than 1 Hz, the equivalent electrical circuit modeling the experimental results is shown in Figure 4 and it consists of a Constant Phase Element (CPE) Q_c related to the non-ideal capacitive behavior of the coating in parallel with the ionic resistance through the paint R_p . The electrolyte resistance can be neglected.

The first parameter, the coating capacitance Q_c , can be expressed by the following formula:

$$Q_c = \epsilon \epsilon_0 A/d \quad (1)$$

where A is the testing area, d the coating thickness, ϵ the dielectric constant of the medium and ϵ_0 the free space permittivity. If the results are measured per unit of area and the coating thickness is constant, the Q_c trend and the ϵ trend are equivalent. Actually the coating thickness can change slightly (+/-10%) from sample to sample and for this reason we have preferred to represent the result in the form of ϵ instead of Q_c in order to minimize the differences due to thickness variations.

The change of Q_c during the immersion time is mainly due to water uptake phenomena inducing an increase of the apparent dielectric constant of the coating. The discussion of ϵ is, therefore, interesting in order to define the change in the water barrier properties of the coating, which can cause electrochemical process on the metal substrate or loss of adhesion at the metal-polymer interface.

The value of R_p is a function of the ion diffusion through any kind of defect in the coating. The chance for a barrier organic coating (without active pigments) to protect against corrosion is mainly due to the aptitude to reduce the ion diffusion in the coating; this is necessary in order to equilibrate and to support the corrosion reaction. From this consideration the importance of the R_p evaluation to understand the protection properties of the coating is evident. The following discussion is based on these two parameters (Q_c and R_p).

In Figure 5 the dielectric constant of both the naturally weathered samples and of the new one versus the time of immersion in NaCl solution is shown in logarithmic scale. During the first 30 minutes of immersion the samples reach an equilibrium with the aqueous environment showing a behavior similar for all the materials with small and insignificant differences. The ϵ values start to increase after the first hours of immersion and they reach a plateau after about 4-5 days. After the initial period the samples showing the higher increase of ϵ (and therefore the higher water uptake) in comparison with the new material are the ones with 10 years of natural weathering;

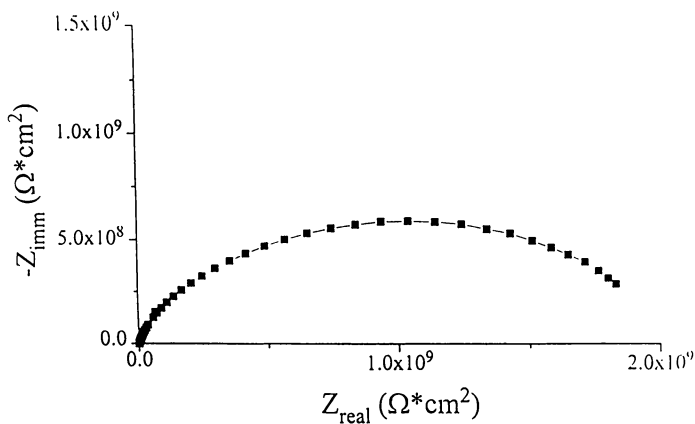


Figure 3: Typical Nyquist plot for natural and artificial weathered samples after some days of immersion in the sodium chlorides solution.

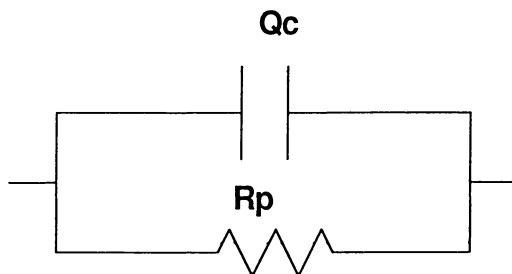


Figure 4: Equivalent electrical circuit modeling the organic coating contribution to the total impedance.

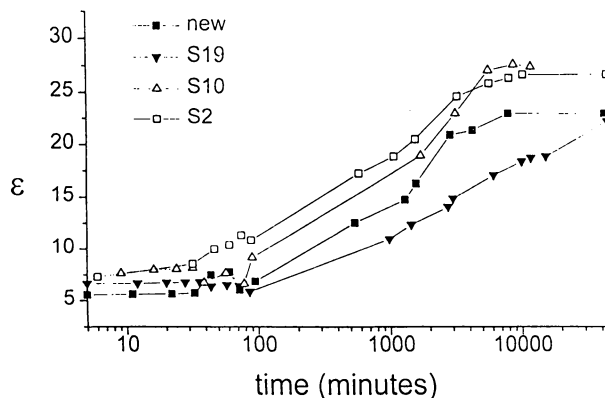


Figure 5: Dielectric constant versus the immersion time trend for the new samples and the samples exposed in the Turin atmosphere for 2 years (S2), 10 years (S10) and 19 years (S19).

the highest being the sample with 2 years of natural weathering. In a previous work (12), it was found that for polyester paints the UV radiation can increase the water uptake process by increasing both the quantity of water (the saturation coefficient) and the kinetics of uptake (the diffusion coefficient). This behavior was explained by considering the microstructural modification in paints due to photo-oxidation and, because of the hydrophilic action of both the free radicals and the products of photo-oxidation.

This result is confirmed by the data of Figure 5, but with a more complex mechanism. There are two competitive phenomena:

- 1) the formation of both free radicals and hydrophilic products of photo oxidation which increase the water uptake;
- 2) the increase of the T_g (more evident for long term exposure, as previously discussed) causing a reduction of the water uptake which induce on its turn a more rigid polymeric structure.

The first aspect is dominant for samples exposed for 2 years in the Turin atmosphere; on the contrary the second mechanism (the reduction of water uptake rate due to the increase of the T_g) is important for samples exposed for 19 years. The result is that for long time UV exposition the water uptake seems to decrease (the values of ϵ are lower after 10 years than after 2 years and after 19 years the values are lower than for the new material). The UV radiation can induce, for long term exposure, a change in the T_g , as previously discussed. The T_g increases (at values higher than the room and testing temperature) and reduces the water uptake rate. The trend in figure 5 is in agreement with the T_g modification.

The results of both the new and the for artificially weathered samples are presented in Figure 6. The behavior is almost the same all the tested materials showing a very similar water uptake process. The absence of differences in the water uptake process is only apparent in contrast with the chemical modifications measured with the infrared characterization. The chemical changes for the studied materials are localized in the upper layers and therefore they do not induce modification in the water barrier properties of the whole coating.

The first conclusion arising from Figures 5 and 6 is that for our samples the UV artificial weathering does not seem to be equivalent to natural weathering. This is shown by the limited effects of artificial UV exposure on water barrier properties.

As previously discussed, the parameter describing the paint barrier properties to ions is the pore resistance R_p . The results obtained on both naturally weathered and new samples are reported in Figure 7. The initial value of R_p is very high (about $10^{10} \Omega \cdot \text{cm}^2$) showing the good corrosion protection properties of this kind of alkydic resin; this is true also after about 20 years of natural exposure. In Figure 7 the starting value of R_p is the first measurable value obtained with the equipment used (it is not possible to measure impedance higher than $10^{10} \Omega \cdot \text{cm}^2$). Due to the interaction of the organic coating with the electrolyte, the value of R_p decreases under the effect of ionic diffusion through the paint.

During the first week of immersion, all the samples, the new and weathered ones, are characterized by the same R_p trend. In the following weeks, the ionic mobility increases (R_p decreases), for the natural weathered materials, while for the new sample it remains almost constant.

This behavior proves the very good protection properties of the alkydic organic coating under investigation because only after several days of immersion in the aggressive solution is it possible to note a difference in the ion resistance which

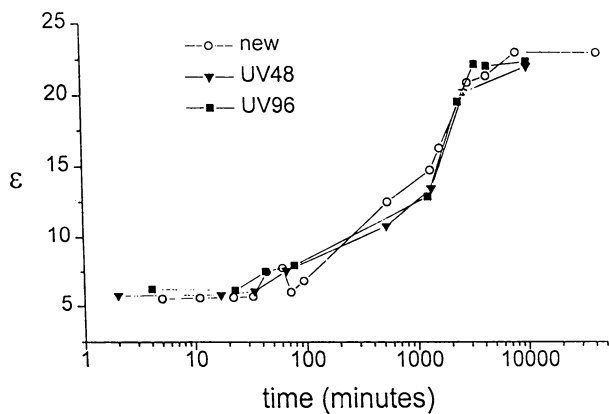


Figure 6: Dielectric constant versus the immersion time trend for the new samples and the samples treated with UV radiation for 48 hours (UV48) and 96 hours (UV96).

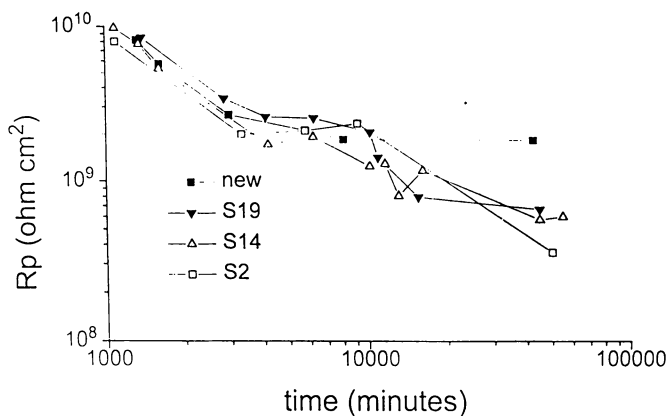


Figure 7: Pore resistance versus the immersion time trend for the new samples and the samples exposed in the Turin atmosphere for 2 years (S2), 10 years (S10) and 19 years (S19).

remains not lower than $5 \cdot 10^8 \Omega \cdot \text{cm}^2$ (also for the naturally weathered samples), According to other authors (6), the UV radiation can produce some microcracks in the coating, inducing the presence of small defects which increase ionic conductivity. This is the case with our samples. The water barrier properties are, therefore, mainly a function of the polymer structure, while the ionic resistance is a function of microscopic defects produced by the UV treatments. We can conclude that the corrosion protection properties of the organic coating are only slightly degraded by 20 years of exposure in the Turin atmosphere, because the chemical and microstructural modification do not induce the formation of any macro-defect but only a limited reduction of ionic barrier properties.

The R_p values obtained by electrochemical impedance data on artificially weathered samples are shown in Figure 8. The initial values are in the order of $10^{10} \Omega \cdot \text{cm}^2$, similar to the same values of the new samples. Also for the UV treated samples there is a decrease in the pore resistance reaching a plateau value after about 7 days of immersion in the NaCl solution. This trend is similar to the behavior of the new samples but the plateau values are different: lower for the weathered samples (about $1.2 \cdot 10^9 \Omega \cdot \text{cm}^2$) and higher for the new ones (about $2 \cdot 10^9 \Omega \cdot \text{cm}^2$). It is important to point out that during the 40 days of testing the naturally degraded samples never actually reach a stationary value of R_p .

Accelerated artificial UV weathering induces a ion barrier degradation in the studied organic coatings. This effect is lower than in the case of natural UV degradation. Moreover, by increasing the time of artificial UV treatment till 400 hours the R_p trend is approximately the same as for 48 or 96 hours of treatment. The lower, but measurable, effect of the artificial weathering can be explained (also for this parameter) considering the limited penetration of the UV degradation in the coating thickness for the artificial UV treated materials and, therefore, also the reduced penetration of microdefects.

Conclusions

- By using infrared, thermal and electrochemical techniques it is possible to characterize the organic coating degradation due to photo-oxidation, comparing the effects of different weathering procedures (natural and accelerated) concerning the microstructural, chemical and corrosion protection properties. This approach could be useful in general for understanding the degradation mechanisms and to explain the possible differences in natural and artificial weathering of paints, in order to improve the efficiency of the accelerated degradation test procedures of organic coatings.
- The chemical bonds in the studied alkyd resin are modified by both artificial and solar UV interaction, as shown by the FTIR characterization, mainly for the degradation of the biuret group. In the case of artificially weathered samples there is also a minor urethane group degradation. However, the chemical modifications are more or less the same for solar or artificial UV treatments.
- There is a noticeable difference between artificially and naturally weathered samples considering the thickness of degradation. The naturally radiated samples are modified in the whole coating thickness, while in the artificially UV treated samples only the superficial layers are photo-oxidized. This difference is due both

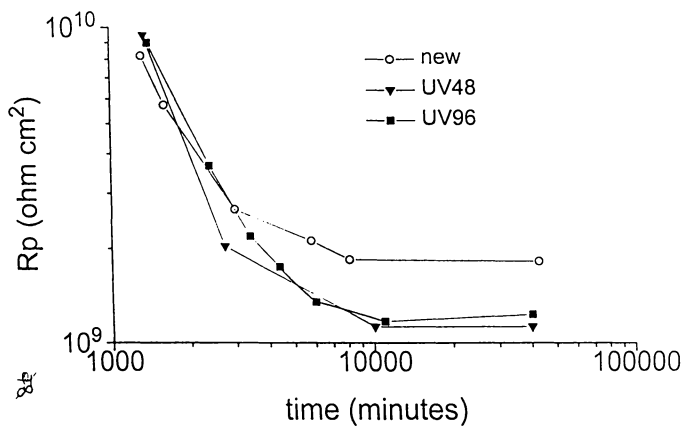


Figure 8: Pore resistance versus the immersion time trend for the new samples and the samples treated with UV radiation for 48 hours (UV48) and 96 hours (UV96).

to the different ozone concentration near the coating surface in the two different cases and to the competition of the propagation and termination reactions of free radicals. For a high intensity of UV radiation (the accelerated test) the high free radical concentration favors the termination reaction, concentrating the chemical modifications in the external layer of the organic coating.

- Because of the differing thickness of degradation, the water barrier properties after the two different UV treatments (natural and artificial) are different. The accelerated UV test does not change the relevance of the water uptake process occurring in new samples. On the contrary, the solar exposure increases both kinetics and amount of the water uptake. There is an inversion of this trend for long term solar exposure, which cause an increase of the glass transition temperature T_g . The more rigid structure causes a reduction of the water uptake kinetics. In conclusion, the accelerated UV test does not correspond to the natural degradation as it does for the water barrier properties.
- The ion barrier properties are reduced by all the UV treatments. However, because of the high protection properties of the studied alkyd resin, it is not possible to distinguish clearly the trend of the ionic resistance as a function of either the solar or the artificial UV exposure time. The only evident result is the minor effect on ion barrier properties of the artificial UV radiation in comparison to the natural photo-oxidation. From the ionic resistance point of view (which corresponds for barrier coatings to the corrosion protection properties) the accelerated UV test corresponds only partially to the natural degradation.

Acknowledgments

The authors thank the Imper S.p.A. in Turin and in particular Dr. Belletti for the samples preparation. The authors acknowledge also Prof. Campostrini of University of Trento and Dr. Fezia of the PPG Italy for the useful discussion about the FTIR results interpretation and Dr. Volcan for the assistance in all the experimental data acquisition and interpretation.

Literature Cited

1. Appelman, B.R. *Journal of Coating Technology* **1980**, 62, p. 57.
2. Kendig, M.; Scully, J. *Corrosion* **1990**, 46, p.22.
3. Clough, R.L.; Shalaby, S.W. In *Radiation Effects on Polymers ACS Symposium Series*, 1991.
4. Pappas, S.P. *Prog. Org. Coat* **1989** 17, p. 107.
5. Armstrong, R.D.; Jenkins, A.T.A.; Johnson, B.W. *Advanced in Corrosion Protection by Organic Coatings II*, The Electrochemical Society, **1994**, p.24.
6. Armstrong, R.D.; Jenkins, A.T.A.; Johnson, B.W. *Corrosion Sci.* **1995**, 37, p. 1615.
7. Bauer, B. *Prog. Org. Coat.* **1993**, 23, p. 105.
8. Monetta, T.; Bellucci, F.; Nicodemo, L.; Nicolais, L. *Prog. Org. Coat.* **1993**, 21, p. 353.
9. Deflorian, F.; Miskovic-Stankovic, V.B.; Bonora, P.L.; Fedrizzi, L. *Corrosion* **1994**, 50, p.446.

10. van Westing, E.P.M.; Ferrari, G.M.; de Wit, J.H.W. *Corrosion Sci.* **1994**, *36*, p. 957.
11. Deflorian, F.; Fedrizzi, L.; Locaspi, A.; Bonora, P.L. *Electrochim. Acta*, **1993**, *38*, p. 1945.
12. Deflorian, F.; Fedrizzi, L.; Bonora, P.L. *Corrosion Sci.* **1996**, *38*, p. 1697.

Chapter 9

Studies of Adhesion and Disbonding of Coatings by Scanning Acoustic Microscopy

J. D. Crossen¹, J. M. Sykes¹, G. A. D. Briggs¹, and J. P. Lomas²

¹Department of Materials, University of Oxford, Oxford OX1 3PH, England

²A.M.TEC Ltd., P.O. Box 501, Warrington WA4 2JP, United Kingdom

The effect of water exposure on the adhesion of an epoxy/polyamide lacquer to mild and stainless steel substrates has been examined. Loss of adhesion is rapid, falling to steady levels within 24 hours. Adhesion is partially regained after drying but maximum values recorded are significantly less than the dry strength. Changes occurring at the interface during exposure and recovery have been examined *in-situ* by Scanning Acoustic Microscopy (SAM) and Time-of-Flight SAM (TOFSAM). During exposure, patches of disbonding at the interface are observed growing rapidly for the first few hours. TOFSAM reveals that after initial disbonding, the coating swells above the disbonded region prior to growth of micro-blisters. During growth, there is little further lateral disbonding. In general, blister growth stops after a period of time. It has been found that drying leads to the disappearance of the majority of the micro-blisters. Observations suggest coating heterogeneities on a microscopic scale.

It has long been recognised that exposure to water of organic coatings on metal surfaces can lead to reduction in adhesion (1,2). In the case of epoxy coatings, this deterioration is particularly rapid (3), leading to failure at the interface between the epoxy and the substrate in an adhesion test (4,5). It has been demonstrated that adhesion loss is partly (1), or fully (3) recoverable if the coating is allowed to dry out.

In previous work (6), it was proposed that the rapid adhesion loss of an epoxy-polyamide lacquer to mild steel during exposure to distilled water was in part due to the formation of discrete regions of micro-blistering at the interface observed by Scanning Acoustic Microscopy (SAM). Drying out samples showed that adhesion recovered rapidly but to a value below the original dry strength. SAM examination revealed that the majority of the blisters disappeared, but a few air-filled micro-voids were left at the interface. It was believed that these voids prevented full adhesion

recovery. Adhesion testing was carried out on mild steel samples but SAM examination was on stainless steel samples to avoid any influence of corrosion during longer exposures. The adhesion test method used, lap-shear testing, is defect-sensitive and therefore is affected by the presence of blisters after drying. Additional work has therefore been carried out to examine more fully the adhesion behaviour on both types of steel substrate in order to further explore the link between adhesion strength and blistering.

In the current work, 90° peel-testing has been used to measure adhesion on mild steel and stainless steel substrates because it is less sensitive to the presence of defects at the interface. It will therefore give a better indication of any more general reduction in interfacial bond strength. The work has also examined blister growth on both substrates in more detail by using Time-of-Flight SAM (TOFSAM) to follow the change in blister dimensions during water exposure.

Experimental Procedure

Adhesion Testing. Substrate samples of size 100 x 25 x 0.8mm were cut from type R mild steel Q-panels and austenitic stainless steel sheets. The test-strips were then vapour degreased in 1,1,1 trichloroethane. A water-break test indicated that the substrates were free from any organic contaminants i.e. complete wetting of the surface, corresponding to a contact angle approaching zero. No other surface preparation was carried out.

The coating studied was an unpigmented 1:1 (by weight) mixture of Epikote-828 type epoxy resin and a Versamid amino polyamide curing agent, thinned with a 3:1 xylene:butanol mixture. The solvent mixture was added in equal amounts to each component prior to mixing in order to reduce viscosity and make preparation easier. The coating was applied on one side of the samples only by flood-spinning for ten seconds and the samples cured at room temperature for 14 days in a dust-free environment prior to testing. The final lacquer thickness was $20 \pm 1 \mu\text{m}$.

To examine adhesion reduction during exposure to distilled water, samples were immersed at 30°C for set periods of time prior to 90° peel-testing in quadruplicate. The testing was carried out on a simple rig where weight was added via a pulley system until a 1.5 x 4cm strip scribed along the coating started to peel continuously. The weight required was then converted to a peel strength using a simple formula.

To measure the recovery of adhesion during drying, samples were exposed to distilled water at 30°C for 24 hours then left to dry out in a desiccator for set periods of time prior to testing.

Scanning Acoustic Microscopy/Time-of-Flight SAM. Sub-surface imaging with a Scanning Acoustic Microscope (SAM) at a resolution approaching that of an optical microscope is possible because the ultrasonic waves generated in the lens are able to propagate below the surface of an optically opaque sample and be brought to a focus within the solid. In addition, the microscope has a confocal imaging system, giving

enhanced depth discrimination in favour of the plane being imaged. Discontinuities such as thin cracks or small unbonded regions at an interface can excite strong contrast in the image due to differences in acoustic wave/sample interaction detected by the lens. Since the lens is generally coupled to the sample by water, true *in-situ* examination in water-disbondment experiments is therefore possible. The technique has been used to examine organic coatings in the past (6-9) and it is evident from this work that the SAM can be used to either study the polymer film itself or to examine processes at the metal-coating interface.

Time-of-flight scanning acoustic microscopy (TOFSAM) is a technique in which extremely short acoustic pulses are sent through the lens to the specimen. The time interval between echoes from the upper and lower surfaces of a coating or defects within it can be measured as the pulsed signal is scanned along a line and changes due to swelling or blistering can be analysed quantitatively: the time being easily converted to a distance if the acoustic velocity is known. The resultant data is a measure of the signal intensity, S , as a function of time, t , and position, y , and is thus referred to as an $S(t,y)$ scan. Full details of TOFSAM and other, more general aspects of scanning acoustic microscopy are given by Briggs (10) and Briggs and Hoppe (11).

Stainless steel and mild steel samples were cut from prepared peel-test specimens and examined on the 'OXSAM' scanning acoustic microscope operating at a frequency of 300-350MHz and using distilled water at 30°C as the acoustic coupling medium. The focus was adjusted so that the interface between the coating and metal was imaged. Micrographs and $S(t,y)$ scans were then taken after increasing lengths of exposure time to record the processes occurring at the interface. For longer exposure times (up to 4 weeks), the areas being observed were marked, the samples removed from the microscope and then immersed in distilled water, again at 30°C. During this time, the samples were periodically re-examined.

Results and Discussion

Wet Adhesion Testing. For both stainless and mild steel samples, reduction in lacquer peel strength was found to be rapid (Figure 1), leading to apparently interfacial failure within 20 minutes exposure. It can be concluded, therefore, that water had penetrated the coating rapidly and disrupted adhesion *uniformly*. Adhesion reduction continued for about 24 hours exposure by which point residual adhesion levels, approximately 3% of the measured dry strength for stainless steel samples and 4% for mild steel samples, had been reached. Residual levels remained constant even after prolonged exposure. Surprisingly, the reduction in adhesion is proportionately greater than that measured during lap-shear testing. For longer term exposure, a visible interfacial water layer could be seen evaporating from the exposed metal surface after peeling.

The rapid loss of adhesion observed corresponds well with the work of Ruggeri and Beck (3) who examined the adhesion of epoxy under similar conditions using a mechanical cutting device. For coatings of similar thickness, they found that reduction

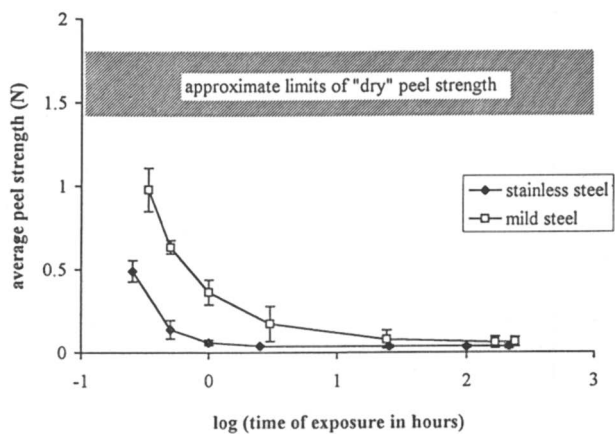


Figure 1. Reduction in lacquer peel strength on mild and stainless steel substrates during exposure to distilled water at 30°C.

of adhesion was rapid and within 30 minutes, the measured value had fallen to approximately 38% of the original dry strength.

Other work by Walker (1) verifies the extreme sensitivity of epoxy-polyamide to water. Using a direct pull-off adhesion test, he found that 50% of the original adhesion was lost within 1 hour of exposure. Again, this is in good agreement with the current work.

Scanning Acoustic Microscopy/Time-of-flight SAM during water exposure. In previous work (6) it was shown that small, distinct patches of bright contrast, corresponding to discrete patches of disbonding at the coating-stainless steel interface, become visible after approximately 30 minutes exposure to water. Figures 2-5 show SAM micrographs of the coating-stainless steel interface during the first few hours of exposure. It should be noted, that the development of disbonded areas does not occur until significant adhesion loss has been measured by peel-testing. During the initial exposure period, the disbonds grow rapidly for the first 2-3 hours, after which point the rate of lateral spreading decreases and, in the majority of cases, becomes negligible.

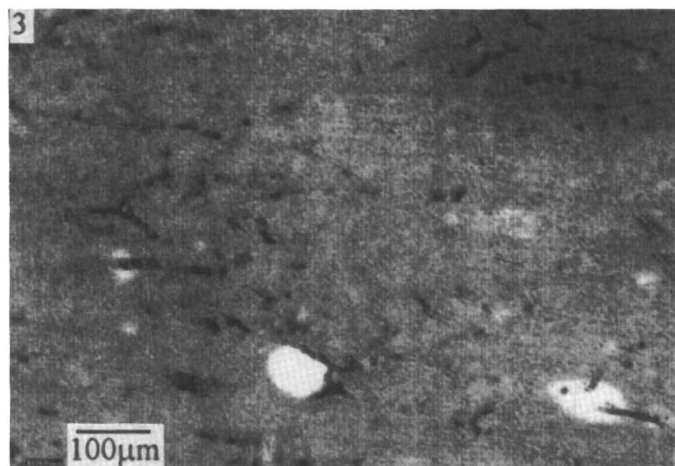
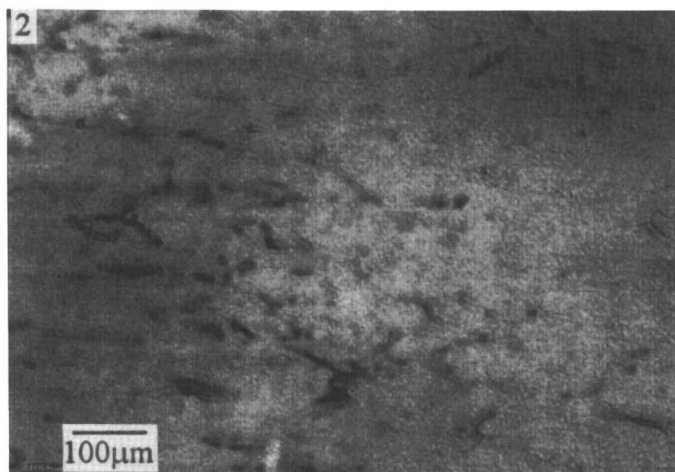
After 2 weeks exposure, (Figure 6), it can be seen that areas of bright contrast cover approximately 50-55% of the total surface area. However, it is also apparent that some regions of the coating still remain in good contact with the substrate (uniform dark contrast). Little further change is observed after 4 weeks exposure.

S(t,y) scans taken across the bright patches after 2 weeks exposure indicate that there is a water filled region between the polymer and the metal. A typical scan, Figure 7, taken across the area marked on Figure 6 shows three groups of fringes, marked (i)-(iii), which in essence display a cross-section of the sample and can be interpreted as follows:

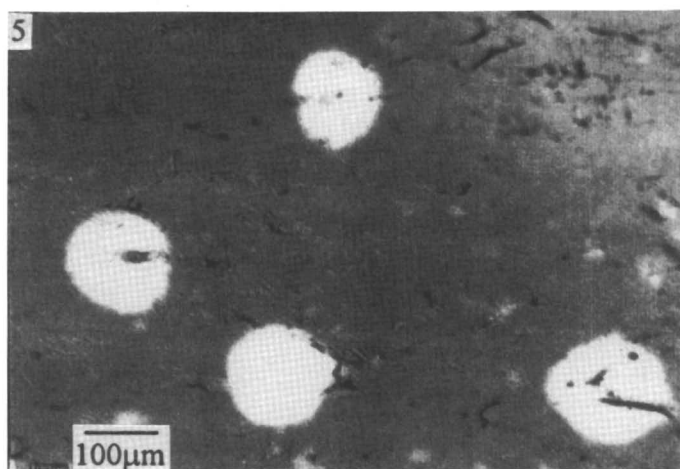
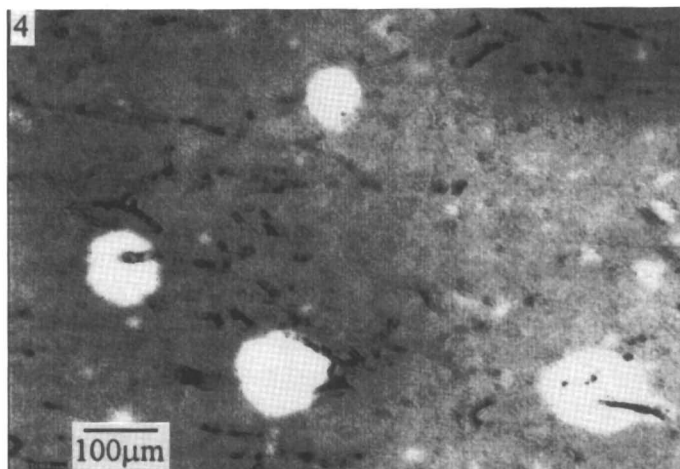
- (i) The first set of fringes corresponds to acoustic wave reflection from the surface of the coating. As can be clearly seen, the time taken becomes shorter above the disbonded region, revealing the profile of a micro-blisters, as the pulse measurement proceeds across the region.
- (ii) The second set of reflections are from the lower surface of the coating which is no longer in contact with the metal. The 180° phase change which can be seen (the fringes are now black-white-black) occurs when acoustic waves travel from a higher velocity medium to a lower velocity medium, in this case from the epoxy to the fluid in the blister.
- (iii) The third (and most intense) set of fringes corresponds to reflection from the metal surface. This requires a medium within the blister (water) to transmit the acoustic waves.

During the first few hours of exposure, S(t,y) scans taken across bright patches show swelling in the coating (raising of the upper surface), but no significant separation of the coating from the substrate.

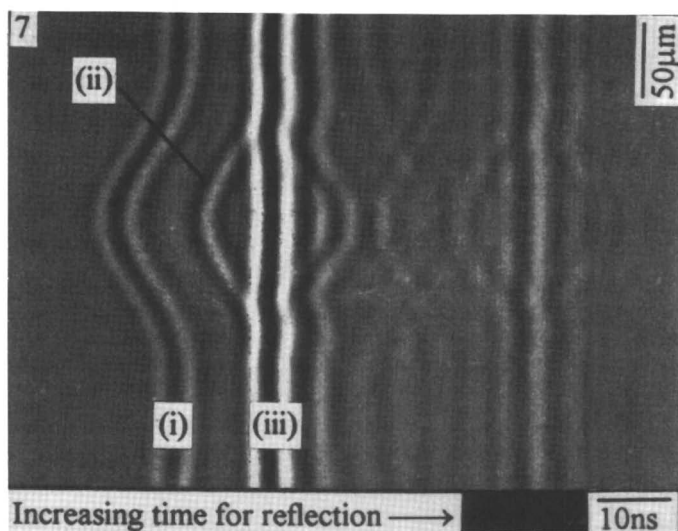
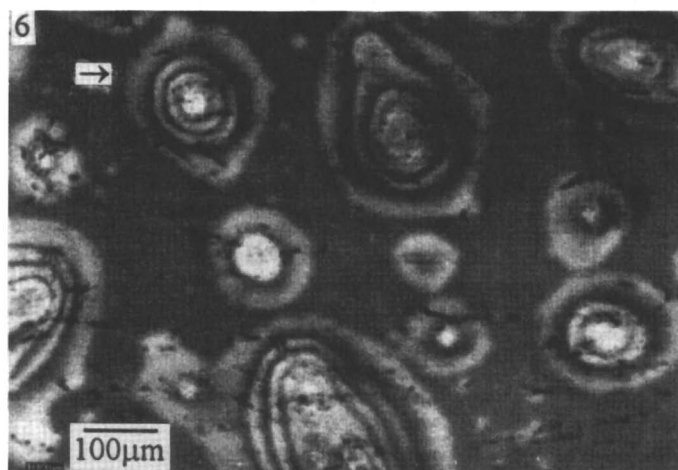
It is also possible to estimate the heights of the micro-blisters by counting fringes arising from interference between acoustic waves within the blister (visible in Figure 6). Each additional fringe corresponds to an increase in height of $\lambda/2$ (2.5 μm with a



Figures 2 and 3. SAM micrographs of the lacquer-stainless steel interface at the start of exposure and after exposure for 30 minutes. (Reproduced with permission from ref. 6. Copyright 1995 The Electrochemical Society.)



Figures 4 and 5. SAM micrographs of the lacquer-stainless steel interface after exposure for 1 hour and 4 hours. (Reproduced with permission from ref. 6. Copyright 1995 The Electrochemical Society.)



Figures 6 and 7. SAM micrograph of the lacquer-stainless steel interface after exposure for 2 weeks and corresponding $S(t,y)$ scan across the microblister indicated. (Reproduced with permission from ref. 6. Copyright 1995 The Electrochemical Society.)

microscope operating frequency of 300MHz). For larger blisters, the estimated value can be verified by examination of $S(t,y)$ scans. Having calculated the height, blister volumes can subsequently be determined by assuming that the blisters have the form of a spherical or ellipsoidal cap. Figure 8 shows a typical result (blister diameter increase, i.e. the rate of lateral disbonding, is also plotted). It should be noted that the measured heights of the blisters is very small compared to the diameters.

Four basic stages in blister growth have been identified:

- 1) rapid lateral disbonding at the interface.
- 2) localised swelling in the coating above the disbonded regions (revealed by $S(t,y)$ scans) before the development of a blister.
- 3) Increase in blister height accompanied by a small amount of additional disbonding at the periphery, with approximately linear increase in volume. This is illustrated in Figures 9-14, showing SAM micrographs and $S(t,y)$ scans across the micro-blisters indicated after increasing time of exposure. The increasing height (and thus volume) can be seen from $S(t,y)$ scans and the increasing number of fringes visible on the micrographs. Note that there is little further growth of the surrounding micro-blisters.
- 4) In the majority of cases, volume increase slows down and blister growth stops.

It has also been found that similar processes occur on mild steel samples, although the micro-blistering is less severe.

In the case of mild steel, both blistering and loss of adhesion might conceivably be linked to the effects of corrosion, specifically generation of alkali, but for stainless steel there is, as expected, apparently no corrosion and therefore osmosis is the most likely mechanism of blister initiation.

The fact that patches of disbondment occur and blisters form at certain sites at the interface suggests that coating adhesion is particularly weak or susceptible to attack by water at these points.

Although adhesion in the regions between blisters is also reduced by water exposure to extremely low levels, the blister volume continues to increase *without* significant additional disbonding at the periphery of the blister. According to van der Meer-Lerk and Heertjes (12) blister growth will continue so long as the internal blister pressure generates sufficient stress at the edge of the blister to detach the coating from the substrate. In the current work, it is clear that most of the peeling off at the edge of the disbond occurs *prior* to the formation of what could be considered a blister. It is therefore apparent that some other process, perhaps swelling of the coating, must be operative during blister growth. This is currently being investigated further.

It should be noted that localised swelling during exposure is only seen above the disbonded regions so it does appear that the nature of the polymer at these points is different from the coating as a whole. The heterogeneous nature of epoxy/polyamide films has been well documented in the past (13) and in the current work, differences in coating properties appear to exist on a microscopic scale. It is therefore also reasonable to suppose that variation in the polymer from point to point should be reflected in changes in the properties of the polymer-metal interface.

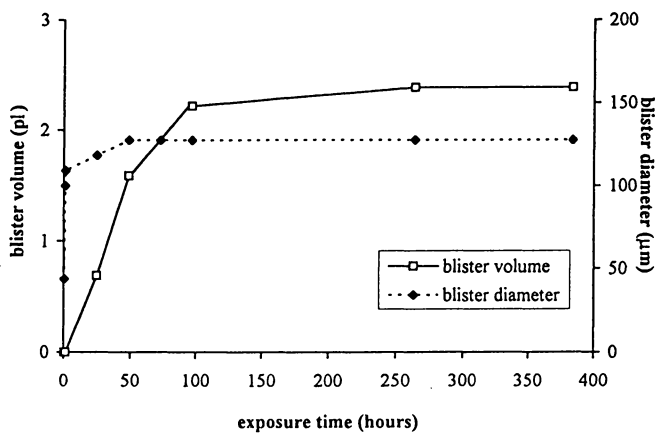
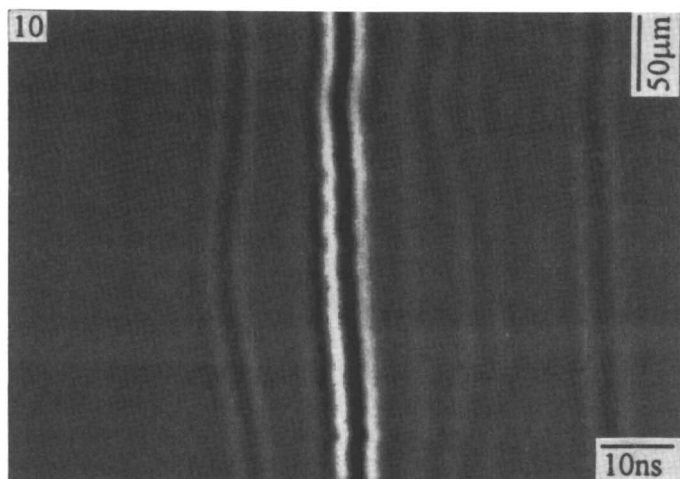
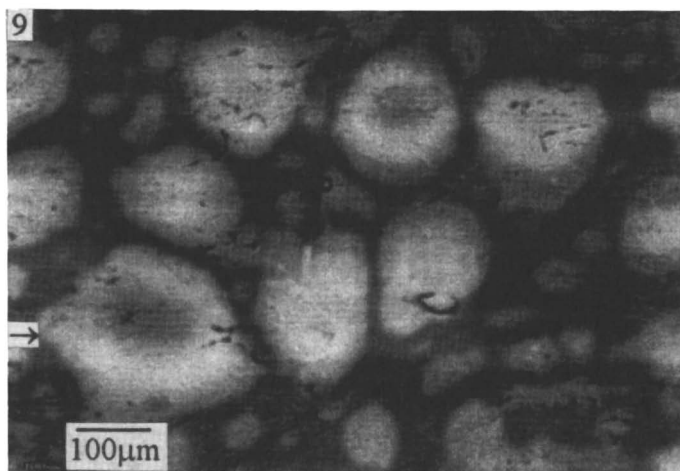
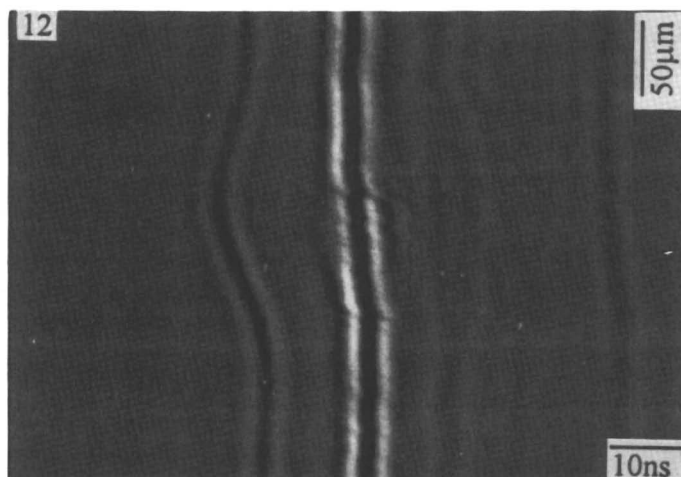
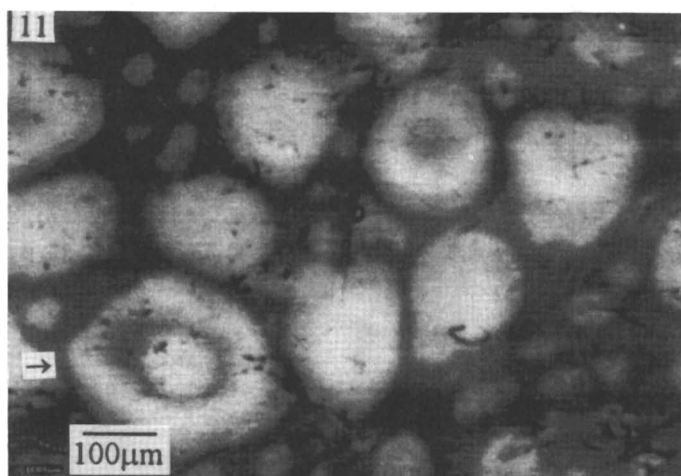


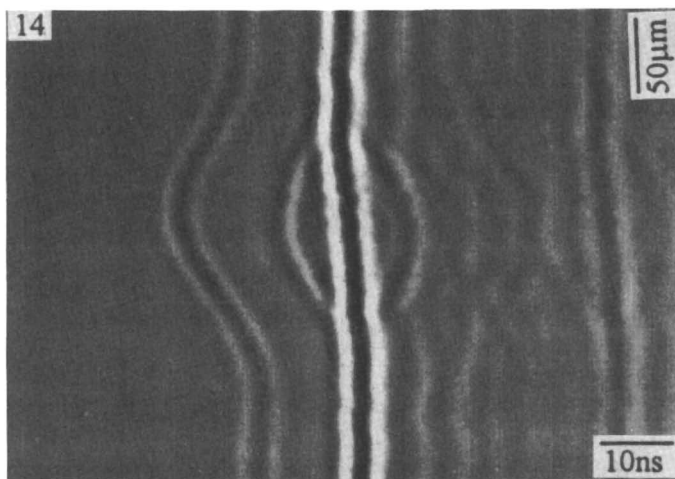
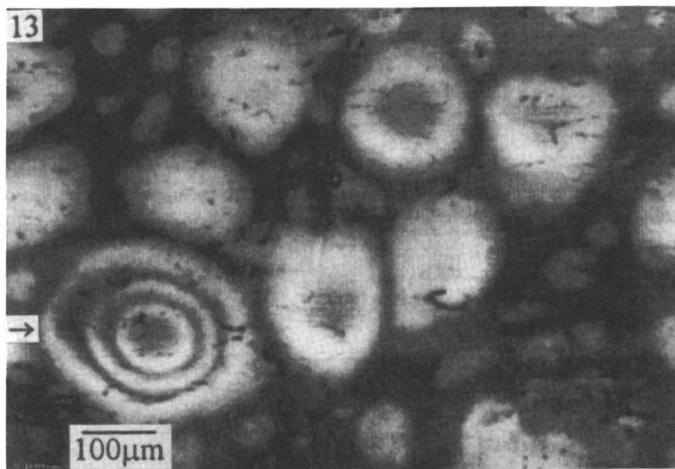
Figure 8. Rate of micro-blister volume increase. Blister diameters are also shown.



Figures 9 and 10. SAM micrograph of the lacquer-stainless steel interface after exposure for 23 hours and corresponding $S(t,y)$ scan across the microblister indicated.



Figures 11 and 12. SAM micrograph of the lacquer-stainless steel interface after exposure for 71 hours and corresponding $S(t,y)$ scan across the microblister indicated.



Figures 13 and 14. SAM micrograph of the lacquer-stainless steel interface after exposure for 239 hours and corresponding $S(t,y)$ scan across the microblister indicated.

Recovery of Adhesion. Figure 15 shows data obtained during the recovery process for each substrate. Adhesion is regained to some extent after drying but the level reached after 1 month is still significantly less than the lowest dry strength measured prior to exposure. Both substrates show similar behaviour, and a high degree of interfacial failure is also noted even after prolonged drying. It is therefore apparent that some process occurs at the interface which prevents full recovery of adhesion during drying. According to Ruggeri and Beck (3) irreversible adhesion loss only occurred when samples were exposed to a corrosive environment. However, since no corrosion was observed on the coated stainless steel samples studied in the current work, some other process must be responsible.

As shown previously (6), drying leads to the disappearance of the majority of the micro-blisters. Figure 16 shows the coating-stainless steel interface after 4 weeks exposure followed by 24 hours drying (same area shown wet in Figure 6). An S(t,y) scan across the area marked, Figure 17, again shows three sets of reflected fringes. In this case however, there is a break in the reflection from the metal surface immediately beneath the blister. This indicates that there is no transmission of acoustic waves through the underside of the coating to the metal (in Figure 7, the reflection from the metal surface is continuous) and it can thus be concluded that these regions are air-filled voids.

From SAM examination, it would therefore appear that recovery had not occurred at these points due to irreversible breaking of the adhesive bonding and localised permanent deformation of the coating. Similar observations have been made on mild steel samples. While these areas undoubtedly contribute to the fact that full adhesion is not regained during drying, they represent a small fraction of the total interfacial area. Peel-test results indicate an additional, more general reduction in recovered adhesion in areas showing recovered bonding to the substrate.

Conclusions

- 1) Peel strength of a epoxy/polyamide coating on both mild and stainless steel samples is reduced rapidly by exposure to distilled water. However, some adhesion is retained even after prolonged exposure.
- 2) Peel strength is partially regained after recovery with both substrate types but values are significantly less than before water exposure.
- 3) SAM examination reveals that localised growth of micro-blisters at the coating/metal interface occurs in much the same way on both mild and stainless steel samples. Disappearance of the majority of micro-blisters during drying has also been observed with both substrates.
- 4) SAM and Time-of-Flight SAM show that micro-blister growth starts with disbonding at the interface, followed by swelling of the coating and then growth in height by water ingress without significant increase in diameter. After an initially rapid rate of volume increase, blister growth slows down then stops.

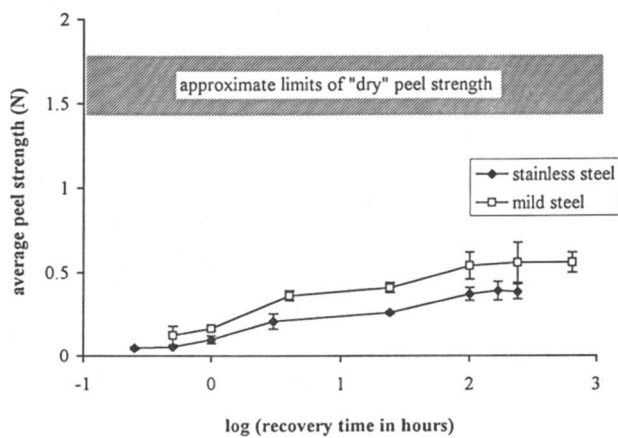
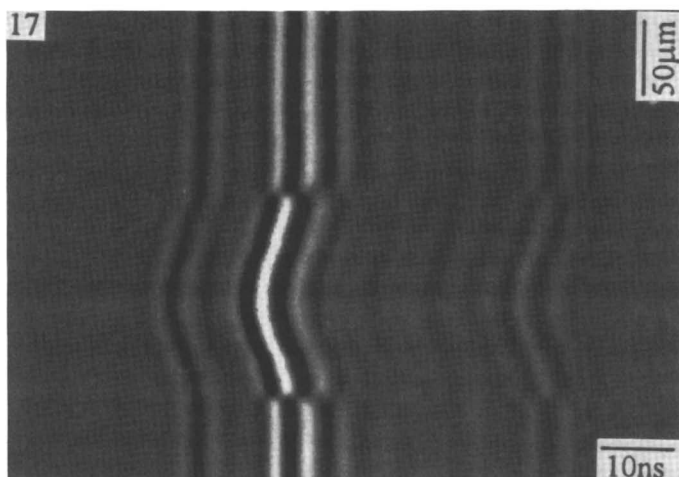
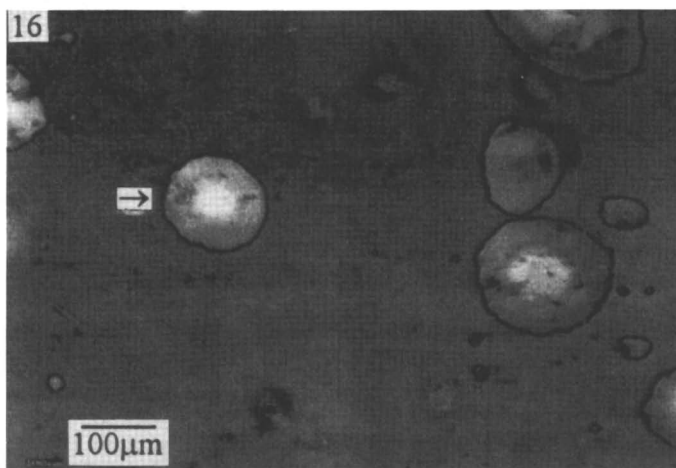


Figure 15. Increase in lacquer peel strength on mild and stainless steel substrates during recovery after 24 hours exposure to distilled water at 30°C.



Figures 16 and 17. SAM micrograph of the lacquer-stainless steel interface after exposure for 4 weeks then drying for 24 hours and corresponding $S(t,y)$ scan across the area indicated. (Reproduced with permission from ref. 6. Copyright 1995 The Electrochemical Society.)

In addition to a link with osmosis caused by soluble contamination at the interface, other factors, such as localised swelling of the coating appear to influence the blister growth.

5) 3) and 4) reveal the existence of microscopic coating heterogeneities.

Acknowledgments

The authors would like to thank Professor B. Cantor for the provision of Laboratory facilities, EPSRC and Courtaulds Coatings for financial support and Dr. L.M. Callow for invaluable discussion.

Literature Cited

- (1) Walker, P. *Off. Digest* 1965, 37, pp1561.
- (2) James, D.M. *J.O.C.C.A* 1956, 39, pp39.
- (3) Ruggeri, R.T.; Beck, T.R. In *Adhesion Aspects of Polymeric Coatings*; Mittal, K.L. Ed.; Plenum Press, N.Y., 1983; pp329.
- (4) Kinloch, A.J. *J.Adhesion* 1979, 10, pp193.
- (5) Gettings, M.; Baker, F.S.; Kinloch, A.J. *J. Appl. Poly. Sci.* 1977, 21, pp2375.
- (6) Crossen, J.D.; Sykes, J.M.; Knauss, D.; Briggs, G.A.D.; Lomas, J.P., In *Proc. of the Symp. "Advances in Corrosion Protection by Organic Coatings II"*, Cambridge 1994; Scantlebury, J.D.; Kendig, M., Eds.; Electrochem. Soc. Inc., 1995, Vol 95-13, pp274.
- (7) Sinton, A.M.; Briggs, G.A.D.; Tsukahara, Y. In *Acoustical Imaging*; Shimizu, H., Chubachi, N., Kushibiki, J., Eds.; Plenum Press, N.Y., 1988, Vol. 17; pp87-95.
- (8) Addison, R.C.; Kendig, M.W.; Jeanjaquet, S.J. In *Acoustical Imaging*; Shimizu, H., Chubachi, N., Kushibiki, J., Eds.; Plenum Press, N.Y., 1988, Vol. 17; pp143-152.
- (9) Kendig, M.; Addison, R.; Jeanjaquet, S. *J. Elect. Chem. Soc.* 1990, 107, No.9. pp2690.
- (10) Briggs, A. In *Acoustic Microscopy*, Clarendon Press, Oxford, 1992.
- (11) Briggs, G.A.D.; Hoppe, M.; In *Images of Materials*; Williams, D.B.; Pelton, A.R.; Gronsky, R. Eds.; Oxford Univ.Press, N.Y., 1991; pp114-141.
- (12) van der Meer-Lerk, L.A.; Heertjes, P.M. *J.O.C.C.A* 1979, 62, pp256.
- (13) Mayne, J.E.O.; Scantlebury, J.D. *Br. Polym. J.* 1970, 2, pp240.

Chapter 10

Defects and Heterogeneities in Corrosion Protective Organic Coatings Films and Their Effects on Film Performance

Gordon P. Bierwagen¹, Dennis E. Tallman², Joel Zlotnick^{3,4},
and Carol S. Jeffcoate¹

¹Departments of Polymers and Coatings and ²Chemistry North Dakota State University, Fargo, ND 58105

³Department of Chemistry, Case-Western Reserve University, Cleveland, OH 44106

A limiting feature of many corrosion protective coatings is how well (defect-free) and how uniformly they can be applied and cured on the metal substrate they are to protect. Failure in coatings/metal systems is very rarely global, and usually occurs at one small site of weakness in the film, and then progresses to give appearance failure or performance failure of the substrate. Careful analysis of film performance often shows that films do not fail in areas where the coating is uniformly applied at the film thickness recommended by the coating manufacturer. The distinct effects of coating heterogeneities have been observed in this laboratory (1) in studies of a multiple sample set of marine coatings by electrochemical noise methods (ENM). It is something which must be considered carefully in choosing the size of the sample set in experimental studies of coating failures (2). One good coating sample definitely does not constitute a representative sample for durability studies. Film thickness fluctuations, local pigment volume concentration fluctuations, local variations in film cross-link density, fluctuations in chemical composition (for example, from a poorly mixed two component system), and locally uncured areas are all local heterogeneities that can cause significant problems. Sampling for lifetime testing of corrosion protective coatings should include coatings with defects that are a representative of those that might be expected in actual practice. Similar arguments have been put forth for the proper analysis of automotive paint film samples that are subjected to exterior exposure testing (3).

⁴Summer undergraduate research associate at North Dakota State University.

metal or coating. If the corrosion is due to local issues in the metal, it is often due to heterogeneities in alloys (4), or local undesirable metal impurities in a metal or

Corrosion of metal substrates in systems protected by organic coatings is almost always a local failure issue, as corrosion occurs at a weak/susceptible point in the alloy. However, in coated metal systems, the corrosion failure can very often be traced to a local defect in the organic coating. As commonly seen in practice, in what appears to be a fairly, uniformly coated system, failure occurs at sharp edges of the object. The film thickness is locally low due to Laplace pressure effects across areas of high radius of curvature (5,6). The coating is also mechanically damaged more easily after application at these sharp edges. Figure 1, taken from Pierce and Schoof (6), illustrates how surface-tension-driven-flows at a sharp edge can generate local thin spots in a coating.

Another common source of corrosion failure is blistering and related defects (7). These often are caused by a coating being applied over a poorly cleaned and prepared substrate or by phase separation and entrapment of solvent during the film formation process in coatings. Because they are often associated with a pre-existing film problem, blistering and subsequent corrosion problems are considered to be caused by film imperfections. It is well known that for successful application and use of corrosion protective coatings, much effort must be made to prepare the surface for coating. Both physical and chemical cleaning are used. A rule of thumb is that 75% of an OEM painting line should be devoted to cleaning and 25% to paint application processes.

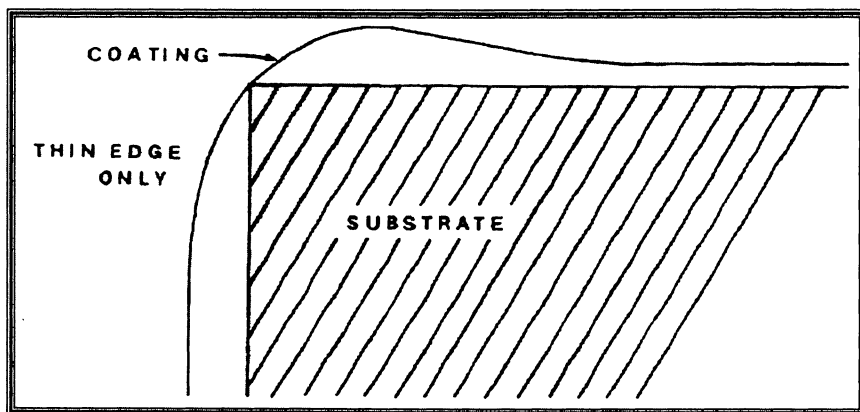


Figure 1. Schematic of Typical Thinning Points in Film-Corrosion Often Occurs at Thin Point at Sharp Edge (with permission from Pierce & Schoof (6)).

Defects can also occur during the application process. Pinholes are caused by foam bubbles trapped in a film during the drying process. Craters are caused by surfactant spreading during the coating application and drying/film formation processes (5,8). Table I gives a summary of defects often seen in coatings and their probable causes. Two or more layers are often used in corrosion protective systems because they significantly reduce the chance of coating imperfections (due to application processes) yielding an imperfection which penetrates directly to the metal substrate. This is illustrated in Fig. 2 (2). Imperfections that

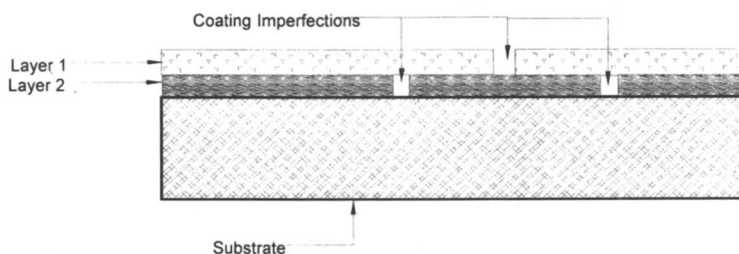


Figure 2. Schematic of Multilayer Coating and Imperfections [with permission from Bierwagen, *Prog. Organic Coatings*, 28 (1996) 43-48 (ref. 2)].

penetrate all the way to the metal surface are often termed “holidays”, and there is a significant market for devices called “holiday detectors” which are used to examine coatings after application, but prior to field use (9).

Fluctuations in film thickness from application processes are a significant cause of poor film performance. These can occur due to poor leveling, ribbing in coil coating processes, and a myriad of other reasons. Film thickness is a very difficult property to measure and control over the entire surface of a coating. Some mapping has been done of fluctuations in film thickness in typical coatings, and these data indicate significant fluctuation in surface profiles (10/11). A qualitative description of film thickness effects on coating corrosion protection was given recently (12), but no quantitative information was provided. Neal gives a discussion of field measurement of corrosion protective coatings (13). Babic, *et al.* (14), discuss briefly the effect of film thickness on film performance, but they are considering only globally average thickness, not local fluctuations.

Film resistance should be linearly related to film thickness if the normal relations observed in resistors hold true and the thickness for example, is equivalent to the length of a resistive wire. The simple relationship (15) for resistance applies

$$R = \rho L/A,$$

where R is the film resistance, ρ the film resistivity, L the film thickness, and A the surface area of the film over which the measurement is made.

Since film corrosion protective performance is often related to resistance, as first noted by Bacon and Rugg, (16), a direct relationship between film performance and thickness should hold. This means that areas of locally low film thickness will give locally poor performance. There is much concern about film thickness control in field use of corrosion protective coatings (17). In general, film thickness variations and the various defects described in Table 1 are the most severe problem faced by the users of corrosion protective coatings. Performance degradation caused by film non-uniformities. Funke has considered much of this in earlier publications (18-19).

Table 1. Film Thickness/Application-Related Defects

Defect	Cause	Reference
Pinholes	Bubbles, Foaming	8
Craters	Surface Contamination	5,8
Ribbing	Flow Instability	5
Scratches	Mechanical Damage	9
Solvent Popping	Solvent Entrapment	3,7
Edge Curvature Thinning	Laplace Pressure Effects	5,6,7
Brushmarks	Leveling Problems	5
De-Wetting	Surface Incompatibility	8,8
Blisters	Sub-Film Contamination	7
Uneven Film Thickness	Poor Application	8

Another defect in coatings related to corrosion failure is the porosity that occurs in pigmented coating films above their critical pigment volume concentration (CPVC). It is very well known that there is a sharp increase in corrosion in coated metals as one increases the pigment volume concentration of the coating (PVC) above the CPVC (20). The rapid development of corrosion in salt spray testing of panels for which the coating was above its CPVC was used as one of the earliest measurements of pigmented coating CPVC. The cause of this effect was assigned to the voids that form in the coating above the CPVC which act as pathways for the electrolyte and oxygen to get directly to the metal/coating interface and support rapid corrosion. By comparison at PVC values below the CPVC the coating has intact barrier properties and materials have to diffuse to the interface through a continuous, closed coating, giving a much reduced corrosion rate. This was more recently considered and discussed by Skerry, *et al.* (21), in a symposium on CPVC related topics. New work of Fishman, *et al.*, (22-23) has shown that local fluctuations in PVC can generate local areas where the PVC exceeds the CPVC, even though the globally $PVC < CPVC$. These local areas of paint film that are above the CPVC will act as a defect with respect to corrosion protection since that portion of the film because it will be locally porous. As shown in Figure 3, the local voids can occur even in a film globally below the CPVC if there is any local volume that is not perfectly mixed, etc. These local voids will provide direct pathways for transport of ions and oxygen and locally destroy barrier properties.

Further, there can be other variations in the properties of films of uniform thickness that lead to variations in performance locally in a film. These include local variations in cross-link density from non-uniform heating or drying of the coating, and local variations in chemical composition due to incomplete mixing of two-component coating systems. Kumins (24) has discussed variations of this type as they effect coating properties. In a thermoplastic film, one could have local variations in the polymer molecular weight (MW) if solubility of the polymer in the casting solvent is MW dependent.

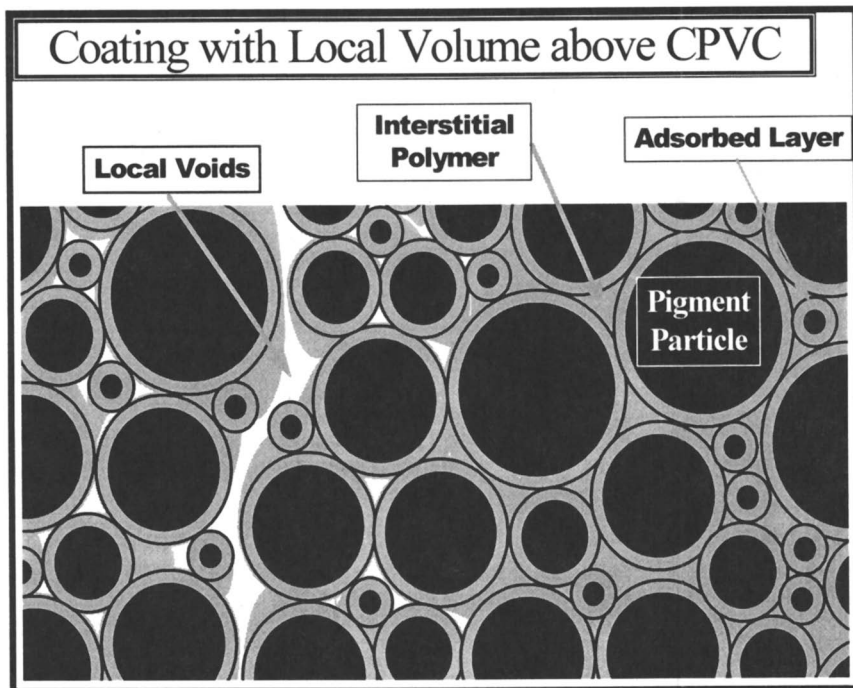


Figure 3. Schematic of Local Voids Occurring in Film Locally above CPVC

The concept of local fluctuations in properties discussed in references 22 and 23 would seem to have generic applicability to all transport properties of film. These include properties such as electrical resistance and diffusion coefficients that are very sensitive to thickness and composition. Certain resistance measurements on films have indicated inhomogeneous behavior upon immersion in electrolyte (25). Mayne and co-workers at Cambridge have studied this in some detail (26). Variations in film properties have been noted in spectroscopic examinations of automotive coatings (10). Some optical methods show variation in polymer properties in the film, but little work has been done to correlate these measurements with film corrosion protective performance. Figure 4 illustrates film property variation in the plane of the film (27).

Another variation in film properties that can occur is the variation in alignment of impermeable flake pigments (such as Al or mica flakes) used to control diffusion in protective coatings. If the alignment of these flake pigments varies from being parallel to the surface of the film, their reduction of diffusion and subsequent improvement of film barrier properties is reduced. Eitzman, et al.(28), have examined this effect in detail theoretically and experimentally for mica in polysiloxane films. They have shown distinct increases in diffusion coefficients as the angle of flake alignment varies from parallel to the plane of the film. This is illustrated in Figure 5.

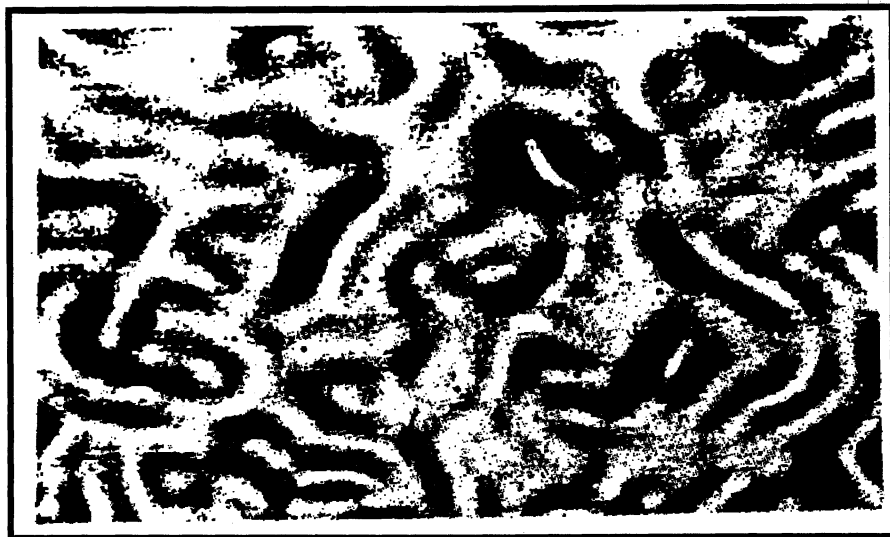


Figure 4. 'Shadowgraph' of Automotive Coating Surface (with permission from ref. 10).

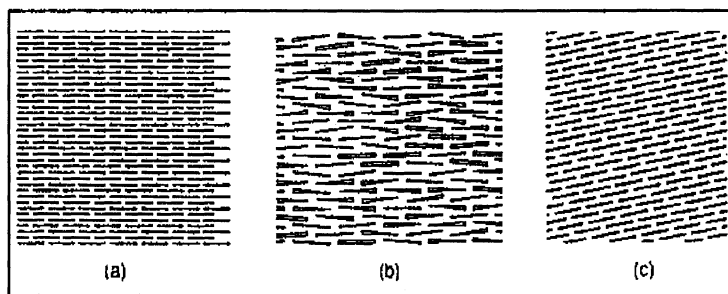


Figure 5. Typical Cross Sections of Flake Filled Films The flakes in (a) are regularly space perpendicular to the diffusion; those in (b) are randomly oriented; those in (c) are all at a fixed angle not perpendicular. [Taken from ref. 28, with permission].

The diffusion is also strongly dependent on the aspect ratio of the flakes and on their size poly-dispersity. The possible sources of variation in film transport properties are summarized in Table II.

Table II. Sources of Local Coating Film Transport Property Variations in Uniformly Thick Films

Film Property Local Variation	Resultant Transport Property Change	Reference
Cross-linking Density	Diffusion	25
Chemical Composition	Ionic & Electrical Resistance	25
	Diffusion	
Flake Pigment Alignment	Ionic & Electrical Resistance	28
	Diffusion	
Molecular Weight	Diffusion	22,23
Crystallinity	Diffusion	
Pigment Volume Concentration	Diffusion	
	Ionic & Electrical Resistance	

The real situation is films applied under use conditions have defects of one type or another. This must be taken into account in the testing and subsequent use of these films. A statistically valid data set of proper size should be used in any test of film performance in order to insure one observes the “true” performance of the coating system under consideration. Choosing only “good” coatings, pre-chosen to have no defects, as samples for testing often fools the user when the resultant test data is used to predict lifetime performance of the system under real application and use conditions. Tait (29) has discussed some of these problems with respect to impedance measurements. Standard statistical methods for choosing sample size for lifetime prediction studies are recommended (30).

Recent Studies on Imperfections - Effects on Electrochemical Measurements

Variations in Application Quality. In this laboratory, we have observed situations where the effects of local defects have created significant problems in the interpretation of corrosion performance test data. In studies of the corrosion of marine coatings (1) we have seen considerable fluctuation of data acquired by electrochemical noise methods (ENM) in two six-sample data sets. This is discussed in some detail in ref. 1, and possible causes for this variation are given therein. Some of the results seen in this study are shown in Figure 6. The data shows that considerable variation occurs in electrochemical characterization of randomly chosen samples, even if care is taken to insure sample uniformity. Visual examination of the immersed samples of ref. 1 after the data was acquired, indicated that there were some defects (e.g., low film thickness in the sample measuring area) in the coatings that performed poorly with respect to the mean of the sample set. Thus, the observed variation was most likely due to sample preparation variation and not in the coating or

substrates themselves. The implications of this data is that the electrochemical performance of coated metal systems is very dependent on the quality of the coating application, and that ENM can distinguish between samples based on their application quality. Also, the data illustrates that the differences in sample quality are not always immediately apparent. The differences in on-going performance between “good” and “bad” samples increases with time, with poorly prepared samples decaying in performance more rapidly than the “good” samples.

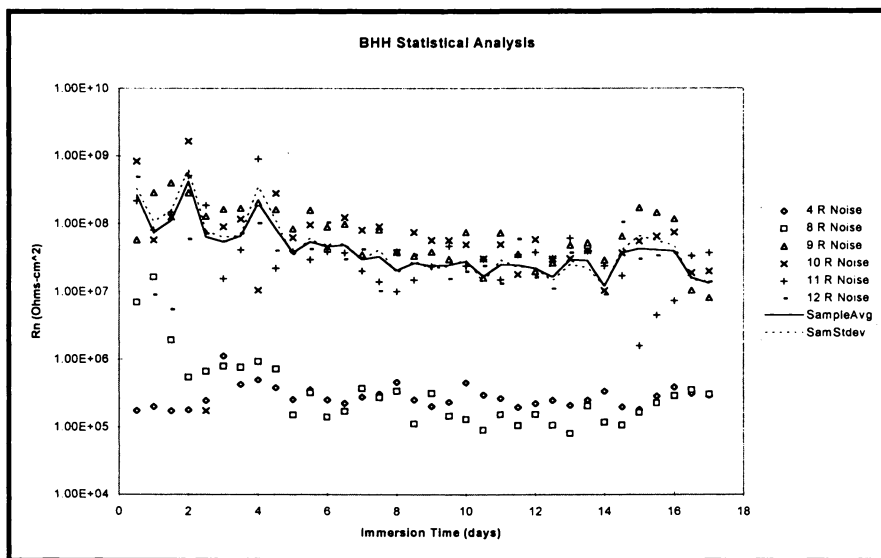


Figure 6. Noise Resistance R_n vs. time for a multiple sample set of a Marine Epoxy coating. (From ref. 1 with permission.)

Effects of Induced Heterogeneities (Damage) on Coating Performance. We further examined the effects of coating damage (analogous to physical damage that can occur to a coating by scratching, dinging, chipping or abrasion) on our data acquisition by ENM. We did this for several reasons. The first is there has been disagreement as to what effect a non-symmetrical pair of electrodes in ENM measurement has on measured results of R_n (reflecting coating performance) and the validity of those results. Cottis and Turgoose (31) claim that the data should be dominated by the electrode with the lowest resistance. Mansfeld concurs with this judgement, and claims to present data to verify this interpretation (32). In our laboratory, by contrast, we have not seen the effects that Cottis and Mansfeld describe. The second reason is to understand what the presence of damage in a coating does to ENM measurements, and to learn how one can identify and interpret ENM data in damaged systems.

Figures 7 and 8 show the comparison of Electrochemical Impedance Spectroscopy (EIS) (Bode plot format for Modulus alone) test results for a damaged

and an undamaged film of the zinc rich primer with a Marine Epoxy topcoat. The data is from systems measured before and after 300 hours exposure in 3% NaCl solution. In inspecting these figures, it is obvious that sample variation, either deliberate or that due to normal sample preparation, has a drastic effect on the data one acquires in electrochemical testing of the corrosion protection. A comparison of initial and final impedance data and several weeks of noise data suggests that mixed pairs of samples (with one panel scratched and the other intact) generally exhibit less scatter in noise resistance data than pairs of un-scratched panels. Furthermore, final noise resistance values were slightly, but significantly, lower for pairs with a damaged panel, and tended to approach a more consistent value than did intact pairs, Figures 9 and 10. We suggest a geometric average,

$$R_{n-pair} = \sqrt{R_{n1}R_{n2}}$$

of asymmetrical pair individual resistances, R_{n1} and R_{n2} , is the best approximation to what is measured by ENM. This follows if ENM monitors transport properties of the films (33). This study of damage effects in coatings will be treated in more detail in future publications from this laboratory.

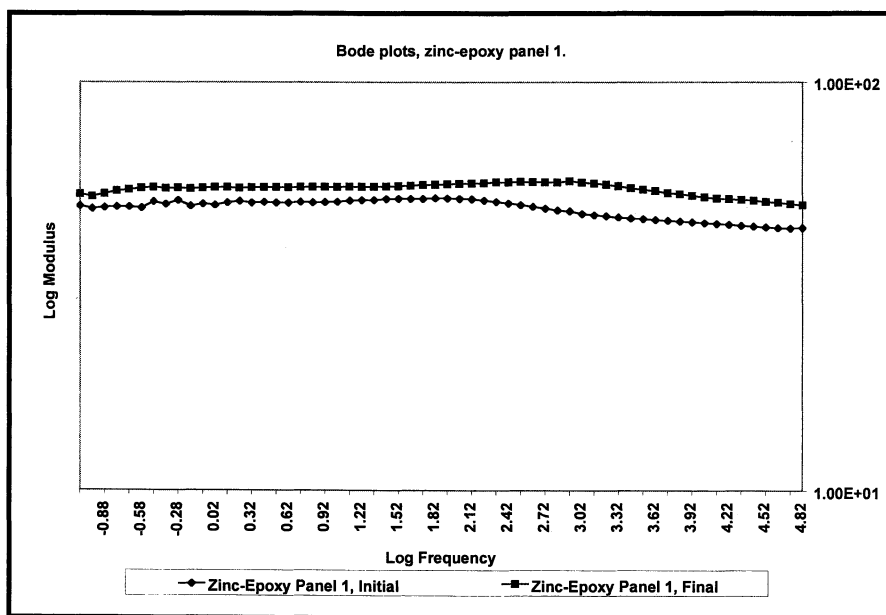


Figure 7. Bode Plot from Damaged Zinc-Marine Epoxy System.

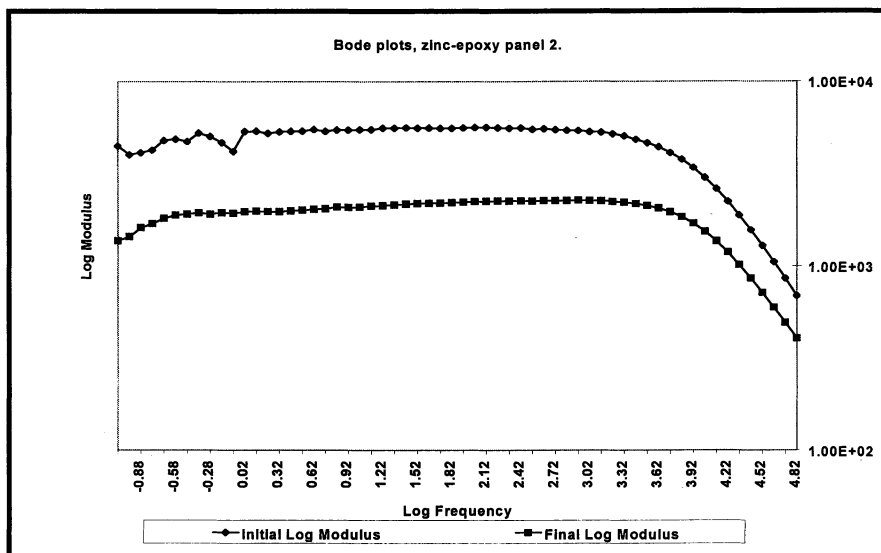


Figure 8. Bode plot for Undamaged Zinc-Marine Epoxy Coatings.

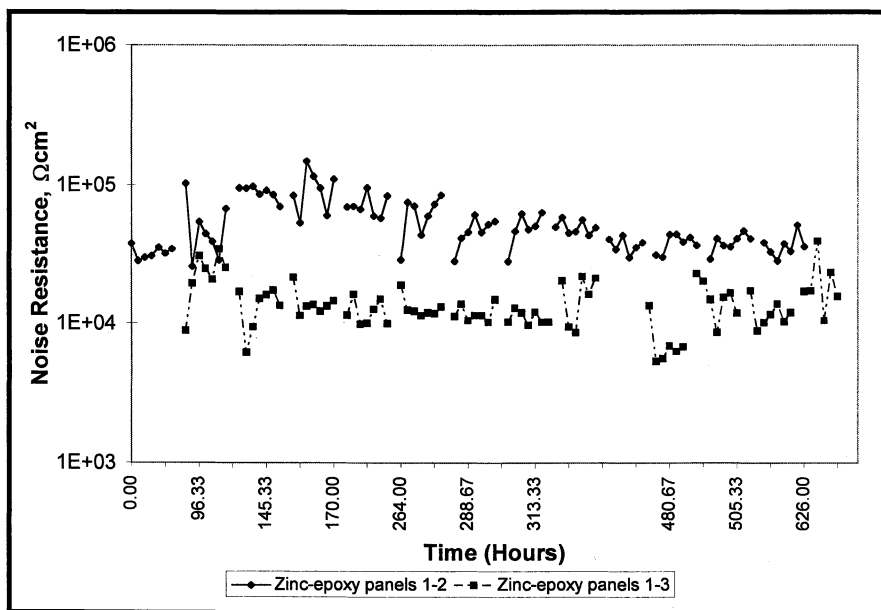


Figure 9. Noise Resistance Plot from Damaged Zinc-Marine Epoxy System.

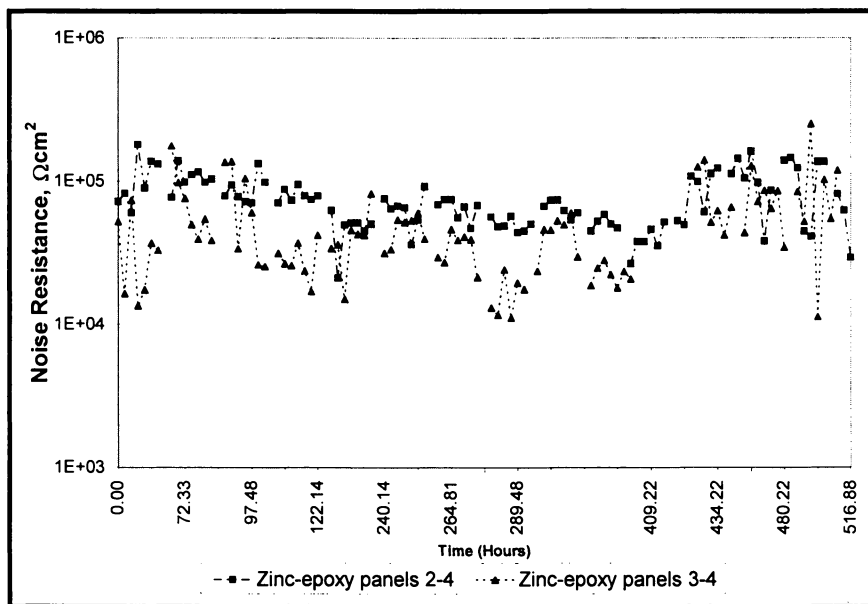


Figure 10. Noise Resistance plot for Undamaged Zinc-Marine Epoxy Coatings.

Though not complete, our studies of heterogeneity/damage effects in electrochemical measurements on coated metals suggests that these effects exist, to a greater or lesser degree, in almost all samples. This means that one must consider the possible effects of measurement area on ENM and EIS measurements of resistance of coating films resistance. If the resistance measurements can be dominated by a single low resistance defect area or area of low cross-link density, there may exist a surface area value above which the measurements are dominated by the probability of having a defect area. At this level, the intrinsic resistance of the properly applied film is not determined. The R_n values measured in larger areas will not increase with area, but level off to an asymptotic value as the area of measurement increases due to the presence of low resistance pathways at defect sites.

Summary and Conclusions

We have shown by both a review of the literature and by results from our laboratory that heterogeneities and damage in coated metal systems are a primary cause of premature corrosion failure of such systems. Corrosion is a local event, which grows from a local to global problem with exposure time. The accumulation of sufficient local corrosion failures leads to total object failure, either in appearance or in performance. Control and elimination of heterogeneities and defects is crucial to obtaining the total performance inherent in a coating/metal system. As higher and higher performance coating systems are developed, measurements need to be made that assess both uniform and non-uniform/damaged applied films in order to properly

test, evaluate, and qualify such coatings. Ideally one would want measurements that determine the “ideally applied” performance of a new coating system, its “as applied” performance, and its “damaged” performance. If the former is extremely high and the latter are low, one must consider new application technology or drastically improved quality control in the current application process. The extremely successful use of electrodeposition primers (34) for corrosion protection suggests that coatings applied by this process (which is self-terminating, is relatively defect free, and has very complete edge coverage) owe almost as much in corrosion performance to the application method as to the chemical nature of the coating (35).

Our lab studies evaluating corrosion protection by means of ENM and EIS indicate the “normal” variation of film thickness and properties within a sample set of test panels prepared by spray application can be extensive. Care must be taken in sampling to insure enough samples for representative behavior. Other studies of deliberately damaged coatings show that, indeed, effects of this nature must be considered in electrochemical analysis of coatings performance. This is especially true in ENM studies where a two electrode pair is required for measurement. Further studies of damaged systems are required to fully determine and document these effects.

Understanding damage effects in systems where chromate pigments and pretreatments are not allowed is especially crucial. This is because one of the major functions of chromates is to provide local inhibition of corrosion about damaged areas; substitutes may not do this as effectively. Such information will be very necessary on all new environmentally compliant systems.

Literature Cited

- 1 Bierwagen, G. P.; Mills, D.J.; Tallman, D.E.; Skerry, B.S. In *Reproducibility Analysis of Electrochemical Noise Data For Coated Metal Systems*; Kearns, J.L.; Scully, J.R.; Roberge, P.R.; Reichert, D.L., Eds.; Electrochemical Noise Measurement for Corrosion Applications, ASTM Special Technical Publication 1277, **Amer. Soc. Testing & Materials** 1996, pp. 427-445.
- 2 Bierwagen, G.P. In “Reflections on Corrosion Control by Coatings” *Prog. Organic Coatings* 1996, 28, 43-48.
- 3 Bauer, David Ford Motor Co., private communication, July 1995.
- 4 Jones, D.A. *Principles and Prevention of Corrosion*; 2nd Edition, Prentice-Hall: Upper Saddle River, NJ, 1996, Ch. 7 and 9.
- 5 Bierwagen, G.P. *Prog. Organic Coatings* 1991, 19, 59-68.
- 6 Pierce, P.E.; Schoof, C.K. *Coating Film Defects*, Brezinski, D., Ed.; Coating Technology Monographs; Fed. Soc. Coating Tech.: Blue Bell, PA 1988.
- 7 Funke, W. "Blistering of Paint Films and Filiform Corrosion" *Prog. Organic Coatings* 1981, 19, 29-46.
- 8 Guthoff, E.B.; Cohen, C.D. *Coating and Drying Defects*; Wiley-Interscience: New York, 1995.
- 9 See, for example, advertisements on pp. 34,49,58 & 74 in **Materials Performance**, 35(#8) August 1996.

- 10 Dubbeldam, G.C. "Visualizing the Topography of Coating Surfaces" *Prog. Organic Coatings* **1992**, 20, 261-272.
- 11 Provder, T. "Application of Profilometry and Fractal Analysis to the Characterization of Coatings Surface Roughness" *Prog. Organic Coatings* **1996**, 27, 219-226.
- 12 Lichtenstein, J. "Thickness Affects the Life of the Coating System" *Materials Performance* **1995**, August, 39-40.
- 13 Neal, D. "Variables in Measuring Coating Thickness" *Materials Performance* **1995**, June, 29-34.
- 14 Babic, R.; Metikos-Hukovic, M.; Rudovic, H. "The Study of Coal Tar Epoxy Protective Coatings by Impedance Spectroscopy," *Prog. Org. Coatings* **1994**, 23, 275-286.
- 15 Halliday, D.; Resnick, R. *Physics*; Wiley & Sons: New York, NY, 1960, Ch. 31, p. 663.
- 16 Bacon and Rugg
- 17 Lichtenstein, J. "Thickness Affects the Life of the Coating System" *Materials Performance* **1995**, August, 39-40.
- 18 Funke, W. "Toward a Unified View of the Mechanism Responsible for Paint Defects by Metallic Corrosion" *Ind. Eng. Chem. Prod. Res. Dev* **1985**, 24, 343-347.
- 19 Funke, W. "How Organic Coatings Systems Protect Against Corrosion" *Polymeric Materials for Corrosion Control In ACS Symposium Series*, 322, *Polymeric Materials for Corrosion Control*; Dickie, R.A.; Floyd, F.L., Eds.: American Chemical Society: 1986, Ch. 20.
- 20 Asbeck, W.K.; Van Loo, M. *Ind. Eng. Chem.* **1949**, 41, 1470 .
- 21 Skerry, B.S.; Chen, C.-T.; Ray, C.J. *J. Coatings Tech.* **1992**, 64(#806), 77.
- 22 Fishman, R.S.; Kurtze, D.A.; Bierwagen, G.P. "Pigment Inhomogeneity and Void Formation in Organic Coatings" *Prog. Org. Coatings* 1993, 21, 387.
- 23 Fishman, R.S.; Kurtze, D.A.; Bierwagen, G.P. "The Effects of Density Fluctuations in Organic Coatings," *J. Appl. Phys.* **1992**, 72, 3116.
- 24 a.)Kumins, C.A, "Fundamental Adhesive and Corrosion Control Studies," *J. Coatings Tech.* 1990, 62 (#781), 63.
 b.)Kumins, C.A., "Electrochemical Properties of Protective Coatings," *Official Digest FSPT* 1960,32, 843-861.
- 25 Mills, D.J., and Mayne, J.E.O. "The Inhomogenous Nature of Polymer Films and Its Effect on Resistance Inhibition", In *Corrosion Protection by Organic Coatings*, NACE: 1981, 12-17.
- 26 a.)Kinsella, E.M., and Mayne, J.E.O. "Ionic Conduction in Polymer Films, I: Influence of Electrolyte on Resistance" *Br. Polym. J.* **1969**, July, 1, 173-176.
 b.)Kinsella, E.M., and Mayne, J.E.O. "Ionic Conduction in Polymer Films, I: Influence of Electrolyte on Resistance", *Br. Polym. J.* 1969, July, 1, 173-176.
 c.)Kinsella, E.M.; Mayne, J.E.O.; Scantlebury, J.D. "Ionic Conduction in Polymer Films, III: Influence of Temperature on Water Absorption" *Br. Polym. J.* 1971, Jan., 3, 41-43.
 d.)Mayne, J.E.O. and Mills, D.J. "Electrical Resistance Measurements in Relation to Protection by Organic Coatings" *JOCCA* 1975, 58, 155.

- 27 Dumbledam, B. *Prog. Organic Coatings* **1992**, 20, 261.
- 28 Eitzman, D.M.; Melkote, R.R.; Cussler, E.L. "Barrier Membrane with Tipped Impermeable Flakes" *AIChE J.* **1996**, 42, 2-9.
- 29a.) Tait, W. S., "A Discussion of the Reliability of Electrochemical Impedance Spectroscopy Data from Coated Metals" *Div. of Polymeric Materials: Sci. & Eng. Preprints*, Vol . Amer. Chem. Soc. National Meeting , Denver, April 1993, p.101.
- b.) Tait, W. S. "Coping with Errors in Electrchemical Impedance Spectroscopy Data from Coated Metals" *J. Coatings Tech.* **1994**, 66(#834), 59-62.
- 30 Martin, J.W.; Saunders, S.C.; Floyd, F.L.; Wineburg, J. *Methodologies for Predicting the Service Lives of Coating Systems*, NIST Building Sciences Series 172, NIST: Gaithersburg, MD, October 1994.
- 31 Cottis, R.A.; Turgoose, S. "The Influence of Electrode Asymmetry on Electrochemical Noise Measurements," NACE 94 Research In Progress Symposium; J. Scully, Ed.; NACE: Orlando, FL, 1994, pp. 90-93.
- 32 Mansfeld, F.; Chen, C.; Lee, C.C.; Xiao, H. "The Effect of Asymmetric Electrodes on the Analysis of Electrochemical Impedance and Noise Data" *Corr. Sci.* **1996**, 38, 497.
- 33 Glasstone, S.; Laidler, K.J.; Eyring, H. "Viscosity and Diffusion" In *Theory of Rate Processes*; New York: McGraw-Hill, 1941, Ch. 23, 477-551.
- 34 Vachlas, Z. "Primers for the Automotive Industry," In *Automotive Paints and Coatings*; Fettis, G., Ed.; VCH Publishers: New York, NY, 1995, pp.28-70.
- 35 Pierce, P., private communication, October 1996.

Chapter 11

Prediction of Blistering in Coating Systems

James M. Pommersheim¹ and T. Nguyen²

¹Department of Chemical Engineering, Bucknell University, Lewisburg, PA 17837

²Building and Fire Research Laboratory, National Institute of Standards and Technology, Gaithersburg, MD 20899

Models based on diffusion and osmotic theory were developed for the growth of water-filled blisters at the substrate beneath organic coatings. Blister growth was considered to occur either over concentrated spots of impurity located at the point of blister initiation, or over a surface containing a uniform distribution of impurity. The solutions to both models had similar mathematical forms: the blister radius, surface area, volume, osmotic pressure, all vary directly as fractional powers of time. Experimental data for KHSO_4 as impurity was used to test the models. Blister volume was found to vary as $t^{0.5}$ (vs. $t^{0.75}$ for the theory) and as M_s (vs. $M_s^{0.75}$), where M_s is the mass of KHSO_4 . Deviations between data and theory were discussed in terms of the contact angle, blister initiation, ion concentrations within the blister, saturation, disbondment, and possible mechanism shifts.

Organic coatings function by protecting substrates from physical and chemical attack. In some instances, however, this attack can be promoted rather than hindered by the presence of the coating. Such can be the case, for example when the substrate is contaminated. Foreign ions, such as chloride or sulfate, present on the surface or leached ions from the coating, can, in the presence of microscopic amounts of water, establish local osmotic cells or blisters. Blisters also form and grow by other mechanisms, for example, e.g.; swelling [1], phase separation during film formation [2], temperature cycling [3], or loss of adhesion [4], but the osmotic mechanism for growth is common [5].

Blister initiation does not occur when the surface is relatively clean, or where water has not penetrated all the way to the substrate surface. Even with water present, the osmotic pressure developed may be insufficient to destroy good adhesion between the film and substrate. Blister initiation can also be prevented by reversing the concentration gradient. Thus, if a concentrated salt solution is kept in the external solution outside the coating, water may be drawn from the coating. This is the principle which makes it possible to store acids and concentrated salts in well-painted vessels made of metals, which would normally corrode. This helps prevent the initiation of blisters and can collapse existing blisters.

Both water and oxygen are capable of passing through the diffusion barrier provided by the organic coating [2, 5, 6]. The actual concentrations of corrosive agents present at the substrate-coating interface will depend on the permeability of the coating, which varies with temperature, partial pressure and the nature of the coating [6]. The film functions as a semi-permeable membrane allowing water to pass through but trapping ions present on the substrate surface within the blister [7]. The high pressures generated within the blisters can cause delamination of the film [7, 8, 9], and more water is osmotically driven into the blister. If oxygen is also present, then the potential for aqueous corrosion exists at the metal surface. Under most service conditions, there is sufficient time for the penetration of water and oxygen [10]. However for more severely corroding systems some evidence suggests that oxygen transfer rates through the coating may be rate limiting so that they determine the progress of corrosion reactions [2, 11]. Corrosion processes can release more ions, principally Fe^{2+} , Fe^{3+} , and OH^- , and provide further blister enlargement by osmosis and cathodic delamination [12]. Blister growth due to corrosion is further complicated by precipitation of corrosion products within the blister (e.g., $\text{Fe}(\text{OH})_3$, Fe_2O_3 , and Fe_3O_4), and by concentration gradients established within the blister between anodic and cathodic regions.

Using time-series color photography and polarized light microscopy, in tests lasting from two to four days, Thomas [13] observed the initiation and growth of blisters beneath a transparent coating on a steel substrate. Small spots of inorganic salt (KHSO_4) placed at the coating-steel interface were found to cause both blistering and corrosion. The corrosion that developed was localized within or near the blister. Cathodes developed near the periphery of the blister while anodes developed within the original spot of salt contamination. Corrosion products (hydrated iron oxides or rust) deposited between the anode and cathode. Results are consistent with the interpretation that anodic regions would tend to form at the center of the blister where oxygen concentrations are higher, while cathodic regions would form at the blister periphery where oxygen concentrations are lower [14]. At later times, blisters grew larger and anode "break-through" was observed. Cathodic blisters were also found to form external to the original salt contamination spot. The observations of Thomas are consistent with those of Leidheiser and Kendig [11] who studied the corrosion mechanism of polybutadiene-coated steel in aerated sodium chloride solutions.

In a series of papers, efforts towards an understanding of the mechanism for osmotic blister formation and growth were made by van der Meer-Lerk and Heertjes [7, 9, 15]. They studied the growth of small blisters under coatings of semi-permeable membranes with KHSO_4 salt deposited on the surface of the substrate. Their results indicated that water transport into the blister was not controlled by the mechanical resistance of the film to deformation [7]. This was demonstrated in an experimental study [9] in which water under pressure was used to artificially create blisters at the surface between different varnish films and substrates. Pressures needed to create blisters were substantially below those calculated to occur within osmotically generated blisters, an atmosphere or so, as compared to many atmospheres. The authors showed that water transport to the blister surface would not be controlled by disbonding or loss of adhesion (peeling) and stiffness. Adhesion loss was seen as a consequence of blister growth rather than a cause. van der Meer-Lerk and Heertjes proposed a mathematical model for the growth of blisters which was based on osmosis [15]. They considered water transport to be driven by the difference in chemical potential between the outside surface of the film and the inside of the blister. The initially high osmotic pressure developed within the blister decreased as it

became diluted with water. The size of the blister was assumed to increase at a rate proportional to the product of its curved (mantle) surface area, and the difference between the osmotic pressure $\Delta\pi$ and a compressive pressure P_k caused by the resistance of the film to deformation. Model results were compared to the data in terms of the product of the mean diffusion coefficient of water in the film \bar{D} and mean concentration of water within the film \bar{C} , i.e., $\bar{D}\bar{C}$, plotted as a function of the water activity coefficient within the blister (a_1). Results for different substrate-film pairs showed that $\bar{D}\bar{C}$ increased only slowly with a_1 at low values of a_1 (less than 0.8), but rapidly for higher values, as the blister filled with water. A comparison was made between results for free films and attached films. Within experimental error it was found that substantially equivalent results were obtained. The authors took this as evidence that the overpressure P_k was negligible in comparison to the osmotic pressure $\Delta\pi$.

Blister Formation and Growth

This paper considers osmotically driven blister growth in the absence of corrosion. For corroding systems the results obtained can be considered to apply at early times, after blister initiation, when oxygen concentrations, and pH levels have not yet reached levels where corrosion is thermodynamically favored [16], or where it has not actually begun. Blistering is considered to initiate at the metal-substrate interface at weak spots randomly distributed over the substrate surface. These can be rough spots, spots with high impurity ion concentrations, or places with incipient adhesion loss. The weakest spots are ones where blisters will first initiate. Blister growth occurs when there is sufficient water present in the vicinity of the metal substrate. With time, the blisters may enlarge to a point where adjacent blisters coalesce. This can lead to complete detachment of the coating from the substrate. This paper is restricted to an examination of the growth of a single blister.

Foreign ions are presumed to be present already at the substrate-film interface as either a locally high spot of impurity or uniformly distributed over the surface of the substrate. Further, water transport to the blister is not limited by film adhesion or stiffness [9] and blisters grow solely by osmosis. The presence of salt contamination at the substrate surface causes a water activity difference between the outside and the interface. This difference induces an osmotic pressure potential causing water to flow from the outside towards the interface. When water has first penetrated to the substrate surface, it mixes with impurity ions present there and small liquid cells of locally high concentration form. Impurity anions, e.g., Cl^- , $\text{SO}_4^{=}$ and HSO_4^- , cannot diffuse out through the coating, which now acts as a semipermeable membrane. Alkali pigments can supply additional species to the ion pool within the blister, and cations, such as Na^+ and K^+ can be leached from glass, stone, or concrete substrates. As a result the osmotic pressure rises and more water diffuses into the cells, gradually enlarging them. In regions where the adhesion between the coating and the surface is poor, or where the concentration of impurity is especially high, the coating can disbond from the metal substrate and a blister can form. The blister continues to enlarge but at a slower rate as the solution is diluted and the osmotic pressure drops. The enlarging blister can also expose additional amounts of surface impurity ions.

Blister initiation and growth are coupled with the processes of adsorption, absorption, and diffusion of penetrants occurring within the organic coating. Adsorption occurs by water uptake in the existing pores. Adsorption occurs by water uptake by the binding sites. Unlike absorption, it can be accompanied by heat release and swelling. Most water uptake in paints and polymers occurs by sorption. The interaction of sorption and diffusion processes depends on both time and distance scales. Thus, if blister initiation and growth is relatively slow compared to the time taken for water to diffuse to the interface, then blisters are more likely to form because of the proximity of water to the surface. The diffusion path for water will be much less than the thickness of the coating and diffusion times will be considerably shortened. If, on the other hand, blister growth is inherently faster than the diffusion rate of water, water will be drawn into the blister from the surface of the coating. The observed rate of blister growth will then be controlled by the uptake and diffusion rates of water. Diffusion of water through the film appears to occur relatively rapidly [5, 6, 10, 17], on a scale considerably faster than the growth of blisters. So although initial formation of blisters may be limited by the local availability of water, by the time blisters begin to grow, there is ample water in their vicinity. In addition, with only a few small blisters, there is minimal demand for more water.

In the models developed in this paper, impurity ions are considered to be either concentrated at specific spots on the surface where blister initiation occurs, or spread uniformly over the whole surface. Figure 1 depicts the two cases. With a uniform distribution of impurity, blister initiation still takes place over weak spots on the surface, but as the blister enlarges, new impurity ions are introduced at the periphery. In both models, it is presumed that adhesion loss and the stiffness of the organic coating do not control the rate of blister growth, so that the effect of the overpressure created by tension in the disbonding film can be neglected [15]. Thus, adhesion loss is considered to be an effect rather than a cause. At later times, the osmotic pressure may fall to the point that the adhesion in the film cannot be overcome. At this point blister growth will stop. It is also assumed that the coating itself contains no impurities that may migrate and change ion concentrations outside the film in the external solution or within the blister itself.

Analysis of Blister Growth

The analysis of the growth of a blister on a substrate beneath an organic coating is based upon a modified Fick's Law for diffusion which takes the flux of water N to be proportional to the product of the effective diffusivity \bar{D} through the coating, the average concentration of water in the coating \bar{C} and the gradient of the logarithm of the water activity coefficient ($d \ln a/dz$) across the coating between the external environment and the interior of the blister [8]:

$$N = -\bar{D}\bar{C} \frac{d \ln a}{dz} \quad (1)$$

Figure 1a depicts the profile of a single blister having the shape of a spherical segment. The contact angle is Θ , the base radius r , and h is the blister height. The contact angle (angle formed between the blister and the flat surface) is assumed to remain constant while both r and h increase as the blister enlarges [15]. The water activity coefficient in the external environment above the free surface is denoted by a_2 ($a_2 = 1$ for pure water). The distance z is measured normal to the coating from the surface. The blister is assumed to remain small relative to the coating thickness ($h \ll L$). This remains true for the initial and middle stages of blister growth. In later stages of growth, the blister may enlarge to the point where its size approaches or exceeds the

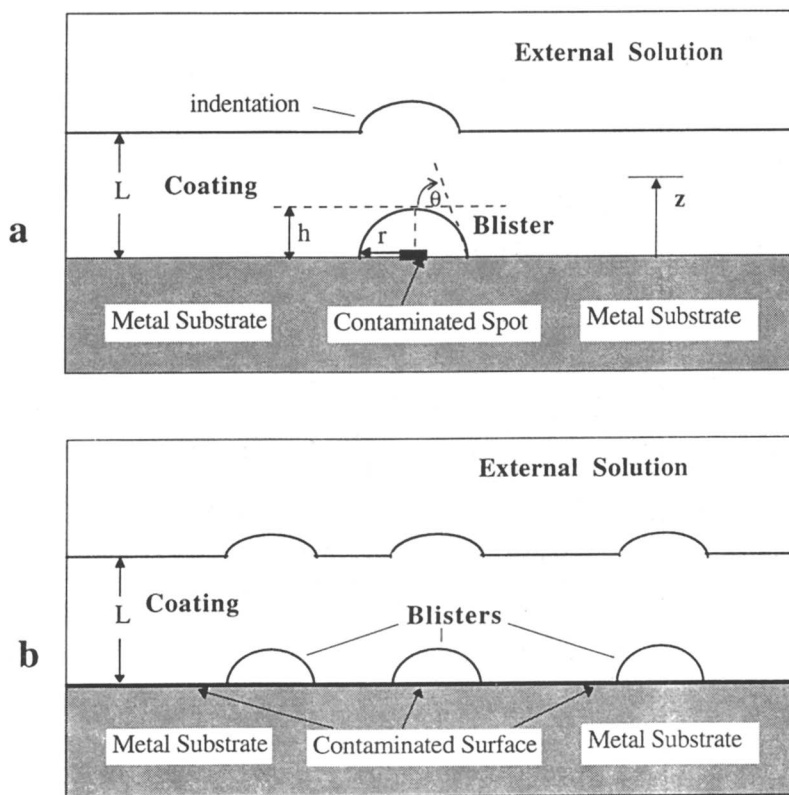


Figure 1. Schematic of blisters on coating surface
a: concentrated impurity, b: uniform distribution

initial film thickness L . In this event, the models presented in this paper may no longer apply.

It can be shown [18] that $d \ln a / dz$ is proportional to the concentration gradient of impurity ion, i.e., (dm/dz) , where m is expressed as moles solute/liter solvent, so that:

$$N = \frac{\overline{DC\phi}}{\ell} \frac{\overline{M}}{1000} \nu \Delta m \quad (2)$$

where:

- m is the concentration of impurity ion
- ℓ is the diffusion path length
- ν is the number of ions formed from one molecule of impurity ion (valency)
- \overline{M} is the solvent molecular weight
- $\overline{\phi}$ is the mean molar osmotic coefficient

The dimension ℓ represents a characteristic diffusion length. In cases where water must be drawn from the external environment, $\ell = L$, the coating thickness. When water is already present as a result of the molecular diffusion process then $\ell = \delta$, where δ represents a characteristic film thickness ($\delta \ll L$) for the diffusion process. With little diffusional resistance, water in the vicinity of the blister would pass freely across the mantle surface and blister growth would be rapid. Equation (2) is based on constant values for D , C and ϕ . These can be considered as average or mean values over the film [15, 19], as denoted by the overbar. The multiplier of Δm on the right hand side of equation (2) is a constant which will be specific to the kind of impurity ion and coating involved. Δm represents the change in the concentration of the impurity ion between the blister and the outside of the coating. The diffusion process can be viewed as being driven by the osmotic pressure difference, $\Delta\pi$, which exists between the inside of the blister and the external environment. Thus:

$$\Delta\pi = \frac{RT}{\tilde{V}} \ell n \frac{a_2}{a_1} = \left(\frac{RT}{\tilde{V}} \frac{\nu \overline{M\phi}}{1000} \right) \Delta m \quad (3)$$

where:

- R is the gas constant
- T is the absolute temperature
- \tilde{V} is the partial molar volume of the solvent in the blister

For most salt solutions, it is reasonable to take \tilde{V} constant and equal to C_1 , the molarity of water. When no impurity ions are present in the external solution outside the coating, then $a_2 = 1$ and $\Delta m = m$. As the blister becomes diluted with water, a_1 rises, the osmotic pressure within the blister drops, and the diffusion process slows.

Concentrated Spots of Impurity. When dissolved impurity ions such as chloride or sulfate are present at a surface together with a sufficient amount of water, then blister initiation and growth occurs. Consider the surface to have a small spot where a high concentration of impurity ions are located, as shown schematically in Figure 1a.

A water balance equates the increase in mass of water within the blister to the amount which fluxes through the mantle (curved) surface:

$$\rho \frac{dV}{dt} = \frac{dM}{dt} = \bar{M} S N \quad (4)$$

where:

ρ is the density of water within the blister
 V is the volume of the blister
 M is the mass of water within the blister
 S is the mantle (curved) surface area

If the dissolution rate of hygroscopic impurity ions is high when compared to the time scale for water diffusion, the dissolution is effectively complete before much water has had a chance to penetrate the blister and the concentration of impurity ions within the blister can be expressed directly as:

$$m = \frac{1000}{M} N_s \quad (5)$$

Here N_s is the moles of salt contained within the blister. Taking the case where no impurity ions are present outside the film ($\Delta m = m$), and substituting equations (2) and (5) into equation (4):

$$\frac{dV}{dt} = \frac{N_s}{C_i^2} \frac{\overline{DC\theta}}{\ell} v \frac{S}{V} \quad (6)$$

This equation predicts blister growth rates that are directly proportional to mantle surface area and inversely proportional to size. It applies to a blister of any shape, e.g., spherical or ellipsoidal segments, such as were observed by van der Meer-Lerk and Heertjes [7]. When the contact angle is not constant (most likely during the initial stages of growth), the theory developed here can be extended to cover these cases. Equation (6) can be integrated numerically, if (θ, r) , (θ, h) , or (r, h) vs. time data are available.

For blisters having the shape of the segment of a sphere (spherical cap), equation (6) can be integrated to give the blister dimensions, surface area and volume as functions of time:

$$r = k_r \left[(1 + 1/2 \cos \theta)^{-2} (1 - \cos \theta)^{-3} \right]^{1/4} \sin \theta \quad t^{1/4} \quad (7)$$

$$h = k_r \left[(1 + 1/2 \cos \theta)^{-2} (1 - \cos \theta) \right]^{1/4} t^{1/4} \quad (8)$$

$$S = 2\pi k_r^2 \left[(1 + 1/2 \cos \theta)^{-2} (1 - \cos \theta)^{-1} \right]^{1/2} t^{1/2} \quad (9)$$

$$V = 2/3 \pi k_r^3 \left[(1 + 1/2 \cos \theta)^{-2} (1 - \cos \theta)^{-1} \right]^{1/4} t^{3/4} \quad (10)$$

where:

$$k_r = \left[\frac{6 N_s}{\pi C_i^2} \frac{\overline{DC\phi}}{\ell} v \right]^{1/4} \quad (11)$$

Details of the derivation of these equations are provided in the Appendix. As stated, the derivation is based on the assumption that the contact angle θ remains constant throughout blister growth [9]. For hemispherical blisters, where $\theta = \pi/2$, all of the angle dependent terms become unity and the equations simplify to previous results [8].

Equation (10) predicts that the blister volume increases as the 0.75 power of time. It also predicts that the rate of blister growth slows with time, being greater at the beginning when the blister is small and contains a concentrated salt solution, and less later when the solution in the blister has become diluted with water.

The osmotic pressure $\Delta\pi$ for concentrated spots of impurity is obtained by combining equations (3), (5) and (10):

$$\Delta\pi = \frac{3RT}{2} C_i^{3/2} \left[\frac{v\bar{\phi}}{\pi} (1 + 1/2\cos\theta)^2 (1 - \cos\theta) \right]^{1/4} \left(\frac{6\overline{DC}}{\ell} \right)^{-3/4} N_s^{1/4} t^{-3/4} \quad (12)$$

Equation (12) predicts that the osmotic pressure varies as the 0.25 power of the amount of salt in the blister and reciprocally with the 0.75 power of time.

Uniform Distribution of Impurity. The second type of blister growth model considers the impurity ion to be uniformly spread across the surface, as shown for several non-interacting blisters in Figure 1b. For the growth of a single blister, this differs from the previous model in one important aspect - as the blister grows, fresh impurity enters through its base. In this case the amount of impurity ion added to the blister N_s is proportional to the (flat) base area of the blister A:

$$N_s = k' A \quad (13)$$

The proportionality constant k' is equal to the surface concentration of impurity ions, mol/cm². For blisters having the shape of the segment of a sphere $A = \pi r^2$.

As in the previous development, it is presumed that the rate of dissolution of impurity ions into the blister is rapid compared to the rate of blister growth. Here, however, N_s will no longer be constant, since, as the blister peels from the surface, exposed impurity ions rapidly transfer into solution. By substituting equation (13) and equation (8) into equation (6), with $\Delta m = m$, it follows that:

$$\frac{dV}{dt} = k' \frac{\overline{DC\phi}}{\ell C_i^2} v \left(\frac{SA}{V} \right) \quad (14)$$

Equation (14) shows that for uniform distribution of impurity the blister growth rate is directly proportional to the mantle surface area, to the base area of the blister and inversely proportional to blister size. It applies to a blister of any shape. Using the expressions for r , S and V provided in the Appendix, equation (14) can be integrated to give the blister dimensions, areas, and volume as functions of time:

$$\mathbf{r} = \mathbf{k}'_r \left[(1 + \cos \theta) (1 - \cos \theta)^{-1/2} (1 + 1/2 \cos \theta)^{-1} \right] \mathbf{t}^{1/2} \quad (15)$$

$$\mathbf{h} = \mathbf{k}'_r \left[(1 + \cos \theta)^{1/2} (1 + 1/2 \cos \theta)^{-1} \right] \mathbf{t}^{1/2} \quad (16)$$

$$\mathbf{A} = \pi \mathbf{k}'_r{}^2 \left[(1 + \cos \theta)^2 (1 - \cos \theta)^{-1} (1 + 1/2 \cos \theta)^{-2} \right] \mathbf{t} \quad (17)$$

$$\mathbf{S} = 2\pi \mathbf{k}'_r{}^2 \left[(1 + \cos \theta) (1 - \cos \theta)^{-1} (1 + 1/2 \cos \theta)^{-2} \right] \mathbf{t} \quad (18)$$

$$\mathbf{V} = 2/3 \pi \mathbf{k}'_r{}^3 \left[(1 + \cos \theta)^{3/2} (1 - \cos \theta)^{-1} (1 + 1/2 \cos \theta)^{-2} \right] \mathbf{t}^{3/2} \quad (19)$$

where:

$$\mathbf{k}'_r = \frac{\mathbf{k}'}{\mathbf{C}_i^2} \frac{\overline{\mathbf{DC}\phi}}{\ell} \nu \quad (20)$$

Again, these equations apply when the contact angle is constant, and reduce to previously derived models for hemispherical blisters [8].

The osmotic pressure for a uniform distribution of impurity is given by:

$$\Delta\pi = \sqrt{\frac{3}{2}} \mathbf{RTC}_i \left(\frac{\mathbf{k}' \ell}{\mathbf{DC}} \nu \right)^{1/2} (1 + \cos \theta)^{1/2} \mathbf{t}^{-1/2} \quad (21)$$

The osmotic pressure does not fall as rapidly in this case because of the continual infusion of salt into the growing blister.

Results and Discussion

Figure 2 presents a logarithmic plot of blister volume V (in μm^3) vs. exposure time (in days). Data were taken from the paper of van der Meer-Lerk and Heertjes [7] for concentrated spots of KHSO_4 having three different initial masses. According to equation (10) the lines should have a slope of 0.75. However a slope of 0.5 fits most of the data well. Since the blister volume can be expressed as $V = k_v t^n$, where $n = 1/2$, the value of k_v , the volumetric growth constant, is found from the intercept of each of the lines in Figure 2. Figure 3 shows a log plot of k_v vs. the mass of KHSO_4 , M_s . The slope of this plot is 1.1 indicating that k_v is nearly proportional to the mass (or moles, N_s) of salt contained within the blister. The model for a concentrated spot of impurity predicts that $k_v \sim N_s^{3/4}$. Thus, theory predicts that $V \sim N_s^{3/4} t^{3/4}$, whereas the experiments give $V \sim N_s t^{1/2}$. So for a fixed amount of salt, blisters grow at a slower rate than predicted, but at any fixed time using more salt results in higher rates of blister growth than is predicted by theory. Blister growth is generally slow enough that it is not limited by the availability of water. However, at longer times lower growth rates would result if the osmotic pressure fell to the point where it approached the disbonding pressure. Lower growth rates would then be the result of increasing film stiffness as the film resisted further disbondment. On the

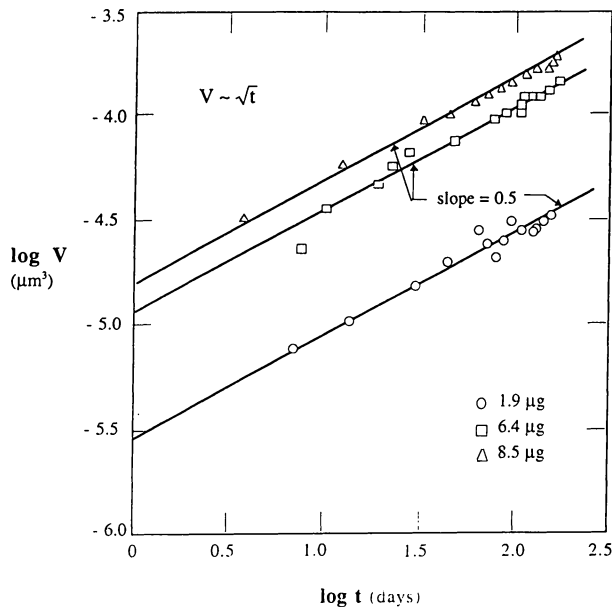


Figure 2. Blister volume (μm^3) vs. time (days) [logarithmic plot]

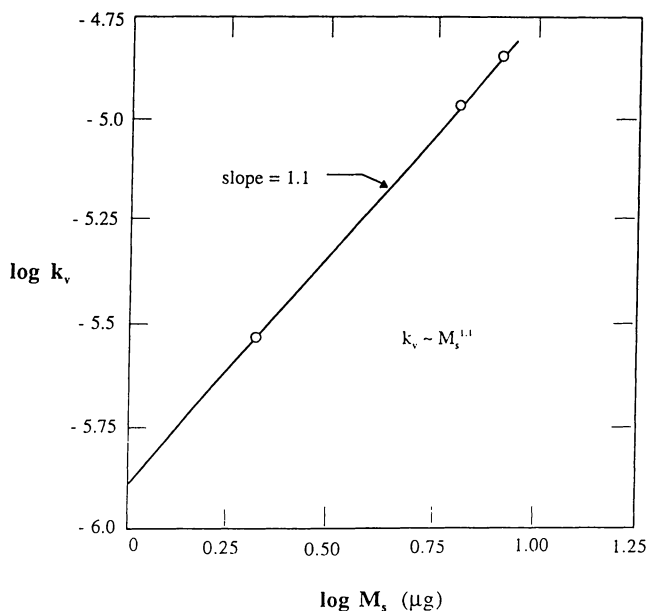


Figure 3. Volumetric growth constant (k_v) vs. mass of impurity (μg) [logarithmic]

other hand, higher blister growth rates may be due to the gradual leaching of water soluble species to the interface as reported by Walkér [20]. Then the concentration of ions in the blisters would be higher, which would drive water faster from the outside to the interface.

Although the exponents are not precisely equal to the theoretical values, these results show that dimensions and rate constants for blister growth can be expressed as simple power law functions of exposure time. Lower growth rates are expected if the blister initially grew very rapidly to the size of the salt patch, or if the concentration within the blister remained constant at the start until all the KHSO_4 had dissolved. With $m = m^*$, the saturation concentration, the volumetric growth rate dV/dt would vary directly as t^2 rather than t until m fell below m^* . At that point (time t_0 , with base radius r_0) growth rates would slow and blister size could be predicted by integrating equation (A - 5), with $r = r_0$ at $t = t_0$. This procedure would handle any case where the initial blister size was not zero, or where such a mechanism shift occurred.

In many cases, the salt spot on the surface is present as a small patch or ring. With the availability of water, surface diffusion gives a more or less uniform salt content over the patch. (It is likely that the center of such a spot has a slightly higher salt concentration so that blister initiation is favorable there.) The model developed for uniform salt distribution is applicable until the blister has grown to the size of the patch, after which the model for concentrated salt distribution applies. At this time, the blister growth rate would abruptly decrease. The experimental data [7, 15] do not show a break in slope, but data were not collected at early times where such a mechanism would be most likely. Both models have the same mathematical form - the radius, surface area and blister volume all vary directly as the time raised to various fractional powers. Comparing model solutions for concentrated impurity distribution with those found for uniform salt distribution predicts that the blister size increases more rapidly with a uniform salt distribution.

For both models, the osmotic pressure is predicted to fall with time as the solution within the blister becomes diluted with water. The models predict an infinite osmotic pressure at time zero. In actuality, the highest osmotic pressure would be one corresponding to the saturation value of the impurity salt in water. The osmotic pressure drops most rapidly when the salt is initially concentrated within the blister rather than being uniformly spread across the substrate. When all the salt is concentrated within the blister, the initial osmotic pressure is much greater than when the salt is uniformly distributed. For uniform salt distributions, osmotic pressure is not predicted to fall as fast because fresh salt is being added at the periphery of the blister. It is best to compare osmotic pressures based on the availability of the same total amount of salt to the blister.

The results of this study can be extended to consider the growth of a field of blisters and to situations where blister formation and growth is coupled with corrosion reactions.

Nomenclature

a_1	water activity coefficient within blister
a_2	water activity coefficient in external solution
A	flat area of blister on metal surface
\bar{C}	mean concentration of water within coating
C_i	concentration of water within blister
D	diffusion coefficient or diffusivity of water in coating
\bar{D}	mean value of D

h	height of blister
k_r	rate constant for blister radius growth
k_v	volumetric growth rate constant for blister volume
k'	surface concentration of impurity ions, based on area
ℓ	effective diffusion path length
L	thickness of coating or film
m	concentration of impurity ion
m^*	saturation value of m
M	mass of water in the blister
M_s	mass of salt present within blister
\bar{M}	solvent molecular weight
\bar{M}_s	salt molecular weight
N	diffusive flux
N_s	moles of salt present within blister
P_k	film pressure
r	radius of base of blister
R	gas constant
S	surface area of blister mantle
t	time
T	absolute temperature
V	volume of blister
\tilde{V}	solvent partial molar volume
z	depth into coating measured from coating-substrate interface

Greek Letters

$\Delta\pi$	osmotic pressure within blister
ν	number of ions formed from one molecule of impurity ion (valency)
$\phi, \bar{\phi}$	molar osmotic coefficient, mean value
ρ	density of water within blister
θ	contact angle

Appendix

Consider a blister having the shape of the segment of a sphere or spherical cap as depicted in Figure 1a. The contact angle, blister height and radius of the base are related by:

$$\frac{h}{r} = \tan(\theta/2) = \frac{1 - \cos \theta}{\sin \theta} \quad (\text{A-1})$$

Equation (A-1) shows that, if the contact angle remains constant during blister growth, there is a simple proportionality between h and r . van der Meer-Lerk and Heertjes [9, 15] found that the contact angle was constant, except at the beginning of their experiments.

The blister volume and mantle surface area S are given by:

$$V = \frac{\pi h^3}{6} \left[1 + 3 \left(\frac{r}{h} \right)^2 \right] \quad (\text{A-2})$$

$$S = \pi h^2 \left[1 + 3 \left(\frac{r}{h} \right)^2 \right] = \frac{2\pi r h}{\sin \theta} = \frac{2\pi r^2}{1 + \cos \theta} \quad (\text{A-3})$$

Combining equations (A-1) and (A-2):

$$V = \frac{2}{3} \pi r^3 \frac{[1 - 3/2 \cos \theta + 1/2 \cos^3 \theta]}{\sin^3 \theta} \quad (\text{A-4})$$

Equation (A-4) has been used to calculate contact angles for small droplets based on experimental measurements of V and r [21].

For concentrated spots of impurity, equation (6) is used. dV/dt is found in terms of r by differentiating equation (A-4), with the contact angle held constant, while S/V is expressed as a function of r using equations (A-3) and (A-4). This leads to:

$$r^3 \frac{dr}{dt} = \frac{3 N_s \overline{DC\phi}}{2\pi C_i^2 \ell} v \frac{\sin^6 \theta}{(1 - 3/2 \cos \theta + 1/2 \cos^3 \theta)^2} \frac{1}{1 + \cos \theta} \quad (\text{A-5})$$

Integration of equation (A-5) with $r = r_0 = 0$ at $t = 0$, leads to equation (7). Expressions for h , S and V (equations 8, 9 and 10) follow directly by substituting equation (7) into equations (A-1), (A-3) and (A-4), respectively.

For uniform distribution of impurity, equation (14) is used. As before dV/dt and S/V are expressed as functions of r , while $A = \pi r^2$. With the assumption that the contact angle remains constant, this leads to:

$$r \frac{dr}{dt} = \frac{3 k' \overline{DC\phi}}{2 C_i^2 M_s \ell} v \frac{\sin^6 \theta}{(1 + \cos \theta)(1 - 3/2 \cos \theta + 1/2 \cos^3 \theta)^2} \quad (\text{A-6})$$

Integration of equation (A-6) with $r = r_0 = 0$ at $t = 0$, leads to equation (15). Expressions for h , A , S and V follow directly.

References

1. Brunt, N.A., *JOCCA*, **47**, 31, (1964)
2. Funke, W., "Toward a Unified View of the Mechanism Responsible for Paint Defects by Metallic Corrosion," *Ind. Eng. Chem. Prod. Res. Dev.*, **24**, 343-347 (1984).
3. Hansen, C.M., "New Developments in Corrosion and Blister Formation in Coatings," *Prog. in Org. Coat.*, **26**, 113-120 (1995).
4. Martin, J.W., Embree, E., and Tsao, W., "Non-Osmotic Defect Controlled Cathodic Disbondment of a Coating from a Steel Substrate," *J. Coat. Tech.*, **62** (790), 25 (1990).
5. Ritter, J. J., and Kruger, J., "Studies on the Sub-Coating Environment of Coated Iron Using Qualitative Ellipsometric and Electrochemical Techniques," *Surface Sci.* **96**, (1980).
6. Nguyen T., Bentz, D., and Byrd, E., "Method for Measuring Water Diffusion in a Coating Applied to a Substrate," *J. Coat. Tech.*, **67** (844), 37-46 (1995).
7. van der Meer-Lerk, L.A., and Heertjes, P.M., "Blistering of Varnish Films on Substrates Induced by Salts," *JOCCA*, **58**, 79-84, (1975).

8. Pommersheim, J., Campbell, P., and McKnight, M., "The Mathematical Modeling of the Corrosion Protective Performance of Organic Coatings", National Bureau of Standards Technical Note 1150, September, (1982).
9. van der Meer-Lerk, L.A., and Heertjes, P.M., "The Influence of Pressure on Blister Growth", P. M., IOCCA, **64**, 30-38, (1982).
10. "Barrier Polymers", Encyclopedia of Polymer Science and Technology, Supplementary Volume 1, 1976.
11. Leidheiser, H., and Kendig, M. W., "The Mechanism of Corrosion of Polybutadiene-Coated Steel in Aerated Sodium Chloride", Corrosion - NACE, **32** (2), 69-76, (1976).
12. Leidheiser, H., and Wang, W., "Some Substrate and Environmental Influences on the Cathodic Delamination of Organic Coating" J. Coat. Tech., **53** (672), 77-84, (1981).
13. Thomas, D., "Initial Degradation of Corrosion Protection by Organic Coatings," Proceedings of the Second International Conference on the Durability of Building Materials and Components, September (1981).
14. Nguyen, T., Hubbard, J., and Pommersheim, J., "Unified Model for the Degradation of Organic Coatings on Steel in a Neutral Electrolyte," J. Coat Tech., **68** (855), 45-56 (1996).
15. van der Meer-Lerk, L.A., and Heertjes, P.M., "Mathematical Model of Growth of Blisters in Varnish Films on Different Substrates," IOCCA, **62**, 256-263, (1979).
16. Uhlig, H. H., Corrosion and Corrosion Control, 2nd edition, John Wiley & Sons, Inc., New York, (1971).
17. Crank, J., and Park G. S., Diffusion in Polymers, Academic Press, New York, (1968).
18. Kemp, M. W., Physical Chemistry, Marcel Dekker, Inc., New York (1979).
19. Robinson, J. M., and Stokes, R. H., Electrolyte Solutions, 2nd edition, Butterworth, London, (1970).
20. Walker, P. "The Effect of Water on the Adhesion of Surface Coating", Official Digest, **12**, 156, (1965).
21. Matijevic, E., (ed.), "Wettability and Contact Angles", in Surface and Colloid Science (Vol. 2), Wiley-Interscience (1969).

Chapter 12

Initial Studies of Electrochemical Comparison of Coating Performance in Flowing versus Stationary Electrolyte

Carol S. Jeffcoate and Gordon P. Bierwagen

Department of Polymers and Coatings, North Dakota State University,
Fargo, ND 58105

Electrochemical impedance spectroscopy (EIS) and electrochemical noise methods (ENM) were used to evaluate the corrosion protection performance of 3 different organic marine coatings (combinations of an alkyd (A), a zinc silicate (Z) and a green epoxy (G) as primers and two top coats were a haze gray epoxy (H) and a silicon alkyd (S).) over mild steel in both static immersion and flowing electrolyte conditions. The calculation of noise resistance (R_n) was made using 3 different set sizes from the accumulated raw data, where the sample set of 40 raw data points gave the best results. The flowing electrolyte has a marked effect upon the performance of a coating system. For the coating systems tested the R_n and low frequency impedance values were significantly lower in the flowing cells, when compared with the values obtained from similar panels in a 'stationary' electrolyte.

Electrochemical methods have long been utilized to assess the corrosion protective performance of coatings. Although the earlier work was with DC resistance (I), recent work has concentrated on more sophisticated techniques(2, 3, 4). The methods used in this study are electrochemical noise measurement (ENM)(5, 6, 7) and electrochemical impedance spectroscopy (EIS)(8, 9).

The primary advantage of ENM is that it is a non perturbing technique i.e. the spontaneous current and voltage fluctuations are measured between two nominally identical panels, with no external potential or current applied(7). The method can be applied as a semi-continuous monitoring technique and with time gives an indication of the overall coating performance. EIS gives more detailed information about the coatings electrical properties but at the sacrifice of perturbing the electrochemical system by applying a scan of AC potentials over a range of frequencies(9).

This work has been designed to test typical marine coating systems for corrosion protection performance in a laboratory environment. The function of a marine coating is two fold. The primary requirement for a coating, of this type, is to provide corrosion resistance. The coating is the primary method for corrosion protection with cathodic protection being used as a secondary method(10). Another function of marine coatings is to provide anti-fouling protection(11, 12). Fouling from animal and vegetable matter is a matter of considerable concern. The increased drag through water causes a drop in maximum speed and efficiency for a given vessel. Environmental restrictions on chromate pretreatment and anti fouling chemicals has spurred on the search and developments of new environmentally compliant coating systems. All new coatings require extensive preliminary laboratory testing and, ultimately, very expensive marine exposure evaluations. Marine exposure, despite the extreme cost, is a very necessary part of the final evaluation.

In an attempt to have a more 'realistic' laboratory assessment, the flowing electrolyte has been added to the testing scheme. The typical laboratory test set-up includes a conductive electrolyte (usually containing chloride) in 'stationary' contact with the test panels. This work investigates, via electrochemical testing the effect of a flowing electrolyte on the degradation of marine coatings.

Experimental

Sample Preparation

The test samples were three layer marine coatings on mild steel. The layers were combinations of three primers: an alkyd (A), a zinc silicate (Z) and a green epoxy (MIL-P 24441 type 1 F-150) (G). The two top coats were a haze gray epoxy (MIL-P 24441 type F-151) (H) and a silicon alkyd (S). Each of the three layers were of approximate equal thickness and gave an average total coating thickness of $200 \pm 10 \mu\text{m}$. The primer/topcoat combinations tested in this investigation were (from substrate interface to electrolyte) AAS, ZAS and GHS. The GHS and AAS combinations were chosen as typical barrier type marine coating systems currently in service. The zinc silicate in the ZAS system works mainly by a sacrificial mechanism, and is non-common for this application. The electrical contact was made through wires which were attached to the test samples. The back and edges of each sample were coated with a colophony rosin / beeswax mixture (3/1) to act as an effective inert, high resistance protective coating. The exposed surface area of the test panel was 50 cm^2 (0.005 m^2).

Cell Design

For both the flowing and the stationary electrochemical cell, a solution of 3% sodium chloride (NaCl, analytical grade) in distilled deionized water was used as the conductive electrolyte. Solutions in both cells were open to the laboratory air and changed monthly to minimize algae growth. The reference electrode for ENM was a saturated Calomel electrode, and for the EIS measurements a platinum secondary electrode was also used.

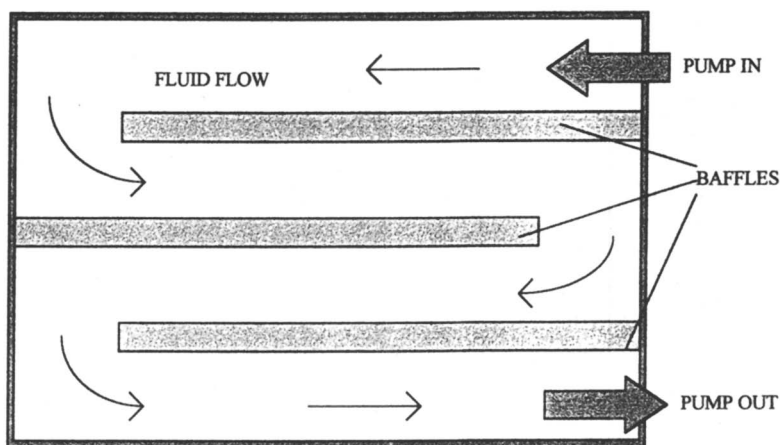


Figure 1 Schematic of the flowing electrolyte electrochemical cell, showing the baffles and fluid flow pattern.

The cell containing the flowing electrolyte was constructed from a 35x25x25 cm high density polyethylene (HDPE) tank with three, 26 cm baffles to obtain a total path length of approximately 95 cm, as shown in figure 1. A constant volume of 10 liters of electrolyte was maintained and a pump circulating at 35 liters/minute provided a flow rate of approximately $0.055\text{m}\cdot\text{s}^{-1}$ ($3.33\text{m}\cdot\text{min}^{-1}$), ensuring laminar flow over the surface of the samples. The stationary electrolyte electrochemical cell consisted of a circular glass dish 18 cm in diameter and 10 cm deep with sufficient electrolyte to cover the exposed surface of the samples. A slotted polystyrene sheet held the samples in position vertically (the pairs facing each other, with a gap of 2cm between them). For the flowing electrolyte cell, the electrochemical measurements were taken after the pump was switched off and flow stopped.

Sample Pairing for Noise Studies

Three nominally identical panels of each of the three types of paint system were immersed into the flowing cell. By cross pairing sample the three panels of each type, it was possible to maximize the number of possible electrode pairs. By cross pairing the three single panels (A, B, C) this allowed three pairs of panels for the electrochemical noise (ENM) studies (AB, AC, BC) for statistical validity.

Experimental Methodology

EIS and ENM measurements were taken right after immersion in the test cells and then at recorded intervals during the immersion time. The fluid pump was switched off during measurements to ensure static conditions.

ENM measurements on the nominally identical panels (paired by AB, AC, BC) were taken on first immersion and at intervals of 15 to 20 days during the extended exposure. Sample acquisition rate for the simultaneous raw potential and raw current data was every 2 seconds (0.5 Hz). The noise resistance (R_n) was calculated using the

standard deviations of the raw potential (σ_v) and the raw current noise (σ_i) as in equation 1.

$$R_n = \frac{\sigma_v}{\sigma_i} \quad (1)$$

Calculations of the standard deviation were made by taking 10, 40 and 128 raw data points and variations in the resultant R_n values recorded.

For the EIS measurements the frequency range was from 65500 to 0.02 Hz and the applied AC voltage was 10 mV RMS.

Results and Discussion

Electrochemical Noise Method

The variation of raw data sample size, i.e. the number of raw data points used to calculate the standard deviation of the simultaneously measured current and potential values, for the calculation of R_n gave varying results, an example of which is given in table I. The smaller sample size of 10 raw data points taken over a time period of 20 seconds gave, at several time intervals, a divide by zero error, i.e. a steady state current was measured over a 20 second sampling period therefore producing a zero standard deviation. The variable R_n observed for the 128 raw data point (taken over 256 seconds) sample size is worthy of caution because the σ_v and σ_i values may be artificially high due to any uncorrected DC drift occurring during the measurement time-span. Therefore a raw data sample size of 40 (taken over 80 seconds) data points was chosen for the calculation of R_n , to minimize the effect of DC drift and divide by zero errors.

Table I Typical noise resistance values for AAS pair 1, calculated using the standard deviation of 10, 40 and 128 raw data points.

Days	R_n , σ of 10 Data Points	R_n , σ of 40 Data Points	R_n , σ of 128 Data Points
0	Divide by Zero Error	1.22×10^{11}	1.28×10^{11}
4	3.25×10^7	3.20×10^7	3.19×10^7
10	3.32×10^7	3.16×10^7	2.90×10^7
25	2.26×10^7	2.25×10^7	2.17×10^7
42	Divide by Zero Error	2.35×10^7	2.83×10^7
66	7.09×10^6	1.17×10^7	1.37×10^7
76	5.18×10^5	2.12×10^5	2.19×10^5

The noise resistance (R_n) vs. time (130 days) plots for all sample pairs immersed in the flowing electrolyte is shown in figures 2 and 3. The trend of R_n for the three samples of each coating type is shown to be very reproducible. The alkyd (AAS) samples show an initial drop of R_n followed by a reasonably steady state reading for the majority of the exposure period. A slight, further, decrease is seen in all the pairs after 96 days. Epoxy sample pairs showed a similar trend. An initial very high value of R_n sharply decreased from 1.1×10^{10} to $6.8 \times 10^8 \Omega \text{cm}^2$ after 10 days of immersion, followed by a relatively constant R_n value for 60 days. The rapid decrease in R_n observed in all the sample systems, on initial immersion, is due to water uptake and consequent swelling of the films. The last of the test systems, ZAS, exhibited slightly different behavior. The initial, immersion, value of R_n ($4.8 \times 10^7 \Omega \text{cm}^2$) was lower with a sharp decrease to R_n values close to values expected for a bare steel electrode after 10 days of immersion.

A similar effect is observed with the samples immersed in the stationary electrolyte. Average R_n values vs. time plots for samples in the stationary electrolyte is shown in figure 4. On immersion in the stationary electrolyte all the coating types exhibited high values of R_n , in the range of $10^9 - 10^{11} \Omega \text{cm}^2$. The AAS samples maintained a high R_n value, above $10^8 \Omega \text{cm}^2$, for the duration of the test. The GHS also maintained the average R_n value above $10^8 \Omega \text{cm}^2$ for the monitoring time. ZAS again proved to be the exception, showing a large drop in R_n value after only 10 days of immersion. After the 70 day immersion time the R_n value dropped further to $10^5 \Omega \text{cm}^2$, similar to that of the flowing electrolyte case.

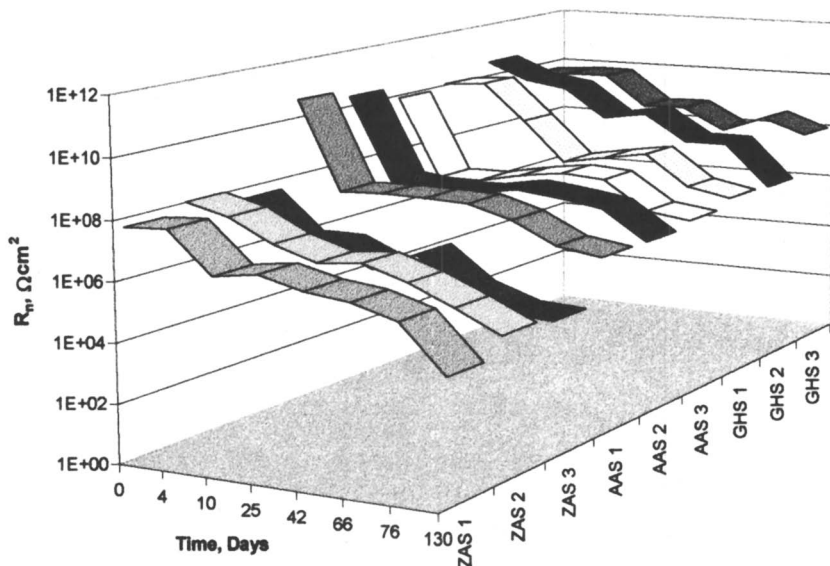


Figure 2 Ribbon graph of noise resistance vs. time, showing the reproducibility between the pairs of panels with identical coatings

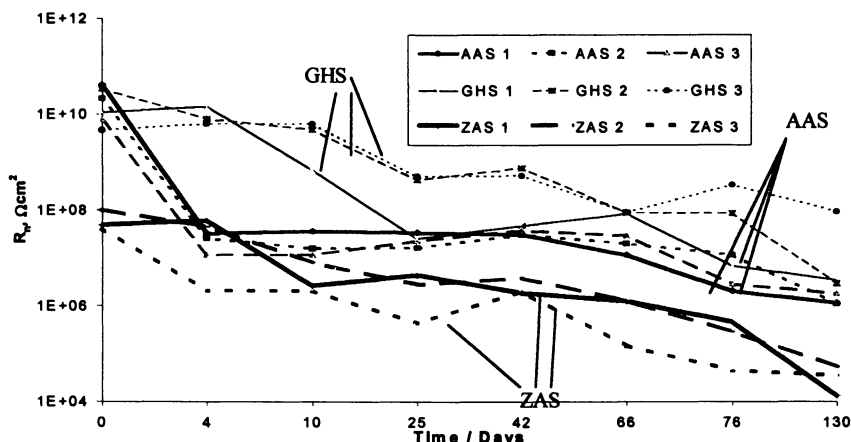


Figure 3 Line graph of noise resistance vs. time, showing the reproducibility between the pairs of panels with identical coatings

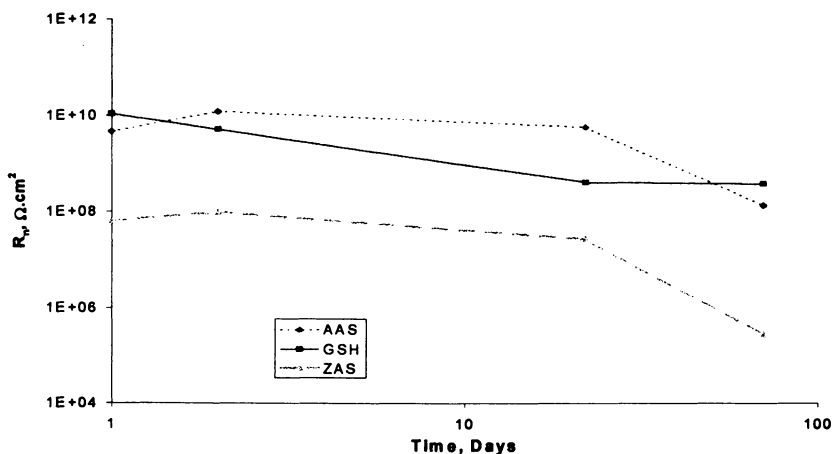


Figure 4 Noise resistance vs. time plot, for the stationary electrolyte electrochemical cell, showing the poor performance of the ZAS compared to the performance of the AAS and GHS panels

It is seen that although the initial (on immersion) R_n values were similar for all three coating systems, for both types of test, the R_n value after a period of 1 month was found to be consistently lower for all samples in the flowing environment. Figure 5 shows a direct comparison of the two cases. Of the three coating systems investigated the most marked difference is seen with the AAS coating system. A variation of nearly three orders of magnitude between the flowing and the stationary R_n values was observed. The GHS samples in the flowing cell showed a drop of R_n values by two orders over the values obtained from stationary electrolyte samples. This reduction in the R_n value for a 'good' coating in the stationary cell re-classifies the coating to 'fair' when the flowing system is considered. The results from both of the ZAS sample sets indicate a presence of conductive pathways to the metal surface. R_n values for both the flowing and stationary electrolyte are shown in table II.

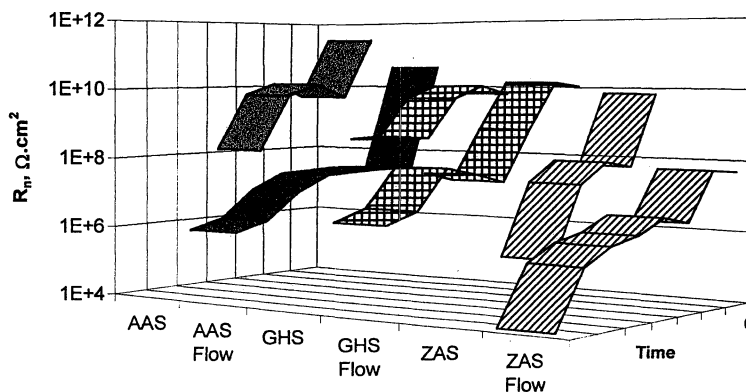


Figure 5 Ribbon graphs showing the difference in noise resistance values for the flowing and the stationary electrolyte electrochemical cell

Table II Average noise resistance values, with time, obtained from the flowing and the stationary electrolyte tests.

	AAS $R_n, \Omega\text{cm}^2$	GHS $R_n, \Omega\text{cm}^2$	ZAS $R_n, \Omega\text{cm}^2$
Stationary on Immersion	2.97×10^{11}	6.11×10^9	6.91×10^9
Stationary after 22 days	5.79×10^9	4.09×10^8	2.69×10^7
Stationary after 70 days	1.33×10^8	3.77×10^8	2.79×10^5
Flowing on Immersion	4.08×10^{10}	1.07×10^{10}	4.82×10^7
Flowing after 25 days	3.42×10^7	2.53×10^7	4.29×10^6
Flowing after 76 days	2.03×10^6	3.4×10^6	1.31×10^4

Electrochemical Impedance Spectroscopy

The impedance spectra were viewed with regard to the shape (one or two time constants) and the value for the maximum stable impedance modulus ($|Z|_{\max}$). The $|Z|_{\max}$ value gives an indication of the barrier properties of the film, the higher this value, the better the barrier type protection for a given coating system.

Monitoring the $|Z|_{\max}$ value over an extended period of time gives observations similar to noise data. Samples in the flowing electrolyte gave values of $|Z|_{\max}$, after an immersion of one month, significantly lower than those obtained from the samples immersed in the stationary electrolyte. Table III lists the $|Z|_{\max}$ values obtained from the EIS measurement for the flowing and the stationary cells.

Table III : Comparison of EIS Data obtained from Stationary and Flowing Electrolytes.

	AAS $ Z _{\max}, \Omega\text{cm}^2$	GHS $ Z _{\max}, \Omega\text{cm}^2$	ZAS $ Z _{\max}, \Omega\text{cm}^2$
Stationary, on Immersion	3.9×10^{10}	7.5×10^9	5.5×10^9
Stationary, after 28 days	2.2×10^7	6×10^9	4×10^6
Stationary, after 96 days	2.0×10^7	2×10^8	7×10^5
Flowing, on Immersion	2.4×10^{10}	2.7×10^{10}	2.8×10^{10}
Flowing, after 35 days	8×10^6	1×10^7	3×10^6
Flowing, after 110 days	3.5×10^5	1.4×10^6	4.2×10^4

The initial $|Z|_{\max}$ values for all the panels were, within an order of magnitude as compared with R_n values obtained from the noise measurements. After immersion in their respective environments for three months the $|Z|_{\max}$ values results from the flowing cell were significantly lower than the values for the stationary electrolyte, shown in figure 6. An exception to this is where the ZAS system, $|Z|$ and R_n values show the same trend in both environments. The ZAS coating system protects the steel substrate by acting in a sacrificial manner. Sacrificial coatings are usually designed and formulated above the critical pigment volume concentration (CPVC) and would therefore be porous in nature. This type of formulation leads to a direct electrolyte connection through the open porous structure of the coating system. As expected, low R_n and $|Z|_{\max}$ values were observed and extensive blistering occurred in both the flowing and stationary electrolyte.

In all there is a good correlation (within an order of magnitude) between the R_n and the $|Z|_{\max}$ values with the exception of the stationary AAS which produced higher R_n values. The flowing environment, although still maintaining laminar flow, is much more aggressive than the stationary cell.

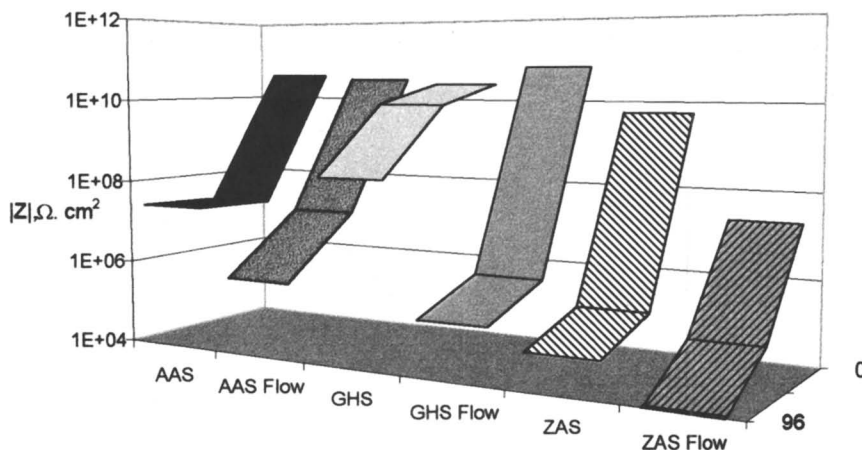


Figure 6 Ribbon graphs showing the difference in impedance modulus values for the flowing and the stationary electrolyte electrochemical cells. As in the previous figure note the large difference in $|Z|_{\max}$ values between the flowing and the stationary electrolyte for the AAS and the GHS systems

Conclusions

When calculating R_n from raw potential and raw current data, the number of data points in the sample size needs to be chosen carefully. An uncompensated DC drift in the potential data results in an artificially high R_n value, conversely a drift in the current signal produces a depressed value of R_n . Too small a sample size, especially for good coating systems, produces divide by zero errors periodically, reducing the effective data size and possibly leads to inaccurate estimations of the coating performance.

The introduction of a flowing electrolyte into an electrochemical experimental set up has a marked effect upon the performance of a coating system. For the coating systems tested the R_n and $|Z|_{\max}$ value were significantly lower in the flowing cells, when compared with the values obtained from similar panels in a 'stationary' electrolyte. The reduction in effectiveness of these barrier type coatings reduces the ranking of both the AAS and the GHS from 'good' to 'fair' (*I*) coatings. The $|Z|_{\max}$ values obtained from EIS measurements show a good correlation to within one order of magnitude, with the R_n values obtained from the ENM method.

Acknowledgments

This work was carried out under the auspices of the Office of Naval Research, Grant No. N00014-95-1-507, and the National Science Foundation - Industry / University Coatings Research Center.

References

1. Bacon R.C., Smith J. J., Rugg F. M., *Ind. Eng. Chem.* **1948**, *40*, pp. 161-167
2. Skerry B.S., Eden D.A., *Prog. Org. Coatings* **1987**, *15*, pp. 269-285
3. Skerry B.S., Eden D.A., *Prog. Org. Coatings* **1991**, *19*, pp. 379-396
4. Chen C.T., Skerry B.S., *Corrosion* **1991**, *47*, pp. 598-611
5. Mills D.J., Bierwagen G.P., Skerry B.S., Tallman D.E., *Proc. of the 12th international Corrosion Congress, 1993, Vol 1* pp. 184
6. Bierwagen G. P., Mills D. J., Tallman D. E., Skerry B. S., *Proc. of Symposium on Corrosion and Corrosion Prevention in Seawater Environments*, E.C.S., Oct. **1993**, Abstract No 81
7. Bierwagen G. P., *J. Electrochemical Soc.*, **1994**, *141*, pp. L155-157
8. *Electrochemical Impedance*, Scully J.R.; Silverman D.C.; Kendig M.W., Eds.; Special Tech. Publ. 1188, ASTM, Philadelphia, PA, **1993**
9. *Impedance Spectroscopy*, MacDonald J.R., Ed.; Wiley-Interscience, New York, NY, **1987**
10. Callow, M. *Chemistry and Industry*, **1990**, pp 123
11. Martin, B. A., *Materials Performance* **1994**, *33*, pp 12
12. Coulson, K.E.W., Barlo, T.J., Werner, D.P., *Oil & Gas Journal*, **1991**, *89*, pp 80

Chapter 13

Transport Properties of Waterborne Polymeric Coatings

H. K. Tay and J. M. Sykes

Department of Materials, Oxford University, Parks Road, Oxford
OX1 3PH, England

Gravimetric sorption curves for water in a water-borne vinyl chloride/vinylidene chloride copolymer coating showed that paint pH had a profound effect on the water uptake. At pH 3, water uptake increases markedly with pigment volume concentration but not for films cast from pH 5 paint. By calculating the amount of water adsorbed on the surface of the pigments, it was found that the water content was influenced by different pigments for different paint pH. pH did not affect water uptake in films cast from latex. The pigment content in the paint influences the rate of and the activation energy for water transport.

Keywords: gravimetric, pH, pigment volume concentration, diffusion coefficient, latex.

When painted metals are exposed to wet corrosive environments the first process leading to the onset of corrosion will be uptake of water by the coating and transport of water to the coating-metal interface. At the interface water will reduce the adhesion of the coating and may lead to development of blisters. The failure of adhesion and development of a separate aqueous phase in contact with the metal is considered by some workers (1) to be essential for the development of corrosion. Water in the coating will also influence the solubilisation of ions and ionic diffusion. Water and oxygen are consumed in the corrosion process, but most paint films are so permeable to water and oxygen that their transport is not usually rate-limiting (2). It may however be an important factor in controlling the deterioration of coatings, for instance by blistering.

This work examines factors influencing water transport in a water-borne coating based on a vinyl chloride / vinylidene chloride copolymer latex (3,4) and the part played by pigments added to make a primer. It seeks to understand controlling factors in water absorption and transport in pigmented water-borne systems. The latex was based on this chlorinated polymer because of its remarkably low permeability to water and oxygen diffusion. It had been found that (5) among typical paint resins (eg. acrylic primer, epoxy/polyamide), 1-coat free films of VC-VDC copolymer latex has the lowest

permeability to water vapour, even when compared to some solvent-borne resins like pigmented alkyd and chloropolymers. The paint is normally formulated at about pH 5 to avoid dehydrochlorination of the polymer (6). Primer formulated at this pH with zinc phosphate pigments provides (5) good corrosion protection.

The influence of pigments on permeability can vary and will depend upon the volume fraction (PVC) added, but flake (or "lamellar") pigments, such as micaceous iron oxide or metallic aluminium, that align themselves parallel to the substrate are commonly added to improve the barrier properties of coatings. Water will be forced to traverse a longer and tortuous path through the pigmented coating as compared to the water transport in an unpigmented coating (7). However, pigment-polymer adhesion is also a crucial factor in determining water transport, because the pigment polymer interface provides a possible easy path for water diffusion. If the particles make contact with one another (the content exceeds the percolation threshold), creating connected pathways, then transport should be facilitated (8). At high volume fractions (exceeding the critical PVC) the polymer matrix fails to fill all the voids between the pigment (9) and barrier properties are gravely impaired.

A convenient way to quantify water transport in polymers is through the determination of sorption curves for free films of paint immersed in water. Interpretation of the results requires solution of the diffusion equation under non-steady state conditions. This is not difficult provided that the diffusion coefficient D can be treated as a constant independent of water concentration in the polymer. Typically sorption curves show a linear water uptake which increases with \sqrt{t} time, but finally levels off when the polymer is saturated with water.

The Fourier transformed solutions for the Fick's equations in the case of sorption into both sides of a thin sheet with D treated as constant and for small times is (10),

$$\frac{M_t}{M_\infty} = 4 \left(\frac{Dt}{l^2} \right)^{1/2} \left[\pi^{-1/2} + 2 \sum_{n=0}^{\infty} (-1)^n \operatorname{ierfc} \frac{nl}{2(Dt)^{1/2}} \right] \quad (1)$$

where, M_t = mass of water absorbed or desorbed at time t ,

M_∞ = mass of water absorbed or desorbed at time ∞ ,

l = thickness of paint film,

$\operatorname{ierfc} = \int \operatorname{erfc} \xi \, d\xi = \{1/(\pi^{1/2} \exp(x^2))\} - x \operatorname{erfc} x$, (11)

$\operatorname{erfc} = 1 - \operatorname{erf}$, where erf is the error function.

For Fickian behaviour and at short times, a linear mass increase relative to \sqrt{t} time is obeyed, eventually the curve becomes concave towards the \sqrt{t} time axis and approaches the final equilibrium value. In ideal diffusion, the penetrant molecules are small compared with the size of the monomer unit of the polymer and the presence of the molecules has negligible effect on the polymer segmental motion. The diffusion of water and gases in soft rubbery polymers (eg. paint films) is usually ideal and the diffusion coefficient can be calculated according to Equation (2) (12) from the gradient, G , of the M_t vs \sqrt{t} plot. Alternatively, using another form of this solution D can be calculated from the time $t_{1/2}$, when $M_t = 0.5 M_\infty$, using Equation (3) (13).

$$D = \frac{\pi l^2 G^2}{16 M_w^2} \quad (2)$$

$$D = \frac{0.049}{(t_{1/2} / l^2)} \quad (3)$$

Experimental

A series of three paints were made containing increasing pigment content (Table I), with the content of the barytes pigment increasing while the contents of zinc phosphate and iron oxide remained the same (Table II). The paint pH was then adjusted to either pH 5 or 3. Films were cast on 100 x 150 mm glass plates (6mm float glass) using a no. 200 Mayer bar, giving a dry film thickness of approximately 100 μm , and dried in flowing filtered air in a cabinet at room temperature for 7 days. Small samples (20 mm x 20 mm) were carefully peeled from the glass plates for testing. The thickness of the paint film was determined using a SHEEN SS.1200 eddy current film thickness gauge. The samples were immersed in distilled water in sealed jars held in a thermostatic water bath at temperatures from 30 - 50° C. Samples were weighed on an analytical balance before immersion, and then at regular intervals after blotting dry.

Results

1. Effect of Pigment (7 days cured coatings)

1(a) Paint pH = 3. Figure 1 shows duplicate results for water uptake as a function of time for three paints containing 15%, 20% and 30% pigment volume concentration (PVC) during immersion in water at 30°C. The 30% PVC paint shows a linear relationship between uptake and \sqrt{t} time, conforming with the diffusion equation, but some curvature is evident for the other two paints. There is a strong dependence of saturation uptake (M_w) with pigment content.

The initial slope, G , increases with increasing PVC. The initial gradient for 30% PVC is about 6 times more than that for 15% PVC. If D values are calculated from this slope using eqn. 2, an even more marked increase with PVC is found because M_w also increases with PVC. The following are duplicate values for G and D .

Table 1. Paint formulation (% by wt) for 15%, 20% & 30% P.V.C.

P.V.C.	15%	20%	30%
Water	8.60	9.97	12.39
Dispersant	0.26	0.34	0.49
Thickener	0.20	0.20	0.20
Micr. red iron oxide	2.71	2.59	2.39
Micr. barytes	9.34	15.62	26.71
Zinc phosphate	6.03	5.77	5.32
Defoamer	0.20	0.20	0.20
Co-solvent	1.98	1.78	1.41
Surfactant	4.52	4.26	3.81
Latex	66.16	59.26	47.08
Total	100	100	100

Table 2. Breakdown of P.V.C. in the paint.

P.V.C. (zinc phosphate)	6.33	6.33	6.33
P.V.C. (micr. iron oxide)	1.98	1.98	1.98
P.V.C. (micr. barytes)	6.69	11.69	21.69
Total P.V.C.	15%	20%	30%

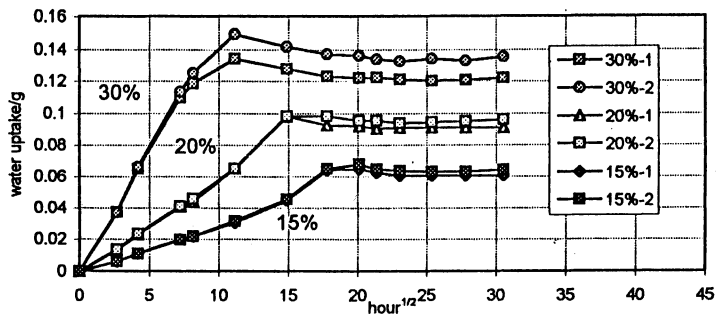


Figure 1. Water Uptake of 15%, 20% and 30% PVC paint films (pH 3, 30°C bath)

PVC / %	Initial Gradient / mg h ⁻¹	Diffusivity / 10 ⁻¹² m ² s ⁻¹
15	2.5	1.24
	2.5	1.11
20	5.3	2.54
	5.4	2.38
30	15.0	10.3
	15.2	8.79

If the pigments are impermeable and do not take up water (14), then water in a pigmented film can be in two places: in the latex or at the pigment-latex interface. The adsorbed "interfacial water" can then be estimated from the total water content (M_w) minus the water dissolved in the latex (calculated from the water uptake in unpigmented films and corrected for reduced volume fraction in the paints). The additional water uptake when pigment is increased from 15% to 30% is significantly greater than when the first 15% is added. Adding barytes has a disproportionately large influence on uptake, as shown when "interfacial water" (calculated by subtracting an appropriate fraction of water taken up by the unpigmented polymer) is plotted against volume fraction of barytes (figure 2). There is a good linear relationship. A plot against total pigment content does not give a good fit. We conclude that a high proportion of the water taken up by coatings formulated at pH 3 is associated with the barytes.

1(b) Paint pH = 5. When a similar experiment was conducted using paint at pH 5, the final water content (M_w) is virtually independent of pigment content (Fig. 3). The pigment content still influences the rate of water uptake, but to a lesser extent; however when D is calculated from initial slopes, an even greater effect of PVC is found than for pH 3 paint films because here the saturation water content (M_w) does not increase with PVC (refer equation 2). The following are duplicate values for G and D .

PVC / %	Initial Gradient / mg h ⁻¹	Diffusivity / 10 ⁻¹² m ² s ⁻¹
15	2.8	1.64
	2.8	1.55
20	4.9	4.47
	4.9	4.29
30	12.7	30.0
	12.7	29.2

The diffusion coefficient for water in unplasticised poly(vinyl chloride) at 25°C is given as $2.4 \times 10^{-12} \text{ m}^2\text{s}^{-1}$ in the Polymer Handbook (15). Poly (vinylidene chloride) will have a much smaller D (16) ($\sim 1/10$) and the value for the copolymer is found to be significantly smaller than for poly(vinyl chloride). One reason why the calculated D

values for "pigmented" films, where water resides at the pigment-latex interface, could be under-estimated is that interfacial water is included in the " M_w " term in eqn. (2) when calculating the diffusion coefficient. Disregarding the "interfacial water" during calculation and taking the value of M_w for the polymer itself will make the D values larger - 2 to 3 times the D values shown above.

When "interfacial water" uptakes were calculated from M_w values and plotted against the PVC of the paint, both M_w and "interfacial water" values showed little change as PVC increased from 15% to 30% (barytes only added), but did increase for the first 15% pigment addition. If non is associated with barytes, water uptake must be associated with one or both of the other two pigments, zinc phosphate and iron oxide (Table II and Figure 4).

1(c) Effect of pH on Latex Films. Sorption curves for pigment-free latex at 30°C were essentially the same for three different pH values with similar saturation water uptake value (M_w) and similar uptake rates (Figure 8).

2. Effect of Temperature

2(a) Paint pH = 3. In this case the total water uptake falls with temperature (Figure 5), contrary to what occurs for water sorption into a typical polymer (17), which increases with increasing free volume. The rate of sorption shows only a small increase with rise in temperature.

2(b) Paint pH = 5. For 20% PVC, there is a very little effect of T (Figure 6) on saturation water uptake value (M_w); but the rate of uptake doubles as T increases from 30°C to 50°C. At 30% P.V.C. (Figure 7), there is a slight increase in water absorbed at 40°C and 50°C but water uptake is little faster than at 30° C.

2(c) Activation Energies for Water Transport. Effective activation energies for water transport in the latex (0% PVC) and paint films were calculated from the sorption curves using the times, t, taken to achieve the same water uptake as a measure of rate at the different temperatures. The least-squares regression line for a graph of $\ln(\text{rate})$ versus $1/T$ were then determined, and the apparent E_{act} value calculated from the gradient. The effective E_{act} values (kJ/mol) are as follows,

	pH 3	pH 5	pH 7
0% PVC	83.9	82.9	84.1
15% PVC		67.0	
20% PVC	40.1	48.5	
30% PVC		9.1	

In the Polymer Handbook (18), the activation energy for diffusion, E_D , for poly(vinyl chloride) at 25°C is given as 41.8 kJ/mol. This is only half the value calculated for the 0% PVC (non-pigmented) film. This is not surprising because the film

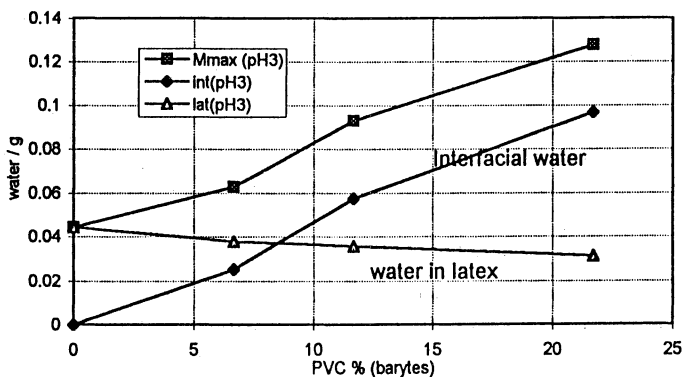


Figure 2. M_{∞} , “latex water” and “interfacial water” vs PVC of barytes (Paint pH = 3)

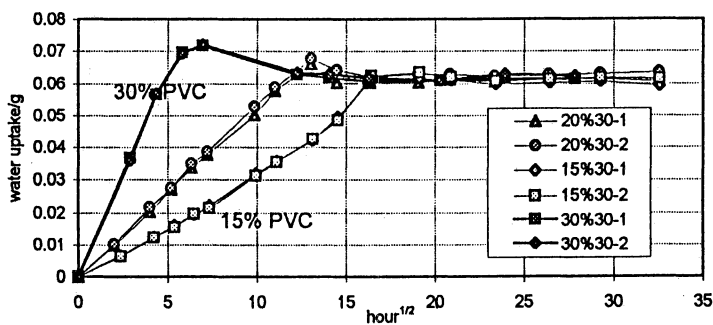


Figure 3. Water Uptake of 15%, 20% & 30% PVC paint films (pH 5, 30°C)

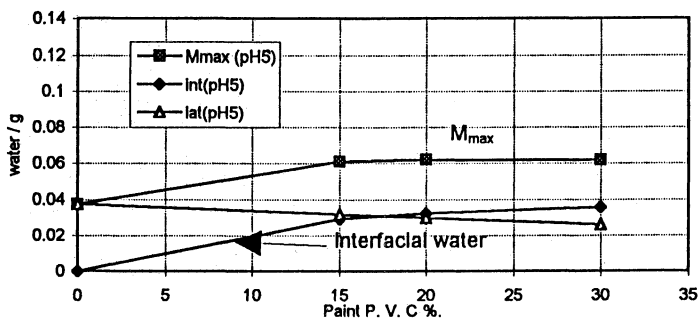


Figure 4. M_{∞} , “latex water” and “interfacial water” vs paint PVC (Paint pH = 5)

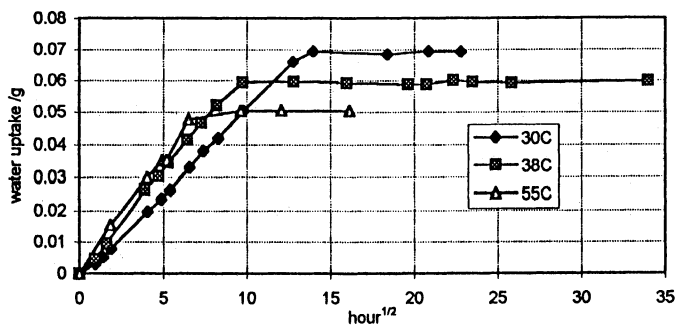


Figure 5. 20% PVC (pH 3) paint films at different T

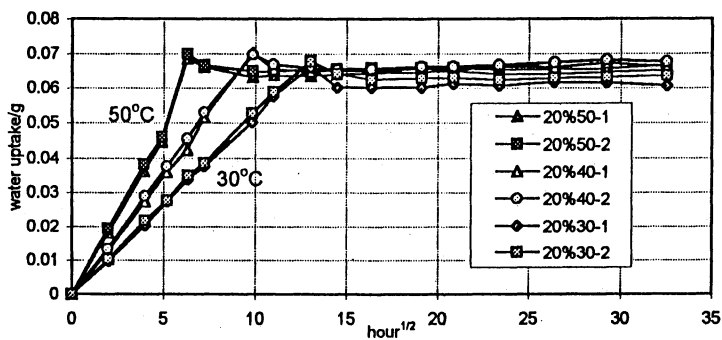


Figure 6. 20% PVC (pH 5) paint films at different T

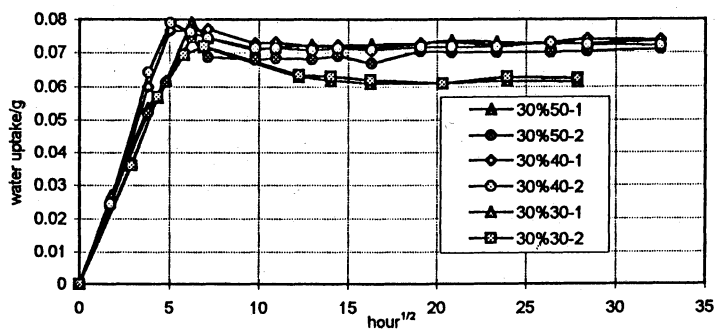


Figure 7. 30% PVC (pH 5) paint films at different T

contains poly (vinylidene chloride) as copolymer. The latter is one of the best barrier polymer to water diffusion.

For pH 5 coatings, there is a steady reduction in activation energy with increased pigment content. The calculated activation energies for latex films formulated to pH 3, 5 and 7 show little change in E_{act} .

Discussion and Conclusions

The results for 7-day cured films at pH 3 (Figure 1) show a strong link between pigment content and water uptake. Comparison with pigment-free films of the same age, which absorb much less water (Figure 8), suggests that here the major part of the water must be adsorbed at the pigment-polymer interface. Breaking down the water uptake data for the different pigment contents show that this water uptake increases essentially linearly with barytes content (Figure 2) independent of the other pigments, so the water must be associated mainly with barytes. That water uptake falls with increase in temperature (Figure 5) is also a good indicator that exothermic surface adsorption is the most important mechanism of uptake, rather than absorption into the polymer itself, where the increase of free volume with temperature would lead to increased water uptake (19).

For pH 5 paint films, the M_w is essentially the same regardless of PVC but higher than in the latex alone (see figure 3); adding barytes now causes no increase in water uptake and little water can be associated with this pigment (see figure 4). All paints contain the same amounts of zinc phosphate and iron oxide so it seems in this case that water is adsorbed on these (or one of these) pigments, with the same additional uptake at all PVC. In this case the amount of adsorbed interfacial water is small and there is little effect of temperature on water uptake. Any decrease in water associated with the pigment is probably compensated by additional uptake within the polymer.

It is difficult to understand why a small adjustment in pH should have so profound an effect. Change in pH will certainly influence the surface charges and colloid stability of both latex particles and pigments, so that the way in which they interact in the paint and as a film forms could be radically altered. Further work is needed to understand the details of how the water-sensitivity of pigment-latex interfaces can be so dramatically modified by this change.

The activation energies for diffusion in pH 5 films show a decrease from the latex films to the paint film with the highest PVC, suggesting a shift from water diffusion in polymer, which is controlled by segmental motion (20), to easier transport along polymer-pigment interfaces as PVC increases. It is clear that water must transport along the polymer-barytes interface even in those cases where the majority of water is associated with the other pigments. The quantity of water taken up into these films (particularly the component associated with the pigments) is sufficient to provide many monolayers of coverage. A few monolayers at the barytes-polymer interface would result in an insignificant weight gain.

At pH 3, where much water adsorbs on the surface of the barytes, easy pathways for water transport should be created, especially at high PVC, yet the table below (duplicate data) shows less effect of pigment increase on the water diffusion coefficient at pH 3 than at pH 5. This is surprising.

	pH 3 paint	pH 5 paint
$D_{15\%}$	$1.24 \times 10^{-15} \text{ m}^2\text{s}^{-1}$ $1.11 \times 10^{-15} \text{ m}^2\text{s}^{-1}$	$1.64 \times 10^{-15} \text{ m}^2\text{s}^{-1}$ $1.55 \times 10^{-15} \text{ m}^2\text{s}^{-1}$
$D_{20\%}$	$2.54 \times 10^{-15} \text{ m}^2\text{s}^{-1}$ $2.38 \times 10^{-15} \text{ m}^2\text{s}^{-1}$	$4.47 \times 10^{-15} \text{ m}^2\text{s}^{-1}$ $4.29 \times 10^{-15} \text{ m}^2\text{s}^{-1}$
$D_{30\%}$	$1.03 \times 10^{-14} \text{ m}^2\text{s}^{-1}$ $8.79 \times 10^{-15} \text{ m}^2\text{s}^{-1}$	$30.0 \times 10^{-15} \text{ m}^2\text{s}^{-1}$ $29.2 \times 10^{-15} \text{ m}^2\text{s}^{-1}$
$G_{15\%}$	$0.0025 \text{ g h}^{-1/2}$ $0.0025 \text{ g h}^{-1/2}$	$0.0028 \text{ g h}^{-1/2}$ $0.0028 \text{ g h}^{-1/2}$
$G_{20\%}$	$0.0053 \text{ g h}^{-1/2}$ $0.0054 \text{ g h}^{-1/2}$	$0.0049 \text{ g h}^{-1/2}$ $0.0049 \text{ g h}^{-1/2}$
$G_{30\%}$	$0.0150 \text{ g h}^{-1/2}$ $0.0152 \text{ g h}^{-1/2}$	$0.0127 \text{ g h}^{-1/2}$ $0.0127 \text{ g h}^{-1/2}$

It should be noted that the initial gradient values at each PVC are roughly the same regardless of pH and the differences in D values arise because M_{∞} (total water content) used as the surface concentration of water in calculating the diffusion coefficients are different. This may give misleading results as there is a large component of interfacial water in the total water content, whereas the water content of the polymer itself is probably the same in all cases. Therefore for pigmented-paint systems where there are two distinct phases, analysis using a simple continuum model may fail to yield realistic parameters. If initial gradient is taken as the basis for comparing rates of water uptake, the 30% PVC paint at pH 3 gives the highest value, but the difference between pH 3 and pH 5 is not as great as might be expected.

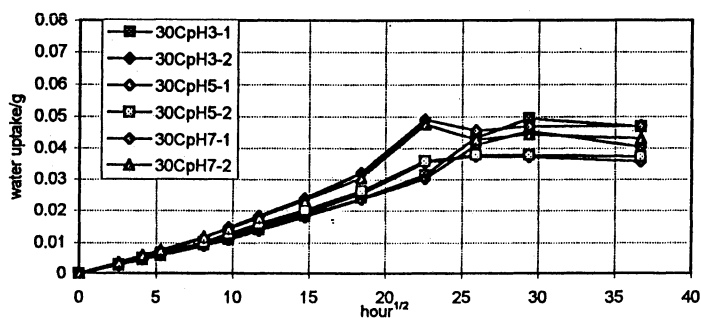


Figure 8. Water Uptake for Latex films (pH 3, 5, 7) at 30°C

From these results we conclude that total water uptake in this water-borne coating is strongly affected by pigment content at pH 3, but not at pH 5. It can be shown that water adsorbs on barytes at pH 3, but not on the other pigments. At pH 5 the situation is reversed. In both cases increased pigment content increases the rate of water uptake, but interpretation of the variation in diffusion coefficient is complex.

Acknowledgement

The authors gratefully acknowledge advice from and helpful discussions with J. C. Padget and P. J. Moreland of Zeneca Resins and Profs. R.J. Brook, D.G. Pettifor and B. Cantor, for provision of laboratory facilities. H. K. Tay would like to thank Zeneca Resins, Runcorn, Cheshire, for a PhD Bursary and CINVESTAV-Merida for their encouragement.

Literature Cited

1. Haagen, H and Funke, W. *J. O. C. C. A.* 1975, **58**, 359
2. Mayne, J. E. O., *Research*, 1952, **6**, 278
3. Padget, J. C., Moreland, P. J. *J. Coat. Tech.*, 1983, **55**, no. 698, 39
4. Humphries, R. G., *J. O. C. C. A.* 1987, **70**, no. 6, pg 150
5. Thomas, N. L. *Prog. Org. Coat.* 1991, **19**, 101-121
6. Burgess, A. J., Caldwell, D., Padget, J. C. *J. O. C. C. A.* 1981, **64**, 175
7. Surface coatings - Raw Materials and Their Usage (vol 1), Chapman and Hall (London), 3rd edition, 1993
8. Lekatou, A., Faidi, S.E., Lyon, S.B., Newman, R.C. *Advances in Corrosion Protection by Organic Coatings*; Kendig, M. W., Scantlebury, J. D. Eds.; Electrochemical Society, 1994
9. *Technology of Paints - Varnishes and Lacquers*; Martens, C. R., Eds.; Reinhold Book Corporation, 1968
10. Crank, J., *The Mathematics of Diffusion*, 2nd ed., Clarendon Press, Oxford, 1979, pp 48
11. *ibid*, pp 376
12. *ibid*, pp 244
13. *ibid*, pp 246
14. Bierganska, B., Zubielewicz, M., Smieszek, E., *Prog Org Coatings*, 1988, **16**, 219 - 229
15. Brandrup, J., Immergut, E. H., *Polymer Handbook*, 3rd edn., section VI: Permeability and Diffusion Data, Wiley-Interscience, New York, 1989
16. Bicerano, J., Burmester, A. F., Delassus, P. T., Wessling, R. A. *ACS Symposium; Series 423 - Barrier Polymers and Structures*, W. J. Koros Ed., ACS, Washington DC, 1990, pp 126
17. Crank, J., Park, G. S., *Diffusion in Polymers*, Chapter 8, Academic Press, 1968
18. Brandrup, J., Immergut, E. H., *Polymer Handbook*, 3rd edn., section VI: Permeability and Diffusion Data, Wiley-Interscience, New York, 1989
19. Atkins, P. W. *Physical Chemistry*, 4th ed., 29.3, Oxford University Press, 1990
20. Cowie, J. M. G. *Polymers: Chemistry and Physics of Modern Materials*, 2nd ed., Chapman and Hall, 1991

Chapter 14

Degradation of Polymer Coatings on Steel Exposed to Seawater

F. Mansfeld, H. Xiao, L. T. Han, and C. C. Lee

Corrosion and Environmental Effects Laboratory (CEEL), Department of Materials
Science and Engineering, University of Southern California,
Los Angeles, CA 90089-0241

The degradation of twelve different polymer coating systems on steel exposed to natural (NS) and artificial (AS) seawater has been monitored using electrochemical impedance spectroscopy (EIS) and electrochemical noise analysis (ENA). The marine test sites were Port Hueneme, California and Key West, Florida. A new approach has been developed to obtain electrochemical impedance spectra and noise data from the remote test sites via modem from the laboratory. Impedance data were collected once a week, while noise data were measured twice a week. Potential and current noise data were determined simultaneously. The experimental approach is described and representative data from exposure to NS and AS are presented for coating systems with different primers and/or topcoats. The aim of this project is to determine the impact of microorganisms on degradation of the protective properties of polymer coatings on steel during exposure to NS.

In a project devoted to the evaluation of the effects of microorganisms on corrosion protection by polymer coatings twelve coating systems applied to steel have been exposed for more than one year to natural seawater (NS) at Port Hueneme, CA and Key West, FL and to artificial seawater (AS) in the laboratory as control electrolyte. Degradation of the protective properties of these coatings has been monitored using electrochemical impedance spectroscopy (EIS), electrochemical noise analysis (ENA) and visual observation. A special monitoring approach has been developed for collection of EIS and ENA data from remote test sites. ENA has been performed for data obtained in the time and the frequency domains. Examples of coating performance at the two marine test sites and in artificial seawater are given for polymer coatings with different types of primers or topcoats.

EXPERIMENTAL APPROACH

Materials and Methods.

Materials. Two different series of coatings systems have been tested. In the CR series (Table I), the nature of the primer, midcoat or topcoat was varied in order to allow comparisons of the effects of coating type on corrosion protection in general and attack by microorganisms in particular. CR 1 and 2 had the same primer, but different mid- and topcoats. CR 5 and 6 had the same primer and midcoat, but different topcoats, while for CR 6 and 7 the midcoat and topcoat were

the same, but the primer was different. A comparison of the results for CR 6 and 7 is expected to allow determination of the effects of the primer, since the midcoat and topcoat were identical, while comparison of the results for CR 5 and 6 will allow to assess the effects of the nature of the topcoat on corrosion protection. The total coating thickness ranged from about 125 μm for CR 2 to 275 μm for CR 5 (Table I) [1].

For the JJ series, three different primers were used (Table II). The coating thickness was less than 100 μm for all coatings [1]. The odd-numbered samples had only a primer and a midcoat, while the even-numbered samples had an additional topcoat of polyurethane. The same midcoat was used for all JJ samples (Table II). The nature of the primer might not only affect the corrosion resistance of the coated steel in abiotic solutions, but might also affect colonization and attack by bacteria due to the different surface potentials.

Methods. Impedance spectra were collected once a week for more than one year at Port Hueneme, CA and Key West, FL. The traditional approach using a frequency response analyzer and a potentiostat was applied in laboratory studies. For collection of electrochemical impedance spectra at remote test sites, a different approach had to be applied in which the potentiostat was eliminated and a multiplexer was used to connect the recording system to the different coating systems (Figure 1) [1,2]. Electrochemical potential and current fluctuations were collected simultaneously for two coated samples of the same type (Figure 1) [1-4]. Relatively large samples (15.2 cm x 10.2 cm) were used in order to lower the impedance of the coating systems. The exposed area was about 250 cm^2 for each sample. Visual observation was performed once a month according to ASTM D 610. Electrochemical impedance and noise data were analyzed using appropriate models and software developed in this laboratory [1].

EXPERIMENTAL RESULTS AND DISCUSSION

The type of information obtained with EIS and ENA during exposure to AS and NS will be discussed in the following for coating systems CR 5, 6 and 7, which have a zinc-rich primer (CR 5 and 6) or an epoxy polyamide primer (CR 7), an epoxy polyamide midcoat and a latex topcoat (CR 6 and 7) or a polyurethane topcoat (CR 5). Polyurethane has been reported to be degraded by microorganisms [5,6].

Figure 2 shows impedance spectra obtained in NS (Port Hueneme, CA) (PH) for CR 5, 6 and 7 for 1, 4 and 7 months. Spectra obtained in AS for the corresponding time periods had similar features [1]. Qualitatively, the continued decrease of the impedance indicated an increase of the delaminated area at which corrosion occurs and an increasing influence of mass transport phenomena as pores developed in the coating and very small rust spots were observed. For CR 5 visual observation after one year indicated a total area of rust spots between 0.03 and 0.1 % of the exposed area (250 cm^2). Both samples of CR 6 and one sample of CR 7 were removed when the total rust area had reached 0.3% after 7 and 9 months exposure at PH, respectively. Removed samples were subjected to observation with an environmental scanning electron microscope (ESEM) [7]. For the remaining CR 7 sample less than 0.03% of rusted area was observed. A comparison of the time dependence of the pore resistance R_{p0} , which is proportional to the delaminated area [8], is given in Figure 3a for the three coating systems exposed at PH. The lowest values of R_{p0} were observed for CR 6 which performed the poorest according to visual observation. The increase of R_{p0} for CR

Table I Composition of Coating Systems (CR series)

Sample Name	CR1	CR2	CR5	CR6	CR7	CR9
Substrate	Hot Rolled Steel	Hot Rolled Steel	Hot Rolled Steel	Hot Rolled Steel	Hot Rolled Steel	Hot Rolled Steel
Primer	Alkyd high solid ¹	Alkyd high solid ¹	Zn-rich Primer ⁴	Zn-rich Primer ⁴	Epoxy Polyamide ⁵	Epoxy Polyamide ⁵
Midcoat	Low VOC Alkyd ²	Silicone Alkyd ³	Epoxy Polyamide ⁵	Epoxy Polyamide ⁵	Epoxy Polyamide ⁵	Epoxy Polyamide ⁵
Topcoat	Low VOC Alkyd ²	Silicone Alkyd ³	Urethane ⁸	Latex ⁷	Latex ⁷	Epoxy Polyamide ⁵

Table II Composition Coating Systems (JJ Series)

Sample Name	JJ1	JJ2	JJ3	JJ4	JJ5	JJ6	JJ7
Substrate	Cold Rolled Steel	Cold Rolled Steel	Cold Rolled Steel	Cold Rolled Steel	Cold Rolled Steel	Cold Rolled Steel	Cold Rolled Steel
Primer	Zinc plate ^a	Zinc plate ^a	Phosphate coat ^d	Phosphate coat ^d	IVD-AI ⁹	IVD-AI ⁹	Epoxy Polyamide ⁵
Midcoat	Epoxy ^b	Epoxy ^b	Epoxy ^b	Epoxy ^b	Epoxy ^b	Epoxy ^b	Epoxy Polyamide ⁵
Topcoat		Polyurethane ^c		Polyurethane ^c		Polyurethane ^c	Epoxy Polyamide ⁵

NOTE:

1. TT-P-645B.
2. TT-E-489H.
3. TT-E-49.
4. SSPC-20, type 2.
5. MIL-P-24441, Formula 150.
6. MIL-C-85285.
7. MIL-P-28578.
8. MIL-P-24441, Formula 151.
9. MIL-P-24441, Formula 152.

- a. Zinc plate per QQ-Z-325 Rev. C (Type II, Class 2).
- b. 2 coats of epoxy polyamide primer MIL-P-23377 Rev. F (Type I class 3) per MIL-F-18264 REV.D AMD.1.
- c. 1 coat of MIL-C-85285 REV.B (AS) AMD.2 polyurethane per MIL-F-18264 REV.D AMD.1 color #36375 lusterless gray of FED-STD-595.
- d. Phosphate coat DOD-P-16232 REV.F (Type Z class 3) ; hydrogen embrittlement relieved for 8 hours at 210-225 degree.
- e. IVD aluminum per MIL-C-83488-C (Notice 1, Type II Class I)

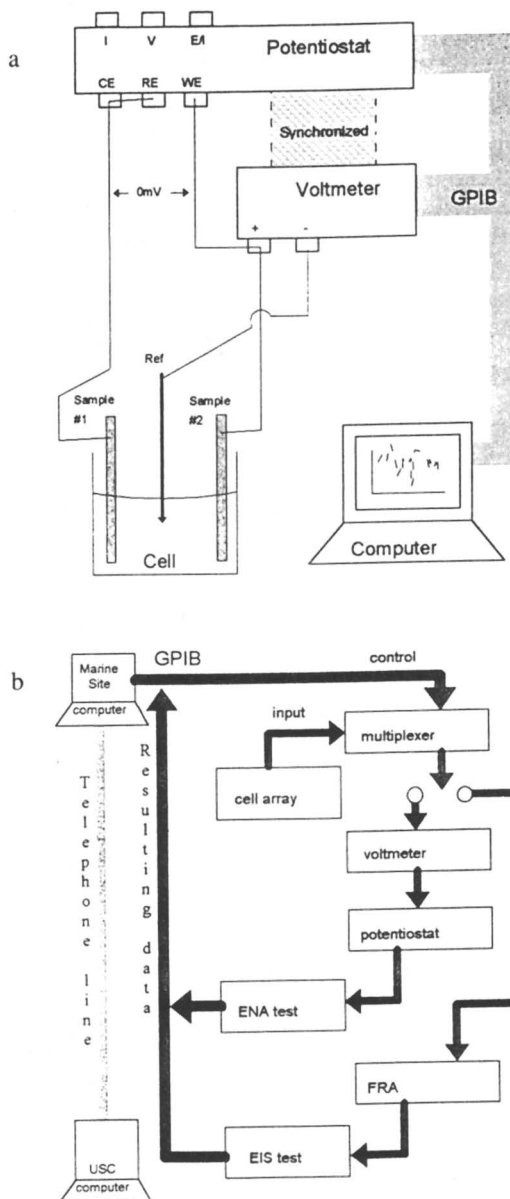


Figure 1. Experimental approach for collection of electrochemical impedance and noise data from a remote test site.

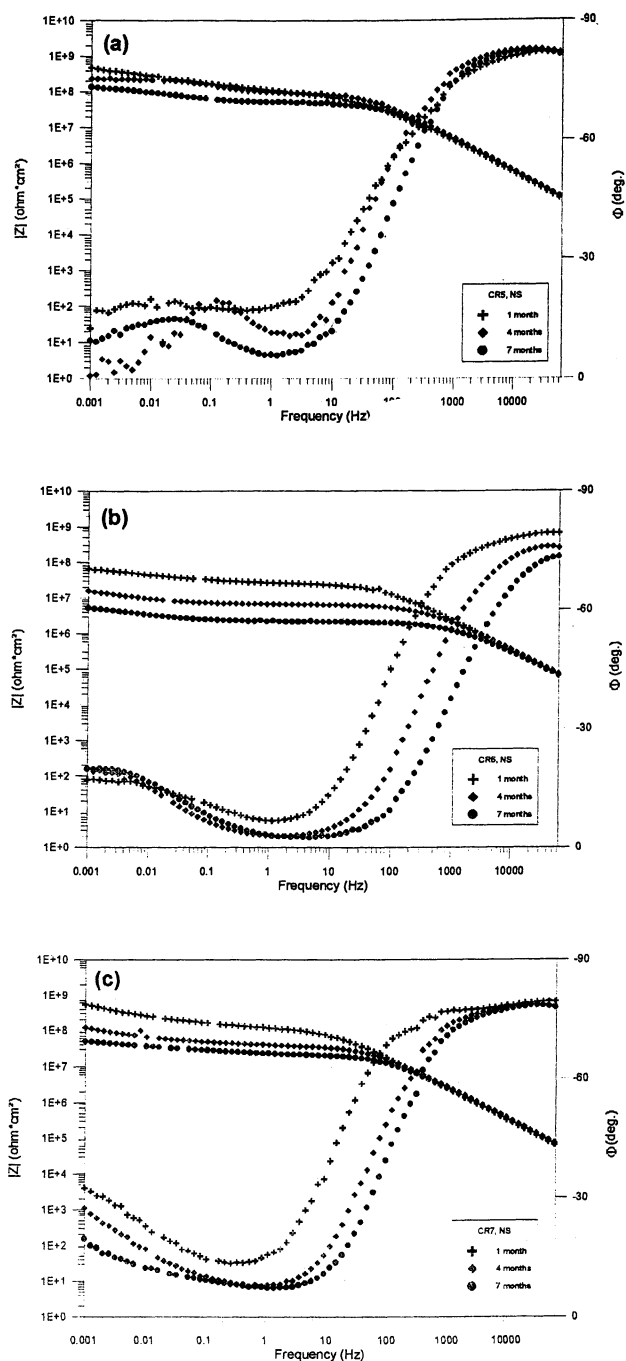


Figure 2. Impedance spectra for CR 5, CR 6 and CR 7 exposed to natural seawater for 1, 4 and 7 months at Port Hueneme (PH), CA.

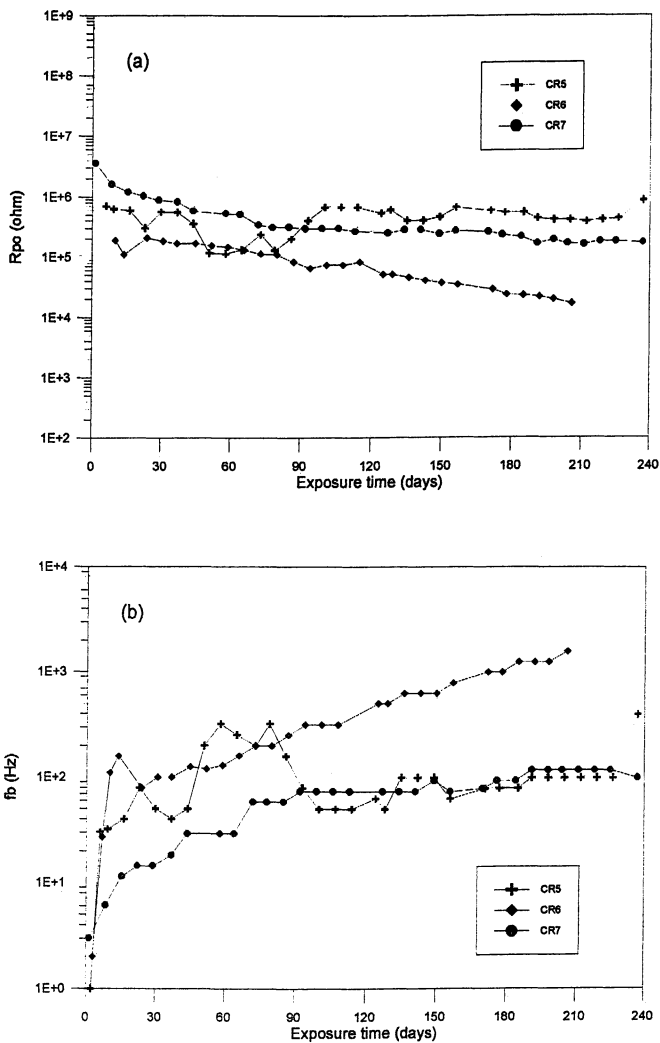


Figure 3. Time dependence of pore resistance R_{p0} (Figure 3a) and breakpoint frequency f_b (Figure 3b) for CR 5, CR 6 and CR 7 exposed at Port Hueneme, CA.

5 after about 80 days seems to be due to plugging of pores in the coating by corrosion products and perhaps also bacteria. Preliminary data obtained by observation with ESEM indicated that bacteria were concentrated in pores of the coating. The breakpoint frequency f_b increased continuously for CR 6, but leveled off at values below 100 Hz for CR 5 and CR 7 (Figure 3b). The delaminated or corroding area A_d can be estimated from f_b which for coating systems with impedance spectra such as those shown in Figure 2 is defined as [8,9]:

$$f_b = (2\pi R_{po} C_c)^{-1} = A_d (2\pi R_{po} C_c)^{-1} \quad (1),$$

where R_{po} is the specific pore resistance in ohm.cm^2 and C_c is the coating capacitance.

The area fraction $D = A_d/A$, where A is the total exposed area, can be estimated based on Eq. 1 provided R_{po} is known. Figure 4 gives a comparison of D values calculated based on Eq. 1 and the results of visual observation for CR 6 exposed at PH and to AS. R_{po} was determined by assuming that the D value obtained by visual observation after about 110 days and that calculated from f_b were the same. This approach resulted in R_{po} values of 1025 and 1250 ohm.cm^2 for PH and AS, respectively, which are very close to the polarization resistance R_p values obtained for bare steel in 0.5 N NaCl by weight loss and impedance measurements. Apparently corrosion occurred mainly in pores filled with rust and therefore R_{po} was close to R_p . Excellent agreement between the D values obtained by the two methods was observed over a four months period (Figure 4). During the entire test period D for CR 6 increased by about a factor of 30 in both media. The validity of Eq. 1 can be checked by comparing the experimental values of $f_b R_{po}$ with those of $(2\pi C_c)^{-1}$, which should be equal according to Eq. 1. Very good agreement was observed.

Figure 5a shows the time dependence of the mean values of the potential of the coupled electrodes E_{coup} for CR 5, 6 and 7 during exposure at PH. E_{coup} increased slowly for CR 5 in the first three months from values typical of zinc to those of actively corroding steel. For CR 6 E_{coup} first increase and then decreased to values close to - 500 mV vs Ag/AgCl. For CR 7, which had an epoxy polyamide primer and midcoat, much more positive values of E_{coup} were observed (Figure 5a). The mean coupling current I_{coup} was usually higher for CR 6 than for CR 5 and 7 (Figure 5b). After about six months the sign of I_{coup} changed for CR 6 (Figure 5b).

From the experimental electrochemical noise data, the noise resistance R_n was obtained by statistical analysis as $R_n = \sigma\{V(t)\}/\sigma\{I(t)\}$, where $\sigma\{V(t)\}$ and $\sigma\{I(t)\}$ are the standard deviations of potential V and current I , respectively. Spectral noise ($R_{sn}(f)$) plots were obtained by analysis in the frequency domain as the ratio of the Fast Fourier Transforms (FFT) of potential and current fluctuations at each frequency f . The spectral noise resistance R_{sn}^0 was defined as the limit of a spectral noise plot for $f \rightarrow 0$ [1-4, 10]. In Figure 6 $\sigma\{V(t)\}$ and $\sigma\{I(t)\}$ are shown as a function of time. The time dependence of $\sigma\{V(t)\}$ was very similar for all three coatings with $\sigma\{V(t)\}$ fluctuating around 1 mV (Figure 6a). After about two months $\sigma\{V(t)\}$ was usually the highest for CR 7. Very low values of $\sigma\{I(t)\}$

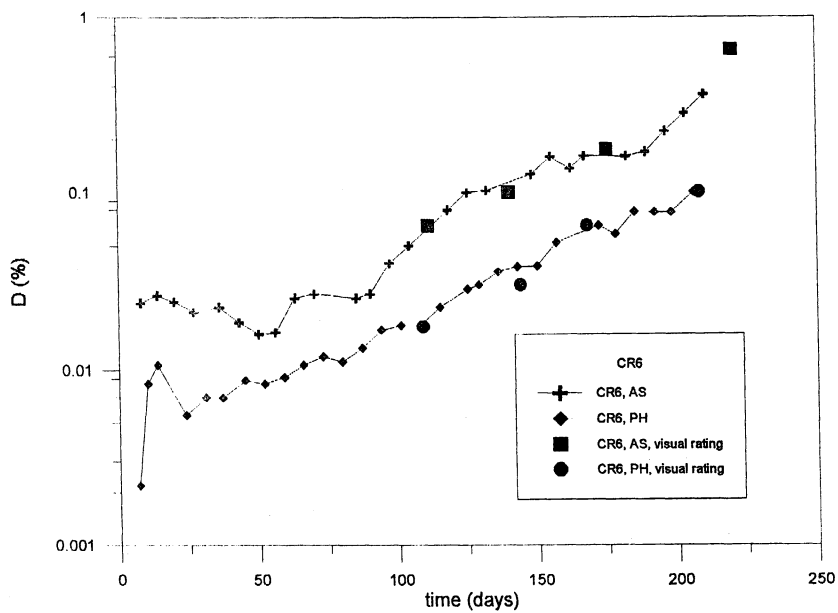


Figure 4. Time dependence of corroding area obtained from f_b and by visual observation according to ASTM D 610 for CR 6 exposed at Port Hueneme, CA.

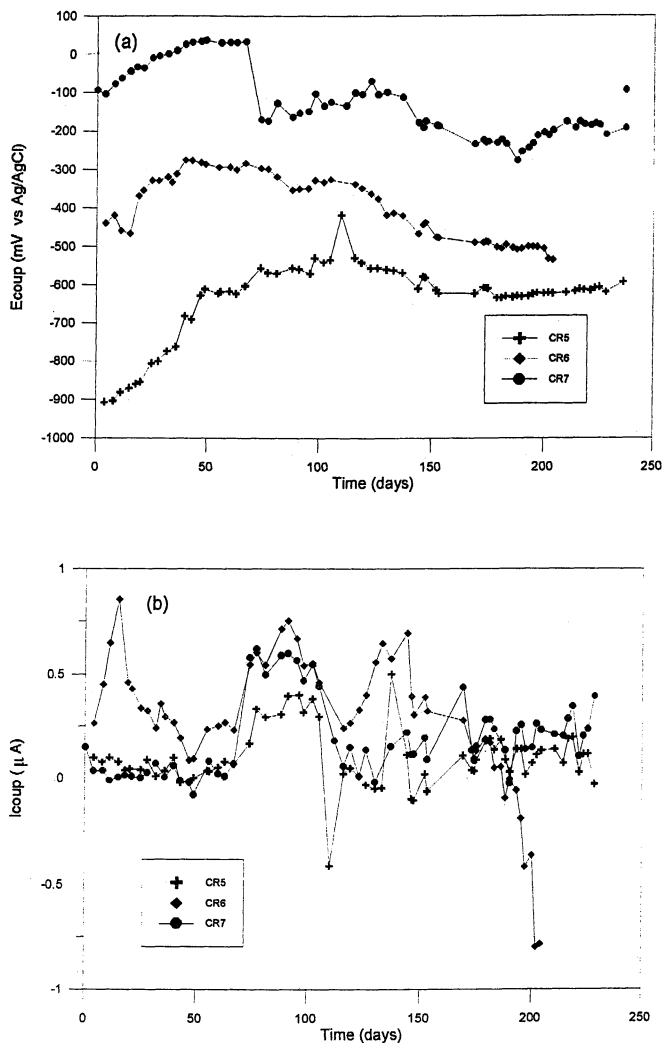


Figure 5. Time dependence of E_{coup} (Figure 5a) and I_{coup} (Figure 5b) for CR 5, CR 6 and CR 7 exposed at Port Hueneme, CA.

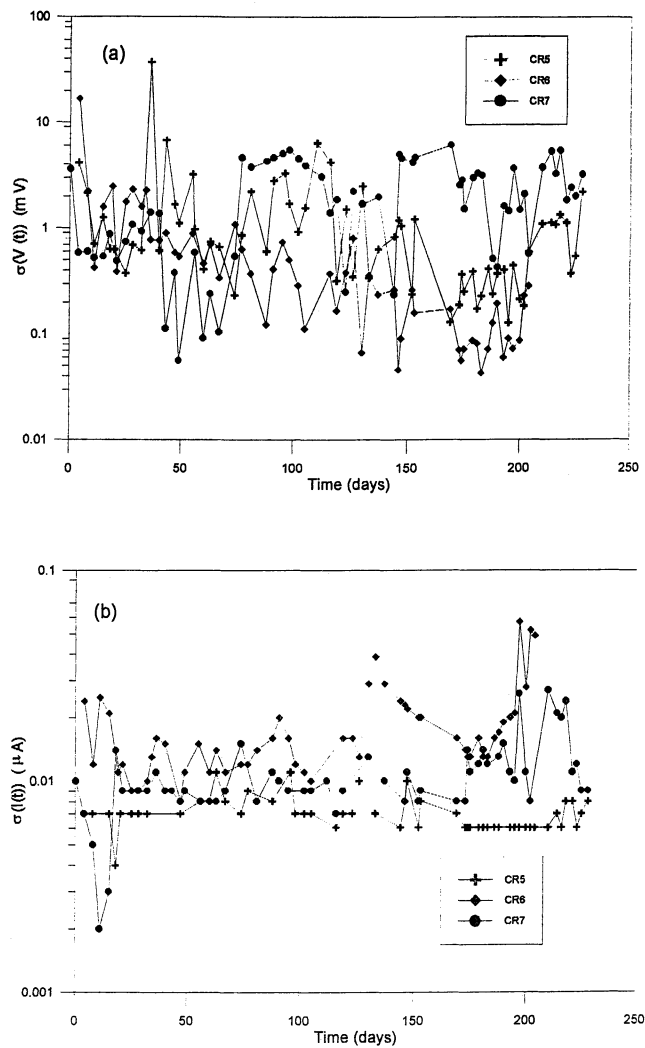


Figure 6. Time dependence of $\sigma\{V(t)\}$ (Figure 6a) and $\sigma\{I(t)\}$ (Figure 6b) for CR 5, CR 6 and 7 exposed at Port Hueneme, CA .

were observed for CR 5 (Figure 6b). This result points to a limitation of the present equipment indicating that the lowest value of $\sigma\{I(t)\}$ which could be detected was about 0.7 nA. Since $\sigma\{V(t)\}$ generally had values close to 1 mV, the maximum values of R_n which could be measured with the equipment used in this project were between 1 and 10 Mohm corresponding to 10^8 to 10^9 ohm.cm². Figure 7 shows the time dependence of R_n and R_{sn}^0 for CR 5, 6 and 7 at (PH). The values and time dependence of these two parameters were similar to those of R_{po} shown in Figure 3. It will be noted that R_n usually had smaller values than R_{sn}^0 (Figure 7).

Additional information can be obtained from power spectral density (PSD) plots which are shown in Figure 8 - 10 for CR 6 at KW for three exposure times. These figures also present comparisons of impedance spectra and spectral noise plots which can be obtained as discussed above or from PSD plots as $R_{sn}(f) = |V_{PSD}/I_{PSD}|^{1/2}$, where V_{PSD} and I_{PSD} are the potential and current power levels, respectively. FFT and PSD plots provide a convenient check of noise data quality which is difficult to obtain in the time domain. In general, V_{PSD} decreased and I_{PSD} increased continuously with constant slope as polymer coatings degraded.

In the PSD plots for polymer coatings exposed to NS and AS no dc limit was observed which probably was due to the very low PSD values. In fact, as shown in Figure 8a, I_{PSD} remained at or below the current power level of about 10^{-20} A²/Hz arising from the potentiostat used as ZRA until coating damage occurred. The slopes of the potential PSD plots remained close to -2, while the slopes of the current PSD plots were also close to -2 once the threshold level due to the instrumentation had been exceeded. For equal values of the slopes of both PSD plots the R_{sn} plots become independent of frequency.

Initially the R_{sn} plots were significantly lower than the impedance plots (Figure 8 - 10) due to the experimental I_{PSD} values which were too high and produced R_{sn} values which were too low. As I_{PSD} exceeded the instrumentation limit, R_{sn} plots approached impedance plots. Figure 8b - 10b also include R_n . After 33 days R_n was lower than R_{sn}^0 and R_p due to the instrumentation threshold discussed above. As time increased, R_n approached R_{sn}^0 and R_p , but always remained below these two values. This result is considered to be due to the manner in which these data were collected. R_{sn}^0 was obtained as the dc limit (or the average of the last 10 lowest frequency points), while R_n was determined at a sampling frequency $f_s = 2$ Hz.

Inspection of spectral noise plots and impedance spectra in Figure 8 - 10 for CR 6 demonstrates the limited frequency range in which spectral noise plots can be obtained. The high-frequency limit could be extended by increasing the data collection rate beyond the presently used 2 points/sec., however instrumentation noise limits this possibility. The low-frequency limit could be decreased by increased time for data collection (1024 sec. at present), however this possibility is not very attractive.

Comparisons of results obtained at the two marine test sites (PH and KW) and in AS will be given next for the coatings systems JJ 3 and JJ 4, which have a phosphate primer and a epoxy polyamide midcoat. JJ 4 has an additional polyurethane topcoat (Table II). The impedance spectra for JJ 3 (Figure 11) have a complicated frequency dependence which, in general, can be explained by

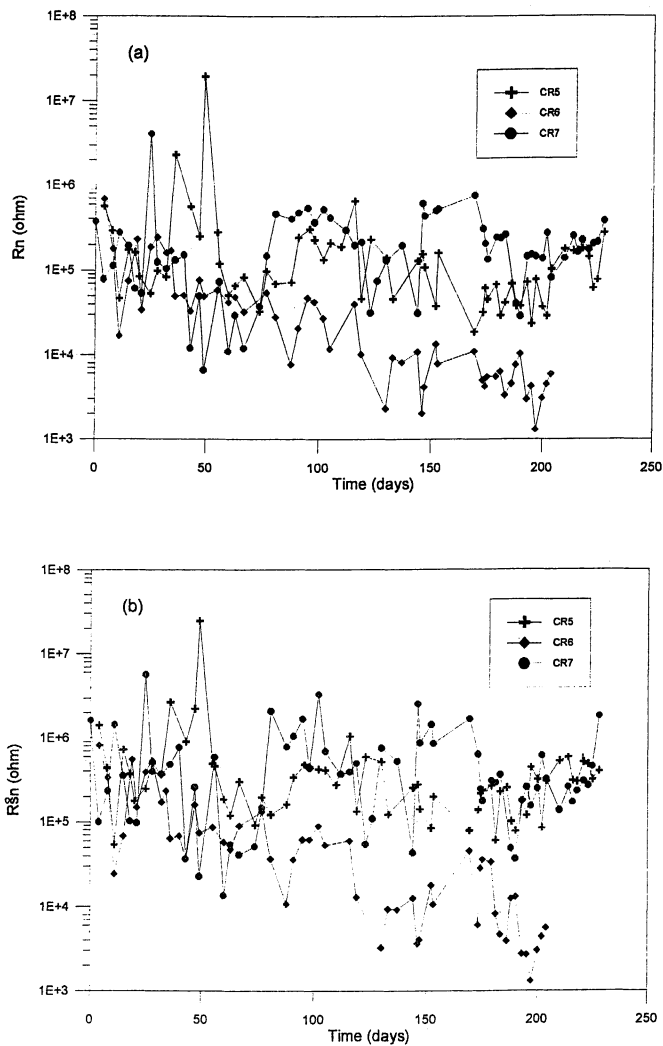


Figure 7. Time dependence of R_n (Figure 7a) and R_{sn}^0 (Figure 7b) for CR 5, CR 6 and CR 7 exposed at Port Hueneme, CA.

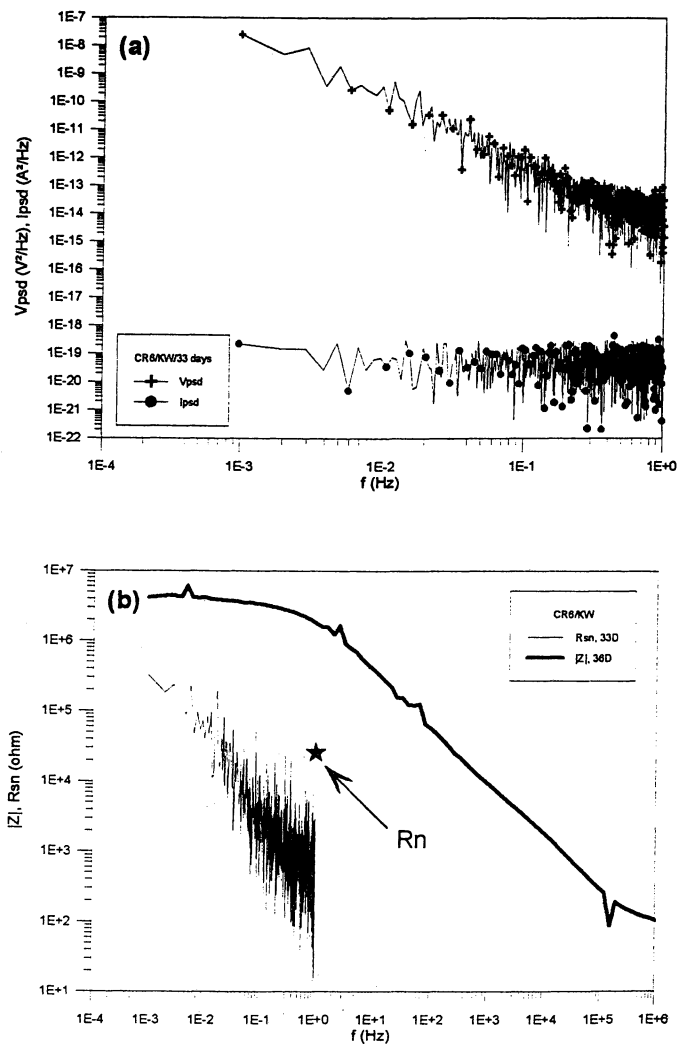


Figure 8. Potential and current PSD plots (Figure 8a) and comparison of impedance spectra (Z), spectral noise plots (R_{sn}) and R_n (Figure 8b) for CR 6 exposed at Key West (KW), FL for about one month.

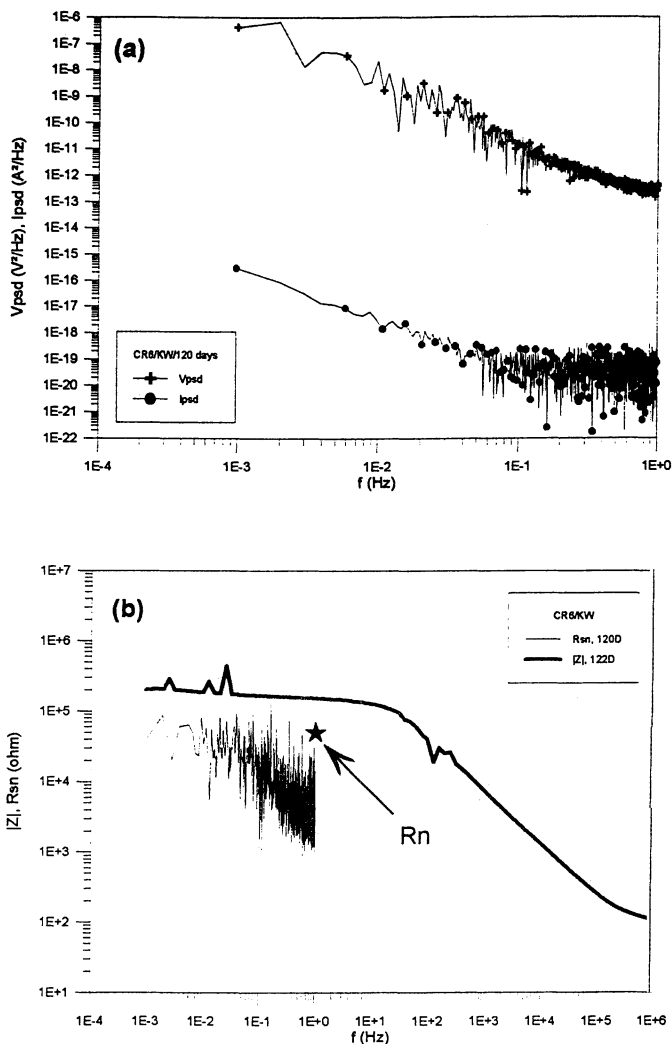


Figure 9. Potential and current PSD plots (Figure 9a) and comparison of impedance spectra ($|Z|$), spectral noise plots (R_{sn}) and R_n (Figure 9b) for CR 6 exposed at KW for about four months.

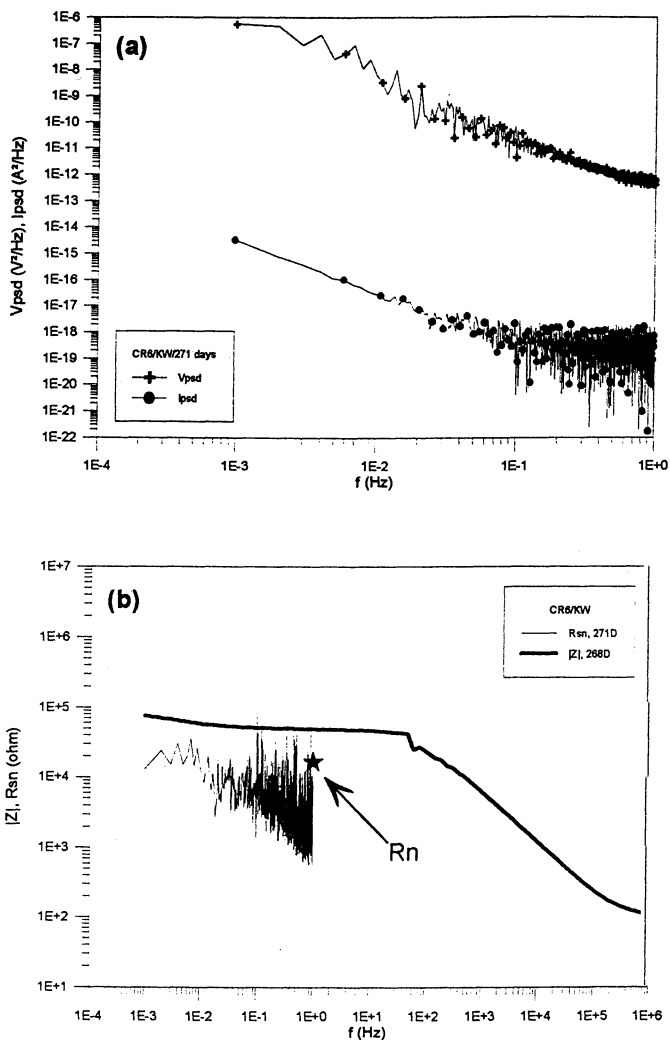


Figure 10. Potential and current PSD plots (Figure 10a) and comparison of impedance spectra ($|Z|$), spectral noise plots (R_{sn}) and R_n (Figure 10b) for CR6 exposed at KW for about nine months.

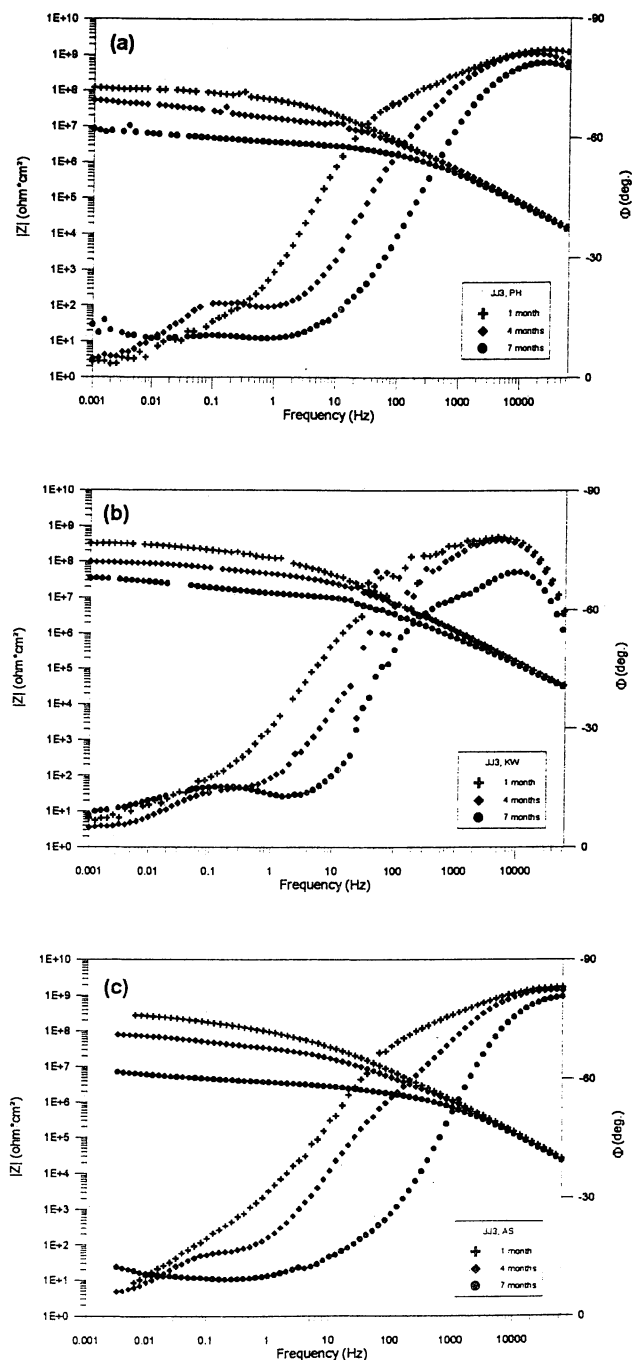


Figure 11. Impedance spectra for coating system JJ 3 exposed to NS (PH and KW) (Figure 11a and b) and AS (Figure 11c).

contributions from changes in the coating properties, delamination, charge transfer and mass transport processes [1]. The impedance decreased gradually for all three exposure conditions with increasing exposure time. The gradual increase of the breakpoint frequency f_b is an indication of coating degradation and initiation of corrosion (Figure 12). E_{coup} decreased in the first month and then remained at values close to E_{coup} for bare steel (Figure 13). Both R_n and R_{sn}^0 decreased continuously with time (Figure 14). Visual ratings of the samples exposed at PH and in AS according to ASTM D 610 decreased to values between 8.5 and 8 ($D = 0.1\%$) after 7 months due to the occurrence of small rust spots.

The impedance spectra for JJ 4 showed little change with time with impedance values remaining at about 10^9 ohm.cm² at 1 mHz (Figure 15). As for the other coating systems, the influences of charge transfer and mass transfer processes are evident from the frequency dependence of the impedance at low frequencies. A gradual increase of f_b was observed (Figure 16), however f_b for JJ 4 remained about a factor of 10 lower than for JJ 3 at all times in all three media (Figure 12). E_{coup} decreased continuously at PH and KW approaching the values for bare steel after 7 months, but remained at values typical for well-protected steel in AS (Figure 17). The R_n and R_{sn}^0 values did not change much with time (Figure 18). Visual rating remained at 9.5 since no rust spots were observed.

SUMMARY AND CONCLUSIONS

The relationship between spectral noise plots and impedance plots is subject to ongoing investigations using the vast amount of data collected for the coating systems exposed at Port Hueneme, CA and in AS for two years and at Key West, FL for more than one year. Recent results with improved instrumentation for current measurements have shown that spectral noise plots and impedance spectra are identical once valid current PSD plots can be obtained [11]. This means that the dc limit of an impedance spectrum corresponds to a spectral noise plot with zero slope in the same frequency range. R_n was found to be close to the average of all R_{sn} data in the measured frequency range which ranged from 1 Hz to 1 mHz in the present investigation [11]. Based on these results no significant relationships between R_n and specific coating properties are to be expected.

Since the performance of CR 6 is inferior to that of CR 5 and CR 7, one can conclude that the nature of both the primer (zinc-rich primer (CR 5 and CR 6) vs. epoxy polyamide (CR 7)) and the topcoat (polyurethane (CR 5) vs. latex (CR 6 and CR 7)) play an important role in corrosion protection. No coating degradation was observed for the epoxy polyamide system CR 9 (Table I) during exposure for almost two years at PH and in AS and for almost one year at KW. Based on the results obtained for all CR coatings with EIS, ENA and visual observation for exposure at Port Hueneme, CA and Key West, FL as well as in laboratory experiments it can be concluded that the effectiveness of corrosion protection decreased in the sequence CR 9 > CR 7 > CR 5 > CR 6 > CR 1 > CR 2 [1]. This conclusion is in general agreement with the results by Murray and Hack [12], who exposed CR 1, CR 5, CR 6 and CR 9 to AS, and by Tsai and Mansfeld [8], who exposed the same materials and CR 2 to 0.5 N NaCl. The relatively poor performance of the alkyd-based paints CR 1 and CR 2 and the excellent corrosion protection by the epoxy polyamide paint CR 9 were found in all cases. However, in the earlier studies [8,12] CR 6 performed better than CR 5.

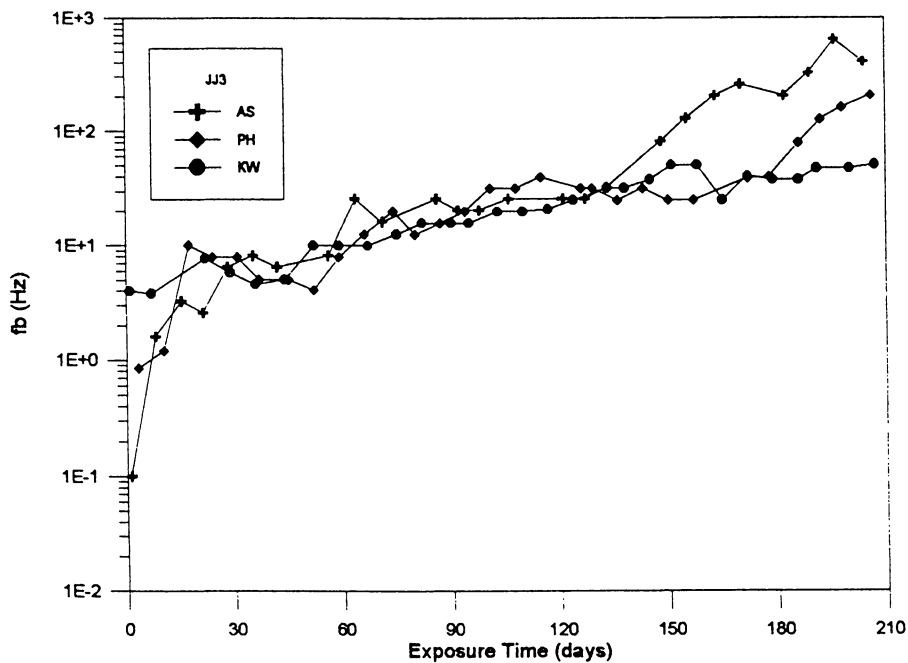


Figure 12. Time dependence of breakpoint frequency f_b for JJ 3 exposed to AS and NS .

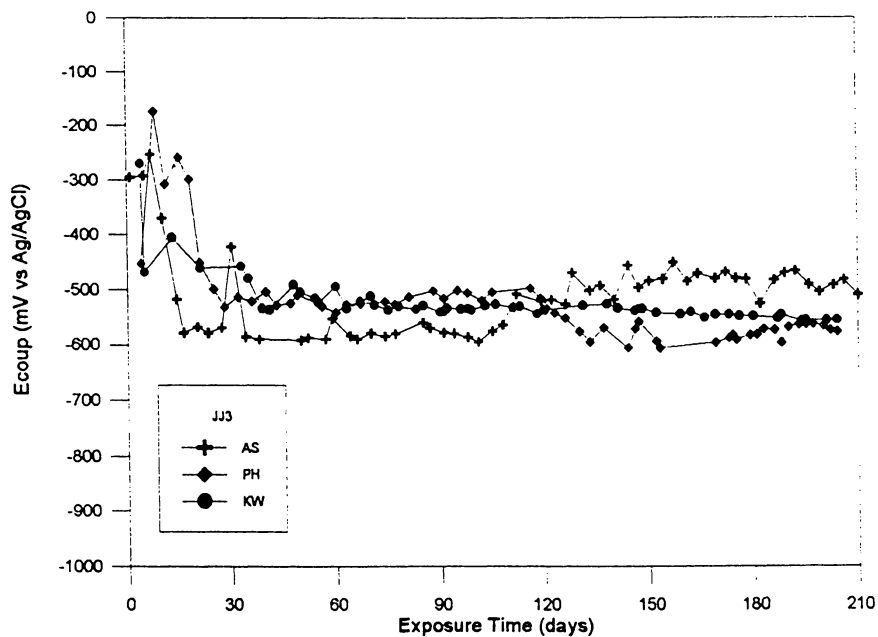


Figure 13. Time dependence of E_{coup} for JJ 3 exposed to AS and NS.

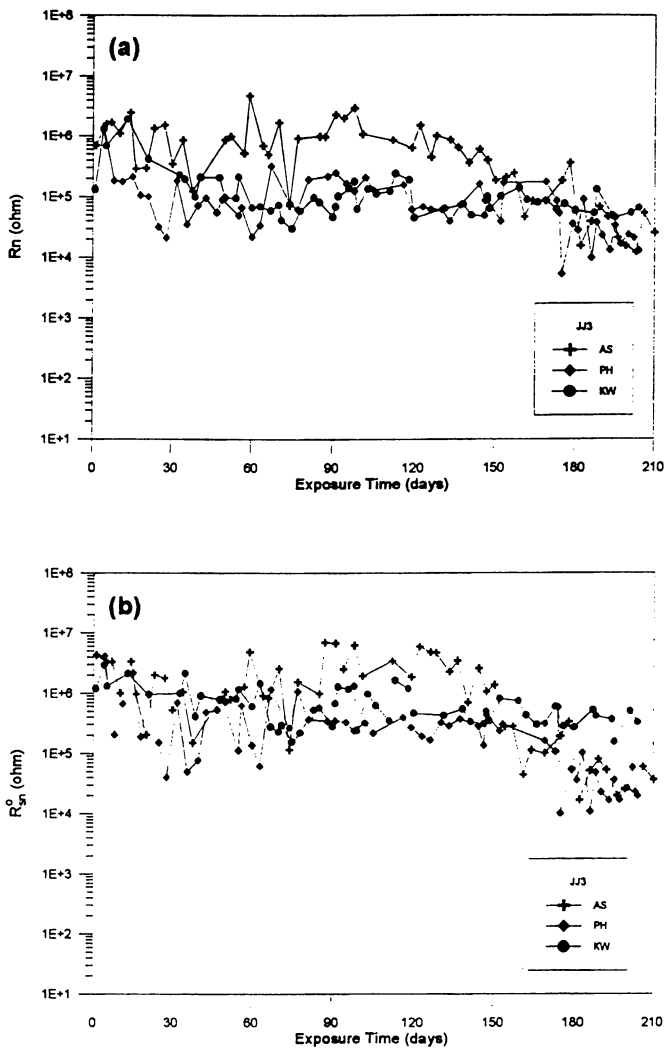


Figure 14. Time dependence of R_n (Figure 14a) and R_{sn}^0 (Figure 14b) for JJ 3 exposed to AS and NS.

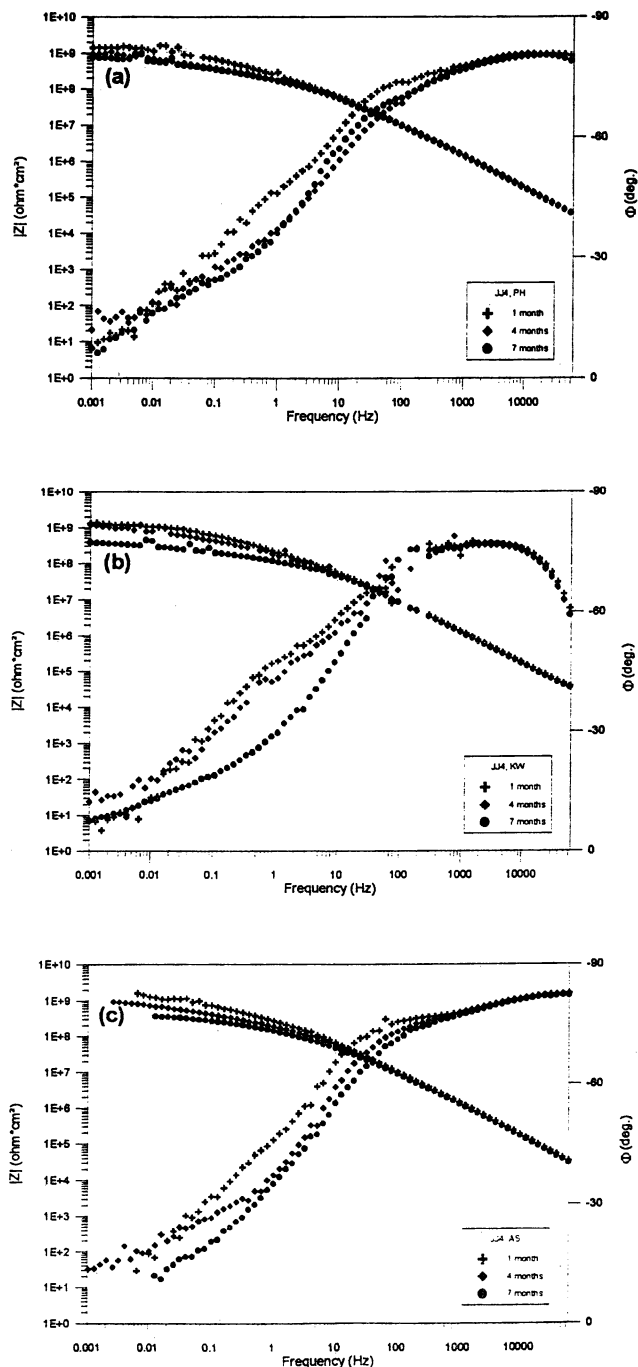


Figure 15. Impedance spectra for coating system JJ 4 exposed to NS (PH and KW) (Figure 15a) and AS (Figure 15c).

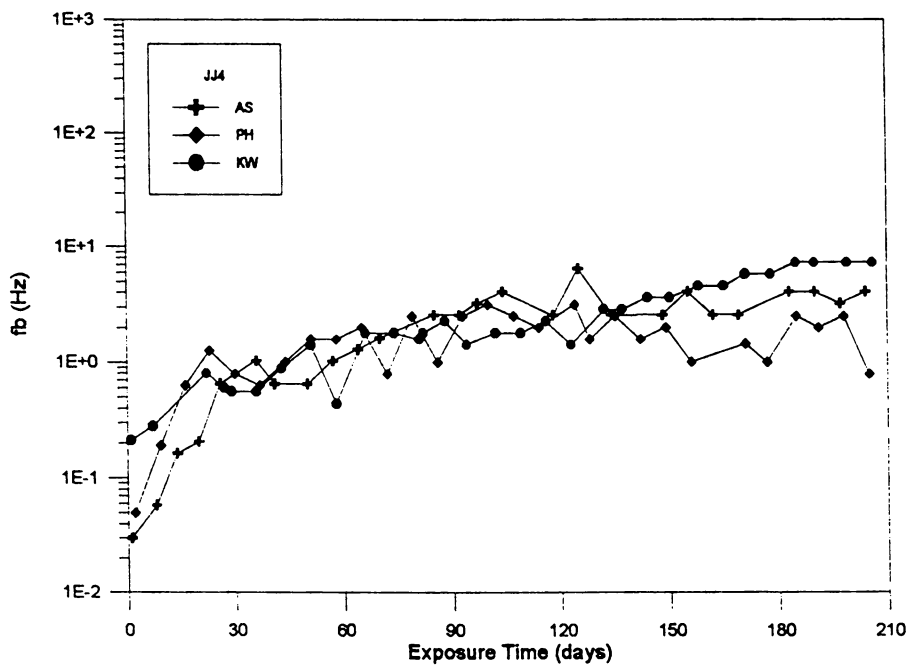


Figure 16. Time dependence of breakpoint frequency f_b for JJ 4 exposed to AS and NS.

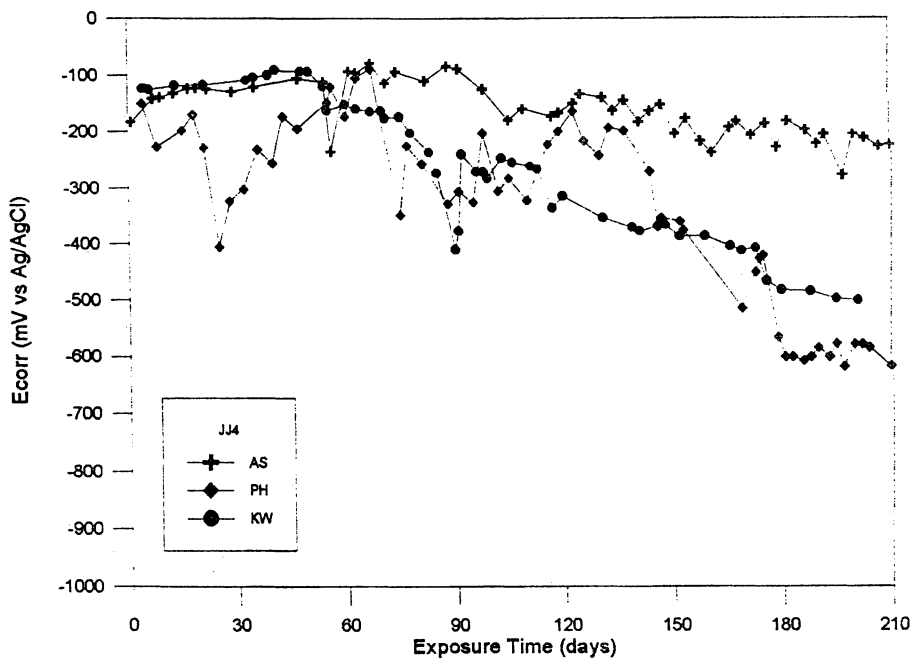


Figure 17. Time dependence of E_{coup} for JJ 4 exposed to AS and NS.

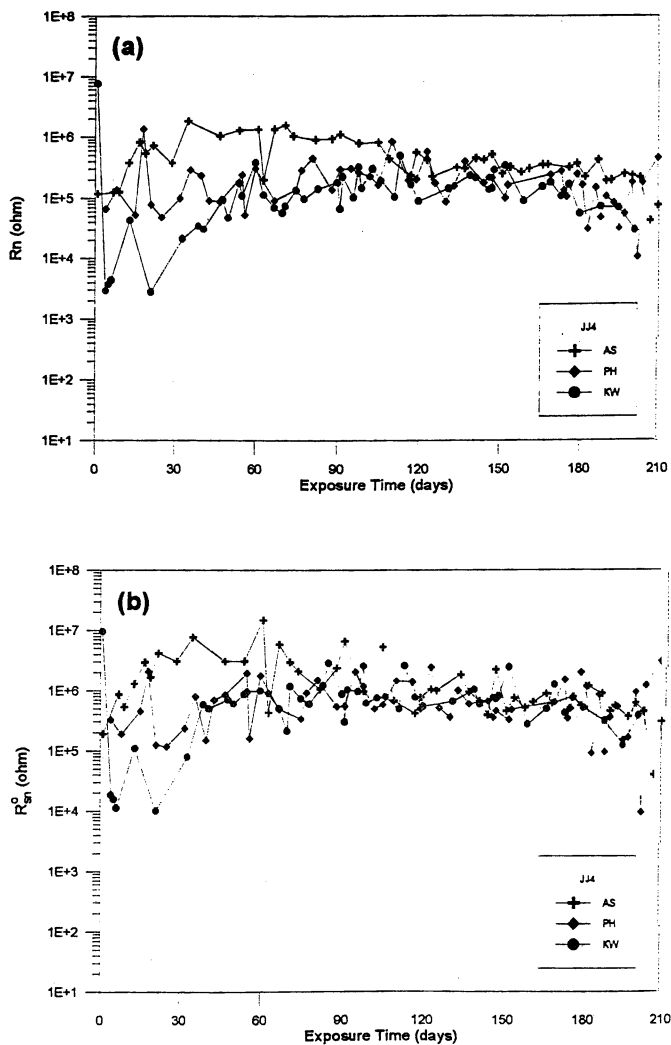


Figure 18. Time dependence of R_n (Figure 18a) and R_{sn}^0 (Figure 18b) for JJ 4 exposed to AS and NS.

For the JJ series it was found that JJ 1 and 2 with a metallic Zn primer (Table I) and JJ 5 and 6 with an IVD-Al primer (Table II) performed well [1,13,14]. No steel corrosion was detected in the first seven months due to cathodic protection by Zn and Al, respectively. However, rusting was observed in NS and AS for JJ 3 with a phosphate primer without a topcoat. The results in Figure 11 - 14 reflect the relatively poor performance of JJ 3. The polyurethane topcoat provided additional protection for JJ 4. However, preliminary analysis of the results obtained in NS and AS for longer exposure periods suggested that microorganisms in NS degraded the polyurethane topcoat of JJ 2, 4 and 6 in agreement with previous reports [5,6]. Corrosion protection provided by the polyurethane topcoat (JJ 2, JJ 4 and JJ 6) was more significant in AS than in NS.

A detailed analysis of the effects of coating properties and microorganisms on corrosion protection of steel by polymer coatings will be performed when all samples have been removed from the test sites in California and Florida and the laboratory.

ACKNOWLEDGMENT

This project is being funded by the Office of Naval Research (Dr. A. J. Sedriks) under Contract No. N00014-94-1-0026.

REFERENCES

1. H. Xiao, "Development of the Electrochemical Noise Analysis Technique and its Application in Monitoring of Localized Corrosion Phenomena", Ph. D. thesis, Univ. Southern California, Sept. 1995.
2. F. Mansfeld, H. Xiao, L. T. Han, C. C. Lee, C. Chen, C. Perez and J. Jones-Meehan, "Evaluation of the Effects of Microorganisms on Corrosion Protection of Steel by Polymer Coatings", Proc. 1995 Int. Conf. on Microbially Influenced Corrosion, New Orleans, LA, May 1995, American Welding Society and NACE, 47-1.
3. F. Mansfeld, C. Chen, C. C. Lee, and H. Xiao, *Corros. Sci.* **38**, 497 (1996).
4. H. Xiao and F. Mansfeld, *J. Electrochem. Soc.* **141**, 2332 (1994).
5. R. G. Baker, G. H. Kitchen and R. R. Welch, *Nat. Bur. Stand. (US) Spec. Publ.* **452**, 25 (1976).
6. K. J. Seal and R. A. Pathirana, *Int. Biodet. Bull.* **18**, 81 (1982).
7. F. Mansfeld, H. Xiao, L. T. Han, C. C. Lee and C. Chen, *Corrosion/96*, paper No. 659, NACE (1996)
8. C. H. Tsai and F. Mansfeld, *Corrosion* **49**, 726 (1993).
9. F. Mansfeld, *J. Appl. Electrochem.* **25**, 187 (1995)
10. F. Mansfeld and H. Xiao, *ASTM STP* **1232**, 42 (1994).
11. F. Mansfeld, C. C. Lee and G. Zhang, "Comparison of Electrochemical Impedance and Noise Data in the Frequency Domain", submitted to *Electrochim. Acta*
12. J. N. Murray and H. P. Hack, *Corrosion* **48**, 671 (1992)
13. F. Mansfeld, L. T. Han and C. C. Lee, "Analysis of Electrochemical Impedance and Noise Data for Polymer Coated Steel in the Time and Frequency Domains", *J. Electrochem. Soc.* (in press).
14. H. Xiao, L. T. Han, C. C. Lee and F. Mansfeld, "Collection of Electrochemical Impedance and Noise Data for Polymer Coated Steel from Remote Test Sites", *Corrosion* (in press).

Chapter 15

Failure Mode Prediction of Organic Coating–Metallic Substrate Systems

L. Nicodemo, T. Monetta, and F. Bellucci

Department of Materials and Production Engineering, University of Naples,
Federico II, Piazzale Tecchio, 80125 Naples, Italy

A mathematical model has been introduced to describe salt uptake and transport through homogeneous and heterogeneous organic coatings. Two approaches have been presented and discussed as far as the heterogeneous systems are concerned. In the first one it has been assumed that the solution filling the heterogeneity or pores is not in thermodynamic equilibrium with the electrolyte solution dissolved in the homogeneous part of the film, while in a second approach thermodynamic equilibrium is assumed. The concept and the role of pores as related to coating's performance has been also addressed. Results obtained in this investigation indicate that the degradation of the metallic substrate can be related to coating's properties such as porosity, tortuosity factor, Cl⁻ ion diffusion and distribution coefficients, and coating thickness. By comparing theoretical results with experimental data it is possible to discriminate between interfacial failure due to adhesion loss (interfacial defects) from failure due to pores present in the coating.

Organic coatings in the form of paints are widely used for protecting metals against corrosion. Changes in electrical properties (dielectric constant and resistivity) during the exposure of organic coating systems to aqueous environments have been the subject of a vigorous research activity in the last decade (see references [1-8], and literature cited therein). An organic coating protects against corrosion by various mechanisms that can be summarised as follows: (i) by depression of the anodic and/or cathodic reaction, (ii) by the introduction of a high electrical resistance into the circuit of the corrosion cell, and (iii) as a barrier to aggressive

species (oxygen, water and ions). Many papers have addressed the physical nature of organic coatings as a barrier to aggressive neutral and ionic permeants (H_2O , O_2 , Cl^-) [1-8]. Main results of the analysis so far presented suggest that water sorption and transport in organic coatings in the early stage of exposure to an aqueous salt solution affects the dielectric constant of the water-coating system, whereas the uptake of salt affects coating's resistivity at later stage of exposure. The concept of a paint film as an impermeable membrane, however, has been largely discredited by permeability data for water and oxygen. In many paint systems, the water and oxygen permeance was found to be high enough to sustain the corrosion rate of the bare substrate, indicating that the rate determining step of the corrosion process is not related to water and oxygen transport to the metal surface [2,8].

This paper examine the possibility to describe salt uptake through organic coatings as related to the coating's structure and properties. A mathematical model will be introduced and discussed to describe salt transport in homogeneous and heterogeneous organic coatings. The concept and the role of "pores" as related to the coating lifetime will be also addressed. Aim of this investigation is to relate the degradation of the metallic substrate to coating's properties such as porosity, tortuosity factor, Cl^- ion diffusion and Cl^- distribution coefficients, and coating thickness. Finally, theoretical results will be compared with experimental data allowing to discriminate between failure due to electrolytes penetration through reduced pathways (defects or heterogeneity) of the coating, from failure due to the interfacial adhesion loss due to the electrochemical process at the metallic interface.

Mathematical Model

In this section an attempt will be made to introduce and to discuss the concept and the role of "pores" as related to the coating lifetime. Two approaches will be presented and discussed. In the first one it will be assumed that the solution filling the heterogeneity or "pores" is not in thermodynamic equilibrium with the electrolyte solution dissolved in the homogeneous part of the film, while in a second approach thermodynamic equilibrium is assumed. Before discussing these models some preliminary concepts will be introduced.

It is generally recognised that coating breakdown is related to the underfilm corrosion process. This process can take place when all the necessary "ingredients", i.e. water, oxygen and electrolyte (Cl^-) are available at the interface. Water, oxygen and ions are taken up into the organic coating film at a rate depending on their diffusion coefficient, D . Each sorption process is based on the following first and second Fick's law:

$$J = -D \frac{\partial C}{\partial x} \quad (1)$$

$$\frac{\partial C}{\partial t} = D \frac{\partial^2 C}{\partial x^2} \quad (2)$$

where J is the solute flux, C the concentration and D is either the water, the oxygen or the chloride ion diffusion coefficient.

In order to obtain the amount of penetrant (water, oxygen and chloride ion) taken up by the coating as a function of the time as well as its equilibrium value, eq. 2 must be solved with the appropriate boundary conditions. The thermodynamic equilibrium rather than the kinetics of solute uptake, will be assumed in this paper as the parameter that affects interfacial coating breakdown.

When a coated metal is immersed in an aqueous salt solution, the first step of the overall degradation process is water, oxygen and salt uptake. Water, oxygen and salt uptake in a homogeneous free standing polymeric film of thickness L can be described according to Fick's law by using the dimensionless time variable $\tau = tD/L^2$ (D is the diffusion coefficient). The thermodynamic equilibrium between the external and internal (film) solution, occurs for $\tau \geq 1$ [9]. Accordingly, the time required to saturate a supported organic coating film of thickness L (neglecting the effect of the metallic substrate), is given by:

$$t \geq \frac{(2L)^2}{D} \quad (3)$$

Since the Cl^- diffuse into an organic polymer at the lowest rate compared to those of water and oxygen, then the time required to reach equilibrium between the Cl^- dissolved into the coating and the Cl^- of the external electrolyte is the rate determining step for corrosion to occur at the coating/metallic interface. This time is defined as the "minimum (coating) life time", MLT and is given by:

$$\text{MLT} = \frac{(2L)^2}{D} \quad (4)$$

In effect, the MLT corresponds to the time required for the electrolyte to reach the maximum concentration at the coating/metallic interface. The time at which this interface fails can be no less than the MLT, but it can be very much larger, depending upon the Cl^- ion concentration at the coating/metal interface, the kinetics of the interfacial corrosion and delamination rate, for example.

If the coating is homogeneous, then the diffusion coefficient to be inserted into eq. 4 is the chloride ion homogeneous diffusion coefficient into the coating fully saturated with water. If the coating is heterogeneous, then the diffusion coefficient to be used in conjunction with eq. 4 must take into account: (i) the salt transported into the pores, (ii) the salt transported into the homogeneous part of the coating, and (iii)

the salt transport between the volume of solution filling the pores and the homogeneous part of the coating. In each of these cases eqs. 1 and 2 must be modified appropriately to account for these additional effects. Before addressing these issues, two extreme cases will be analysed first: (i) a homogeneous film of thickness L fully saturated with water, and (ii) a stagnant water layer of thickness L separating the metallic interface from the environment. The latter case can be considered equivalent to that of a coating fully porous. In the first case $D=D_{s,f}$ while in the second case $D=D_{s,w}$, where $D_{s,f}$ and $D_{s,w}$ represent the Cl^- diffusion coefficient in the homogeneous film and in water, respectively. The minimum lifetime of a coating, therefore, varies between $\text{MLT}_w=(2L)^2/D_{s,w}$ and $\text{MLT}_f=(2L)^2/D_{s,f}$.

The real situation differ from the above two limiting cases. The coating will contain, to some extent, "pores" of not well defined geometry and structure such as those schematically reported in Fig. 1 as "a", "b", "c", "d", and "e". It should be appreciated that the MLT for cases "a", "d", and "e", are expected to be of the same order of magnitude since in each case the electrolyte must penetrate the same effective path length through homogeneous film. On the other hand, the ultimate failure of the interface is likely to occur more readily for case "a", which includes the interface between the coating and substrate than for either case "d" or "e" which are removed from the interface. In order to account for the presence of such "pores" in the mathematical model, the coating porosity θ can be defined as: $\theta=V_p/V_T$, where V_p and V_T are the volume of "pores" and the nominal volume of the coating, respectively. No pores size distribution will be considered in the present investigation.

In the first approach it is assumed that only "pores" of the type "b" and "c" exist. In addition it is further assumed that the pores diameter, d_p , is large enough to neglect the flux of Cl^- from the solution filling the pores to the pores wall (homogeneous part of the coating). According to the schematic of Fig. 1, the flux N is assumed to be much less than the flux J . First and second Fick's law describing salt uptake into these "pores" are still given by eqs. 1 and 2. The time to saturate the continuous pores is much smaller than the time required to saturate the homogeneous part of the film. In this case the MLT, is given by:

$$\text{MLT} = \frac{(2L)^2 \tau_p}{D_{s,w}} \quad (5)$$

where τ_p is a pore tortuosity factor defined as the ratio between the real path length and the nominal thickness ($\tau_p=1$ for "c" type "pores" and $\tau_p>1$ for "b" type "pores"). The MLT is, thus, a function of τ_p and of L^2 not on the porosity θ .

As second approach, it is assumed that equilibrium exists at any time t between the homogeneous part of the coating and the electrolyte solution

filling the pores. The unsteady state processes of interest are, in this case, those occurring into the homogeneous part and into the pores of the film. The solute flux into the homogeneous film, J_f , and into the pores, J_p , (first Fick's law) can be written as:

$$J_f = -D_{s,f} \frac{(1-\theta)}{\tau_f} \frac{\partial C_f}{\partial x} \quad (6)$$

$$J_p = -D_{s,w} \frac{\theta}{\tau_p} \frac{\partial C}{\partial x} \quad (7)$$

where τ_f and τ_p are the tortuosity factor of the film and of pores, respectively. Due to the thermodynamic equilibrium between the solution filling the pores and the solution homogeneously dissolved into the film, the electrolyte concentration into the film, C_f , is given by: $C_f = KC$, where K is the distribution coefficient that is assumed constant with the concentration.

After some manipulations, the second Fick's law describing the uptake of salt into the pores can be written as:

$$\frac{\partial C}{\partial t} = D_{cq} \frac{\partial^2 C}{\partial x^2} \quad (8)$$

where D_{cq} is an equivalent diffusion coefficient given by:

$$D_{cq} = \frac{D_{s,f} \frac{K}{\tau_f} (1-\theta) + D_{s,w} \frac{\theta}{\tau_p}}{K(1-\theta) + \theta} \quad (9)$$

Due to the assumption made on the constancy of K with the concentration, eq. 8 is equivalent to eq. 2. The MLT is, thus, given by:

$$MLT = \frac{(2L)^2}{D_{cq}} \quad (10)$$

Eq. 10 shows that the MLT depends, in this case, on L^2 and on the equivalent diffusion coefficient, D_{cq} that is depending on the porosity θ , on the distribution coefficient K , on the tortuosity factors, τ_f and τ_p , and on the Cl^- diffusion coefficient in the water and into the homogeneous part of the film. Eq. 9 well describes the two limiting cases of $\theta \rightarrow 1$ and $\theta \rightarrow 0$ mentioned above. In the former case $D_{cq} \rightarrow D_{s,w}$ (layer of water of thickness L), in the latter case $D_{cq} \rightarrow D_{s,f}$ (homogeneous film of thickness L).

It must be pointed out, however, that this model does not account for

the presence of osmotic stresses at the interface due to the absorption of electrolyte in the film.

Results and Discussion

The organic coating investigated in this paper was a commercially available PMDA-ODA made from pyromellitic dianhydride (PMDA) and oxydianiline (ODA). The polymer film of interest was deposited on pure aluminium and iron as metallic substrate using the spin coating technique (6000 rpm for 90 s) and then cured. A β -stage cure (135 °C for 10 minutes in air) followed by a final curing step at 400 °C for 45 minutes in nitrogen was adopted. The electrochemical impedance spectroscopy technique (EIS) was used to follow the degradation of the polymer coating system in the test solution (0.5 M air saturated sodium chloride at the temperature of 20 ± 1 °C). EIS was performed by using a Schlumberger Solartron 1250 Frequency Response Analyser (FRA) connected to a Solartron 1286 potentiostat. The analyser was controlled by a Hewlett-Packard desktop computer. During data acquisition, samples were potentiostatically held at the corrosion potential, E_{corr} , and a sinusoidal perturbation of 20 mV was applied to the system. The current response was generally measured over a range of frequencies from 65 kHz to 0.1 Hz at 10 steps/decade. EIS spectra were recorded, at ambient temperature, as a function of immersion time.

Figs. 2 and 3 show the Bode plot for two 1.2 μm thick PI/Al samples ("A" and "B") while Fig. 4 shows the Bode plot for a 2.4 μm film as a function of immersion time in aerated 0.5 M NaCl solution at room temperature, respectively. As can be seen from these figures all samples exhibit the same features but on a different time scale. A capacitive behaviour at early immersion followed by a more complex spectrum for prolonged immersion in the test solution is observed. In this latter case the Bode angle plot shows two time constants (τ_f for the film and τ_{ct} for the metal), given by:

$$\tau_f = R_f C_f^* ; \quad \tau_{\text{ct}} = R_t C_d^* \quad (11)$$

where R_f and C_f^* are the film resistance and capacitance, R_t the charge transfer resistance, and C_d^* the double layer capacitance, respectively. The time constant at higher frequencies is due to the film if $\tau_f < \tau_{\text{ct}}$, which is usually the case.

The impedance response over the lifetime of the film reported in Figs. 2, 3 and 4 can be related to the various stages of degradation at the PI/Al interface. Initially, the film acts as a pure dielectric separating the metallic substrate from the aggressive external environment. This behaviour results in purely capacitive behaviour (see for example Fig. 2 after 1 day immersion, Fig. 3 for immersion times up to 30 days and Fig. 4 for immersion times up to 25 days). The second step is water and ion

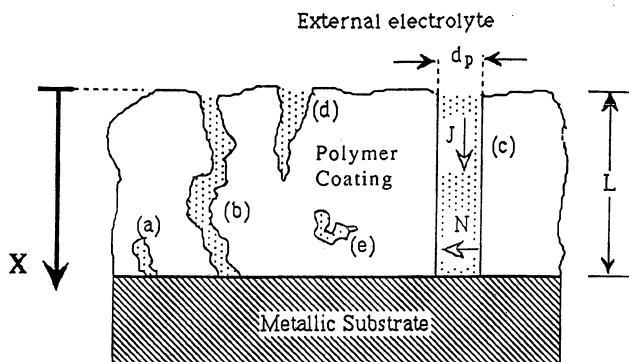


Figure 1. Schematic of the coating-metallic interface showing the different type of "pores".

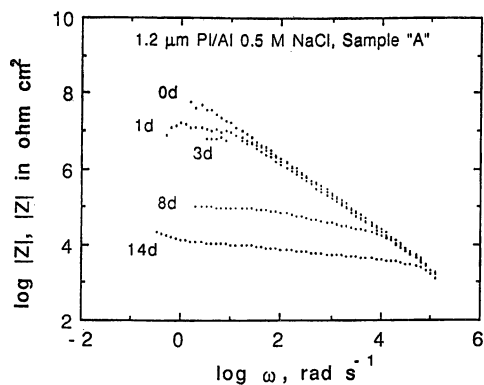


Figure 2 Bode plot as a function of immersion time for the 1.2 μm thick PI/Al system (sample "A") in air saturated 0.5 M NaCl at room temperature.

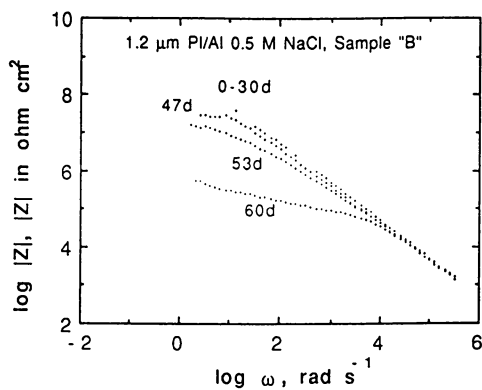


Figure 3. Bode plot as a function of immersion time for the 1.2 μm thick PI/Al system (sample "B") in air saturated 0.5 M NaCl at room temperature.

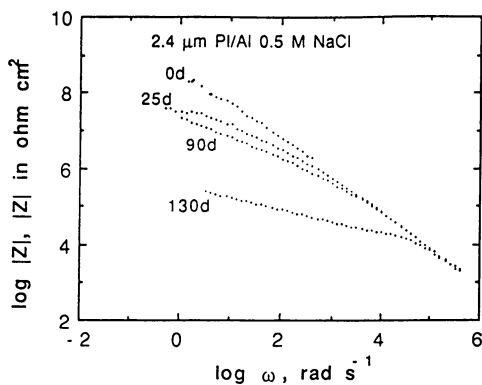


Figure 4. Bode plot as a function of immersion time for a 2.4 μm thick PI/Al system in air saturated 0.5 M NaCl at room temperature.

uptake within the film, either homogeneously through the film or heterogeneously due to defects. At this stage the water and ion uptake can modify the capacitive response leading to either one (see Figs. 2, 3 and 4 up to 3, 47 and 25 days of immersion, respectively) or two time constants (Figs. 2, 3 and 4 after 8, 53 and 130 days, respectively). Two time constants are indicative of the first separation of film and metal substrate properties. Similar results were also obtained for the PI/Fe system. Two time constants were observed after 1 and 5 h of immersion for the 5 and 15 μm film in the latter case, respectively.

To compare results from the mathematical model with experimental findings a criteria for coating's failure should be available. Different criteria have been reported in the literature to assess coating breakdown as related to water or salt taken up by the coating for prolonged immersion in NaCl solutions [10-12]. Two different paint behaviour types were described in the literature, which were independent of the method to determine coating lifetime [11,12].

The first showed a decrease in lifetime with an increase in NaCl concentration [11], while the second showed the opposite behaviour [12]. The appearance of a second time constant in the Bode (or phase angle) plot was used as the criteria to determine lifetime in this paper. The second time constant is associated with an electrochemical reaction at the coating/metallic interface. On this basis, the sample "A" exhibits a life time ranging between 3 and 8 days, the lifetime of sample "B" ranges from 47 to 53 days while the lifetime of a 2.4 μm thick film is equal to 130 days (PI/Al system). The 5 μm coated Fe sample exhibits a lifetime of 1 h, while the lifetime for the thicker sample is 5 hrs (PI/Fe system). These values are shown in Fig. 5 as a function of the film thickness on a log-log plot.

The difference in the lifetime experimentally observed in the case of PI/Al (samples "A" and "B") and PI/Fe systems could be ascribed, according to eq. 5, to the presence of macroscopic defects characterised by a difference (by orders of magnitude) of the tortuosity factor. It is reasonable, however, that due to the small values of the thickness L , τ_p is, likely, on the order of 1, therefore the experimental lifetime values cannot be ascribed to different tortuosity factors among the samples investigated. At the same time it should be pointed out that "pores" with $d_p \sim L$ can be considered as large defects. Although this approach fails in describing the experimental lifetime findings, an estimate of τ_p and of d_p were obtained. These estimate will be used to evaluate the MLT values as shown below.

To compare the MLT as calculated by the second approach (eqs. 9 and 10) with the experimental lifetime, it is reasonable to assume, $\tau_f \sim \tau_p \sim 1$ as described above. The diffusion and distribution coefficient of Cl^- across PI have been reported in the literature as $1 \times 10^{-13} \text{ cm}^2 \text{ s}^{-1}$ and 0.01 [13], while the Cl^- diffusion coefficient in water is equal to $1.5 \times 10^{-5} \text{ cm}^2 \text{ s}^{-1}$. On these basis, the theoretical MLT values as a function of L are reported in Fig. 5 for different values of the porosity θ . As can be seen, the experimental

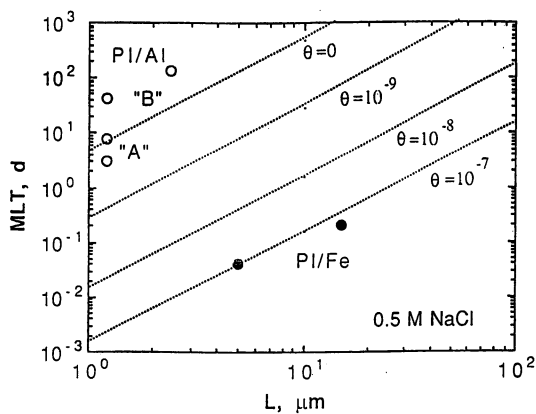


Figure 5. MLT in days as a function of L for different values of θ for the PI in presence of 0.5 M NaCl. In the same Figure the experimental lifetime for the PI/Al (samples "A" and "B") and the PI/Fe system in air saturated 0.5 M NaCl at room temperature are also reported.

lifetime data for the sample "A" (PI/Al system), lie in the vicinity of the MLT values for $\theta=0$, while those of sample "B" lie well above the MLT values for $\theta=0$. This result indicates that both the PI/Al samples ("A" and "B") can be assumed as homogeneous as far as the Cl^- ion diffusion across the PI is concerned in spite of the shorter lifetime exhibited by sample "A". If, on the other hand, heterogeneity such as pores "b" are present in the case of sample "A", the order of magnitude of these invisible "holes" must be very low as will be shown later.

As reported above, the time at which failure is observed can be larger than the MLT depending on the type and on the "pores" distribution into the PIs. The macroscopic difference in the lifetime observed for samples "A" and "B", could be attributed, therefore, to a greater number of "a" type pores in sample "A". Unreleased water or solvent trapped at the interface, may have acted as source of stress reducing the adhesion between the polymer and the metallic substrate leading to such interfacial defects. In these defects water can easily accumulate thus providing the medium in which the Cl^- ions coming from the homogeneous part of the coating can concentrate up to its equilibrium value that is 0.5 M. In presence of this high Cl^- ion concentration, Al corrodes at high rate leading to the early failure of the PI/Al system. Although it is not possible at this time to discriminate between the two possible degradation mechanism (via distributed thin type "b" pores or via interfacial "a" type defects), it is remarkable to point out that the early failure observed for sample "A" can be attributed to a poor interfacial adhesion rather than originated from large coating defects due to processing.

Quite different is the behaviour of the PI/Fe system. The experimental lifetime values lie well below the MLT values for $\theta=0$. The experimental lifetime well coincide with the MLT values obtained assuming a porosity $\theta=10^{-7}$. The presence of "b" and "c" type "pores" can, thus, account for the early failure observed in this case. An estimate of the "pores" size diameter, d_p , can be attempted on the basis of the following argument. A coating containing n "c" type pores of diameter d_p (for 1 cm^2 of nominal coating surface) is characterised by a value of $\theta \approx n d_p^2$. SEM carried out on PI of comparable thickness showed that there are no pores larger than $0.1 \mu\text{m}$. It can, thus, be concluded that a porous film with $d_p \sim 0.1 \mu\text{m}$ and $\theta=10^{-7}$ is compatible with a number of "pores" $n \sim 10^3$. Diffuse heterogeneity rather than macroscopic defects are, therefore, responsible for the corrosion behaviour of the PI/Fe system. Such invisible "pores" formed during the processing of the PI dramatically affect the PI/Fe lifetime.

It is worthwhile to mention that the theoretical analysis presented above allows to predict that heterogeneity as small as $0.1 \mu\text{m}$ (that are difficult to detect even at SEM) can reduce the MLT of thin films by orders of magnitude. In addition, a method has also been suggested to distinguish between failure due to defects into the coating ("b" and "c"

pores), from failure due to the loss of interfacial adhesion ("a" defects) depending upon their position with respect the MLT values for $\theta=0$. The closer are the experimental lifetime data to the MLT values for $\theta=0$, the larger is the metallic surface involved in the interfacial corrosion process the greater are the number of "a" type heterogeneity.

It should be pointed out, however, that the validity of the model discussed so far is restricted to the assumptions of: (i) validity of Fick's law, (ii) equilibrium between the solution filling the "pores" and that homogeneously dispersed into the film, (iii) constant distribution coefficient K with the concentration, and (iv) absence of fixed charge in the polymeric matrix.

Conclusions

From the results reported in this paper, the following conclusions can be drawn:

1. The role of pores and the concept of MLT is introduced and used to explain the lifetime experimentally observed in the case of PI/Al and PI/Fe systems.
2. Interfacial failure due to adhesion loss (interfacial defects) can be discriminate from failure due to pores present in the coating if use is made of the MLT concept.

Acknowledgements

The financial support of MPI 40% is gratefully acknowledged.

Literature Cited

- 1) Bellucci, F.; Kloppers, M.; Latanision, R.M.; *J. of Elect. Soc.*, **1991**, *138*, p.40.
- 2) Funke, W.; Haagen, H.; *I&EC Prod. Res. Devel.* **1978**, *17*, p.50.
- 3) Perera, D.Y.; Heertjes, P.M.; *J. Oil Col. Chem. Ass.*, **1977**, *54*, p. 774.
- 4) Corti, H.; R. Fernandez-Prini, R.; *Progr. in Org. Coat.*, **1982**, *10*, p. 5.
- 5) M. Buller, M.; Mayne, J.E.O.; D.J. Mills, *J. Oil Col. Chem. Assoc.* **1976**, *59*, p.351.
- 6) Kinsella, E.M.; Mayne, J.E.O.; Scantelebury, J.D.; *Br. Polymer J.* (**1971**), *3*, p.41.
- 7) McBane, B.; *J. of Paint Technology*, **1970**, *12*, p.730.
- 8) Haagen, H.; Funke, W.; *J. Oil Col. Chem. Assoc.*, **1975**, *58*, p. 359.
- 9) Crank, J.; *The Mathematics of Diffusion*, University Press, Oxford, GB, 1968.
- 10) Brasher, D.M.; Kingsbury, A.H.; *J. Appl. Chem.*, **1954**, *4*, p.62.
- 11) Brasher, D.M.; Nurse, T.J.; *J. Appl. Chem.*, **1959**, *9*, p.96.
- 12) Walter, G.W.; *Corros. Sci.*, **1986**, *26*, p.27.
- 13) Schussler, A.; Bellucci, F.; Senturia, S.D.; Latanision, R.M.; *J. of Appl. Poly. Sci.*, **1991**, *42*, p.1567.

Biodegradation of Polyimide-Coated Chromium Substrates

D. B. Mitton¹, S. Toshima^{1,5}, S. S. Chang¹, R. M. Latanision¹, F. Bellucci²,
T. E. Ford³, J.-D. Gu⁴, and R. Mitchell⁴

¹The H. H. Uhlig Corrosion Laboratory, Department of Materials Science and Engineering, Massachusetts Institute of Technology, Cambridge, MA 02139

²Department of Materials and Production Engineering, University of Naples, Federico II, Piazzale Tecchio, 80125 Naples, Italy

³Department of Environmental Health, Harvard School of Public Health, Boston, MA 02115

⁴Division of Engineering and Applied Sciences, Harvard University, Cambridge, MA 02138

The biodegradation of polyimide-coated chromium substrates has been investigated by electrochemical and optical techniques. All samples were sterilized prior to exposure and experiments were accomplished in either inoculated or non-inoculated (sterile conditions maintained) 0.5 M NaCl solutions. Electrochemical impedance spectra reveal that specimens exposed to inoculated solutions experience deterioration in a shorter time than samples exposed to sterile conditions. These spectra indicate deterioration of the coating and, probably, corrosion of the substrate. In addition, photographic evidence suggests that there is an effect on the polymer as a result of the presence of the microorganisms. These results strongly suggest that the polyimide-chromium system tested during this study is subject to premature breakdown in this inoculum as a result of microbial activity.

Due to their thermal stability, chemical resistance and low dielectric constant (≈ 3.0 - 3.5), polyimides are employed as intermetallic dielectric layers, passivants and overcoats. One disadvantage of such organic dielectrics is their intrinsic permeability to moisture and contaminants, which may result in the degradation of the protective properties of the coating and, ultimately, in the corrosion of the metallic substrate. The corrosion rate of a polymer-coated metal is usually related to the absorption of water and dissolved species into the coating, charge transfer processes at the metal-coating interface and changes in the composition of the organic matrix. However, there is also evidence suggesting that polymers are subject to

⁵Current address: Department of Material and Biological Engineering, Tsuruoka National College of Technology, Tsuruoka, Yamagata 997, Japan.

biodegradation (1, 2) and that polymer-coated materials exposed to inoculated solutions may exhibit deterioration in a shorter time than in non-inoculated solutions (3, 4).

Even meticulous cleaning procedures may be unable to remove all viable organisms or their resistant spores from a material surface and fungal spores have even been located in clean rooms (5). Fungi are a group of organisms mainly composed of linear and/or branched filaments, which are termed hyphae. These filaments are either long tubes without cross-walls or they have, at intervals, cross-walls termed septa, each with a central pore. A tangled mass of filaments is termed a mycelium. In the presence of microorganisms such as fungi, degradation may result from the following: (i) the fungus may directly attack and assimilate a material as a nutrient, or (ii) even if a material is resistant to direct attack, metabolic products such as organic acids may influence its chemical and physical properties, (iii) oxygen gradients or pH changes resulting from microbial activity may influence corrosion reactions and finally, (iv) a synergistic relationship may be formed with other organisms such as bacteria, which may find that the fungal growth provides a good anchorage or a favorable microhabitat (6). The potential for deleterious influence on the dielectric properties of thin polymeric films, such as those employed in the electronics industry, may be very significant due to small amounts of microbial products dissolved or transported into or across the material and should not, therefore, be neglected.

Electrochemical impedance spectroscopy (EIS) is used as a tool in the study of the performance of organic coatings in corrosive environment (7-9). In addition, it has been suggested that the activity of microorganisms on a polymer-coated metal may be revealed by EIS (3-4, 10). The purpose of the current research is to define the susceptibility of a selected metal/polymer system to a consortium consisting of a mixture of bacteria and fungi that are common contaminants of air and water. This has been accomplished by employing a combination of electrochemical and optical techniques.

Experimental

Materials. Polyimide-coated samples were prepared by electron-beam depositing chromium (3000 Å) onto a 4 inch silicon wafer. The wafers were then spin-coated with BTDA-ODA/MPDA (benzophenone tetracarboxylic acid dianhydride oxidianiline / *m*-phenyldianiline). The coating procedure was carried out twice in order to minimize the occurrence of pinholes and to provide a final thickness of 2.6-2.8 μm . An intermediate cure (135° C for 30 minutes) was performed for each layer. This was followed by a final cure at 435° C for 15 minutes.

Electrochemical and Microscopic Measurement. The electrochemical cell configuration used during the current study is presented in Figure 1. Acrylic tubing was attached to the sample using an epoxy paint to construct a solution container providing a working electrode surface area of 7.065 cm^2 . Electrochemical cells were sterilized in a nitrogen-purged oven at 100° C for a minimum of 6 hours. After sterilization, all cells were stored in a desiccator prior to use to prevent absorption of water from the ambient environment.

The electrolyte employed was 0.5 M sodium chloride, which was prepared using reagent-grade chemicals and deionized water. This was autoclaved for 20 minutes at 121° C at a pressure of 0.11 MPa (16 lb/in²), which is the accepted condition for sterilization of liquid media (11). This solution was subsequently used for both sterile and inoculated electrolytes. Thus, except for the introduction of an aliquot of inoculum to the inoculated samples, all solutions employed during experiments were identical. The fungal culture used as the inoculum was previously isolated from the surface of naturally deteriorating polyimide. We have already reported (2, 4) that the most common microorganisms detected in this culture belong to the fungal species, *Aspergillus versicolor* and a *Chaetomium* sp. Although this consortium has not yet been thoroughly characterized, it undoubtedly consists of a mixture of bacteria and fungi that are common contaminants of air and water. The inoculated cells were incubated at ambient temperature.

Electrochemical measurements were accomplished in the modified three electrode cell that is presented in Figure 1 using a Solartron potentiostat (1286) and frequency response analyzer (1250). Prior to initiating measurements, the saturated calomel reference electrode (SCE) and platinum counter electrode were sterilized by rinsing thoroughly with ethanol solution, which was then allowed to evaporate. EIS analysis was generally conducted over the range from 65 kHz to 1 mHz by superimposing a 40 mV sinusoidal perturbation at the potentiostatically held open-circuit potential. All electrochemical measurements were performed in a clean box through which air flowed continuously via two types of Sterile Acrodiscs® (Gelman Sciences, pore size: 0.45 μm and 0.2 μm) to maintain sterilized conditions.

In-situ microscopic observations were conducted with either a stereo microscope or with a confocal scanning laser microscope. This provided information on the degree and location of growth on the surface of selected polyimide coatings.

Results and Discussion

Criterion for Failure of a Coating. Values of R_f above $10^8 \Omega \text{ cm}^2$ have empirically been associated with coatings displaying good protection while values below $10^7 \Omega \text{ cm}^2$ are typically considered to reflect a poorly protective coating (12). Others (13) have also associated coating failure with a precipitous decrease in R_f . Additionally, in our experience with polyimides, when R_f values fall below $10^7 \Omega \text{ cm}^2$, corresponding EIS data are generally observed to exhibit two time constants. The latter phenomenon is related to degradation and theoretical curves have been produced (14) which follow with time, the change in the Bode plots as coating porosity and corrosion increase. This treatment of the subject clearly reveals the development of a second time constant with the occurrence of corrosion. Additionally, work carried out in our laboratories (15) has identified a correlation between the appearance of a second time constant and the visual detection of corrosion spots. Finally, a correlation between the appearance of a second time constant and under film corrosion has also been assumed by others in the case of microbially enhanced degradation (10). During this study, therefore, samples were considered to have failed when a second time constant was observed in the electrochemical impedance spectra and the R_f value decreased to values below $10^7 \Omega \text{ cm}^2$.

Electrochemical Data. EIS measurements were carried out in both control and inoculated solutions to generate statistically significant experimental data. In general, EIS data revealed that samples behaved essentially as pure dielectrics just after exposure to the test solution, primarily revealing capacitive character over a wide frequency range. Occasionally, after very short immersion times, regardless of the presence or absence of microorganisms, some samples exhibited a rapid decrease in film resistance (R_f) by several orders of magnitude. Such behavior is assumed to be attributable to a defective polymer coating or poor cell preparation and was, thus, considered spurious.

Figure 2 is generally recognized as being representative of a deteriorating polymer-coated metal system (7). This circuit comprises the solution resistance (R_s), film resistance (R_f), film capacitance (C_f), charge transfer resistance (R_{ct}) and double layer capacitance (C_{dl}).

When a coating/metal system is first immersed in an electrolyte, water and ionic species will permeate into the coating. Depending on the quality and nature of the coating as well as the metal substrate, a substantial time interval may elapse prior to the initiation of detectable corrosion processes. During the time dominated by diffusion of these species into the intact coating, the equivalent circuit is composed of the solution resistance (R_s), film resistance (R_f) and film capacitance (C_f). According to this circuit, a semi-circle with a diameter equivalent to the film resistance (R_f) should be observed in the Nyquist plot; however, due to initial very high film resistance values and an instrument limitation ($\approx 10^9 \Omega$), only a portion of this semi-circle is, typically, observed for short exposure times. Thus, initially the film behaves, essentially, as a pure dielectric exhibiting a -1 slope on the Bode plot and a high and constant phase angle as a function of frequency. With time, ionic paths develop at pores (or virtual pores) and as the coating degrades, an in-phase (R_f) component develops (13). The appearance of a first time constant ($\tau=R_f C_f$) corresponds with the time at which this in-phase component is observed. There is a general consensus that this time constant is associated with ionic penetration into the polymer (16). At extended times, the parallel combination of R_{ct} and C_{dl} (Figure 2) corresponds to the active interface between solution and metal surface, and it appears as a second time constant at low frequency in EI spectra. The appearance of this additional time constant is generally considered to be related to the initiation of corrosion at the polymer-metal interface (15-18).

The performance generally observed for the non-inoculated samples is presented in Figure 3. The decrease in impedance as a function of exposure time apparent in Figures 3 (a) reflects an increase in C_f as a result of the penetration of water into the film. However, even after immersion times in excess of 7 months, non-inoculated cells can exhibit essentially capacitive behavior revealing a phase angle approaching 90° (Figure 3 (b)) and apparently the protective properties may not be degraded even after extended exposure.

The typical behavior of an inoculated sample is presented in Figure 4. In general, EI data revealed behavior similar to the non-inoculated samples during the first two weeks (see 15 day curve) exhibiting capacitive behavior with a -1 slope on

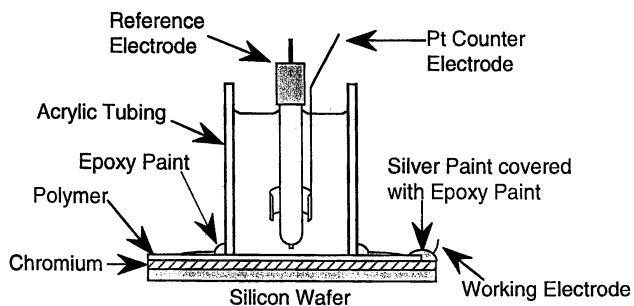


Figure 1. The electrochemical cell configuration employed during the current study.

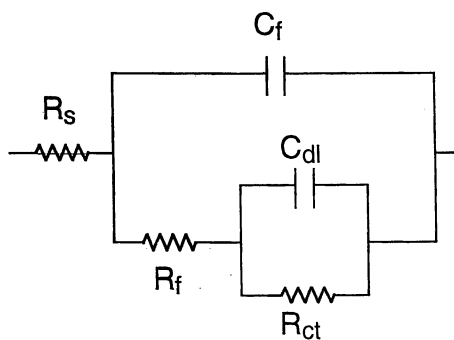


Figure 2. The equivalent circuit model employed during data analysis.

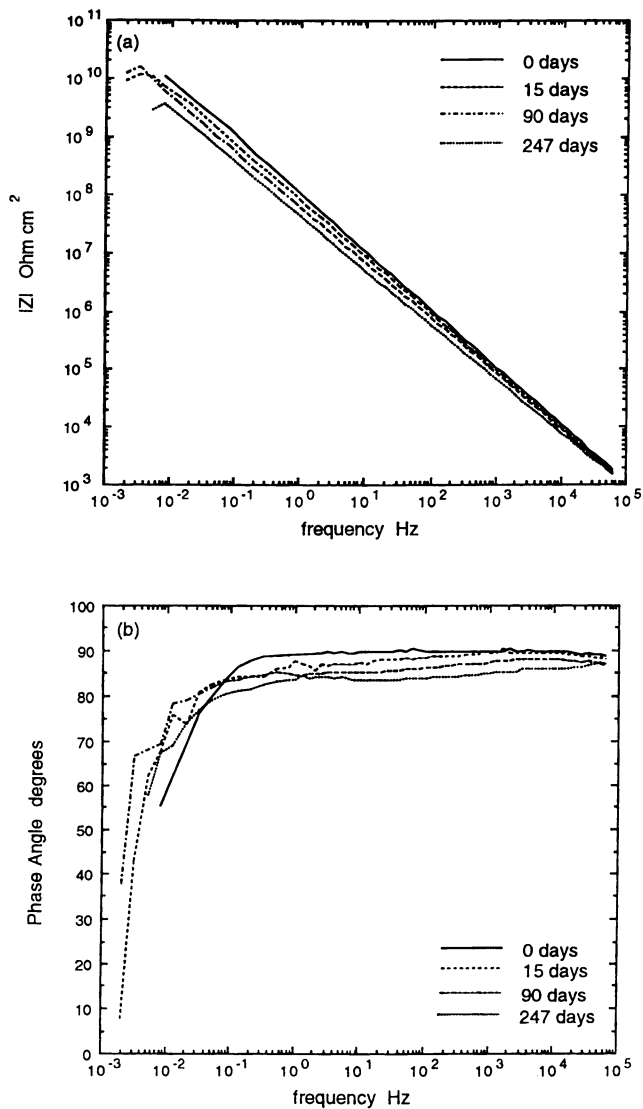


Figure 3. The Bode Magnitude (a) and phase angle (b) plots for one of the non-inoculated samples.

the Bode plot (Figure 4 (a)) and a phase angle approaching 90° (Figure 4 (b)). Unlike the non-inoculated samples, however, approximately one month after initiating experiments, some spectra deviated from purely capacitive behavior exhibiting a second time constant ($R_f C_{dl}$) associated with the active interface between solution and metal surface (see Figure 2) and the R_f decreased to values below $10^7 \Omega \text{ cm}^2$, which is interpreted as sample failure.

The dry film capacitance C_0 of the polymer coating is given by:

$$C_0 = \epsilon \epsilon_0 A / d \quad (1)$$

where ϵ is the dielectric constant of the coating, ϵ_0 is the dielectric constant of empty space ($8.84 \times 10^{-14} \text{ Fcm}^{-1}$), and A and d represent the surface area and thickness of the coating, respectively. Using a dielectric constant of 3 and a coating thickness of 2.8 μm provides a dry film capacitance of approximately $6 \times 10^{-9} \text{ Fcm}^{-1}$. For applied coatings, C_0 represents more a measure of the capacitance of the dry film/metal system, including a contribution from oxides, which may be at the interface between the metal and the polymer. Capacitance values determined from data generated during the test carried out on the first day are, however, on the same order of magnitude ($\approx 2 \times 10^{-9} \text{ Fcm}^{-1}$) as those calculated for the dry film. In addition, there is no systematic difference between the values for the inoculated and non-inoculated cells.

Figure 5 presents the R_f data obtained using the equivalent circuit presented in Figure 2. There is an obvious tendency for the inoculated cells to fail at times that are significantly shorter than for corresponding non-inoculated cells. While half of the inoculated samples failed within the first 40 days (insert Figure 5), none of the sterile cells exhibited failure during the same period. Such behavior strongly suggests an influence on the protective nature of the polymeric coating as a result of the presence of the microorganisms. In another set of experiments to assess the degradation characteristics of polyimide sheet (4), the inoculated system also exhibited failure earlier than the sterilized system.

Figure 6 presents the incidence of failure for inoculated and non-inoculated cells as a function of exposure time. These results reveal a major difference in the time to failure for the inoculated and non-inoculated samples. Although after 300 days of exposure both inoculated and non-inoculated samples display the same number of failures, this results from the finite sample size and, ultimately, all samples will fail. There is, nevertheless, an obvious trend in which the inoculated samples fail at shorter times than the non-inoculated samples. As presented in this figure, approximately 50% of the inoculated samples failed after an exposure time of one month. A similar level of failure was not reached until after a further six months of immersion for the non-inoculated samples. Likewise, while 67% of inoculated samples had failed after about five months, non-inoculated samples reveal a similar number of failed samples only after immersion times in excess of eight months. Clearly, when 67% of the inoculated samples tested had failed after 164 days and the first failure of a non-inoculated sample occurred only after 140 days, there is strong

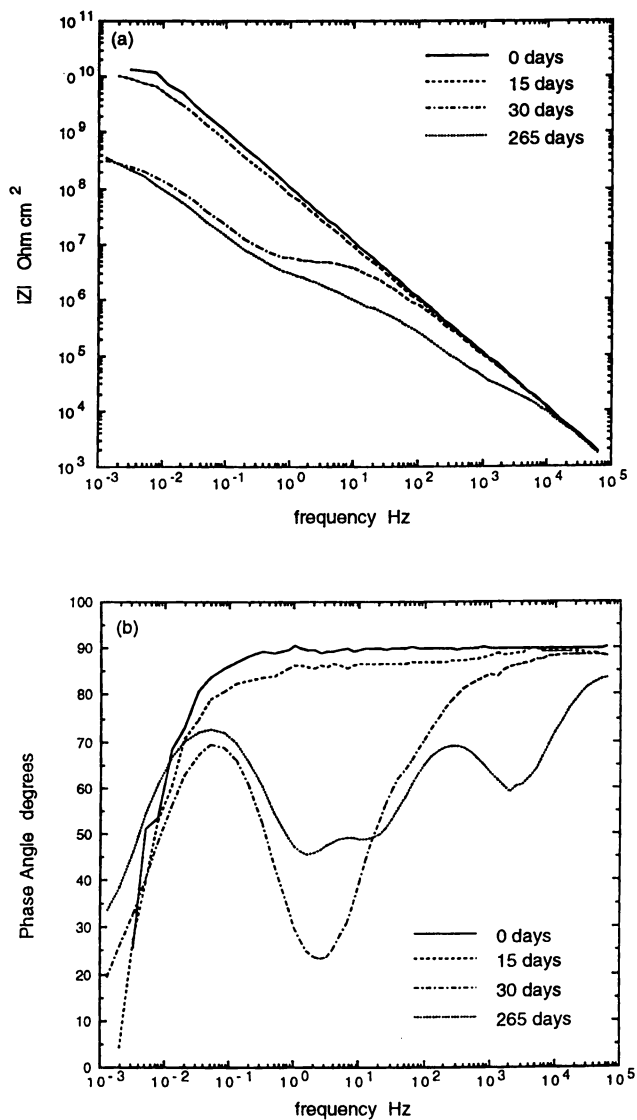


Figure 4. The Bode Magnitude (a) and phase angle (b) plots for one of the inoculated samples.

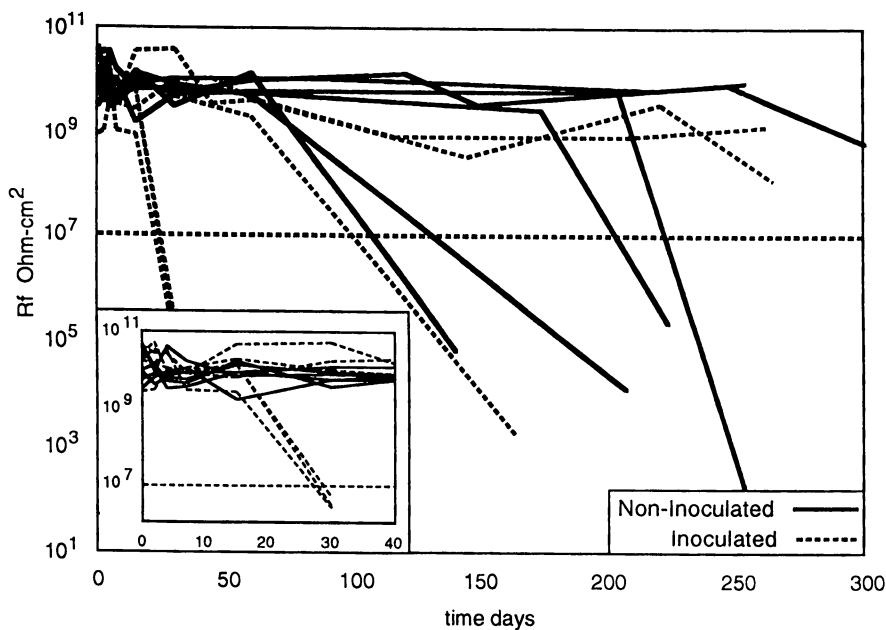


Figure 5. Change in R_f as a function of exposure time for polymer coated metallic substrates exposed to inoculated and non-inoculated electrolytes.

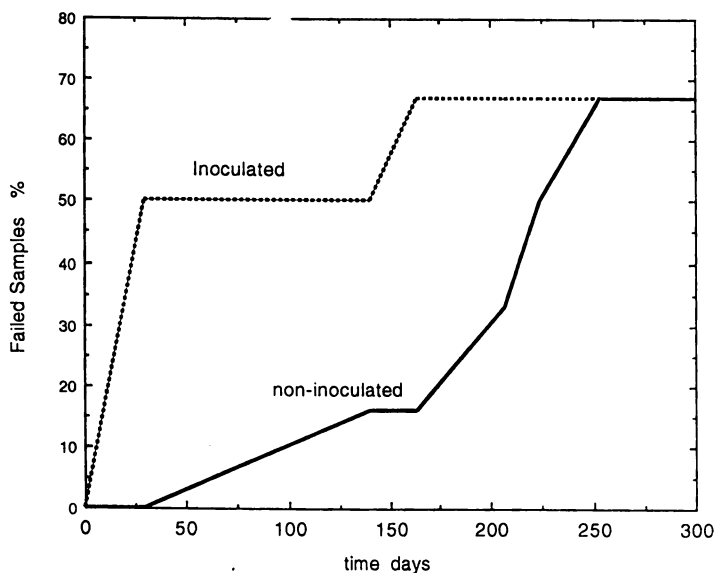


Figure 6. This figure reveals the incidence of failure for inoculated and non-inoculated cells over a 300-day exposure period.

evidence to suggest an influence of the microorganisms on the performance of these samples.

Figure 7 is an in-situ confocal laser scanning micrograph of fungal growth on the polymer surface of one of the inoculated samples. The septa are apparent at many locations within the various hyphae. Figure 8 reveals an in-situ stereo micrograph of the surface of a polyimide sample, which also exhibited failure during another set of EIS experiments (Mitton, D.B.; Gu, J.-D.; Ford, T.E.; Mitchell, R. and Latanision, R.M., unpublished data). This sample exhibits significant colonization and the dark regions that appear at the base of a number of fungal growths suggest that there is an (as yet unidentified) effect on the polymer. This could be the result of organic acids or other microbial metabolites produced by fungi or other components of the microbial consortium (19).

The current research strongly suggests that the presence of the fungal culture used during this study influenced the degradation of the polyimide-chromium samples. It is uncertain, however, if the origin of the breakdown of the polyimide by the microorganisms results from direct use of specific components in the polyimide as nutrients or if it is a result of the production of metabolic products.

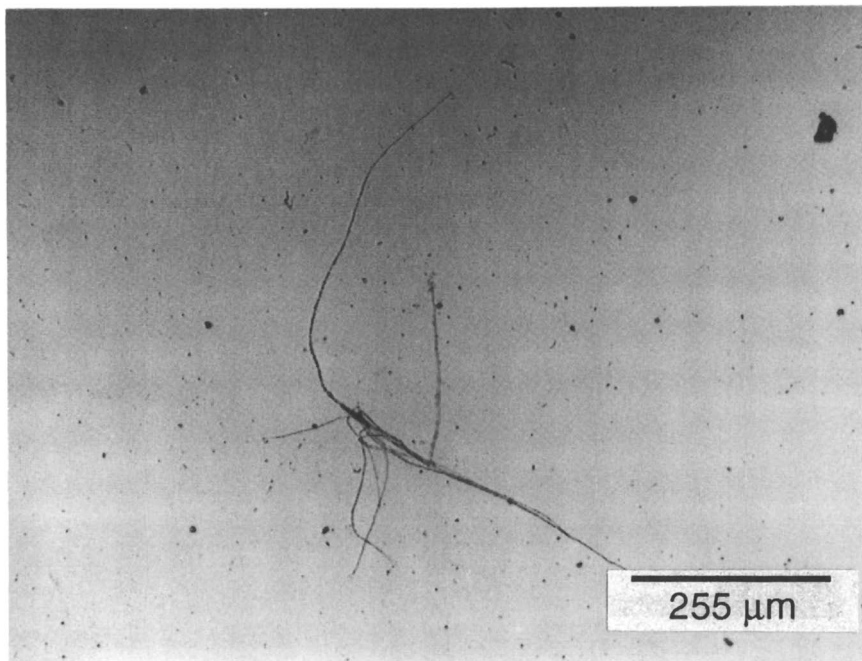


Figure 7. In situ confocal scanning laser micrograph image of the surface of one of the inoculated samples revealing the presence of microbial growth.

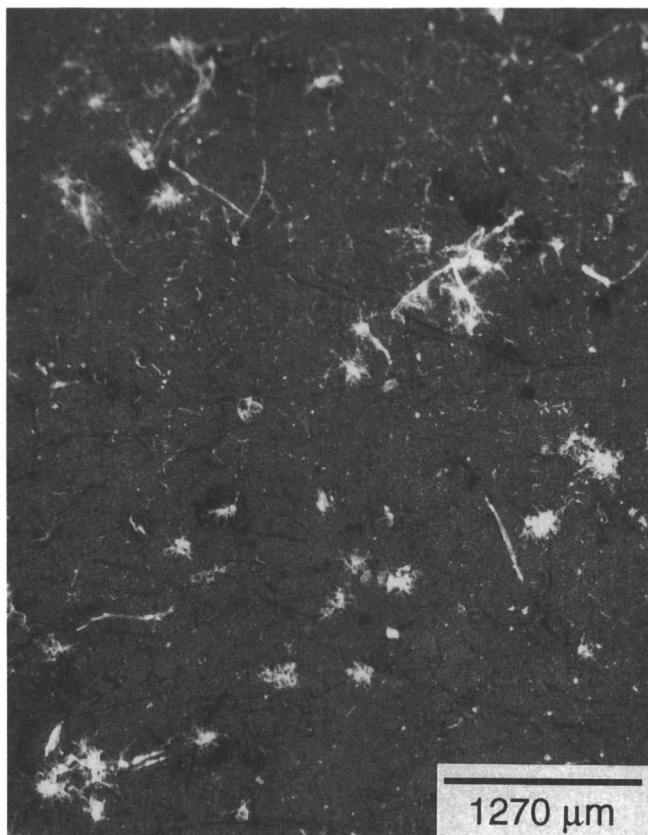


Figure 8. In situ stereo micrograph of the surface of a polyimide sample revealing the presence of microbial growth. Dark regions at the base of fungal growth suggest some effect on the polymer.

Conclusions

EIS data reveal a trend suggesting that inoculated samples fail at shorter times than the non-inoculated samples. Photographic evidence reveals the presence of microorganisms on the surface of inoculated samples and, additionally, dark regions at the base of fungal growths suggest some effect on the polymer.

It is apparent from the data that major differences exist between the behavior of the non-inoculated and inoculated samples. Ultimately, all samples will fail; however, there is an obvious tendency for the inoculated cells to fail at times that are significantly shorter than for corresponding non-inoculated cells. Such behavior strongly suggests an influence on the protective nature of the polymeric coating as a result of the presence of the microorganisms.

Literature Cited

- 1 *Biodegradable Polymers and Packaging*, Ching, C.; Kaplan, D.L. and Thomas, E.L., Editors, Technomic Publishing: Lancaster, PA 1993.
- 2 Gu, J.-D.; Ford, T.E.; and Mitchell, R. *J. Appl. Polym. Sci* **1996**, 62 1029.
- 3 Mitton, D.B.; Ford, T.E.; LaPointe, E. and Mitchell, R. *CORROSION* **93**; Paper No. 296; National Association of Corrosion Engineers: Houston, TX 1993.
- 4 Gu, J.-D.; Ford, T.E.; Mitton, D.B. and Mitchell, R., *CORROSION* **95**; Paper No. 202; National Association of Corrosion Engineers: Houston, TX 1995.
- 5 Inoue, Mayumi, *7th International Biodeterioration Symposium*, 1987, p.580.
- 6 Wagner, P.A.; Little, B.J.; Hart, K.R. and Ray, R.I. *Biodeter. Biodegr.* **1996**, 38, 125.
- 7 Mansfeld, F. and Kendig, M.W. in *Laboratory Corrosion Tests and Standards*, ASTM STP 866, Haynes, G.S. and Baboian, R., Editors, American Society for Testing and Materials: Philadelphia, PA, 1985, p.122.
- 8 Titz, J.; Wagner, G.H.; Spähn, H.; Ebert, M.; Jüttner, K. and Lorenz, W.J.; *Corrosion* **1990**, 46, 221.
- 9 Hack, H.P. and Skully, J.R. *J. Electrochem. Soc.* **1991**, 38, 33.
- 10 Jones, J.M.; Walch, M. and Mansfeld, F.B. *CORROSION* **91**; Paper No. 108; National Association of Corrosion Engineers: Houston, TX, 1991.
- 11 *Methods for General and Molecular Bacteriology*; Gerhardt, P., Editor-in-Chief; American Society for Microbiology: Washington, D.C., 1994, p.730.
- 12 Bacon, R.C.; Smith, J.J. and Rugg, F.M. *Ind. Eng. Chem.* **1948**, 40, 161.
- 13 Kendig, M. and Scully, J. *Corrosion* **1995**, 46, 22.
- 14 Mansfeld, F. and Kendig, M.W. *International Congress on Metallic Corrosion*; National Research Council of Canada: 1984, Vol. 3, p. 74.
- 15 Bellucci, F.; Kloppers, M. and Latanision, R.M. *J. Electrochem. Soc.* **1991**, 138, 40.
- 16 Mansfeld, F. *J of Appl. Electro.* **1995**, 25, 187.
- 17 Bellucci, F.; Nicodemo, L.; Monetta, T.; Kloppers, M. and Latanision, R.M. *Corr. Sci.* **1992**, 8, 1203.
- 18 Walter, G.W. *Corr. Sci.* 1986, 26, 681.
- 19 Ford, T.E. and Mitchell, R. *Advances in Microbial Ecology*, Marshall, K.C., Editor; 1990, Vol. 11, 231-261.

Quantitative Methods of Predicting Relative Effectiveness of Corrosion-Inhibiting Coatings on Aircraft Aluminum

K. J. Lewis, J. H. Aklon, and J. D. Zook

Courtaulds Aerospace, International Research Center, Burbank, CA 91504

The aerospace industry visually evaluates results from salt spray and filiform exposures to judge the effectiveness of chromate-inhibited coatings. These methods, however, do not provide enough information for non-chromate-inhibited coatings. Quantitative tests are needed and are described in this paper. Electrochemical impedance spectroscopy (EIS) and galvanic current (I_{galv}) are two such tests. EIS response on bonded films measures barrier properties (R_{pore}) of coatings. EIS on corresponding nonbonded films measures the electrochemical passivation activity (R_{ct}) of the inhibitors they contain. Accurate prediction of field performance requires knowing both R_{pore} and R_{ct} . Measuring I_{galv} with a tightly spaced titanium cathode gradually creates the anaerobic acidic conditions of crevice and pit environments. Inhibiting corrosion of aircraft aluminum alloys in these conditions is a rapid predictor of inhibitor performance in real crevice or pit environments. Both methods require comparing non-chromate candidates to uninhibited and chromate-inhibited controls. These tests, along with the traditional ones, will provide the greatest confidence in predicting real world performance.

Corrosion-protective paints and sealants for aircraft must protect high strength, copper-containing aluminum alloys, which are more susceptible to corrosion than pure aluminum. A polymeric coating protects a metal from corroding in two ways. First, it serves as a barrier to water, oxygen, and corrosive ions. Second, it serves as a reservoir of electrochemically active inhibitors with low, but finite, water solubilities.

The following characterize the total corrosion process for a coated metal:

1. Transport properties of a coating or sealant for water, oxygen, and ions (permeability/mechanical integrity)
2. Water collection at the polymer/metal interface (hydrolytic stability or wet adhesion)
3. Availability or escape rates of inhibitors from resin matrix to metal surface (solubility/dispersion/wetting)
4. Activity of inhibitors in passivating a metal surface through adsorption, precipitation, or otherwise plugging pores in a coating
5. Susceptibility of the alloy surface for localized vs. uniform corrosion

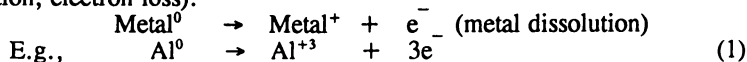
Number one and two comprise the barrier properties of the coating or sealant. Number five involves the electrochemical activity of the inhibitor(s) toward the active sites on a particular alloy. Three and four contribute to both. An active inhibitor must also not interfere with resin stability or cure chemistry.

The aerospace industry uses visually evaluated test methods such as salt spray, filiform, and Prohesion exposures. Fortunately, solvent-borne epoxy coatings have excellent barrier properties, and chromate inhibitors give excellent electrochemical passivation of copper-containing aluminum alloys. Since most current coatings use chromate, only barrier properties differentiate available materials.

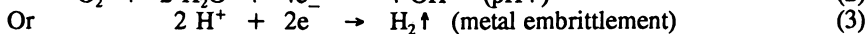
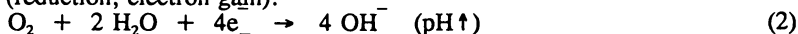
Environmental regulations mandate removal of solvents and toxic additives, including the carcinogenic chromate inhibitors. Suppliers have been unable to develop ultra high solids materials that deliver film and application performance comparable to current solvent-borne systems. Thus, the aerospace industry is looking to water-borne coatings to solve their VOC problems. Water-borne coatings commonly exhibit weaker barrier properties than solvent-borne coatings. Thus, aerospace must develop new test methodologies to adjust to these technology changes. Further, new methods should enable understanding of the separate contributions barrier properties and the electrochemical activity of the corrosion inhibitors each make. Electrochemical passivation will become more important in water-borne coatings and must be measured accurately. Finally, these methods should extrapolate laboratory data to real world performance without field history. Visual tests for limited times do not separate the two contributions and may not reliably predict long-term field behavior. Quantitative electrochemical methods must now be added to accepted visual evaluations to improve confidence in predicting field performance from accelerated lab tests.

The basic corrosion reactions for aluminum can be expressed as follows:

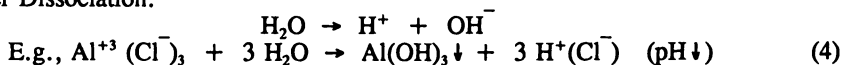
Anode (oxidation, electron loss):



Cathode (reduction, electron gain):



Water Dissociation:



Oxygen-rich areas electrically coupled to anaerobic areas provide the cathode reaction supporting continued anode metal dissolution in crevice areas (Fig. 1) (1). The continued formation of metal ions then locally dissociates water to form insoluble hydroxides (Eq. 4). Chloride ions are drawn in to maintain electrical balance while H^+ ions build up. Thus, pH drops, ultimately to an equilibrium level of ~ 3 for aluminum.

The presence of a polymeric film on metal creates a differentially aerated environment under the film as it starts to delaminate. Acidic conditions develop in anaerobic underfilm areas and lead to accelerated corrosion. This occurs in edge filiforms, underfilm blisters, and in pits on bare metal areas exposed upon coating loss. We test inhibitors under acidic conditions and in neutral environments. Others have reported correlation of increased resistance to localized pitting and crevice corrosion in field tests, with measured metal passivation under acidic conditions (2).

Disbondment can also occur in alkaline cathode areas, depending on the adhesion mechanism. Small localized pH changes in either direction can come from incipient corrosion in the presence of moisture. These changes can reverse adhesion based only

on polar acid/base interactions (such as from organosilanes). Disbondment allows water to collect at the interface, leading to corrosion. We found strong mechanical adhesion of a coating to aluminum's own high surface area oxide to be very important in preventing corrosion. A good, adhesion-promoting conversion coating achieves this. Others have also documented this need on aluminum, even in the presence of chromate inhibitor in the subsequent primer coating layer (3).

Experimental

We used 14 methods to compare corrosion inhibitors on aircraft alloys. Testing was done on solutions and on coating or sealant formulation films. These methods include:

1. pH Range immersion exposures of aluminum alloys in inhibited aqueous salt solutions. Visual comparisons are made.
2. Galvanic current measurements (I_{gal}) (4) of salt solutions containing dissolved inhibitors. Solutions are held between tightly spaced titanium and bare aluminum alloy electrodes. Quantitative and visual comparisons are made.
3. The method in No. 2, but with inhibitors entering salt solutions from patterned or scribed formulation films bonded to the aluminum.
- 4,5. Electrochemical impedance spectroscopy (EIS) (5) of dissolved inhibitors in neutral or acidic aqueous salt solutions contacting bare aluminum alloys. Quantitative and visual comparisons are made.
6. EIS persistence testing of salt-solution-deposited inhibitors on aluminum alloy. Measurements are made before and after removal of inhibitors from contact solutions. Quantitative and visual comparisons are made.
- 7-10. EIS testing of formulated films containing inhibitors, (a) where the films are bonded to aluminum alloy, and (b) where they are laid against bare alloy after casting and curing on a nonadhering surface. Neutral or acidic salt exposure solutions are used. Quantitative and visual comparisons are made.
- 11,12. Salt fog or acidic salt fog exposure (6) of flawed (scribed) formulation films bonded to aluminum alloy. Visual comparisons are made.
13. Prohesion (alternating wet/dry) exposure (7) of flawed formulation films bonded to aluminum alloy. Visual comparisons are made.
14. Filiform exposure (8) of flawed coatings bonded on aluminum alloy. Semi-quantitative visual comparisons are made, measuring filiform length/frequency.

Inhibitors are screened by dissolving them in salt solution in five of the methods (Nos. 1, 2, 4, 5, and 6). The other nine methods test them in actual formulas. Corroboration among several methods gives confidence that formulas will protect alloys for the life of an aircraft, in a variety of exposure environments. Those environments differ with location on an aircraft and with the aircraft's geographical routes. The above tests also create varying environments, from high humidity to total immersion, and from aerated (neutral/alkaline) to deaerated (acidic) crevice conditions.

Inhibitor-Containing Solution Tests. The solution tests are screening tools for finding electrochemically active inhibitors. The pH range immersion test (No. 1) visually evaluates pieces of aluminum alloy sheet immersed in inhibitor-containing aq. NaCl or AlCl₃ solutions. Inhibitor concentrations are ~1mM, or saturated for low solubility materials. Solutions are buffered from pH 3-10. AlCl₃ is used for pH 3, acetic acid/sodium acetate for pH 4-6, nothing for pH 7 and NH₄Cl/NH₄OH for pH 8-10.

Chromates inhibit aluminum alloys for many months, over the full pH range. Non-chromates, showing protection at low pH for as little as a few days, usually inhibit for

months in neutral conditions. They perform better than uninhibited controls in most other tests as well.

The remaining tests with inhibitors added to solution, measure I_{galv} or are variations of EIS tests. They are described later.

Tests on Formulated Coatings and Sealants. I_{galv} and two types of EIS are run on formulated coatings and sealants to compare and corroborate results of standard salt fog, filiform, and Prohesion exposure tests. Non-chromate inhibitors are always compared to uninhibited and chromate-inhibited controls, as well as to each other.

I_{galv} Measurement. To measure I_{galv} , a titanium cathode is electrically shorted to the active metal, usually Al alloy, in 3.5 percent aqueous NaCl solution for up to 1000 hours. Figure 2 illustrates the modified EIS cell used for I_{galv} measurements. The I_{galv} method was adapted from one introduced in 1968 for corrosion testing chromate-containing sealants for aircraft (4). Stainless steel, cadmium plated steel, and carbon composite can also serve as cathodes. Titanium is preferred because of the convenient signal level (μ amp range) and because titanium rivets are used extensively on aircraft.

On Solutions and Formulated Coatings and Sealants. In the I_{galv} cell configuration, the two metals are directly shorted electrically, except during the brief periods of measurement. They are separated in the immersion area with "O" ring spacers. Liquid fills the gap through holes in the titanium.

When inhibitors are added in the salt solution, bare aluminum is used. With formulated films, the aluminum is coated on the side facing the titanium cathode. A pattern of bare area is left to produce the galvanic signal. Uninhibited NaCl solution is used and the inhibitors leach from the film. The "up" side of the uncoated cathode has access to renewing dissolved oxygen. In the closely spaced gap between the metals, oxygen gets depleted, creating a crevice environment.

A Keithley picoammeter (Model 485) measures current between anodes and cathodes at programmed intervals. It is connected through a computer-controlled, multichannel scanning/switching device (Keithley Model 706) that controls up to 49 cells. The computer feeds the data to a spreadsheet program and plots current vs. time.

EIS Measurement. EIS measurements are made in the cell shown in Figure 2, using the setup with no titanium counterelectrode. Instead, a passivated stainless steel counterelectrode and calomel reference electrode are held ~ 1 inch above the working aluminum electrode with a rubber stopper. A potentiostat (Schlumberger Model 1286), with a frequency response analyzer (Model 1255), makes the measurements.

On Solutions. In solution tests, dissolved inhibitors or formula-extracts are added to neutral or pH-adjusted, NaCl solutions. These solutions act on "O"-ring-defined areas of bare metal. Results are judged on the magnitude and stability over time of the charge transfer resistance (R_{ct}). R_{ct} is measured before and after removal of inhibitor-containing aq. NaCl, followed by replacement with uninhibited aq. NaCl.

The retention of high R_{ct} ($> 10^6 \Omega \cdot \text{cm}^2$) after removal of inhibitor-containing salt solution is described as "persistence." It suggests whether passivated metal will remain passivated after depletion of inhibitor from a coating, i.e., in grooves. Chromates form a "persisting," insoluble passivation layer on aircraft aluminum.

On Formulated Coatings and Sealants. EIS is run with two setups to separate measurement of a coating's barrier properties from determination of electrochemical activities of inhibitors contained in the coating. Exposure solutions are 3.5 percent NaCl. To determine barrier properties, EIS is run on fully covering samples of equal

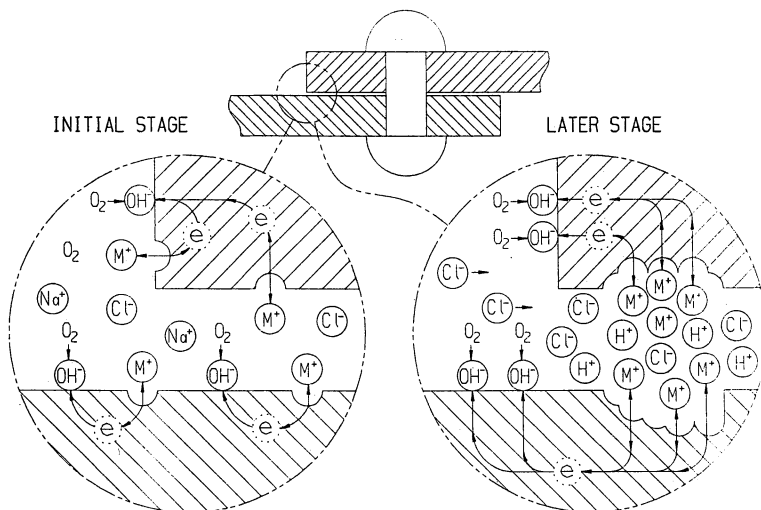
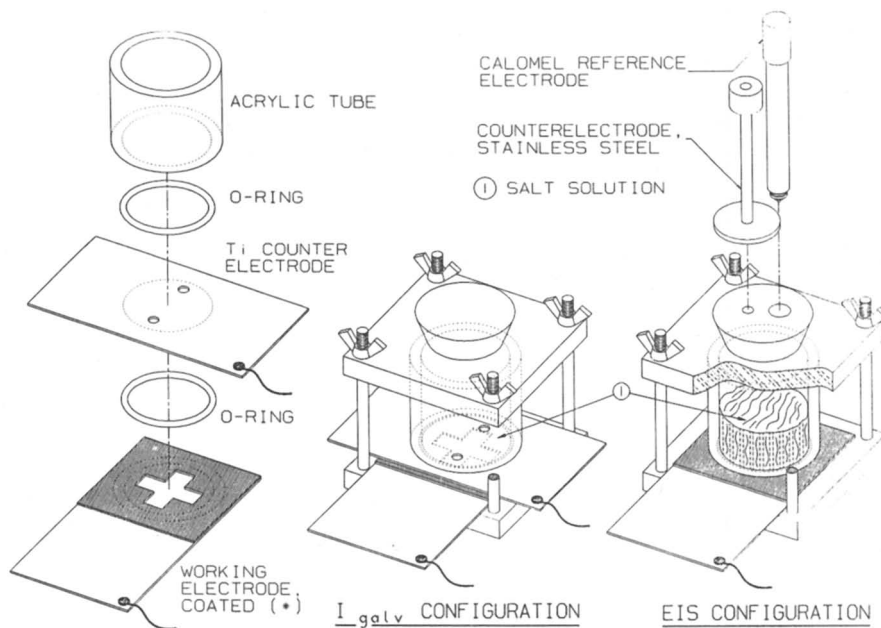


Figure 1 - Crevice (or Pit) Corrosion Mechanism (Reproduced with permission from ref. 1. Copyright 1986, The McGraw-Hill Companies.)



* WITH BARE AREA FOR I_{galv} CONFIGURATION. FULLY COVERED FOR BONDED OR NON-BONDED EIS CONFIGURATION.

Figure 2 - I_{galv} and EIS Test Cell Configuration

film thickness, bonded to similar substrates. Pore resistance (R_{pore}) is measured over time. The diameter of the highest frequency semicircle in a Nyquist plot, or the resistance of the lowest horizontal plateau in a Bode plot, yields R_{pore} .

R_{ct} quantifies the electrochemical activity of inhibitors contained in a formulated film. The exposed metal/electrolyte interface area must be known to determine comparative values. We test cast, cured films. They are simply laid against the substrate and an "O" ring seals around the edges. Once the "nonbonded" film is penetrated, the inhibitor-carrying liquid spreads, by capillary action, over the whole sealed area under the film.

Some buckling usually occurs with rigid films as they swell. Often some areas do not get wetted, but water marks are then visible, whether corrosion has occurred or not. Dry areas are determined with grid paper laid over the outlines.

Simple corrections to "wetted" areas are always less than an order of magnitude. They are at least as accurate as determining pore and delaminated areas in a bonded film, following current literature techniques. These techniques make controversial mathematical assumptions (9, 10, 11) and use curve fitting, or they use complicated optical techniques (12). Errors can be especially large when delaminated areas are orders of magnitude less than the total exposed area of a bonded film.

The resistance computed from the diameter of the second highest frequency semicircle in the Nyquist plot for a nonbonded film is adjusted for the correct metal/electrolyte interface area under the film. R_{ct} for inhibitors leached through the films are then compared accurately.

Alternatively, extracts of these cast films can be used to expose bare substrates to determine R_{ct} . Neither method precisely represents real concentrations because cast films are usually 2-4 times thicker than the films used on aircraft. Nevertheless, the dissolution process from the film will simulate actual use.

Substrate Effects. Inhibitor corrosion protection must be compared on the same substrates. Large differences in corrosion resistance of the various aluminum alloys (including clad and conversion-coated surfaces), often give more variation in test results for the same coating, than differences between inhibitors (including none), in the same coating, on the same substrate. On the more corrosion-resistant substrates, differences in inhibitor behavior are difficult to discern. Clean Alclad surfaces are pure aluminum and inherently resistant to corrosion, unless contaminated. They differentiate inhibitors poorly. Alloy 2024 pits and crevice corrodes more readily than 7075. Both are active because of their copper sites. As bare substrates, both differentiate inhibitors well.

Matrix Effects. Inhibitors should always be compared in the same resin matrix, loaded to the same total pigment volume concentration (PVC). This holds water permeability and adhesion of the polymer phase as constant as possible. The kinetics of inhibitor escape from a resin into the aqueous environment is an important parameter, especially in certain use environments. Damage-exposed bare metal areas, next to coated areas, should be protected as well as underfilm areas. Healing of established pits and crevice areas is difficult, even for chromate. Fast-leaching materials generally protect better, by passivating bare areas before corrosion processes become well established.

Results and Discussion

I_{galv} . The I_{galv} test cell configuration accelerates the development of acidic crevice conditions. This happens after ~100-1000 hours in the narrow, air-deficient gap between the "O"-ring-spaced anode and cathode metals. Figure 3 shows an I_{galv} data comparison for noncuring sealants. The effectiveness of inhibitors in suppressing galvanic current is compared, both initially and with up to 1000 hours of exposure.

Acidic conditions gradually develop in prolonged exposure, unless corrosion is totally suppressed. Acidity accelerates the corrosion rate.

Four of the samples contained (1) no inhibitor, (2) a low level of SrCrO_4 , (3) a neutral-inhibiting, non-chromate system, and (4) an acid-condition-inhibiting, non-chromate system. These four were in the same noncuring sealant matrix. The fifth sample contained BaCrO_4 at a higher level. A slower inhibitor dissolution rate is seen in the expanded X-axis plot on the right of Figure 3.

Low pH Current Acceleration. The measured pH of gap liquids is always 3-4 in uninhibited or poorly inhibited I_{galv} cells opened after the current rate has steeply climbed. The aerated side of the titanium cathode provides an accelerated cathode reaction to drive development of anodic crevice conditions in the confined gap.

The accelerating currents of such samples come from both building acidity and increasing exposure area from edge spots of underfilm corrosion. The latter occur especially on 2024 alloy. Hydrogen reduction ultimately occurs. Accelerated currents then level off or fall if the gap becomes gas-bound or clogged with corrosion product.

Chromate-inhibited controls rarely climb in current unless too low a level is used. The pH usually stays steady at the starting level of 6-7. However, crevice blisters have been seen with inadequately-inhibited chromate systems, following inhibitor depletion.

Acid-resistant Inhibitors. Some non-chromate corrosion inhibitors resist I_{galv} cell crevice conditions longer than others. We found such results to follow the timing for appearance of acidic crevice blisters in salt spray exposure.

We compared the I_{galv} results of Figure 3 with salt spray results on the same noncuring sealants, on 2024 alloy. Acidic crevice blisters formed on the uninhibited sample by 500 hours. They appeared in the neutral-condition-resistant, non-chromate sample by 1200 hours. They did not appear with the acid-resistant non-chromate system until 2000 hours.

At higher loading, in cured sealant, a related, acid-resisting, non-chromate system lasted over 4000 hours in salt spray. No crevice blisters formed. This salt spray sample also exhibited no corrosion of adjacent bare metal areas within 1/8 inch of the sealant edge. I_{galv} results for this material are shown in Figure 4. EIS measurements of a nonbonded film of it are shown in Figure 5. Both tests indicate good electrochemical passivation by the inhibitor system.

Figure 6 shows I_{galv} data for three other, related, acid-resisting, non-chromate inhibitors in an amine-cured, water-borne epoxy primer. Chromate-inhibited and uninhibited controls are included. Long-term crevice current was suppressed.

Inhibitor Passivation of Bare, Damaged Areas Next to Coating or Sealant. Surface Transport Properties of Inhibitors in a Damp Environment. SrCrO_4 and CaCrO_4 , in the uncured and cured sealants in Figures 3 and 4, prevented blisters up to 2000 and 4000 hours, respectively, in salt spray. Pits formed in 1/4"-wide bare metal areas next to the sealants, however, as early as one week on alloy 2024. Alloy 2024 is prone to localized corrosion. Chromate does not migrate well onto bare areas unless the matrix is immersed.

The acid-resistant non-chromate system in Figures 3 and 4 actually protected adjacent bare metal areas against pitting better than chromate in these sealants. They exhibited surface migration in a damp, but not immersed environment. Protecting adjacent, exposed damage sites is an issue to consider since such sites will pit and corrode vertically into the metal, compromising its structural integrity. Daimler Bena Aerospace Airbus in Europe does a crevice test where both vertical and lateral corrosion penetration are measured from a damage site. Inhibitors able to migrate from a coating or sealant to passivate adjacent bare areas in a "damp but not immersed" environment provide a performance advantage.

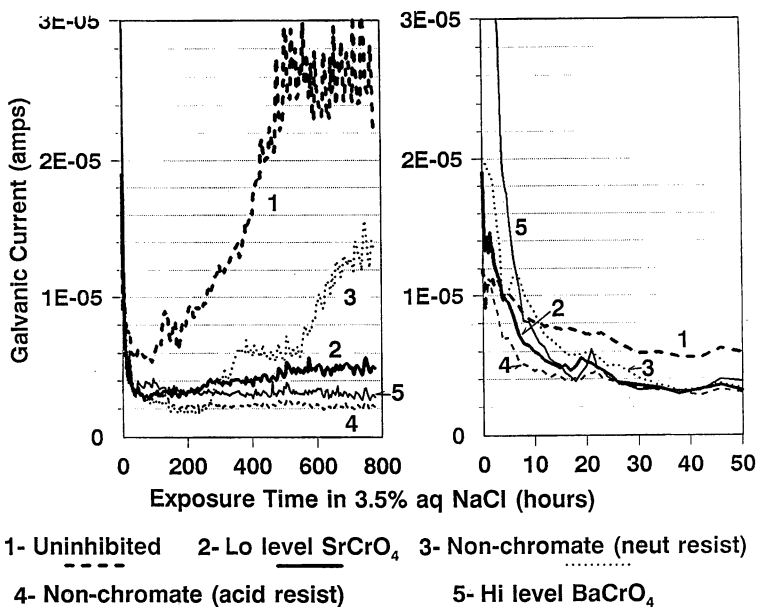


Figure 3 - I_{galv} Measurements, Noncuring Sealant, 2024 Alloy

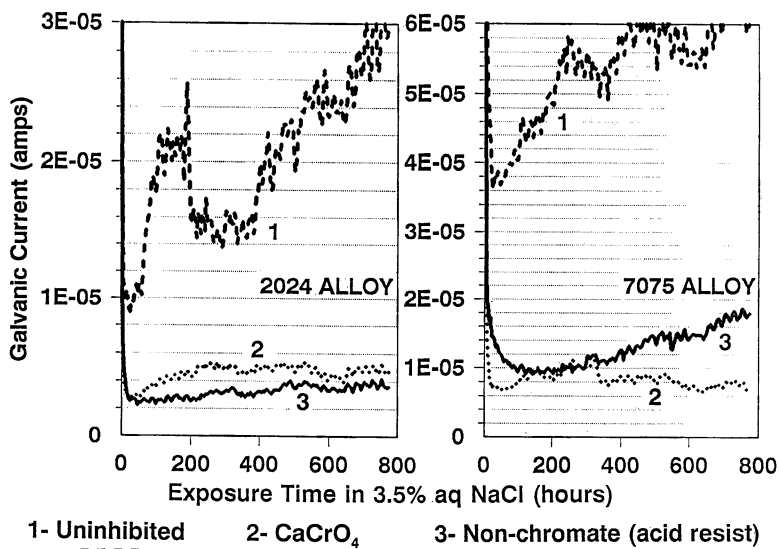


Figure 4 - I_{galv} Measurements, Cured Sealant, Both Alloys

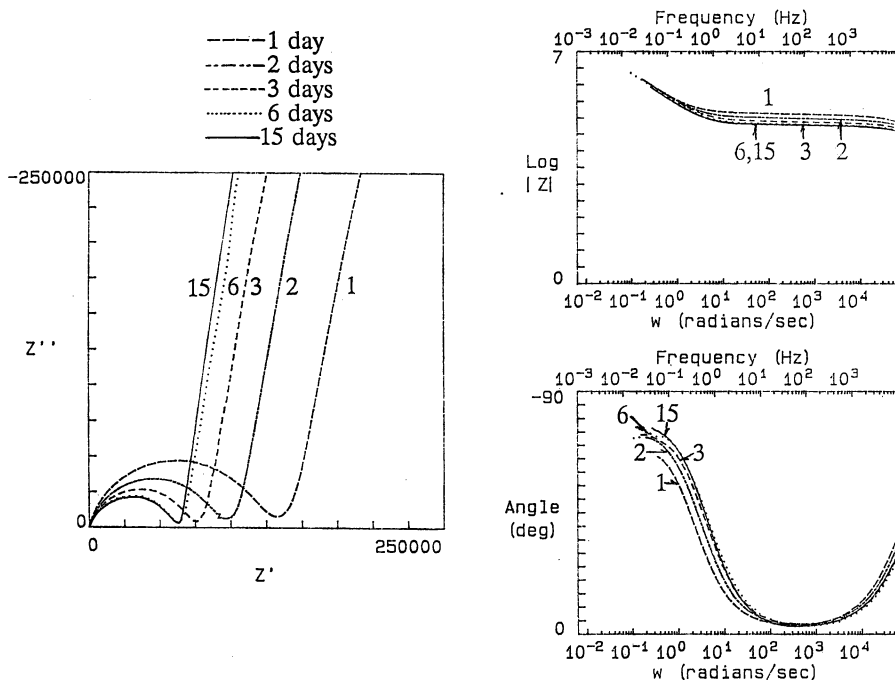


Figure 5 - EIS Measurements, Nonbonded Polythioether Sealant, 7075 Alloy

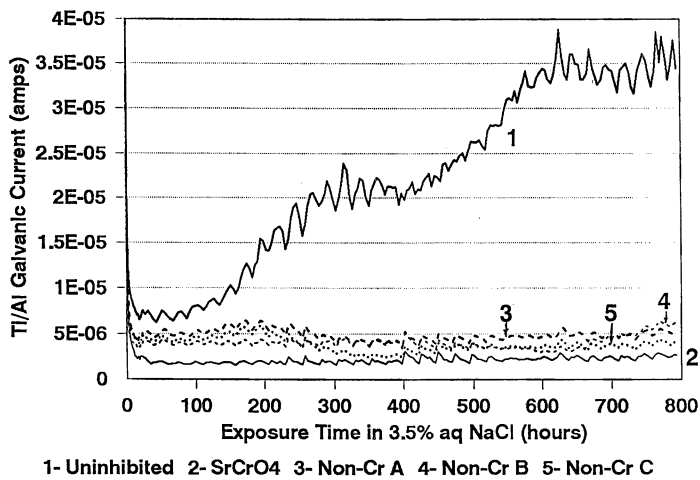


Figure 6 - I_{galv} Measurements, Water-Borne Epoxy Primers, 2024 Alloy

EIS. On Solutions. EIS testing of inhibitor solutions at both neutral and acidic pH was used as a screening tool on bare metal substrates. Along with pH range immersion tests and I_{galv} measurements on solutions, solution EIS identified electrochemically active inhibitors and combinations for further testing in formulas.

Beyond looking for high initial R_{ct} ($> 10^6 \Omega \cdot \text{cm}^2$), we screen for "persistence" of high R_{ct} . Recall we remove the inhibitor-containing solution after exposure from 1 day to 1 month, replace it with uninhibited NaCl, and remeasure R_{ct} over time.

Figure 7 shows EIS data for SrCrO_4 and for both persisting and nonpersisting non-chromate inhibitors, in NaCl solution, on 2024 Al alloy. For chromate and for the persisting non-chromate system, initial R_{ct} is $> 10^6 \Omega \cdot \text{cm}^2$, and it remains essentially unchanged after removing the inhibitor(s). With a nonpersisting inhibitor, a high initial R_{ct} can last for weeks in an undisturbed, sufficiently concentrated solution. The equilibrium adsorption is destroyed, however, when the inhibitor-containing NaCl solution is removed and replaced with just NaCl. R_{ct} drops to $\leq 10^5 \Omega \cdot \text{cm}^2$, and the aluminum then corrodes as if no inhibitor were present.

On Coatings and Sealants. Recall inhibitors should be compared in the same resin matrix, at the same PVC (or PVC/CPVC ratio), at equal thickness, on the same alloy substrate. Meaningful conclusions can then be drawn as to the inhibitor's contributions to both barrier properties and electrochemical passivation activity.

Measured resistance is inversely proportional to corrosion current, so both R_{pore} and R_{ct} should be as high as possible. Generally, the lower the resistance to pore formation (low R_{pore}), the poorer a coating system performs, especially if the measurement is on a primer/top coat combination. However, a high R_{ct} within the pores of a primer (at the metal/electrolyte interface) can go far in overcoming a pore formation problem with a "water-sensitive" inhibitor. Good corrosion protection can still result, provided enough inhibitor is present and good adhesion is maintained, especially if that adhesion is mechanical. We found this to be the case with all the SrCrO_4 -loaded epoxy primers we tested. Not surprisingly, we also found the loading level, dispersion quality, and water solubility of added pigments to greatly influence R_{pore} of the primers we tested.

Figure 8 compares uninhibited and SrCrO_4 -inhibited, bonded primers, made from the same solvent-borne, amine-cured epoxy formula, at the same total PVC. Both were coated on 2024 alloy at the same ~ 4 -mil thickness, without topcoat.

The barrier performance of the SrCrO_4 -loaded sample (determined from R_{pore}) was seen to degrade more rapidly than that of the uninhibited one. In the uninhibited sample, the pigment volume which was occupied by SrCrO_4 in the original formula, was replaced with less-water-sensitive, hydrophobic silica. This improved R_{pore} compared to the original SrCrO_4 formula.

At the same time, R_{ct} , represented by the second semicircle diameter in each of the Nyquist plots, is uncorrected for actual metal/electrolyte exposure area since it is unknown. The exposure areas for the chromate sample have to be larger because of their lower R_{pore} values (taken from the first semicircle diameters). Thus the real, area-corrected R_{ct} values for the SrCrO_4 sample would be larger multiples of the measured resistances than those for the uninhibited sample. Since the measured R_{ct} values for the chromate sample are already much larger without correction than for the uninhibited one, the real differences are huge.

On Topcoats (or Unicoats). EIS can be used to measure barrier properties (porosity) and water uptake of topcoats. Porosity (R_{pore}) changes will profile the UV resistance of an exterior coating. EIS will corroborate measured gloss changes on films exposed to normal or accelerated weathering.

- 1 - SrCrO_4 - original, after 1dy & after 1mo w/NaCl only
- 2 - Persisting non-chrome, original
- 3 - Persisting non-chrome, after 4hr w/NaCl only
- 4 - Persisting non-chrome, after 1mo w/NaCl only
- 5 - Non-persisting non-chrome, original
- 6 - Non-persisting non-chrome, after 4hr w/NaCl only

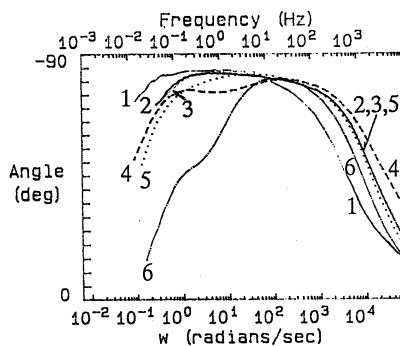
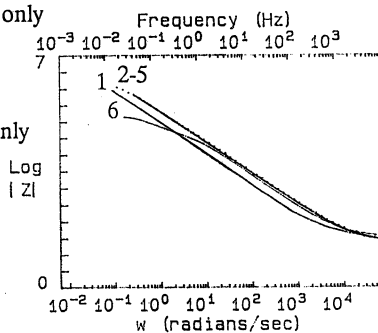
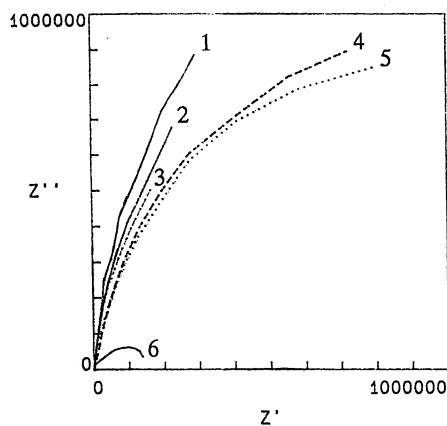


Figure 7 - EIS Persistence Measurements - SrCrO_4 and Persisting and Non-persisting Non-chromate Inhibitors, in Solution on 2024 Alloy

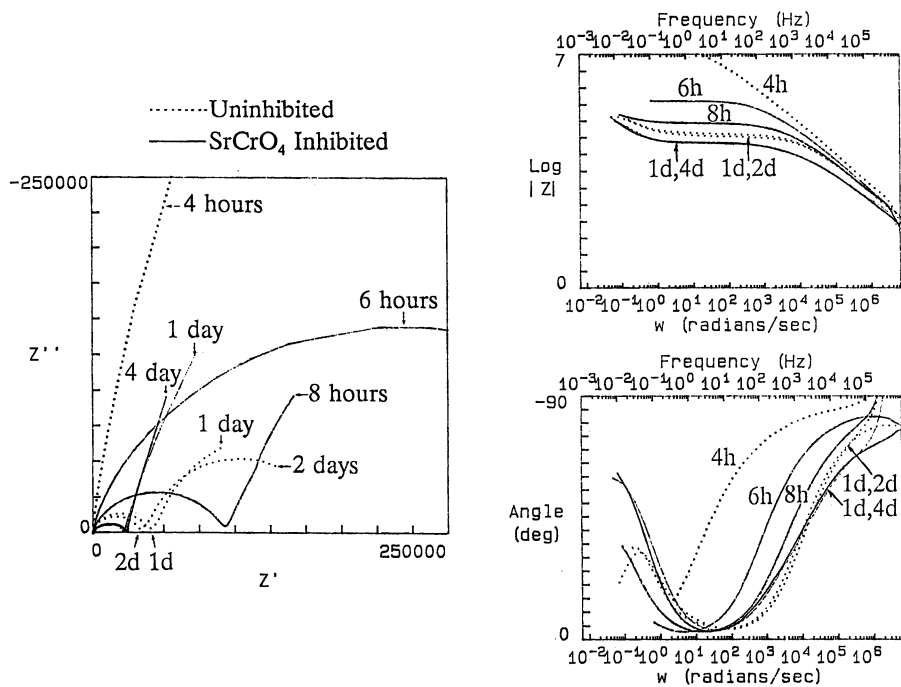


Figure 8 - EIS Measurements - Bonded Epoxy Primers, 2024 Alloy

For topcoats providing corrosion protection in addition to cosmetics, the issue of porosity changes in terms of barrier properties is critical. Another paper in this symposium (13) presented data comparing conventional salt fog, filiform, and Prohesion results with corrosion data from outdoor exposure at various USA sites. There was no correlation at all (coefficients were <0.1). If the lab tests included periods of UV exposure, however, such as in a QUV chamber, correlation rose to 0.4-0.7. While still of questionable significance, this was a vast improvement.

UV-induced porosity changes in coatings lower their barrier properties and therefore their corrosion protective capability. UV-exposed corrosion test samples should correlate better with outdoor exposure than when tested in dark chambers only. For exterior coatings, combined exposure is recommended.

For interior coatings seeing immersion in service, with no outdoor light, lab immersion tests will best mimic real use. Immersion results in faster pore penetration, providing an acceleration factor for intermittent, liquid-exposed applications.

Comparison of Primer Coatings by EIS and Filiform Testing. Barrier Property vs. Electrochemical Inhibition. An early, poorly controlled filiform test in our lab emphasized the importance of EIS in determining the separate contributions of film barrier properties and inhibitor electrochemistry. When we first ran filiform exposure on the formulations seen in Figure 8, an uninhibited film performed better than one with SrCrO_4 . The test was the usual 1 hour HCl vapor exposure, followed by 1000 hours at $80 \pm 5\%$ relative humidity (RH). Recall EIS showed the uninhibited film to have better barrier properties than the one with SrCrO_4 .

Our humidity chamber was poorly sealed. A new monitor showed the RH was 70% instead of the required $80 \pm 5\%$. At 80%, RH is high enough for liquid water (dew) to form with small temperature fluctuations. Chromated samples always perform better than uninhibited ones, in solution and in immersed coating tests. Electrochemistry dominates in liquid water. With insufficient liquid water, barrier properties evidently dominated in this test, especially in the first few days, while HCl remained in the film. The chromated samples performed better than their uninhibited counterparts once the chamber was sealed and the RH raised to $80 + \%$ from the onset.

Discrepancies in filiform results from low humidity may be smaller with water-borne coatings since barrier properties will likely be less effective. Nevertheless, a dichotomy exists. Loading a hydrophobic polymer film with hydrophobic fillers can preserve its water resistance or barrier properties. Conversely, loading a hydrophobic polymer film with effective inhibitors that are water-soluble enough to enter the electrochemical environment to stop corrosion will always compromise barrier properties to some extent. Barrier properties are the first line of protection against corrosion and should be at a maximum as long as possible.

We have consistently observed the R_{pore} of bonded and nonbonded films to drop more quickly when loaded with SrCrO_4 or other effective, but water-sensitive inhibitors, than when uninhibited. Nevertheless, the "area-normalized" R_{α} for effectively inhibited primer films will be $\geq 10^6 \Omega \cdot \text{cm}^2$, a level several times higher than for uninhibited films. They show good metal protection, especially if their mechanical adhesion to the substrate is good and good barrier topcoats cover them.

EIS on Nonbonded Films. Recall Figure 5 shows EIS spectra of a nonbonded film of cured polythioether sealant. The film was pliable. Uniform liquid wetting beneath the film was seen upon cell disassembly. Measured film resistance (R_{pore}) dropped quickly at the high loading of non-chromate inhibitor, suggesting weak barrier properties. Polythioether sealants are water-permeable. Nevertheless, the corrected metal/electrolyte interface resistance (R_{α}) for this sample was $> 10^6 \Omega \cdot \text{cm}^2$, suggesting good passivation. Recall this sealant performed well as a bonded film in salt spray.

Table I shows bonded and nonbonded film data on uninhibited, SrCrO₄-inhibited, and non-chromate-inhibited versions of an amine-cured, water-borne epoxy. They were air-dried and measured without topcoats.

While film thicknesses were not exactly the same, all were penetrated quickly. A low R_{pore} was measured on each bonded coating, from the high-frequency-semicircle diameters of Nyquist plots, or the high-frequency, lowest-plateau values of Bode plots.

An area-corrected R_{ct} was determined for each nonbonded coating from the Nyquist next-lower-frequency-semicircle diameters. Values for both chromate- and non-chromate-inhibited films were 1-2 orders of magnitude higher than for uninhibited films, even after 50 days. Where values were $> 10^7$, it was difficult to extrapolate the semicircle diameters accurately. Measuring to very low frequency to improve accuracy was often not possible. Noise from "autointegration failure" in the software computations begins to compromise the low frequency data when R_{ct} is very high.

Conclusions.

The aerospace industry currently uses visually evaluated salt spray and filiform exposures to judge the effectiveness of chromate-inhibited coatings. Current coatings differ mainly in their barrier properties for protecting aluminum alloys since most contain SrCrO₄, although some BaCrO₄ and ZnCrO₄ are used. Salt spray and filiform alone do not provide enough information for non-chromates. Quantitative tests such as electrochemical impedance spectroscopy (EIS) and galvanic current measurement (I_{galv}) are needed. To make valid rankings of non-chromate inhibitors, they should be compared against uninhibited and chromate-inhibited controls, as well as to each other. Matched matrices, with equal pigment volume concentrations, should be used at the same thickness, on the same selection of aluminum alloy substrates.

A dichotomy exists in formulating films for corrosion protection of metal. Loading a hydrophobic polymer film with hydrophobic fillers can preserve its water resistance and barrier properties. Conversely, loading a hydrophobic polymer with effective inhibitors that are water-soluble enough to enter the electrochemical environment to stop corrosion will always compromise barrier properties to some extent. Barrier properties are the first line of protection against corrosion and should be at a maximum as long as possible.

EIS response on bonded films measures barrier properties (R_{pore}) of inhibited coatings. EIS on corresponding nonbonded films measures the electrochemical passivation activity (R_{ct}) of the inhibitors themselves. Accurate prediction of field performance requires knowing both R_{pore} and R_{ct} . Both should be as high as possible. R_{pore} for a non-chromate coating should be no worse than for a similarly-loaded chromate control. However, it may be poorer than for an uninhibited control, as is SrCrO₄. R_{ct} for a non-chromated coating should exceed R_{ct} for an uninhibited control, and should approach a similarly-loaded chromate control.

When using filiform testing for corroborating electrochemical tests, relative humidity should be kept high enough for some liquid water to form during cycling. This appears necessary for electrochemical properties to be a factor in the corrosion resistance measured in this test. Lower humidity favors barrier property domination, especially while HCl vapor is present in a film.

Inhibitor passivation of aircraft aluminum alloys in acidic solution is useful in predicting suppression of localized corrosion. Measuring I_{galv} between aluminum alloy and a tightly spaced titanium cathode is recommended for 100-1000 hours, to accelerate development of acidic crevice conditions. With this method, inhibited formulas can be ranked as to capability to retard crevice and pit corrosion.

In salt spray, inhibitors that migrate from a formulation and passivate adjacent exposed metal areas, in a damp environment, can provide a performance advantage.

Table I - EIS Coating Measurement Results, Water-borne Epoxy Primers

Inhibitor	Exposure Time	Film Thickness (mils)		$R_{\text{pore}} (\Omega \cdot \text{cm}^2)$	$R_{\text{ct}} (\Omega \cdot \text{cm}^2)$	
		Bonded	Nonbonded	from Bonded Films	from Nonbonded Films	
				(24 cm ²)	(24 cm ²)	(1 cm ²)
None	1 hr	1.5-1.8	5-7	-	-	1x10 ⁵
	3 hr			> 10 ⁸	1.5x10 ⁵	-
	1 day			7x10 ⁵	-	2x10 ⁵
	2 day			-	3.5x10 ⁵	-
	6 day			2500	4x10 ⁵	7x10 ⁵
	50 day			1000	2x10 ⁵	3x10 ⁵
SrCrO ₄	1 hr	1.8-2.0	8-9	-	-	3x10 ⁵
	3 hr			> 10 ⁸	1x10 ⁶	-
	1 day			5x10 ⁶	-	2x10 ⁶
	2 day			-	4x10 ⁶	-
	6 day			1000	3-4x10 ⁷	> 10 ⁸
	50 day			500	2x10 ⁷	1x10 ⁸
CA Non-chromate	1 hr	2.5	6-10	-	-	8x10 ⁶
	3 hr			5x10 ⁴	1-2x10 ⁷	-
	1 day			8000	-	> 10 ⁷
	2 day			-	1x10 ⁷	-
	6 day			1500	1x10 ⁷	1x10 ⁷
	50 day			1200	8x10 ⁵	1x10 ⁷

Acknowledgments.

The authors thank T. Dang at Courtaulds Aerospace for his fine artwork in Figures 1 and 2. We also thank Courtaulds Coatings, UK for providing us with EIS equipment for this project.

Literature Cited.

1. Fontana, M.G., *Corrosion Engineering*, McGraw-Hill, 54 (1986).
2. Szklarska-Smialowska, S., *Reviews on Corrosion Inhibitor Science and Technology*, *NACE*, I-9-1 (1989).
3. Evans, A.T., Scantlebury, J.D. and Callow, L.M., *Proceedings of the Symposium on Advances in Corrosion Protection by Organic Coatings II*, *Electrochem. Soc.*, 95-13, 266 (1995).
4. Morris, L., "Corrosion of Galvanic Couples Found on Aircraft and the Effects of Inhibitive Sealants", *Report to NACE Technical Unit Committee T-9c, Fuel Systems Corrosion*, Cleveland, OH (1968).
5. MacDonald, J.R., Ed., *Impedance Spectroscopy*, Wiley & Sons, 1987.
6. ASTM B 117-85.
7. Cremer, N.D., "Prohesion Compared to Salt Spray and Outdoors", *Presentation to Federation of Societies for Coatings Technology, 1989 Paint Show*, UK, Reprint from Q-Panel Co., 1989.
8. ASTM D 2803-70 (reapproved 1974) and MIL-P-23377G (1994).
9. Haruyama, S., Asari, M. and Tsuru, T., *Proceedings of the Symposium on Corrosion Protection by Organic Coatings*, *Electrochem. Soc.*, 87-2, 197 (1987).
10. Mansfeld, F. and Tsai, S., *Corrosion*, 47 (12), 958 (1991).
11. Kendig, M., Mansfeld, F. and Tsai, S., *Corrosion*, 47 (12), 964 (1991).
12. Kendig, M., Ryang, H., Liao, T., Cunningham, M. and Jeanjaquet, S., "Corrosion Induced Adhesion Loss-Low Volatile Organic Content (VOC) Coatings", *Final Report to Material Interfaces Div., Office of Naval Research, Contract #N00014-90-C-1011*, March 1993.
13. Simpson, C.H., "The Replacement of Chromate Inhibitors in Protective Coatings", this volume (1997).

Inhibition Properties of Some Aircraft Corrosion Protective Coatings

A. W. Fangmeier¹, E. Kock¹, F. Vohwinkel², and C. P. Brandt²

¹Department of Surface Protection and Chemistry, Daimler-Benz Aerospace, Airbus GmbH, 28199 Bremen, Germany

²Department of Material Science and Processes, Fachhochschule Osnabrück, 49076 Osnabrück, Germany

Starting from the general Airbus corrosion prevention philosophy requiring a certain leachability of the corrosion protective pigments of the coating, extracts of several chromate containing and chromate-free primers were prepared. The extracts were used to run special alternate immersion/emersion (A.I.E.) tests as well as electrochemical measurements such as equilibrium potential and polarisation resistance measurements. These results enable a classification of the primers into types of different efficiency and mechanism and can be compared to results of standard filiform corrosion tests.

In the past, most of the approaches to qualify chromate-free corrosion inhibiting primers for aircraft application failed. These efforts were the starting point for some further general investigations of chromate-free primers without needing too much detail as to the primer formulation. Following the general Airbus corrosion prevention philosophy which requires a certain solubility of the corrosion inhibiting pigments of the coatings, water based extracts of several chromated and chromate-free primers were prepared.

Chromated and Chromate-Free Primers

Chromated primers have been applied in the aerospace industry for over 30 years. One of their most important properties is the leachability of the corrosion inhibiting pigment, the chromate. In addition to under the primer this promises good protection on areas which are not directly covered by the primer such as drill holes, scratches or other damaged sites. It is known that chromate acts on both cathodic and anodic site inhibiting pit formation as well as corrosion propagation.

¹Daimler-Benz Aerospace Airbus GmbH, Huenefeldstr. 1-5, D-28199 Bremen.

²Fachhochschule Osnabrück, Albrechtstr. 30, D-49076 Osnabrück.

Due to its long use, the behavior of numerous chromated primers under many of the world wide applied corrosion test conditions is well characterized.

In contrast the numerous chromate-free corrosion inhibitive primers which have been developed during the last few years are not so well understood. Their corrosion prevention behavior has been evaluated mainly by standard salt spray tests, filiform corrosion tests, a few alternate immersion/emersion (A.I.E.) and crevice corrosion tests.

In Figure 1 the representative leaching behavior of a chromated primer is shown. Although there are some primers which have an initial leaching rate of only ten percent of the shown value, these primers are still active showing the same inhibition behavior.

Even if the leaching rate starts at a level comparable to that of the specimen leached for 29 days, there is still a corrosion protective effect. This can be illustrated by observing the leaching rates of old aircraft parts shown in Figure 2. These parts were in service in an aircraft for over 15 years but still do not show any corrosion. Even when scratched after 22 days immersion in distilled water, a significant rise of the leaching rate appears.

For the investigation described, the most commonly applied, chromated primers of the european aerospace industry and the most promising chromate-free ones of the qualification attempts of the past years were used (Table I).

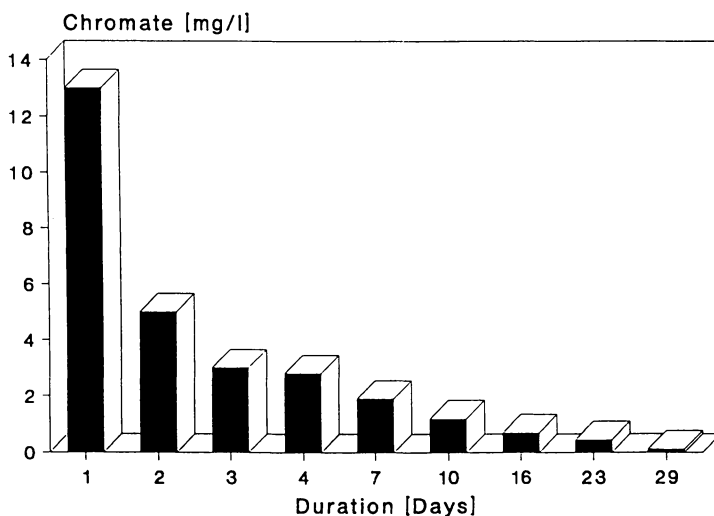


Fig. 1. Chromate leaching of a primed specimen.

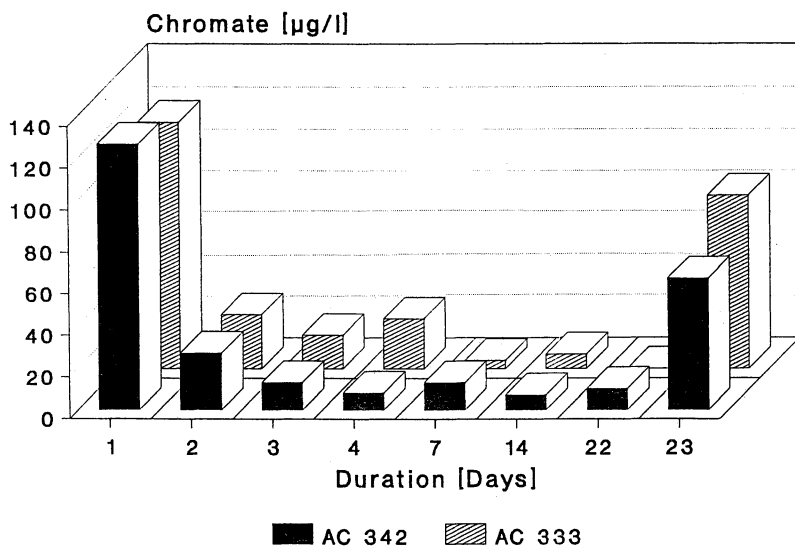


Fig. 2. Chromate leaching of old aircraft parts.

Table I: Types of Primers under Investigation

Polymer base	Number of primers	Designation
Epoxy (EP), chromated	2	A,B
Polyurethane (PUR), chromated	2	C,D
Epoxy (EP), chromate-free	4	E,F,G,H
Polyurethane (PUR), chromate-free	1	I

While both EP-primers (A,B) and one of the PUR-primers (C) are inhibited by 20-25% zinc- or strontium chromate, the PUR-primer (D) is only inhibited by about 5% barium chromate. The inhibiting pigments of the chromate-free primers in most cases are not known at this time.

Extract Preparation and A.I.E. tests

As a first screening, an attempt was made to prepare extracts with acetone from the different paint base compounds. Although this approach was successful with some primers for some A.I.E. tests, it was judged to be

- An unrealistic procedure compared to in service conditions.
- Not applicable to some primers.
- Uncertain due to the unknown solubility of the different pigments in acetone.

Therefore this method was replaced by preparing aqueous extracts from cured paint films which is more realistic and easier to perform.

Extract Preparation. Cured and powdered primer was stirred for three days with distilled water and then filtered. Conductivity measurements showed that after three days the conductivity of the extract became constant for all primers under investigation.

In order to get a suitable electrolyte for A.I.E. tests the extracts were diluted 1:10 with distilled water and sodium chloride was added to give a 3% solution. To half the solution a part of the insoluble residue of the extraction process was again added to determine the influence of the water insoluble part of the primer on the A.I.E. test results.

After preparation of the extracts, A.I.E. tests were performed on the substrates and with the conditions given in Table II.

Table II. Test Conditions

Characteristic	Property
Temperature	20-25°C
Duration	1000 hrs.
Cycle	2 hrs. wet / 2 hrs dry
Substrate	Al alloy 2024 (bare) Al alloy 2024 (Al clad)
Treatment	Chromic acid anodizing (CAA) Chrome sulfuric acid pickling (CSA)

Results. Without discussing any specimen individually, the results of the A.I.E. test can be summarized as shown in Table III.

While the chromated primers do not show any significant difference on pure aluminium clad (Al-clad) and unclad (bare) material or CAA and CSA pretreated substrates, the chromate free ones in general show a better protection behavior on clad than on bare material and on CAA than on CSA surfaces.

Table III. A.I.E. test Results

Primer	Test series with residue	Test series without residue
A,B,D	+	+
C	0	+
E	+	0
F,G,I	0	-
H	-	-

+ = very good corrosion protection

0 = poor corrosion protection

- = very poor corrosion protection

The reason for this behavior is assumed to be the lower protection performance of these primers such that the anodic protection by the cladding and the passivation by the CAA layer become more important for the test results. Although well recognizable, these effects are not strong enough to change the classification given in Table III.

It is remarkable that most of the chromate-free primers, especially primer (E) give a better corrosion protection if some insoluble primer residue is present which means that there must be still some interaction. This was not observed with the chromated primers.

Electrochemical Measurements

For the electrochemical measurements (determination of the equilibrium potential and the polarisation resistance), primer extracts were used which were prepared as previously described. Different dilution ratios were prepared from these extracts. They included from full concentration to 1:1000 extract/water. Sodium chloride was added to give a 0.1M NaCl electrolyte solution. The measuring equipment used was a VersaStat 250-1.

As shown in Table IV, the chromated primers in general give an initial high polarisation resistance at a low concentration. There is a drop when going to the chromate-free primers which even at a high concentration give a significantly lower polarisation resistance. Thus these results corroborate those found in the A.I.E. tests.

Table IV. Results of the Polarisation Resistance Measurements

Primer	Dilution ratio [extract/water]	Polarisation resistance [kΩ]
A	1:10	780
B	1:100	660
C	-	800
D	1:15	660
E	1.5:0.5	690
F	1:10	390
G	-	350
H	-	400
I	-	200

Second Test Cycle

Following this first test cycle, more detailed investigations were started (in order to get a better correlation to in service conditions) to take into account the real situation in scratches, well defined scratches were prepared and the chromate leaching out of these artificial damage sites was measured.

For this purpose, 80x150mm specimen with primer and top coat, were prepared and scratched twelve times. Measuring the leached chromate gave 8.5 mg/l. This

value was taken to define the chromate concentration of at least one of the solutions used in the following electrochemical and A.I.E. tests.

As there was nothing known about the leachability of inhibitors from the chromate-free primers, the extracts prepared from them were diluted to the same extent as the extracts of the chromated primers. So all concentrations given in the following for chromate-free systems are based on these dilution ratios and do not represent real concentrations.

A second question to be answered by the following tests was that of the importance of the relative chloride to inhibitor concentration ratio.

For steel it was reported (1) that $\log [\text{chloride}/\text{chromate}]$ should not exceed two, or the inhibitor loses its effectiveness. This was the second point considered in diluting extracts used in the following tests:

1. Modified A.I.E. test
2. Polarisation resistance measurement
 - with oxygen aeration
 - with nitrogen aeration
3. Equilibrium potential measurements

The composition of the electrolytes prepared from an extract of primer A is given in Table V. The concentration is based on a measurement which gave 560 mg chromate/l $\approx 4.8 \times 10^{-3}$ mol/l. All other extracts were diluted in the same way without measuring the real inhibitor concentration which was not possible without knowing the exact inhibitor composition.

Table V: Composition of Electrolytes Prepared from Primer A

Dilution	NaCl [mol/l]	$\log [\text{Cl}^-]/$ [inhibitor]	Abs. chromate conc.
A1	0.05	1.00	4.80×10^{-3}
A2	0.05	1.50	1.60×10^{-3}
A3	0.05	2.00	5.00×10^{-4}
A1	0.10	1.30	4.80×10^{-3}
A2	0.10	2.15	7.10×10^{-4}
A3	0.10	2.50	3.16×10^{-4}

Results. The results of some of the electrochemical measurements are given in Tables VI-VIII (different test conditions) and Figures 3 and 4 (different primers).

The results given in Tables VI-VIII show that chromate inhibits the anodic process as well as the cathodic process while the chromate-free systems preferably influence the cathodic reaction.

A summary of the test results of the A.I.E.-tests of this second cycle are given in Table IX and Figures 5-7. The corrosion categories which are essential for the understanding of the above mentioned figures, as they are not yet standardized, are defined in Table X.

All results from the previously described corrosion tests corroborate the electrochemical measurements and confirm the somewhat poorer corrosion inhibition properties of the chromate free primer systems.

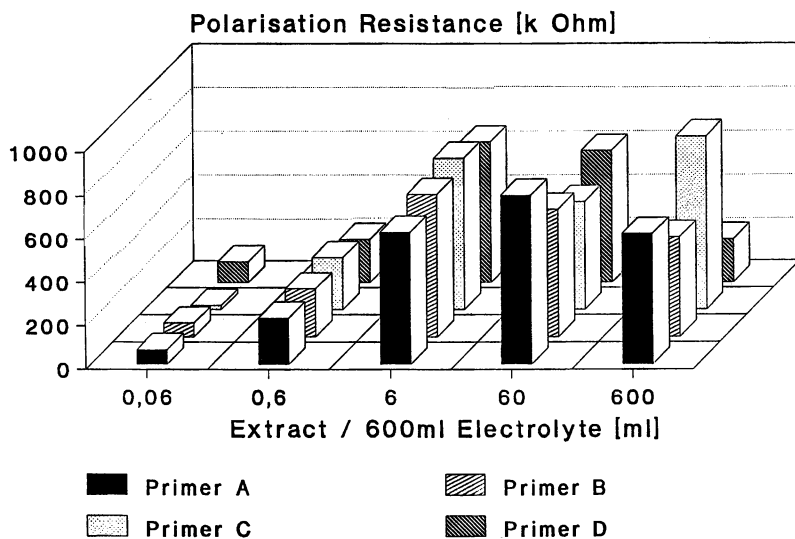


Fig. 3. Polarisation resistance of chromated primers (0.1M NaCl).

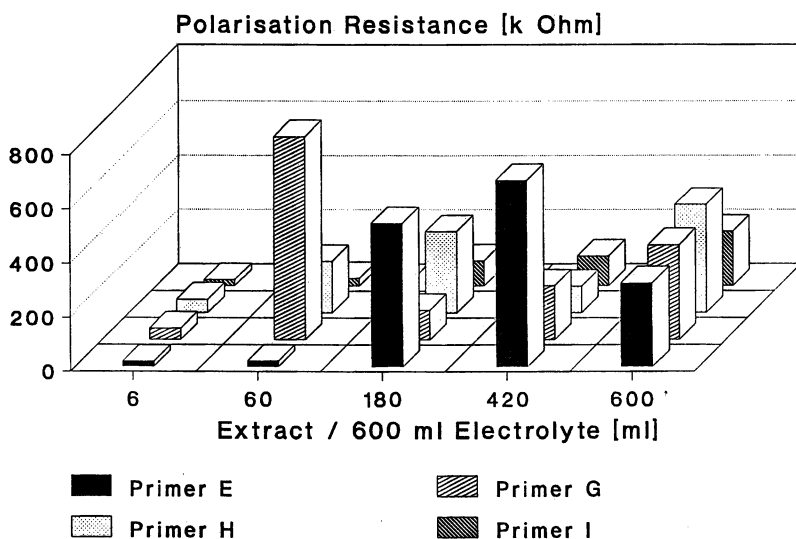


Fig. 4. Polarisation resistance of chromate-free primers (0.1M NaCl).

Table VI: Polarisation Resistance and Equilibrium Potential of a Chromated Primer

O ₂ aeration				
Dilution	0.05M NaCl		0.1M NaCl	
	Polarisation resistance [kΩ]	Equilibrium potential [volt]	Polarisation resistance [kΩ]	Equilibrium potential [volt]
A1	400	-0.645	530	-0.569
A2	300	-0.681	450	-0.686
A3	900	-0.872	400	-0.668
N ₂ aeration				
A1	600	-0.705	630	-0.688
A2	800	-0.787	830	-0.700
A3	1000	-0.867	510	-0.680

Table VII. Polarisation Resistance and Equilibrium Potential of a Chromate-Free Primer

O ₂ aeration				
Dilution	0.05M NaCl		0.1M NaCl	
	Polarisation resistance [kΩ]	Equilibrium potential [volt]	Polarisation resistance [kΩ]	Equilibrium potential [volt]
A1	5.8	-0.526	6.5	-0.529
A2	100	-0.507	7.3	-0.544
A3	400	-0.563	100	-0.532
N ₂ aeration				
A1	1200	-0.748	590	-0.605
A2	1300	-0.789	900	-0.633
A3	1400	-0.712	670	-0.714

Filiform Corrosion Test Results

One of the standard qualification test procedure run on the primers evaluated in this study was filiform corrosion. The results on CSA pretreated Al-specimen are given in Figure 8 as they reflect the tendencies of all other corrosion test results run during these qualification test attempts. They also corroborate the other reported investigation results.

Table VIII. Polarisation Resistance and Equilibrium Potential of Reference Electrolyte

0.05M NaCl		0.1M NaCl	
Polarisation resistance [$k\Omega$]	Equilibrium potential [volt]	Polarisation resistance [$k\Omega$]	Equilibrium potential [volt]
4.3 / 15.2	-0.540 / -0.540	4.2 / 90	-0.554 / -0.560
O ₂ aeration / N ₂ aeration			

Table IX. A.I.E. Test Results (Summary)

Primer	0.05M NaCl	0.1M NaCl	0.5M NaCl
A	+	+	+
E	+	0	0
F	-	-	-
H	-	-	-

+ / 0 / - = good / low / very poor corrosion inhibition

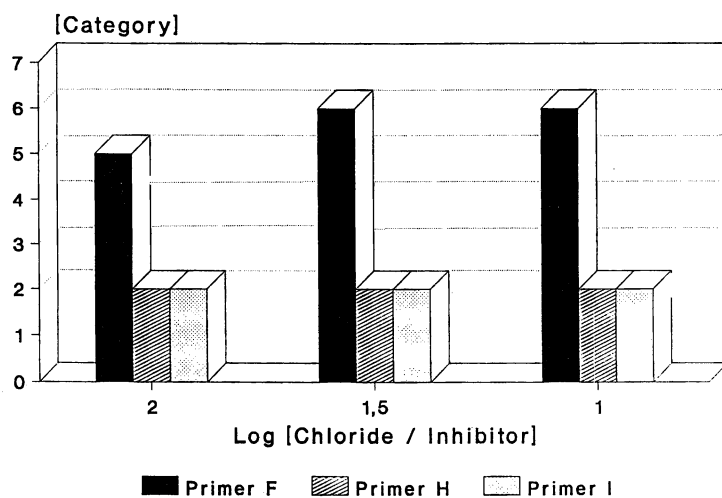


Fig. 5. A.I.E. test results with 0.05M NaCl.

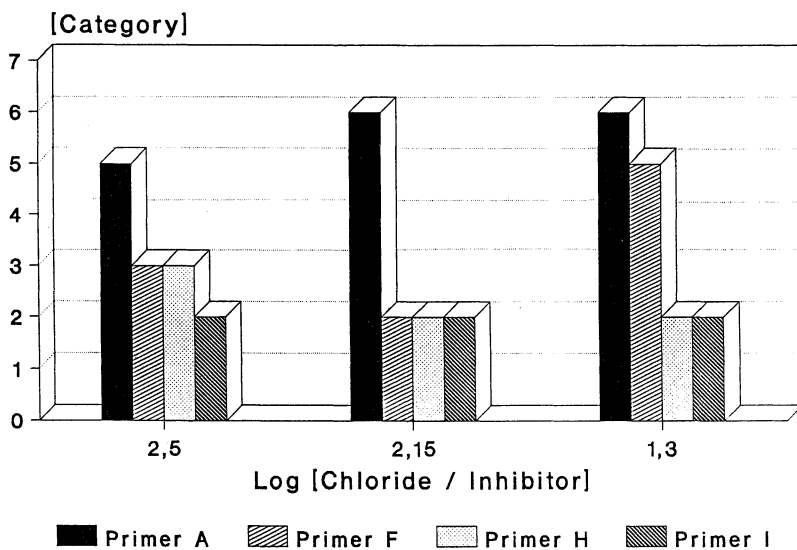


Fig. 6. A.I.E. test results with 0.1M NaCl.

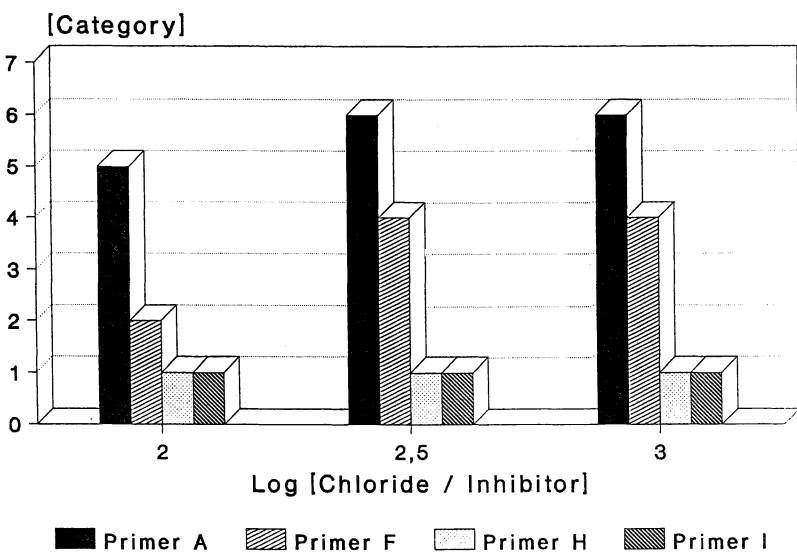


Fig. 7. A.I.E. test results with 0.5M NaCl.

Table X. Corrosion Categories

Categories
1 = complete area corroded, covered with tightly adhering corrosion products
2 = complete area corroded, nearly no tightly adhering corrosion products
3 = < 50 % of area corroded
4 = < 20 % of area corroded
5 = corrosion visible by eye
6 = no visible corrosion

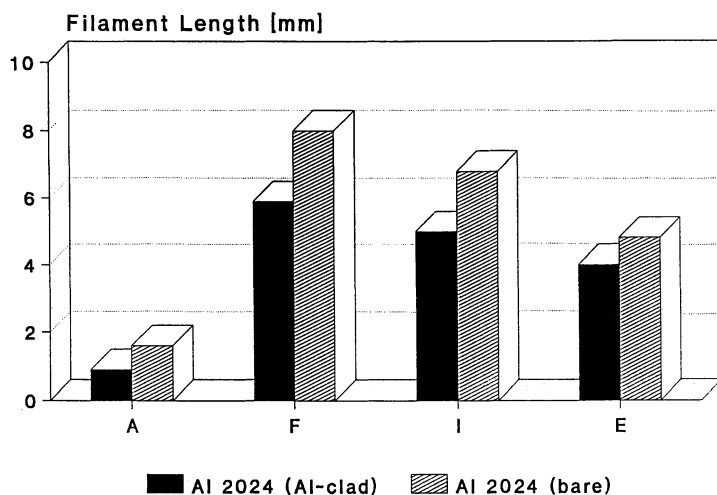


Fig. 8. Filiform corrosion results on CSA pretreated Al-specimen.

Conclusion

Chromated and chromate-free primers exhibit a completely different behavior. A significant influence of chloride / inhibitor ratio on the effectiveness of the corrosion tests could not be proven. The A.I.E. tests and the electrochemical measurements show the same trends and also corroborate the results of filiform corrosion testing. The extraction method, together with the described electrochemical measurements, demonstrated the capability of a good screening test for corrosion inhibiting primers. These methods may be used prior to qualification testing to preclude running costly corrosion tests on poor corrosion inhibiting primer systems and to choose inhibitor systems for further primer development.

Literature Cited

[1] Mc Lafferty, E., "A Competitive adsorption Model for the Inhibition of Crevice Corrosion and Pitting", *J. Electrochem. Soc.*, Vol. 137, No. 12, 3731 (1990)

Chapter 19

Testing of Coating Materials in Industrial Practice

Otto Vogt

Sika Chemie GmbH, D 70432 Stuttgart, Germany

Accelerated test procedures for assessing the performance of coating materials are very common in the coating industry. Compared with exposure to service conditions, accelerated tests yield results within a much shorter period of time. But they suffer the drawback that laboratory and field conditions frequently disagree. However, at present there is no alternative to the use of accelerated tests. Examples will demonstrate their application in industrial practice. It will be shown that, despite reservations, accelerated testing can still be a good tool.

Accelerated corrosion testing has been used for many years as a means for evaluating the performance of coatings, when exposure to actual conditions is too time consuming. However, due to frequent differences between test conditions and service environment, the validity of results obtained by laboratory tests is not beyond any doubt.

This point has been dealt with in detail by numerous scientists. They all agree that exposure to service conditions would be the definitive test for assessment of a material's performance. Concerning accelerated tests the opinions are rather controversial. In particular, the widely used salt spray test has been seriously questioned (1 - 2), because the majority of materials are not exposed to the conditions of this test in their working environment. In a literature survey the results of accelerated tests have been compared with natural weathering (3). Some correlations but also a number of inconsistencies have been encountered. For coatings designed for long-term immersion service it has been reported (4), that immersion tests of several months revealed tendencies which standard laboratory tests failed to show. On the other hand it has been pointed out that a combination of thoroughly selected accelerated tests can provide quite satisfactory results (5).

This discussion is not very encouraging to the tester, who depends on accelerated laboratory tests, but experience has proved that in most cases allowance for such discrepancies is possible.

The following presents a few examples of laboratory testing in industrial practice. It should be emphasized that these investigations were conducted in order to solve relevant problems rather than to compare testing methods.

Examples

Influence of surfactants adhering to the steel substrate. Dry blast cleaning is generally accepted to be the most effective means of surface preparation for subsequent coating. But the heavy dust evolution is a serious disadvantage of this procedure, rendering its use increasingly difficult. One should bear in mind that blast cleaning is most frequently used in the course of maintenance work in order to remove old paint layers, which are likely to contain hazardous components, e.g. red lead or asbestos.

Efforts are made to minimize dust formation by addition of water in different amounts to the blast-cleaning abrasive, which can be very effective. For example, in case of the moisture injected blast cleaning (6 · 7), which uses only a relatively small quantity of injection water, dust formation is dramatically reduced, though not completely prevented. In cooperation with the Bau-Berufsgenossenschaft, Wuppertal, Bayer AG, Leverkusen, Märkische Fachhochschule, Labor für Korrosionsschutztechnik, Iserlohn, and Peiniger GmbH, Leverkusen, a new approach was made to further improve this method. Preliminary experiments revealed that dispersions as well as surfactants, added to the injection water, can result in an additional dust reduction. Our task was to find out whether the surfactants will be harmful to subsequent coating or not. Since the blast equipment needed adaptations for handling the different admixtures, and also because the dust measuring turned out demanding and expensive, a screening by means of accelerated tests was decided in order to avoid unnecessary cost and work by excluding inappropriate admixtures during an early stage of the investigation.

Five surfactants, supplied by Henkel KGaA, were examined. Their chemical constitution is given in Table I. The test procedure was as follows: Steel panels, prepared by using modified moisture injected blast cleaning, were coated. Two coating systems essentially according to the technical terms of delivery 918 300 page 677 (PVC combination) and 687 (EP/PUR) of the Deutsche Bundesbahn were chosen. As reference samples standard blast cleaned panels (Sa 2^{1/2} or better) were contemporarily prepared and tested. Since surfactants adhering to the steel substrate were expected to increase the susceptibility to water and, consequently, to affect the adhesion, tests comprising the influence of liquid water or high relative humidity were selected:

- Condensation water test DIN 50 017.
- Salt spray test DIN 50 021.
- A cyclic climatic test according to own specifications (8).

In addition, both test and control samples were exposed to natural weathering, which, of course, was unable to make any contributions to the screening. However, if during a later stage of the investigation some surfactants had turned out to be appropriate, then results of long-term testing would have been very helpful.

After three weeks of testing the specimens were removed from the cabinets and evaluated. The rating criteria were: (a) rust spots, (b) blistering, (c) undercutting at the scribe, (d) cross-cut test, and (e) pull-off test for adhesion. The evaluation was simply done by comparing each individual test specimen with the corresponding control sample. From this, relative rating numbers ranging from 0 (= breakdown of the coating system) to 10 (= no damage) were derived. Figure 1 shows the results.

It can be derived from Figure 1, that surfactant (4) exhibited the best performance, nearly equalled by (2). Consequently all but these two were excluded from further consideration. The behaviour of the other surfactants ranged from indifferent to bad.

This result will be quite understandable if the chemical constitution of the surfactants is taken into account. The best performing surfactants are non-ionic, whereas the other ones are ionic. And, not too surprising, the worst behaving surfactant (3) is a quarternary ammonium chloride. Thirty three months of natural weathering confirmed the results of accelerated testing. This leads to the following conclusions:

- Despite of reservations, laboratory and long-term testing can agree.
- Conclusions drawn from accelerated tests are not necessarily misleading.

Performance of coatings on aluminium substrates. In connection with the filiform corrosion tests, (see below), the performance of a variety of coating systems on aluminium substrate, in general, and the adhesion in particular, were investigated. Along with outdoor exposure four accelerated tests were conducted:

- Test in condensation water without SO₂ DIN 50 017.
- Test in condensation water with SO₂ (Kesternich test) DIN 50 018.
- Salt spray test DIN 50 021.
- Cyclic climatic test.

Table II shows the coating systems. It has been already mentioned, that the main objective of this investigation concerned the adhesion on aluminium substrate. The results have been recorded elsewhere (8). Another point should be scrutinized here.

Standard laboratory tests are not commonly adapted to the specific problems. Because of this it can be risky to rely on one single test which, in individual cases, can yield misleading results. Performing several different tests and combining their results is more promising, because the combined result is likely to be balanced out. In Figure 2 the combined result of all accelerated tests is compared with the result of outdoor exposure (for the rating numbers

Table I. Chemical constitution of surfactants

No.	Chemical constitution
1	Triethanolaminolauryl sulfate
2	Alkylaminopolyglycol ether
3	Lauryldimethylbenzylammonium chloride
4	Fatty alcohol ethoxylate
5	Turkey red oil

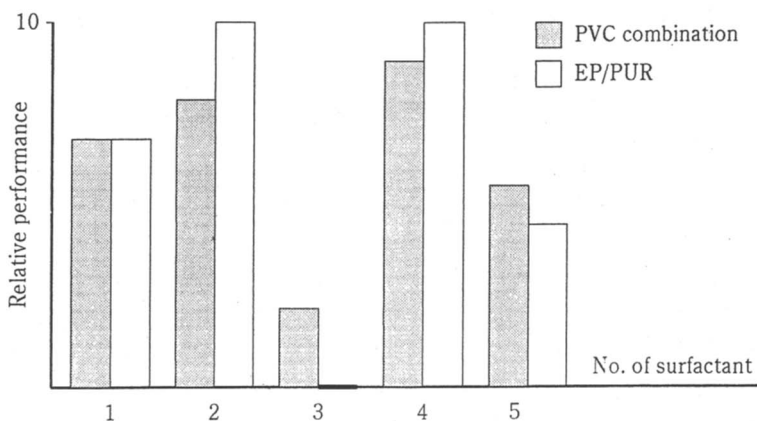


Figure 1. Influence of surfactants on the performance of coatings.

Table II. Materials for adhesion testing on aluminium substrate

No.	Primer	Top coat
1	Modified epoxy resin (2 layers)	
2	Epoxy resin	Polyurethane
3	Epoxy coal-tar (2 layers)	
4	Epoxy resin ester (zinc rich)	Polyurethane
5	Epoxy resin (zinc rich)	Polyurethane
6	Bituminous coat (2 layers)	
7	Tar pitch coat (2 layers)	
8	Zinc silicate	Polyurethane

SOURCE: Adapted from ref. 8.

see example 1). On the basis of accelerated testing the systems (1) and (2) are the best. The performance of (3) - (5) is quite acceptable, whereas (6) - (8) are unusable for aluminium substrate. This corresponds with natural weathering as well as with practical experience.

If exclusively the salt spray test is regarded, the result would be different (Figure 3). For systems (1) - (3) the assessment remains valid. The other systems generally perform worse, but there are some inconsistencies. In contrast to the outcome of accelerated testing and natural weathering, (7) outperforms (4) and (5), which for their part exhibit a remarkably poor performance. Hence, relying exclusively on the salt spray test would have led to an unjustified rejection of (4) and (5) as well as to an equally unjustified acceptance of (7). From this, the following can be reached:

- Individual laboratory tests not adapted to the specific conditions can yield questionable results. Therefore, running several different tests and combining their results is advisable.

Filiform corrosion. Filiform corrosion is generally accepted to be a type of differential oxygen concentration cell (see (9) and therein cited literature), in which the head is anodic, whereas the tail acts as cathode. Therefore, the liquid in the head should be acidic and in the tail it should be alkaline.

In attempting to make this visible, aluminium panels were pretreated with a pH indicating dye prior to coating with a colourless acrylic varnish. Finally filiform corrosion was initiated as reported below, with two exceptions: only one single immersion procedure was done, and the specimens were stored at ambient temperature instead of 40°C.

Photo 1 shows a small thread, which clearly exhibits the anodic and cathodic sites. The colour film, used to photograph the panel, does not truly reproduce the vivid colours observed under the microscope, but it gives a fairly good representation of the pH changes involved. There were filaments too, which showed only a red coloured head or even remained without colour changes. In some cases it may have been that these rather short-lived events were simply not noticed. No cathodic (i.e. blue coloured) areas surrounding the head (10 - 11) could be detected.

In the past, filiform corrosion, though well known to the car and aeroplane manufacturers, did not play any role in the sector of corrosion protection of constructions. Today the situation is different. For several years powder coated aluminium facades in industrial environment near the coast have been attacked by filiform corrosion. During the search for repair materials coating systems with zinc rich primers turned out to be remarkably resistant to this type of corrosion (12).

In order to verify this finding, a lot of different materials were examined within several test series. Only one of this series shall be dealt with here. Table III shows the coating materials. The topcoats of systems (1) - (4) are identical. The binders of systems (1) - (3) and the varnishes (5) - (7), respectively, were of the same type but not exactly identical. It should be mentioned, that systems (1) and (4) are the same as systems (5) and (4) of Table II.

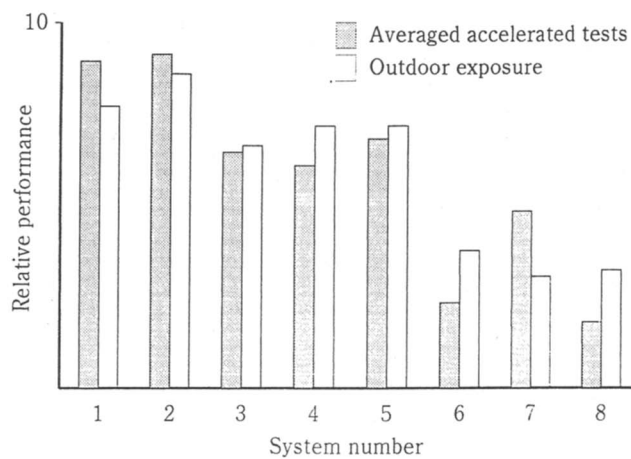


Figure 2. Averaged accelerated tests and outdoor exposure.

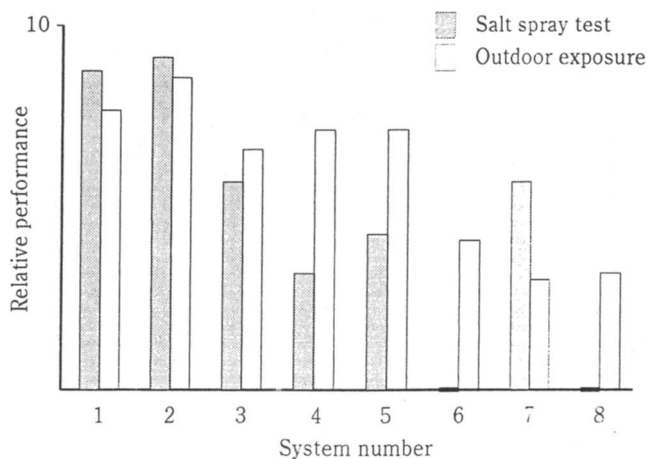


Figure 3. Salt spray test and outdoor exposure.



Photo 1. Thread of filiform corrosion on aluminium substrate pretreated with a pH indicating dye. Length approximately 6 mm.

Table III. Materials for filiform corrosion testing

No.	Primer	Top coat
1	Epoxy resin (zinc rich)	Polyurethane
2	Epoxy resin (zinc phosphate)	Polyurethane
3	Epoxy resin (micaceous iron oxide)	Polyurethane
4	Epoxy ester resin (zinc rich)	Polyurethane
5	Binder of primer 1 (single layer varnish)	
6	Binder of primer 2 (single layer varnish)	
7	Binder of primer 3 (single layer varnish)	
8	Binder of primer 4 (single layer varnish)	

In this case, we had to rely exclusively on a laboratory test, because outdoor exposure causes filiform corrosion only at particular sites. It seems that both conditions, industrial and coastal environment, have to meet. This does not apply to our test racks, neither in Stuttgart nor in Gelsenkirchen. In order to be as close as possible to reality, filiform corrosion was not initiated by means of hydrochloric acid fumes, which have been reported to be very effective (12). Instead of this the following simple test procedure was set up: Once a week the X-scribed aluminium panels were immersed in artificial sea water for 5 minutes at ambient temperature. Otherwise the specimens were stored in a cabinet with 80% relative humidity at 40°C. The pH value of the artificial sea water was adjusted to 4-5 by means of sulfuric acid. During the immersion procedure the panels were visually inspected for signs of filiform corrosion.

The intention of this test series was not only to confirm the already known good performance of (1) and (4) but also to examine possible influences of pigmentation and type of binders.

Already after 2 weeks the first signs of filiform corrosion became visible. Later, all systems apart from (1) and (4) were gradually attacked by filiform corrosion. After 26 weeks the test was finished. Only systems (1) and (4) and, for comparison, (5) and (8) remained under examination.

Photo 2 shows the appearance of systems (4) and (8) after 33 weeks of testing. After such a long time some undercutting and flaking at the scribe of (4) is not significant. However, it is worth noting that only (8) suffered filiform corrosion, though both, (4) as well as (8) are based on the same vehicle. The comparable pair of systems (1) and (5) performed equally.

Even after 91 weeks of testing systems (1) and (4) exhibited no signs of filiform corrosion attack. Hence, zinc rich primers, as far as tested, turned out to be indeed resistant to filiform corrosion. This property is strongly related to the zinc dust pigmentation. This finding is in accordance with outdoor exposure recorded in (12) as well as with practical experience gained in the meantime with system (4). From this the following can be deduced:

- Even a single laboratory test can yield reliable results, provided it is well adapted to the specific situation.

Conclusions

The validity of results achieved by means of accelerated tests is not beyond any doubt, because the correlation with service conditions can be questionable. Despite of this, appropriate testing strategies make accelerated tests a valuable tool.

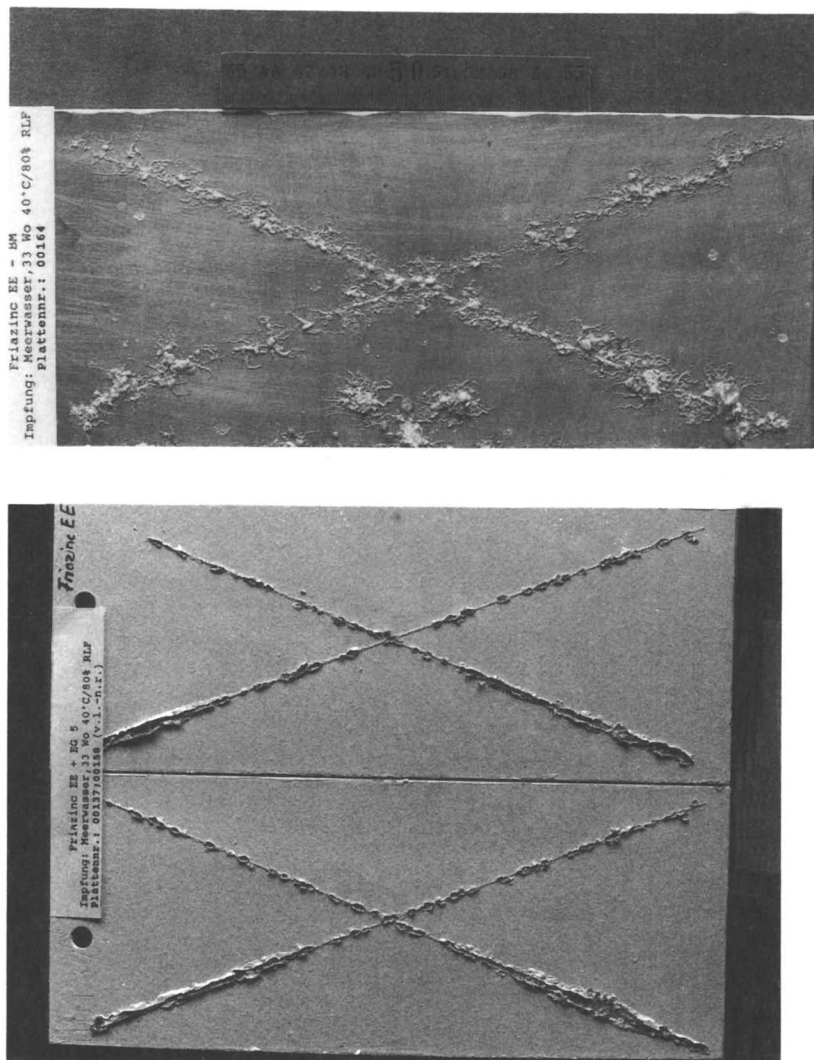


Photo 2. Appearance of systems (4) and (8) after 33 weeks of filiform corrosion testing. Left: system (4), right: system (8).

Acknowledgement

The cooperate project referred to in the first example was financially supported by the German Bundesminister für Forschung und Technologie, DLR Projektträgerschaft Arbeit und Technik, Kennzeichen 01 HK 199/2.

Literature Cited

1. Cremer, N. D. *Pittura Vernic. Eur.*, Dec. 1992, 68, (12), pp. 27-32, 35-36.
2. Montle, J. F.; Korobov, Y. *American Paint & Coatings Journal* 76, No. 29, Dec. 23, 1991, pp. 36-44.
3. Boelen, B.; Schmitz, B.; Defourny, J.; Blekkenhorst, F. *Corros. Sci.*, Nov. 1993, 34, (11), pp. 1923-1931.
4. Pawel, S. J. *Materials Performance* 34, 10 (1955), pp. 37-42.
5. Padinha, E. A.; Ferreira, M. G. S.; Maia, M. A. *8th European Congress of Corrosion, Vol. 2, (Proc. Conf.)*, Nice, France, 1985, pp. 40.1-40.10.
6. Gieler, R. P. *Stahlbau* 3/1984, pp. 79-82.
7. Vogt, O. *XIXth Patitepec Congress*, Aachen, Germany, 1988, Vol II, pp. 319-327.
8. Vogt, O. *UK Corrosion & Eurocorr 94, Vol I (Proc. Conf.)*, Bournemouth, England, 1994, pp 20-29.
9. Kobayashi, K.; Shimizu, K.-i.; Tanabe, H.; Masuda, K., *Steps into the 90 's, Vol 1 (Proc. Conf.)*, Queensland, Australia, 1989, pp. 243-249.
10. Leidheiser, H., Jr., *Corrosion Nace, Vol. 38, No. 7, 1982*, pp. 374-383.
11. Hoch, G. M.; Tobias, R. F. *Corrosion/71*, paper no. 19 (Houston, TX: Nace 1971).
12. Heinrich, M.; Haagen, H.; Schuler, T. *farbe + lack* 100 (1994), No. 4, pp. 249-252.

Chapter 20

Realistic Performance Testing of Internal Coatings for Oilfield Production

G. R. Ruschau

Materials Technology Group, ARCO Exploration and Production Technology, 2300
West Plano Parkway, Plano, TX 75075

Internal coatings for petroleum production must perform in severely corrosive environments. The two components to a successful coating test are exposure to corrosive environments actually seen in service, and correct evaluation of the performance of the coating after exposure to the test media. Proper accelerating factors must be applied without being unrealistic.

Simulation of the corrosive environments is best accomplished by duplicating the most severe field service conditions in one of three test cells: the standard atlas cell (corrocell), the pressured atlas cell, or the rocker arm. In all of these tests, a thermal gradient is present across the coated steel sample. Acceleration of the test is best accomplished by increasing the thermal gradient across the coating, using deionized or distilled water as the water phase, and evaluating the subtle changes which occur within coating if failure is not evident.

The use of internal coatings for corrosion protection in the petroleum production industry is well established. In many cases, proper coating selection can allow the use of carbon steel for construction instead of corrosion resistant alloys (CRA's); the initial cost of even the most inexpensive CRA vessels is 2x-5x more than carbon steel. As the CRA becomes more specialized, the material cost can go up tenfold; in addition, other issues such as welding, machining, and availability add to the cost and problems.

Internal corrosion protection of oilfield gathering and distribution systems can be divided into four classes of service: downhole tubing, line pipe, production vessels, and storage tanks.

Downhole tubing generally sees the most corrosive environments of all; it is not unusual to encounter temperatures which range from a low of 100°F to over 400°F in high temperature/high pressure developments. Pressures encountered are nominally in the range of 2000 psi to 10,000 psi. The typical corrosive fluids and gases are H₂S, water, and CO₂; hydrocarbons are not corrosive to steel but raw gas and crude oil will always contain significant amounts of water and usually CO₂ as well; H₂S may or may not be present in significant amounts. In isolated cases, strong acids or bases may come into contact with the tubing for short duration (several hours).

Line pipe normally is of larger diameter (4" to 60" is used, 10" to 24" most common) than downhole tubing (normally 2"-3"). Crude oil and multiphase production lines run at pressures of 100 psi to 2000 psi; gas production lines can run up to 4000 psi. The possible corrosive environments are similar to the downhole conditions, except that they tend to be lower temperature and pressure. For cross-country product transportation lines, the temperatures are seldom above 120°F and generally have been stripped of most of the produced water and corrosive gases; however, process upsets and malfunctioning separation equipment can result in a corrosive fluid or gas being transported. Chemical treatment is often used in lieu of coatings or to supplement coatings.

Production vessels include separators, treaters, slug catchers, and miscellaneous pressurized tanks into which crude oil and gas are dumped at line pipe pressures and temperatures. They can be as small as a few hundred gallons or can hold tens of thousands of gallons of fluid. In addition to coatings, many production vessels use cathodic protection anodes mounted internally for corrosion control; like chemical treatment, anodes can also be used to supplement coatings and vice-versa.

Storage tanks are most often found grouped at pipeline terminals; they may contain crude oil (and associated water), salt water, potable water, refined products, manufactured chemicals, or alternate between these fluids. Near oilfield production, these tanks can operate at temperatures over 200°F, but most storage tanks operate below 100°F at atmospheric or even less than atmospheric pressures.

STANDARD TESTS

Standard industry tests for internal linings include, in order of increasing aggressiveness, simple immersion, elevated temperature immersion, and autoclave immersion. Simple immersion normally can distinguish only gross chemical incompatibilities unless the test is run for a very long period of time.

Performing a simple immersion test at elevated temperatures accelerates a test in two ways: increases the solubility of the solvent (including water) in the coating by increasing the entropy contribution to solubility, and increases the free volume of the polymer so that the solvent may penetrate more easily and more quickly. In the autoclave immersion, pressure is added to further increase the solubility of the solvent in the coating. In addition, gas mixes can be introduced in the autoclave to test compatibility of the coatings with aggressive gases.

For all immersion tests, the coating is visually checked for signs of dissolution, blisters, discoloration, and softening. These are not quantitative tests, and most manufacturers rank this data as "satisfactory" or "unsatisfactory" for a given service.

Quantitative results are difficult to obtain with immersion tests. The standard pull tab adhesion tests (ASTM D-4541) rarely result in meaningful numbers when high performance epoxy linings are tested. Because these epoxies are developed for superior adhesion, only linings which are severely affected by the test environment will fail adhesively at the steel surface in the pull tab device. More often than not, the sample will break at the glue on the pull tab, or appear as a cohesive failure within the coating. Likewise, crosshatch adhesion testing (ASTM D-3359) is inadequate for high performance epoxies for the same reason.

Electrochemical evaluation is gaining popularity not only as a measure of coating performance but as a research tool to determine the mechanisms by which coatings protect steel and/or fail. DC Resistance, electrochemical impedance spectroscopy, and electrochemical noise are commonly employed methods¹⁻⁴; however, extracting significant information from electrochemical measurements requires great skill unless the system has been fully characterized. Also, evaluation without a good electrolyte is an extremely complicated problem; some of the more aggressive fluids are not conductive.

Depending on the intended service, cathodic disbondment tests (ASTM G-95) may also be run. Because coatings in storage and production tanks often are used in

conjunction with installed sacrificial anodes, the cathodic reaction taking place at any coating holiday produces hydrogen gas which causes disbondment. This test ideally should be run in combination with some type of immersion testing in order to determine the extent to which the immersion fluid/gas has affected adhesion in the area surrounding the coating holiday.

PREFERRED TESTS

The preferred method of testing varies for each of the oilfield production services. The emphasis is on process simulation, so the test which most closely duplicates field conditions is always preferred.⁵

The standard glass atlas cell or corrocell, shown in Figure 1, is used

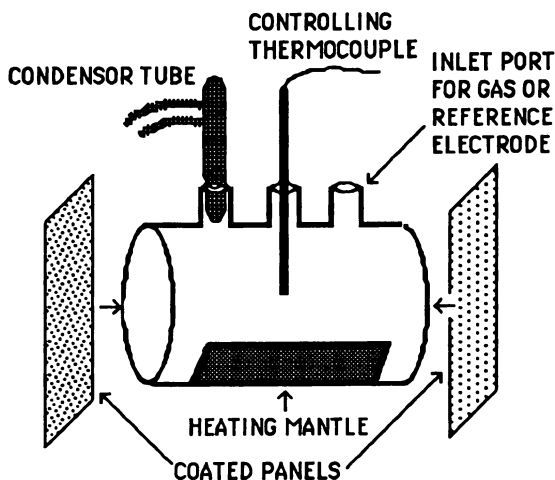


Figure 1: The standard Glass Atlas Cell (Corrocell) setup; the specification for linings testing is detailed in NACE TM-01-74, "Laboratory Methods for Evaluation of Protective Coatings as Lining Materials in Immersion Service."

to evaluate coatings for storage tanks and low pressure pipelines such as drain lines. Gases may be bubbled through the liquid in the cell to simulate sealed storage tanks in which there will be dissolved gases in the water. An advantage of the standard atlas cell is that because it is transparent, the condition of test coating can be visually inspected in-situ; therefore, the time dependence of events such as blister formation can be studied.

Tubular coatings are best evaluated in a rocker arm test, diagrammed in Figure 2. The rocker test uses a small (2'-4') section of 2"-3" coated tubing which is filled with the production environments and pressurized to the test pressure using actual production gas mixes. Temperature is controlled using an immersed heating element and thermocouple; the external wall of the sample is not insulated or heated except by heat transfer from the production fluids. This sample is slowly (10-20 cycles/minute) rocked back and forth at an amplitude of 6" to 12", which produces a stratified motion of fluid in the pipe. At the conclusion of a test (usually 30-60 days), the sample is split and the coating condition examined.

For production vessels, the pressured atlas cell provides the most useful data. This cell, diagrammed below in Figure 3, is quite similar to the standard atlas cell in concept except that it is normally sealed from ambient and pressurized with a production gas mix like the rocker arm. However, unlike the rocker arm, it is a

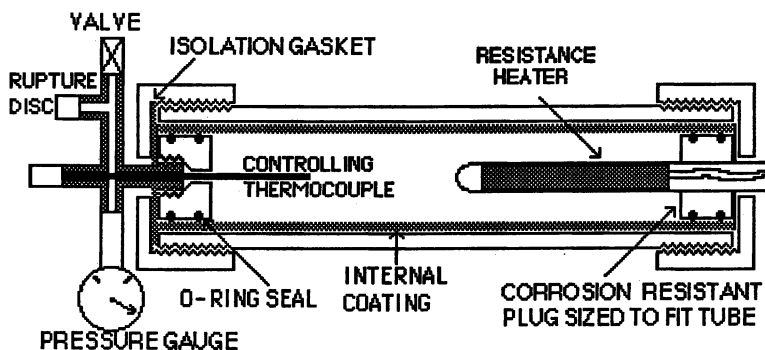


Figure 2: Test sample setup for the Rocker Arm coating evaluation. This test sample is rocked back and forth with test fluids and gases inside to simulate flowing production.

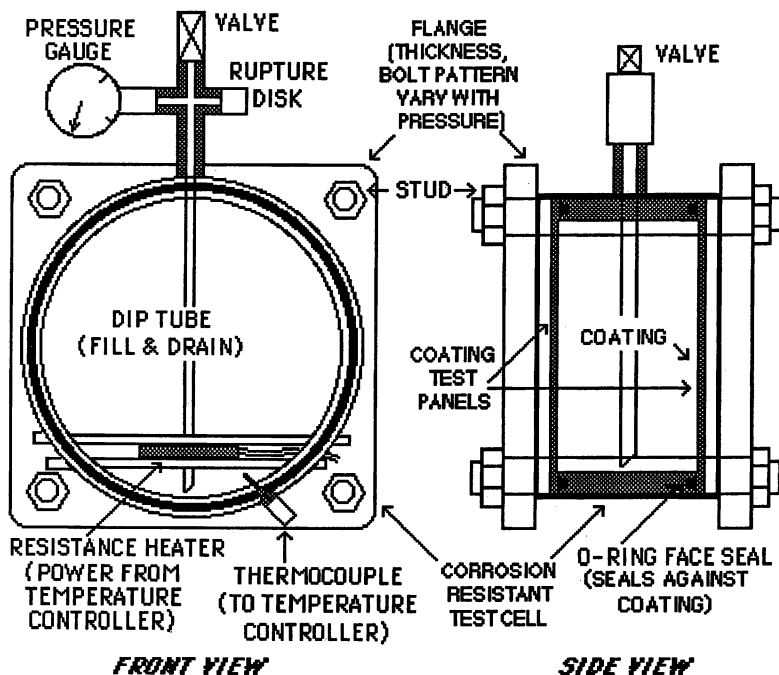


Figure 3: The Pressured Atlas Cell

stationary test, allowing the test fluids/gases to separate. In this way, the effect of individual phases on the coating can be examined. Because most production coating failures occur in water-filled areas, this can provide significant information as to where to inspect for coating damage and/or corrosion in previously coated tanks and vessels.

A common feature of these tests is perhaps the most significant degradative factor in a coating test: the presence of a negative thermal gradient across the coating to the steel, often referred to as the cold wall effect. Figures 4 illustrates the magnitude of this temperature gradient for the standard atlas cell, rocker arm, and pressured atlas cell.

The effect of the cold wall is not exactly understood, but appears to be most dependent on the temperature of the steel - coating interface. For a case in which the coating is "saturated" with water, the water in the coating will condense on the colder steel substrate. This driving force for condensation can overcome the adhesive bonds between the coating and the steel, resulting in disbondment or blistering.

The reason for the difference in the magnitude of the temperature gradients between these three test methods is mostly a function of the cell design. Pressurized cells contain a greater mass of alloy for strength purposes, and heat transfer through the metal is more rapid than heat transfer from the metal surface to the ambient air. This higher thermal mass coupled with slower heat transfer translates into a higher steel temperature in a pressurized cell. For a rocker arm test, heat transfer from the fluid to the coating and steel is greater still because of the convective heat transfer resulting from the rocking motion.

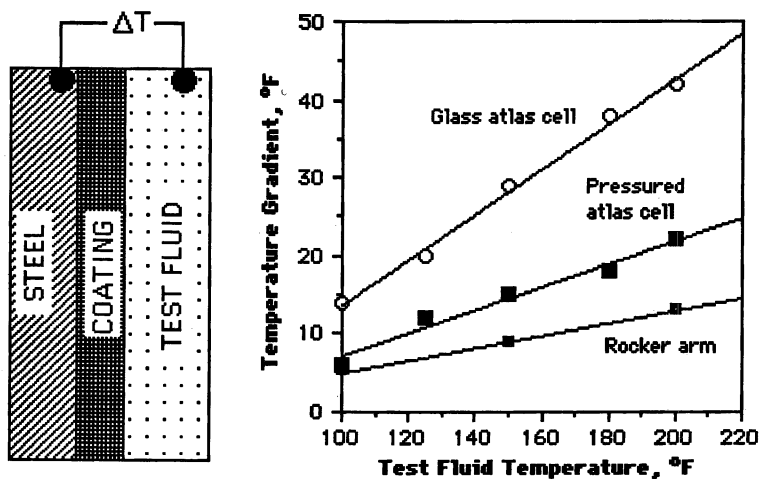


Figure 4: Magnitude of temperature gradients from the test fluid to the steel under the coating in preferred coating performance tests.

In addition to condensation, a thermal gradient increases the thermal expansion mismatch between the steel and the coating. The magnitude of this stress can be estimated if the material constants (elastic modulus, thermal expansion coefficient) are known for a particular coating; however, the elastic modulus of a coating bonded to steel will often be different from the modulus of a free-standing coating film because the bonded coating will be pre-stressed due to shrinkage upon drying and curing. Therefore, a thorough investigation of the magnitude of thermal stresses becomes a more difficult task. However, it is clear that the adhesive bond is subjected to a shear stress because of a difference in thermal expansion coefficients; this shear stress is in addition to the force of cold-wall condensation disbondment.

DISCUSSION OF TEST METHODS AND ACCELERATING FACTORS

One thing that needs to be understood when evaluating both coating performance and test protocol is that end-user coating evaluation is normally not designed to eliminate all but the best coatings. On the contrary, it is designed to determine which coatings will qualify for a given service. Therefore, when testing a number of coatings for a mild service, it is perfectly reasonable to have a 90% passing rate. When the service conditions are highly corrosive, it is reasonable when no coatings survive the test; in this case other corrosion mitigation / prevention methods must be considered.

The real key to a successful coating evaluation is to include all the degradative factors in a test and to maintain the test until a sort of "equilibrium" is reached in reference to the response of the coating to the forces acting upon it. In reality, equilibrium is not reached in a short term coating test since polymers undergo other forms of degradation over long periods of time. The type of equilibrium referred to here is pseudo-steady state with the test environment in terms of water absorption and stress relaxation in the coating film (via disbondment). Failure appears to be time-dependent but not linear. A coating will be put in a state of stress early on in a coating test, and will seek to relieve this stress by blistering and buckling. Once the stress is relieved, further blistering and disbondment only occurs as the coating film thermally degrades, a much slower process than stress relaxation. Therefore, a coating which can withstand a large amount of residual stress without disbonding in an accelerated test will normally last for many years without disbondment.

1. Increased Temperature

The most obvious accelerating factor for coatings testing is increasing the test temperature. Indeed, this will cause tremendous differentiation among coatings and is probably the most effective accelerator to cause failures. However, in many cases it is unrealistic and unfairly punishes coatings which may be of an excellent formulation but are not intended for high temperature use.

When polymers are heated, the various thermal transitions encountered (such as glass transition temperature, T_g) may or may not have a detrimental effect on the performance of the coating. If it can be verified that increased temperature is purely an accelerating factor in a given coating system in a specific temperature range, then the temperature can be safely increased. The increase in temperature in this case will accomplish three separate things: (a) Increase the solubility of the solvent in the coating, (b) Increase the diffusivity of the solvent through the coating, and (c) Increase the thermal gradient across the coating, as was shown in Figure 4 (for test methods in which the air surrounding the coated panel is at ambient temperature).

Mathematically, each of these factors can be examined through some fundamental relationships:

(a) Solubility:

$$\Delta G_{\text{mix}} = \Delta H_{\text{mix}} - T\Delta S_{\text{mix}} \quad (1)$$

where G = energy of mixing, H is the enthalpy of mixing, T is temperature, and S is entropy of mixing. Increasing T decreases the energy of mixing by increasing the entropy contribution, thus providing a more favorable condition for dissolution of the polymer by the diffusing species.

(b) Diffusivity:

$$\frac{\partial C}{\partial t} = \frac{\partial}{\partial t} (D \frac{\partial C}{\partial x}) \text{ (Fick's Second Law)} \quad (2)$$

where $\partial C/\partial t$ = concentration of diffusing species at time t , D = diffusion coefficient, and $\partial C/\partial x$ = concentration gradient. Empirically, it is known that D is dependent on temperature by an Arrhenius-type relationship of the form:

$$D = D_0 e^{-E/kT} \quad (3)$$

where D_0 = pre-exponential factor, E = activation energy for diffusion, and k = Boltzmann's constant. Increasing temperature will increase D and therefore increase the diffusion rate of solvent through the coating film.

(c) Thermal Gradient

$$\frac{\partial Q}{\partial t} = -K \frac{\partial T}{\partial x} \quad (4)$$

where $\partial Q/\partial t$ = heat flux, $\partial T/\partial x$ is the temperature gradient, and K = thermal conductivity. Obviously, an increase in the temperature increases $\partial T/\partial x$ provided that the ambient temperature is not affected.

While these factors are understood, both conceptually and in terms of magnitude, there is another factor which is often not considered. The introduction of a solvent into a polymer is known to shift transition temperatures (such as T_g) so that an apparently "safe" elevated temperature may be unrealistic. For this reason, it makes sense to conduct coating tests at the highest possible temperature that the coated area in the system will reach, even if only a small amount of the coated equipment (e.g. the inlet port area on a water tank) will actually see that temperature.

2. Increased Thermal Gradient

An increased cold wall is a seldom used acceleration factor for testing. This is accomplished by cooling the back side of a coated panel with moving air or circulating fluid to draw more heat away from the steel panel and increase the driving force for condensation disbondment. The quantitative significance of the cold wall effect as shown in Figure 4 deserves further discussion.

Condensation and thermal expansion mismatch are each a function of the temperature difference between the coating film and the steel, not the test fluid and the steel. Figure 5 illustrates the actual magnitudes of the various thermal gradients across

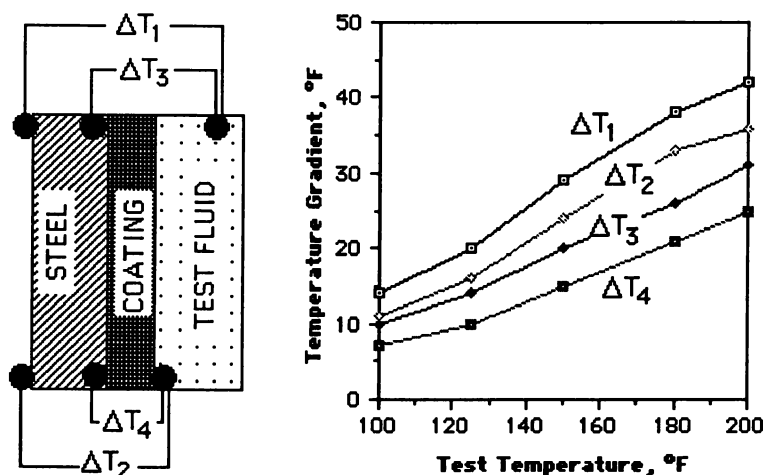


Figure 5: Description of the cold wall effect as it applies to different regions of a tested coated panel.

the different regions of the glass atlas cell. The gradient across the coating, ΔT_4 , is what should be monitored when accelerated cold wall effect is used. Figure 6 shows this number as a function of test temperature for different cooling schemes applied to the back side of the coated panel.

Like other accelerating factors, the increased thermal gradient can be unfair to a coating, particularly for coatings which have less inherent ability for stress relaxation. In this case, the thermal expansion mismatch alone could disbond the coating. The proper magnitude for a fair thermal gradient depends on the intended application (e.g. outdoor arctic service, thermally insulated pipelines and vessels, underground tanks

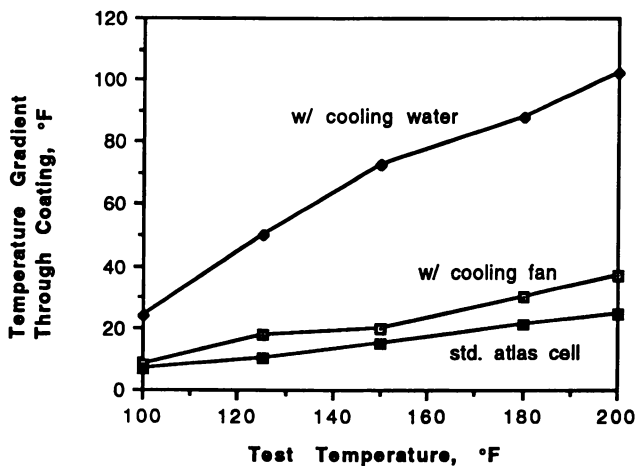


Figure 6: Thermal gradient in the glass atlas cell for accelerated cold wall experiments.

and pipelines, etc.), and the validity of the test results is left to the researcher to determine.

3. Use of Deionized or Distilled Water

A more controversial method to accelerate coatings testing is the use of deionized or distilled (DI) water instead of tap water or salt water in a test. DI water is an extremely aggressive solvent for coatings on steel; only the most advanced coatings can withstand elevated temperature DI water.

Because DI water has a higher osmotic pressure than salt water, it will seek out ions from within the coating film or on the steel surface to become saturated. It is also believed that ionic species such as chlorides and carbonates dissolved in non-DI water effectively block diffusion of H_2O through the coating film. This creates a tortuous path for diffusion, which slows the disbondment or in some cases may even prevent disbondment if the driving force for diffusion and solution is not sufficiently strong.

For oilfield production most of the water encountered is a brine of some composition. In three-phase production, the gas phase carries less heat so the top areas of pipelines and vessels will be cooler than the bottoms. Because of this, water will condense on the walls in the vapor regions of the pipeline or vessel; this condensed water will be deionized and attack coatings, causing blisters in the vessels very similar to those observed in laboratory tests.

4. Adhesion Evaluations

As stated earlier, quantitative measurements of adhesion are difficult to obtain for high-performance epoxy coatings because they seldom break at the adhesive bond to the steel. Therefore, tracking adhesion changes qualitatively yields the best results. There have been other methods developed to quantitatively measure adhesion, such as blister inducement time⁶, but the brittle nature of high performance internal linings makes this impractical. Also, there is great interest in correlating results of electrochemical test methods to adhesion, but the applicability of these techniques to general coating performance evaluation has not been proven.

When there are no visual signs of deterioration, a simple knife adhesion test can provide much information about the affect of the test environment on the coating/steel

interface. The knife adhesion test is quite simple; an "X" scribe is cut through the coating to the steel, as shown below in Figure 7. The knife cut is applied at an angle to induce shear stress, which will tend to cause the coating to lift at the scribe. This sheared quadrant is then popped off the steel, revealing the condition of the interface. It has been postulated that residual stress alone in a coating relates

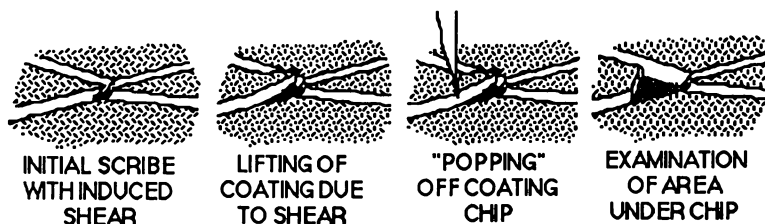


Figure 7: Qualitative adhesion estimation using knife scribe technique

directly to coating performance⁷. Other techniques, such as a parallel scribe method, can also be used but the same factor is being examined: the relative amount of coating remaining on the steel after the coating chip has been removed.

Poor adhesion is indicated when the coating pulls completely away from the substrate, leaving no remnants in the etch pattern on the steel. Most coatings leave some amount in the etch pattern; the relative surface area of etch pattern containing coating is compared to untested samples and to samples tested in other conditions, especially other test temperatures. This evaluation allows for a detailed examination of exactly what changes take place during exposure.

Changes in adhesion are often precursors to blistering and disbondment. Therefore, adhesion evaluation used in combination with aggressive exposures (such as atlas cells) becomes a useful tool for obtaining early indications of coating performance.

CONCLUSIONS

Because long term exposure of internal linings for test purposes is impractical, it becomes important to rely on accelerated testing. The best coating tests are those which correctly simulate the intended corrosive service. For oilfield production, the preferred tests are the standard glass atlas cell (for simulating storage tanks and low pressure pipelines), the rocker arm (for simulating downhole tubing and high pressure pipelines), and the pressured atlas cell (for simulating production pipelines and vessels). The best accelerating factors are increased temperature (if carefully administered), increased thermal gradient, use of deionized or distilled water for any water phase present, and a detailed qualitative observation of adhesion changes.

REFERENCES

- (1) Popov, B.N.; Alwohaibi, M.A.; White, R.E.; *J.Electrochem.Soc.* **1993**, *140*, 947-951.
- (2) Lillard, R.S.; Kruger, J.; Tait, W.S.; Moran, P.J.; *Corrosion* **1995**, *251-259*.
- (3) Chen, H.J.; *Corrosion* **94**, **1994**, #437.
- (4) Mills, D.J.; Bierwagen, G.B.; Tallman, D.; Skerry, B; *Proc.12th Int.Corr.Cong.*, **1993**, Houston, TX, 182-194.
- (5) Ruschau, G.R.; Bone, L.; and Moghissi, O.C.; *Proc.12th Int.Corr.Cong.*, **1993**, Houston, TX, 2601-2611.
- (6) Elbasir, A.; Scantlebury, J.D.; Callow, L.M.; *JOCCA* **1985**, *67*, 282-285.
- (7) Korobov, Y.; and Salem, L.; *Mat. Perf.* **1990**, *29*, 30-35.

Chapter 21

An Aspect of Concrete Protection by Surface Coating

J. B. Johnson¹ and B. S. Skerry²

¹Johnson-Thomas Associates, 36 Cedarway, Bollington, Cheshire SK10 5NS,
United Kingdom

²Cleveland Technical Center, The Sherwin-Williams Company, 601 Canal Road,
Cleveland, OH 44113

The effectiveness of polyisocyanate and alkoxy-silane coatings on concrete is investigated. Good and poor quality concrete samples were evaluated with or without surface chemical contamination (representing sea/road salts or acid rain conditions) after exposure to a natural outdoor environment cyclic test for 3 years. Concrete degradation was assessed visually and by; surface wetting; leaching of calcium from the cement; and depth of carbonation. The most significant factor was the quality of the concrete. Contaminants also decreased concrete performance in the order $\text{H}_2\text{SO}_4 \gg \text{Na}_2\text{SO}_4 > \text{NaCl}$. To some extent, both coatings ameliorated concrete degradation even when pre-contaminated. Here, the alkoxy-silane was somewhat more effective. In conclusion, when protecting concrete by coatings, all surfaces and sub-surfaces should be contaminant free. The effectiveness of remediation of poor quality or contaminated concrete may be limited.

Concrete, a building material composed of cement, stone, sand and water, has been in use since Egyptian and Roman times. In the 20th century, it has been used as an economical alternative to materials such as natural stone, brick and wood. For many years now, steel reinforcing bars have been molded into concrete to increase its structural strength. Unfortunately, a common type of failure of steel reinforced concrete is cracking and spalling loss of the concrete mainly due to the corrosion of the steel reinforcement inside the concrete. Galvanized steel or steel encased in epoxy based coatings have been attempts to isolate the reinforcing bars from the ingress of aggressive chemical agents.

Another important aspect about the preservation of concrete is the complementary use of coatings on the outside surfaces of the concrete. Acrylic, epoxy, silane and

polyurethane coatings have all been used for this purpose. The idea is that if access to and ingress of contaminants into the concrete can be minimized, then the useful life of a reinforced concrete structure can be increased (1, 2). Thus, coatings may inhibit the direct interactions between environmental components and a concrete substrate surface as well as slow the rate of penetration of any such components within the concrete. Despite the obvious apparent advantages of coating the surfaces of concrete structures, several factors affecting concrete durability can still be overlooked. For example, whether the coating is compatible with the chemical nature of the substrate as well as whether it is stable in sunlight (*i.e.*, whether it is alkali and UV radiation resistant). Further, is the coating maintainable, repairable, renewable and cost effective? (3)

Yet another complication arises when, as is becoming increasingly commonplace, a concrete structure of several years standing requires maintenance, repair and a new surface coating. In this case, the question arises as to what is the likely efficacy of the protection of concrete by the surface coating if contaminant salts from the environment are already on the surface of the concrete, or worse, penetrated *into* the concrete prior to the coating application. Even if a specification calls for 'blast-back' to sound concrete, sub-surface permeation may make it difficult to achieve a 'clean' surface for painting. The practical requirement is, therefore, that a coating should remain on a concrete surface and be effective against soil, water and atmospheric reactivity even when applied to a surface already contaminated and deteriorating.

Most laboratory evaluations of concrete and concrete coatings have used non-contaminated and good quality concrete. The purpose of this work has been to investigate four factors of practical significance, (i) concrete quality, (ii) chemical contamination, (iii) type of protective surface coating and (iv) different environmental exposure conditions, and to determine how these factors influence the likely long term performance and durability characteristics of coated concrete.

Experimental

Concrete Preparation. Two grades of concrete (*i.e.*, good and poor quality) were produced by using washed sand, limestone aggregate (graded between 5 and 15 mm), ordinary portland cement and water in the following ratios; (2:4:1:0.5 [*good quality*] and 2:4:1:0.65 [*poor quality*]).

Slabs of these mixtures were made in plastic molds (approx. 70 cm long x 35 cm wide x 5 cm thick). The slabs were allowed to cure at a temperature of 8-13°C protected from sunlight and wind for 35 days. Each slab was then cut across the longitudinal axis into 6 samples, each approximately 11 cm wide. A total of 48 samples were made; 36 representing good quality and 12 representing poor quality concrete.

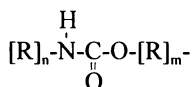
Surface Contamination. Three pre-treatments for concrete contamination were investigated. These treatments were intended to represent the effects of sea or road salts (chlorides and sulfates) and of natural acid rain (dilute sulfuric acid). The 48 concrete samples were numbered and divided into four groups of 12, each group having 3 good quality and 1 poor quality concrete samples, and were then treated as follows:

- i) Primary controls - *not contaminated with chemical treatments.*

- ii) Contaminated with chloride ions by immersion in 2wt% NaCl for 21 days, then removed and exposed for drying in ambient air for 7 days. The immersion was repeated with a fresh solution of NaCl. Samples were then allowed to dry again and any surface salts brushed off.
- iii) Contaminated with sulfate ions by the same procedure as for chloride ions but substituting a 2wt% solution of Na₂SO₄·10H₂O.
- iv) Contaminated with dilute sulfuric acid at pH 3 by immersion for 2 days in a fixed volume of acid (so as to produce a concrete surface loading of 3 mls acid per 1 cm² surface area), followed by removal and drying by outdoor exposure for 5 days. This procedure was repeated 10 times.

Surface Coatings. All the concrete samples were again separated; this time into three groups and treated as follows;

- i) The first series was left uncoated as secondary controls.
- ii) Samples in the second group were triple coated on all exposed surfaces by alkoxy-silane [R]Si[OR]₃ (where R, for example, may be a methyl group); prepared as a 20-30wt% solution in ethanol.
- iii) Samples in the third group were triple coated on all exposed surfaces by polyisocyanate prepared as a 20-30wt% solution in butyl acetate



where R, for example, may contain ether or ester groups.

In all cases, the coatings were applied by a hand held ½" broad brush using approximately 0.02 ml/cm² of the alkoxy-silane or polyisocyanate solution per application with 4 hours air drying allowed between first, second and third coats. All the coated samples were then left standing in a fume hood to cure for 21 days.

Exposure Test. Test exposure was in a natural outdoors (-rural) environment. Samples were half buried in soil (*i.e.*, to a depth of approximately 17cm) facing southwest. After six months exposure, they were removed from the soil and immersed to a depth of approximately 4 cm (along the vertical length) in de-ionized water also facing south-west for a further six months. This sequence was repeated for a total period of 3 years. Samples were therefore exposed to varying environmental factors including wind, rain, frost, pollutants and sunlight whilst being partially buried in soil or partially immersed in de-ionized water. Available or measured environmental conditions pertaining to the exposure test are noted in Table 1. Within the overall matrix of test panels in this program, for each test condition and surface state, good quality concrete samples were tested in triplicate and poor quality concrete samples were tested as single samples.

Table I. Exterior Exposure Program, Soil and Atmospheric Environment Characteristics

A) Soil

Cl ⁻	25 - 35 mg/g
SO ₄ ²⁻	25 - 35 mg/g
Water	20 - 30wt%

For a 1 liter d.i. water extraction from 100 g dry soil;
pH = 8.2; conductivity = 85 - 87 μ S (20°C)

B) Atmospheric Conditions

Annual sunlight: 750 - 850 hrs,
Temperature: -4°C to 25°C,
Average rainfall: 800 mm/yr (pH 4.5 - 5.6),
Humidity range; 55 - 100%,
Pollutants; SO₂ 5 - 20 ppb; NO₂ 5 - 15 ppb

Concrete performance assessment methods. Concrete performance was investigated by the following methods;

- i) Visual observations. All samples were inspected visually and photographed prior to and again after the 3 year exposure test.
- ii) Water surface capillary rise measurements. Selected samples from the program were immersed to a depth of 4 cm in de-ionized water at 25°C both before and after the 3 year exposure test. Any linear rise of water on a sample surface was measured with respect to time up to a period of 3 hours duration. The objective of this test was to assess the relative susceptibility and affinity to water ingress for the different test sample conditions both before and after exposure.
- iii) Calcium leachability. Other selected samples from the program were immersed to a depth of 4 cm in de-ionized water (*i.e.*, 120 cm² exposed surface area in 600ml H₂O) at 25°C for two separate periods of 36 hours after which, each water sample was analyzed for calcium content by atomic absorption spectroscopy. These measurements were made both before and after the 3-year exterior exposure program. The objective was to assess the effectiveness of the coatings in inhibiting concrete degradation through loss of calcium from the cement.
- iv) Depth of carbonation. After the 3-year exterior test program, representative samples were cross-sectioned and sprayed with a 1 vol% alcoholic solution of phenolphthalein. The depth of the non-colored band was taken as the depth of carbonation. The objective here was to assess the effectiveness of the coatings in preventing concrete degradation by acidification caused by diffusion of environmental CO₂ combined with water.

Results

Visual Observations. Prior to exposure testing, other than the presence of one of the surface coatings where present, all the samples were equivalent in appearance. After the 3-year exposure, clear visual differences became apparent. However, the blocks which had most obviously deteriorated were all those mixed using the 'poor concrete' recipe.

Representative degradation is illustrated in Figure 1(a) for the poor quality concrete sample contaminated with dilute H_2SO_4 and treated with the polyisocyanate coating. All poor quality concrete samples showed significant deterioration of this nature, irrespective of contamination or surface coating type. In contrast, Figure 1(b) shows the equivalent result for a sample of good quality concrete also contaminated with H_2SO_4 and coated with polyisocyanate which remained in remarkably good condition at the end of the 3-year exterior test. This suggests that concrete recipe is a more important factor than either damage due to contamination or protection via surface coating type. However, significant differences in properties likely to affect long term durability can escape detection by simple visual inspection as reported below.

Water Surface Capillary Rise Measurements *before Exterior Exposure.* Figure 2 shows the measured surface capillary water rise results before environmental exposure testing for all clean and contaminated samples (both good and poor quality concrete) which were not surface coated.

Scale:  5.0cm

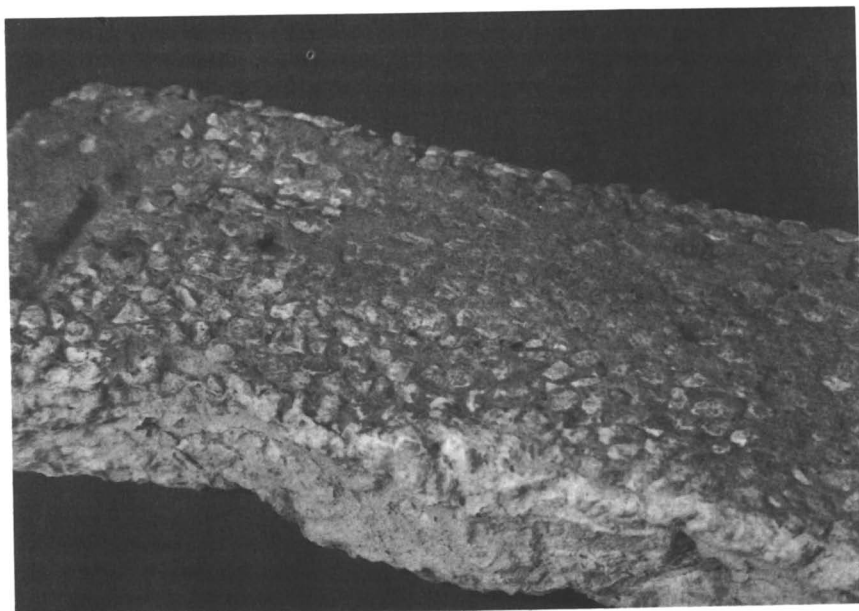


Figure 1(a). Poor Quality Concrete – Preconditioned with Dilute H_2SO_4 , Polyisocyanate coated.

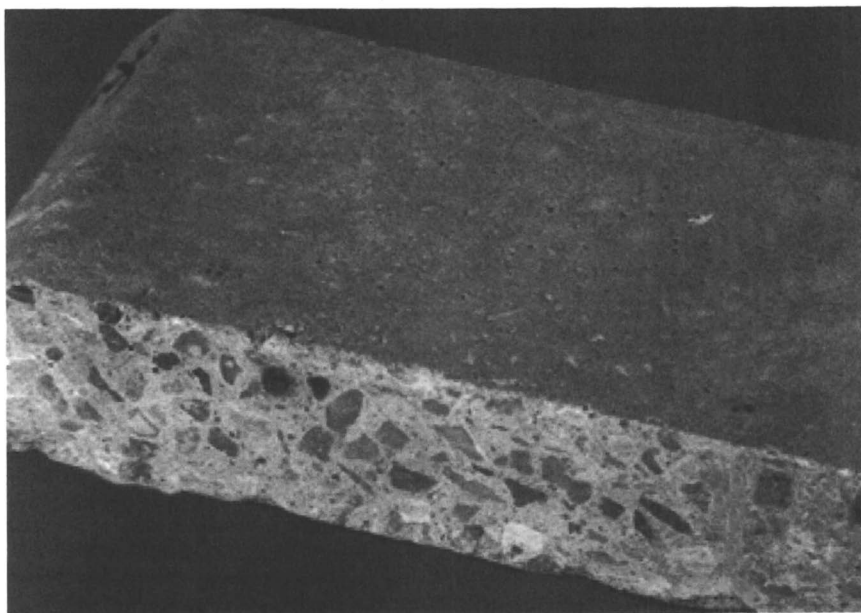


Figure 1(b). Good Quality Concrete – Preconditioned with Dilute H_2SO_4 , Polyisocyanate coated.

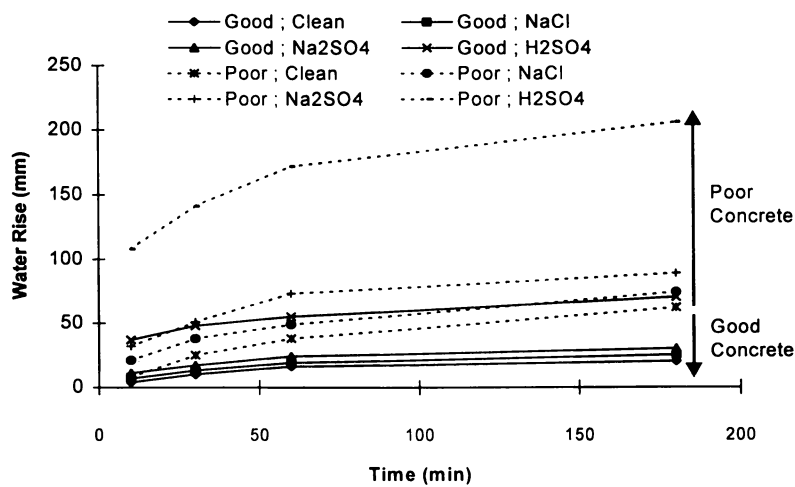


Figure 2. Surface Capillary Water Rise before Exposure – No Surface Coatings.

Here, the strong dependence on concrete quality recipe can be seen. Figure 2 shows that the poor quality concrete samples had surface capillary water rise values approximately 3x the rate of the good quality samples. Also apparent from Figure 2 is that, irrespective of concrete quality, the dilute acid treated samples were rather more wettable than the chloride, sulfate or non-contaminated samples. Almost none of the alkoxy-silane or polyisocyanate treated samples showed any signs of water wettability before environmental exposure. The only exceptions to this were some of the samples contaminated with dilute H_2SO_4 which wetted very slightly, but not enough to register significantly on Figure 2.

Water Surface Capillary Rise Measurements after 3 Years Exterior Exposure Testing. Results obtained after 3 years of environmental exposure testing for good quality concrete samples are shown in Figure 3(a).

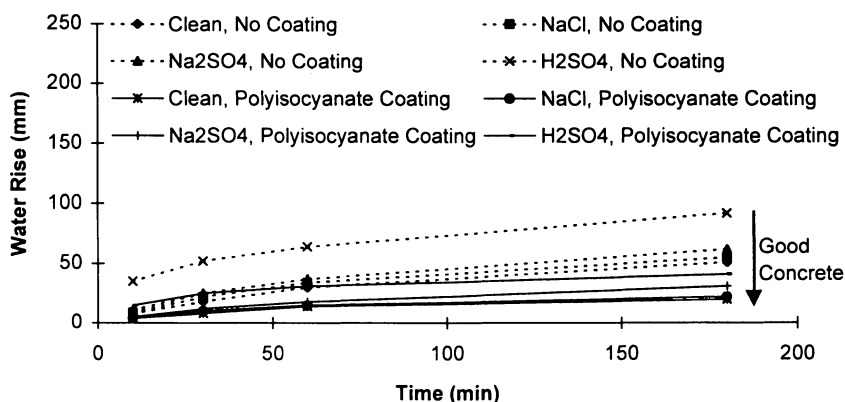


Figure 3a. Surface Capillary Water Rise after 3 Years of Exposure – Good Quality Concrete.

These data are plotted on the same scale for direct comparison with Figure 2 (before exposure). Only the alkoxy-silane coated samples retained their complete water non-wettability after exposure, insufficient to register above the x-axis minimum on Figure 3(a). All other good quality concrete samples, including those coated with polyisocyanate were found water wettable. Poor quality concrete sample results after exterior exposure are shown in Figure 3(b).

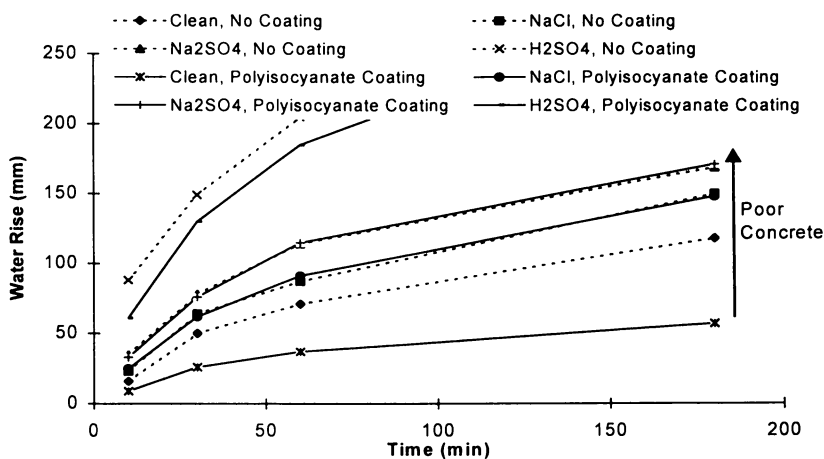


Figure 3b. Surface Capillary Water Rise after 3 Years of Exposure – Poor Quality Concrete.

Again, all the alkoxy silane treated samples retained their non-wetting characteristics. All other samples, whether coated with the polyisocyanate or not coated, permitted water wetting as shown, Figure 3(b), to a considerably greater degree than for the equivalent good quality concrete samples, Figure 3(a).

From Figures 2 and 3, it is clear that surface capillary water rise measurements on exposed samples show increases over the initial values obtained before environmental exposure. The effects of surface pre-contamination were also significant. Water rise measurements rose in the following order; non-contaminated (least detrimental effect), NaCl, Na₂SO₄ and finally dilute H₂SO₄ (most detrimental effect). Further, whereas the alkoxy silane coated samples showed no surface capillary water rise either initially or after exposure, the polyisocyanate samples did exhibit water capillary rise after exposure testing.

Calcium Leachability before Exterior Exposure. Calcium leaching data before test exposures are shown in Figure 4(a) for clean concrete and those pre-contaminated with NaCl or Na₂SO₄, and in Figure 4(b) for the samples contaminated with dilute H₂SO₄. (These data are plotted separately because of the much larger extent of Ca leaching caused by the dilute acid contamination treatment.)

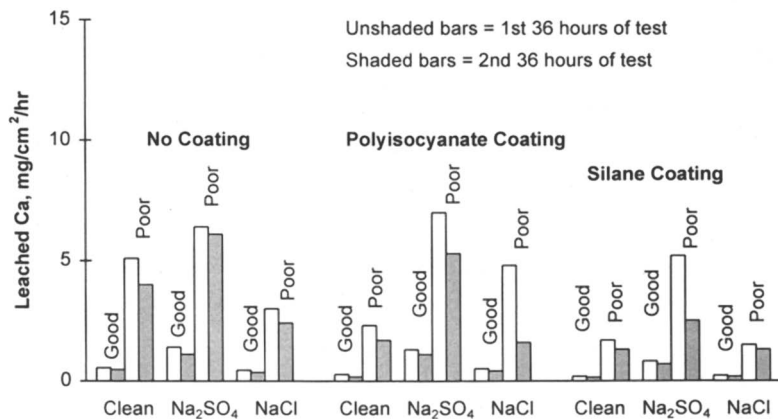


Figure 4a. Calcium Leachability before Exposure - Clean Concrete and NaCl/Na₂SO₄ Contamination.

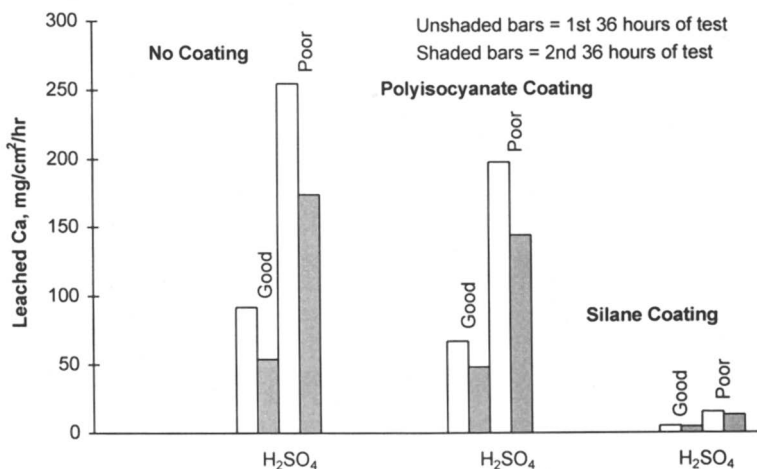


Figure 4b. Calcium Leachability before Exposure - H₂SO₄ Contamination.

Again, concrete recipe quality is clearly an important issue, as is the deleterious effect of pre-contamination with H₂SO₄. However, before exposure testing, these two factors were mitigated by use of the alkoxy-silane coating. Within the sequence, clean, NaCl and Na₂SO₄, the more severe effects were caused by Na₂SO₄ rather than by NaCl.

Calcium Leachability after 3 Years Exterior Exposure Testing. After exterior exposure testing, Figures 5(a) and (b), broadly similar results were obtained. Thus, similar conclusions were drawn regarding the effects of concrete quality, NaCl, Na₂SO₄ and H₂SO₄ contamination. Again, the alkoxy-silane coating proved effective.

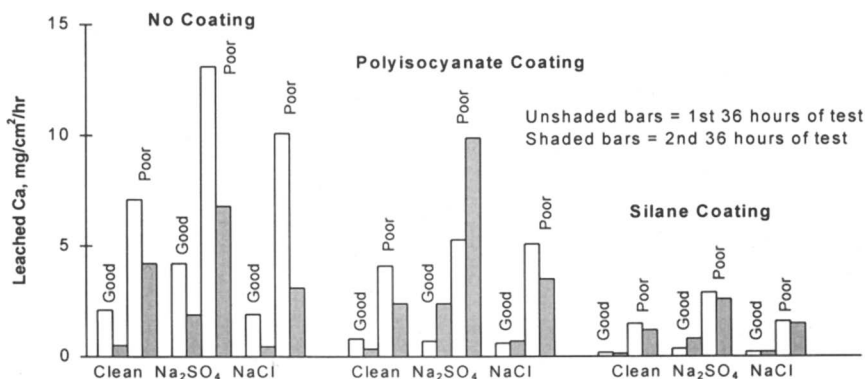


Figure 5a. Calcium Leachability after 3 Years of Exposure – Clean Concrete and NaCl/Na₂SO₄ Contamination.

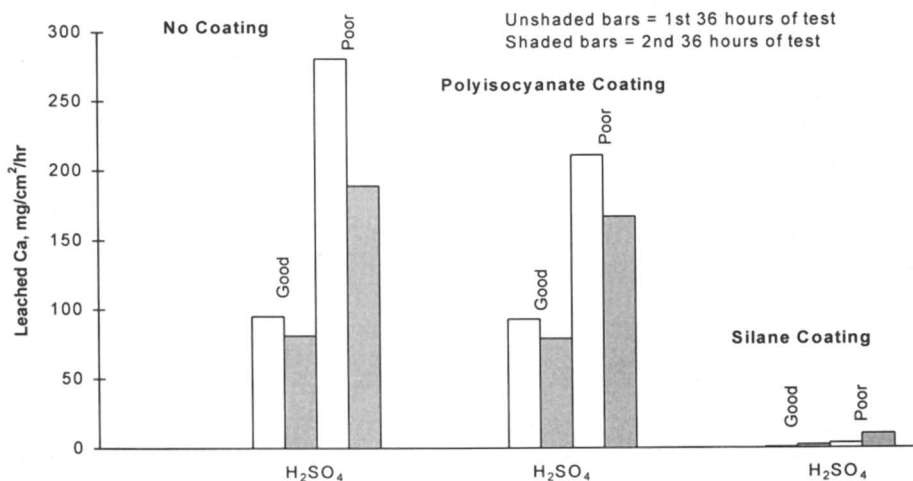


Figure 5b. Calcium Leachability after 3 Years of Exposure – H₂SO₄ Contamination.

Carbonation Depth after 3 Years Exterior Exposure Testing. Carbonation depths after 3 years exterior testing were obtained from cross-sectioned samples. The results are shown in Figure 6.

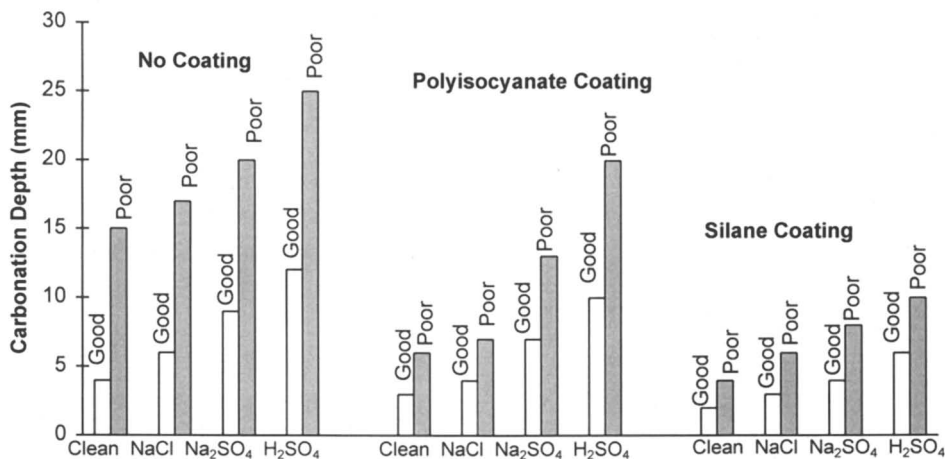


Figure 6. Carbonation Depth after 3 Years of Exposure.

Once again, the impact of concrete quality is clear as is the worsening effects of contaminants in the sequence; NaCl, Na₂SO₄ and H₂SO₄. Also apparent is that both coatings types, polyisocyanate and alkoxy silane, resist the extent of carbonation for all concrete samples for both good and poor quality concrete. Overall, the alkoxy silane based coatings gave the lowest carbonation depths.

Discussion

There are three major considerations in this work; firstly, the impact of correct concrete recipe mix, secondly, the relative behavior characteristics of pre-contaminated samples compared to non-contaminated (clean) samples and thirdly, the relative effectiveness of two types of concrete surface coatings. The results of all the examinations, whether by water wettability (by surface capillary rise), calcium leachability or by depth of carbonation showed a general consistency.

The most striking information generated in this work is of the critical importance of mixing the concrete to the correct recipe. Errors here lead clearly to decreased concrete performance properties and likely long term reduced durability. However, results obtained in this work suggest that a good surface protective coating can compensate, to some extent, for a poorer quality concrete mix.

Precontaminated samples all exhibited increases in wettability (capillary rise), leachability and carbonation over the non-contaminated samples. The degree of increase was in the order; NaCl (least effect) to Na₂SO₄ to dilute H₂SO₄ (most effect). That is, the presence of inorganic salts is detrimental to the life of the concrete, perhaps

due to decreases in surface mechanical properties and increases in permeability characteristics of the concrete.

Both coating systems tended to produce reduced water wettability (capillary rise), calcium leaching and carbonation compared with non-coated equivalent samples. However, the presence of inorganic salt contaminants reduced, to some degree, the efficacy of the protective coatings, possibly due to factors such as enhanced osmosis and reduced adhesion. Of the two coatings investigated in this work, the alkoxy-silane apparently remained hydrophobic for the 3 year exterior exposure period and protected the concrete samples rather more efficiently than the polyisocyanate. However, it is important to note that generalizations regarding different coating types should not be made based on the limited data presented here. Rather, since coatings behave differently in different environments, when considering the use of surface coatings, a recommendation should be given to conduct exposure trials with a variety of generic coating types to select the most appropriate for the specific circumstances expected.

Conclusions

- 1) The importance of correct recipe concrete mix is clearly a critical issue. In this work, it was the overriding factor determining performance properties of the concrete samples as tested.
- 2) The surface application of protective coatings reduces the rate of degradation of both clean as well as contaminated concrete samples. Here, polyisocyanate produced some benefits but not as great as those brought about by the alkoxy-silane treatment.
- 3) The presence of contaminating inorganic salts either on, or within the surface layers of concrete substrates reduces the protection sought by the use of organic overcoatings. This reduction in protection is particularly apparent with poor quality concrete.
- 4) When organic surface coatings are applied to concrete, the surfaces and subsurfaces should be contaminant free. Any attempted use of coatings to 'cover up' poor quality concrete or to try to extend significantly the life of such concrete should be recognized as having limitations.

Literature Cited

1. D. Starke & W. Perenchio, 'The Performance of Galvanized Reinforcement in Concrete Bridge Decks'. Project No. ZE-206, International Lead Zinc Research Organizations & American Hot Dip Galvanisers Association Construction Technology Laboratories, Skokie, Illinois, 1975.
2. 'Epoxy Coated Reinforcing Bars', Engineering Data Report No. 14, CRSI, Schaumburg, Illinois, USA.
3. A. Baba & O. Senbu, 'A Predictive Procedure for Carbonation Depth of Concrete with Various Types of Surface Layers', Proc. 4th Int. Conf. On Durability of Building Materials and Components. Singapore, 1987, Pergamon, Oxford, Vol. II, p.679.

Chapter 22

Formulations and Field Performance of Fluorinated Polyurethane Coatings

Robert F. Brady, Jr.

Materials Chemistry Branch, Naval Research Laboratory,
Washington, DC 20375-5342

Heavily-fluorinated polyurethane coatings have been formulated and tested in demanding marine applications. In addition to the chemical and weather resistance typical of polyurethane coatings, these coatings have an anti-adhesive surface which permits the facile removal of water, ice and soil. This paper describes the chemistry of the polyol resins, the formulation of these resins into tough, anti-adhesive polyurethane coatings, and performance of these coatings in rigorous marine and industrial applications.

A continuing basic research program on the synthesis of fluorinated polymers has yielded a series of tough, chemically-resistant polymers with unusual and useful properties. The polymers are soluble in common solvents and can react with the biuret trimer of hexamethylene diisocyanate to form a series of polyurethane coatings. These coatings are applied by conventional brush and spray techniques and cure at room temperature to form tough, uniform, integral films. The coatings may be pigmented to any desired shade with inorganic or organic pigments or employed as clear films. In fact, because the low surface energy of the polymer is comparable to that of poly(tetrafluoroethylene) (PTFE), up to 38 volume percent of finely-powdered PTFE can be incorporated as a pigment to form homogeneous paints having high fluorine content and extreme resistance to adhesion and penetration.

Coatings based on this chemistry are being used in specialized defence applications (*1*). Several of these uses which are relevant to industrial applications will be described. Tests of these coatings in US Naval vessels and shore facilities began in 1977 and continue to the present day. Each test has a unique objective, and these new materials have performed successfully in a broad spectrum of applications, demonstrating their endurance and desirability. The coatings offer retention of appearance properties, ease of maintenance, protection of

the substrate from corrosion, long service life, and superior resistance to heat, actinic radiation and chemicals.

Background

Fluoropolymers are among the most chemically inert of organic compounds. They demonstrate outstanding thermal stability and resist oxidative attack. These properties can be attributed to the presence of the fluorine atom (2):

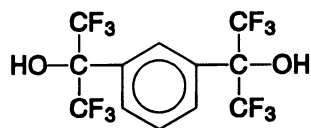
★The carbon--fluorine bond energy (540 kJ mol⁻¹ in fully-fluorinated aliphatic hydrocarbons) exceeds that of the carbon--hydrogen bond (435 kJ mol⁻¹ in aliphatic hydrocarbons).

★Carbon--carbon backbone bonds are strengthened when fluorine is attached to the backbone. Carbon--carbon bond energies are 406 kJ mol⁻¹ in perfluoroethane and 368 kJ mol⁻¹ in ethane.

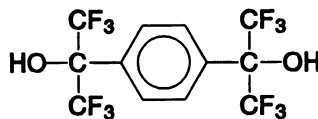
★The covalent atomic radius of fluorine (7.2 nm) is nearly twice that of hydrogen (3.7 nm). A fluorine atom screens the polymer backbone from attack without more effectively than a hydrogen atom, without introducing steric strain to the backbone.

Compared to an unfluorinated analog, a polymer containing fluorine has a lower equilibrium moisture absorption, a lower dielectric constant, a lower index of refraction leading to intriguing optical properties, and frequently increased thermal stability.

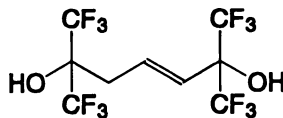
A fluorinated polymer also has a low surface energy. Pioneering studies by Zisman (3) demonstrated that the surface energy of a polymer is determined by the functional groups on the polymer surface. Zisman showed that substitution of fluorine causes the surface energy to decrease in the order -CH₂- > -CH₃ > -CF₂- > -CF₃. This is readily observed in the surface energies of polymers with surfaces composed or ordered single groups such as poly(ethylene) (33.7 mJ m⁻²), poly(dimethylsiloxane) (21.2), poly(tetrafluoroethylene) (18.6), and poly[di(3,3,3-trifluoropropyl)siloxane] (6.0).



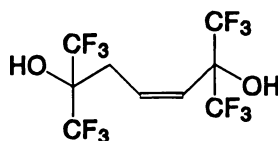
1



2



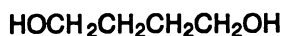
3



4



5



6

Figure 1. Diols used in the synthesis of the fluorinated polyols.

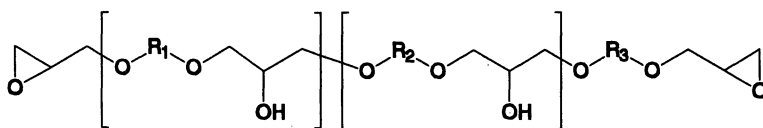
Griffith was first to apply these findings to the synthesis of fluorinated polyol resins suitable for the production of coatings with low surface energy (4). He used a number of fluorinated diols (Figure 1) in his work. The aromatic diols 1 and 2 were synthesized by the reaction of benzene with two moles of hexafluoroacetone using the method of Farah et al. (5); the reaction product contained 90% of 1 and 10% of 2. The unsaturated diols 3 and 4 were obtained in yields of 82% and 4%, respectively, from the reaction of propene with hexafluoroacetone at 170 °C for 48 hours (6). 2,2,3,3,4,4-Hexafluoropentanediol (5) was prepared by the reduction of diethyl perfluoroglutarate with lithium aluminum hydride (7). Butane-1,4-diol (6) is available from commercial sources.

The polyols are synthesized by refluxing the mixture of diols 1 and 2 with an equimolar amount of either the mixture of diols 3 and 4, or 5, or 6 with epichlorohydrin and a large excess of sodium hydroxide in a solution of acetone containing a small amount of water. The reaction is monitored by gas chromatography, and reflux is discontinued as soon as the starting diols have disappeared. The resulting viscous polymers are washed with water until free of base and dried at 120 °C, producing light amber solids in yields of 87 to 97 percent. The generic structure of the polyol is shown in Figure 2, and properties of the neat polyols are given in Table I. The products are dissolved in methyl isobutyl ketone at 50 weight percent and filtered, and the solution is used directly in coatings.

Formulation of Coatings

We have formulated fluorinated polyurethane coatings containing powdered PTFE which exhibit not only the hardness and toughness of conventional polyurethane coatings, but also the low surface energy and easy cleanability of PTFE. Formulations containing up to 38 percent by volume of PTFE have been successfully tested in field applications. Our standard coating contains 24 volume percent PTFE; fluorine comprises 41.7% of the dry weight of this coating. Clear coatings in flat, semigloss, or gloss finished can be formulated with these fluorinated resins, and conventional pigments can be used without difficulty.

Basic formulations for fluorinated polyurethane coatings were devised using the polyol of Figure 2. The biuret 8 of hexamethylene diisocyanate (HMDI) shown in Figure 3, made by the reaction of three moles of HMDI with one mole of water, was chosen as the curing agent in order to maximize the resistance of the coating to chemicals and to weather. Titanium dioxide was used as a hiding pigment, and dibutyl tin dilaurate (DBTDL) was used at levels of 0.01 to 0.07 percent by weight of the curing agent to catalyze the cure. In early work the solvent consisted of a 20:20:60 volume percent blend of ethyl acetate, methyl isobutyl ketone (MIBK), and ethylene glycol monoethyl ether acetate, but we no longer use this solvent blend. Current formulations use a 50:50 volume percent mixture of *n*-butyl acetate and xylene, or methyl isobutyl ketone alone. All solvents are urethane-grade.



7

Figure 2. The structure of the fluorinated polyols. R_1 is a 90:10 mixture of diols 1 and 2; R_2 is as shown in Table I; R_3 may be either R_1 or R_2 .

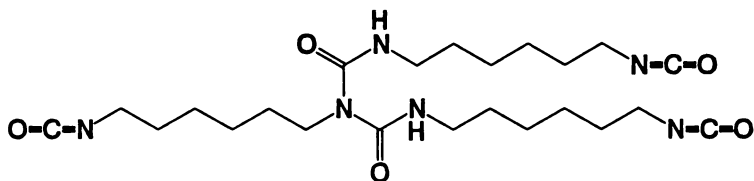
Table I. Properties of fluorinated polyols

R_2	Fluorine content, %	Equivalent weight ¹
3 & 4 (82:4)	48.84	700
5	44.22	579
6	34.09	487

¹Hydroxy or epoxy equivalent weight, based on two of each functional group.

Formulated binders such as these have surface energies of about the same magnitude as poly(tetrafluoroethylene). PTFE can be easily incorporated into the liquid coatings but, because it contributes no hiding in this resin, it must be considered as an extender pigment. Coatings containing up to 38 percent by volume of PTFE can be made, but these are somewhat soft and easily marred. We have found that 24 percent by volume is the optimum level for whiteness, hardness, and chemical resistance. A formulation for a typical fluorinated urethane coating filled with 24 volume percent of PTFE is given in Table II. Sources of ingredients used in the formulation are shown in Table III, and the ranges of composition acceptable for manufactured coatings are given in Table IV. This formulation is normally applied to a dry-film thickness of 75 μm (0.003 inch); at this spreading rate, 270 square feet may be covered with one gallon of paint.

The fluorinated urethane is the topcoat in a three-coat system. After abrasive blasting of the steel, a primer and intermediate coat are applied. Both contain polyester polyols and aliphatic polyisocyanates. The time between blasting and priming must be less than four hours; times between the prime and intermediate coats, and between the intermediate and top coats must be less than sixteen hours. When these intervals are observed, no difficulties with the adhesion of the topcoat have been experienced. The fluorinated topcoat may even be overcoated with itself; procedures customary for overcoating fully cured crosslinked coatings (*i.e.*, epoxies or urethanes) must be observed.



8

Figure 3. The curing agent used in the formulation of the fluorinated polyurethane coating.

Applications

Tank Linings (8). An organic lining in a steel fuel storage tank helps to maintain the purity of the fuel and helps to prevent minor fuel leaks. Large tanks always contain water at the bottom of the tank which accumulates naturally from condensation. The lining also forms a barrier to prevent this water from corroding the bottom of the tank.

Fluorinated urethane coatings are being used as linings in shore-based petroleum storage tanks containing between 10,000 and 12,000,000 US gallons of fuel. The costs of emptying and cleaning these tanks, preparing their surfaces for coating, and applying three or more coats of a lining system are so great that the cost of the topcoat is not an overriding consideration. Significant savings can be achieved by using linings with very long service lives. Tests of fluorinated urethane tank linings began in 1978 at the US Naval Air Station in Norfolk Virginia. By comparison with other linings a service life of 30 or more years is anticipated for these materials.

Fluorinated linings also expedite required periodic cleanings. The surface of the fluoropolymer permits most cleaning jobs to be performed with high pressure water hoses alone. No detergent is needed and oily waste may be processed in an oil-water separator, eliminating the high cost of waste water disposal. Linings of this type have been installed in fuel storage tanks at US Naval Air Stations in Norfolk, Virginia, Patuxent River, Maryland, Corpus Christi, Texas, Koshiba, Japan, Hakozaki, Japan, and Pearl City, Hawaii. They have been certified by the US Navy as their standard lining for fuel storage tanks, and are now being used in new tanks in Craney Island Virginia and Pensacola Florida.

Ship Hulls. Although the coating which never fouls is not yet a reality, significant strides have been made in the formulation of low surface energy coatings which are easy to clean, and in the demonstration of their performance on various US Naval vessels (9). Fluorinated polyurethane coatings have been extensively trialed as non-toxic foulant release coatings for ships' hulls. These coatings are intended to

facilitate the release of barnacles, grass, dirt, algae and other fouling from hulls by permitting the formation of only weak bonds to the surface. These bonds are usually broken by the weight of the fouling or by the motion of the ship through the water.

Table II. Composition of PTFE-pigmented fluoropolyurethane coating

Ingredient	Weight ¹	Volume ¹
Component A		
Poly(tetrafluoroethylene) ²	248.5	13.15
Titanium dioxide ³	98.3	2.99
Fluoropolyol resin ⁴	224.3	16.38
Methyl isobutyl ketone	324.0	48.59
Dibutyl tin dilaurate solution ⁵	5.3	0.79
Component B		
Biuret of hexamethylene diisocyanate solution ⁶	160.0	18.10

¹Measuring weight in pounds produces 100 gallons of coating; measuring weight in grams produces about one Liter of coating.

²Pigment-grade poly(tetrafluoroethylene), less than 6 microns average particle size.

³American Society for Testing and Materials, Specification D-476, Type IV.

⁴Different fluoropolyols have different equivalent weights, depending on composition (see Table I). This formulation is based on the copolymer having a hydroxy equivalent weight of 579.

⁵A solution of 1.7 percent by weight of DBTDL in MIBK.

⁶A solution of 75 percent by weight of the biuret of HMDI in a solvent containing equal weights of *n*-butyl acetate and xylene.

Table III. Sources of ingredients in the fluorinated urethane coating

Titanium dioxide	Ti-Pure R-960 (E. I. duPont de Nemours & Company) Kronos 2160 (Kronos, Inc.); formerly Titanox 2160 (NL Industries) Tioxide UF02 (Tioxide Specialties, Ltd.) Tiona RCL-6 (SCM Chemicals)
PTFE	Polymist F-5A (Allied Signal) TL-102 (Liquid Nitrogen Processing) SST-3 (Shamrock)
Company)	Teflon MP 1200 (E. I. duPont de Nemours &
Dibutyl tin dilaurate	M&T Chemicals, Inc.; Aldrich Chemical Company
Biuret of hexamethylene diisocyanate	Desmodur N-75 (Bayer) Luxate HB 9075 (Olin Chemicals)

Early work with sheets of PTFE was discouraging, for the PTFE accumulated all types of marine fouling with astonishing speed (10). This is due to the porosity of PTFE: marine adhesives invade cavities in the surface and cure inside them, creating a secure mechanical interlock even in the presence of chemical incompatibility (11). However, the fluorinated urethane binder fills these cavities and creates a smooth, low-energy surface which resists but does not escape attachment of fouling organisms. Tests of the various formulations have included conventional laboratory performance tests as well as the evaluation of static panels immersed at Chesapeake Beach Maryland, Key West Florida, and at Naos Island in the Bay of Panama.

Trials of the fluorinated hull coating began in 1977, when a tugboat at the Norfolk, Virginia Naval Base was coated (12). This coating lasted until the boat was destroyed in an accident in 1989. During this time the coating did indeed accumulate fouling. Cleaning, if accomplished at 4- to 6-week intervals during the fouling season, could be accomplished by water from a standard fire hose, but left to accumulate, fouling became quite difficult to remove. The coating was rugged and sturdy, and effectively protected the hull from corrosion during its 12-year lifetime. Subsequently, the coating was applied to a 65-foot patrol boat and to a patrol hydrofoil vessel. Again, the coating proved durable and effective when cleaned regularly, but it did not remain free of fouling.

Table IV. Quality control test ranges for the PTFE-pigmented fluoropolyurethane coating in Table II

	Component A		Mixture A and B	
	min	max	min	max
Grind, Hegman	5	--	--	--
Viscosity, Krebs Units	35	85	--	--
Pigment, percent by weight	39.8	40.0	32.7	32.9
Volatiles, percent by weight	35.9	36.1	34.0	34.2
Nonvolatiles, percent by weight	63.9	64.1	65.8	66.0
Weight per gallon, pounds	11.0	11.2	10.5	10.7
Drying time, tack-free, hours	--	--	--	4
Flash point [Seta], °C	--	82	--	79

The introduction of foulant release coatings to the operating Navy involves several new concepts. Sailors are accustomed to having unfouled underwater hulls, and tend to dismiss the idea of a coating that will not resist fouling. In addition, an easily-cleanable coating has no value if it is not cleaned regularly; so to make the use of this coating realistic and practical, it has been necessary to implement a regular program of underwater hull maintenance wherever this coating is used.

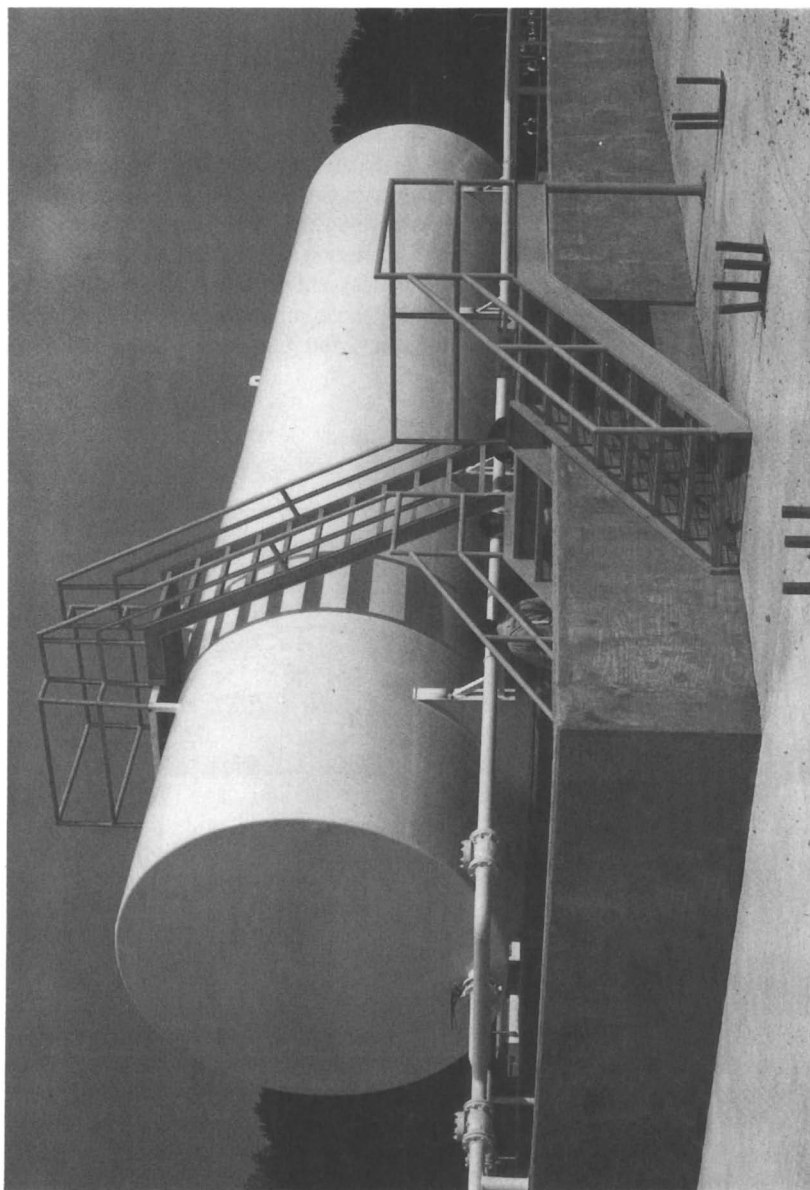


Figure 4. A new tank at Patuxent River Naval Air Station, Maryland, lined with the NRL fluoropolymer anticorrosive coating

Submarine Radome Coatings. Films of water on antenna housings interfere with the transmission and reception of signals. Antennas must be retuned as water drains from their surface, and a strong and steady signal is obtained only when water is absent. Antennas on submarines are therefore more effective when they have a coating that allows water to drain from the surface rapidly.

A standard submarine radome is about 22 feet long and has an oval cross-section with chords of 22 and 14 inches. The radome is raised and lowered against high density polyethylene bearings which are frequently contaminated with sand, and the long axis is vertical during use. The previous coating, an amidoamine-cured epoxy, retained a uniform film of water when new and was easily abraded. An unpigmented fluorinated polyurethane coating causes water to bead and run down the side of the radome, and has proven to be practical and effective in this application.

It allows a one-third reduction in the time needed to achieve a constant signal because of its superior water-shedding properties, and delivers an extended lifetime due to its excellent abrasion resistance.

Collection, Holding and Transfer (CHT) Tanks. The system aboard US Naval ships for accumulating, transporting, storing, and discharging septic waste is called the CHT system. Septic waste is contained aboard ship in CHT tanks until it can be discharged. The periodic opening and cleaning of these tanks is an unusually distasteful chore. Fluoropolymer coatings extend the interval between cleanings, reduce the time needed for cleaning, and preserve the steel walls and floor of the tank from corrosion.

Fluoropolymer coatings have been trialed in septic tanks in the USS MCCANDLESS (FF 1084) and the USS MANITOWOC (LST 1180). The former ship is a Knox-class frigate with a standard displacement of 3,000 tons and a crew of 282; the test coating was installed in a cubic tank measuring about five feet on a side. The latter ship is a Newport-class tank landing ship with a standard displacement of 4,800 tons and a crew of 253; the tank with the test coating measured about 30 x 15 x 6 feet. On each ship the service life, corrosion protection, and cleanability of the fluorinated urethane coating very substantially exceeded that of the epoxy--polyamide coating it replaced.

Anticorrosive Coatings for Ships' Bilges. Fluoropolymer coatings have demonstrated extended service life in the bilge of the aircraft carrier USS FORRESTAL (CV 59). Test areas were cleaned by hand using a wire brush or a chemical cleaner; half of each section was primed with an epoxy--amidoamine primer, and half was left unprimed. The fluoropolyurethane coating was applied by brush to a dry film thickness of 5 mils over each of the four test areas. The coating was inspected regularly for 8 years, during which time all of the coatings remained intact and tightly bonded to the steel. At the final inspection, it was estimated that less than 5 percent of the coating had been removed, all of this apparently by mechanical damage. During its service life the coating was easily cleaned by hand scrubbing with detergent and water.

Future Work

The special properties of these fluoropolymers suggest many applications. The resins are hydrophobic and oleophobic, and thus produce coatings and composites that can be easily cleaned. They offer promise as flame-resistant coatings because of their low heat-release characteristics. Fluoropolyols with low molecular weights react through their epoxy groups to form tough polymers useful as laminating resins, solution adhesives, and conformal coatings. The polymers also have a low refractive index which makes them especially attractive for applications in optics and electronics. The market for anticorrosion coatings in ship and shore applications will provide the initial impetus for sales of this coating while secondary markets develop.

Conclusions

Fluorinated polyols have been synthesized from a range of aliphatic and aromatic fluorinated diols. These polyols react with aliphatic polyisocyanates to form urethane coatings which retain their appearance, are easy to maintain, protect the substrate from corrosion, and provide superior resistance to heat, ultraviolet radiation and chemicals during a long service life. Seventeen years of tests in the marine environment have proven the outstanding endurance and cost-effectiveness of these coatings.

References

1. Griffith, J. R.; Brady, Jr., R. F. *Chemtech* **1989**, *19*, 370-373.
2. Brady, Jr., R. F. *Chemistry in Britain* **1990**, *26* (5), 427-430.
3. Zisman, W. A. In *Contact Angle, Wettability, and Adhesion*. Advances in Chemistry Series 43, American Chemical Society, Washington, DC, 1964, 1-51.
4. Field, D. E.; Griffith, J. R. *Indus. Eng. Chem., Prod. Res. Dev.* **1975**, *14*, 52-54.
5. Farah, B. S.; Gilbert, E. E.; Sibilica, J. P. *J. Org. Chem.* **1965**, *30*, 998. (1965).
6. Urry, W. H.; Niu, J. H. Y.; Lundsted, L. G. *J. Org. Chem.* **1968**, *33*, 2302.
7. McBee, E. T.; Marzluff, W. F.; Pierce, O. R. *J. Am. Chem. Soc.* **1952**, *74*, 444.
8. Brady, Jr., R. F.; Griffith, J. R.; Thomas, R. *Navy Civil Engineer* **1993**, *23* (2), 23-25.
9. Brady, Jr., R. F.; Griffith, J. R.; Love, K. S.; Field, D. E. *J. Coatings Technology* **1987**, *59* (755), 113-119.
10. Saroyan, J. R.; Lindner, E.; Dooley, C. A.; Bleile, H. R. *Indus. Eng. Chem., Prod. Res. Dev.* **1970**, *19*, 123-128.
11. Brady, Jr., R. F. *Nature* **1994**, *32* (2), 23-25.
12. Griffith, J. R.; Bultman, J. D. *Naval Engineers Journal* **1980**, *92* (2), 129.

Chapter 23

Electrochemical Studies of Vinyl Ester Coatings for Fuel Tanks

V. N. Balbyshev¹, Gordon P. Bierwagen¹, and R. L. Berg²

¹Department of Polymers and Coatings, North Dakota State University, Fargo, ND 58105

²Xerxes Corporation, 7901 Xerxes Avenue, Minneapolis, MN 55431

Several types of vinyl ester coatings, known for their outstanding corrosion resistance properties, have been subjected to immersion and evaluated for corrosion resistance by electrochemical noise methods (ENM) and electrochemical impedance spectroscopy (EIS). The test solution was chosen to emulate the water bottoms found in underground fuel storage tanks. Electrochemical noise Impedance, calculated from electrochemical noise data, has been used to supplement the ENM and EIS techniques and for a better understanding of low-frequency behavior of these coating systems. The data for first three months of exposure shows good agreement between the ENM test results and electrochemical noise impedance. The DC resistance and EIS values have been found to deviate from equivalent parameters obtained from the above two techniques. The results from four different electrochemical methods are interpreted, and the correlation among them is discussed.

Corrosion in fuel tanks of crude oil and refined products is closely associated with the presence of water. Petroleum and refined products themselves do not enter in the corrosion reaction but may pick up water and other corrodents such as oxygen, chlorides, sulfates, and others. Therefore, reducing the availability of one or several of these species would also tend to reduce corrosion (1).

The family of vinyl ester resins is earning increasing commercial use in the fabrication of industrial equipment. Vinyl esters provide a number of advantages over those made with conventional metal and polyester materials. Their outstanding resistance to corrosion by many different chemicals makes them well suited for industrial corrosion resistant applications.

Chemical attack of polyester resins occurs through hydrolysis of the ester groups or the splitting of unreacted carbon-to-carbon double bonds through oxidation

or halogenation. In vinyl ester resins, the double bonds are at the ends of the molecular chain (unlike the conventional polyesters where the double bonds occur throughout the molecular chain). These react completely on polymerization, giving a more chemically resistant structure. Also because the unsaturation in vinyl ester resins is terminal, the double bonds are extremely active, and as a result, the resins cure rapidly and consistently. Cured vinyl ester resins contain only terminal cross-linking, and the entire length of the molecular chain is available to elongate under stress and thus absorb mechanical or thermal shocks.

We investigated several type of vinyl ester coatings using electrochemical methods (2,3,4) such as electrochemical noise measurement (ENM) (5) and electrochemical impedance spectroscopy (EIS) (6,7). Both methods were used to evaluate protective properties of the coatings. The test electrolyte solution we used for this electrochemical testing was rather unique. We designed an immersion electrolyte based on the information from gasoline suppliers and reference literature as a worst-case scenario for water condensate in the bottoms of tanks storing ethanol/methanol modified gasolines (1,8,9). This is described in detail in the experimental section.

The electrochemical noise method is a powerful technique for assessing corrosion resistance of steel alloys, and possibly for determining mechanisms of corrosion. One of the major advantages of the ENM is that it is non-intrusive, i.e. it does not perturb in any way the system being investigated. The EIS is somewhat intrusive: a small amplitude sinusoidal signal is applied to the system. A resistance noise parameter, R_n , obtained from the ENM is used to give rapid ranking of the coating performance (10,11).

The R_n value can be correlated with the low-frequency limit impedance modulus obtained directly from the EIS measurements. However high impedance coatings such as the vinyl esters investigated in this study show a lot of scatter in the low-frequency region of the EIS spectrum. Using FFT and Maximum Entropy Spectral Analysis (MESA) algorithms, it is possible to derive the power spectral density functions (PSD) of current and potential noise from the ENM time series and calculated a noise impedance value, Z_n . Using this approach it is possible to eliminate the low-frequency scatter and get a better extrapolation of the low-frequency impedance modulus (12,13).

Experimental

The individual specimen preparation for the Electrochemical Noise (ENM) studies was identical to the one for the Electrochemical Impedance Spectroscopy (EIS) tests. All measurement were made at room temperature.

Cell Preparation. The 6"x 6" coated carbon steel panels were supplied by Xerxes Corporation (Minneapolis, MN). The panels had been coated with the following vinyl ester resins: 470 (470-2000) - one, two, and three coat systems; 8084 with 470, and Dion 367. Very little technical information could be obtained about the resins. For ENM measurements each of the original panels was cut half to produce two 3" x 6" specimens. The film thickness was measured on each specimen with Elcometer® 345 Digital Coating Thickness Gauge (Table I).

Table I. Film Thickness of Investigated Systems

<i>Coating System</i>	<i>Film Thickness^a (μm)</i>
470-2000, 1 Coat	200 (±30 μm)
470-2000, 2 Coat	400 (±30 μm)
470-2000, 3 Coat	600 (±50 μm)
8084 with 470	300 (±40 μm)
Dion 367	75 (±10 μm)

^aaveraged over several measurements

A piece of 1-1/2" PVC pipe was affixed to each panel with Marine Goop™ adhesive to form a tested area of approximately 11 cm². The position of the PVC pipe on the panel was chosen such as to achieve similar film thickness for the two specimens comprising a pair for the ENM experiment. The film thickness variation between the two panels in an ENM pair was 50 μm on the average.

The test solution, duplicating the aqueous bottoms found in tanks, was prepared based on the information found in the literature and obtained from the major gasoline suppliers (8,9). It contained 2% NaCl, 2% Na₂CO₃, and 1.5% (NH₄)₂SO₄.

Electrochemical Tests. The ENM tests were performed on a semi-continuous basis using a three-electrode setup with two 3"x 6" coated carbon steel panels (working electrodes) and an SCE reference electrode (Figure 1). The two working electrodes were electrically connected via the agar/KCl salt bridge. The potential noise was measured between the pair of nominally identical working electrodes and the reference electrode. The current noise was monitored between the two working electrodes. The measurements were made using Gamry Instruments potentiostat and CMS 100/120 software package. The current and potential noise were sampled at 2 second intervals for 512 seconds producing 256 raw data points per cell. From each individual record of 256 points, a potential and current noise standard deviation were calculated. The resistance noise value, R_n , was derived using Ohm's law as the ratio of the potential to current noise standard deviation (14):

$$R_n = \frac{\sigma_I}{\sigma_V}$$

The R_n value is an important ENM parameter that allows one to rapidly rank the system's protective properties. Data was typically acquired over 12 hours to produce one R_n value per hour per cell. The ENM experiment was repeated every few days.

The EIS measurements were made on each working electrode separately using an SCE reference electrode and a Pt counter electrode (Figure 2). The EIS spectra were obtained in the region from 65 kHz to 100 mHz (10 mV applied AC potential) using Gamry Instruments potentiostat, Schlumberger 1250 Frequency Response Analyzer (FRA), and CMS 100/300 software from Gamry Instruments. The low-frequency impedance modulus values, obtained from the two working electrodes being part of an ENM pair, were averaged using the geometric mean to obtain a single

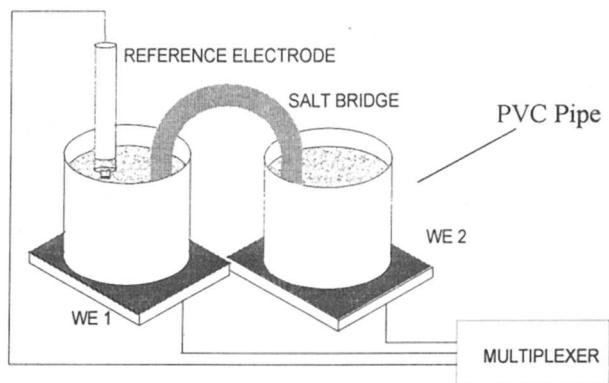


Figure 1. ENM Cell Setup.

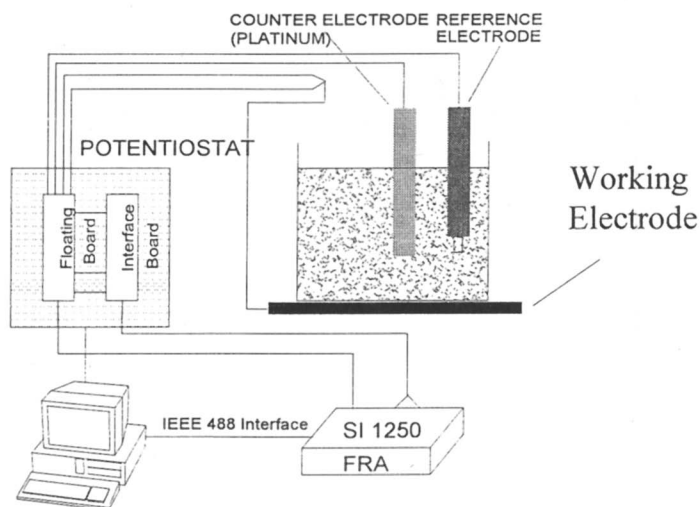


Figure 2. EIS Cell Setup.

value, $\lim_{f \rightarrow 0} |Z(f)|$, that could be compared to the R_n value for the particular system (15):

$$\lim_{f \rightarrow 0} |Z(f)|^2 = |Z_1| \cdot |Z_2|$$

where $|Z_1|$ and $|Z_2|$ are low-frequency limit impedance moduli for individual specimens.

For noise impedance (Z_n) calculation, the DC and drift components of the signal was subtracted before performing Fourier transform and MESA. The noise impedance spectrum was obtained as the ratio of the power spectrum density functions of potential and current (16):

$$|Z_n(f)|^2 = \frac{PSD_V(f)}{PSD_I(f)}$$

The low-frequency limit of noise impedance, $Z_n(0)$, was compared to the values of R_n and low-frequency limit of impedance modulus, $\lim_{f \rightarrow 0} |Z(f)|$ obtained from direct EIS measurement. All calculations were performed using Mathcad™ PLUS 6.0.

The DC resistance measurements were made after each ENM run, not before, to ensure that the applied during DC resistance measurement potential does not perturb the system by polarizing the electrodes.

All the specimens were visually assessed at the end of each ENM test.

Results and Discussion

The composition of the test electrolyte solution was one of the most important modifications of our standard test protocol that we introduced into this electrochemical study of underground storage tank coatings. Most tests of this kind utilize the 3% NaCl solution which emulates the sea water environment. However, as it has been shown in the literature (1,8,9) the content of other salts in the water bottoms of fuel tanks is rather significant and comparable to that of sea water (Table II).

Table II. Corrosion Products Found in Fuel Tanks

<i>Product</i>	<i>%wt.</i>
Iron, total	39.0
Sulfur, total	0.9
Sulfide	<0.1
Sulfate	1.1
Chloride	1.4
Carbonate	1.0
Carbon, total	26.2

Although our test solution did not include sulfides and organic sulfur, its composition is believed to give a more realistic picture of what the composition of the water bottoms of fuel tanks. The net salt concentration of our electrolyte was 5.5%

and the electrical conductivity was found to be higher than that of 3% NaCl: 56 mS vs. 44 mS. This clearly indicates the more aggressive nature of the water bottoms electrolyte, and therefore the solution used in this study may give a better tool for studying corrosion protection afforded by organic coatings.

Using ENM we were able to rank the coatings after one week of immersion. The plot in Figure 3 clearly identifies two groups of coatings: the ones with the R_n values greater than 10^{10} Ohm-cm² (squares) and the ones with much lower R_n values of about 10^7 Ohm-cm² (diamonds).

The first group of coatings maintained high R_n values for almost four months of continuous immersion in corrosive electrolyte, while the R_n values for the coatings in the second group dropped significantly after 2 months of immersion. While none of the coatings showed any visible signs of corrosion, the coatings with the lower R_n did show some discoloration.

The high R_n coatings are the 2 and 3 coat 470-2000 and 8084 with 470. The first two have very thick films and were expected to outperform the other systems. However the R_n values for 8084/470 are not entirely due to the film thickness. The main reason is the different resin. The 8084 resin is enhanced with a reactive elastomer. The result, 8084 offers increased adhesive strength, which combined with superior corrosion resistance of 470 gives an overall better performance at lower film thicknesses. It is obvious that the 470 1 coat system is inadequate for corrosion protection, whereas a 3 coat system may be an overkill, and there exists a maximum film thickness above which there is no increase in protective properties of a given system. A multi-coat system gives better protection than a system of the same film thickness but with fewer coats.

The impedance spectra for the vinyl esters showed considerable scatter of the low-frequency components after 7 days of immersion (Figure 4). The low-frequency limit, $\lim_{f \rightarrow 0} |Z(f)|$, is equivalent to the DC resistance and gives us important information about the performance of the system, in a similar way R_{DC} and R_n do. It should be pointed out that the EIS technique did not quite differentiate the systems after 7 days of immersion while as ENM did. According to the EIS results, Dion 367 performed just as well as the 470-2000 2 and 3 coat systems. The 470-2000 1 coat system did show lower impedance but not by much. The fact that even at 0.1 Hz the EIS spectra show a lot of scatter makes the interpretation of the graph difficult and somewhat unreliable. Increasing the applied AC potential may produce more readable spectra, but this approach must be taken with caution: large perturbations may cause non-linearities in system response.⁷

It turns out that it is possible to obtain the low-frequency information from the noise data. There are a couple of things that need to be taken into consideration though. First, the impedance obtained in this fashion corresponds to an overall impedance, i.e. the events act as perturbation and are not analyzed individually. And second, only one impedance spectrum is obtained for a pair of working electrodes. (The EIS gives one spectrum for each electrode.)

Both the Fast Fourier Transform (FFT) algorithm and Maximum Entropy Spectrum Analysis (MESA) are very advantageous for the calculation of the power spectral densities of the signals: they require no hypothesis about the signal's physical

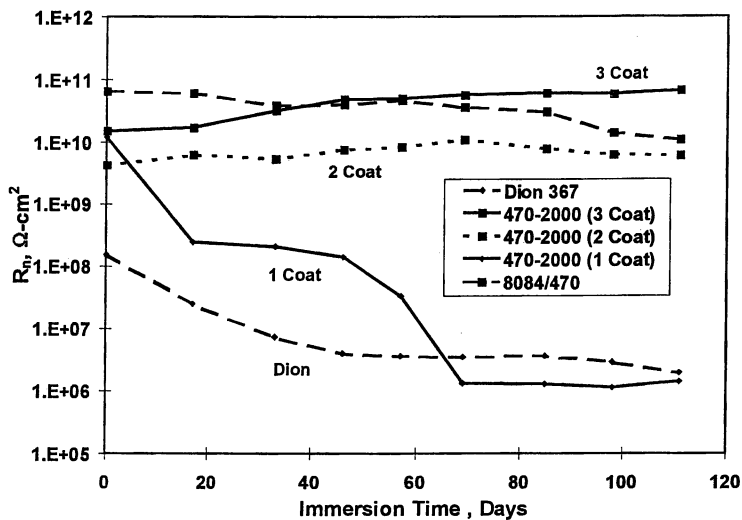


Figure 3. R_p vs. Immersion Time.

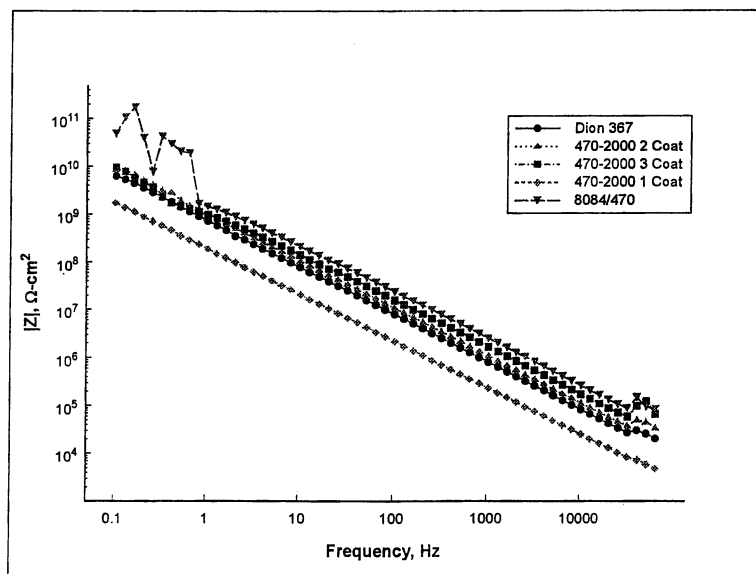


Figure 4. Impedance Spectra after 7 days of immersion.

structure. However the results in Figure 5 show that FFT suffers from high variance in the low-frequency region of the spectrum and was therefore unsuitable for analysis of noisy signals at low frequencies. On the other hand, MESA can handle the low frequencies better than FFT (Figure 6). The low-frequency noise impedance values, $Z_n(0)$, correlate well with the coating ranking using R_n . Dion 367 and 470-2000 1 coat systems show lower resistance than 8084/470 and 470-2000 2 and 3 coat systems. Although the noise impedance value for 8084/470 appears to be lower than that for the 2 coat 470-2000, it is still in the region where the coatings are said to afford excellent performance (3).

The summary of four different electrochemical techniques is given in Table III.

The R_{DC} values could only be measured with the shown accuracy. All R_{DC} values appear to be lower than the corresponding R_n values. DC Resistance is the most intrusive method of the four. The potential, applied during the measurement, forces the charge through the coating making the resistance seem lower than the R_n value measured in the unperturbed system.

The R_n values correlate very well with the noise-derived impedance, $Z_n(0)$. There is somewhat poor correlation between these two noise techniques and the EIS. The reason is many-fold. First, the direct EIS value is a geometric mean of two individual EIS measurements (15). (The particular choice for the geometric mean comes from empirical observation.) Second, we are looking at low-frequency limits at different frequencies. With impedance noise, it is possible to go to much lower frequencies than can be reliably measured by direct EIS. Another possible explanation for the discrepancy would be two different mechanisms for data acquisition: time-domain noise signal and frequency-domain impedance spectrum. Any kind of mathematical transform is an approximation based on a better or poorer model, and therefore it introduces some distortion of the original signal information.

The visual method of assessment did not detect any significant differences in the appearance of the test panels. No blistering or rust was observed on the surface however all five system did show some discoloration.

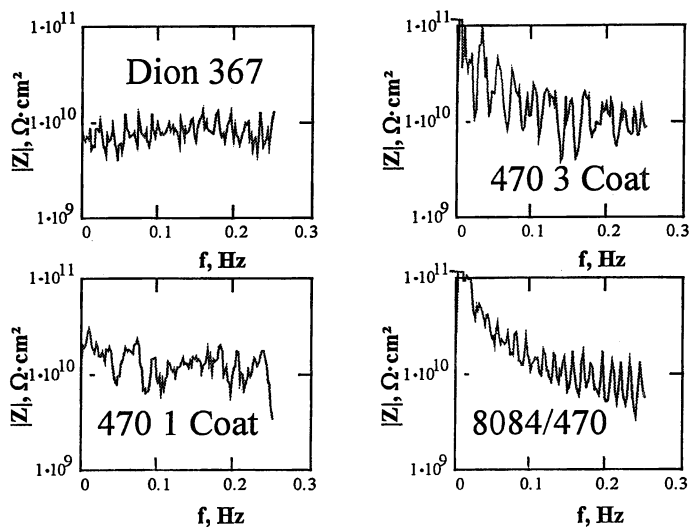


Figure 5. Noise Impedance, Z_n , vs. frequency, f , obtained by FFT.

In Organic Coatings for Corrosion Control; Bierwagen, G.;

ACS Symposium Series; American Chemical Society: Washington, DC, 1998.

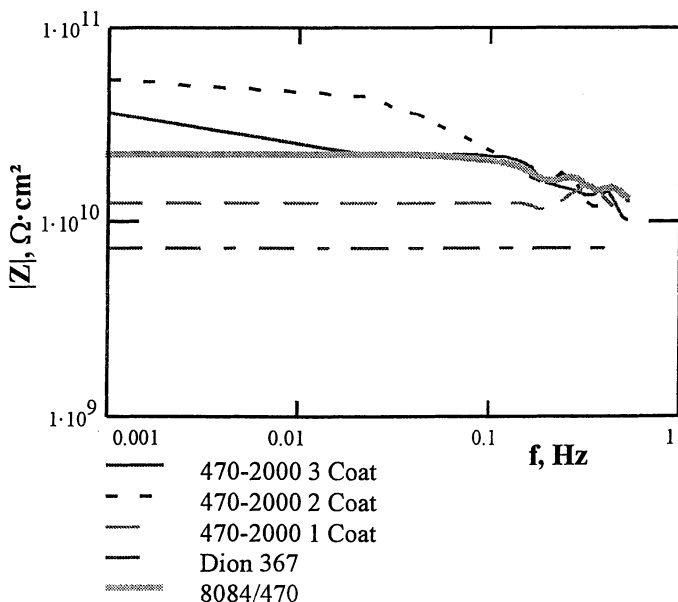


Figure 6. Noise Impedance, Z_n , vs. frequency, f , obtained by MESA.

Table III. R_n , Noise Impedance $Z_n(0)$, R_{DC} , and EIS ($\lim_{f \rightarrow 0} |Z(f)|$)

Coating System	R_n	$Z_n(0)$, MESA	R_{DC}	$(\lim_{f \rightarrow 0} Z(f))$
470-2000 1 Coat	$1.2 \cdot 10^{10}$	$1.5 \cdot 10^{10}$	$1 \cdot 10^9$	$1.0 \cdot 10^9$
470-2000 2 Coat	$4.3 \cdot 10^{10}$	$4.0 \cdot 10^{10}$	$1 \cdot 10^9$	$1.0 \cdot 10^{10}$
470-2000 3 Coat	$1.5 \cdot 10^{10}$	$3.5 \cdot 10^{10}$	$1 \cdot 10^9$	$1.0 \cdot 10^{10}$
8084-470	$6.5 \cdot 10^{10}$	$1.0 \cdot 10^{10}$	$1 \cdot 10^{10}$	$1.0 \cdot 10^{11}$
Dion 367	$1.6 \cdot 10^8$	$7.5 \cdot 10^8$	$1 \cdot 10^8$	$1.0 \cdot 10^{10}$

Conclusions

The test solution used in this study is found to better emulate the composition of the water bottoms found in underground fuel storage tanks. It is unclear at this point if the introduction of small amounts of alcohol, which is often present in recent gasolines, will affect the rate of corrosion or whether it will affect the electrochemical measurements. Some preliminary results obtained in our group suggest a negative answer, but more investigation needs to be conducted.

The study on the effect of film thickness on protective properties of coatings may need further development. While it is obvious that a multi-coat system protects better than a single coat, there may be some optimal combination of the number of coats and their thickness.

The electrochemical noise method and electrochemical impedance spectroscopy can be used to rapidly rank corrosion resistance properties of coated

steel electrodes. The derivation of the noise impedance supplements the results obtained with R_n and EIS. Electrochemical noise impedance, Z_n , allows one to quantitatively link the signals' spectral content and the nature and rate of corrosion. Z_n characterizes the correlation between the potential and current noise signals.

At this point the question really is about "which technique better describes the electrochemical changes of the system and which technique to trust." While there is no definite answer to those questions, one thing is obvious: the four electrochemical methods utilized in this study complement each other, and by having information obtained in several different ways, one gets a more reliable set of tools to rank the corrosion protection of coating systems.

Acknowledgments

We acknowledge Xerxes Corporation for preparation and supply of the investigated samples and for partial funding of this work.

References

1. Foroulis, Z.A. *Anti-Corrosion* Sept. 1981, 4.
2. Thomas, N.L. *Prog. Organic Coatings* **1991**, *19*, 101.
3. Bacon, R.C.; Smith, J. J.; Rugg, F. M. *Ind. Eng. Chem.* **1948**, *40*, 161.
4. Simpson, T.C. *Proc. 12th International Corrosion Congress*, Houston, TX, Sept. 1993, Vol. 1, pp 157.
5. Skerry, B.S.; Eden, D.A. *Prog. Organic Coatings* **1991**, *19*, 379.
6. Scully, J.R. *J. Electrochem. Soc.* **1989**, *136*, 979.
7. *Impedance Spectroscopy*; MacDonald, J.R., ed.; Wiley-Interscience: New York, NY, 1987; Chapter 4.3, pp 260-308.
8. Shitova, E.M.; Batrakov, V.P. *Khimiya I Tekhnologiya Topliv I Masel* **1976**, *3*, 22.
9. Wieland, R.; R.S. Treseder *Corrosion - National Assoc. of Corrosion Engineers* **1954**, *10*, 401.
10. Bierwagen, G.P.; Balbyshev, V.N.; Mills, D.J.; Tallman, D.E. *Proc. of the Symposium on Advances in Corrosion Protection by Organic Coatings II, Special Publication of The Electrochemical Society* **1995**, *95*, 69.
11. Mills, D.J.; Bierwagen, G. P.; Tallman, D.E.; Skerry, B.S. *Material Perf.* **1995**, *34*, 33.
12. Peebles, P.Z. *Probability, Random Variables, and Random Signal Principles*; McGraw-Hill, New York, NY, 1980; Chapter 8, pp199-202.
13. Priestly, M.B. *Spectral Analysis and Time Series*, Vol 1: Univariate Series, Academic Press, New York, NY, 1981.
14. Bierwagen, G.P. *J. Electrochemical Soc.* **1994**, *141*, 155.
15. Mills, D.J. Private Communication, North Dakota State University, October 1994.
16. Mayet, H.; Marsolais, R.; Baroux, B. Paper presented at *ASTM Symposium on Electrochemical Noise Measurement for Corrosion Applications*, Montréal, Canada, May 1994.

Chapter 24

Control of the Protective Properties of Polyethylene Coatings Using Molybdenum Disulphide Filling

V. Yu. Barinov, V. E. Panasyuk, and S. R. Prots

Department of Mechanics of Composite Materials, Physico-Mechanical Institute of the National Academy of Sciences of Ukraine, Lviv 290601, Ukraine

Control of the powder polyethylene coatings' properties using molybdenum disulphide filling has been studied. A powder blend of high-density polyethylene and filler was applied on a steel substrate by electrostatic spraying. The coatings as well as the isolated composite films 0.15 mm in thickness were formed. The influence of molybdenum disulphide on the stress-strain relationship of films as well as on adhesion, thermoplastic and electrical properties of coatings has been investigated. The majority of tested parameters achieve their maximum values in the narrow range of fillers concentrations. The highest resistance of coatings to an acid effect is achieved at the same content of additive.

Molybdenum disulphide filling is successfully used to increase the wear resistance of polymer coatings. The lubricating effect of such additive is determined by its lamellar structure (*l*). To select a filler concentration for practical use, it is necessary to take into consideration the diverse effect of molybdenum disulphide on the structure of polymer. Introduced additive must maximally optimise the definite composite properties. Other operational characteristics of coatings must be improved on or kept constant.

This article describes the possibilities of regulating the corrosion-protective and mechanical properties of powder polyethylene coatings using molybdenum disulphide filling.

Experimental Procedures

The Samples. High-density polyethylene (PE) and molybdenum disulphide were used as the subjects of research. The powder compositions of polymer and filler at

concentrations within the range up to 2.5 volume percent (%) were obtained by mixing the powders. The coatings 0.15 mm thick were formed from the mentioned composite powders. The powders were applied by electrostatic spraying over a steel substrate with the following fusion. The isolated films of filled PE were obtained from melt in hot moulding.

Electrical Measurements. The corrosion-protective resistance of coatings was studied by measuring the electrical characteristics. The 10% solution of hydrofluoric acid (HF) was served as a liquid electrode. The choice of such a medium was connected mainly with its high activity to PE. The changes in conductance (G) / resistance (R) and capacitance (C) of coatings under an acid effect were determined as a function of \sqrt{t}/d , where t is an exposing time; d is a coating thickness. The changes in the values of G and C characterize the existent specificity of liquid penetration into a polymer sample. Procedure based over (2, 3) describes such changes as follows

$$\frac{G_t - G_o}{G_t} = \frac{R_o - R_t}{R_o} \quad \text{and} \quad \frac{C_t - C_o}{C_t}$$

where G_o , R_o , and C_o are the values obtained by extrapolation, which correspond to the moment of contact beginning between electrolyte and coating; G_t , R_t , and C_t are the values measured in time t after the contact has begun. The measurement was carried out at the frequency of 1 kHz.

Tension of the Films. Yield point (σ_y) and elongation at failure (λ_f) of filled PE isolated films were calculated from the data, which were obtained by registration of the stress-strain relationship (tension at the rate of $4 \cdot 10^{-2} \text{ s}^{-1}$).

Adhesion Strength (A) was measured at peeling a steel foil strip (0.1 mm thick and 10 mm in width) from a coating.

A Flow Temperature (T_f) was assessed from a flow curve as a function of temperature (weight pressure is 25 kPa; rate of temperature increase is $0.25 \text{ }^\circ\text{C/s}$). It assumed to be equal to the temperature at the inflection point in this curve. Analysis of the way of changing in the value of T_f makes possible to apprise the influence of filler concentration on the thermochemical destruction of macromolecules.

Results and Discussion

Protective Properties. The results of measurement of the electrical characteristics of coatings are shown in Figure 1. The values of G and C rise during the effect of 10% solution of HF. However, the rates of their changes differ from one another. The considerable increase in G is observed during the first one to two hours a sample is affected by the liquid medium. The value of G can be used as a porosity index of coatings. According to this inference, the conclusion may be drawn concerning presence of pores in PE. In this case the quantity of pores is sufficient for alteration in polymer's conductivity. Within the time range of 40-400 hours the influence of electrolyte becomes stabilized. Partial blocking of coating pores with some

decomposition products (4) may be the cause of such stabilization. The second stage of corrosion activation, leading to the final loss of corrosion-protective properties of coatings, is observed after 400 hours of a sample staying under the acid effect. The variations in the value of C are comparatively less intensive. Nevertheless, the quick increase in C at the initial stages of medium effect is also observed as in the case with G . Since the value of C may be presented as an index of integral liquid penetration into the polymer volume. Its change reflects the swelling processes.

The filling influences on the protective properties of coatings. The liquid penetration into the composite reduces with the enhancement in additive content up to 0.8%. The reduction spreads over both the above-mentioned schemes. At a higher filler concentration the degradation of corrosion-protective properties is observed.

An introduction of molybdenum disulphide leads mainly to the physical modification in PE. From this point the corrosion-protective properties of such coatings should be examined just in the context of physical characteristics of composite itself and its specific interaction with the substrate.

Mechanical Properties. As shown in Figure 2, for the composite with the filler content more than 0.4-0.6% the value of λ_f is far less than this value for the initial polymer. Simultaneously the maximum value of σ_y is achieved in the area of the upper limit of this concentration range. To a slight degree these changes are connected with the influence of molybdenum disulphide on the crystallization in PE, as well as with the presence of additive in the deformed specimen. The presence of filler particles raises the amount of crystallization centers in the polymer. An increase in this amount is followed by a reduction in the average spherulite dimensions. Moreover, molybdenum disulphide acts as an internal lubricant in the volume of fused composite. This causes a plasticizing effect in the area of temperatures approximating to the crystallization temperature of PE. As a result of these factors more homogeneous spherulitic structure is formed in such composite, what is followed by the enhancement in σ_y . Filler particles are acting as defects in the supermolecular structure of polymers. The dependence of deformation on the existence of these defects becomes essential for PE containing more than 0.6-0.8% molybdenum disulphide. Such dependence leads to lesser stresses during deformation of the composite. The result is the peak of σ_y versus concentration is existing on the curve. Besides that, introduction of fillers leads to an increase in polymeric chains' stiffness (5), which is reflected in the sharp decrease of λ_f .

Thus, the strength and straining properties of composite are basically defined by the diverse and opposite influence of additive on the structure and properties of PE. On the one hand, filling leads to more homogeneous spherulitic structure forming and to a plasticizing effect during crystallization, as well as to a rise in macromolecules' stiffness. On the other hand, the presence of molybdenum disulphide raises the amount of faults in the supermolecular structure. Specifically, the effect of increase in the polymeric chains' stiffness becomes dominant when the filler content in PE is in the range of 2.0-2.5% or more. The failure of such

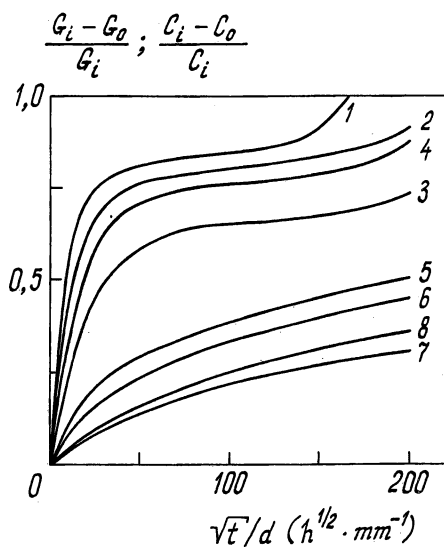


Figure 1. $\frac{G_i - G_0}{G_i}$ and $\frac{C_i - C_0}{C_i}$ versus \sqrt{t}/d curves for a polyethylene coating affected by the 10% solution of hydrofluoric acid as a function of molybdenum disulphide concentration: 0% (1, 5); 0.2% (2, 6), 0.8% (3, 7); 1.4% (4, 8).

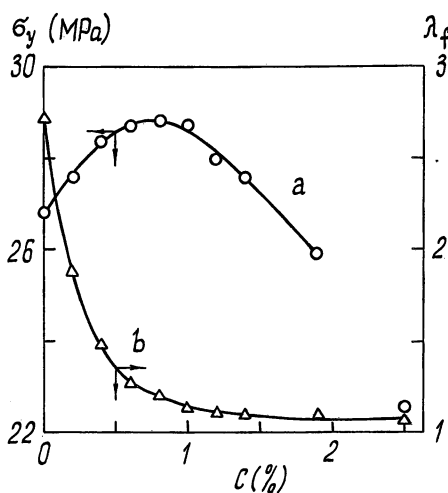


Figure 2. The dependence of the values of yield point (a) and elongation at failure (b) of polyethylene film on the concentration of molybdenum disulphide. The point for the film with the filler content of 2.5% is out of the graph a (see text).

composites occurs at σ still before achieving the value of σ_y (see the point situated out of the graph *a* in Figure 2).

As shown in Figure 3 (curve *a*), the value of A has a complicated dependence upon the additive content in polymer. The maximal value of A is achieved by filling within the concentration range of 0.6-0.8%. At the filler content near or more than 2.0% the non-continuous coatings are formed. The lower limit of this range can be established visually at the appearance of considerable amount of cavities still at the stage of the powder spraying. Heat treatment fixes these defects. Adhesion of such samples cannot be measured by the method used.

A peeling of polymer coatings depends on the ratio of cohesion forces to internal stresses (δ). The enhancement in cohesion forces leads to the σ_y rise and in such a way becomes a reason for increase in the cohesive constituent part of adhesion. Besides, as shown in Figure 3 (curve *b*), the value of T_F reduces when the filler content goes up. The increase in molybdenum disulphide concentration heightens the fraction of heat energy that is absorbed by a powder coating under the definite conditions of heat treatment. The thermochemical destruction of macromolecules is intensified as a result of changes in the fusion conditions. This process also contributes to a rise in adhesion.

Conclusions

The existence of concentration range in which the corrosion-protective and mechanical properties of filled PE reach the optimal values is established. Considering the data of electrical and adhesive experiments, the conclusion is made about increased homogeneity and continuity in coatings with the additive content of 0.6-0.8%. The study of the mechanical properties of isolated films resulted in showing that the specificity of filler's influence is typical not only for coatings, but, probably, could be such a basic characteristic of the present material. An introduction of molybdenum disulphide in PE allows one to choose the production

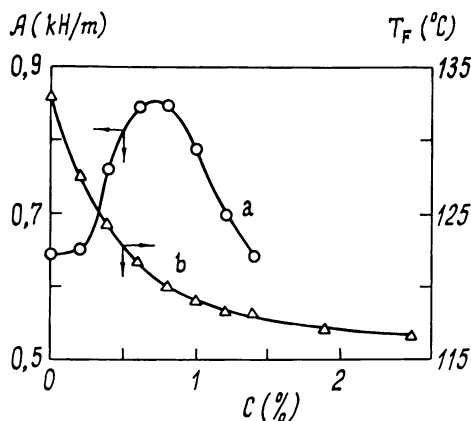


Figure 3. Adhesion strength (*a*) and flow temperature (*b*) versus the concentration of molybdenum disulphide in a polyethylene coating.

conditions of the powder composite coatings with heightened resistance to environment effect as well as with better adhesive and strength properties.

Literature Cited

1. Vadasz, E. *The Plastic Coatings Used for Carrying Out and Restoring the Machine Details*; Books: Budapest, 1978; chapter 3.
2. Emanuel, N. M.; Buchachenko, A. L. *Chemical Physics of Ageing and Stabilization in Polymers*; Science: Moscow, 1982; chapter 2.
3. Panasyuk, V. E.; Prots, S. R.; Barinov, V. Yu. *Phys.-Chem. Mech. Mater.* **1995**, vol. 31, p. 118.
4. Frechette, E.; Compere, C.; Ghali, E. *Corrosion Sci.* **1992**, vol. 33, p. 1067.
5. Vettegren', V. I.; Bashkarev, A. Ja.; Lebedev, A. A. *Mech. Comp. Mater.* **1990**, vol. 26, p. 978.
6. Farris, R. J.; Goldfarb, J.; Maden, M. *Makromol. Chem. Macromol. Symp.* **1993**, vol. 68, p. 57.

Chapter 25

Defect Area Calculated from Electrochemical Noise and Impedance Measurements

R. L. Twite and Gordon P. Bierwagen

Department of Polymers and Coatings, North Dakota State University,
Fargo, ND 58105

The uses of electrochemical methods to estimate the defect area on steel substrates under an organic coating have been proposed in the literature. These citations suggest that the defect area can be estimated using electrochemical impedance spectroscopy (EIS) parameters from an equivalent circuit or extracted from the "raw" data of an electrochemical noise (ENM) test. In this investigation, these methods are applied to estimate the defect area on Al 2024-T3 substrate coated with a number of different aerospace primers. The results are compared with image analysis data from scanning electron micrographs (SEM). It is found that the method utilizing the ENM measurements agrees best with scanning electron microscopy / image analysis data. EIS methods only apply to systems when coating resistance values are low and coating failure is detectable. Although the different methods disagree with respect to the numerical values for defect area fractions, each predict a time dependent increase in defect area and can be used qualitatively to estimate the amount of system deterioration and its rate.

Electrochemical impedance spectroscopy (EIS) and electrochemical noise methods (ENM) are the two techniques currently used for relatively rapid evaluation of corrosion protection offered by coating systems [metal substrate/pretreatment/primer/topcoat]. Traditional tests such as salt spray (ASTM B-117) and Prohesion™ test provide qualitative data and are used for ranking coatings systems (1,2,3,4). ENM and EIS can provide quantitative information on both the extent and mechanism of coating degradation due to corrosion. Furthermore, these methods can be used to estimate the defect area at the coating/metal substrate interface. Four methods currently used to estimate the defect area using data from either EIS or ENM are described briefly.

The first three methods discussed are based on values obtained from electrochemical impedance spectroscopy. The equivalent circuit (EC) method of data analysis provides a method to estimate capacitance (C), resistance (R) and "pseudo" inductance (L) values from an EIS spectrum. The most common EC used to represent a coated metal substrate is shown in Figure 1 (5).

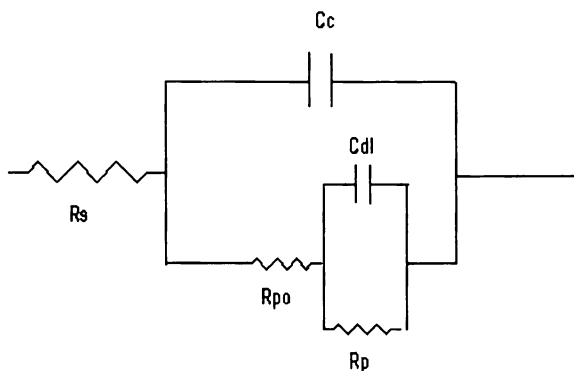


Figure 1. Equivalent circuit used for interpretation of EIS data.

R_s ($\Omega \text{ cm}^2$) is the solution resistance, R_{po} ($\Omega \text{ cm}^2$) the pore resistance, C_c ($\mu\text{F}/\text{cm}^2$) the coating capacitance, R_p ($\Omega \text{ cm}^2$) the polarization resistance and C_{dl} ($\mu\text{F}/\text{cm}^2$) is the double layer capacitance. The corresponding Bode plots from such an EC are shown in Figure 2.

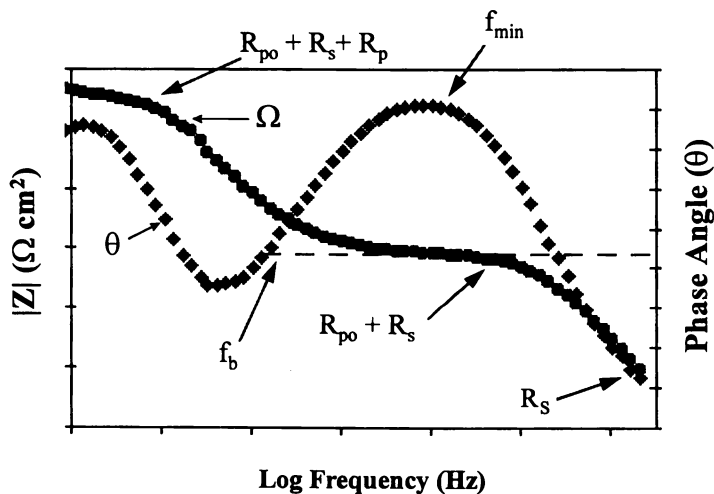


Figure 2. EIS phase angle (\bullet) and log modulus (\blacklozenge) vs. log frequency plots for degraded coating on a metal substrate.

The pore resistance value is a measure of the resistance of microscopic and / or virtual pores in a coating. Virtual pores are local areas of low film resistance caused by effects such as low crosslink density or high pigment volume concentration (PVC) in the continuous film. A plot of R_{po} vs. immersion time gives a good indication of coating degradation. It is defined as

$$R_{po} = \frac{R_{po}^o}{A_d} \quad (1)$$

where

$$R_{po}^o = \rho d \quad (2)$$

A_d is the defect area, ρ is the coating resistivity and d is the total coating thickness. The ingress of ions into coating defects is slower than water so that, unlike capacitance values, R_{po} cannot be measured accurately at very short and long exposure times. Therefore, it is necessary to understand that R_{po} cannot be used independently to determine the defect area of a coating, but must be combined with capacitance values. The following method introduced by Hirayama and Haruyama combines both capacitance and resistance terms to calculate the defect area of a degrading coating.⁶ The method proposed by Hirayama and Haruyama is the first of two techniques discussed that utilizes the break point frequency method as defined below. It is designated as BPF1.

Break Point Frequency (1) [BPF1]. The BPF method utilizes the break point frequency in the high frequency region of the EIS spectrum. The break point frequency is the frequency at which the phase angle (Φ) equals 45° . It is accepted as being the point when the coating's resistive and reactive impedances are equal and is defined by equation 3:

$$f_b = \frac{1}{2\pi C_c R_{po}} = \frac{1}{2\pi C_c^o R_{po}^o} \left(\frac{A_d}{A} \right) \quad (3)$$

where

$$C_c = C_c^o A \quad (4)$$

$$C_c^o = \frac{\epsilon \epsilon_o A}{d} \quad (5)$$

Where ϵ is the coatings dielectric constant and ϵ_o is the permittivity of free space. The coating capacitance is also dependent on the total exposed area A of the sample. Equation 1 shows that R_{po} is dependent on the coating resistivity, ρ , which is likely to change with exposure time. Due to this, it has been argued that BPF1 falls short for a

good estimation of defect area since both ρ and ε change with immersion time (5). Mansfield and Tsai recognized the coating resistivity dependence and proposed a new calculation using the break point frequency but also being independent of ρ (7,8).

Break Point Frequency (2) [BPF2]. BPF2 combines both resistance and capacitance terms in the calculation, but also incorporates a second frequency term. The second frequency term is the frequency at minimum phase angle, f_{\min} . Mansfield *et. al.* found experimentally that f_{\min} could be defined as (7,8).

$$f_{\min} = \left(\frac{1}{4\pi^2 C_c C_{dl} R_{po}^2} \right)^{\frac{1}{2}} \quad (6)$$

where

$$C_{dl}^o = \frac{C_{dl}}{A_d} \quad (7)$$

By taking the ratio between f_b and f_{\min} , the defect area can be determined independent of the coating resistivity, as shown by equation 8.

$$\frac{f_b}{f_{\min}} = \left(\frac{C_{dl}}{C_c} \right)^{\frac{1}{2}} = (a_3 D)^{\frac{1}{2}} \quad (8)$$

where

$$D = \frac{A_d}{A} \quad (9)$$

and

$$a_3 = \frac{C_{dl}^o}{C_c^o} \quad (10)$$

It was mentioned that it is necessary to incorporate capacitance terms with resistance terms in order to obtain an accurate account for the defect area of a degrading coating, as was done with BPF1 and BPF2. The third method uses only pore resistance values to determine the defect area of a coating and will be used as a comparison with the previous two methods.

Pore Resistance Method. The defect area due to pores in the film can be measured using R_{po} independent of the capacitance values (9). This procedure tends to give defect area values five orders of magnitude lower than the defect area values

obtained from calculations involving capacitance terms (9). Another way of defining pore resistance is shown in equation 11.

$$R_{po} = \frac{d}{\kappa N A_{po}} \quad (11)$$

where κ is the solution conductivity ($\Omega^{-1} \text{ cm}^{-1}$), d is the total film thickness, N is the number of pores and A_{po} is the size of each pore assuming all pores are of the same dimension. The effective resistance of a layer of the electrolyte solution occupying the same area as that of the coating is defined as R_e , where:

$$R_e = \frac{d}{\kappa N A} \quad (12)$$

The ratio of the R_{po} to R_e gives the porosity of the coating.

$$\frac{R_e}{R_{po}} = \frac{N A_{po}}{A} \quad (13)$$

Again, these calculations are based on a constant ρ value during the period of immersion.

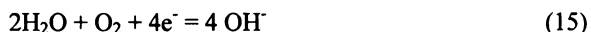
As mentioned earlier, R_{po} only provides reasonable measure of defect area for intermediate exposure. R_{po} values, however, can vary by up to two orders of magnitude among "identical" test samples (9). It is also important to note that pore resistance values can increase during exposure time. Such an increase is due to the blockage of pores by corrosion products and / or other insoluble contaminants. An increase in pore resistance values is commonly detected for aluminum alloy substrates where it is common for the oxide layer thickness to increase with time. The final method discussed is based on data retrieved from electrochemical noise measurements.

Electrochemical Noise Method (ENM). Skerry and Eden proposed a method that uses the coupling current from ENM data to assess the defect area of a coating on a metal substrate (10). The coupling current is the resultant current induced by corrosion or thermal effects occurring spontaneously in the paired sample set-up. They suggested that the total blister volume could be approximated by determining the total charge passed through the coating system during the immersion period (4). The total charge (Q) is calculated using the DC coupling current obtained from the ENM measurement and can be written as:

$$|Q| = \sum |i| \Delta t \quad (14)$$

where Δt is the time increment between measurements and $|i|$ is the absolute value of the coupling current. The charge can also be related to equivalent OH^- groups formed

in the galvanic cell. The following half-cell equations represent the reactions at the metal surface:



With the assumptions that 1) the ionic concentration in the blister is equal to that of the bulk solution ($\kappa_0(\text{mho cm}^{-1}) = \kappa_{\text{blister}}(\text{mho cm}^{-1})$) and 2) the blister assumes a hemispherical shape, the total blister volume (V) is calculated as:

$$V = \frac{|Q|}{0.0615F} = \frac{2}{3}\pi r^3 \quad (17)$$

where F is Faraday's constant and r is the cross sectional radius of the blister. The defect area is estimated by determining the value of r. Since the blisters are assumed to be hemispherical in shape the cross sectional area is that of a circle and the defect area is defined as

$$A_d = \pi r^2 \quad (18)$$

The ratio of defect area to total area is calculated by dividing equation 18 by the total exposed area (A).

Results from electrochemical monitoring of three different organic coatings on Al-2024-T3 were used to estimate the defect areas after 9 days of immersion in dilute Harrison's solution (11). The results obtained from each technique were compared with each other and with data obtained by image analysis of SEM micrographs.

Experimental

Coating Systems The coating systems used in this study were received from McDonnell Douglas Aerospace, St. Louis, MO. The representative coatings systems were a spray coat epoxy/polyamide solvent borne (MIL-C-23377), a spray coat epoxy/polyamide water borne (MIL-C-85582) containing chromated pigments and an epoxy / blocked isocyanate electrocoat containing no inhibitive pigments. Each primer system was applied to a 3 inch by 6-inch aluminum alloy 2024-T3 panel. The substrate was cleaned and degreased prior to paint application. No conversion coating was used for any of the coating systems investigated. The film thickness (primer only) ranged from 10 to 20 μm .

Electrolyte Solutions Three different electrolyte solutions are commonly used in the laboratory to study corrosion inhibition of coating systems. These solutions are i) 5% NaCl, ii) 3% NaCl and iii) dilute Harrison's solution ((8.5 mM $(\text{NH}_4)_2\text{SO}_4$ and 26 mM (NaCl)). The 5% NaCl solution is used by researchers to compare their results with the ASTM standard B-117 salt spray test. The 3% NaCl solution has

been widely used as a simple electrolyte representative of marine salt water. Dilute Harrison's solution has been used by Skerry and others as the closest electrolyte representative of outdoor atmospheric conditions (12). This solution is also used in the ASTM standard G85-00 Annex A5 Prohesion™ Weatherometer⁸ test. Two of the primers used in this study are current military specification primers and the third (e-coat) is an experimental aerospace primer, therefore dilute Harrison's solution was the electrolyte solution used to reproduce conditions specific to an aircraft fleet. The specific conductance of the solution was measured using a Labcraft™ Digital Conductivity Meter with an accuracy of $\pm 0.3\%$. The specific conductance values of the individual solution obtained at the time of measurement ranged from approximately $7 \Omega^{-1}\text{cm}^{-1}$ to $14.5 \Omega^{-1}\text{cm}^{-1}$.

Prohesion™. Replicates of three of each sample were placed in a Q-Fog Prohesion™ Weatherometer for 2000 hours following ASTM standard G85-00 Annex A5(2). Tests consisted of cycling between dry conditions at 35 °C and wet (with electrolyte solution) conditions at ambient temperature. The cycle was repeated every 2 hours.

Electrochemical Analysis. ENM and EIS measurements were conducted using a Gamry Potentiostat controlled by Gamry CMS100 software. A Schlumberger® 1250 frequency response analyzer was used for frequency control during impedance measurements. The details of the analysis can be found in reference (13).

Scanning Electron Microscopy. SEM samples of the coated panels were mounted on regular stubs, examined and photographed on a JEOL, JSM-6300V scanning electron microscope. Scanning areas were $600 \mu\text{m}$ by $300 \mu\text{m}$ in most cases and micrographs with magnification of 1000 X were taken.

Digital Image Analysis. SEM pictures are analyzed using Optimus® version 5.0 digital image analysis package on a P-90 workstation. Defect area estimations were based on the contrast between the filled pores and continuous resin portions.

Results and Discussion

The corrosion protection behavior of a solvent borne and a water borne epoxy/polyamide spray coat along with an epoxy / blocked isocyanate electrocoat (e-coat) primer was monitored using EIS and ENM. Figure 3 is the log modulus vs. log frequency plot for the three coatings after 9 days of exposure in dilute Harrison's solution.

It is evident from Figure 3 that the e-coat system maintains capacitive behavior and displays no break point frequency. As observed by Tsai and Mansfeld, neither BPF1 nor BPF2 offer good prediction for high resistance coatings ($> 10^7 \Omega$) (7). For this reason, defect area calculations for the e-coat were not made using BPF1 or BPF2. Table I lists the values obtained from ENM and EIS analysis that were used for calculation of the defect area. Table II lists the equations and the percent defect area for each sample. It must be noted that ENM measurements are done on two panels to obtain one value, which is an average of the two panels. Each ENM estimation will

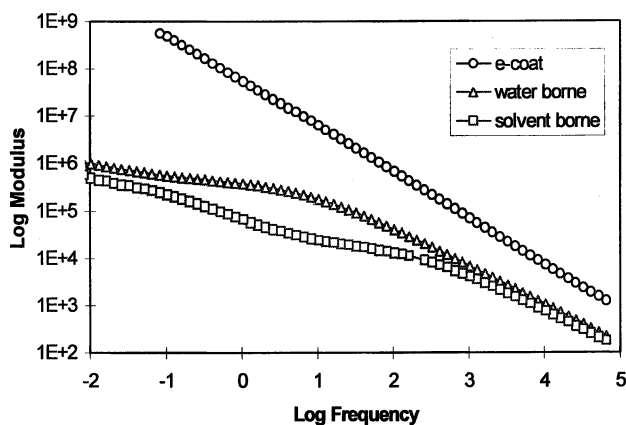


Figure 3. Log Modulus vs. Log frequency for water borne (Δ), solvent borne (\square) and e-coat (\circ) primer systems after 9 days exposure in dilute Harrison's solution.

have two corresponding EIS values. Also included in Tables I and II are values and equations used for the R_{po} method.

The standard deviations of the coupling current from ENM measurements are shown in Figure 4. The values displayed are on the average 2 orders of magnitude lower than the actual coupling current values. The higher values for the solvent borne spray coat are indicative of a more pronounced extent of corrosion taking place in the system.

The standard deviations are used to highlight the trend displayed from ENM measurements. According to the results presented in Figure 4, the defect areas increase in the order of solvent borne > water borne > e-coat. The results displayed in Table 2 also show the above trend when using ENM values for defect area estimations. The trend is not the same when using EIS data to estimate the defect areas. In the cases where the BPF techniques are used for calculations, the e-coat could not be evaluated and the water borne system displayed a higher defect area with respect to the solvent borne system. The defect area estimations from the ENM and the BPF techniques give values, which vary from slightly under 1% up to 8%. Values from the R_{po} method are very low compared to the previous estimations. These low values quantitatively suggest that no delamination is occurring. As was mentioned earlier, R_{po} cannot be used alone to measure the defect area because the coatings display both capacitive and resistive properties. All of the estimations obtained from ENM, BPF1 and BPF2 lie within one order of magnitude. Several aspects may be addressed to explain the slight ambiguity in the numbers. First the differences between estimations from the BPF methods and the ENM method may be accounted for by analyzing what is actually measured when using EIS compared to ENM. When using ENM, as described in this paper, the resistive and capacitive components of a coating system cannot be separated, but instead are measured as a whole. Therefore the ambiguity can only be solved when these components from an ENM measurement can actually be separated and the data re-evaluated. Secondly, the ENM calculations are based on several assumptions. To reiterate what was mentioned earlier, these

Table I. EIS and ENM parameters extracted from electrochemical analysis after 9 days immersion.

Parameter / File	Solvent Borne #1	Solvent Borne #2	Water Borne #1	Water Borne #2	E-coat #1	E-coat #2
R_s (Ω)	101	101	77	73	13	10
R_p (Ω)	2.75E+05	3.93E+04	1.00E+06	5.50E+06	n/a	n/a
C_f (F)	3.18E-06	2.97E-06	5.00E-05	5.31E-05	n/a	n/a
C_c (F)	3.04E-08	2.83E-08	2.18E-08	5.10E-08	2.50E-09	2.80E-09
R_c (Ω)	1.58E+04	2.50E+03	4.50E+05	4.40E+05	2.08E+09	2.20E+09
f_b (Hz)	335.00	3257.00	11.00	12.90	n/a	n/a
f_{min} (Hz)	32.57	258.00	0.26	0.26	n/a	n/a
f_b/f_{min}	10.29	12.62	42.64	50.00	n/a	n/a
Φ	27.70	24.57	17.40	17.70	n/a	n/a
R_c at $t=0$ (Ω)	3.86E+03	8.59E+03	6.63E+05	7.66E+05	n/a	n/a
R_c^o ($A_d / A = 1e-4$) at $t=0$ ($\Omega \text{ cm}^2$)	4.323	9.621	742.560	857.920	n/a	n/a
C_{dl} at $t=0$ (F)	5.30E-06	4.17E-06	1.00E-05	3.00E-05	n/a	n/a
C_{dl}^o ($A_d / A = 1e-4$) at $t=0$ (F/cm ²)	4.73E-03	3.72E-03	8.93E-03	2.68E-02	n/a	n/a
C_c ($t=0$) (F)	2.5E-08	1.92E-08	2.47E-08	2.33E-08	n/a	n/a
$C_c^o = C_c$ ($t=0$) * A (F/cm ²)	2.8E-07	2.15E-07	2.77E-07	2.61E-07	n/a	n/a
d (cm)	1.80E-03	1.80E-03	7.50E-04	7.50E-04	2.10E-03	2.10E-03
κ (mho/cm)	9.60E-03	9.60E-03	9.60E-03	9.60E-03	9.60E-03	9.60E-03
A_{total} (cm ²)	11.20	11.20	11.20	11.20	11.20	11.20
$ Q $ (C/cm ²)	0.05	0.05	0.03	0.03	0.016	0.016

Table II. Defect area calculations and percent defect area for each coating system after 9 days immersion.

Parameter/file	ncylw1b	ncylw2b	ncgm1b	ncgm2b	ncgry1b	ncgry2b
$d/(R_c * \kappa) = NA_d$ (cm ²)	1.06E-06	6.70E-06	1.55E-08	1.59E-08	9.39E-12	8.88E-12
$d/\kappa A = R_c$ (Ω/cm^2)	0.017	0.017	0.007	0.007	0.020	0.020
NA_d/A	9.46E-08	5.98E-07	1.38E-09	1.42E-09	8.38E-13	7.93E-13
R_c/R_c (Ω)	1.06E-06	6.70E-06	1.55E-08	1.59E-08	9.39E-12	8.88E-12
$A_d/A_{total} = fb * (2\pi C_c^o R_c^o)$ (BPF1)	0.003	0.042	0.014	0.018	n/a	n/a
$A_d/A_{total} = (f_b/f_{min})^2 * C_c^o / C_{dl}^o$ (BPF2)	0.006	0.009	0.056	0.024	n/a	n/a
% Defect Area ENM	8	8	5	5	2	2
% Defect Area BPF1	0.3	4.2	1.4	1.8	n/a	n/a
% Defect Area BPF2	0.6	0.9	5.6	2.4	n/a	n/a
% Defect Area R_{po}	9×10^{-6}	6×10^{-5}	1×10^{-7}	1×10^{-7}	8×10^{-11}	8×10^{-11}

estimations are based on the fact that $\kappa_o = \kappa_{\text{blister}}$, the shape of the defect is hemispherical, the only cathodic reaction is the reduction of water, and the reactions involved are irreversible. When dealing with blisters, the conductivity of the solution inside the blister is usually different from that of the solution. Blisters are caused by impurities or corrosion product at the coating/metal interface. When the impurity is ionic or from a corrosion product the conductivity of the blister solution is higher than the bulk solution. When the impurity is from an organic species, the conductivity of the blister solution is lower than that of the bulk. Two of these assumptions can be eliminated by assuming that pores or breaks in the film rather than blisters are the major source of film defects. Thus one can say that $\kappa_o = \kappa_{\text{pore}}$ and the volume is estimated by using the volume of a cylinder with a hemispherical shaped defect onto the substrate (where $r(\text{cylinder}) = r(\text{hemisphere})$). This does not account for outward spread of the defect or a pit deeper than the radius of the pore. The values obtained using this assumption were within 0.5% of the estimations made using a hemispherical shape. Thirdly, the two break point frequency methods also are based on several assumptions. BPF1 assumes constant film thickness, d , and coating resistivity, ρ . Mansfeld and Tsai's calculations correct the coating resistivity by defining an equation that is independent of ρ , but BPF2 is also dependent on C_{dl} . Amirudin and Thierry (9) observed that the double layer capacitance is more a measure of the electroactive area of the substrate rather than the defect area. C_{dl} is therefore different for passive substrates such as aluminum alloys. Since these equations were all developed based on an equivalent circuit that corresponds to a coated steel substrate, the effects of the highly capacitive oxide layer are not accounted for. It would be beneficial to modify the EC to include elements for the oxide layer. Twite and Bierwagen have noticed that after long exposure time, a coated aluminum substrate starts to display three clear RC time constants. The Bode plot of such a system is shown in Figure 5. It is believed that after long exposure time the organic coating becomes saturated and separate time constants between the organic coating and the inorganic oxide layer emerges. The three time constants are attributed to the double layer, the oxide layer and the organic coating.

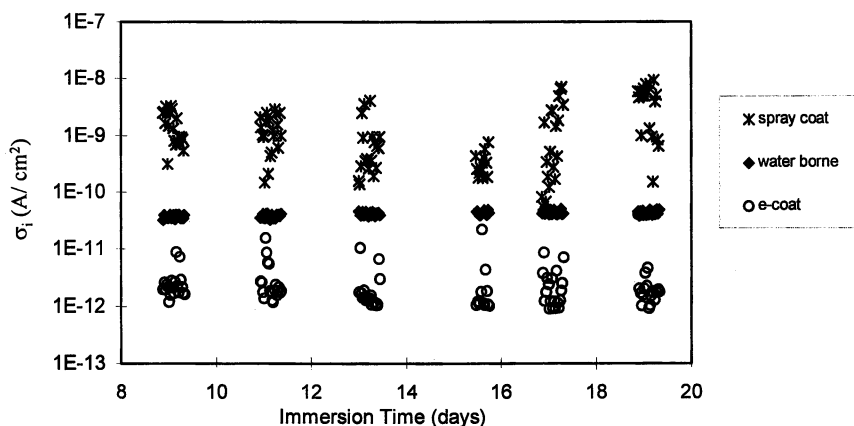


Figure 4. Standard deviation of the coupling current, $|i|$, for a 20 day immersion period for spray coat (*), water borne (♦) and e-coat (o).

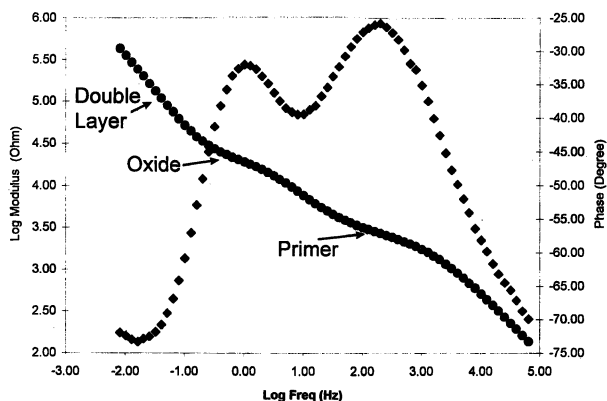


Figure 5. Bode plot of coated aluminum substrate showing three distinct time constants.

SEM was used to monitor changes in the surface morphologies of the coatings as they were exposed to the electrolyte environment. The electron micrographs revealed the porous nature of the spray coatings and the relatively uniform film obtained for the electrocoat system. SEM micrographs (1000X magnification) for the solvent borne spray coat before and after exposure to a) dilute Harrison's solution and b) after 2000 hours in the Prohesion™ weatherometer (approximately 83 days) are shown in Figures 6 and 7a & b. There is a clear indication of the pores in the primer coat throughout the surface of the sample even before conditional exposure as shown in Figure 6. Upon exposure, the pores were filled with corrosion products and / or with precipitated salts from the electrolyte. The micrographs of samples from the Prohesion™ study are shown because they show more contrast between pores and the continuous coating. Preliminary elemental analysis of the surface using EDAX indicates higher amounts of Na, S and Cl with respect to the unexposed film. These are all elements found in dilute Harrison's solution. Figure 7-b was analyzed using digital image analysis (DIA) techniques. DIA is a technique that is now being used to supplement traditional corrosion testing methods which rely on visual analysis (14,15,16). It allows the user to quantify defects by size, shape and number through digital filters and arithmetic operations. DIA was not used to determine the approximate pore area for the coating in its initial state because the contrast between the pores and the continuous film was not high enough for proper estimations. The SEM/DIA analysis provided a quantitative estimation of the area of each pore and the total pore area of the film. If one assumes that the pore area at the surface of the coating is equal to the pore area at the interface, this method can be used for defect area estimation. The total pore area from Figure 6 was estimated to be $14.85 \pm 1.24\%$ and each pore had an area of approximately 0.10%. There has not been any known study done to provide a reasonable correlation between constant immersion and Prohesion™ exposure. The analysis using SEM / DIA was used to show that defect areas can also be estimated using optical methods, although an accurate correlation between the optical and electrochemical methods cannot be made. Although the values obtained from SEM / DIA analysis are still relatively close (within 1 order of

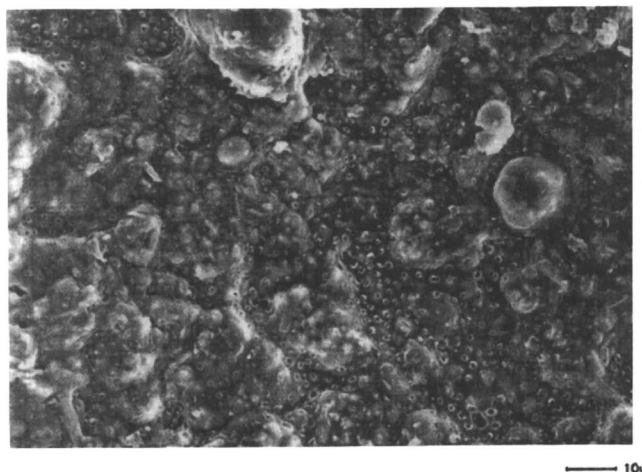


Figure 6. SEM of spray coat in original state.

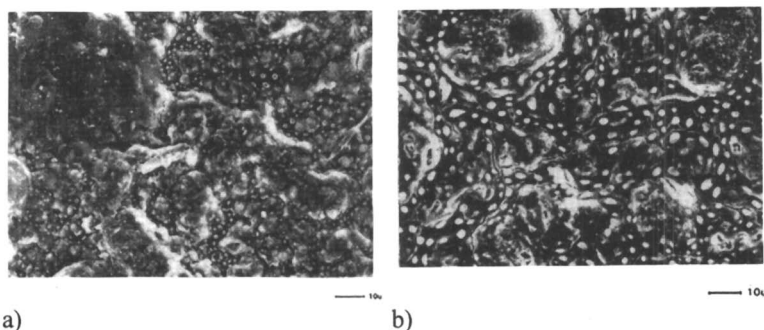


Figure 7. SEM of spray coat after a) immersion in dilute Harrison's solution and b) exposure in a Prohesion™ weatherometer.

magnitude) to the estimations from electrochemical analysis, these studies were included mainly to provide an independent method other than electrochemical testing to monitor the delamination of organic coatings on metal substrates. The results from the SEM micrographs also indicate that there is a higher degree of defects present than estimated by the pore resistance method. The findings confirm that the pore resistance method should only be used to monitor changes in the coating but not for defect area estimations.

Conclusions

The rapid estimation of the defect area of a coated metal substrate by means of electrochemical testing provides a quantitative value to the degree of degradation of the coating system. The methods presented are dependent on the type of substrate (e.g. steel vs. aluminum) and the test method used to derive the defect area values. As opposed to results presented using steel alloys, coated aluminum samples show a

noteworthy variance among the procedures. When using the pore resistance value alone, very low values of defect area values were obtained. The defect area values obtained from BPF1, BPF2 and ENM methods were all within one order of magnitude for each system with values ranging from slightly less than 1% up to 8%. The variance between the values for each method makes it difficult to distinguish between the actual state of degradation between the three coatings systems. The SEM / DIA analysis gave a defect area of approximately 15% of the total exposed area for the solvent borne spray coat as compared to values ranging from 0.6% to 8% calculated from electrochemical data. The ambiguity in the results among all estimation procedures is due to the several assumptions made in each method.

Acknowledgments

The research was supported with an ASSERT Grant supplemental to the Office of Naval Research: Grant # N00014-93-1-0013, while G. Bierwagen was supported by the primary ONR grant. Digital image analysis was performed with the aid of P. Elliot of Polymers and Coatings and Prof. K. Ebling in the Department of Industrial Engineering at NDSU. Scanning electron microscopy was performed with the assistance of personnel in the Electron Microscopy laboratory at NDSU.

Literature Cited

- 1 ASTM Standard B-117, Annual Book of ASTM Standards 1990.
- 2 ASTM G85-00, Annual Book of ASTM Standards, 1994.
- 3 Cremer, N.D. *Federation of Societies for Coatings Technology: Paint Show*, 1989.
- 4 Skerry, B.S. and Simpson, C.H. *Corrosion* 91, Cincinnati, OH, March 1991, Paper 412.
- 5 Amirudin, A.; Jernberg, P.; Thierry, D. *12th International Corrosion Congress Preceedings:Coatings*, 1, Houston, Texas, 171, Sept. 1993.
- 6 Hirayama, R.; Haruyama, S. *Corrosion* 1991, 47 (12), 952.
- 7 Mansfeld, F.; Tsai, C.H. *Corrosion* 1991, 47 (12), 958.
- 8 Tsai, C.H.; Mansfeld, F. *Corrosion* 1993, 49 (9), 726.
- 9 Amirudin, A.; Thierry, D. *Progress in Organic Coatings* 1995, 26, 1.
- 10 Skerry, B.S.; Eden, D.A. *Progress in Organic Coatings* 1987, 15, 269.
- 11 Harrison, J. B.; Tickle, T. C. K. *J. Oil and Colours Chemists Assoc.* 1962, 45, 571.
- 12 Skerry, B.S.; . Simpson, C.H *Corrosion* 1993, 49 (8), 663.
- 13 Twite, R.L.; Balbyshev, S.; Bierwagen, G.P. Electrochem. Soc. 188th National Meeting, Chicago, IL, Oct. 1995, Abstract #189.
- 14 Cohen, E.D.; Grotovsky, R. *Progress on Organic Coatings* 1993, 22, 125.
- 15 Bentz, D.P.; Martin, J.W. *Journal of Protective Coatings and Linings* 1987, 4, 38.
- 16 Van De Mark, M.R. *J. of Coatings Technology* 1993, 65 (827), 45.

Chapter 26

Novel Pretreatments of Metals for Corrosion Protection by Coatings: Part I, Plasma Polymerized Hexamethyldisiloxane on Cold-Rolled Steel

W. J. van Ooij and K. D. Connors

¹Department of Materials Science and Engineering, University of Cincinnati, Cincinnati, OH 45221-0012

In an attempt to replace metal pretreatments that produce toxic by-products with more environmentally friendly treatments without sacrificing the degree of corrosion protection, the use of plasma pretreatments and plasma-polymer films has been investigated. Cold-Rolled Steel (CRS) panels were treated in a plasma of oxygen or a mixture of argon and hydrogen, or both sequentially. A film of plasma-polymerized hexamethyldisiloxane (PPHMDS) was then deposited in the same plasma reactor. The panels subsequently had a cathodic E-coat applied over the PPHMDS. These panels, a phosphated CRS panel, and an untreated CRS panel, were then subjected to a cyclic accelerated environmental corrosion test, after which they were tested using Electrochemical Impedance Spectroscopy (EIS). The EIS tests were also conducted over an extended period of time, during which the panels were continuously exposed to a 1.0 M solution of NaCl. The results indicate that under certain pretreatment conditions, PPHMDS, when used as a primer for E-coating, can perform as well or better than standard phosphating.

Current technology for the corrosion protection of cold-rolled steel (CRS) involves the incorporation of a phosphate layer on a solvent cleaned surface, followed by a chromate rinse. This treatment is used to ensure good adhesion of the cathodic electrocoat primer (E-coat) to the metal substrate. Due to the toxic wastes produced by this process, pressure from EPA has prompted research efforts focusing on the replacement of this system with a more environmentally friendly system. Any new system must also provide a comparable degree of corrosion protection achieved by the phosphating/chromating system.

One possible replacement system being investigated is the use of a plasma cleaning procedure followed by the application of a plasma polymer film in the same reactor.

A plasma treatment using a non-reactive gas, such as oxygen, has been found to be effective in removing carbon contamination from the surface of CRS [1]. The carbon contamination is thought to be a major contributor in the lack of adhesion between metals and polymer coatings. Plasma polymers have properties ideally suited for use as a corrosion protection coating [2]. If the CRS is first plasma treated, and a plasma polymer film is applied over this clean surface in the same reactor, this film can then act as a corrosion protection coating, and also as a primer coating for subsequent coatings, such as the E-coat and the topcoat. The authors have shown that these plasma polymer films do provide corrosion protection in an aggressive environment [3]. It has also been stated that these films are conductive enough to allow the application of an E-coat [4]. Therefore, the entire system of the plasma cleaned surface, covered by a plasma polymer coating and an E-coat should provide the same adhesion and corrosion protection characteristics of the phosphated/chromated surface covered with an E-coat.

Electrochemical Impedance Spectroscopy (EIS) has gained popularity as the technique of choice for investigating the corrosion protection capabilities of polymer coatings on metals [5,6]. This technique, which measures the current response to a fluctuating applied potential as a function of the AC frequency, can provide a quick assessment of the corrosion protection capabilities of a coating in a laboratory or in-situ environment. This is best achieved by fitting the collected EIS data to the performance of an Equivalent Circuit Model (ECM) subjected to the same current and frequency as used in the test of the coated CRS panel. The difficulty lies in the design of the ECM. Only if the ECM chosen for comparison contains elements that are analogous to the physical properties of the coating/metal system can the analysis be taken as representative of the performance of the system.

As well as the pre-assessment of a coating system, the deterioration of a coating can also be investigated using EIS [7]. This is again best achieved by fitting the collected EIS data to the performance of the ECM, and monitoring the changes in the values of the ECM elements with time. Correlation of the EIS analysis with data from environmental corrosion performance tests can be used for verification of the conclusions drawn from the EIS analysis.

Historically, EIS has been used to investigate the properties or the deterioration of polymer coatings. However, if the parameters of the plasma polymerization and the E-coating are held constant, any differences in the performance of the prepared samples should be attributable to the plasma treatment.

This work shows that the system using plasma treatments followed by the application of a plasma polymer coating provides corrosion protection of CRS that is comparable to the phosphating/chromating system. It also shows that EIS can be used to investigate the effectiveness of the pretreatments applied to CRS prior to the application of polymer coatings.

Experimental

Materials. The CRS panels used were automotive grade, type 1010 low carbon sheet material obtained from Armco Research & Technology. The gases used in the plasma cleaning, (oxygen, argon, and hydrogen), were obtained from Wright Bros.,

Inc. The HMDS was obtained from Aldrich Chemical Co.. The E-coat used was an ED-5000 type obtained from PPG Inc.

Sample Preparation. The CRS panels were ultrasonically cleaned in acetone for 20 minutes, and placed in a parallel plate DC plasma reactor. In this reactor, the substrate to be treated or coated is the cathode, and is placed between two anodes. This allows both sides of the sample to be treated or coated simultaneously. The size of the anodes, approximately 22 cm by 22 cm, is larger than the size of the cathode, which in this work was 10 cm by 15 cm. This electrode arrangement is shown schematically in Figure 1.

After placement in the reactor, these panels were first cleaned using a plasma of oxygen, and/or a plasma of an argon/hydrogen mixture. The type of plasma cleaning used in this research was based on results of previous work by the authors [1, 3, 8]. The details of this step are given in Table I. After plasma cleaning, a thin film of plasma-polymerized hexamethyldisiloxane (PPHMDS) was deposited on both sides of the substrate. During the deposition, the chamber pressure was held constant at 125 mtorr, the monomer flow rate was 2.5 sccm, and the power was 20 mA and 1200 volts. The plasma cleaned/plasma polymer coated samples then had a cathodic electrocoat primer applied by immersing in a bath of the paint at a voltage of 180 V for 3 minutes. The panels were then removed from the bath, rinsed using DI water, and then cured at 175°C for 30 minutes. A plain CRS panel, and a phosphated CRS panel were similarly E-coated to be used as a baseline in this study.

Analysis/Characterization. EIS was carried out using the CMS300 system from Gamry Inc., with a Stanford Research Systems model SR810 Lock-In Amplifier.

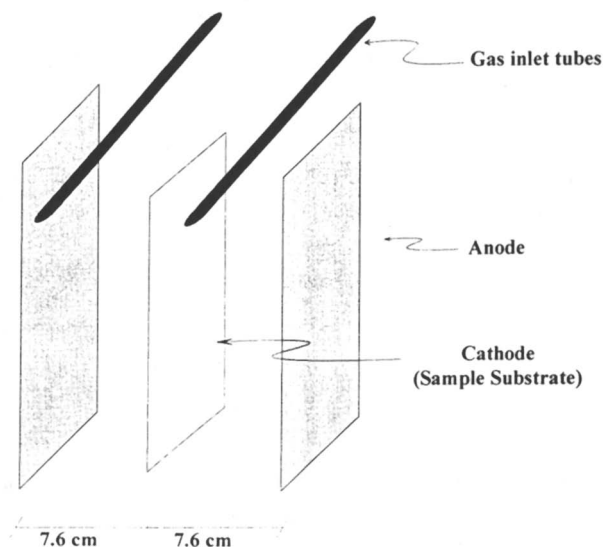


Figure 1. Plasma Reactor Electrode Schematic.

Table I. Plasma Cleaning Conditions

Sample #	Plasma Cleaning Process
CRS	NA
Phosphated CRS	NA
912-D	None
914-A	20 minutes O ₂ , 10 minutes
923-C	10 minutes Ar/H ₂ , 10 minutes

The sample was connected to the equipment using a three electrode cell. The counter electrode was a screen mesh of platinum, whose surface area is much greater than the working electrode surface area of 1.78 cm², which is the coated metal being tested. A reference electrode (Ag/AgCl) is used to measure the polarization potential of the system. The electrolyte used was a 1 M NaCl solution.

The samples were then subjected to a modified version of a cyclic accelerated environmental exposure test (GM-scab test). In this test, the samples are first scribed diagonally across the face of the sample through the E-coat and the plasma polymer to the metal. They are then placed in racks so that the orientation of the scribed face of the sample is approximately 45° to horizontal, and exposed to 60°C and 85% RH for 23 hours in a humidity/temperature chamber. Once removed from the chamber, they are placed in a solution of 5% NaCl for 15 minutes. After soaking, they are removed from the solution and allowed to air dry for 45 minutes. This procedure defines one cycle. The samples are put through a minimum of 25 cycles. The samples are analyzed by measuring the amount of delamination of the coating away from the scribe as indicated by the "bubbling up" of the coating as a result of corrosion product build up at the plasma-polymer/metal interface. Usually, six measurements are taken along the length of the scribe, and the average of these measurements is given as the average delamination value. If the samples show no major difference in the average delamination value after 25 cycles, additional cycles may be used.

After the GM-scab test was completed, the samples were exposed to a 1M NaCl solution for an extended period of time. This long term exposure test was conducted to investigate the deterioration of the coating, or the deterioration of the adhesion between the coating and the CRS. The samples were exposed to the salt solution using a glass joint approximately 15 cm long. A three electrode cell was used, with the counter electrode being a graphite rod, and a Ag/AgCl reference electrode. EIS data was collected daily for the first week, and weekly or bi-weekly thereafter.

For all the EIS tests, data was collected over a frequency range of 0.001 Hz to 100 kHz. This data was then plotted in a Bode plot format, which plots the impedance and the phase angle as a function of the frequency. This format allowed a simple graphical analysis of the data [6]. Additional analysis of the EIS data was also performed using Equivalent Circuit Modeling (ECM) (Figures 2-3). An ECM was designed based on the graphical analysis, as well as the possible relationship

between the Bode plots analysis and the physical characteristics and properties of the sample being tested. The arrangement of the ECM was determined by the shape, and the number of slope changes in the impedance modulus and the phase angle vs. frequency curves.

Results and Discussion

In previous work by the authors, various combinations of plasma cleaning were investigated [9]. From that investigation, the samples that ranked the best, the worst, and intermediate in corrosion performance in EIS tests and in the GM-scab test were chosen, along with plain CRS and phosphated CRS samples, to undergo the long term exposure test.

The impedance modulus of the EIS data taken at the initiation, after 15 days, and again at 107 days of the solution exposure are shown in Figures 4-8. A comparison of the maximum value of the modulus shows that the samples that were plasma cleaned with an oxygen treatment have better corrosion protection parameters than all other samples in the set. This value can be related to the total resistance of the system. This resistance can further be correlated with the corrosion protection properties of the coating system. Realizing that the deposition of the PPHMDS and the E-coating were both carried out under identical condition for all samples, this comparison is then a comparison of the pretreatment. It can thus be

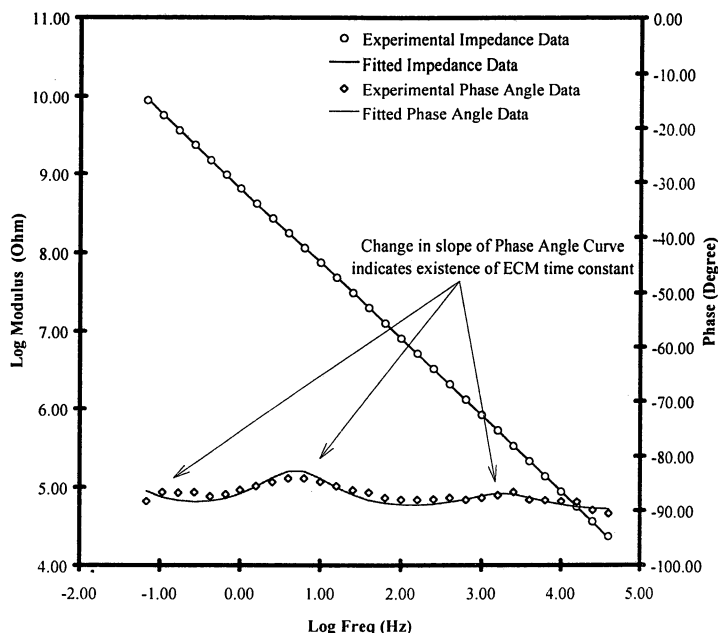


Figure 2. Bode Plot of plasma cleaned/plasma-polymer coated/E-coated CRS.

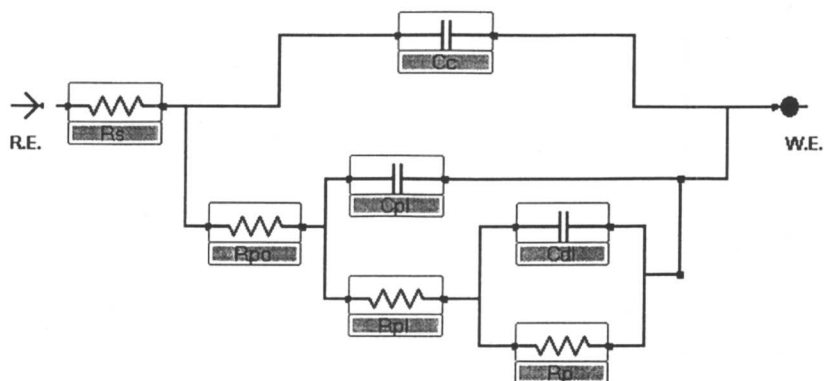


Figure 3. Equivalent Circuit Model used to analyze EIS data of plasma cleaned/plasma-polymer coated/E0coated CRS.

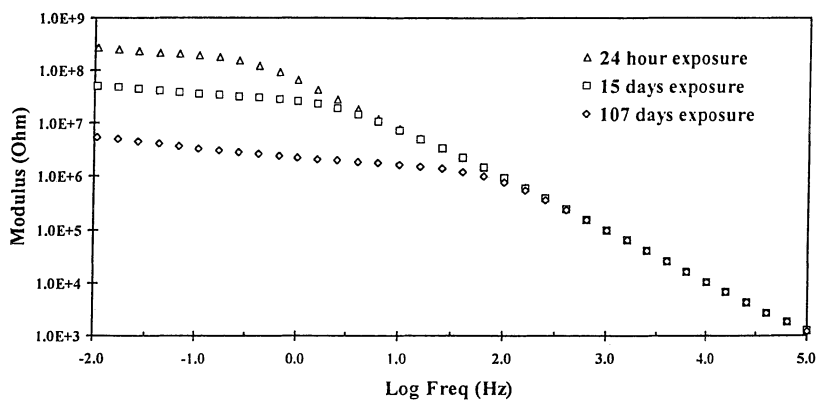


Figure 4. Modulus of Impedance for Phosphated CRS.

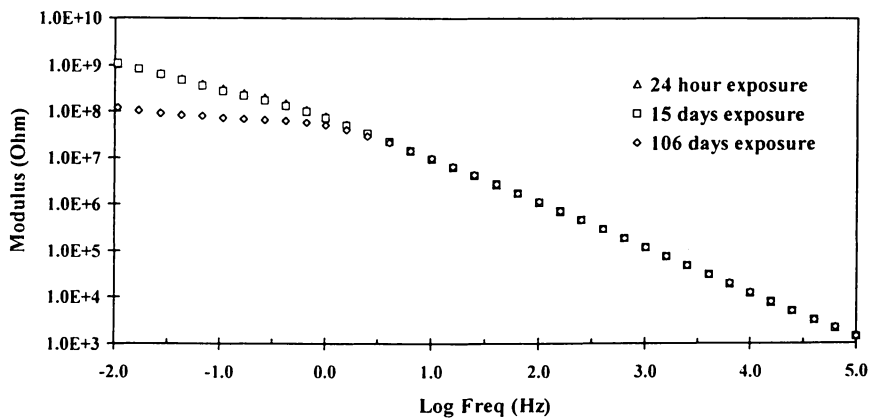


Figure 5. Modulus of Impedance for CRS.

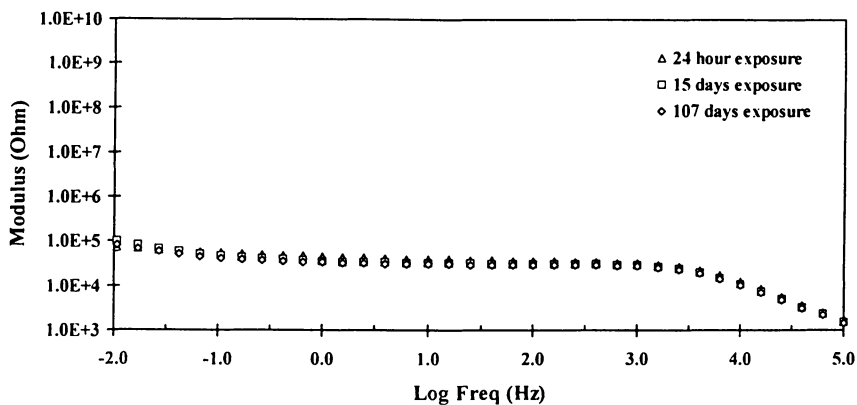


Figure 6. Modulus of Impedance for Sample 12-D.

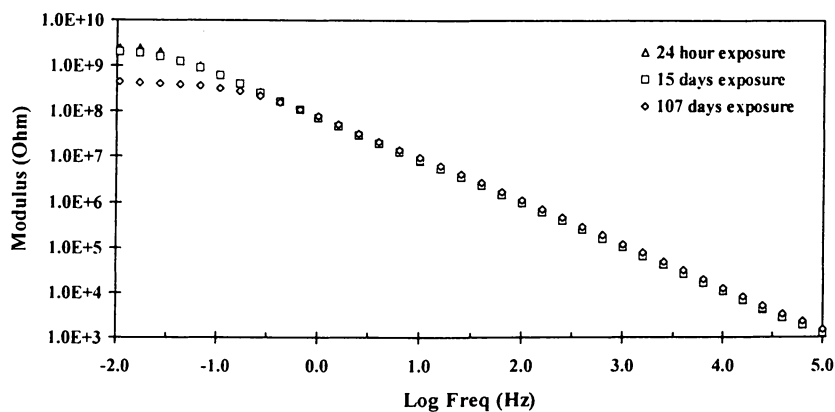


Figure 7. Modulus of Impedance for Sample 14-A.

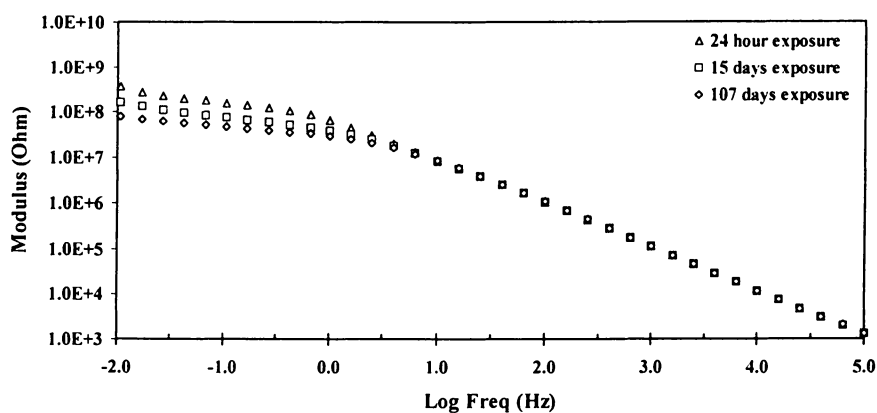


Figure 8. Modulus of Impedance for Sample 23-C.

concluded that the oxygen treated samples show corrosion protection properties that are superior to the two baseline samples, plain CRS and phosphated CRS. These trends also carried through the long term exposure testing of the samples. However, we can also see from this preliminary analysis that not plasma treating the CRS prior to depositing the PPHMDS coating is actually detrimental to the corrosion protection properties of the coating system.

An alternative method for analyzing this data graphically is to note the change in the maximum modulus of impedance value for each sample. We can see that the phosphated CRS shows the greatest change in the maximum modulus, with a change of more the 1 ½ decades during the length of the test. The plasma treated samples, as well as the CRS sample, show a change of less than 1 order of magnitude. This would seem to indicate that there is less deterioration of the coating and/or the interface in these samples than with the phosphated sample.

An exception to this trend is seen in the sample with no plasma treatment, and a plasma polymer coating (sample 12-D). With this sample, it seems that the deterioration of the interface was more or less complete prior to the solution exposure test. This deterioration was due to the exposure in the humidity chamber. This resulted in very low values of a maximum impedance modulus, which stayed more or less constant during the entire period of the test.

A more detailed analysis of impedance data involves the use of an Equivalent Circuit Model, or ECM. In this approach, a simple electrical model is chosen based on the graphical analysis of the impedance data presented in the form of a Bode plot, in conjunction with the known properties of the system being studied. This approach has been used previously by Mansfeld et al. in the investigation of polybutadiene coated metals [10, 11], and Hirayama and Haruyama in the general investigation of degraded coated steel with pores [12]. Figure 2 shows a representative plot of the data from all the samples in this set prior to the GM-scab test. Although the values of the slopes and the position of the breaks in the curves vary from sample to sample, the general shape of the curve is the same for all samples tested. This plot shows that there are essentially three time constants in the EIS data gathered. The high frequency portion of the plot represents the resistance and capacitance of the top polymer layer, the E-coat in this system. The mid frequency range of data represents the resistance and capacitance of the intermediate polymer layer, the plasma polymer in this system. The low frequency portion of the data represents the corrosion reactions taking place at the plasma-polymer/metal interface. Based on this information, the ECM that best represents the plasma cleaned/plasma polymer coated/E-coated CRS is shown in Figure 3.

The parameter R_s represents the resistance of the electrolyte solution. R_{po} and C_c represent the pore resistance and capacitance of the cathodic E-coat. The pore resistance represents the integrity of the coating, i.e., the density of pinholes and defects over the area tested. The value of the C_c is dependent on the thickness of the coating and the degree of solution saturation of the coating. The two parameters, R_{pl} and C_{pl} , represent properties similar to the C_c and R_{po} , only in this case they are representative of the plasma-polymer coating. R_p represents the polarization resistance, which is a property of the polymer/metal interface. C_{dl} represents the double layer capacitance present at the interface of a saturated polymer and a metal

substrate. The parameters C_{pl} and R_{pl} were also used in the data analysis of the two baseline samples so that a comparison of the parameter values of the entire sample set could be achieved. In the phosphated CRS sample, these values would represent the phosphate layer of the coating system. It is not quite clear what the physical correlation of these parameters represent in the CRS sample. It is possible, and probable, that they represent the inherent oxide layer found on CRS. In all cases, including the baseline samples, the fit of the experimental data to the model data using this third time constant was exceptional.

In this work, the pretreatment of the CRS samples was investigated. Therefore, the values of R_p and C_{dl} , which are related to electrochemical processes that occur at the metal/plasma-polymer interface, were used for comparison of the corrosion protection properties of the coating system [10, 11]. This is the area that would be most significantly affected by the pretreatment. The double layer capacitance, C_{dl} , is established once the aqueous solution has penetrated the coating to the plasma-polymer/metal interface. For the aqueous solution to spread at the interface, there must be some delamination of the plasma-polymer from the metal. This delamination is caused by the corrosion of the metal and causes a Faradic charge transfer process to occur, which can be measured as R_p . The changes in these values over the length of the exposure test are shown graphically in Figures 9 and 10, and listed in Table II.

In Figure 9, we see that the initial value of R_p was virtually identical for all samples except 12-D, which received no plasma treatment prior to plasma-polymer deposition. Over the length of the solution exposure test, the value of R_p dropped for all samples. We see in Table II that the phosphated CRS sample had the largest drop in R_p , while the CRS sample and 23-C had drops of approximately 33% of the phosphated sample. Sample 14-A showed a significant drop in R_p , but not quite as great as the phosphated CRS sample.

In Figure 10 we see that values of C_{dl} range between 10^{-7} to 10^{-9} farads, with sample 14-A having the lowest, or best value, and the phosphated CRS having the highest, or worst value. The change in these values is listed in Table II. As with the values of R_p , we see that the phosphated CRS had the greatest change, while sample 23-C had the least change.

The changes in both values discussed above indicate a deterioration of the adhesion of the plasma-polymer to the metal substrate. This causes a decrease in the R_p and an increase in C_{dl} . As water penetrates through the E-coat and the plasma-

Table II. Changes in R_p and C_{dl} for Solution Exposure Test

Sample #	ΔR_p	ΔC_{dl}
Phos CRS	1.81	1.54
CRS	0.61	1.18
12d	0.64	-0.05
14a	1.38	1.79
23c	0.70	0.73

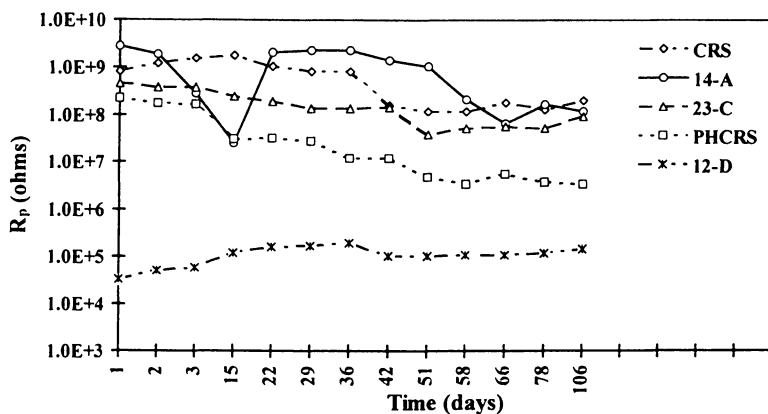


Figure 9. Change in R_p with time for solution exposure test.

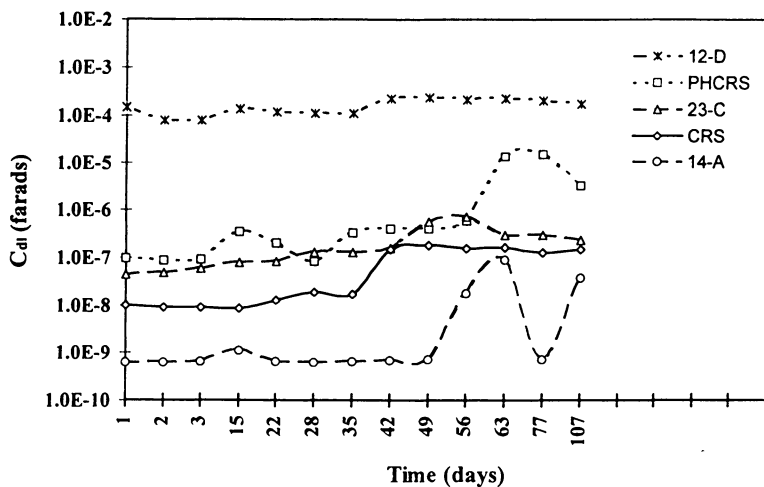


Figure 10. Change in C_{pi} with time for solution exposure test.

polymer, it attacks the chemical species responsible for the adhesion of the plasma-polymer to the metal, thereby affecting the adhesion of the plasma-polymer to the metal substrate. It is postulated that this breakdown in the adhesion is due to hydrolytically unstable species at the plasma-polymer interface. Exactly what causes the instability, and what the exact form of the unstable species are is still unclear. This phenomenon, and the chemical nature of the interface which produces it is currently being investigated.

Sample 12-D, which showed very little change in both R_p and C_{dl} , was the exception to the trends mentioned above. It is seen, however, that the absolute values of both R_p and C_{dl} are so much poorer than all the other samples, that we can only conclude, as we did with the graphical analysis, that the interface of this sample had already significantly deteriorated prior to the start of the solution exposure test. This deterioration was due to the exposure in the humidity chamber, and indicates that this sample had very poor adhesion of the plasma-polymer to the metal substrate prior to any testing.

The results of the GM-scab test show that the oxygen treated sample performed comparably to the CRS and the phosphated CRS. These results also confirm that the results of the preliminary EIS data analysis can be used to assess the corrosion performance of these plasma cleaned/plasma polymer coated/E-coated samples, without the need for any long term environmental exposure tests. It must be remembered, however, that the EIS was performed on samples with no defects, while the GM-scab tests were performed on samples with a three inch scribe. It would thus be difficult to compare the results of the two tests, and make any general conclusions based on these comparisons.

Conclusions

1. Plasma cleaning by an oxygen plasma and the application of a plasma polymer on CRS prior to E-coating provides corrosion protection properties comparable to that of phosphating/chromating treatments.
2. The important step in this environmentally friendly treatment is the plasma cleaning, and in fact, deposition of a plasma-polymer without a plasma pretreatment is actually detrimental to the corrosion performance.
3. EIS and Equivalent Circuit Modeling of the EIS data can be used as an assessment of a system's corrosion protection properties, as well as for long term exposure testing, as long as the proper ECM is chosen for the EIS data analysis.

References

1. K.D. Conners, W.J. van Ooij, S.J. Clarson, and A. Sabata, *Journ. Appl. Polym. Sci.: Appl. Polym. Symp.*, **54**, 167 (1994)
2. N.M. Morosoff, in, R. D'Agostino, ed., "Plasma Deposition, Treatment, and Etching of Polymers, Academic Press, San Diego, CA (1990)
3. K.D. Conners and W.J. van Ooij, *CORROSION '95 Proceedings, Paper #379*, NACE International, Houston, TX (1995)

4. T.J. Lin, B.H. Chun, H.K. Yasuda, D.J. Yang and J.A. Antonelli, *J. Adhesion Sci. Technol.* **5**, 893 (1991)
5. H.P. Hack, and J.R. Scully, *J. of Electrochem. Soc.*, **138**, (1), 33 (1991)
6. M. Kendig and J. Scully, *Corrosion* **46**, 22 (1990)
7. E.P.M. van Westing, G.M Ferrari and J.H.W. de Wit, *Corrosion Science*, **36**, 979 (1994)
8. W.J. van Ooij and K.D. Conners, in D. Scantlebury and M. Kendig, eds., "Advances in Corrosion Protection by Organic Coatings II", **95-229**, The Electrochemical Society, Pennington, NJ (1995)
9. W.J. van Ooij, K.D. Conners and P.J Barto, Paper submitted for Presentation at ICAST '95, Amsterdam, The Netherlands, Oct. 16-21,
10. F. Mansfeld, M.W. Kendig, and S. Tsai, *Corrosion*, **38**, 478 (1982)
11. F. Mansfeld and C.H. Tsai, *Corrosion*, **47**, 958 (1991)
12. R. Hirayama, and S. Haruyama, *Corrosion*, **47**, 952 (1991)

Novel Pretreatments of Metals for Corrosion Protection by Coatings: Part II, Plasma Polymerized Hexamethyldisiloxane Films on Galvalume

W. J. van Ooij¹, N. Tang¹, S.-E. Hörnström², and J. Karlsson

¹Department of Materials Science and Engineering, University of Cincinnati, Cincinnati, OH 45221-0012

²Dalarna University, S-78188 Borlänge, Sweden

Thin films of plasma-polymerized hexamethyldisiloxane were deposited on Galvalume substrates. The films were analyzed by AES. The corrosion performances of the coil-painted plasma samples were tested in the new Volvo indoor corrosion test. The test results were compared with those of the samples with standard chromate and zirconium pretreatments. It was found that a plasma cleaning step prior to deposition of the films had a marked effect on the corrosion performance of the painted system. The plasma deposition conditions had a significant effect on the composition and thickness of the films but their effect on the corrosion performance of the painted samples was minor. The optimized plasma coating had a performance comparable to that of the chromate pretreatment.

Galvalume is a trade name of steel strip hot-dip-coated with an Al-43.4Zn-1.6Si alloy. The metal-coated steel strip can be coil-coated to achieve a decorative and corrosion-resistant material. It is a general experience that painted Galvalume provides a better corrosion protection than painted hot dip-galvanized steel, but that, initially, it is more sensitive to edge corrosion propagation (edge creep) (1,2). The coil-painted sheet is given its final shape by a forming process after painting. The industrial coil paint process today usually uses chromate in pretreatment and in primer in order to achieve a high degree of adhesion and corrosion performance (3). However, the chromate solution is a potential health hazard during handling and also undesirable from an environmental point view.

In recent years, plasma polymerization of organic monomers has been proven to be a useful method for surface modification of a variety of materials (4). Plasma-polymerized thin films deposited on metal surfaces are highly crosslinked, pinhole-free, thermally stable, well adhered to substrates and compatible with paints (5). It was reported that plasma polymerization of organosilicon monomers can be

an effective pretreatment of cold-rolled steel (CRS) giving corrosion protection comparable to that obtained by a fine-grained automotive phosphate (6,7).

The objective of the research described in this paper was to utilize plasma-polymerized hexamethyldisiloxane (HMDS) films as a pretreatment for Galvalume panels prior to painting. This work is part of our ongoing efforts to develop novel, environmentally compliant pretreatments of metals to replace chromates and phosphates. Another pretreatment of Galvalume prior to painting on the coil line, namely by organofunctional silanes, is also being studied in our laboratory (8). In this paper, we report results of our study of the effects of plasma cleaning and plasma film deposition conditions on the composition of the plasma film as well as the corrosion performance of the painted metal systems. The corrosion performance of the plasma pretreated samples were compared to those of two standard pretreatments: a conventional chromate rinse and a commercial zirconium treatment that has been proposed as a replacement of the chromate.

Experimental

HMDS (99.3%) was purchased from United Chemical Technologies. The 55% Al-Zn-coated steel panels were supplied by SSAB Tunnpå AB (Borlänge, Sweden). The metal substrates were first cleaned with acetone in an ultrasonic cleaner for 15 minutes and were dried in air. The plasma polymerization of HDMS on Galvalume panels was conducted in a custom-built DC reactor which is shown in Figure 1. Rotary and diffusion pumps were used for pumping down the pressure. The flow rates of gases were controlled by three Brooks 5850 mass flow controllers. In this experiment, the Galvalume panels were placed between two stainless steel plates. The Galvalume substrate was either a cathode with two stainless steel (SS) panels placed as anodes on both sides of the cathode, or, alternatively, was disconnected electrically, i.e., was floating. In that case, one SS plate was the cathode and the other one was the anode. The sample to be coated was then placed in the full glow of the plasma. Before deposition, the metal surface was cleaned with a plasma of oxygen or a mixture of hydrogen and argon. The plasma cleaning and deposition conditions are listed in Tables I and II, respectively. Two pretreatments from Chemetall GmbH were used for comparison; a standard chromate pretreatment (9) used in coil painting lines and a pretreatment based on alkaline oxidation and an after rinse in a hexafluorozirconic acid based solution (10). The panels were finally painted with a chromium-free polyester coil-line primer and a polyester topcoat.

A Perkin-Elmer PHI 660 Scanning Auger Microprobe was used to record elemental depth profiles of the samples. A 200 nA electron beam accelerated to 10 keV was used for excitation. Sputtering was performed with argon ions accelerated to 1 keV. The sputtering rate was calibrated using a Ta₂O₅ film of known thickness.

Reflection-Absorption IR (RAIR) spectra of PP-HMDS films were acquired on a Bio-RAD FTS-40 FTIR Spectrometer with a deuterated triglycine sulfate detector, using a resolution of 4 cm⁻¹ and were averaged over 128 scans.

A new cyclic accelerated indoor corrosion test designed by Volvo was used to test the performance of the samples after painting. One test cycle included one hour of spraying with a 1% NaCl solution followed by a cycling of the relative humidity between 90 and 45% during 3½ days. The length of the periods at 90%

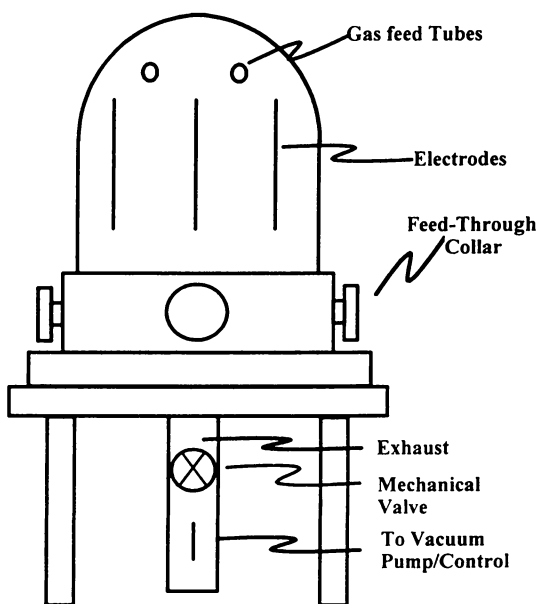


Figure 1. Schematic diagram of the DC plasma reactor.

Table I. Plasma Cleaning Conditions of the Galvalume Panels*

<i>Sample ID</i>	<i>H₂ sccm</i>	<i>Ar sccm</i>	<i>O₂ sccm</i>	<i>P Pa</i>	<i>V volts</i>	<i>I mA</i>	<i>Time min.</i>
PPF1	–	–	–	–	–	–	–
PPF2	2	4		8	700	80	30
PPF3			7.5	16	530	80	30
PPF4	2	4		8	600	80	30
PPF5	2	4		8	1100	80	30

*all panels were connected to the cathode

Table II. Deposition Conditions of HMDS on Galvalume Panels

<i>Sample ID</i>	<i>HMDS sccm</i>	<i>P Pa</i>	<i>On Pulse μs</i>	<i>Off Pulse μs</i>	<i>V volts</i>	<i>I mA</i>	<i>Time min.</i>
PPF1 ^a	2.5	26			500	20	10
PPF2 ^a	2.5	13	331	331	700	20	10
PPF3 ^a	2.5	13	331	331	630	20	10
PPF4 ^a	2.5	13	331	331	700	20	10
PPF5 ^b	2.5	13	331	331	900	20	10

a: the sample was connected as a cathode in between two stainless steel anodes.

b: the sample was floating in the plasma between the anode and cathode.

relative humidity was seven hours and the length of the periods at 45% relative humidity, including the transition times, was five hours. The temperature was 35°C throughout the test. The samples were tested for 19 weeks (38 cycles). A 5 cm vertical scribe down to the steel base was applied to each panel. The performance in the corrosion test was evaluated by measuring the average edge and scribe creep after removing loose paint by an industrial adhesive tape.

Results and Discussion

The AES depth profiles of the films PPF1-5 are shown in Figure 2. The profiles show that the different cleaning and deposition conditions had a pronounced influence on the chemical composition of the plasma films. PPF4 had a well-defined film containing Si, O, N and C. The O/Si ratio was approximately 2.5 and fairly

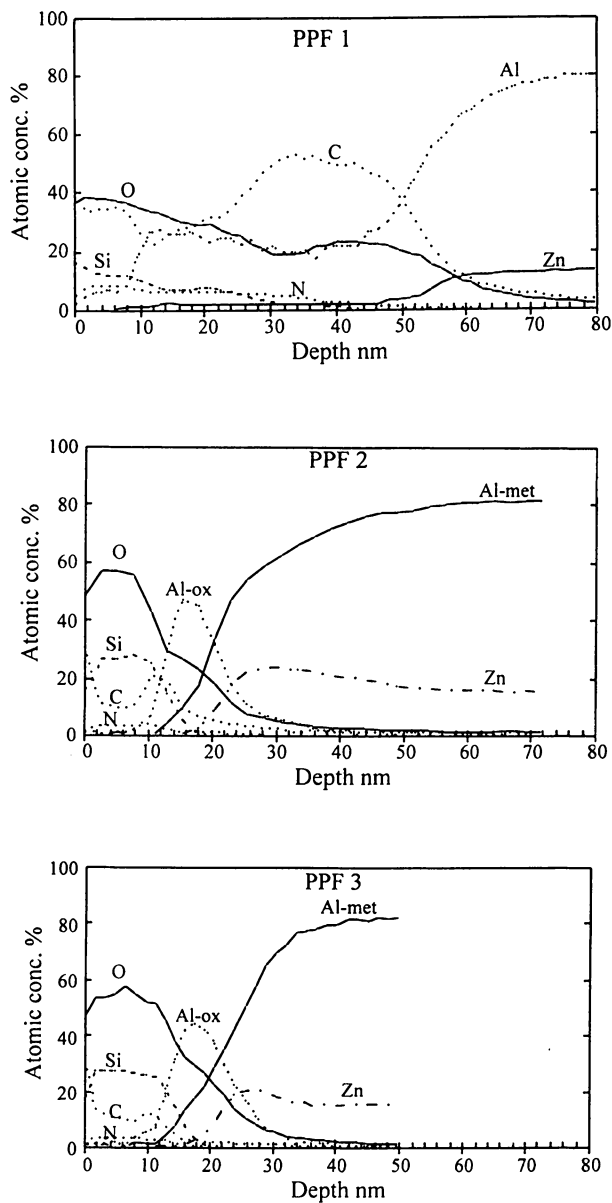
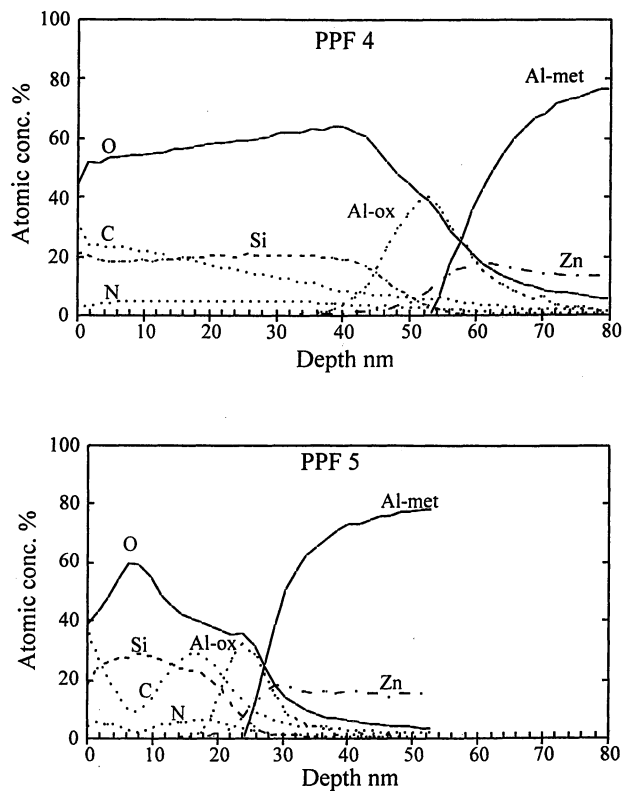


Figure 2. AES depth profiles of Galvalume sheets coated with plasma-polymerized films PPF 1-5.

Continued on next page.

Figure 2. *Continued.*

constant in the film, while the carbon concentration decreased slowly towards the metal substrate. The inner parts of the film thus seemed to contain a higher concentration of Si and O, while the outer part of the film contained more alkyl groups. The small amount of nitrogen present in the film was probably incorporated in the plasma film due to residues in the vacuum which was purged with pure N_2 before cleaning the substrates and again before depositing the films.

At the metal-plasma film interface a layer of Al oxide was detected. This oxide formed during solidification of the alloy coating as a result of the high affinity of aluminum to oxygen. The amount of zinc oxide was very small at the interface and was not included in the depth profiles.

Sample PPF1 had a much lower Si concentration and a higher carbon concentration. Al was detected in the entire layer here. It was in this case not possible to separate the Al spectra in a metal and an oxide component. The origin of the Al detected in the plasma film could be a non-uniform coating caused by the occurrence of sparking during deposition of the PPF1 film. The high carbon concentration could also be a result of this effect. Sparking during deposition of the PPF1 film was considerably higher than in the other samples, as the power during deposition of the PPF-1 film was not pulsed. In all other depositions, the power was pulsed (Table II). In general, sparking and arcing is much reduced in a DC discharge if the voltage is pulsed. The fact that no plasma cleaning was performed on this sample could also have an effect on its composition, as has been shown in previous work (5).

PPF2 and PPF3 had about the same chemical composition as PPF4 but the thickness of the coatings was only about one fourth of that of PPF4. PPF5, which was floating in the plasma during deposition, had a somewhat higher silicon concentration than PPF2-4. This effect may be related to the mode of deposition which in this case was on a substrate at floating potential. Under such conditions, the intensity of positive ion bombardment on the growing plasma film is much reduced (7).

Figure 3 shows typical RAIR spectra of PP-HMDS films prepared under different conditions of power and pressure (11). The main peaks are assigned as follows: 810 and 840 cm^{-1} are the Si-C rocking in $>Si(CH_3)_2$ and $-Si(CH_3)_3$, respectively; the peaks in the range of 1075-1085 cm^{-1} are the asymmetric stretch in the Si-O-Si group. The differences in frequency of this band are related to the degree of crosslinking and the length of the -Si-O-Si- chain. The band at 1260 cm^{-1} is the Si-CH₃ symmetric deformation and its intensity indicates the degree of retention of methyl groups bonded to silicon. The band at 2960 cm^{-1} is the asymmetric and symmetric stretch of the -CH₃ group, whereas the band at 2890 cm^{-1} is the asymmetric and symmetric stretch of the methylene group, -CH₂-. The absence of the band at 1260 cm^{-1} and the presence of the one at 2890 cm^{-1} indicate that the PP-HMDS film is crosslinked via -CH₂- or -CH₂CH₂- groups. As the figure indicates, this effect occurs under more severe deposition conditions of higher power and lower pressure. These conditions are more severe as both an increase of the power and a decrease of the pressure result in a higher flux and a higher energy of positive ions bombarding the growing film on the cathode. The spectra thus show that the composition of PP-HMDS films can be manipulated reproducibly by varying the plasma deposition conditions. Pulsing of the discharge power tends to

result in films that are slightly less crosslinked and softer, i.e. the effect is about the same as reducing the power and increasing the pressure.

In Figure 4 the edge corrosion and corrosion creep from the scribe are presented for the different samples. It was observed that among the plasma-polymerized samples PPF4 had the lowest edge creep and PPF1 the highest. Samples PPF2-5 were comparable or slightly better than the chromate and zirconium pretreated samples. The chromate-rinsed sample had the lowest scribe creep but not the lowest edge creep. The zirconium-rinsed sample had an edge creep comparable to the chromated sample but a larger scribe creep. No signs of blistering or corrosion were observed on the surface of the panels away from the edges or the scribe.

It can be assumed that the plasma polymer film will act as a physical barrier to the diffusion of corrosive species to the metal surface (6). Also, a high degree of adhesion is important as poor adhesion between metal and paint will lead to spreading of water and delamination of the paint coating during the corrosion process.

The poor performance of PPF1 can be related to its composition or structure which are determined by the plasma cleaning and deposition conditions. It has been suggested that a plasma cleaning before film deposition removes residual hydrocarbons and a loose oxide layer on the metal surface (7). Without such a cleaning step, the above substances will remain on the metal surface and may decrease the adhesion between the plasma-polymerized HMDS film and the metal substrate. Further, no corrosion-resistant covalent bonds can be formed in such conditions (7). In addition, sparking during deposition probably resulted in a non-homogeneous film, as the presence of Al in the film (Figure 2a) suggests that this film was porous.

The differences in performance between the films PPF2-5 are hardly significant, despite their pronounced differences in composition and thickness. Thus, we may conclude that the major factor that determines the performance of plasma-polymerized HMDS films on Galvalume is the plasma cleaning process prior to film deposition. Without such a cleaning process, no covalent bonds can be formed. Such bonds are more hydrolytically stable than hydrogen bonds normally formed at metal-paint interfaces. This conclusion confirms our previous findings with CRS substrates (7).

Conclusions

1. Plasma-polymerized HMDS films provide excellent corrosion protection to painted Galvalume® substrates.
2. A plasma cleaning step prior to plasma deposition is very important for the corrosion performance of the painted plasma-film coated sheets.
3. The corrosion performance of plasma-polymerized coatings is comparable to that of a standard chromate pretreatment.

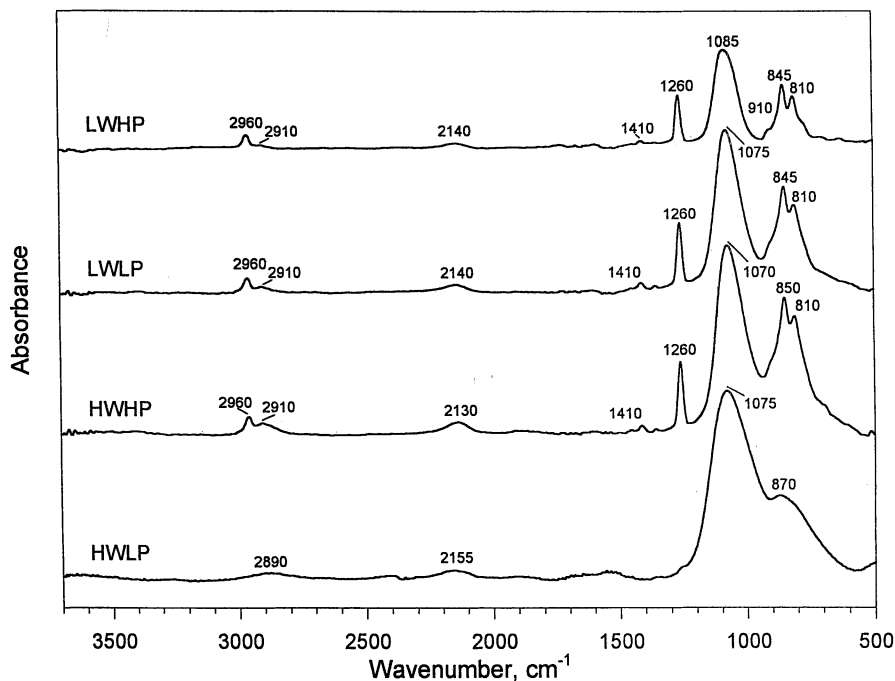


Figure 3. RAIR spectra of PP-HMDS films deposited on stainless steel substrates; the power and pressure were varied; the monomer flow rate was 4.2 scc per minute. LW - 1 W; HW = 22 W
LP = 6 Pa; HP = 65 Pa

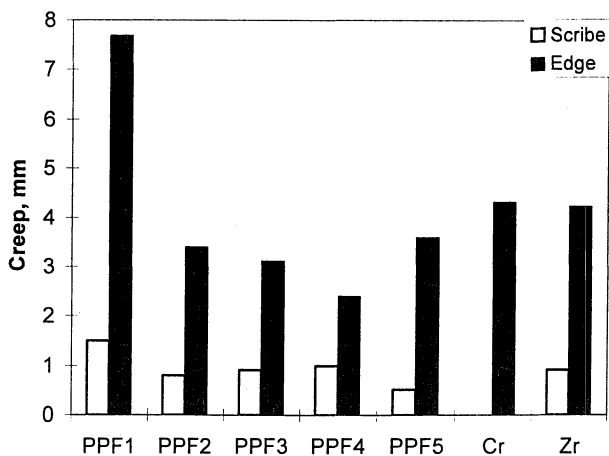


Figure 4. Volvo test results of the painted Galvalume panels.

Acknowledgments

The authors are indebted to Kirk Conners for his help in preparing the plasma-polymerized coatings and for providing Figure 1. The assistance of Stephan Eufinger for acquiring the RAIR spectra of Figure 3 is also gratefully acknowledged.

Literature Cited

1. Oka, J. and Tagasugi, M., *J. Iron Steel Inst. Japan*, 1991, 77, 1130.
2. Harvey, G.J., *Revue de Métall.*, 1990, 87, 183.
3. Townsend, H.E., Proc. 3rd Int. Conf. on Zinc and Zinc Alloy-Coated Steel Sheet, GALVATECH '95, 1995, 171.
4. Yasuda, H., "Plasma Polymerization", Academic Press, Orlando, 1985.
5. van Ooij, W.J. and Sabata, A., *Surf. Interface Anal.*, 1993, 20, 475.
6. van Ooij, W.J.; Edwards, R.A.; Sabata, A. and Zappia, J., *J. Adhesion Sci. Technol.*, 1993, 7, 897.
7. van Ooij, W.J. and Conners, K.D., *J. Electrochem. Soc.*, 1995, 95-13, 229.
8. Hörnström, S.E.; Karlsson, J.; van Ooij W.J.; Tang, N. and Klang, H., *J. Adhesion Sci. Technol.*, 1996, 10, 883.
9. Hörnström, S.E.; Hedlund, E.G.; Klang, H.; Nilsson, J-O. and Backlund, M., *Surf. Interface Anal.*, 1993, 20, 427.
10. Hörnström, S.E.; Karlsson, J. and Östling, A., Proceedings of the UK Corrosion & Eurocorr 94 Conference, 31 Oct. – 3 Nov. 1994, Bournemouth, UK, Vol. 1, p. 35.
11. Eufinger, S.; van Ooij, W.J. and Conners, K.D., *Surf. Interface Anal.*, 1996, 24, 841.

Chapter 28

Improvement of Wet-Adhesion on Stainless Steels by Electrolytic Polymerization Treatment with Triazine Thiol Compounds

H. Yamabe

ABB Asea Brown Boveri Industry K. K., Shimada, Shizuoka, Japan

The surface treatment of stainless steels by electrolytic polymerization with 1,3,5-triazine-2,4,6-trithiol (TTN) in aqueous solution was investigated. This surface treatment improved the adhesion durability of epoxide resin adhesive joints in wet environment.

Structural adhesive bonding for metallic materials is now established as indispensable industrial technology for construction of airplanes and cars (1) (2). Nevertheless, several technological problems of strategic importance are left unsolved in this important industrial technology. The most important problem includes "loss of adhesion strength in the presence of humidity." This unsolved problem is actually identical in quality to the problem of adhesion of the corrosion protective coating layer to a metallic substrate in a humid environment. Loss of adhesion between layers is believed to be a result of water to the adhered interface between two layers. In the case of corrosion protective coating, surface modification of the metal substrate is practiced to inhibit undesired loss of adhesion between coating layer and metal substrate in humid environments (3).

It is well known that stainless steel exhibits inferior adhesion property to organic coatings as compared with other metals such as cold rolled steels or aluminum. Various pretreatments for stainless steel have been used to enhance the physical properties of the steel. Several different types of pretreatments for stainless steel have been used in aerospace industry (mechanical, chemical, and a combination of mechanical and chemical) (4). If a chemical pretreatment process is employed, a residue (smut) is deposited on the surface. This residue must be removed with another chemical treatment, a desmutting solution. For this reason such a chemical pretreatment process is environmentally not very attractive.

In this study, the surface treatment of stainless steel by electrolytic polymerization with 1,3,5-triazine-2,4,6-trithiol monosodium salt (TTN) in aqueous solution was investigated in an attempt to improve adhesion in humid environment. Three types of surface analysis techniques were employed in an attempt to ascertain the bonding mechanism with this surface treatment.

Experimental

Functionality of Triazine Thiol Compounds. This triazine thiol compound has various advantages as shown in Figure 1. For instance, if R represents a thiol group, this compound gives adhesion properties to polymeric materials such as epoxide resin, as the thiol can react with the glycidyl group of the epoxide resin (5).

Thiol groups can polymerize radically with formation of disulfide bonding (S-S). If one of the thiol groups is in the form of salt (SNa, SK), the triazine thiol compound is soluble in water (6). Therefore, 1,3,5-triazine-2,4,6-trithiol monosodium salt (TTN) in water was employed as an adhesion promoting agent for stainless steel.

Pretreatment Procedure. Figure 2 shows a schematic diagram of the pretreatment procedure. Before pretreatment with TTN, the stainless steel was degreased and rinsed by deionized water. Then the fresh stainless steel was pretreated electrolytically with TTN.

Figure 3 shows a schematic diagram of the electrolytic polymerization process of TTN for stainless steel. The stainless steel at the anode was pretreated electrolytically in 5 mM TTN (99.9% purity, supplied by Toa Electric Co., Japan) in water at constant current. In this case, the current density was kept constant at 5 mA/cm².

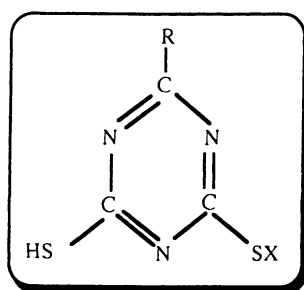
Coating Thickness. The dry coating thickness of TTN was measured by ellipsometry. The coating thickness of TTN depends on the time of electrolysis. As shown in Figure 4, the almost linear relationship between time of electrolysis and coating thickness of TTN was shown.

Adhesion Study. The pretreated specimens for lap joint were bonded using the epoxide (Epikote 828)/polyamide (Versamid 140) adhesive. The adhesive was cured for 7 days at room temperature and then for 1 hour at 100° C. The thickness of the adhesive layer was 100–150 μm.

The joints were then drawn in an Enstron Universal Testing Instrument. The load required to break the joints was determined in accordance to JIS K6850. Figure 5 shows the effect of the polymerization time on adhesion strength of stainless steel bonded by an epoxide polyamide adhesive. In this case, the optimal adhesion strength was obtained at the thickness between 10 and 20 Å. In the range of higher coating thickness, the cohesive destruction in pretreated layer was observed. From these results, the polymerization time was fixed to 20 seconds, which corresponds to the thickness of 100 Å.

The effect of humidity exposure (70° C., 98% r.h.) on adhesion strength is shown in Figure 6. Significant improvement in adhesion durability can be achieved by the application of electrolytic polymerization treatment with TTN.

Similar thiol compounds have also been developed for pretreatment of metallic materials to be subjected to adhesion bonding. For example, Schmidt and Bell (7) reported improved adhesion performance for steel achieved with an ethylene-mercaptop ester copolymer-coupling agent.

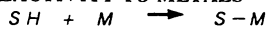


FUNCTIONALITY

ADHESION TO POLYMERS : $R = SH$

ANTIFOULING : $R = NH(CF_2)_3CF_3$

REACTIVITY TO METALS



POLYMERIZABILITY

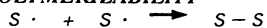


Figure 1. Functionality of triazone thiol compounds (5).

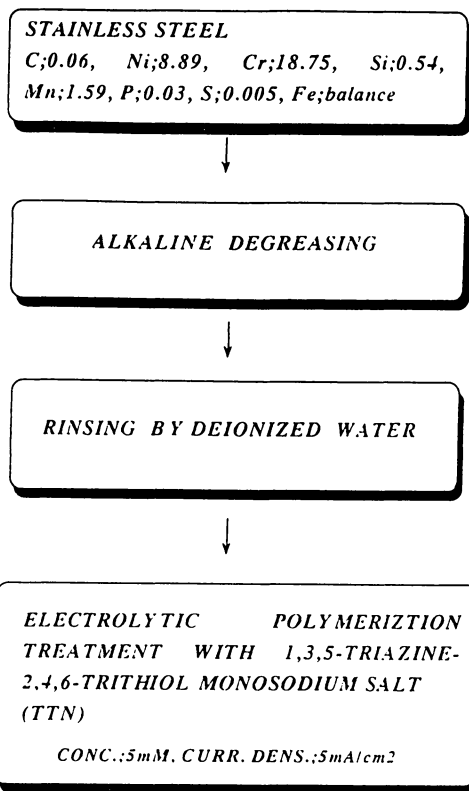


Figure 2. Procedure for sample preparation

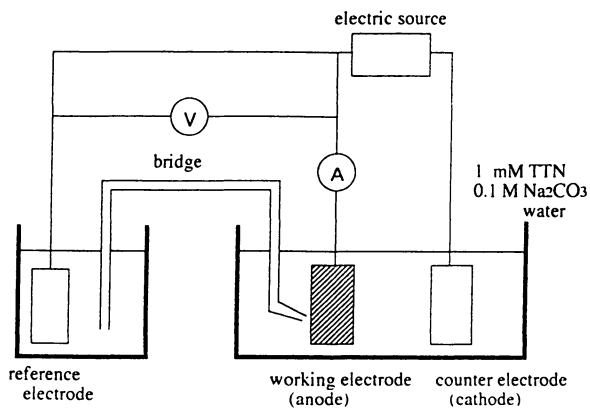


Figure 3. Schematic diagram of electrolytic polymerization equipment

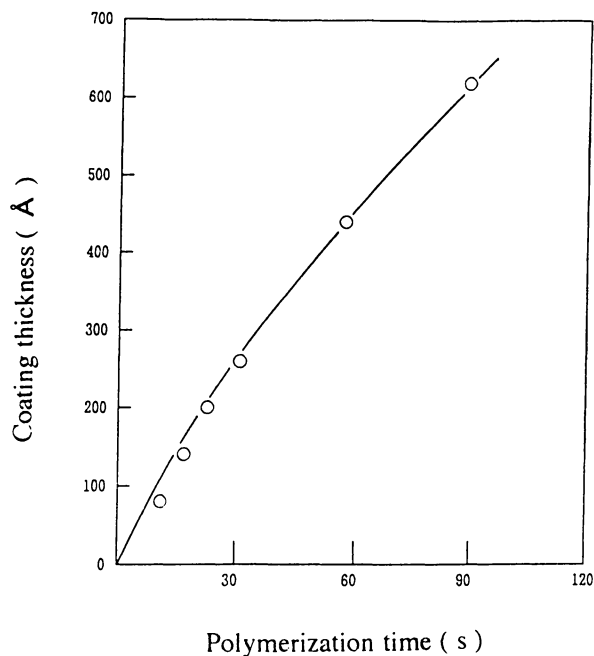


Figure 4. Effect of TTN polymerization on coating thickness.

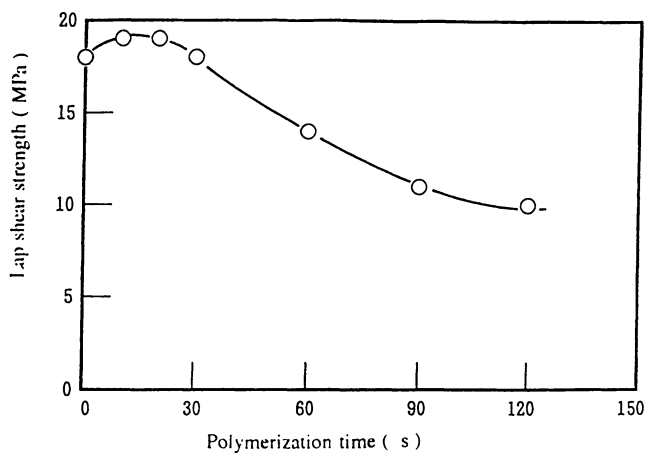


Figure 5. Effect of TTN polymerization time on the adhesion strength of bonded stainless steel.

Interface Characterization. As described above, the electrolytic polymerization of a layer of TTN improved adhesion durability of stainless steel. In order to characterize the interface between the TTN layer and the stainless steel, three surface characterization techniques were employed:

- A Perkin-Elmer Model 257 spectrometer was used for reflection-absorption Fourier transform infrared (RA-FTIR) spectroscopic analysis.
- A Perkin-Elmer PHI Model 5500 was used for X-ray photoelectron spectroscopic (XPS) analysis. The exciting radiation was provided by magnesium K α X-ray source operated at a constant power of 200W (10 kV, 20 mA).
- An ATOMIKA Model A-DIDA3000 was used for static secondary ion mass spectroscopic (SIMS) analysis. In this technique, a 3 keV Argon ion beam irradiated an elliptical area and current densities were kept at $\sim 10^{-6}$ A/cm².

RA-FTIR Analysis. RA-FTIR spectra from stainless steel treated with TTN are shown in Figure 7. As seen in this figure, in the case of immersion only, the IR spectrum of the TTN layer can not be observed. On the other hand, in the case of electrolytic polymerization treatment, the apparent spectrum of the TTN layer can be observed. Absorbance at 1510 and 1460 cm⁻¹ can be assigned to the stretching vibration of -N=C< in the triazine ring. Absorbance at 1260 and 1220 cm⁻¹ is assigned to the stretching vibration of C-N in the triazine ring.

XPS Analysis. XPS is employed as a meaningful analytical method in the field of surface characterization (1). As the chemical environment of an atom changes, the photoelectron spectrum undergoes changes in peak shape, position or intensity. Since the adhesion durability in a wet environment is a fundamental local phenomenon involving only a few atom layers of substrate and organic coatings, the resultant data from the XPS studies should contribute toward an understanding of chemical interaction behavior at the interface of TTN film and stainless steel. Figure 8 shows XPS high resolution examinations of the S(2p) region from stainless steel, which was electrolytically treated with TTN. The peak at a binding energy of 162 eV indicates the presence of covalent bonding between the thiol of TTN and the stainless steel surface. This kind of covalent bonding was also observed between n-decanthiol and mild steel by Stratmann (8) (9). He came to the conclusion that the thiol group has a relatively high reactivity with the metal surface and forms a covalent bond with metal such as Fe. This type of interfacial structure is responsible for the stability of TTN/stainless steel interface in a wet environment.

The peak at binding energy of 165.5 eV may indicate the disulfide (S-S) bonding, from which a polymerized structure of TTN can be expected. The peak separation of thiol and disulfide is so difficult that further investigation is needed. However, the polymerization of TTN can be assumed because the TTN film formed was not soluble in tetrahydrofuran.

Figure 9 shows XPS high-resolution examinations of the S (2p) region from fractured stainless steel after water vapor exposure for 72 hours. On both the adhesive and substrate sides, a polymerized TTN layer can be detected. This analysis also revealed the presence of the covalent bonding between thiol and metal. From

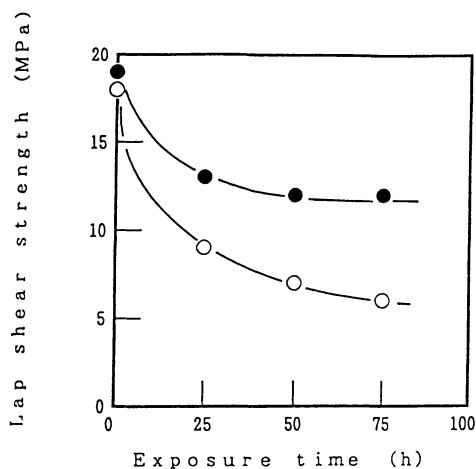


Figure 6. Effect of TTN polymerization treatment on the adhesion strength of bonded stainless steel after high-humidity test.

● : treated with TTN, ○ : untreated.

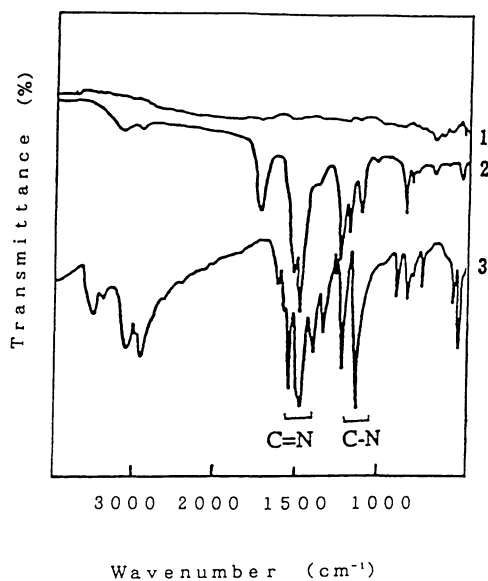


Figure 7. RA-FTIR spectra of stainless steel (SUS304 2B) treated with TTN.
1. Immersion 2. Polymerized film 3. TTN crystal/KBr

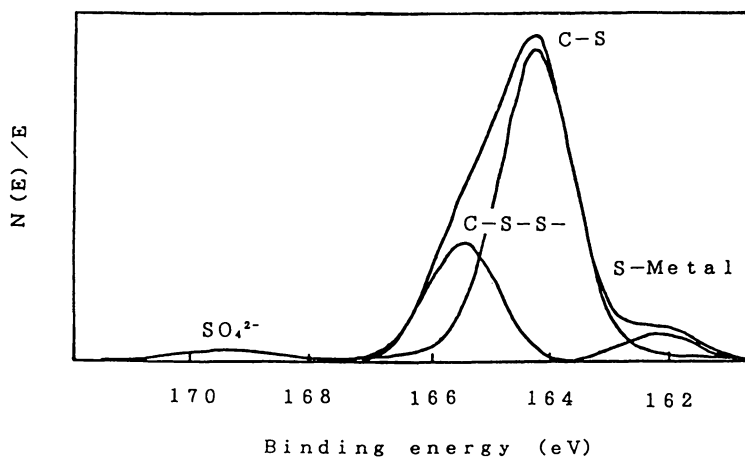


Figure 8. S_{2p} XPS spectra of stainless steel (SUS304 2B) treated with TTN.

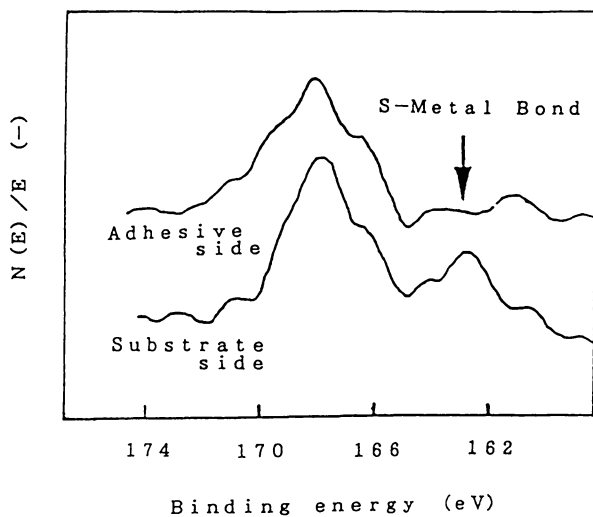


Figure 9. S_{2p} XPS spectra of bonded stainless steel (SUS304 2B) fractured after high-humidity test for 72 hours.

these results it is concluded that thiol/metal bonding resists water penetration and that fracture occurred within the polymerized TTN layer.

Static SIMS (SSIMS) Analysis. In SIMS, ionized particles are ejected from the surface by the action of an argon beam. They are analyzed according to their masses. As the current densities are very low in the static mode, only the surface layer can be investigated. Either atoms or molecules can be ionized, and thus, details about the chemical state of atoms in the surface can be inferred (10).

It is evident from Figure 10 that the surface of the stainless steel contains traces of many elements. At 84 amu and 88 amu the molecular ions CrS^+ and FeS^+ can be observed, respectively. These two molecular ions may be associated with the covalent bonding between thiol of TTN and metallic elements of stainless steel, such as Cr and Fe.

Gettings and Kinloch (11) investigated performances of several silane-coupling agents over a stainless steel sheet surface and observed that increased stability for the adhered interface with a coupling agent varied appreciably from one agent to another. They also used SSIMS for characterization of the bonding state of a silane-coupling agent/metal oxide interface. In this case, similar SIMS characterization was undertaken and ions indicative of the presence of FeOSi and CrOSi were detected. The silane-coupling agent, which gave such ions successfully, improved the adhesion performance for the stainless steel. As such, formation of a primary covalent bond in addition to a secondary bond seemed to be essential for enhancement of interface stability in a humid environment.

Polymerization Mechanisms of TTN on Metal Surfaces. Figure 11 shows polymerization and adhesion mechanisms of TTN on a metal surface. The TTN molecules exist in ionized form as seen in this figure. This molecule can be oxidized and leaves an electron. The oxidized S radical reacts with another S radical. In this way, the polymerized layer will be formed on stainless steel. The terminal of polymerized TTN can form covalent bonding with metal atoms, such as Cr and Fe, on stainless steel surfaces. The outermost thiol can react with epoxide and combine stainless steel and epoxide by covalent bonding.

Conclusion

There are some important conclusions that can be drawn from this work:

- The electrolytic polymerized TTN layers are excellent pretreatment for stainless steel/epoxide bonding.
- The results of RA-FTIR, XPS and SSIMS gave information regarding the polymerized layer. Especially, the evidence of polymerization and covalent bonding with stainless steel that was observed for XPS analysis.
- In conclusion, it is clear that the use of polymerized TTN allows a better understanding of surface treatments and allows the choice a priori of the best treatment of stainless steel to be bonded to the organic polymer.

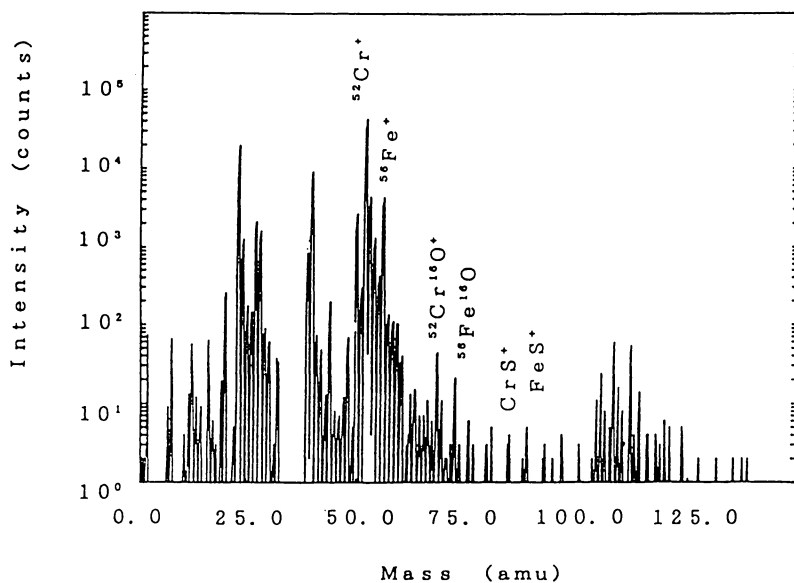


Figure 10. Static SIMS spectra of stainless steel (SUS304 2B) treated with TNN.

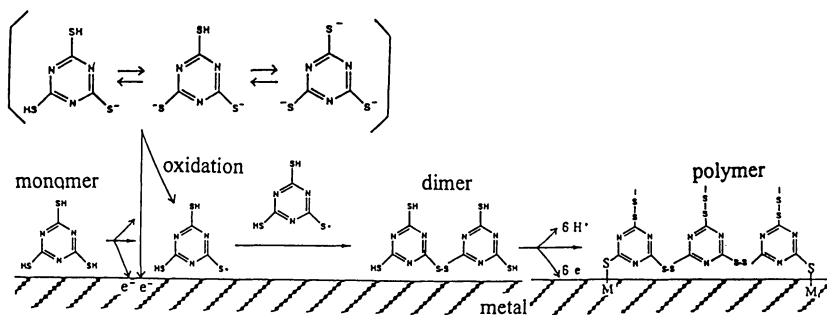


Figure 11. Polymerization and adhesion mechanism of TTN on metal.

Literature Cited

- 1 Yamabe, H. *Zairyo-gizyutu* **1996**, 14(10), 288.
- 2 Yamabe, H. *Japan Adhesion Society* **1993**, 29, 12.
- 3 Yamabe, H.; Funke, W. *Farbe und Lack* **1990**, 96, 497.
- 4 Yamabe, H.; Hirahara, H.; Mori, K. *J. Japan Society of Color Material* **1995**, 68, 404.
- 5 Yamabe, H. *ibid.* **1993**, 66(10), 605.
- 6 Mori, K.; Nakamura, Y. *J. Polymer Science: Polymer Chemistry Edition* **1985**, 23, 315.
- 7 Schmidt, R. G.; Bell, J. P. *J. Adhesion* **1988**, 25, 85.
- 8 Stratmann, M. *Farbe und Lack* **1993**, 99, 16.
- 9 Stratmann, M. *Adv. Mater.* **1996**, 2, 191.
- 10 Yamabe, H.; Tsutsumi, A. *Farbe und Lack* **1993**, 99, 16.
- 11 Gettings, M.; Kinloch *J. Mater. Sci.* **1977**, 12, 2511.

Chapter 29

The Replacement of Chromate- and Lead-Based Inhibitors in Protective Coatings

Charles Simpson

Sherwin-Williams Chemicals, 101 Prospect Avenue, NW, Cleveland, OH 44115

Health and environmental hazards associated with the use of corrosion inhibitors based on hexavalent chromium and lead has prompted considerable interest in effective, nontoxic replacements for these pigment materials. Molybdate pigments represent an important class of nontoxic corrosion inhibitors that have been successfully applied to the development of high performance lead and chromate free coating. Since first being introduced to industry over 20 years ago, the value of these unique materials has been demonstrated through considerable field and laboratory testing.

In addition to the requirement for effective replacements for chromate and lead pigments, however, the reformulation of coatings for environmental compliance also requires the availability of reliable short term test methods that provide meaningful indications of exterior durability. Test methods based on a cyclic salt-spray/UV-condensation procedure (recently designated ASTM D5894) have been shown to provide close correlation with outdoor exposure testing, particularly when compared to results obtained by older industry methods (e.g., ASTM B117 salt-spray) still in widespread use. It is suggested that the development of effective chromate and lead free coatings will be most successful when based on the use of corrosion inhibitors

having documented field histories, in conjunction with evaluation techniques known to provide good correlation with outdoor results.

Chromate and Lead Based Inhibitors

Historically, paints designed to protect steel and other metals have been based on the use of slightly soluble lead and chromate based corrosion inhibitive pigments. Table 1 list some of the most important chromate and lead based inhibitors. Such pigments have been found to be highly effective corrosion inhibitors in various coating applications.

Government regulations, concerning both protection of the environment and protection of industrial workers, have prompted paint manufacturers and end-users alike to favor the use of non-chromium and lead based pigments. In the US, an important example is the regulation of hazardous wastes by the Environmental Protection Agency (EPA). The EPA has established limitations on the maximum leachable concentration of certain metals that may be present in industrial waste materials (e.g., spent abrasive/coating debris from blasting operations to remove old coatings). This is measured using the Toxicity Characteristics Leaching Procedure or TCLP (Table 2). Materials found to exceed these requirements must be handled as hazardous waste for disposal purposes.

The protection of workers who handle lead and chromium based pigments and paints is also an important consideration. In the workplace, specific measures must be taken to maintain airborne concentrations of hazardous materials below permissible exposure levels established by the Occupational Safety and Health Administration (OSHA). The use of anticorrosive pigments free of lead and chromates can eliminate the need for many such measures. Anticorrosive molybdate pigments, for example, are regulated only as a nuisance dust material, as are other nontoxic materials like calcium carbonate.

Anticorrosive Mechanism of Molybdates

Corrosion is an electrochemical process involving the oxidation of a metal, known as the anodic reaction, and the corresponding reduction of another material, known as the cathodic reaction. The ability of molybdates to effectively inhibit the corrosion process has been recognized for many years in the field of corrosion science.⁽¹⁾

Molybdates are classified as anodic or passivating inhibitors.

When a coating film that contains molybdate pigments becomes exposed to water, small quantities of molybdate ions will be released into the coating film. When these ions contact the metal substrate they are known to promote formation of a protective, passive oxide layer on the metal which prevents corrosion of the underlying substrate. This can be demonstrated using the Pourbaix diagram for iron in contact with water (Fig. 1). The presence of molybdate ion raises the electrode potential and moves iron into a region of passivation. The interaction of molybdates with other metal substrates (e.g., aluminum) has been studied less extensively, but can be expected to be similar to iron, in principle.

In this respect, molybdates function in a similar way to chromate inhibitors. Such similarities are not surprising considering the relative position of chromium and molybdenum on the periodic table of elements (Fig. 2).

Molybdate Based Inhibitors

There are three main types of nontoxic inhibitors that have been used commercially to develop lead and chromate free systems. These include borates, phosphates, and molybdate pigment products. Molybdates are of particular importance, given that these pigments have been in commercial use for over twenty years. Considerable testing has demonstrated that the performance capabilities of molybdates are comparable and in some cases exceed that provided by chromate and lead based pigments. Additionally, molybdates are white pigments and provide for the development of white or tintable primers, topcoats and direct to metal systems.

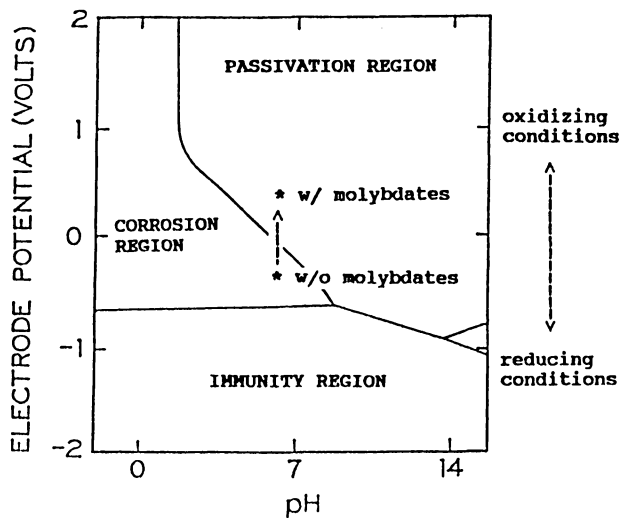
Table 1 - Lead and Chromate Based Corrosion Inhibitors

<u>name</u>	<u>chemical composition</u>
zinc chromate (zinc yellow)	$4\text{ZnOK}_2\text{O} \cdot 4\text{CrO}_3 \cdot 3\text{H}_2\text{O}$
zinc tetroxy chromate (basic zinc chromate)	$5\text{ZnO} \cdot \text{CrO}_3 \cdot 4\text{H}_2\text{O}$
strontium chromate (strontium yellow)	SrCrO_4
red lead	Pb_3O_4
basic lead silicochromate (BLSC)	$3\text{PbO} \cdot \text{PbSiO}_3 \cdot \text{PbO} \cdot \text{PbCrO}_4 \cdot \text{SiO}_2$

Table 2 - Requirements of EPA Toxicity Characteristics Leaching Procedure

<u>metal</u>	<u>maximum leachable concentration (ppm)</u>
Arsenic	5.0
Barium*	100.0
Cadmium	1.0
Chromium*	5.0
Mercury	5.0
Lead*	0.2
Selenium	5.0
Silver	5.0

*indicates metals present in some anticorrosive pigments

**Figure 1 - Pourbaix Diagram for Iron**

There are three main types of commercially available molybdate pigments, (1) zinc molybdates, (2) calcium molybdates and (3) phospho-molybdates (Table 3). Zinc molybdates are primarily used in solvent based coatings, particularly alkyd and epoxy systems. Calcium molybdates have been used most widely in water-based coatings, including latex emulsion and water-reducible systems. Calcium molybdates are considered to be more compatible and stable in water-based coatings, due to their lower solubility versus zinc molybdates.

Phospho-molybdates are the most recently developed type of molybdate based inhibitors. These pigments incorporate a synergistic combination of phosphate and molybdate compounds, and have exhibited cost and performance advantages over their earlier molybdate counterparts. Products include zinc phospho-molybdate, which is generally recommended for solvent based coatings, and calcium zinc phospho-molybdate, which is effective in water and solvent-based systems.

Phospho-molybdates represent the fastest growing type of molybdate pigment finding applications today.

Application of Molybdate Inhibitors

The uses of molybdate pigments in U.S. Federal and Military Specification coatings provides for documented formulation examples of molybdate-based coating systems. Table 4 list some of these specifications along with a brief description. Detailed formulation information for these specifications can be obtained through the General Services Administration (GSA).

The US Navy recently patented a number of self-priming, corrosion inhibitive coating systems for steel and aluminum that all reference the use of molybdate inhibitors (Table 5). These systems were developed to replace existing chromate and lead based coatings, and offer the additional advantage of being self-priming, eliminating the need for a two step primer and topcoat application process.

group	<u>IVB</u>	<u>VB</u>	<u>VIB</u>	<u>VIIB</u>	<u>VIIIB</u>
	Ti	V	Cr	Mn	Fe
	Zr	Nb	Mo	Tc	Ru
	Hf	Ta	W	Re	Os

Figure 2 - Group VIB Transition Series Metals

Table 3 - Types of Commercially Available Molybdate Inhibitors

<u>description</u>	<u>active agent</u>	<u>application note</u>
zinc molybdates	ZnMoO ₄	solvent based coatings
calcium molybdates	CaZn _x (MoO ₄) _y	water and solvent based coatings
phospho-molybdates	ZnCa _x (PO ₄) _y (MoO ₄) _z	water and solvent based coatings

Table 4 - US Federal and Military Specification Paints Referencing Molybdate Inhibitors

<u>designation</u>	<u>effective date</u>	<u>description</u>
MIL-P-28577A	June 1977	latex primer with calcium molybdate
MIL-P-85658	May 1986	silicone alkyd primer with zinc molybdate
TT-P-645B	February 1990	low VOC alkyd primer with zinc molybdate
TT-P-2756	September 1990	self-printing polyurethane with zinc molybdate

Table 5 - US Navy Patents for Self-Priming Coatings Referencing Molybdate Inhibitors

<u>US Patent No.</u>	<u>title</u>	<u>date</u>
5,100,942	Corrosion Resistant Acrylic Coatings	Mar. 31, 1992
5,089,551	Corrosion resistant Alkyd Coatings	Feb. 18, 1992
5,059,640	Epoxy Corrosion Resistant Coatings	Oct. 22, 1991
5,043,373	High-Gloss Corrosion Resistant Coatings	Aug. 27, 1991
4,885,324	Combination Primer/Top Coat Coatings	Dec. 5, 1989

Improved Test Methods for Corrosion

The most widely used accelerated test for corrosion resistant paints is the ASTM B117 salt-spray test. Because this method has shown very poor correlation with actual outdoor exposure results, there has been much interest in the identification and development of more meaningful test procedures. One test method, often referred to as Prohesion/QUV incorporates wet/dry cyclic salt-spray (using an ammonium sulfate based electrolyte) with UV/condensation cycles (Table 6).

Based on independent studies reported by the Steel Structures Painting Council⁽³⁾ and the Cleveland Society of Coatings Technology,⁽⁴⁾ the Prohesion/QUV test provided outdoor exposure correlations considerably higher than that obtained with other new methods being proposed to industry (Table 7 and 8). In both studies, standard salt-spray testing was found to have a negative correlation with outdoor exposure. The ASTM has recently approved and published a standard procedure for Prohesion/QUV testing. This is now designated ASTM B5894, "Standard Practice for Cyclic Salt Fog/UV Exposure of Painted Metal."

A study was conducted to determine the statistical correlation of Prohesion/QUV and outdoor exposure, specifically in the evaluation of molybdate and other types of anticorrosive pigments (Table 9). In this work, a total of fourteen different high-solids alkyd primes (each formulated using a different inhibitor, but otherwise identical) were prepared and applied to steel panels. One set of panels was exposed for two years at a marine testing site, while another set was exposed in Prohesion/QUV for 1,008 hrs. After testing, correlation plots were prepared for scribe undercutting and general surface rust as shown in Figures 3 and 4, respectively. Qualitatively, a reasonable good degree of correlation is indicated.

To get a better understanding of the statistical significance of the data, the ranking of the panels after the two exposure conditions were then compared using a statistical Spearman Ranking procedure. Correlation coefficients obtained (Table 10) did show that the test was quite useful in providing meaningful indicators of exterior

Table 6 - 'Prohesion/QUV' (cyclic salt-spray/UV-condensation) Test Procedure1 week (168 hrs) UV-condensation

4 hr UV (bulb type: A340) exposure at 60 C

4 hr condensation exposure at 50 C

1 week (168 hrs) cyclic salt-spray1 hr salt-spray (0.35% (NH₄)₂SO₄, 0.05% NaCl) at room temp.

1 hr. dry-out period at 35 C

Table 7 - Correlation Coefficients (Steel Structures Painting Council)

<u>test method</u>	<u>correlation coefficient*</u>
ASTM B117 Salt-Spray	-0.110
KTA Envirotest Type 1	0.485
KTA Envirotest Type 2 (w/UV)	0.481
KTA Envirotest Type 3	-0.043
KTA Envirotest Type 4 (w/UV)	0.619
Prohesion	0.065
Prohesion/QUV	0.699

*marine exposure site

Table 8 - Correlation Coefficients (Cleveland Society of Coatings Technology)

<u>test method</u>	<u>correlation coefficient*</u>
ASTM B17 Salt-Spray	-0.107
Cyclic Salt-Spray	0.046
KTA Envirotest Type 2 (w/UV)	0.213
Prohesion	-0.091
Prohesion/QUV	0.459

*average from nine industrial and marine exposure sites located across the US

Table 9 - Anticorrosive Pigments Studied

zinc chromate	zinc phosphate
barium modified zinc phosphate	strontium zinc phosphosilicate
zinc hydroxy phosphite	zinc phospho-molybdate
calcium zinc phospho-molybdate	zinc molybdate grade 1
ion exchange pigment	zinc molybdate grade 2
barium metaborate	zinc molybdate grade 3
aluminum triphosphate	calcium carbonate (blank control)

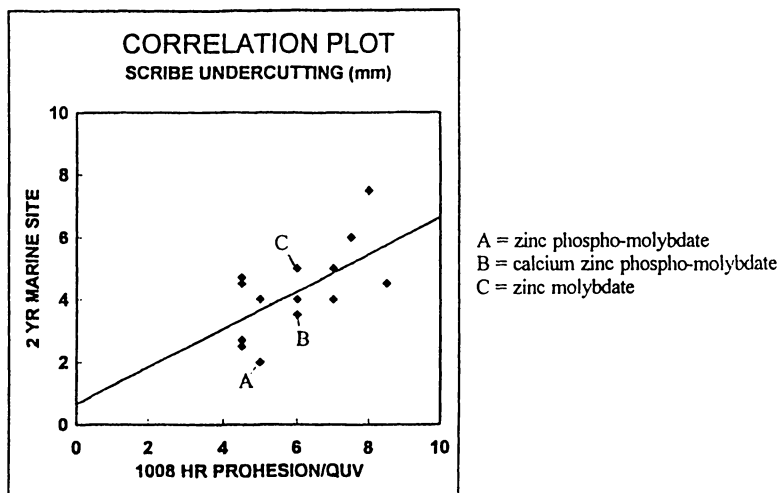


Figure 3 - Correlation Plot for Scribe Line Undercutting (mm)

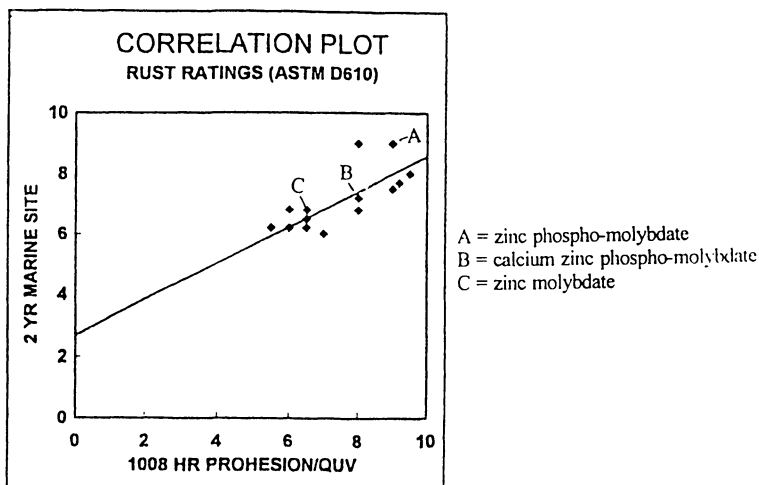


Figure 4 - Correlation Plot for Surface Rust Ratings (ASTM D610, 10=best)

Table 10 - Calculated Spearman Rank Correlation Coefficients for Prohesion/QUV

	<u>correlation coefficient</u>
scribe undercutting	0.88
surface rust	0.92

performance. These test results also demonstrated the performance advantages of the more recently developed phospho-molybdate pigment grades. In Figures 3 and 4, zinc phospho-molybdate (A) and calcium zinc phospho-molybdate (B) formulations can be seen to provide improved resistance to surface rust and scribe line corrosion versus the zinc molybdate (C) formulation.

Conclusions

Molybdates represent an important, field-documented alternative to lead and chromate based corrosion inhibitors. Newly developed phospho-molybdate pigments offer improved cost effectiveness versus earlier molybdate counterparts. Test methods base on cyclic salt-spray in combination with UV/condensation provide high degrees of correlation with outdoor exposure in the evaluation of anticorrosive pigment products.

References

- (1) "Performance of Molybdate Pigments in Primer Paints," D. R. Robitaille, unpublished report, 1978.
- (2) "Accelerated Test Method for Assessing Corrosion and Weathering of Paints for Atmospheric Corrosion Control," B. S. Skerry and C. H. Simpson, *CORROSION*, Vol. 49, No. 8, 1993, p. 663.
- (3) "A Report on SSPC Programs to Research Performance Evaluation Methods," S. K. Boocock, *JPCL*, Vol. 11, No. 10, 1994, p. 51.
- (4) "Correlation of Accelerated Exposure Testing and Exterior Exposure Site," Cleveland Society of Coatings Technology Technical Committee, *JCT*, Vol. 65, No. 837, 1994, p. 49.

Nontoxic Spinel-Type Pigments in Anticorrosive Coatings

A. Kalendová¹, J. Snupárek², and P. Kalenda¹

¹Departments of Paints and Organic Coatings and ²Synthetic Polymers and Resins, Institute of Polymeric Materials, University of Pardubice, 532 10 Pardubice, Czech Republic

The present paper is directed to replacing the toxic anticorrosive pigments based on chromium(VI) and lead compounds by new advanced pigments showing no harmful effects. These new pigments consist of spinels, the preparation of which runs via a method used in the preparation of high-temperature pigments. By the isomorphous exchange reaction comprising bivalent Mg, Ca, and Zn elements and trivalent Fe and Al elements the following element combinations were used: Mg-Zn-Fe, Zn-Fe-Al, Ca-Zn-Fe, Ca-Mg-Fe, and Zn-Mg-Ti. In order to examine the anticorrosive properties the individual pigments prepared were added to epoxy, alkyd, and styrene-acrylate coating compositions. Not only the anticorrosion efficiencies but also the mechanisms of action of the pigments were followed. The results achieved showed that the spinel-type pigments could be a good replacement for hitherto usual ecologically harmful pigments.

A majority of metallic and nonmetallic materials, the production of which is steadily rising, are exposed during their application to ever increasing mechanical and chemical strain, which entails their premature deterioration and loss of lifetime. A considerable fraction of such premature deterioration effects can be ascribed to corrosion, which is actually a damage of the material due to chemical or physicochemical influences. The most universal way of protection from corrosion consists in applying organic coatings to the respective material surface. The development of new protection systems based on organic coatings and their application are affected by a number of factors, the most important ones being at present those related to environmental acceptability and low energy consumption. In the early days of ecological consciousness the attention was primarily focused on volatile organic solvents present in coating compositions. At present the coating compositions as a whole are addressed, special attention being directed to toxic anticorrosive pigments, mainly those based on Pb and insoluble chromate compounds. The current-time task is devoted to the investigation of such anticorrosive pigments which are considered harmless from the environmental point of view and, at the same time, highly efficient in their corrosion-inhibitive power.

Protection against Corrosion Using Organic Coatings

Pigmented organic coatings, which do not contain any corrosion-inhibitive matter (an anticorrosive pigment or organic corrosion inhibitor) can exhibit only the so-called barrier effect if attacked by corrosion-initiating species. This effect is, to a large extent, connected with the nature of chemical binder, the size and shape of pigment particles, the additive content and, eventually, with the fractions of individual components being present in the coating formulation. The protective power secured by the barrier mechanism alone would be low in the case of organic coatings. Therefore, securing the long-term protection of metal surface with respect to the corrosion effects requires to combine the barrier mechanism with an inhibition mechanism. A further prerequisite of securing the long-term protective power of the coating comprises the study/knowledge of the adhesion mechanism. The necessary precondition for appearance of corrosive action comprises the presence of an electrolyte at the metal surface. A basic prerequisite from the angle of the protecting coating for a high protective efficiency involves a high resistance performed by the coating towards diffusion and penetration of the surrounding medium. The components of the surrounding medium - solutions of electrolytes, water, and gases are supposed to penetrate via diffusion processes through the organic film towards the metal surface. When the metal substrate has been, prior to coating, contaminated with soluble salts then below the coating layer corrosion processes are running, which result in deteriorations of the covering coating film so as in disturbing the metal substrate. At present no organic coating is known which alone would be absolutely impermeable for water and aqueous solutions. As far as a binder exhibits a high barrier efficiency then its protective function can be improved by means of corrosion inhibitors (1-8). Among the corrosion inhibitors both inorganic and organic compounds can be found.

Penetration of water through the organic coating can run via two mechanisms. The principal and also determining mechanism consists in diffusion processes running at the molecular level. The other mechanism involves penetration of aqueous solutions and water through pores and channels formed in the films during the drying processes (9-11). Penetration of surrounding water through the coating is accompanied with a reduction of adhesion between the coating and the substrate metal. The loss of adhesion results in appearance of osmotic blisters containing electrolyte solution. In the blisters electrochemical processes are running under simultaneous corrosion processes in the electrolyte. The osmotic blisters reduce significantly adhesion of coating to substrate metal (12). The barrier effect, which characterizes primarily the protection mediated by nonpigmented coatings, is also in a direct relation to the coating-film thickness.

Classification of Pigments Active from the Reduction of Corrosion Point of View

Generally, the anticorrosive pigments can be divided, according to their action, to the following classes:

- pigments acting in terms of the barrier mechanism - the pigments characterized by a flake-like structure increasing the diffusion path of the medium to the substrate surface;
- pigments showing inhibitive activity with respect to corrosion - the pigments reacting with the binder, metal substrate, or diffusing medium in terms of giving compounds acting as inhibitors (13);
- pigments showing electrochemical activity - the pigments provide a cathodic protection to the metal substrate.

Effective protection of metals with respect to the corrosion requires that the coating compositions contain anticorrosive pigments (14, 15). At present when the chromate and lead pigments (zinc yellow, zinc tetraoxychromate, strontium chromate, red lead, lead suboxide, and calcium plumbate) were abandoned with respect to ecological and toxicological reasons the phosphates have become the most frequently used pigments.

Also, phosphates have been the first anticorrosive pigments of nontoxic nature. Anticorrosive phosphate pigments are at present available in three development types, which differ from one another in their structures, cations contained (16), and also efficiencies (zinc phosphate, modified phosphates, and condensed phosphates).

Spinel-Type Pigments. The spinels involve a large group of double metal oxides characterized by a general formula AB_2X_4 and a crystal structure similar to that of the natural spinel mineral, which is a magnesium aluminate ($MgAl_2O_4$). These mixed metal oxides are solid solutions or compounds consisting of two or more metal oxides (17). The spinel lattices are rather stable, and the oxides showing this structure are characterized by high thermal and chemical stabilities and a high refractive index. A new compound is formed on the base of the isomorphous substitution principle in the basic spinel structure when a minor or total parts of the original cations are replaced with other cations without a change in the original structure. In such a way it is possible to affect some properties, the structure and basic properties remaining unchanged. Based on A, B and X ions, the spinels can be divided into three categories as follows: 2-3, 4-2, and 6-1 types with oxygen as the most usual anion (cf. Table I).

Table I. Types of Spinel Compounds

Type	A ions	B ions	X ions	Examples
2-3	A^{2+} : Mg, Ca, Zn Mn, Ni	B^{3+} : Al, Fe, Cr	X^{2-} : O, Se	$MgAl_2O_4$, $ZnFe_2O_4$, $MgFe_2O_4$
4-2	A^{4+} : Sn, Ti, Mn	B^{2+} : Mg, Zn, Mn	X^{2-} : O, S	$TiZn_2O_4$
6-1	A^{6+} : W, Mo	B^+ : Li, Na, Ag	X^{2-} : O	$MoAg_2O_4$

The first 2-3 type, with oxygen anions, is the most common and colorful spinel pigment category used in the ceramic and plastic industries (17). As a replacement of standard anticorrosive pigments of the equal activity but without harmful effects the spinel-type ferrites $MeFe_2O_4$ or mixed metal oxides show to be prospective candidates (18-19). The appropriate cations for the use in anticorrosive spinel-type compounds comprise Zn, Mg, and Ca.

Effect of Polymeric Binders on the Inhibitive Efficiency of Coatings. An appropriate formulation of the protective coating creates a general protection by increased life expectancy of the operational coating on the substrate. A key component determining the coating quality is the polymer matrix. No protective high-quality system can be obtained if no anticorrosive high-quality pigment is used in a combination with a high-quality binder. Properties of the binder, such as hydrolytic stability, chemical resistance (20), glass-transition temperature, cross linking degree, and polymer purity in certain limits are the parameters affecting principally the functional properties of coating.

For determining the anticorrosive efficiency of newly developed pigments the coating compositions containing an alkyd ethylene glycol-fumarate resin, epoxy-type resin, and water-dilutable dispersion of styrene-acrylate copolymer were prepared. All the samples contained in addition to the anticorrosive pigment also a filler and inert pigments so as further additives required to give a high-quality film. The compositions prepared were coated on test steel (220x50x0.8 mm) sheets using the standard type depositing bar (applicator for producing uniform films of paints, Byk.-Labotron, D), the test sheets had been subjected to sand-blasting and degreasing procedures. The samples thus processed were conditioned for 30 days at a temperature of 23 ± 2 °C and a relative humidity of $50 \pm 5\%$ prior to starting the corrosion tests.

Table II describes the characteristic properties of the binder used in the present paper for investigating the effects of spinel-like pigments. Tables IIIa, IIIb, and IIIc contain the formulation data for individual anticorrosive coating compositions, completed with the values of non-volatile contents, PVC, CPVC, and Q parameter(=100.PVC/CPVC) and information on the suppliers of raw materials.

Table II. Characteristic Properties of the Binders Used

<i>Binder resin</i>	<i>Properties of the coatings obtained</i>				
	<i>chemical resistance</i>	<i>UV-radiation resistance</i>	<i>watertightness</i>	<i>heat resistance</i>	<i>ecological harmless.</i>
alkyd	-	+	o	-	o
acrylate (latex)	-	+	o	-	+
epoxy	+	-	+	o	+

Key: + = very good, 0 = insignificant, - = poor; * aromatic epoxy type

Table IIIa. The Formulation of Alkyd-Based Coating Composition Used

<i>Components</i>	<i>Amount (wt.%)</i>
anticorrosive pigment	5.00
ferric oxide ¹	18.20
*CHS-Fenalkyd KLD ²	36.90
Co-octoate 5% ³	0.25
Ba-octoate 2% ³	0.94
Ca-octoate 4% ³	0.31
Millicarb ⁴	6.20
Plastorit ⁵	18.19
mineral spirit	3.85
xylene	9.98
Siloxid ⁶	0.17
solid content (vol.%): 70	1 Precheza a.s. Přerov, CZ
PVC (%): 34	2 Spolchemie a.s., Ústí n. L., CZ
CPVC (%): 57	3 Setuza a.s., Lovosice, CZ
Q (%): 60	4 Omya GmbH, Köln, D
	5 Naitsch Mineralwerke, A
	6 Silchem s.r.o. Neštětice, CZ

Table IIIb. The Formulation of Epoxy-Based Coating Composition Used

<i>Components</i>	<i>Amount (wt.%)</i>
<i>Component A:</i>	
anticorrosive pigment	5.0
zinc oxide ¹	13.56
Blanc-fixe ²	43.36
ferric oxide, black ³	0.73
butanol	1.37
^b ChS Epoxy 1/33 (60%) ⁴	18.28
Melform ⁴	12.18
xylene	5.51
<i>Component B:</i>	
hardening agent Telalit 150 ⁴	100 A : 50 B
solid content (vol.%): 80	1 Slovliak a.s., Košeca, SR
PVC (%): 34	2 MCHZ a.s., Ostrava, CZ
CPVC (%): 56	3 Precheza a.s., Přerov, CZ
Q (%): 60	4 Spolchemie a.s., Ústí nad Labem, CZ

Table IIIc. The Formulation of Styrene-Acrylate-Based Coating Comp. Used

<i>Components</i>	<i>Amount (wt.%)</i>
anticorrosive pigment	5.47
ferric oxide, red ¹	8.66
Millicarb ²	26.48
Dehydran 1293 ³	0.17
Aditol XW 330 ⁴	0.26
Preventol D6 ⁵	0.09
water	8.89
^c Sokrat 2403 LX ⁶	44.17
butylene glycol acetate	1.71
Latekol D/25% ⁷	3.42
Butrol 35 ⁸	0.98
solid content (vol.%): 65	1 Precheza a.s. Přerov, CZ
PVC (%):23	2 Omya GmbH., Köln, D
CPVC (%):46	3 Henkel KGaA, Düsseldorf, D
Q (%):50	4 Vianova, Vien, A
	5 Bayer AG., Leverkusen, D
	6 CHZ a.s. Sokolov, CZ
	7 Eastman Chemical, CH
	8 BASF, D
	9 Buckman Laboratories, Gent, Belgie

¹Fenalkyd KLD/50 LBX; a product of the Spolchemie, a.s. (Ústí nad Labem, Czech Republic), a solution of glycerol modified with fatty acid of linseed and tung oil and alkyd-formaldehyd resin.

^bChS Epoxy; epoxy resin of a medium molecular weight (50% solution in an 1:1 isopropyl alcohol-toluene mixture, a product of the Spolchemie, a.s.(Ústí nad Labem, Czech Republic).

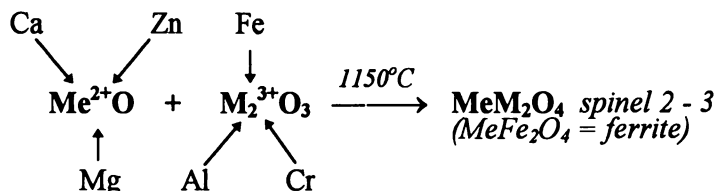
^cSokrat 2403 LX; an aqueous dispersion of styrene-acrylate copolymere, a product of CHZ a.s. (Sokolov, Czech Republic).

Preparation of the Spinel-Type Pigments. As the spinel-type pigments there have been prepared the compounds using possibility of isomorphous substitution in a spinel lattice of the bivalent magnesium ion by bivalent ions of other elements. Similarly, the trivalent aluminum ions can also be replaced by trivalent ions of other elements.

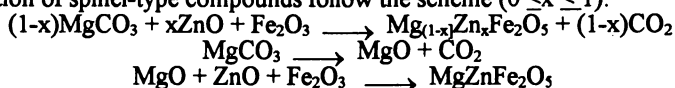
These pigments representing a group of high-temperature inorganic pigments were prepared using a procedure which consists of synthesizing a structure stable at high temperatures. The procedure is determined or influenced by a number of thermodynamic and kinetic factors (such as the Hedvall magnetocatalytic effect and the Tamann temperature). The spinel structure is formed at high temperatures via solid-phase reactions. The process of preparing the pigments consists of 4 operational steps:

- **Homogenization of starting compound mixtures.** In this stage of preparation the starting materials are not only mixed intimately, but the starting substances are also subjected to mechanical/chemical activations, where the reactivities are increased by increases in the contact area.
- **Calcination procedure.** The calcination is accomplished via a nonisothermal furnace/calcination process run in an electric resistance furnace operated in a temperature range of 1100 to 1150°C, as derived from the DTA results. In the first stage the starting materials comprising the respective metal carbonates and hydroxides undergo a decomposition process; in the second stage the oxides thus formed react with one another giving the final product.
- **Leaching the calcination products by washing with water**
- **Adapting the product** to obtain the size of particles as necessary by a wet grinding process using a vibration ball mill for about 60 hours.

The preparation of 2-3 type spinels can be represented by the following simplified equation:



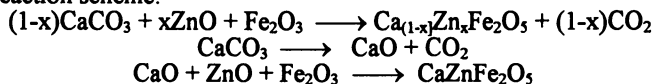
Preparation of the Mg-Zn-Fe-Type Spinel. The starting materials for the preparation contained the appropriate metal carbonates and oxides: MgCO_3 , ZnO , and red Fe_2O_3 . The calcination temperature was kept at 1150°C . The reactions leading to the formation of spinel-type compounds follow the scheme ($0 \leq x \leq 1$):



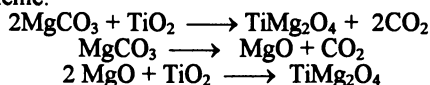
Preparation of the Zn-Fe-Al-Type Spinel. The starting materials contained Al_2O_3 , ZnO , and red Fe_2O_3 . The calcination temperature was kept at 1140°C . The reaction leading to the formation of the spinel-like compounds runs in agreement with the equation:



Preparation of the Ca-Fe-Zn-Type Spinel. The starting materials for the syntheses contained CaCO_3 , Fe_2O_3 , and ZnO . The calcination temperature was kept at 1150°C . The preparations of the spinel-type compounds run in agreement with the following reaction scheme:



Preparation of the Zn-Mg-Ti-Type Spinel. The starting materials for the syntheses contained MgCO_3 , TiO_2 , and ZnO . The calcination temperature was kept at 1150°C . The preparations of the spinel-type compounds run in agreement with the following reaction scheme:



Methods of Testing the Anticorrosive Pigments.

For testing the properties of spinel-like pigments prepared the model coating compositions were formulated using the polymers given in Table II as binders. The activities of spinels as inhibitors were tested by using accelerated laboratory-scale procedures for determining the corrosion resistance (the so called direct methods). Certain characteristic properties of individual spinels (as the pH values of aqueous extracts, the content of water-soluble matters, the densities, and the Critical Pigment Volume Concentration values, as necessary for formulating the coating compositions) were measured. The parameters characterizing an inorganic pigment-organic binder system, given as the CPVC were determined by measuring the binder consumption by a gravimetric method under standard conditions defined in an appropriate ISO CSN standard. Further a series of measurements were done starting with the so called indirect methods (21, 22) for evaluating the corrosion effects (used for describing the action mechanisms of anticorrosive pigments). Table IV gives some characteristic properties of individual spinels prepared.

Table IV. Results of Evaluating Some General Physicochemical Properties of the Synthetized Pigments

<i>Pigment</i>	ρ [g.cm ⁻³]	<i>pH value in the extract</i>	<i>Water-soluble parts [%].10³</i>	<i>CPVC [%]</i>
Zn - Mg - Fe type				
ZnFe ₂ O ₄	5.110	8.2	10.60	56.6
MgFe ₂ O ₄	4.577	10.3	119.80	48.4
Zn _{0.8} Mg _{0.2} Fe ₂ O ₄	4.961	10.4	29.54	55.8
Zn _{0.2} Mg _{0.8} Fe ₂ O ₄	4.761	10.2	41.04	56.8
ZnMgFe ₂ O ₅	4.416	10.3	90.51	43.8
Ca - Mg - Fe type				
CaFe ₂ O ₄	4.259	10.2	160.90	43.2
Ca _{0.4} Mg _{0.6} Fe ₂ O ₄	4.184	11.0	127.17	44.7
CaMgFe ₂ O ₅	3.874	10.5	130.20	40.4
Ca - Zn - Fe type				
Ca _{0.3} Zn _{0.7} Fe ₂ O ₄	4.695	10.9	140.50	54.2
Al - Fe - Zn type				
ZnAl ₂ O ₅	3.445	8.7	118.43	63.1
Ti - Zn - Mg type				
Ti ₂ MgO ₅	3.823	9.0	110.92	54.6
TiMgZnO ₄	4.485	7.8	101.15	67.3

Accelerated Corrosion Tests. (a) Accelerated corrosion tests run in a condensation chamber operating with SO₂-containing atmosphere with condensing water vapor at a temperature of 35±1°C (the so-called humidity test). The testing conditions were adapted according to the appropriate ISO standard. The sample exposure conditions were adjusted as a continuous cycle taking 1000 h for the alkyd-binder samples and 500 h for the styrene-acrylate binder ones.

(b) Accelerated corrosion tests run in a salt spray chamber operating with a NaCl solution at 35±2°C. (the so called salt spray test). The testing conditions were adapted according to ISO CSN 1227 standard. The 5% NaCl spray exhibited a neutral pH value. The sample exposures were adjusted as a continuous cycle taking 800 h for the alkyd binder systems and 400 h for the styrene-acrylate ones.

Microscopic Determination of the Diffusion of Corrosive Media into Coating Films. The diffusion methods of investigating the anticorrosive pigments start with existence of barrier effects and binding the aggressive compounds penetrating the organic coating. The diffusion of corrosively active compounds into the epoxy coating samples prepared was treated mathematically using an expression going out of the base diffusion equation (the Fick law II), which formulated for the diffusion in *x*, *y*, *z* axes-directions reads as follows:

$$\frac{\partial c}{\partial t} = D \frac{\partial^2 c}{\partial x^2} + D \frac{\partial^2 c}{\partial y^2} + D \frac{\partial^2 c}{\partial z^2};$$

Adapting and simplifying procedures applied to the basic equation result in the Einstein formula for calculating the diffusion coefficient:

$$D = \frac{x_0^2}{\pi \cdot t};$$

where *D* is coefficient of diffusion [mm².s⁻¹]; *t* is time [s]; *x*₀ is the depth of diffusion [mm].

Microscopic investigation of the diffusion of aggressive acid medium into pigmented films consisted in measuring the depth of penetration of the medium. When a suitable form of test pieces was used the condition of diffusion in a single direction was satisfied, and the diffusions along the y and z axes could be disregarded (23). The depth of diffusion can be measured microscopically as a function of time, the time being considered as the time of exposure of the samples to the corrosive medium being investigated.

Determination of the Corrosion Inhibitive Activity of Coatings. (a) Determination of the losses by corrosion obtained from steel samples in aqueous extracts of stripped coating films or individual anticorrosive pigments

The testing procedure comprised an aqueous extract of stripped coating films or, occasionally of pigmented powders. The testing steel samples of precisely defined dimensions were exposed to a system consisting of a water and 10 wt.% stripped film (cut in pieces) for a definite time period, the corrosion products formed being afterwards removed by treating the sheets with a standard pickling agent. The experimental results processed mathematically can give the quantities characterizing the weight losses caused by corrosion effects such as :

$$K_m = \frac{(m - m_1) \cdot 10^4}{S}$$

K_m - the loss of weight per a surface unit due to the corrosion [g/m^2]

m - the weight of clean metal sheet [g]

m_1 - the weight of the sheet after the exposure [g] and

S - the surface area of the sheet [cm^2]

(b) Determination of pH values and water-soluble matter in aqueous extracts of the coating films. The data thus obtained can give information on the mechanisms of anticorrosive pigments applied to coating films. The measurements were done by using 10% stripped coating films suspended in redistilled water.

Anticorrosive Actions of Spinel in Coatings

Let us start with the assumption that the primary cause of corrosion at the metal substrate under the protective coating consists in the penetration of surrounding medium through the heterogeneous film created by a polymer matrix with pigment particles which are usually of inorganic nature. From this point of view we can appreciate the importance of the study of transport processes comprising water and corrosive acidic media into the coatings pigmented with spinel pigments.

All the binders pigmented to a variable PVC (Pigment Volume Concentration) with spinel like pigments showed a similar behavior for the penetration of acidic (1.0M HCl, 0.5M H_2SO_4 , and 1.0M CH_3COOH) medium through the coating. The curves obtained indicate that the diffusion of water through the coating layer depended not only on the kind (defined by chemical composition) of the pigment, but also the pigment volume concentration in the system. Titanium dioxide, which was used as a representative of inert towards acid media pigments, showed a rising coefficient of diffusion, which entails a higher degree of penetration of coating by the medium and, eventually, a reduction of corrosion resistance of the system as a whole.

Figure1 depicts the influence of the pigment volume concentration on the diffusion coefficient for various spinel-type pigments. The curve/development dependence shows how the cations present in the spinel-crystal lattice affect the transport of acidic medium into the epoxy resin-based coating film. The CPVC values of all the pigments tested lie in a range of 45-55 vol.% and it can be concluded that at such a pigment concentration a sharp growth can be observed for the diffusion of liquid medium. The PVC = 40vol.% value is an optimum condition for the minimum diffusion of liquids into the coating films.

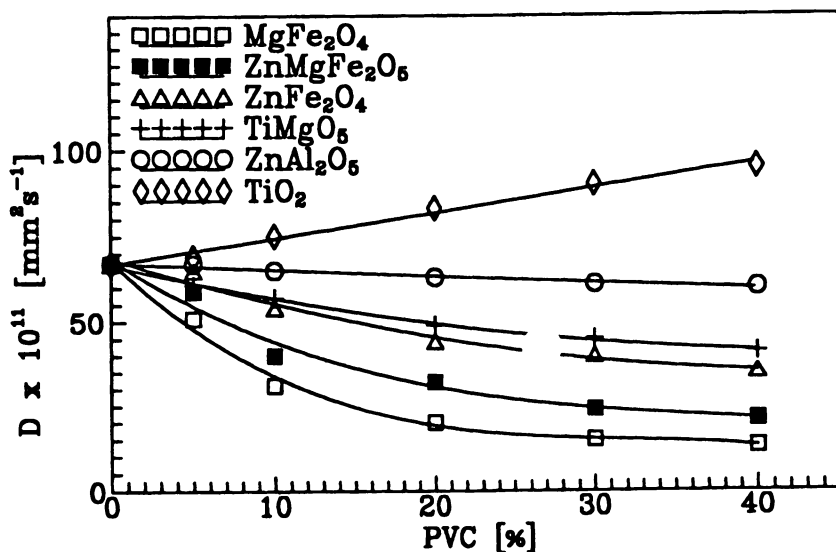


Figure 1. PVC Dependence of the Coefficient of Diffusion (D) for Various Media Diffusing into the Coatings Characterized by the Respective PVC Values.

Quite generally, the transport phenomena take part in all corrosion processes, and the appropriate pigmentation can reduce the diffusion of medium and thus prevent appearance of the primary corrosion cause. The capacity to neutralize the penetrating substances protects also, to a certain extent, the binder, by stopping chemical attacks on the molecular chain thereof.

Based on the results obtained a model situation can be assumed, according to which at the surface of spinel pigment particles the salts (of appropriate acids) are formed. This eliminates the chemical diffusion component. Also, an important role is here played by the degree of wetting of the pigment particle by the organic binder. An objective representation of the diffusion of corrosive media at the pigment/binder interface for both inert and reactive (spinel-type) pigment is given in Figure 2.

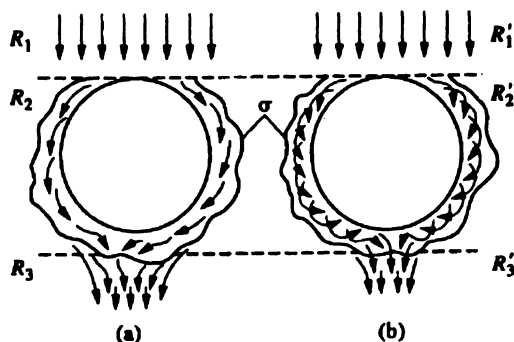


Figure 2. Scheme of Diffusion of Corrosive Media at the Pigment/Binder Interface; (a) Inert Pigment, (b) Reactive Pigment.

In the first stage the physical diffusion through the coating takes place, the diffusion running at a rate R_1 . At a moment when the diffusion field contacts an inert pigment (TiO_2) particle a change in the rate of diffusion takes place to a rate R_2 , which is determined by the degree of wetting of the pigment achieved during the dispersion process. The pigment particles act in this case as heterogeneities at a rate of diffusion $R_2 \gg R_1$. If we consider the diffusion running only in one direction (along axis \bar{x}) the rate of diffusion R_3 will be higher than or equal to the rate R_1 . If spinel-type pigments are used then in the phase of diffusion $R_1 = R_1$. On contacting a reactive spinel and an acidic medium the reaction to the appropriate salt will take place, which also binds several water molecules. The particle surface becomes afterwards a coating consisting of these reaction products, which considerably reduces the diffusion process for the original medium. The rate of diffusion $R_2 \ll R_2$.

Formation of Metal Soaps. The spinel-type pigments are also capable of reacting with the carboxyl binder groups, which results in the formation of metal soaps. The reactions are similar to those encountered with red lead (lead orthoplumbate), a standard anticorrosive pigment, however with significantly higher toxicity. The formation of metal soaps can considerably reduce the tendency to saponification exhibited by the binder concerned, a reaction, in which primarily the hydroxyl ions produced by the corrosion processes and also the outside media diffusing through the film take part. Also, the anticorrosive activity of the metal soaps formed does not seem to be negligible (24).

The formation of metal soaps becomes evident from the hardness values, which increase with the time. Figure 3 shows the hardness values of coatings changing with the time of hardening (method PERSOS) for an alkyd resin-based coating composition (the binder is a maleinized alkyd with an acid number of 159) pigmented to a PVC value of 30 % using either titanium dioxide or zinc or calcium ferrite. The formation of metal (both calcium and zinc) soaps can be deduced indirectly from the time dependence of growing hardness of the alkyd films. All the samples were desiccated in presence of constant amounts of Co^{2+} , Ca^{2+} , or Ba^{2+} -based siccatives. Due to the fact that the hardness of coatings pigmented with TiO_2 is lower than that of those pigmented with spinel-type pigments the formation of the zinc and calcium soaps can be supposed to take place.

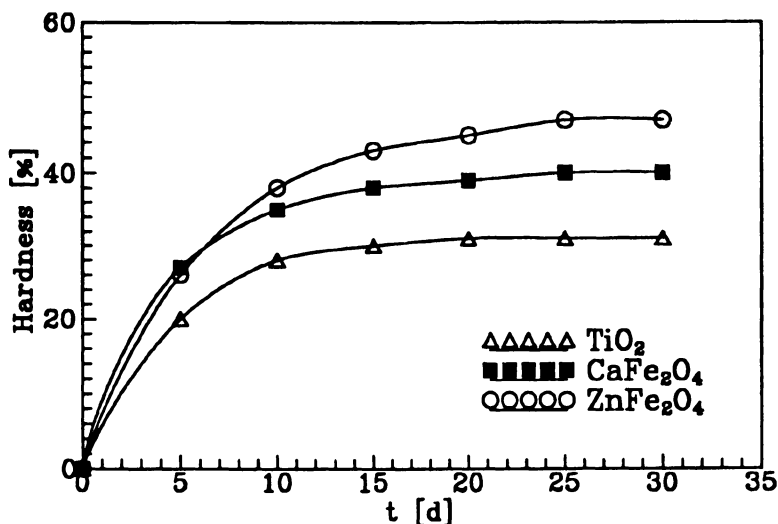


Figure 3. Time Dependence of Hardness of the Film.

Results of the Corrosion Resistance Tests Performed with the Coatings Containing Spinel-Type Pigments. The efficiencies of synthesized spinel pigments with respect to anticorrosive activities were evaluated by the two testing procedures: that working in an SO₂-containing atmosphere (35±1°C and 100 % relative humidity) and that working in the NaCl-fog atmosphere (35±2°C and 5 % NaCl spray).

The results obtained were to be objectively evaluated and quantified to get the form of clear and demonstrable data. Using the method of evaluating the corrosion effects by appropriate standard procedures several parameters were determined: osmotic blisters having appeared at the coating surface with respect to size and frequency, corrosion at a scratch (of the cross form) in the coating, and surface corrosion of the substrate. ASTM D 714-87 Method classifies the osmotic blisters formed to groups defined by the sizes designated by 2, 4, 6 and 8 values (2 denoting the highest size, 8 the lowest size). To the blister size an information is attached giving the respective frequency of appearance. The highest frequency of appearance is designated as D (denoting dense), a lower one as MD (denoting medium density) and as F (denoting few). This approach can give a series starting with a surface showing the lowest corrosion attack by few osmotic blisters of small size up to dense large-size blisters. ASTM D 1654-92 Method describes a procedure evaluating the extent of corrosion appearing along a cut line and the „subsurface“ corrosion appearing under the coating in the cut-line vicinity. ASTM D 610-85 Method: By means of this method the results obtained can be compared to appropriate standards. The standards are related to the corrosion degree at the surface under the protective coating. The result is defined as a certain degree of the substrate-surface corrosion given in %. Tables V-VII give some results of the tests performed.

Table V. Results of the Humidity Test (ASTM D 1654-92)

<i>Pigment</i>	<i>Corrosion in a scratch [mm]</i>	<i>Frequency and size of blisters [degree]</i>	<i>Corrosion of substrate [%]</i>
Alkyd resin - based coating composition			
ZnFe ₂ O ₄	0	8F	0.03
MgFe ₂ O ₄	2 - 3	8MD	10
Zn _{0.8} Mg _{0.2} Fe ₂ O ₄	0 - 0.5	8M	0.1
Zn _{0.2} Mg _{0.8} Fe ₂ O ₄	0.5 - 1	8F	0.3
ZnMgFe ₂ O ₅	0 - 0.5	8F	0.3
CaFe ₂ O ₄	7 - 10	4MD	16
Ca _{0.4} Mg _{0.6} Fe ₂ O ₄	0.5 - 1	4M	10
CaMgFe ₂ O ₅	2 - 3	4M	16
Ca _{0.3} Zn _{0.7} Fe ₂ O ₄	1 - 2	4M	10
ZnAl ₂ O ₅	7 - 10	4MD	33
Ti ₂ MgO ₅	0 - 0.5	8M	1
TiMgZnO ₄	0 - 0.5	8M	3
Aqueous styrene-acrylate dispersion - based coating composition			
ZnFe ₂ O ₄	0	8F	0.03
MgFe ₂ O ₄	0 - 0.5	8MD	0.1
Zn _{0.8} Mg _{0.2} Fe ₂ O ₄	0 - 0.5	8F	0.1
Zn _{0.2} Mg _{0.8} Fe ₂ O ₄	0.5 - 1	8F	0.1
ZnMgFe ₂ O ₅	0 - 0.5	8F	0
CaFe ₂ O ₄	7 - 10	8F	16
Ca _{0.4} Mg _{0.6} Fe ₂ O ₄	0.5 - 1	4M	10
CaMgFe ₂ O ₅	2 - 3	8M	16
Ca _{0.3} Zn _{0.7} Fe ₂ O ₄	0.5 - 1	8M	10
ZnAl ₂ O ₅	7 - 10	4M	16
Ti ₂ MgO ₅	0 - 0.5	8M	0.1
TiMgZnO ₄	0 - 0.5	8M	3

Table VI. Results of the Salt - Spray Test (ASTM D 7654-92)

<i>Pigment</i>	<i>Corrosion in a scratch [mm]</i>	<i>Frequency and size of blisters [degree]</i>	<i>Corrosion of substrate [%]</i>
Alkyd resin - based coating composition			
ZnFe ₂ O ₄	0.5 - 1	8M	10
MgFe ₂ O ₄	1 - 2	8MD	16
Zn _{0.8} Mg _{0.2} Fe ₂ O ₄	0	10F	0
Zn _{0.2} Mg _{0.8} Fe ₂ O ₄	0.5 - 1	8F	10
ZnMgFe ₂ O ₅	0	10F	0
CaFe ₂ O ₄	7 - 10	4MD	33
Ca _{0.4} Mg _{0.6} Fe ₂ O ₄	2 - 3	4MD	16
CaMgFe ₂ O ₅	7 - 10	8MD	33
Ca _{0.3} Zn _{0.7} Fe ₂ O ₄	5 - 7	8MD	10
ZnAl ₂ O ₅	10 - 13	4D	33
Ti ₂ MgO ₅	0 - 0.5	4F	1
TiMgZnO ₄	0 - 0.5	8M	3
Aqueous styrene-acrylate dispersion - based coating composition			
ZnFe ₂ O ₄	7 - 10	8D	33
MgFe ₂ O ₄	5 - 7	8MD	16
Zn _{0.8} Mg _{0.2} Fe ₂ O ₄	2 - 3	8MD	10
Zn _{0.2} Mg _{0.8} Fe ₂ O ₄	5 - 7	8MD	16
ZnMgFe ₂ O ₅	7 - 10	8MD	33
CaFe ₂ O ₄	2 - 3	8MD	16
Ca _{0.4} Mg _{0.6} Fe ₂ O ₄	7 - 10	8MD	33
CaMgFe ₂ O ₅	0.5 - 1	6M	10
Ca _{0.3} Zn _{0.7} Fe ₂ O ₄	7 - 10	8MD	16
ZnAl ₂ O ₅	10 - 13	6D	33
Ti ₂ MgO ₅	7 - 10	8D	16
TiMgZnO ₄	10 - 13	8D	33

Table VII. Weight Losses (K) of Steel Samples Exposed to 10%. Suspensions of Coating Films in Water (for 10 Days)

<i>Pigment</i>	<i>K [g/m²]</i>	
	<i>Alkyd film</i>	<i>Styrene-acrylate film</i>
ZnFe ₂ O ₄	8.69	13.68
MgFe ₂ O ₄	3.96	10.96
Zn _{0.8} Mg _{0.2} Fe ₂ O ₄	8.81	10.73
Zn _{0.2} Mg _{0.8} Fe ₂ O ₄	9.58	11.47
ZnMgFe ₂ O ₅	8.27	18.37
CaFe ₂ O ₄	8.88	10.81
Ca _{0.4} Mg _{0.6} Fe ₂ O ₄	9.92	18.38
CaMgFe ₂ O ₅	8.19	16.27
Ca _{0.3} Zn _{0.7} Fe ₂ O ₄	10.63	15.54
ZnAl ₂ O ₅	15.55	15.38
Ti ₂ MgO ₅	18.22	10.16
TiMgZnO ₄	16.71	11.21

These tests give an image of appropriate effects of the individual pigments contained in the coatings as depending on the given corrosion environment. Tendency to higher formation of osmotic blisters in the film coating is low in the anticorrosive spinel-type pigments, which is connected to low contents of water-soluble matter in the pigments. The anticorrosive efficiency of spinels with respect to attacks taking place under film surface and the subsequent corrosion of the metal surface is high. It does not mean, however, that the pigments of this type reach a high efficiency in hindering the

surface corrosion taking place under the coating film due to blistering effects occurring at the organic coating. This is a difference to the chromate pigments. The corrosion and corrosion spreading in the vicinity of a cross cut give an evidence of the electrochemical action of anticorrosive spinel-type pigments. In the NaCl-containing atmosphere, $Zn_{0.8}Mg_{0.2}Fe_2O_4$, $ZnMgFe_2O_5$ and Ti_2MgO_5 (contained in the alkyd binder) and $CaMgFe_2O_5$ (contained in the styrene-acrylic binder) show to be the most effective pigments. In the SO_2 -containing atmosphere, $ZnFe_2O_4$, $ZnMgFe_2O_5$ and $Zn_{0.8}Mg_{0.2}Fe_2O_4$ (contained in the alkyd binder), and $ZnMgFe_2O_5$, $ZnFe_2O_4$ and Ti_2MgO_5 (in the styrene-acrylic binder) give the best corrosion protection results. As evidenced the results obtained from various tests can differ from one another. The corrosion-test results obtained in both SO_2 and NaCl media indicate the following combinations of Mg and Zn-based pigments as the best pigments: $Zn_{0.8}Mg_{0.2}Fe_2O_4$ resp. $ZnMgFe_2O_5$. The styrene-acrylate coating compositions withstand the corrosive atmospheres worse than the alkyd ones evidently due to the binder nature. Nevertheless, also here individual pigments were distinguished with respect to their protective action roughly in the same order as in the first case. The NaCl-containing atmosphere acts more intensely than the SO_2 -containing atmosphere as evidenced by the more severe substrate corrosion. Evaluations of the corrosion-induced losses observed for the steel sheets exposed to the media of aqueous extracts of free/stripped coating films give evidence of the possible reactions running in the organic coatings. The weight losses of steel samples having been exposed to aqueous suspensions containing 10% free coating films for 10 days are lower for the alkyd coating films than for styrene-acrylate films. It can be said that the weight loss observed for individual coating compositions drops with increases in pH of the aqueous extracts (and with a high content on water-soluble matter). The lowest weight loss was found with Ti_2MgO_5 resp. $Zn_{0.8}Mg_{0.2}Fe_2O_4$ as pigments.

Conclusions

Spinel-type pigments of the Mg-Zn-Fe, Ca-Mg-Fe, Ca-Zn-Fe, Al-Fe-Zn, and Ti-Zn-Mg series were prepared via high temperature synthesis procedure operating at a temperature of 1140-1150 °C. These pigments are compounds characterized by a medium density value, a low content of water-soluble matter, and a pH value of the aqueous extract in the alkaline region.

The corrosion-inhibiting properties have been verified by the accelerated corrosion tests in simulated corroding atmospheres and by indirect laboratory methods. The results obtained indicate that coating films of the alkyd-type modified with vegetable oils work on the principle of neutralization of the acidic binder components. The alkyds subjected to drying liberate the fatty acids present, which causes low pH values of the aqueous extracts of the binders concerned. These acids can accelerate the course of corrosion running under the organic coating. The data show clearly a high neutralizing power of a series of the spinel pigments having been developed. The pH values of extracts are, however, not at such a level to affect the properties of otherwise saponifiable binder and are, at the same time, appropriate to the manifestation of inhibition effects of the zinc, calcium, and magnesium soaps having been formed by the reaction of spinel with the acidic groups present in the binder. In epoxy resin-based protective films the anticorrosive effects of spinels are secured by the electrochemical action of cations on the metal substrate and by the active participation of spinels in the penetration of corrosive media through the film. It has been found that the diffusion of liquid and gaseous substances through the film pigmented with spinel-like compounds is lower than in absence of the pigments. This phenomenon explains why such anticorrosive pigments are active also in the binders of alkaline and neutral nature, wherein their neutralizing effects cannot manifest themselves. Also in the tests performed with styrene-acrylic binders no reactions between such a binder and a spinel-like pigment take place, and only effects of electrochemical nature and active participation of the pigment in diffusion of the medium through the film can be

considered. The corrosion tests performed with the prepared pigments allow to conclude that from the protection point of view the zinc and magnesium containing spinels appear to be more effective than the calcium-containing ones. The highest anticorrosion efficiency is shown by the pigments containing simultaneously Zn and Mg cations. The spinel-like pigments prepared and tested are prospective pigments with respect to their high anticorrosion activity and primarily with respect to the absence of any toxicity.

References

1. Fletcher, T. *Euro Coat* 1991, 9, 553.
2. Jackson, M.A. *Polym. Paint Col. J.* 1991, 180, 608.
3. Beland, M. *American Paint and Coatings J.* 1991, 76, 43.
4. Beland, M. *American Paint and Coatings J.* 1991, 76, 92.
5. Wleeshouwens, A.R. *Polym. Paint Col. J.* 1988, 178, 788.
6. Draper, P.A. *JOCCA* 1989, 68, 243.
7. Seavell, A.J. *JOCCA* 1992, 75, 293.
8. Kalenda, P. *Dyes and Pigments* 1993, 23, 215.
9. Carter, E. *Polym. Paint Col. J.* 1981,
10. Leiheiser, H.JR. *Corrosion*, 1982, 38, 374.
11. Kalenda, P.; Kalendová, A. *Dyes and Pigments* 1995, 27, 305.
12. Kalendová, A.; Kalenda, P. *Kor. Ochr. Mater.* 1994, 38, 81.
13. Ruf, J. *Korrosion Schutz durch Lacke und Pigmente*, Verlag W.A.Colomb, 1972 pp 73-74.
14. Šrank, Z. *Chem. Prum.* 1990, 40, 190.
15. Jackson, M.A. *Polym. Paint Col. J.* 1984, 174, 281.
16. Kalendová, A.; Šňupárek, J.; Kalenda, P. *Dyes and Pigments* 1996, 30, 129.
17. Ullman's Encyclopedia of Industrial Chemistry, „Pigments, Inorganic“, Vol. A20; VCH, 1992, pp 308.
18. Kresse, P. *Farbe & Lack* 1977, 83, 85.
19. Kalendová, A.; Kalenda, P.; Šňupárek, J. *Nichttoxische antikorrosive Pigmente vom Spineltyp, XXIII. FATIPEC Congress, Brussels 10.-14.June 1996, Book of conferences volume D*, pp 134-142.
20. Kalenda, P. *J.Appl. Pol. Sci.* 1992, 45, 2235.
21. Melville, I.; Simpson, L.A. *JOCCA* 1989, 72, 434.
22. Kalendová, A. *Kor. Ochr. Mater.* 1996, 40, 8.
23. Doležel, B. *Chem. prům.*, 1957, 7, 447.
24. Goldie, B.P.F. *JOCCA* 1988, 71, 257.

Anticorrosion Organic Coatings Prepared from Aniline Oligomers and Their Epoxy-Cured Derivatives

Yen Wei¹, Chuncai Yang¹, Jui-Ming Yeh¹, Tianzhong Ding¹, Gu Wei¹,
Danliang Jin¹, Jianguo Wang^{1,3}, Xinru Jia^{1,4}, and Susan A. Jansen

¹Department of Chemistry, Drexel University, Philadelphia, PA 19104

²Department of Chemistry, Temple University, Philadelphia, PA 19122

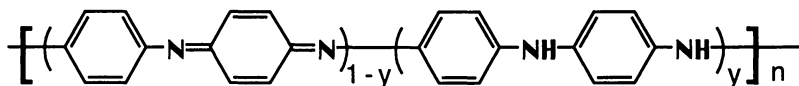
Aniline trimers and higher oligomers with primary amine as end-groups have been prepared by a simple, one-step oxidation of aniline or substituted anilines in the presence of 1,4-phenylenediamine with ammonium persulfate as oxidant in acidic media. Similar to conventional polyaniline, the emeraldine base of the oligomers offers good corrosion protection as coatings on cold rolled steel based on electrochemical measurements of corrosion potential, polarization resistance and corrosion current in aqueous 5 wt% NaCl electrolyte. Both the trimers and the higher oligomers can be used as crosslinking agents for curing epoxy resins to afford new epoxy polymer systems. The trimer- and oligomers-cured epoxy coatings on CRS all exhibit excellent electrochemical anticorrosion effects.

Currently, one of the standard industrial practices against metal corrosion is to treat and/or coat the surface of metals with chromium-containing compounds. However, the concern on the known adverse health and environmental effects of the chromium compounds is ever increasing. In the past decade, the use of electroactive organic polymers as corrosion inhibiting coatings has been explored for the potential replacements of chromium-containing materials (*1-11*). One of the most interesting electroactive polymers is polyaniline because it can be readily prepared by oxidative polymerization of inexpensive aniline and has a relatively good solubility for solution-coating applications (*12,13*).

³Current address: DuPont Central Research, Wilmington, DE 19880.

⁴Current address: Chemistry Department, Peking University, Beijing 100871, China.

The structures of polyaniline in base form can be schematically represented by the following formula(13):



The oxidation state of polyaniline is determined by the y values. Pernigraniline is the completely oxidized form with $y = 0$, whereas leucoemeraldine is the fully reduced form ($y = 1$). Emeraldine contains an equal fraction of both reduced and oxidized forms ($y = 0.5$). Upon doping with a protonic acid (e.g., hydrochloric acid), the emeraldine base (EB) exhibits a moderate electric conductivity (e.g., 10 S/cm) (13). Recently, we reported that the non-conductive base form of polyaniline as coatings on cold rolled steel (CRS) offers good corrosion protection based on the electrochemical measurements under various conditions (10). The results obtained by us and by others suggest that the observed corrosion protection by the polyaniline base may not originate merely from the physical barrier effect of the coatings (5,9,10). Since small amine compounds have long been used as corrosion inhibitors (14), we became interested in the use of the oligomers of aniline as the active materials for coating applications. Oligomeric aromatic amines with amino groups at both ends are of particular interest in polymer science and industries because of their applications as monomers to prepare polyamides, polyimides and epoxy polymers. However, the synthesis of amino-terminated oligomers of aniline via conventional routes is often very complicated, if it is possible at all. *N,N'*-Bis(4'-aminophenyl)-1,4-phenylenediamine, a reduced form of *N,N'*-bis(4'-aminophenyl)-1,4-quinonediimine, was synthesized by catalytic hydrogenation of *N,N'*-bis(4'-nitrophenyl)-1,4-phenylenediamine (15) and was used as a trimer of aniline in elucidating the structure-semiconductivity relationship of the aniline oligomers (16,17). Gebert et al. (18) developed another method to prepare this oligomer in order to use it as a building block in their attempt to achieve a total unambiguous synthesis of polyaniline via Schiff base chemistry. Both methods involve multiple synthetic steps and reduction of the nitro groups in the precursors. Hence, it is difficult to generalize these methods in the synthesis of its derivatives and for industrial applications.

In our earlier studies of aniline polymerization (19,20), we found that a small amount of aromatic amine additives, such as 1,4-phenylenediamine, 1,4-aminodiphenylamine, *N,N'*-diphenylhydrazine, benzidine, etc., could drastically increase the rate of the oxidative polymerization of aniline monomers. According to the mechanism we have proposed, the growth of polymer chains is mainly achieved via electrophilic aromatic substitution on neutral monomers by the oxidized growing polymer chain ends. The polymerization process is neither a classical step nor a

classical chain polymerization but something in-between. The additives function essentially as chain initiators in the polymerization and, therefore, the molecular weights of polyaniline can be reduced by increasing the amount of the additives relative to aniline in the system (11,19-21). The number-average degree of polymerization (X_n) should be inversely related to the molar ratio of the initiator ([I], i.e., the additive in this case) to the monomer ([M]): $X_n \sim [M]/[I]$. At high additive-to-aniline ratios, more soluble and processible oligomers with designed end-groups could be obtained (11,21). At the molar ratio of the additive 1,4-phenylenediamine to aniline being 1 to 2, we should expect the trimeric species such as N,N'-bis(4'-aminophenyl)-1,4-quinonenediimine to form in an appreciable yield under favorable reactions conditions. It should be noted that the both amino end-groups in 1,4-phenylenediamine may react with aniline monomers.

In this paper, we present the synthesis of a series of electroactive aniline oligomers and electrochemical studies of the anti-corrosion effects of the oligomers as coatings on CRS. The results are compared with those obtained on uncoated and the conventional polyaniline-coated CRS as well as the CRS coated with commercial chromium-containing primer. Since the aniline oligomers can be made to have primary amino groups at the chain ends by employing 1,4-phenylenediamine as the additive, we also evaluated the corrosion protection performance of the coatings formed by curing epoxy resins with the oligomers as the crosslinking agents (i.e., hardeners).

Experimental Section

Materials and Instrumentation. Aniline, substituted anilines and 1,4-phenylenediamine (Aldrich) were distilled or recrystallized. Tetrahydrofuran (THF, HPLC grade from Aldrich), dimethyl formimide (DMF, Fisher), 1-methyl-2-pyrrolidinone (NMP, HPLC grade, Aldrich), ammonium persulfate (Aldrich), epoxy resin (Araldite GY2600 from Ciba-Geigy or bisphenol-A-diglycidyl ether from Dajac Lab) were used as received. The cold rolled steel (CRS) coupons were received from Akzo-Nobel Coatings in Columbus, OH, in both uncoated and chromium-containing primer-coated forms. The uncoated coupons were prepared prior to use with fine polishing paper (LECO Corp. 400 Grit, #183) followed by washing thoroughly with distilled water, acetone and ethanol. Melting points were determined with a Mel Temp apparatus and were uncorrected. Infrared spectra were recorded on a Perkin-Elmer Model 1600 FTIR spectrophotometer. The NMR spectra were measured on a Bruker WM 250 FTNMR spectrometer. Regular mass spectra were recorded on a Finnigan-450 mass spectrometer. Exact mass spectra were determined on a VG ZAB-HF high resolution mass spectrometer. UV-Vis spectra were recorded on a Perkin-Elmer HP8451 spectrophotometer. Gel-permeation chromatography (GPC) measurements were performed on a Waters GPC-IIA with THF (HPLC grade, Aldrich) as eluant. The

molecular weights were calculated directly from a calibration curve of monodispersed polystyrene standards. The electrochemical corrosion measurements were performed on an EG&G PAR 273 potentiostat/galvanostat in a standard corrosion test cell equipped with two graphite rods (diameter: 6.15 mm) as counter electrodes, a saturated calomel reference electrode (SCE) and the gas purge tube as well as the coated or uncoated CRS working electrode.

Synthesis of the Aniline Oligomers. As a typical procedure, 4.75 g (51 mmol) of freshly distilled aniline and 0.25 g (2.3 mmol) of 1,4-phenylenediamine were dissolved in 350 mL of 1 M HCl (aq.) and the solution was cooled to below 5 °C in an ice bath. A solution of 3 g (13 mmol) $(\text{NH}_4)_2\text{S}_2\text{O}_8$ in 150 mL 1 M HCl (aq.) precooled to below 5 °C was poured into the monomer solution with vigorous stirring. The reaction was maintained at 0-5°C for 1.5 h. The blue precipitate was collected by filtration under reduced pressure and washed thoroughly with distilled water until the filtrate formed no precipitation with silver nitrate solution, indicating a complete removal of HCl. The product was then treated with 0.1 M aqueous ammonia at room temperature for 3 h. Upon filtering and drying under dynamic vacuum at 50°C for 48 h, a blue powder of the amino-terminated oligomer in emeraldine base (EB) form was obtained. The number-average molecular weight was ca. 2300 based on GPC measurements with polystyrene calibration.

Synthesis of the Aniline Trimers, i.e., N,N'-Bis(4'-aminophenyl)-1,4-quinonene-diimine and Its Derivatives. In a typical procedure for the synthesis of compound 1 (Scheme 1), 0.86 g (8 mmol) of 1,4-phenylenediamine was dissolved in a solution of 100 mL aqueous 1 M HCl and 40 mL ethanol. The solution was then cooled to about -5 °C in a NaCl-crushed ice bath. To this solution was added 1.8 g (8 mmol) of ammonium persulfate in one portion with stirring under air. After about 5 min, the reaction solution became dark brown and 1.5 mL (16 mmol) of doubly distilled aniline was added quickly. Several minutes later, a blue particle suspension was formed and the reaction mixture was stirred vigorously for additional 30 minutes. The solid product was collected by filtration through a Buchner funnel under a reduced pressure and was washed with 30 mL 1 M HCl followed by 80 mL distilled water. The product was then treated with 40 mL 1 M aqueous solution of ammonium hydroxide for 1 to 2 h. The mixture was filtered under a reduced pressure and the remaining solid was washed with distilled water until the filtrate became neutral in pH. Upon drying at 40 °C overnight under vacuum, 0.93 g of the product 1 was obtained as a blue powder in 40% yield. It is important to note that when the amount of the oxidant was increased to, e.g., two equivalents (16 mmol) in the reaction, higher yields (e.g., >80%, Table 1) were obtainable by otherwise identical procedure. However, the product needed to be purified by dissolution in THF followed by column chromatography over silica gel with a 1/3 (v/v) mixture of ethyl acetate/hexane or diethyl ether alone as eluant.

Preparation of Coatings and Electrochemical Measurements. The conventional polyaniline-EB fine powder was dissolved in NMP to give typically 1-2 wt% solutions. With better solubility, 5-10 wt% solutions of the oligomer in NMP were prepared readily. The solutions were cast dropwise onto the CRS coupons (1x1 cm) followed by drying in air for 48 h to give coatings of ca. 20-130 μm in thickness. The oligomer-cured epoxy resin coatings were prepared by mixing the oligomer solution in NMP with 10 wt% epoxy resin (Araldite GY2600, Ciba-Geigy) followed by spreading the solution onto CRS coupons and heating at 100°C for 1 h. The thickness of the oligomer-cured epoxy resin coatings was approximately 100 μm . The trimer-cured epoxy coatings were made in a similar manner from the trimer solution in DMF and bisphenol-A-diglycidyl ether (Dajac Lab) with a curing temperature of 120°C. The coated and uncoated coupons were then mounted to the working electrode so that only the coated side of the coupon was in direct contact with the electrolyte. The edges of the coupons were sealed with super fast epoxy cement (Elmers). All the electrochemical measurements(10,22,23) were made at room temperature. The electrolyte was NaCl (5 wt-%) aqueous solution. The open circuit potential (OCP) at the equilibrium state of the system was taken as the corrosion potential (E_{corr} in V vs. SCE). The polarization resistance (R_p in Ω/cm^2) was measured by sweeping the applied potential from 20 mV below to 20 mV above the E_{corr} at a scan rate of 0.2 mV/s. The Tafel plot was obtained by scanning potential from 250 mV below to 250 mV above the E_{corr} at a scan rate of 0.2 mV/s. The corrosion current (i_{corr}) was determined by superimposing a straight line along the linear portion of the cathodic or anodic curve and extrapolating it through E_{corr} . The corrosion rate (R_{corr} , in milli-inches per year, MPY) was calculated from the following equation (14):

$$R_{\text{corr}} \text{ (MPY)} = [0.13i_{\text{corr}} \text{ (E. W.)}]/[A \cdot d]$$

where $E. W.$ is the equivalent weight for iron (in g/eq.), A is the area (in cm^2) and d is the density (in g/cm^3).

Results and Discussion

The amino-terminated aniline trimers, i.e., N,N'-bis(4'-aminophenyl)-1,4-quinonediimine (**1**) and its derivatives (**2-4**), were prepared in good yields by oxidation of 2 eq. aniline and substituted anilines with ammonium persulfate as oxidant in the presence of 1 eq. 1,4-phenylenediamine. The oxidation state of the products can be readily interconverted by simple chemical or electrochemical redox reactions. The synthesis is depicted in Scheme 1 and the yields are summarized in Table 1. All the trimers were found to be electroactive by the cyclic voltammetric studies. Reduction of compound **1** with hydrazine under nitrogen atmosphere afforded quantitatively a white solid, which was characterized as N,N'-bis(4'-aminophenyl)-1,4-phenylenediamine (**5**) with melting point 198 °C, exactly the same as reported in the literature(15). All

the compounds were characterized by means of infrared, electronic absorption, exact mass and NMR spectroscopy and the results are consistent with the proposed structures.

Scheme 1

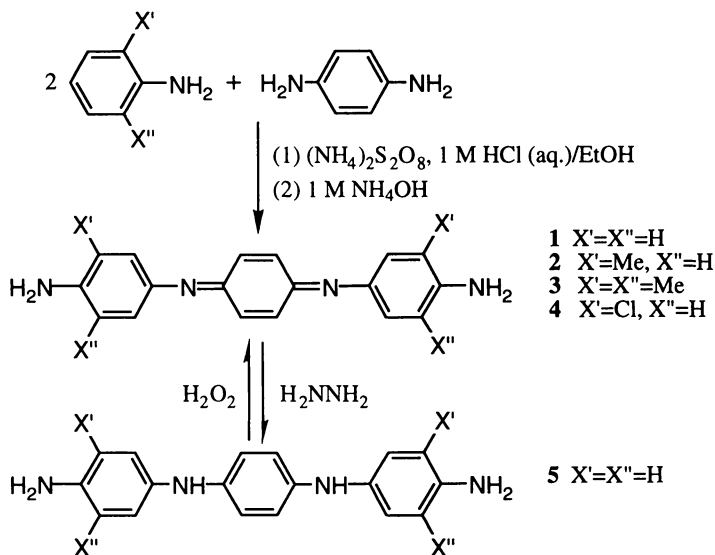


Table 1. Yields and wavelengths of maximum absorption (λ_{\max}) of N,N'-bis(4'-aminophenyl)-1,4-quinonediimine (1), its derivatives (2-5) and higher aniline oligomer (6) as well as conventional polyaniline.

compound	[I]/[M] ^b	yield(%) at [O]/[M] ^a		λ_{\max} (nm) in		
		1:2	1:1	DMF	THF	CH ₂ Cl ₂
1	1:2	40	77	572	556	532
2	1:2	42	83	578	558	539
3	1:2	42	64	578	560	546
4	1:2	28	---	554	544	520
5	1:2	---	---	312	310	307
6	1:22	24 ^c	---	613 ^e	---	---
Polyaniline ^d	0	20 ^c	---	630 ^e	---	---

a) [O]/[M] is the molar ratio of ammonium persulfate to aniline or substituted aniline that was employed in the synthesis. b) [I]/[M] is the approximate molar ratio of the additive 1,4-phenylenediamine to aniline or substituted aniline that was employed in the synthesis. c) [O]/[M] = 1:4. d) Emeraldine base prepared in the absence of additives. e) Measured in NMP solution.

As expected, all the trimers exhibit excellent solubility in most of common organic solvents. It is particularly interesting to note that the methyl ring-substituted trimer (**3**) is soluble in the solvents like methyl amyl ketone and *n*-butyl acetate, which are widely used in the coatings industry. The wavelengths of maximum UV absorption (λ_{\max}) were measured in various solvents as listed in Table 1. The electron-donating groups on the phenyl ring (e.g., **2** and **3**) tend to increase the λ_{\max} value while the electron-withdrawing groups (e.g., **4**) to decrease the λ_{\max} value. Such a tendency remains the same regardless of polarity of solvents. For the same compound, the increase in the polarity of the solvent apparently leads to a bathochromic shift of the λ_{\max} . The reduced form of the compounds (e.g., **5**) have much lower λ_{\max} values than their corresponding oxidized counterparts (e.g., **1**). The reduced form undergoes oxidation by air or by other oxidants such as hydrogen peroxide to regenerate the oxidized form of the compounds.

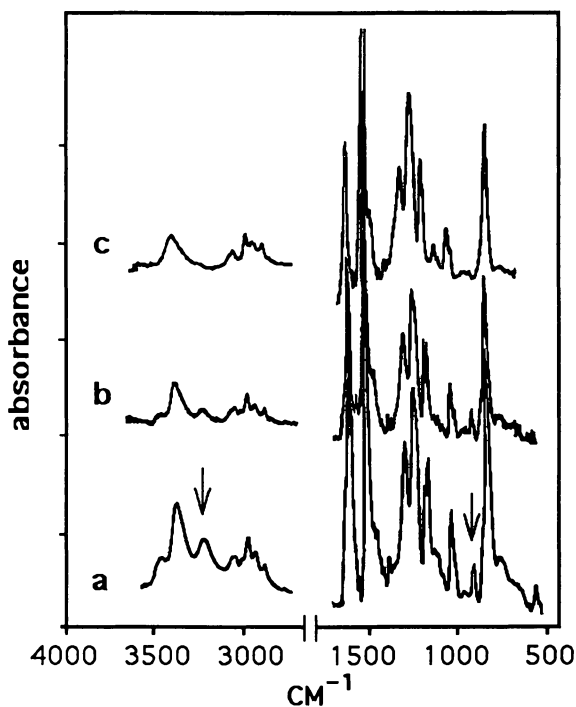


Fig. 1. Infrared spectra of the epoxy resin cured with *N,N'*-bis(4'-aminophenyl)-1,4-quinonediimine at 120 °C for (a) zero, (b) 10 and (c) 35 minutes.

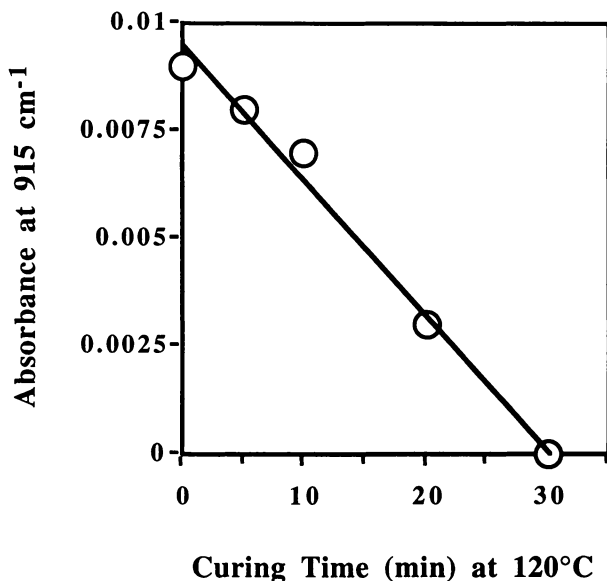


Fig. 2. Plot of absorbance of the IR band at 915 cm^{-1} against curing time at 120°C .

The primary amino-terminated trimers were used as hardeners to cure epoxy resins (Araldite GY2600 from Ciba-Geigy and bisphenol-A-diglycidyl ether from Dajac Lab) under various conditions. For example, 0.144 g (0.5 mmol) of **1** was dissolved in 3.0 mL of DMF followed by mixing thoroughly with 0.17 g (0.5 mmol) of the epoxy resin. The resultant solution was coated on various substrates including silica glass slides, KBr pellets (for IR and curing kinetic studies) and CRS coupons (for corrosion studies). Fig. 1 shows some representative IR spectra of the coatings before and after curing at a curing temperature of 120°C . The extent of curing was monitored by the intensities of characteristic infrared absorption bands at 915 cm^{-1} for epoxy ring and at 3210 and 3340 cm^{-1} for primary amino end-groups (24). The absorbance of both IR bands decrease rapidly with curing time at 120°C . The bands at 915 and 3210 cm^{-1} almost disappeared after 30 min (Fig. 1c), indicating the achievement of complete conversions of the epoxy rings and the primary amino groups in the system, respectively. This trend is further demonstrated in the plot of absorbance of the IR band at 915 cm^{-1} against the curing time (Fig. 2). The trimer-cured epoxy polymer films have excellent thermal and mechanical properties as well as a good adhesion to the CRS substrate.

The oligomer (**6**) with X_n of approximately 20 in this study was prepared similarly by oxidation of aniline in the presence of ca. 5 mol% (with respect to aniline) of 1,4-phenylenediamine with ammonium persulfate as oxidant in 1 M HCl solution followed by neutralization with 0.1 M aqueous ammonia (Scheme 2). The conventional procedures for chemical oxidative polymerization of aniline in 1 M HCl in the absence of the additive usually favor the chain growth reactions to yield polyaniline products with molecular weights as high as 10^5 and with a bimodal type of molecular weight distribution (25). As the amount of the additives is increased (e.g., 1 to 5 mol%), the molecular weight of polyaniline decreases accompanying with narrower molecular weight distributions. The oligomer prepared in the presence of 5 mol% of 1,4-phenylenediamine has a number-average molecular weight (M_n) of about 2,300 and a polydispersity (M_w/M_n) of about 1.5 based on GPC measurement with polystyrene calibration. The UV-vis spectroscopic study shows that the λ_{\max} value (613 nm) of the oligomer is quite close to that (630 nm) of the conventional polyaniline (26) (Table 1). This oligomer exhibited a much higher solubility than the conventional polyaniline and it could be readily dissolved in 1-methyl-2-pyrrolidinone (NMP) to yield a 10 wt% solution. It is noteworthy that unlike conventional polyaniline, the solution of the oligomer is very stable and does not gelate over a long period of time (e.g., >3 days). The solution was then cast onto CRS coupons and dried in air to give smooth and uniform coatings (ca. 130 μm in thickness). The oligomer-epoxy coatings were made by spreading the mixture of the oligomer solution with epoxy resin (10 wt% with respect to the oligomer) on the CRS coupons followed by curing at 100 $^\circ\text{C}$ for 1 h.

Scheme 2

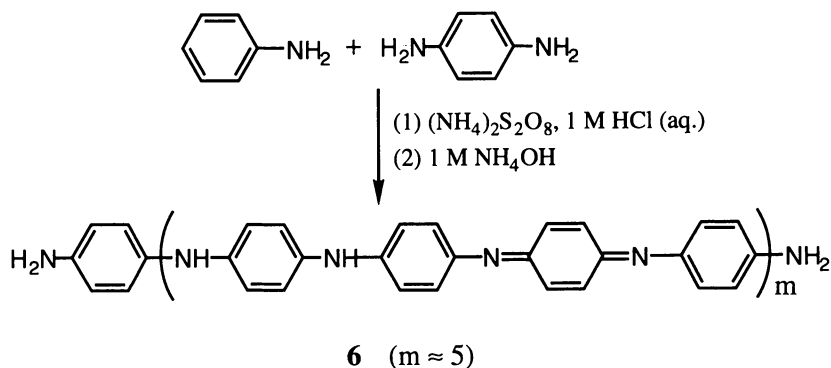


Fig. 3 shows plots of the corrosion potential (E_{corr}) against time for various coated and uncoated CRS in 5 wt% NaCl aqueous solution. After about 60 min, the corrosion potentials in all the system become relatively stabilized. The CRS coupon

coated with conventional polyaniline EB (Fig. 3b) shows a higher E_{corr} value than the uncoated CRS (Fig. 3a), which is consistent with our previous observation (10). However, it has a lower E_{corr} value than the specimen coated with chromium-containing primer (Fig. 3c) or with the primer plus topcoat (Fig. 3d). The oligomer-coated CRS (Fig. 3e) exhibits a high corrosion potential of ca. -110 mV at 60 min. Even after 5 h measurement, the potential remained at ca. -130 mV. Such a high E_{corr} value suggests that the oligomer-coated CRS is very noble towards electrochemical corrosion. The oligomer-coated CRS showed a polarization resistance (R_p) value of $1.7 \times 10^5 \Omega/\text{cm}^2$ in 5 wt-% NaCl, which is about 2 orders of magnitude greater than the uncoated CRS.

The Tafel plots for (a) uncoated, (b) EB-coated and (c) the oligomer-coated CRS are shown in Fig. 4. The corrosion current (i_{corr}) of the oligomer-coated CRS is ca. $0.27 \mu\text{A}/\text{cm}^2$, which is correspondent to a corrosion rate (R_{corr}) of ca. 0.13 millinches per year (MPY). These values are significantly lower than the conventional polyaniline EB-coated CRS (ca. $3 \mu\text{A}/\text{cm}^2$ and 1.3 MPY) and the uncoated CRS (ca. $10 \mu\text{A}/\text{cm}^2$ and 4.3 MPY). The trimer (1) was found to have similar effects as the oligomer. Again, the oligomer coatings offer good corrosion protection and show a better anti-corrosion performance than the conventional polyaniline coatings. Such a better performance might be attributed to the possibility that the electroactive oligomer could have better "adhesion" (i.e., stronger interactions) with the metal surface.

Both the oligomer-cured and the trimer-cured epoxy coatings appeared to have the best corrosion protection effect in this study. The CRS coated with the oligomer-cured epoxy resin showed positive E_{corr} values and very high R_p values ($>10^7 \Omega/\text{cm}^2$). The i_{corr} values were too low to be measured reproducibly, suggesting very slow rates of electrochemical corrosion of the CRS specimen. Similar results were obtained for the trimer-cured epoxy coatings. These corrosion protection effects may not originate merely from the barrier effect of the coatings, because the conventional epoxy coatings as prepared from Araldite GY2600 with HY265 (Ciba-Geigy) as hardener did not show the same electrochemical behavior and gave a high corrosion current (ca. $4.5 \mu\text{A}$). We are currently evaluating the corrosion protection effects of the oligomers and their epoxy derivatives by means of other electrochemical (e.g., impedance spectroscopy) and industrial (e.g., salt spray) techniques (14,23,24).

In summary, we have described the synthesis of amino-terminated aniline trimers and higher oligomer by oxidation of aniline and substituted anilines in the presence of various amount of 1,4-phenylenediamine in an acidic aqueous medium. Similar to conventional polyaniline, the emeraldine base of the oligomer with X_n of approximately 20 offers good corrosion protection as coatings on CRS based on the electrochemical corrosion measurements of E_{corr} , R_p and i_{corr} values in aqueous 5 wt% NaCl electrolyte. This oligomer seems to have better anti-corrosion performance than

conventional polyaniline. Both the trimers and the higher oligomer can be used as crosslinking agents for the curing of epoxy resins to afford new epoxy polymer systems. The oligomer-cured and the trimer-cured epoxy coatings on CRS all exhibit excellent electrochemical corrosion protection effects.

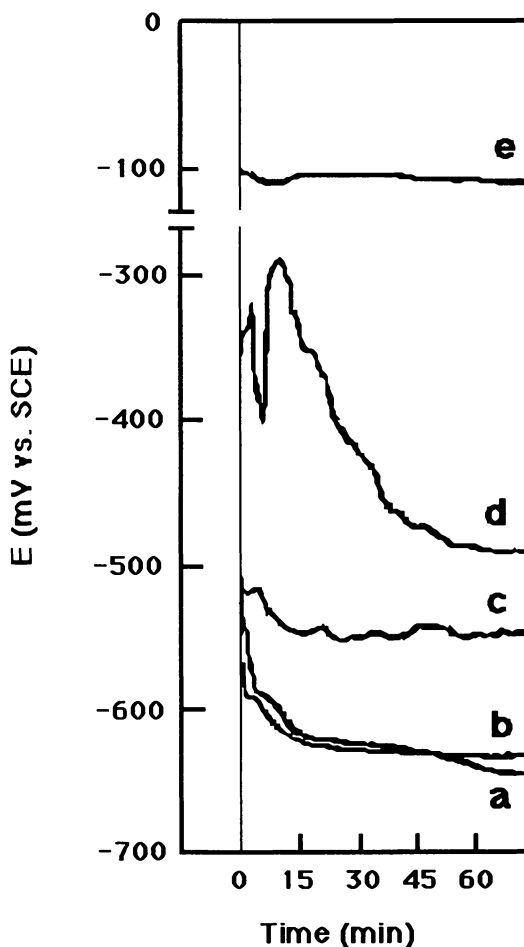


Fig. 3. Plots of open circuit potential against time measured in aqueous 5 wt% NaCl electrolyte on CRS coupons (a) uncoated, (b) coated with conventional polyaniline EB, (c) coated with chromium-containing primer, (d) coated with chromium-containing primer plus topcoat, and (e) coated with the aniline oligomer.

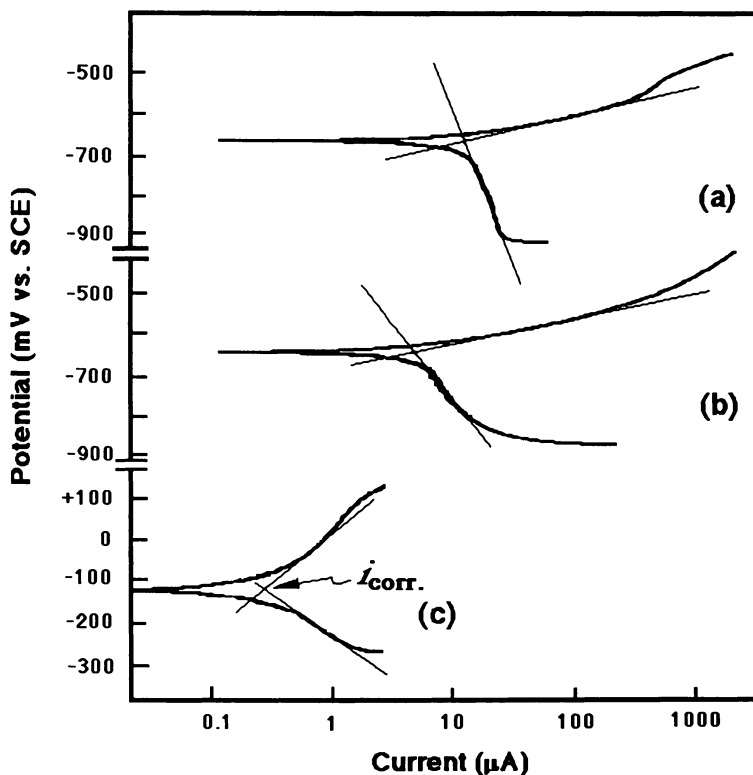


Fig. 4. Tafel plots for (a) uncoated, (b) EB-coated and (c) the oligomer-coated CRS coupons measured in 5 wt-% NaCl aqueous solution.

Acknowledgments. This work has been supported in part by Akzo-Nobel Corporate Research America, Inc. and by Harry Stern Foundation. We are grateful to Dr. A.J. Epstein of Ohio State University, Dr. E.D. Weil of Polytechnic University and Dr. P. Spellane of Akzo-Nobel for many valuable discussions. We thank Dr. J. Honovich and M. Lalevic of Drexel University for measuring the mass spectra.

References and Notes

1. Jain, F.C.; Rosato, J.J.; Kalonia, K.S.; Agarwala, V.S. *Corrosion* **1986**, *42*, 700.
2. DeBerry, D.W. *J. Electrochem. Soc.* **1985**, *132*, 1027.
3. Sathiyarayanan, S.; Dhawan, S.K.; Trivedi, D.C.; Balakrishnan, K. *Corrosion Sci.* **1992**, *33*, 1831.

4. MacDiarmid, A.G., personal communication, 1986.
5. (a) Elsenbaumer, R.L.; Lu, W.K.; Wessling, B. *Int. Conf. Synth. Met.* Seoul, Korea, Abstract No. APL(POL)1-2, 1994. (b) Lu, W.K.; Elsenbaumer, R.L.; Wessling, B. *Synth. Met.* **1995**, *71*, 2163.
6. Wroblewski, D.A.; Benicewicz, B.C.; Thompson, K.G.; Bryan, C.J. *Polym. Prepr. (Am. Chem. Soc., Div. Polym. Chem.)* **1994**, *35(1)*, 265.
7. Wessling, B. *Adv. Mater.* **1994**, *6*, 226.
8. Deng, Z.; Smyrl, W.H.; White, H.S. *J. Electrochem. Soc.* **1989**, *136*, 2152.
9. Jasty, S.; Epstein, A.J. *Polym. Mater. Sci. Eng.* **1995**, *72*, 565.
10. (a) Wei, Y.; Wang, J.; Jia, X.; Yeh, J.-M.; Spellane, P. *Polym. Mater. Sci. Eng.* **1995**, *72*, 563. (b) Wei, Y.; Wang, J.; Jia, X.; Yeh, J.-M.; Spellane, P. *Polymer* **1996**, *36*, 4535. (c) Vallerio, R.; Keyer, R.; Jansen, S.A.; Wei, Y. *Mater. Res. Soc. Symp. Proc.* **1996**, *413*, 523.
11. Wei, Y.; Wang, J.; Jia, X.; Yeh, J.-M.; Yang, C.; Ding, T. unpublished results and US patents pending.
12. (a) Genies, E.M.; Boyle, A.; Lapkowski, M.; Tsintavis, C. *Synth. Met.* **1990**, *36*, 139 and references therein. (b) MacDiarmid, A. G.; Epstein, A. J. *Faraday Discussion, Chem. Soc.* **1989**, *88*, 317. (c) Diaz, A. Z.; Logan, J.A. *J. Electroanal. Chem.* **1980**, *111*, 111. (d) Focke, W. W.; Wnek, G. E.; Wei, Y. *J. Phys. Chem.* **1987**, *91*, 5813. (e) Wei, Y.; Focke, W. W.; Wnek, G. E.; Ray, A.; MacDiarmid, A. G. *J. Phys. Chem.* **1989**, *93*, 495.
13. MacDiarmid, A. G.; Chang, J. C.; Richter, A. F.; Somasiri, N. L. D.; Epstein, A. J. In *Conducting Polymers*; Alcacer, L., Ed.; Reidel Publishing Co.: Holland, 1987, p. 105.
14. Jones, D.A. *Principles and Prevention of Corrosion*; 2nd ed., Prentice-Hall: Upper Saddle River, NJ, 1996.
15. Honzi, J.; Ulbert, K.; Hadek, V.; Tlustakova, M. *Chem. Commun.* **1965**, 440.
16. Ulbert, K.; Hadek, V. *Collection Czechoslov. Chem. Commun.* **1967**, *32*, 1118.
17. (a) Hadek, V.; Ulbert, K.; Honzi, J. *Collection Czech. Chem. Commun.* **1969**, *34*, 3139. (b) Nespurek, S. *Czech. J. Phys.* **1973**, *B23*, 368.
18. Gebert, P. H.; Batich, C. D.; Tanner, D. B.; Herr, S. L. *Synth. Met.* **1989**, *29*, E371.
19. (a) Wei, Y.; Sun, Y.; Jang, G.-W.; Tang X. *J. Polym. Sci., Part C: Polym. Lett.* **1990**, *28*, 81. (b) Wei, Y.; Tang, X.; Sun, Y. *J. Polym. Sci., Part A: Polym. Chem.* **1989**, *27*, 2385. (c) Wei, Y.; Jang, G.-W.; Chan, C.-C.; Hsueh, K. F.; Hariharan, R.; Patel, S. A.; Whitecar, C. K. *J. Phys. Chem.* **1990**, *94*, 7716. (d) Wei, Y. U.S. Pat. No. 4,940,517 (1990). (e) Wei, Y.; Hariharan, R.; Patel, S. A. *Macromolecules* **1990**, *23*, 758.
20. Wei, Y.; Hsueh, K. F.; Jang, G.-W. *Polymer* **1994**, *35*, 3572.

21. Wei, Y.; Yang, C.; Ding, T. *Tetrahedron Lett.* **1996**, *37*, 731.
22. (a) Rothstein, M.L. *EG&G PAR Appl. Note CORR-5* from *Plating & Surface Finishing*, Nov., 1986; *EG&G PAR Appl. Note CORR-4*. (b) Evans, U.R. *The Corrosion and Oxidation of Metals: Scientific Principles and Practical Applications*; St. Martin's Press: New York, 1960.
23. (a) Leidheiser, Jr., H. *J. Coat. Tech.* **1991**, *63*, 21. (b) Bierwagen, G.; Mills, D.; Tallman, D. *Proc. 12th Int. Corrosion Congr.* **1993**, *6*, 4208.
24. (a) Younes, M.; Wartewig, S.; Lellinger, D.; Strehmel, B.; Strehmel, V. *Polymer* **1994**, *35*, 5269. (b) Sykora, V.; Spacek, V.; Dobas, I. *J. Appl. Polym. Sci.* **1994**, *54*, 1463. (c) Nigro, J.; Ishida, H. *J. Appl. Polym. Sci.* **1989**, *38*, 2191. (d) McAndrew, T.P.; Gilicinski, A.G.; Robeson, L.M. US Pat. No. 5,441,772 (1995).
25. Tang, X.; Sun, Y.; Wei, Y. *Makromol. Chem., Rapid Commun.* **1988**, *9*, 829.
26. (a) Kim, Y. H.; Foster, C.; Chiang, J.; Heeger, A. J. *Synth. Met.* **1989**, *29*, E285. (b) Shacklette, L. W.; Wolf, J. F.; Gould, S.; Baughman, R. H. *J. Chem. Phys.* **1988**, *88*, 3955. (c) Wei, Y.; Hsueh, K.F.; Jang, G.-W. *Macromolecules* **1994**, *27*, 518.

Polyaniline in Corrosion-Resistant Coatings

T. Page McAndrew¹, Susan A. Miller², Andrew G. Gilicinski³, and
Lloyd M. Robeson^{2,4}

¹Polymer Chemicals Technology, ²Corporate Science and Technology Center, and
^{2,3}Corporate Research Services—Analytical, Air Products and Chemicals, Inc., 7201
Hamilton Boulevard, Allentown, PA 18195-1501

During the past two decades, one of the most active fields of solid-state science has been that of electrically conductive polymers. Electrically conductive polymers are polymers which, though insulators as prepared, can be converted to polymers having many or all of the properties of a metal through appropriate chemical/electrochemical oxidation or reduction. Typical applications considered for electrically conductive polymers have been in areas such as rechargeable batteries and electrochromic devices. Recently it has been reported that polyaniline, in its electrically conductive, protonated form, displays excellent performance as a coating for preventing the corrosion of carbon steel. The present research has shown that in fact, the non-conductive, unprotonated form of polyaniline displays even better performance in corrosion prevention than the conductive form. Moreover, it has been shown that polyaniline can be blended with other polymers (e.g., polyimides) to improve their corrosion resistance performance, or used as a hardener for epoxides or diisocyanates to give very good corrosion resistant coatings. Polyaniline performance is discussed in terms of its ability to form dense, adherent films, and create a basic surface on carbon steel.

Electrically Conductive Polymers. During the past two decades, one of the most active fields of solid-state science has been that of electrically conductive polymers. Electrically conductive polymers (ECP's) may be generally characterized as polymers that, though insulators as prepared, can be converted to polymers having many or all of the properties of a metal through appropriate chemical/electrochemical oxidation or reduction (processes usually referred to as *doping*). For example, with the prototype ECP, polyacetylene [(CH)_x], oxidative doping with I₂ vapor raises electrical conductivity (σ) from ca. $10^{-9} \Omega^{-1}\text{cm}^{-1}$ to ca. $200 \Omega^{-1}\text{cm}^{-1}$ -- a change from the insulating regime to the metallic regime (1-3). For the present discussion, ECP's are

⁴Corresponding author.

distinguished from extrinsic electrically conductive polymers -- insulating polymers in which metallic properties are produced by inclusion of metal fillers (e.g., Ag-filled epoxy or graphite-filled polyethylene).

Electrically Conductive Polymers in Coatings. The major applications investigated for ECP's have been typically in areas such as rechargeable batteries, electrochromic devices and charge dissipative coatings -- applications that take advantage of the high electrical conductivity of ECP's and their ability to undergo facile oxidation/reduction (1-3). One potential use of ECP's, that recently has received considerable attention is in corrosion resistant coatings. Notable among research in this area has been that by a joint group from the National Aeronautics and Space Administration (NASA, Kennedy Space Center, FL) and the Los Alamos (NM) National Laboratory (LANL). It describes the use of the protonated, conductive, emeraldine form of polyaniline (PAn) as a coating for the protection of carbon steel from corrosion (4-8). See Figure 1. It is noted that reports discussing the use of ECP's in corrosion resistant coatings date to 1981(9-15). However, the cited NASA/LANL report was the first to categorically claim utility in the protection of carbon steel. Subsequent to these reports, other reports have been issued regarding the utility of PAn in corrosion resistant coatings (16-24).

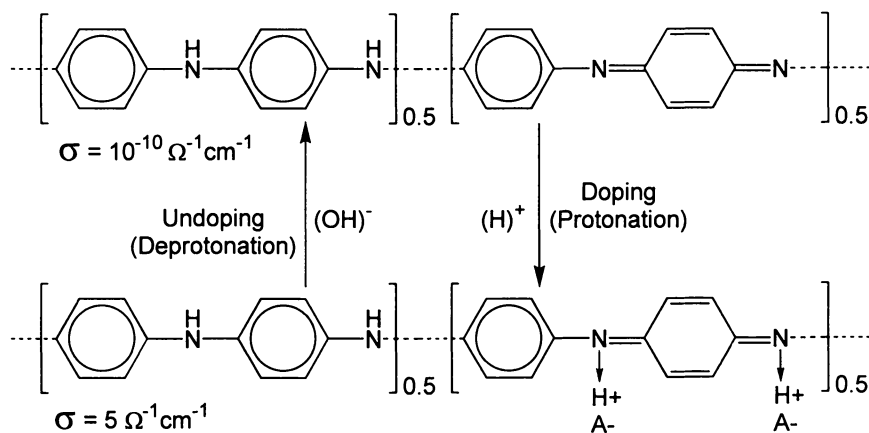


Figure 1. Structures of the Emeraldine Forms of Polyaniline: Unprotonated and Protonated

In view of reports claiming very good corrosion resistance performance, it was considered worthwhile to examine the utility of PAn as a corrosion resistant coating -- in particular as an additive for specialty corrosion resistant coatings. This report describes that research.

Experimental

Synthesis of Polyaniline. The conductive, protonated (i.e., doped), emeraldine form of PAN was prepared according to standard methods, by polymerization of aniline with ammonium persulfate in aqueous 1.0 M HCl (25,26). Electrical conductivity (4-point measurements on compressed pellets) of such dried, doped PAN was ca. $5 \Omega^{-1} \text{cm}^{-1}$. Note that PAN is somewhat different from most ECP's, in that it is prepared, ordinarily, in the conductive form, as opposed to the non-conductive form. The non-conductive, unprotonated (i.e., undoped), emeraldine form of PAN was prepared by deprotonating finely ground, protonated PAN, by agitated immersion for ca. 24 hours in excess aqueous 0.1 M NH_4OH , followed by vacuum drying at room temperature for ca. 24 hours (26). The structures of the unprotonated and protonated emeraldine forms of PAN are shown in Figure 1.

Preparation of Solutions. Solutions (5% by weight) of non-conductive PAN in N-methylpyrrolidinone (NMP) were prepared by slow addition of finely ground, dried PAN with vigorous stirring, and subsequent vigorous stirring (under N_2 atmosphere) for ca. 24 - 48 hours. Solutions were filtered and stored under N_2 atmosphere at room temperature. Such storage was found to reduce the rate of solution gelation, as compared with storage under air atmosphere. Blend solutions of PAN with the amic acid form of pyromellitic dianhydride oxydianiline (DuPont Kapton RC-5019, 5% by weight in NMP) or styrene - acrylic acid copolymer [SAA, 85 mole percent styrene, prepared at Air Products and Chemicals, Inc. (APCI), 5% by weight in NMP] were prepared by combining solutions. Blend solutions of PAN with epoxide (bisphenol-A diglycidyl ether, Ciba-Geigy GY-2600) or urethane-linked diisocyanate (ULDI, APCI PPT-95A) were prepared by neat addition to PAN solution. Solutions of comparative systems of epoxide with standard hardener (Ciba-Geigy XU-265, mixture of diamines) or ULDI with standard hardener (methylene dianiline, MDA), were made in NMP (5% by weight, total). Stirring of all blend solutions was very vigorous and for less than ca. 15 minutes -- to enable film preparation prior to a substantial amount of any reaction.

Preparation of Films. Films were prepared by dispensing solutions (with pipette) onto washed (hexanes), carbon steel panels (Q-Panel Co., Type S-35, 1 inch by 4 inches) in quantity such that final films (i.e., NMP removed) were ca. 0.005 cm (2 mils) thick. Removal of NMP was achieved by treatment for ca. 24 hours at ca. 110°C under partial vacuum (ca. 250 mm Hg with flowing N_2) followed by ca. 24 hours at the same temperature under full vacuum. For Kapton and Kapton blends, this NMP removal cycle was followed by treatment for ca. 16 hours at ca. 250°C under full vacuum. Films for dynamic mechanical analysis were prepared in the same manner, except on glass or Teflon[®] substrates. Removal of such films was by water immersion.

Protonation of non-conductive PAN films (on steel panels) with p-toluenesulfonic acid (PTSA) was done by immersion in a 0.5 M solution of PTSA in tetrahydrofuran for ca. 24 hours, followed by washing with fresh tetrahydrofuran and air drying at room temperature (27). No conductivity measurements were made on

PTSA-doped PAn films. Air oxidation of non-conductive PAn films (on steel panels) was by treatment for ca. 3 days at ca. 110 °C in flowing air.

Electrochemical Impedance Spectroscopy. Electrochemical impedance spectroscopy measurements were made with a system consisting of: (1) a Model 5208 (or 5210) lock-in analyzer, a Model 273 potentiostat, and impedance software package M388 -- all by EG&G Princeton Applied Research and (2) a standard electrochemical flat cell (having an exposed sample area of ca. 1.0 cm² and employing aqueous 1.0 M NaCl as electrolyte) with a Pt gauze and a Ag/AgCl electrode as the counter electrode and reference electrode, respectively. Nyquist plots were constructed from measurements made over the range of 0.01 Hz to 100,000 Hz, using either a 5 mV or 10 mV oscillation from open circuit potential. Pore resistance values were taken as the low frequency, x-axis (real impedance) intercept of said Nyquist plots. This was a preliminary analysis of the data. Further, more detailed analysis would be worthwhile.

Immersion Testing and Salt Fog Testing. Immersion testing was performed in aqueous 3% (by weight) NaCl solutions. To insure good aeration, immersion solutions were changed approximately every 3 days. Salt fog testing was performed in accord with ASTM specification B-117. For each type of test, panels were scribed (through coating into metal to create fresh metal surface) prior to commencement. Performance in each type of test was determined, qualitatively, by visual examination. Examined was the level of peeling, blistering or delamination that occurred with time.

Dynamic Mechanical Analysis. Dynamic mechanical analysis measurements were made with a Rheometrics Solid Analyzer (RSA II), in tension at a frequency of 6.28 radians/second, under a dry N₂ atmosphere. The temperature range was -150 °C (start) to 500 °C. Note in Figures 3-5 that E' = Young's storage modulus and $\tan \delta$ = loss tangent (i.e., E''/E' , where E'' = Young's loss modulus).

Results and Discussion

Performance of Polyaniline. Preliminary electrochemical impedance spectroscopy (EIS) examination showed that on steel panels, the pore resistance (PR) of undoped PAn films was very high -- 100-fold higher than that of PTSA-doped PAn films. See the Table. EIS is a commonly used method for evaluation of coatings. PR has been demonstrated to be a good predictor of long-term coating performance in corrosion prevention. (28) PR can be regarded as a measure of how easily electrolyte solution can move through a film. Therefore, higher PR values indicate that some of the components needed for corrosion to occur (i.e., aqueous electrolyte, see Equation below) will have a more difficult time moving through to access the underlying metal surface. Consequently, higher PR values experimentally relate well to better corrosion resistance performance. Note that EIS examination of PAn has been made previously, but not with a focus on corrosion prevention. (29,30)

The performance results for undoped PAn were surprising at first, because as described above, previous research had indicated very good corrosion resistance

performance for doped PAN (4-8). Upon consideration, however, it can be understood why undoped PAN would show better corrosion resistance performance than doped PAN. Doped PAN is a polyelectrolyte -- a polymer containing a substantial amount of charge (for fully doped PAN, ca. one (+) or (-) charge for each aniline mer, see Figure 1). It would well be expected that aqueous electrolyte ingress into such a polyelectrolyte film would be much easier (resulting in a lower value of PR) than into an undoped PAN film, that contains no charge. As such, corrosion resistance performance of undoped PAN is better. It is noted that air-oxidized PAN showed a PR value even higher than that of undoped PAN. Understandably, such a crosslinked PAN structure would provide for even greater resistance to electrolyte solution ingress.

Table. Pore Resistance Values of Films

Sample (a)	Pore Resistance (Ω)
PAn (undoped)	2×10^8 exp 8
PTSA-Doped PAn	2×10^6 exp 6
Air-Oxidized PAn	5×10^8 exp 8
Kapton	2×10^4 exp 4
PAn/Kapton (1:1)	3×10^6 exp 6
PAn/Kapton (1:3)	6×10^7 exp 7
PAn/Kapton (1:9)	9×10^6 exp 6
PAn/ Epoxide (2:1)	2×10^9 exp 9
Hardener/Epoxide (2:1)	2×10^9 exp 9
PAn/ULDI (1:1, mole)	1×10^8 exp 8
MDA/ULDI (1:1, mole)	6×10^8 exp 8
SAA	3×10^4 exp 4
PAn/SAA (1:1)	1×10^7 exp 7

- a. All films were nominally 0.0050 cm (2 mils) thick. All compositions are on a weight basis, unless stated otherwise.

Performance of Polyaniline Blends. Given the very good corrosion resistance performance observed for undoped PAN, the natural question to arise concerned the most cost-effective manner in which undoped PAN could be used. Limitations to the large-scale use of PAN are the facts that PAN is soluble only in select high boiling solvents, such as NMP, and that PAN cost is likely to be relatively high, given its current status as a specialty chemical. In view of these issues, consideration was given to PAN blends -- to determine if PAN could be used to improve the performance of a system already suited for coatings.

In order to determine the phase behavior of PAN blends, and assess reactions that might occur with temperature excursions higher than those employed during film preparation, dynamic mechanical analysis was performed on blend film samples.

Polyimide Blends. The first system considered for blending with PAN was a polyimide -- pyromellitic dianhydride oxydianiline (DuPont Kapton RC-5019, the

amic acid form of which is shown in Figure 2). The Table shows PR values for films of PAN, Kapton and PAN/Kapton blends. It can be seen clearly that the presence of PAN in Kapton raised PR values, as compared with Kapton. It was observed also that the presence of PAN in Kapton improved performance in immersion testing and salt fog testing. In immersion testing, Kapton showed more than ca. 25% delamination after 4 weeks, whereas PAN/Kapton blends did not show such a level of delamination until after 7-13 weeks. In salt fog testing, Kapton showed clear blistering after 1 week, whereas PAN/Kapton blends showed only minor blistering after 1 week.

Thus, it seems clear that PAN can improve the corrosion resistance performance of Kapton. Moreover, the presence of PAN in Kapton did not

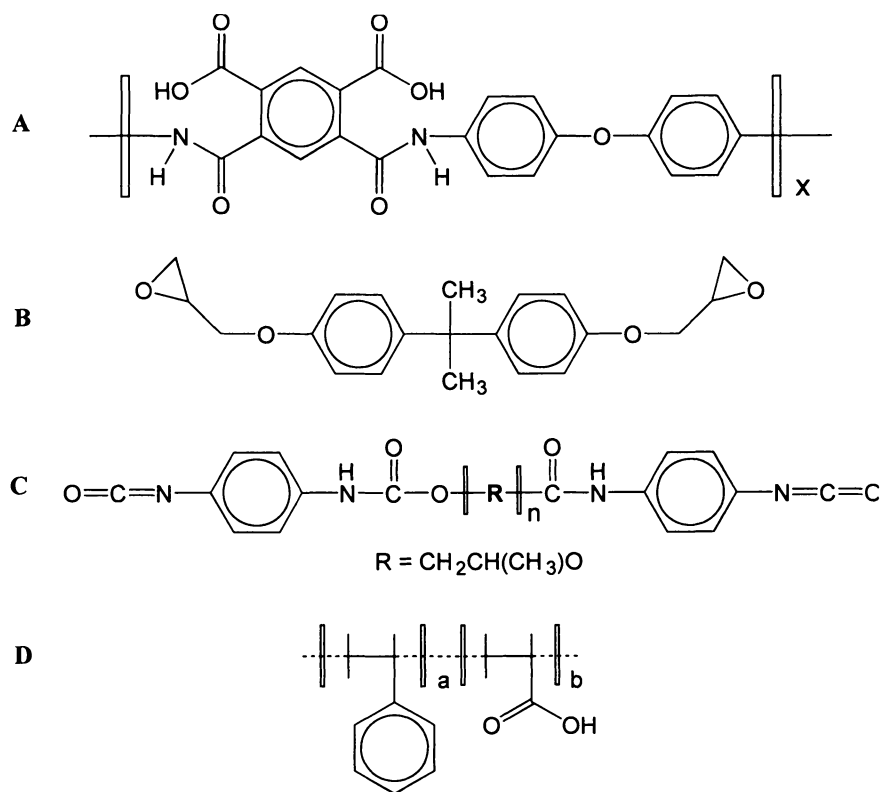


Figure 2. Structures of: **A.** Amic Acid Form of Pyromellitic Dianhydride Oxydianiline (DuPont Kapton RC-5019). **B.** Bisphenol-A Diglycidyl Ether. **C.** Urethane Linked Diisocyanate (ULDI, APCI PPT-95A). **D.** Styrene - Acrylic Acid Copolymer (SAA, $a = 0.85$, $b = 0.15$).

substantially reduce thermal stability. This combination of features suggests utility in applications where polyimide thermal/dielectric performance is required, but some

measure of corrosion resistance is required also. It is noted that previous discussion of PAN/polyimide blends has been made. (31)

The dynamic mechanical properties of a PAN film, Kapton film and PAN/Kapton (1:1, weight basis) film are shown in Figures 3A and 3B. PAN shows a T_g of 140 °C (tan δ). At T_g , there occurs a large decrease in modulus that continues up to 180 °C, above which an increase in modulus occurs -- presumably due to interchain reaction (e.g., crosslinking). The peak at 225 °C is due to crystallization. Kapton shows a T_g of 390 °C (tan δ). PAN/Kapton (1:1) does not show a T_g characteristic of either PAN or Kapton, but rather shows two transitions, intermediate between the T_g values of PAN and Kapton. The shoulder at 250 °C (tan δ) probably indicates either a PAN rich phase, or the onset of a reaction involving the amic acid group of Kapton with PAN (that would result in the observed increase in modulus). T_g of the probable resultant network is 350 °C (tan δ). The shoulder at 250 °C (tan δ) for PAN/Kapton (1:1) is different from the peak at 225 °C (tan δ) for PAN, since no evidence of crystallization is present for PAN/Kapton (1:1) (E'). Dynamic mechanical analysis results are consistent with the hypothesis that a homogeneous PAN/Kapton blend is formed by reaction between constituents. Supporting this hypothesis is the observation that, at room temperature, a PAN/Kapton blend solution gels within hours of mixing. Determining whether it is ideal miscibility, or partial miscibility, that exists within this blend would require further analysis.

Epoxide Blends. The second system considered for blending with PAN was an epoxide -- bisphenol-A diglycidyl ether (Ciba-Geigy GY-2600, structure shown in Figure 2). The Table shows the PR values for a PAN/epoxide (2:1, weight basis) film, and a comparative epoxide film made with a standard hardener (Ciba-Geigy XU-265, mixture of diamines) (2 parts hardener, 1 part epoxide, weight basis). Clearly, the presence of epoxide in PAN substantially increased (10-fold) the value of PR, as compared with PAN. However, the PR value of PAN/epoxide (2:1) was essentially the same as that of epoxide with standard hardener (2:1). In immersion testing, PAN/epoxide (2:1) showed performance equivalent to that of PAN -- small levels of blistering after 32 weeks and performance slightly better than that of epoxide with standard hardener (2:1) -- small levels of blistering after 18 weeks. In salt fog testing, PAN/epoxide (2:1) and epoxide with standard hardener (2:1) showed equivalent performance -- over ca. 25% delamination after 12 weeks. In contrast, PAN showed over ca. 25% blistering after only 3 weeks. A recent literature report is in good agreement with the present observation that addition of epoxide to PAN results in improved corrosion resistance performance. (23)

The dynamic mechanical properties of a PAN/epoxide (2:1, weight basis) film and a PAN/epoxide (1:2, weight basis) film are shown in Figure 4. T_g for PAN/epoxide (2:1) is 175 °C (tan δ), and for PAN/epoxide T_g (1:2) is 160 °C (tan δ). For either blend, a transition in the range of 270 °C - 290 °C is observed, followed by a decrease in modulus at higher temperatures. This decrease may result from the onset of thermal degradation of a crosslinked network. The observations for PAN/epoxide (2:1) and PAN/epoxide (1:2), as compared with PAN, indicate that epoxide has

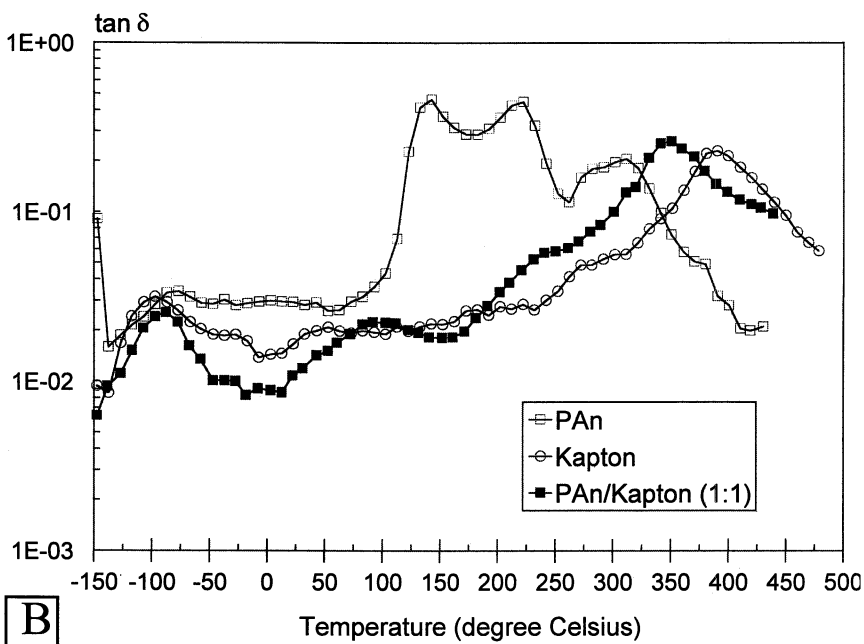
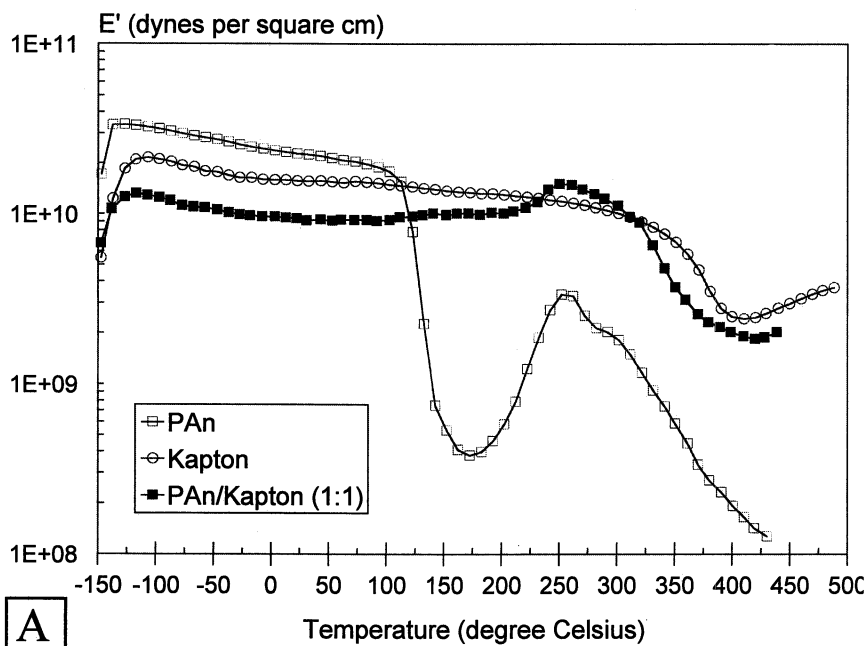


Figure 3. Dynamic Mechanical Properties of PAn, Kapton and PAn/Kapton (1:1, weight basis). E' = Young's storage modulus, $\tan \delta$ = loss tangent.

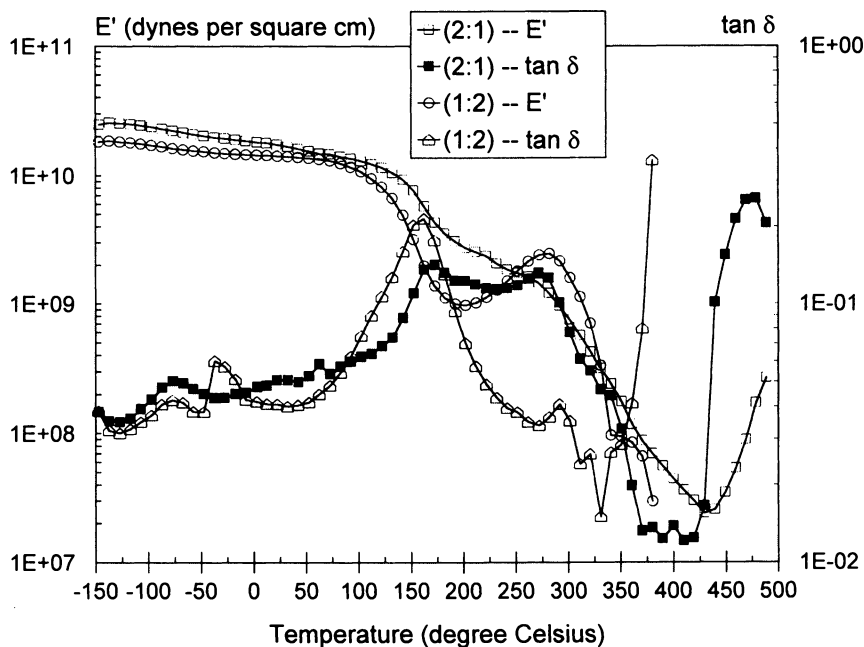


Figure 4. Dynamic Mechanical Properties of PAN/Epoxy (2:1, weight basis) and PAN/Epoxy (1:2, weight basis). E' = Young's storage modulus, $\tan \delta$ = loss tangent.

reacted with PAN to form a crosslinked network. This hypothesis is supported by the observation that a PAN film swells substantially when immersed in NMP, whereas a PAN/epoxy (2:1) film does not swell at all.

Urethane Linked Diisocyanate Blend. The third system considered for blending with PAN was a urethane-linked diisocyanate (APCI PPT-95A, structure shown in Figure 2). The Table shows the PR values for a PAN/ULDI (1:1, mole basis) film and a comparative ULDI film made with a standard hardener (methylene dianiline, MDA) (1:1, mole basis). PAN/ULDI showed a PR value lower than that of either PAN or MDA/ULDI. As was the case with Kapton or epoxy blending, ULDI reacts with PAN to yield a material with substantial crosslinking. This is indicated by the observation that a PAN film swells substantially in NMP, whereas a PAN/ULDI film does not swell at all.

The dynamic mechanical properties of a PAN/ULDI (1:1, mole basis) film are shown in Figure 5. A broad T_g is observed with a peak at 165 °C ($\tan \delta$). Above T_g , the increase in modulus indicates an increase in crosslink density that is probably caused by further reaction of PAN with ULDI. Although reaction does occur upon constituent mixing, further reaction above T_g presumably occurs because of increased constituent mobility. The broad transition for PAN/ULDI indicates less

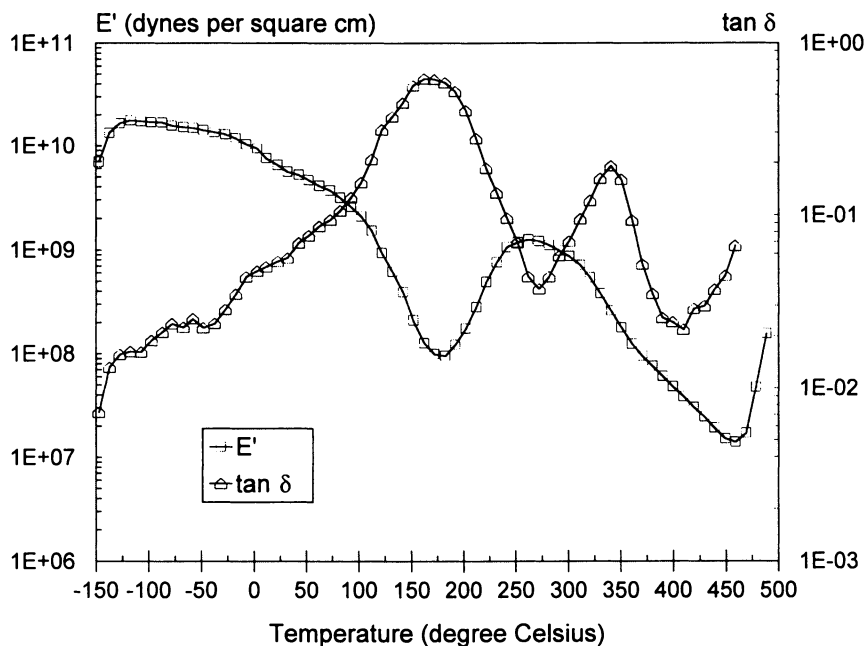


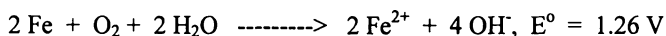
Figure 5. Dynamic Mechanical Properties of PAN/ULDI (1:1, mole basis). E' = Young's storage modulus, $\tan \delta$ = loss tangent.

than ideal miscibility. Presumably, the poly(propylene oxide) block of ULDI is partially phase separated -- resulting thus in a microheterogeneous blend. The presence of phase separated poly(propylene oxide) may explain why the PR value of PAN/ULDI was lower than that of PAN.

Styrene - Acrylic Acid Copolymer Blend. The last system considered for blending with PAN was a styrene - acrylic acid copolymer (SAA, 85 mole percent styrene, structure shown in Figure 2). The Table shows how the PR value of a PAN/SAA blend (1:1, weight basis) was improved, as compared with SAA. In immersion testing, PAN/SAA (1:1) showed neither blistering nor peeling after 13 weeks. In contrast, SAA showed over ca. 25% delamination after only 7 weeks. In salt fog testing, PAN/SAA (1:1) and SAA showed equivalent performance -- over ca. 25% delamination after 1 week. Thus, it seems clear that PAN can improve the corrosion resistance performance of SAA. This is analogous to what was observed with Kapton. Contrasted with the other systems considered, however, it is unlikely that PAN underwent any chemical reaction with SAA.

Mechanism of Polyaniline Performance. Previous research has attributed the very good corrosion resistance performance of PAN coatings to either alteration of the oxidation potential of metal, or the formation of a passivating layer of metal oxides on the surface of metal. Either of these explanations would seem to be inconsistent with

the present observation -- that non-conductive, unprotonated (i.e., undoped) PAN gives better corrosion resistance performance than conductive, protonated (i.e., doped) PAN. A non-conductive coating would be expected neither to alter the oxidation potential of a metal (since it would not be in electrical contact with said metal), nor foster the oxidation of a metal surface to form oxides. Based upon the present observations, the following explanation is offered. From the high PR values observed, it must be concluded that PAN forms a dense, non-porous film on carbon steel panels, and adheres very well thereto. Such a dense film would restrict access to the underlying steel surface of some of the components necessary for corrosion to occur (see the Equation below). Also, it is noted that aniline itself is a corrosion-inhibiting agent (32). A film coating of PAN is essentially a very dense collection of aniline molecules mechanically held against a carbon steel surface. These aniline molecules serve to effectively scavenge any protons, and foster a local basic surface (from reaction with water molecules present). The summation of both effects is that the corrosion reaction shown below is forced to the left, according to Le Chatelier's Principle -- fostering the maintenance of an unoxidized carbon steel surface.



It is noted that a recent report has stated that undoped PAN offers better corrosion resistance performance than doped PAN -- in agreement with the present research. (21)

Summary

Preliminary research has demonstrated that non-conductive, unprotonated (i.e., undoped) PAN performs very well as a corrosion resistant coating -- better than conductive, protonated (i.e., doped) PAN. Moreover, it has been demonstrated that PAN can be added to other polymer systems to improve corrosion resistance performance. Benefit is obtained whether or not PAN chemically reacts with the second system. A U.S. Patent has been awarded to Air Products and Chemicals, Inc. for the technology described herein regarding non-conductive PAN and PAN blends (33-35). Note however, that no PAN system considered gave performance substantially better than available with the commercially available epoxy system described. PAN may show utility as an additive for water based coatings. Some literature reports have already described the manufacture of PAN emulsions (36-38).

Acknowledgments

Thanks are extended to: M.S. Vratsanos and S.C. Voth for mechanical property analyses, J.A. Kuphal for styrene - acrylic acid copolymer, J.R. Stets for electron microscopy analyses, M.L. Achenbach and F.M. Prozonic for thermal analyses, and M.S. Brenner for many literature citations.

Literature Cited

1. *Handbook of Electrically Conducting Polymers*; Skotheim, T.E., Ed.; Marcel Dekker: New York, NY, 1986; Vol. 1 and 2.

2. Chien, J.C.W. In *Polyacetylene: Chemistry, Physics and Materials Science*; Academic Press: New York, NY, 1984.
3. Kanatzidis, M.G. *Chem. Eng. News* December 3, 1990, 36.
4. Thompson, K.G.; Bryan, C.J.; Benicewicz, B.C.; Wroblewski, D.A. Los Alamos (NM) National Laboratory Report LA-UR-92-360, 1991.
5. *Chem. Eng. News* January 20, 1992, 20.
6. *Inside R&D* January 22, 1992, 21 (4).
7. *The Wall Street Journal* April 4, 1994, B1.
8. *Popular Science* June 1994, 38.
9. Mengoli, G.; Munari, M.T.; Bianco, P.; Musianai, M.M. *J. Appl. Polym. Sci.* **1981**, 26, 4247.
10. Mengoli, G.; Musiani, M.M.; Pelli, B.; Vecchi, E. *J. Appl. Polym. Sci.* **1983**, 28, 1125.
11. Musiani, M.M.; Mengoli, G.; Furlanetto, F. *J. Appl. Polym. Sci.* **1984**, 29, 4433.
12. DeBerry, D.W. *J. Electrochem. Soc.* **1985**, 132, 1022.
13. Zhi, D.; Smyrl, W.H.; White, H.S. *J. Electrochem. Soc.* **1989**, 136, 2152.
14. Mattson, G.C. Final Report of NASA Contract with the University of Central Florida, NASA-NGT-60002, N89-14159, August 1988, 118.
15. Troch-Nagels, G.; Winand, R.; Weymeersch, A.; Renard, L. *J. Appl. Electrochem.* **1992**, 22, 756.
16. Ren, S.; Barkey, D. *J. Electrochem. Soc.* **1992**, 139, 1021.
17. Wroblewski, D.A.; Benicewicz, B.C.; Thompson, K.G.; Bryan, C.J. *Polym. Prepr., Am. Chem. Soc. Div. Polym. Chem.* **1994**, 35 (1), 265.
18. Wessling, B. *Adv. Mater.* **1994**, 6 (3), 226.
19. Phillips, M. *New Sci.* October 29, 1994, 24.
20. Wei, Y.; Wang, J.; Jia, X.; Yeh, J.-M.; Spellane, P. *Polym. Mater. Sci. Eng.* **1995**, 72, 563.
21. Jasty, S.; Epstein, A.J. *Polym. Mater. Sci. Eng.* **1995**, 72, 565.
22. Lu, W.-K.; Elsenbaumer, R.L.; Wessling, B. *Synth. Met.* **1995**, 2163.
23. Wei, Y.; Yeh, J.-M.; Wang, J.; Jia, X.; Yang, C.; Jin, D. *Polym. Mater. Sci. Eng.* **1996**, 74, 202.
24. Wei, Y.; Yang, C.; Ding, T.; Yeh, J.-M.; Wei, G. *Polym. Mater. Sci. Eng.* **1996**, 74, 209.
25. Huang, W.-S.; Humphrey, B.D.; MacDiarmid, A.G. *J. Chem. Soc., Faraday Trans. 1* **1986**, 82, 2385.
26. MacDiarmid, A.G., University of Pennsylvania, personal communication, 1991.
27. Wroblewski, D.A., Los Alamos National Laboratory, personal communication, 1992.
28. Jones, D.A. *Principles and Prevention of Corrosion*; Macmillan Publishing: New York, NY, 1992, 491.
29. Glarum, S.H.; Marshall, J.H. *J. Electrochem. Soc.* **1987**, 134, 142.
30. Musiani, M.M. *Electrochim. Acta* **1990**, 35, 1665.
31. Patel, N.; Saraf, R.; Angelopoulos, M. In *Advances in Polyimide Science and Technology*; Feger, C.; Khojasteh, M.M.; Htoo, M.S., Eds.; Technomic Publishing: Lancaster, PA, 1993, 165.
32. Granata, R.D., Lehigh University, personal communication, 1992.
33. McAndrew, T.P.; Gilicinski, A.G.; Robeson, L.M. U.S. Patent 5 441 772, 1995.

34. McAndrew, T.P.; Miller, S.A.; Gilicinski, A.G.; Robeson, L.M. *Polym. Mater. Sci. Eng.* **1996**, 74, 204.
35. McAndrew, T.P. *Trends Polym. Sci.* **1997**, 5, 7.
36. Beadle, P.; Armes, S.P.; Gottesfeld, S.; Mombourquette, C.; Houlton, R.; Andrews, W.D.; Agnew, S.F. *Macromolecules* **1992**, 25, 2526.
37. Stejskal, J.; Kratochvil, P.; Gospodinova, N.; Terlemezyan, L.; Mokreva, P. *Polymer* **1992**, 33, 4857.
38. Kinlen, P.J. International Patent WO 96/14343, 1996.

Corrosion Inhibition Using Self-Assembled Monolayers of Alkanethiols on Copper

G. Kane Jennings and Paul E. Laibinis¹

Department of Chemical Engineering, Massachusetts Institute of Technology,
Cambridge, MA 02139

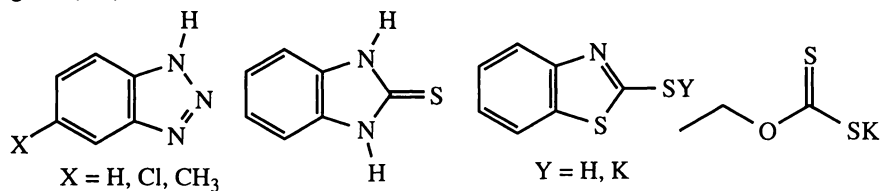
Alkanethiols adsorb onto copper surfaces and form densely packed monolayer films that inhibit corrosion of the underlying copper substrate. The hydrocarbon chains in these chemisorbed assemblies are highly crystalline and provide a transport barrier for small molecules (including agents of corrosion such as oxygen and water) to the copper substrate. Angstrom-level increases in the thickness of the hydrocarbon layer -- effected by selection of the chain length of the alkanethiol -- produced superior barrier film properties. With longer-chained adsorbates, the coatings exhibited barrier properties that were insensitive to the moisture content of the oxidizing environment. Films prepared by the self-assembly method effectively inhibited corrosion during weeklong immersions in oxygen-saturated water without the addition of corrosion inhibitor molecules to the water phase. Siloxane-based bilayer assemblies offered improved film stability; however, their effectiveness as corrosion inhibitors was less than that for monolayers due to synthetic difficulties in preparing suitably high quality bilayer films on copper.

Organic coatings are often used as barriers against corrosion or as primers that facilitate adhesion of a barrier layer to a metal substrate (1-13). Polymeric films allow the construction of thicker, more robust layers for these operations (7), where multiple points of physical contact are largely responsible for the adhesion and stability of the coating. In heat transfer applications and the microelectronics industry, these same properties are required from sub-micron-thick films (1). Difficulties in the preparation of uniform coatings on this dimension from polymers -- particularly on the convoluted geometries within heat exchanging equipment and on the highly patterned surfaces of semiconductor devices -- preclude their use for these applications. Molecular precursors are often used as corrosion inhibitors where their function is to adsorb onto the metal surface -- in either mono- or multilayer quantities -- and restrict transport of oxidants to the underlying substrate (1-13). In some applications, these species also serve as mild reducing agents and return the metal surface back to its oxide-free state.

¹Corresponding author.

Copper is a commonly used material in heat transfer applications due to its high thermal conductivity, malleability, and low cost (14). In the electronics area, copper has become a material of great interest due to its low resistivity ($1.67 \mu\Omega\text{-cm}$) than metals such as gold ($2.35 \mu\Omega\text{-cm}$) and aluminum ($2.65 \mu\Omega\text{-cm}$), particularly as line widths in integrated circuits continue to decrease. Corrosion of the copper surface negatively impacts its use in these applications by lessening the rate at which heat can be transferred into a contacting medium (often water or steam) in heat exchanging operations and by decreasing the electrical conductivity of the microfabricated wires that provide connections within an integrated circuit. Copper corrosion occurs more rapidly in the presence of water (14), and the frequent exposure of copper in these applications -- be it towards aqueous circulating streams or aqueous processing and etching solutions -- exacerbates this problem.

Present efforts to lessen the corrosion of copper use a variety of molecular agents (1-7):



These compounds are frequently low molecular weight aromatic compounds and contain basic sulfur or nitrogen sites for ligation to the surface. They are sufficiently soluble in water that they can be added directly to the aqueous stream; however, this property requires their presence in the stream to maintain a barrier layer on the copper surface. Another function for some of these molecules is as reducing agents that can remove oxides from the copper surface as they form and regenerate the native metal. Despite the importance of the corrosion problem and the numerous studies that have been reported on these systems (1-6), there is little agreement regarding their exact function, the mechanisms by which they operate, and even whether these films form mono- or multilayer films on the copper surface. As monolayers, these films provide relatively thin films where a benzene ring is largely responsible for providing a barrier between an oxidizing species and the copper surface. Their rigid structures can limit their effective packing and result in the formation of films that can contain many pinholes.

An increasing problem with the current molecular strategies is the requirement that these additives have sufficient concentration in the contacting aqueous stream to maintain a barrier film on the copper surface. The constant presence of these additives in the water streams (typically at the 10 to 100 ppm level) is an increasingly important environmental problem. Their disposal and the regeneration of the water streams present the need for undertaking new strategies that can overcome the limitations of this approach. Further, better defined systems would also allow exploration of the fundamental properties associated with the design of barrier films and in turn, lead to films with superior properties. Our goal is the formation of single-application barrier layers that do not require the constant presence of additives in order to achieve their inhibitory properties. This strategy would simplify current operational procedures and offer the aforementioned environmental benefits. This paper describes the application of self-assembled mono- and multilayers on copper as barrier films, their current abilities, their limitations, and opportunities for further improvements.

Self-Assembled Monolayers

Recent advances in the preparation of self-assembling molecular films have provided a synthetically flexible strategy for derivatizing a number of metal surfaces with densely packed, often highly crystalline, organic layers (15-18). These systems are the product of the spontaneous adsorption of ligating molecules (from solution or the vapor phase) onto a reactive metal (or metal oxide) surface. The most studied system has been the assembly of alkanethiols, $\text{HS}(\text{CH}_2)_n\text{X}$, onto gold surfaces due to its synthetic flexibility and ease of use (16, 17). Thiols also assemble onto silver and copper surfaces to form oriented, densely packed monolayer films with related properties (18, 19). On copper and silver, the hydrocarbon chains of the adsorbate exist in a crystalline, trans-zig-zag-extended structure, with the axis of the chain orienting close to the surface normal (cant angle $\approx 13^\circ$) (18, 19). The assembly on these metals can accommodate a wide range of polar and non-polar tail groups, thereby allowing formation of both hydrophilic and hydrophobic surfaces (20). The resulting assemblies are stable in polar solvents and under vacuum. They can provide an organic platform on the metal for the attachment of other species, in essence, using the self-assembled monolayer as a molecular primer between the metal and organic phases (21-23).

For use as barrier layers, self-assembled monolayers provide a convenient system for investigating the roles that structure and chemical functionality play in imparting corrosion inhibition to a layer. The reliance on an adsorption process for the assembly of these films provides a convenient method for applying these barrier layers uniformly to surfaces (15). In addition, the adsorption process should be largely insensitive to the contour of the surface, providing a straightforward means for coating the convoluted inner surfaces frequently encountered in heat exchanger equipment. Examinations of the barrier properties of such films have largely focused on their abilities to impede electron transfer on gold (24-26). Studies on the use of these layers as barriers for corrosion have been an area of recent development (8-13), with related efforts focusing on their application in lithographic procedures as barriers to chemical etchants (27).

Experimental Section

Sample Preparation. Cr (150 Å) and Cu (1000 Å) were sequentially evaporated from resistively heated tungsten filaments onto Si wafers in a diffusion-pumped evaporation chamber. Immediately following evaporation of copper, the chamber was backfilled with N_2 , and the freshly evaporated samples were transferred under a positive flow of N_2 to 1 mM deoxygenated isooctane solutions of the alkanethiols that were brought inside the evaporator. After remaining in solution for 40 min, the samples were removed, rinsed with ethanol, and blown dry in a stream of N_2 .

Bilayer films were prepared on copper via a two-step process: as above, copper samples were instead derivatized with a mercapto-alcohol — $\text{HS}(\text{CH}_2)_{11}\text{OH}$ or $\text{HS}(\text{CH}_2)_{22}\text{OH}$ (20) — and then treated with a mixture of 0.5 mM isooctane solution of octadecyl trichlorosilane ($\text{C}_{18}\text{H}_{37}\text{SiCl}_3$) and solid Na_2CO_3 for 5 min, rinsed with isooctane and blown dry. All manipulations involving the silane were performed in a glove box using dry air.

Oxidation Studies. Immediately after assembly of the monolayers, the Si wafers were cut into $1 \times 3 \text{ cm}^2$ samples, and the samples were exposed to ambient conditions

(air) or were placed into either a "dry" (10% R.H.) or a "humid" (100% R.H.) chamber at room temperature. Humidity levels were determined using a digital hygrometer (Fisher). A steady stream of O_2 flowed through each chamber at $10\text{ cm}^3/\text{min}$ during the experiments. Within the "humid" chamber, a subset of samples was immersed in vials that contained deionized water. Exposures to air and O_2 were performed in the dark to minimize any possible effects due to light. After various periods of exposure, samples were rinsed with ethanol, dried in a stream of N_2 , and characterized by either wetting or XPS. After characterization by either method, the samples were discarded. Data in the figures represent measurements on individual slides that had been continuously exposed to the listed oxidation conditions and had undergone no previous analysis. In most cases, the data represent at least two independent preparations and oxidations of the SAMs.

Wetting Measurements. Advancing contact angles were measured on both sides of a static drop using a Ramé-Hart manual goniometer. The drop was advanced prior to measurement by a Matrix Technologies electro-pipette ($1\text{ }\mu\text{L/s}$). The pipette tip remained in the drop during measurement. The data represent the average of at least three measurements, with the reproducibility across a sample being $\pm 3^\circ$.

X-ray Photoelectron Spectroscopy (XPS). XPS spectra were obtained with a Surface Science X-100 spectrometer using a monochromatized $Al\text{ K}\alpha$ X-ray source. Copper spectra were accumulated over 5 scans ($\sim 10\text{ min}$), and the spectra were fitted using 70% Gaussian/30% Lorentzian profiles and a Shirley background. For spectra where signals for Cu(II) species could not be distinguished from baseline, the thickness of the Cu(II) layer, $d_{\text{Cu(II)}}$, is presented as 0 \AA but may have a value up to 0.5 \AA .

Results and Discussion

Figure 1 displays a schematic illustration of our experimental approach. In our experiments, we used evaporated copper films supported on silicon as substrates. Immediately after evaporation of the copper, the chamber was backfilled with N_2 and the samples were transferred anaerobically to a deoxygenated solution of the adsorbate. These conditions produce well-defined self-assembled monolayer films on the copper surface (19, 20); the wetting properties of these films were similar to those formed from these compounds on gold (20). XPS spectra for these samples exhibit no peaks in the

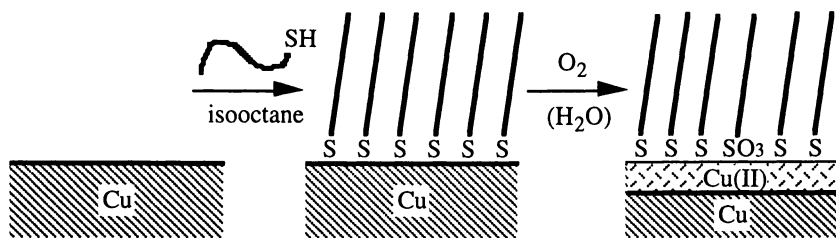


Figure 1. Schematic illustration of the formation of a self-assembled monolayer on copper and the species produced after exposure to oxidizing conditions. The assembly of the thiols (step 1) was conducted under anaerobic conditions.

Cu(2p_{3/2}) region due to Cu(II) species (Figure 2) and provided the starting point for our corrosion studies. After exposure of these samples to various oxidizing conditions, we characterized them by wetting measurements and x-ray photoelectron spectroscopy (XPS). These measurements provided information regarding the structural integrity of the barrier film and the extent of oxidation for the underlying copper substrate.

In these studies, we relied heavily on XPS to quantify the extent of oxidation for the copper substrates. XPS is well suited for these studies as it is highly surface sensitive and allows the detection of Cu(II) oxidation products at the sub-angstrom-level. In the Cu(2p_{3/2}) spectral region, Cu(0) and Cu(I) species exhibit a single peak at a binding energy of 932.6 eV while Cu(II) species exhibit a peak that is shifted positively to a position of ~934.7 eV and also display shake-up satellite peaks at 941.5 and 943.8 eV that are readily distinguished and well-separated from the primary Cu(2p_{3/2}) peaks (28). The relative intensities of the peaks in the Cu(2p_{3/2}) spectral region can be related to thicknesses through eq 1 (8),

$$d_{\text{Cu(II)}} = -\lambda \cos \phi \ln [1 - \% \text{Cu(II)}] \quad (1)$$

where $d_{\text{Cu(II)}}$ is the thickness of the layer that contains Cu(II) species, λ is the inelastic mean free path of Cu(2p_{3/2}) photoelectrons through the CuO layer ($\approx 10.7 \text{ \AA}$) (29), ϕ is the angle at which the detector is positioned relative to the surface normal (so-called "take-off angle" = 55°), and %Cu(II) is the percentage of the integrated peak area of the Cu(2p_{3/2}) spectral envelope that is due to Cu(II) species (both the primary and shake-up peaks). This analysis assumes that the Cu(II) species in the copper substrate are present in a uniform layer nearest the sample/air interface (8). The use of thickness measurements derived from eq 1 for the Cu(II) species allows direct quantitative comparison of the spectral results for different samples and oxidizing conditions.

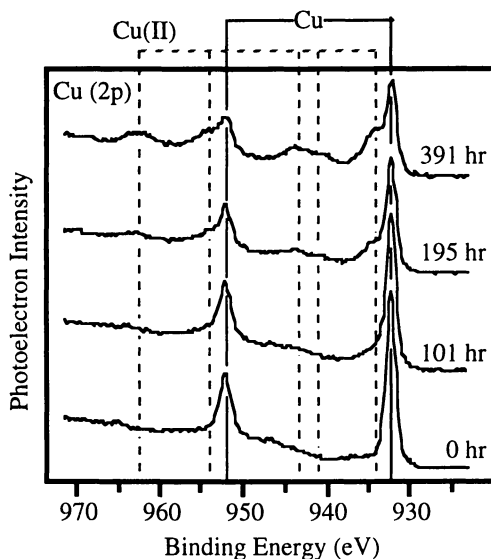


Figure 2. XPS spectra of the Cu(2p_{3/2}) region for copper samples derivatized with hexadecanethiol after various lengths of exposure to atmosphere.

Figure 2 displays an XPS spectrum for a freshly prepared copper sample that had been derivatized with hexadecanethiol and minimally exposed to atmosphere. This sample displayed no peaks due to Cu(II) species. Upon exposure of the copper surface to air, the XPS spectra exhibit peaks due to Cu(II) species that increase in intensity with

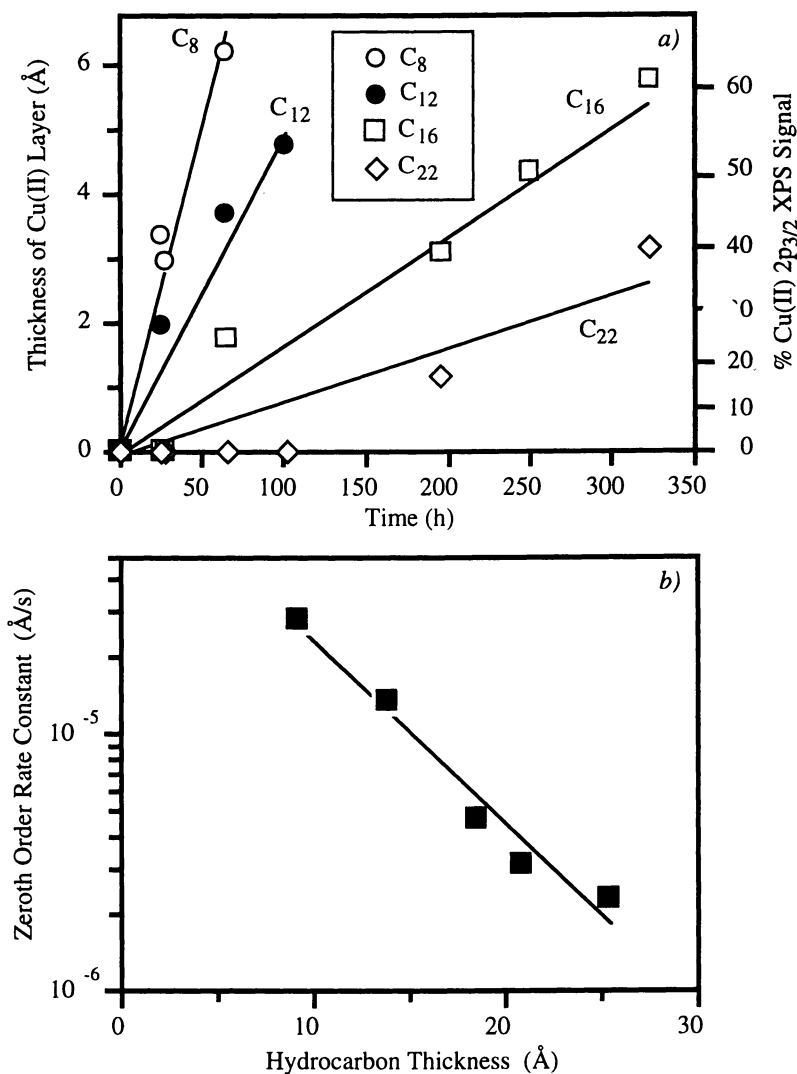


Figure 3. Extent of oxidation of the copper surface for various *n*-alkanethiolate monolayers on copper as a function of exposure time to the atmosphere. a) XPS-derived thicknesses of Cu(II) species for the samples; the lines represent zeroth-order best fits to the data. b) Relationship between the slopes of these lines and film thickness.

continued exposure (Figure 2). A comparison of the level of oxidation for different samples or different conditions provides information about the resistance of the system toward corrosion.

We investigated the relative differences that could be obtained in the barrier properties of these films as a function of their thickness. Figure 3a compares the corrosion resistance of copper samples that had been derivatized with alkanethiols varying in chain length between C_8 and C_{22} and exposed to air. Despite the small differences in the thickness of these layers (10 to 30 Å), we readily observed differences in the corrosion rates of the underlying copper substrates. With increasing chain length, the films exhibited superior levels of inhibition. A simple kinetic analysis of the data (Figure 3b) revealed that the rate of oxidation of the underlying copper decreased by 50% for every 4 Å (or roughly 3 CH_2 units) increase in the thickness of the monolayer film. Complementary studies of the oxidation of the adsorbed thiulates to sulfonates by XPS revealed similar conclusions that the thicker films are more effective as barrier films and they provide roughly twice the level of inhibition for thickness increases of 4 Å.

For use as barrier layers in heat exchanger operations, we examined the abilities of these films to inhibit corrosion under oxidizing conditions of high humidity levels and direct contact with oxygenated water. Bare copper rapidly oxidizes in these aqueous environments (14), and we expected that these conditions would provide a more difficult test for the self-assembled monolayers. Figure 4 displays the oxidation results for a docosanethiolate monolayer on copper that has been exposed to 1 atm O_2 under different levels of water exposure. Remarkably, we observed no differences in

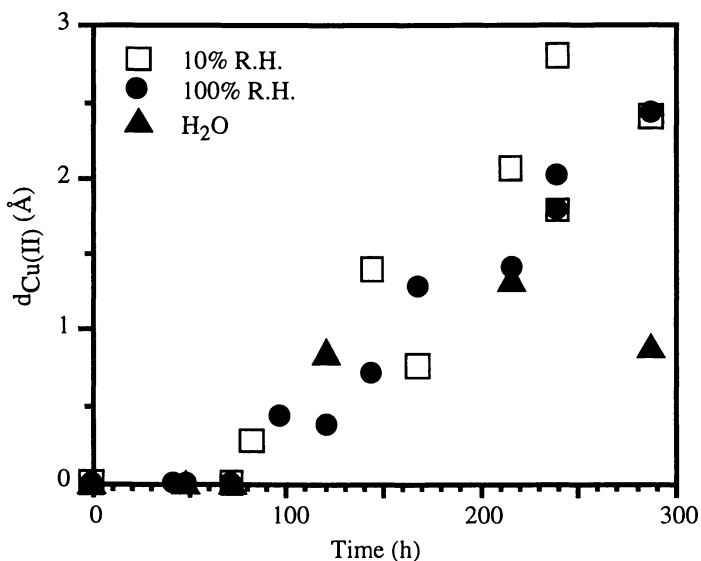


Figure 4. Comparison of the extent of oxidation for copper samples derivatized with $C_{22}H_{45}SH$ and exposed to 1 atm of O_2 at 10% and 100% relative humidity and to oxygen-saturated water at 1 atm. For comparison, untreated copper had a value for $d_{Cu(II)}$ of ~ 10 Å after 24 h of exposure to 100% relative humidity.

the corrosion rate for these samples suggesting that the densely packed alkanethiolate monolayer provides a useful hydrophobic barrier that prevents contact between water and the copper surface. Despite the presence of grain boundaries and defects that are expected to be present in the film, these factors seemingly do not appear to affect the barrier properties of the films. One reason may be that the selection of alkyl chains -- that become densely packed and adopt trans-zig-zag-extended structure upon adsorption -- provides some floppiness to the molecules and allow them to better accommodate the presence of imperfections within the layer. Such results may be difficult to obtain with the rigid aromatic molecules that are more often used as corrosion inhibitors on copper (vide supra).

To increase the thickness of the layer and its stability, we have begun investigation into the use of multilayer strategies for improving the barrier properties of thin films on copper. An advantage of the self-assembly method on copper is that it can produce films that express reactive functionalities at the monolayer/air interface that can be further functionalized. This strategy has been used successfully on gold to assemble alkyltrichlorosilanes onto hydroxyl-terminated monolayers (21-23). By analogy, we assembled $\text{HS}(\text{CH}_2)_{22}\text{OH}$ onto copper (to form a chemisorbed layer expressing a hydrophilic OH surface) and subsequently reacted it with octadecyltrichlorosilane from solution (Figure 5). The high level of reactivity of copper for the chloride that was

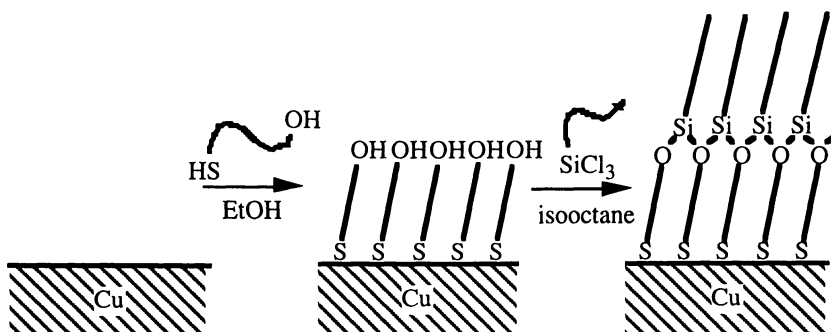


Figure 5. Schematic illustration of the formation of bilayer films on copper by the sequential adsorptions of an alkanethiol and an alkyltrichlorosilane.

produced during the reaction impeded our ability to form high quality films on the copper surface. By XPS, these films exhibited peaks due to chlorine. Using scavenger agents in the reaction mixture -- NaOH , Na_2CO_3 , etc. -- and dilute reaction conditions, we were able to form bilayers on copper that exhibited no chlorine peaks by XPS.

Figure 6 displays a comparison of the inhibition properties of the bilayer assembly and a shorter dodecanethiolate monolayer to 100% relative humidity at 1 atm O_2 . Despite its greater thickness, the bilayer proved to be an inferior barrier towards oxidation. The reaction process used to form the bilayer, despite the lack of chlorine by XPS, appears to affect the integrity of the initially formed copper sample as evidenced by the presence of $\text{Cu}(\text{II})$ species in the sample before its exposure to the oxidizing conditions. We examined a variety of conditions to improve the barrier characteristics of the bilayer and concluded that chlorine-based methods of forming self-assembled

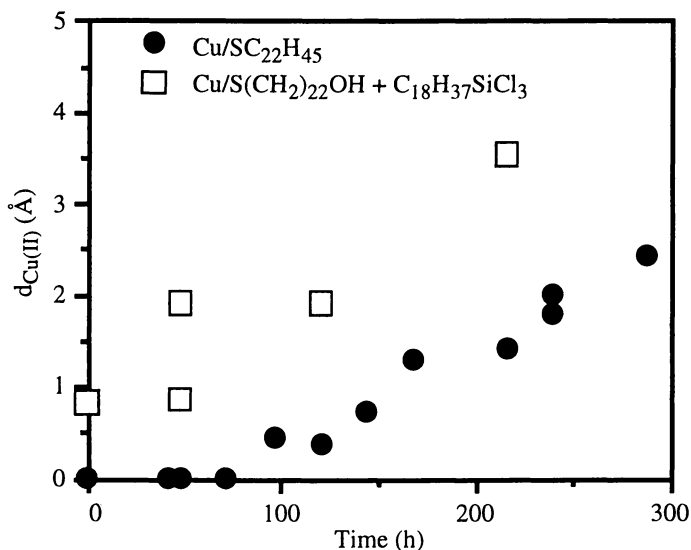


Figure 6. Extent of oxidation of the copper surface for samples derivatized with C₂₂H₄₅SH or a bilayer formed from sequential treatments with HS(CH₂)₂₂OH and C₁₈H₃₇SiCl₃ as a function of exposure time to 1 atm of O₂ at 100% relative humidity.

multilayers should be avoided on copper. Although the barrier properties of the bilayer were inferior to those of the monolayer, we observed that the stability of the bilayer -- as evidenced by the retention of its initial wetting properties (oleophobicity) -- was greatly improved over that for the monolayer (Figure 7). In Figure 7, decreases in the wetting properties by hexadecane on these layers indicate an increased level of disorder within the film (8, 30). As the silane treatment results in the formation of a cross-linked siloxane network within the bilayer, this network appears to stabilize the film and increase its lifetime. With the development of cross-linking strategies that are compatible with the reaction chemistry of copper, self-assembly methods should allow formation of high quality barrier films on copper with the improved lifetimes and thermal stabilities needed for practical application.

Summary

This study demonstrates that self-assembled monolayers formed from alkanethiols can be used to inhibit corrosion of copper in dry, humid and wet oxidizing conditions. Their similar performance under these conditions suggests that the layers are effective in screening the interaction between water and the metal substrate. This result is important for the potential application of these systems as barrier layers that contact aqueous streams. Longer-chained *n*-alkanethiols yielded thicker SAMs on the copper substrate that exhibited superior abilities to impede corrosion than did shorter-chained adsorbates. Efforts using existing multilayer strategies can produce thicker, more robust films on the copper surface; however, fine tuning of reaction chemistry is required to achieve superior levels of corrosion resistance. The development of such

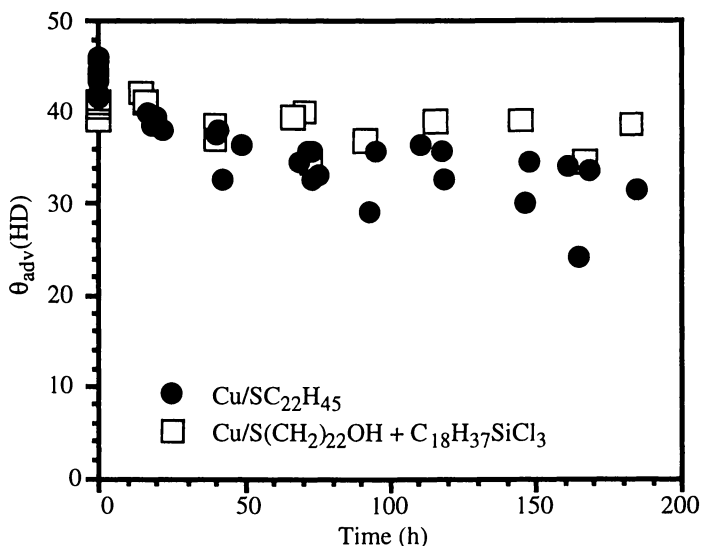


Figure 7. Extent of film integrity as probed by the advancing contact angle of hexadecane for copper samples functionalized with C₂₂H₄₅SH or a bilayer formed from sequential treatments with HS(CH₂)₂₂OH and C₁₈H₃₇SiCl₃ as a function of exposure time to 1 atm of O₂ at 100% relative humidity.

strategies should allow formation of corrosion resistant coatings on copper that remain stable under a wide variety of oxidizing conditions and require one-time chemical application for their generation and effective operation

Acknowledgments

This work supported by Sloan Funds administered by MIT and the Henry and Grace Doherty Career Development Chair to PEL through the MIT Sea Grant Program.

Literature Cited

- Holm, R.; Holtkamp, D.; Kleinstück, R.; Rother, H.-J.; Storp, S. *Fresenius Z. Anal. Chem.* **1989**, *333*, 546.
- Hashemi, T.; Hogarth, C. A. *Electrochimica Acta* **1988**, *33*, 1123.
- Brusic, V.; Frisch, M. A.; Eldridge, B. N.; Novak, F. P.; Kaufman, F. B.; Rush, B. M.; Frankel, G. S. *J. Electrochem. Soc.* **1991**, *138*, 2253.
- Aramaki, K.; Kiuchi, T.; Sumiyoshi, T.; Nishihara, H. *Corros. Sci.* **1991**, *32*, 593.
- Brunaro, G.; Parmigiani, F.; Perboni, G.; Rocchini, G.; Trabaneli, G. *Brit. Corros. J.* **1992**, *27*, 75.
- Gonzalez, S.; Laz, M. M.; Souto, R. M.; Salvarezza, R. C.; Arvia, A. J. *Corrosion* **1993**, *49*, 450.
- Carron, K. T.; Lewis, J.; Dong, J.; Ding, J.; Xue, G.; Chen, Y. *J. Mater. Sci.* **1993**, *28*, 4099.
- Laibinis, P. E.; Whitesides, G. M. *J. Am. Chem. Soc.* **1992**, *114*, 9022.

9. Yamamoto, Y.; Nishihara, H.; Aramaki, K. *J. Electrochem. Soc.* **1993**, *140*, 436.
10. Itoh, M.; Nishihara, H.; Aramaki, K. *J. Electrochem. Soc.* **1994**, *141*, 2018.
11. Itoh, M.; Nishihara, H.; Aramaki, K. *J. Electrochem. Soc.* **1995**, *142*, 1839.
12. Ishibashi, M.; Itoh, M.; Nishihara, H.; Aramaki, K. *Electrochimica Acta* **1996**, *41*, 241.
13. Jennings, G. K.; Laibinis, P. E. *Colloids and Surfaces A* **1996**, *116*, 105.
14. Torigoe, Y.; Ichino, T.; Nakano, Y. *Corros. Eng.* **1979**, *28*, 343.
15. Ulman, A. *An Introduction to Ultrathin Organic Films from Langmuir-Blodgett to Self-Assembly*; Academic Press: Boston, MA, 1991.
16. Dubois, L. H.; Nuzzo, R. G. *Annu. Rev. Phys. Chem.* **1992**, *43*, 437.
17. Bain, C. D.; Troughton, E. B.; Tao, Y.-T.; Evall, J.; Whitesides, G. M.; Nuzzo, R. G. *J. Am. Chem. Soc.* **1989**, *111*, 321.
18. Walczak, M. M.; Chung, C.; Stole, S. M.; Widrig, C. A.; Porter, M. D. *J. Am. Chem. Soc.* **1991**, *113*, 2370.
19. Laibinis, P. E.; Whitesides, G. M.; Allara, D. L.; Tao, Y.-T.; Parikh, A. N.; Nuzzo, R. G. *J. Am. Chem. Soc.* **1991**, *113*, 7152.
20. Laibinis, P. E.; Whitesides, G. M. *J. Am. Chem. Soc.* **1992**, *114*, 1990.
21. Netzer, L.; Iscovici, R.; Sagiv, J. *Thin Solid Films* **1983**, *99*, 235.
22. Tillman, N.; Ulman, A.; Penner, T. L. *Langmuir* **1989**, *5*, 101.
23. Ulman, A.; Tillman, N. *Langmuir* **1989**, *5*, 1418.
24. Porter, M. D.; Bright, T. B.; Allara, D. L.; Chidsey, C. E. D. *J. Am. Chem. Soc.* **1987**, *109*, 3559.
25. Chidsey, C. E. D.; Loiacono, D. N. *Langmuir* **1990**, *6*, 682.
26. Chidsey, C. E. D. *Science* **1991**, *252*, 668.
27. Xia, Y.; Kim, E.; Whitesides, G. M. *J. Electrochem. Soc.* **1996**, *143*, 1070.
28. Briggs, D.; Seah, M. P., Eds. *Practical Surface Analysis: Volume 1 Auger and X-ray Photoelectron Spectroscopy*; Wiley: Chichester, 1990.
29. Tanuma, S.; Powell, C. J.; Penn, D. R. *Surf. Interface Anal.* **1988**, *11*, 577.
30. Laibinis, P. E.; Nuzzo, R. G.; Whitesides, G. M. *J. Phys. Chem.* **1992**, *96*, 5097.

Chapter 34

Corrosion Protection with Organic Acid Sealants for Anodized Aluminum

Garson P. Shulman and Albert J. Bauman

Alumitec Products Corporation, Torrance, CA 90503

Long chain carboxylic acids applied to anodized aluminum react with the surface and fill the pores, providing excellent corrosion resistance. The best results are obtained using isostearic acid. Salt spray (ASTM B -117) lifetime of 2000 hours for corrosion prone alloys such as 2024 are achieved. Bath stability is improved by adding chelating agents such as benzotriazole. The acid-treated surface is hydrophobic but can be painted if applied from dilute solutions. Plating of other metals with aluminum provides equivalent protection.

Following the 1963 discovery by Kramer (1) that long chain carboxylic acids applied in the hot molten state greatly increased fatigue life and corrosion resistance of anodized aluminum, we have developed systems which provide corrosion protection with slight improvement in fatigue life when applied at ambient temperature (2). Typical data are summarized in Table I.

Conventional sealing of anodized aluminum results from conversion of an oxyhydroxide, boehmite, to aluminum trihydroxide. This process increases the volume of the oxide layer, closing the pores, which make up about half its volume. Carboxylic acid sealants form a water repellent aluminum soap on the surface, while the pores remain open, but filled with residual acid. Solvent extraction removes 90% of the isostearic acid, 10% is not soluble in isopropyl alcohol. For high copper corrosion-prone alloys (e.g. 2024 and/or 380 diecast), superior corrosion resistance as measured by ASTM B-117 salt spray testing of 2000 to 4000 hours can be obtained using stearic or isostearic acid. Certain conventional tests, Dye Stain (failed) and Acid Dissolution testing (416 mg/dm^2), which measure the integrity of a solid oxide coating, are not applicable to this organic type of sealing. Better results are obtained from Electrical Impedance Spectroscopy (26 megohm/cm^2) and Galvanic corrosion tests. These tests should be used for quick evaluation of organically sealed coatings.

EIS testing was conducted by Martin Kendig at Rockwell Science Center. Galvanic corrosion testing was performed by Kathy Lewis at Cortaulds Aerospace by

placing titanium and coated aluminum plates in an electrolyte anodized aluminum panels, the aircraft industry standard, and anodized aluminum panels treated with isostearic acid-0.1% benzotriazole reduced the current by about the same amount.

Table I. Salt Spray Testing of Sulfuric Acid Anodized 2024 Treated with Chelating Agents Dissolved in Isostearic Acid

CHELATING AGENT	AMOUNT (%)	TIME TO FAILURE (hours)
BZA*	saturated	816
BZT**	0	2050
BZT	0.1	1650
BZT	0.5	1400
BZT	1.0	1200
BZT	3.0	1056
BZA PRETREAT	0	2050
BZT***	0.1	1650

* = BENZOTRIAZOLE-5-CARBOXYLIC ACID

** = BENZOTRIAZOLE

*** = SANODAL DYED BEFORE SEALING

Most alloys of aluminum can be protected in this way, and most long chain carboxylic acids provide at least some corrosion resistance. Salt spray life increases steadily from 12 to 18 carbons in the acid, with good results also from 12-hydroxystearic acid and azelaic acid. Perfluorinated benzoic and octanoic acids did not provide protection. Alloys which have been tested include 1100 (pure aluminum), 2014, 2024, and 380 (high copper corrosion prone alloys), 5354, 6061, and 7075.

The copper content of 2000 series aluminum alloys would be expected to have a catastrophic effect on bath life if any dissolved. Copper is a well-known catalyst for oxidation of fatty acids. Kramer observed rapid degradation of linear 18 and 22 carbon acids. Branched acids would be more prone to oxidation. Benzotriazole was added to chelate copper, in an attempt to increase bath stability. Accelerated aging tests, 90 days at 90° C., resulted in less than 25% decomposition of the isostearic acid, assuring a multi-year bath life at ambient temperatures

Cleaning

Liquid high molecular weight acids are similar to light mineral oil in their physical properties. After immersion of the aluminum in sealant, an oily film adheres to the surface. In the laboratory, this film can conveniently be removed by wiping with a soft cloth or paper towels-this method is obviously not satisfactory for large-scale production. N-Methylpyrrolidone (NMP) is a good solvent for the excess acid, but used neat it also removes material from the pores. A mixture of 40% to 50% water in NMP allows for excess removal without extracting liquid from the pores. For small parts, tumbling with absorbent materials has proven satisfactory. Mineral absorbents (cat litter) have been used successfully. Sawdust, ground cork, and similar materials should also be usable.

Paintability

Methods for coloring and protecting aluminum surfaces were also developed. Following up on the NMP excess removal, it was found that 15% to 25% solutions of isostearic acid in NMP could be used to seal anodized aluminum, with some loss of corrosion resistance (Table II). The NMP is soluble in water and can be removed by rinsing. Surfaces treated in this way will accept epoxy primers or topcoat without further treatment.

Table II. Paintability after NMP/Isostearic Acid Sealing

ISOSTEARIC ACID (%)	SALT SPRAYWET TAPE TEST (Hrs)	(Epoxy)
10	300	Pass
15	500	Pass
25	1400	Pass
50	--	Fail
100	2000	Fail

A preferred method of imparting color is with use of water-soluble dyes or inks before sealing. The amount of dye and sealant needed to fill the pores of an anodized coating 0.3 mil thick is the equivalent of 0.15 mil, compared to 1 to 2 mil for paint. This allows for significant savings of weight, paint and labor costs.

Protection of Other Metals

The excellent corrosion resistance achievable on aluminum can be extended to other metals. A thin (0.8 to 1 mil) coating of aluminum, applied by dip, electroplate, or thermal decomposition can be anodized, then sealed (3). Porous coatings, such as those from ion vapor deposition, can not be anodized. Steel panels treated in this way have survived over 3600 hours of ASTM B-117 salt spray.

Literature Cited

1. Kramer, I.R. and Burrows, C.F, U.S. Patent 3,510,411, 1970.
2. Shulman, G.P. and Bauman, A.J. *Metal Finishing* **1995**, 93, No. 7, 16.
3. Shulman, G.P.; Bauman, A.J. and Frömberg, W. *Metal Finishing* **1996**, 94, No. 6, 93.

Chapter 35

Electrochemical Properties of Coatings from Renewable Natural Products

U. G. Hermann, Gordon P. Bierwagen, D. J. Mills, and V. H. Hauser

Department of Polymers and Coatings, North Dakota State University,
Fargo, ND 58105

Organic coatings based on renewable natural products were investigated using DC Resistance Measurements, Electrochemical Impedance Spectroscopy and Electrochemical Noise Measurements. The binder component was an alkyd diluted by variable amount of modified linseed oil (Dilulin[®], Cargill Co. Ltd.). Unpigmented films on mild steel initially showed a moderate resistance (consistently for Resistance Noise, Impedance and DC Resistance around $10^8 \Omega \text{cm}^2$) decreasing after 8 weeks of immersion in 3% NaCl solution to approximately $10^6 \Omega \text{cm}^2$. Corrosion inhibitive pigments (chromate replacements) were added to the binder to improve the protective properties and the resultant coatings were investigated by the aforementioned methods. Zinc molybdates and zinc phosphates increased the resistance slightly and maintained this higher film resistance for a longer time of exposure, while borosilicates were detrimental to the coating and phosphosilicates showed an only mediocre increase in performance.

Linseed oil is from renewable resources, a natural product coming from flax, and grown in the Great Plains of the USA and southern Canada. Linseed oil or modified linseed oil products can be added to organic resins as an environmentally friendly reactive diluent, as they are classified as being 100% solids. These products can produce durable and protective coatings, which are non-sticky and air-drying (1). Also, linseed oil can act as a replacement for volatile organics (VOC), the reduction of which is demanded by the Clean Air Act of 1990 (2).

In this respect, paints containing reactive diluents can be superior to waterborne coatings as the latter usually contain small amounts of organic solvents (3). Also, for water borne systems, the strong polar groups needed for solubility in water may make the film water sensitive and permit other corrosion promoting species to penetrate a coating system.

Linseed oil, in comparison to other unsaturated vegetable oils e.g. sunflower oil, has a very high cross-linking rate after the addition of a cobalt or zirconium catalyst and exposure to the air. This is due to the high content of linolenic acid (approximately 55%). Linolenic acid contains three double bonds in 9,12 and 15 position in the fatty acid moiety of the oil forming triglyceride (4). Dilulin[®] (Cargill, Inc), used as a modified linseed oil (MLO) product, is formed by a controlled reaction of linseed oil with cyclopentadiene (under formation of bicyclic moieties and retention of the double bonds) and is a low molecular weight copolymer (5) with low tendency to yellowing. MLO was added to an alkyd resin (VOC: 10 % mostly as hydrocarbons) in order to produce ultra-low VOC and simultaneously "high solids" coatings with a relatively long lifetime. The concentration of MLO ranged from 0 to 50% w/w.

The objective of this work is to study electrochemical properties of unpigmented and pigmented alkyd coatings with a variable content of modified linseed oil product on mild steel substrates. The following electrochemical methods were applied: a) DC Resistance Measurements (6) (giving a first and fast insight into the corrosion protective power of a coating), b) Electrochemical Impedance Spectroscopy (EIS, giving deeper, electrochemical information (7-8) related to the capacitive/imaginary part of resistance/impedance by measuring the frequency dependence of impedance), and c) Electrochemical Noise Methods (ENM, Current and Voltage Noise are measured simultaneously while the Noise Resistance R_n is calculated by division of the standard deviations of Voltage and Current Noise) (9-12). AC Impedance and especially the capacitive resistance are determined by the exposed coatings' physical and chemical properties and are strongly dependent on the frequency of the applied AC voltage. A transition from capacitive to resistive (Ohmic) behavior is observed at the breakpoint frequency. A high (Ohmic) resistance is characteristic for good and protective coatings. A low breakpoint frequency (range: 10^{-2} - 10^0 Hz) over several weeks of exposure is a diagnostic criterion for good coatings. Therefore, EIS and ENM Spectra allow, at least partially, a lifetime prediction of coatings (7-8). Films with an Ohmic Resistance higher than 10^9 Ohm cm^2 mostly show a good performance and a long lifetime, while coatings with a resistance below 10^6 Ohm cm^2 are not considered to be long-term protective. Protective coatings for industrial purposes are expected to show an initial Ohmic Resistance higher than 10^8 Ohms.

Since the alkyd coatings used in this paper are inexpensive, but provide only a mediocre protection for steel substrates, corrosion inhibitive pigments like borosilicates (CW-291[®] of Halox), zinc molybdates/phosphates (Moly-White ZNP[®] of Sherwin-Williams) and zinc phosphates (Phosguard Hispafos J-0853[®] of Mineral Pigments) were used at different pigment volume concentrations (PVC) in order to further improve our coatings.

EXPERIMENTAL

The Binder. A long oil alkyd resin (product 57 5866, McWhorter Technologies) was used (VOC: 10% as petroleum, heavy naphtha, xylene and ethylbenzene). Dilulin[®] (Cargill, Inc. Minneapolis, MN) was employed as reactive diluent; it is a low-molecular copolymer of linseed oil with cyclopentadiene (M_w : 2500 Dalton; containing 98% minimum non-volatile organics) (5). The following catalysts (Nuodex, Inc.) were used as driers: (a) Zirconium (1.5% w/w in binder): Nuocure

Zirconium 12% Catalyst as through-drier and (b) Cobalt (0.05 % w/w in binder): NuXtra Cobalt 12% Catalyst as top-drier. A higher top-drier (Co) content caused wrinkled coating surfaces if the layer thickness exceeded 45 μm . Dry coatings were stored for at least 3 weeks in air prior to use for measurements. The Stormer viscosity ranged from 128 k.u. (10% MLO) to 70 k.u. (50 MLO) for diluted alkyd solutions. After admixture of the pure binder, pigments were added in the specified volume concentrations. The following pigments were used:

- CBSP CW-291[®] (Halox, Hammond, IN, USA)
 - properties: formula $1.2 \text{ CaO} \cdot 0.2 \text{ B}_2\text{O}_3 \cdot \text{SiO}_2 \cdot 0.5 \text{ H}_2\text{O}$ (150.3 g/mol)
 - mean particle size (avg.): 3.4 micron Hegman Grind: 5.0
 - spec. grav. (g/mL): 2.71 oil absorption: 27.0 g/100g pigment
- basic ZM/P Pigment Moly-White ZNP[®] (Sherwin-Williams Chemicals)
 - properties: formula $\text{ZnMoO}_4 \cdot \text{ZnO} \cdot \text{Zn}_3(\text{PO}_4)_2$
 - mean particle size (avg.): 1.17 micron Hegman Grind: 5.0
 - spec. grav. (g/mL): 4.0 oil absorption: 13.5 g/100 g pigment
 - appearance: white odorless powder solubility: 0.30g/100mL water
- ZP pigment Phosguard Hispafos J 0853 (Mineral Pigments, Beltsville, MD, USA)
 - properties: formula $\text{Zn}_3(\text{PO}_4)_2 \cdot 2-4 \text{ H}_2\text{O}$
 - mean particle size (avg.): 1-5 micron spec. grav. (g/mL): 3.4
 - oil absorption: 50g/100g pigment solubility: 0.0052g/100mL water
 - Critical Pigment Volume Concentration (CPVC): 35%
- CPP pigment CW-491[®] (Halox, Hammond, IN, USA)
 - properties: formula $2 \text{ CaO} \cdot 0.5 \text{ P}_2\text{O}_5 \cdot \text{SiO}_2 \cdot \text{H}_2\text{O}$
 - mean particle size (avg.): 2.6 micron Hegman Grind: 5.0
 - spec. grav. (g/mL): 2.69 oil absorption: 49g/100g pigment
 - solubility: 0.02g/100 mL water pH: 7.8

Substrates and their treatment. Test panels “Bonderite[®] 1000” (25 polished, cold rolled steel), 3”x9” (di. water rinse), Parker Chemical Co., were used. Steel substrates were cleaned by a fine emery paper and washed in pure toluene and acetone prior to use.

Layer Thickness Measurement. The layer thickness of coatings was measured by an Elcometer[®] 345 FS (battery) for ferrous substrates (range 0-1250 micron).

DC Resistance Measurements. A Keithley 617 Programmable Electrometer was used (Automatic Ohmic Mode). Reference electrode was a Saturated Calomel Electrode (SCE).

Electrochemical AC Impedance Spectroscopy (EIS). Smooth alkyd coatings on steel substrates were investigated by EIS (GAMRY Corrosion Measurement System and Potentiostat; Schlumberger SI 1250 Frequency Response Analyzer) in the potentiostatic mode. An electrochemical cell was built by attaching a polyvinylchloride pipe (ASTM D 1785) on the coating using a silicon adhesive (area: 11.8 cm^2). After drying of the adhesive, the pipe was filled with 3% w/w NaCl solution and equipped with a Counter Electrode (Platinum foil) and a Saturated Calomel Electrode (SCE) as Reference. The applied AC Voltage Amplitude was mostly 100 mV and the frequency ranged from 65500 Hz to 0.01 Hz. The Ohmic resistance, measured by Impedance Spectroscopy via log Z (modulus of impedance) vs. log frequency plots (Bode plots) at zero frequency, was confirmed by DC

Resistance and always showed a very good agreement. Generally, three identical samples were measured.

Electrochemical Noise Measurements (ENM). Two electrochemical cells were built by attaching polyvinylchloride pipes as for the EIS measurements. After drying of the adhesive, the pipes were filled with 3% w/w NaCl solution and the two cells were connected by a salt bridge. The cell on one of the coated substrates acting as Working Electrode 1 was equipped with an Ag/AgCl Reference Electrode, while the other substrate acted as the Working Electrode 2. The measurement system was the same as described earlier (10). The Noise Resistance was calculated from the current and voltage noise by division of the standard deviations of voltage and current noise (9-10). Current and voltage noise were obtained in 7 time series with 128 datapoints each (recorded every two seconds) with a total block time of 256 seconds.

RESULTS AND DISCUSSION

Unpigmented Films. In preliminary investigations it was found that unpigmented long oil alkyd coatings diluted by variable amounts of MLO showed a low DC Resistance of roughly $10^5 \text{ Ohm} \cdot \text{cm}^2$ if the layer thickness was low at around 10-20 μm which decreased in inverse proportion to modified linseed oil content. In contrast, unpigmented films with a layer thickness around 50 μm showed a much higher DC Resistance of roughly 10^8 - $10^9 \Omega \text{cm}^2$. So, a layer thickness in the range of 50 micron and higher was chosen for the following experiments with a variable content of Dilulin[®] from 0 to 50% w/w (corresponding VOC: 10-5% mainly as aliphatic hydrocarbons). In the following, Noise Resistance, DC Resistance and EIS Spectra were measured.

DC Resistance and Noise Resistance of unpigmented films containing 0-50% w/w MLO stayed almost constant at a moderately high level for approximately eight weeks of exposure to 3% w/w NaCl solution (as electrolyte and corroding reagent). The log average value of 3 representative and nominally identical samples dropped only slightly from around 10^8 to 10^7 - $10^6 \Omega \text{cm}^2$ (cf. Figure 1 giving a synopsis over the variable MLO contents and showing a plateau-like region). This level of resistance is typical for good coatings - but not for excellent coatings. The observed behavior seems to be a general tendency for all measured unpigmented coatings with varying MLO content. A slightly faster decay was only observed for coatings with a MLO content of 40% and 50% where the resistance mostly fell to the $10^6 \Omega$ level after 40-50 days. This effect can be ascribed to a slight deterioration of the film properties with increasing content of the modified LO. For the most part, some tiny rusty spots could be observed visually after an exposure time of 3-4 weeks. All resistance values are given as logarithm or as arithmetical average of logarithmic values. The standard deviation of log noise resistance was mostly between 0.1 and 1 this indicates a fair to good reliability of the data. In each case, a good correlation with DC Resistance values was obtained, i.e. Noise Resistance was in the same order of magnitude as DC Resistance and no significant contributions of frequency dependent parts (impedance) were observed at this point of our investigations (especially after averaging over 3 samples).

Electrochemical Impedance Spectra support the aforementioned results: Initially, a relatively high impedance at zero-frequency (extrapolation to left R-axis with

slope ~ 0) of around $10^8 \Omega$ was measured which dropped slightly with the immersion time and which is consistent with DC Resistance and Noise Resistance measurements. Figure 2 shows the observed log impedance vs. log frequency plots (Bode plots) of a coating containing 20% w/w MLO with a layer thickness of 40 μm directly after immersion and after 1, 3, 5 weeks of immersion. After this exposure time a slight decrease of resistance at low or zero-frequency of roughly one order of magnitude occurred. Generally, a shift of the "breakpoint frequency" in Bode plots, i.e. the transition from capacitive (slope: -1) to resistive behaviour (slope: ~ 0), from roughly 10^{-1} to 10^0 Hz was observed after several weeks of immersion - indicating a slight deterioration of the coating and the beginning of corrosion.

Pigmented Films/Coatings

The alkyd binder containing 10% w/w MLO as described above was pigmented by corrosion inhibitive pigments to achieve a better protection and a longer lifetime of coated substrates. Again, a layer thickness around 40-50 μm was chosen. However, higher pigment contents provided thicker layers because shrinkage on curing was reduced by pigment particles.

Borosilicate Pigments

The pigment CW-291[®] (Borosilicate of Halox) was investigated. Pigment volume concentration of 10-40% at a MLO content of 10% w/w was chosen and the paint was applied onto steel substrates. The VOC was 6.5-3.0% in the pigmented paint and 9% in the clear binder. The layer thickness of the pigmented films changed with the pigmentation level. However, a significant increase was only found for the highest PVC. An increase from 35 μm (10%, 20% PVC) to 42 μm (30% PVC) and 74 μm (40% PVC) was observed due to higher pigment content.

Generally, DC Resistance measurements showed only poor results: initially, with PVC 10-30% coatings a resistance around $10^5 \Omega \text{cm}^2$ was measured which dropped after 1-2 days below the electrode resistance ($\cong 10^3 \Omega \text{cm}^2$). Noise Resistance measurements (cf. Figure 3) showed similar results: a decrease from around $10^6 \Omega \text{cm}^2$ to around $10^4 \Omega \text{cm}^2$ was observed for a PVC between 10 and 30% after one day of immersion. However, a much thicker film with 40% PVC showed only a slight decrease from around 10^7 to $10^6 \Omega \text{cm}^2$ within 7 days, but small rusty spots and discoloration were observed visually after 3 days. Additionally, the average potential in ENM measurements (from 7 time blocks averaged over 3 samples) decreased to the corrosion potential of bare iron (appr. -720mV) after 1 day of immersion. These results are supported by EIS Spectra: log impedance vs. log frequency plots (Bode plots) of the investigated coatings mostly showed low resistance at extrapolated zero-frequency and high breakpoint frequencies at around 10^2 - 10^5 Hz directly after immersion - what is typical for poor coatings. Only the thicker PVC 40% coating initially showed a higher Ohmic resistance around 10^7 Ohms which however, decreased after few days to 10^{5-6} Ohms while the breakpoint frequency was high at appr. 10^3 Hz (cf. Figure 4).

Finally, a pigmentation with the borosilicate pigment did not show an improvement of corrosion protective properties in comparison to unpigmented films.

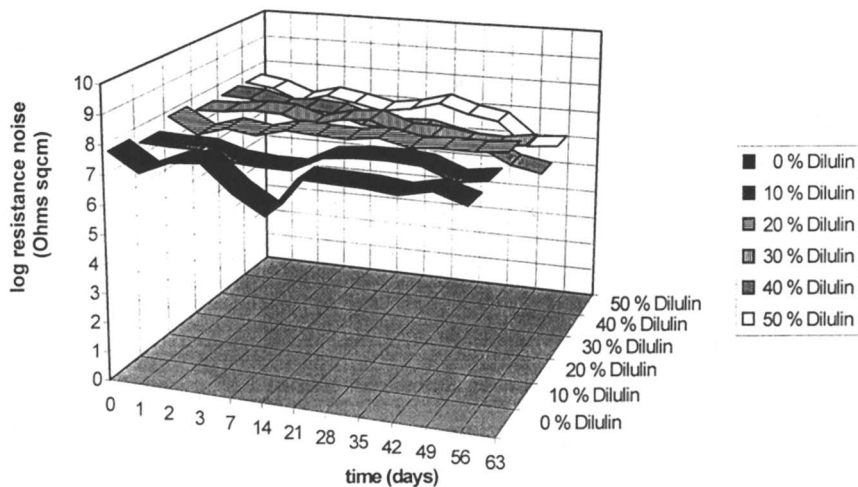


Figure 1. Synopsis of log resistance noise vs. modified linseed oil content vs. immersion time of long oil alkyd coatings containing 0 - 50% w/w MLO (layer thickness: 40-60 micron; VOC 10 - 5 %).

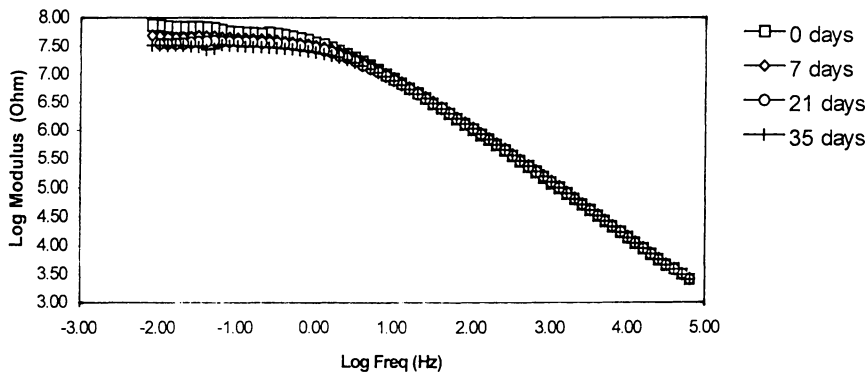


Figure 2. Log impedance (modulus) vs. log frequency plot (Bode plot) of a 40 μm alkyd film containing 20% MLO on steel after 0, 7, 21 and 35 days of immersion in 3% NaCl solution.

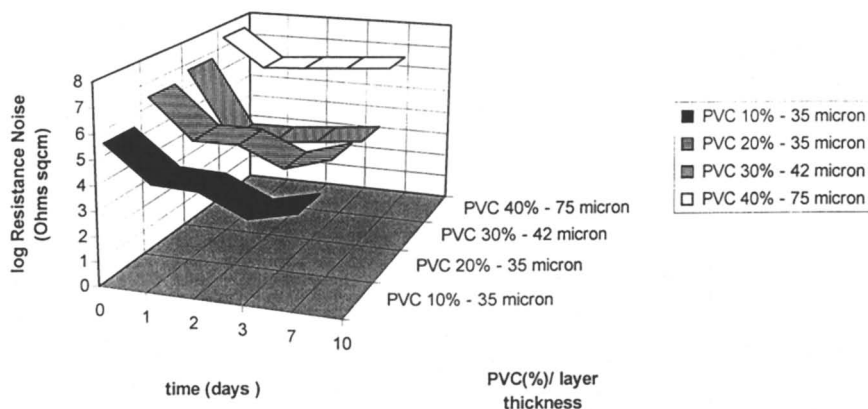


Figure 3. Synopsis of log resistance noise vs. immersion time (vs. PVC/layer thickness) of long oil alkyd coatings containing 10% MLO and a PVC of 10-40% of borosilicate pigment (VOC 6.5-3%; 9% in clear binder).

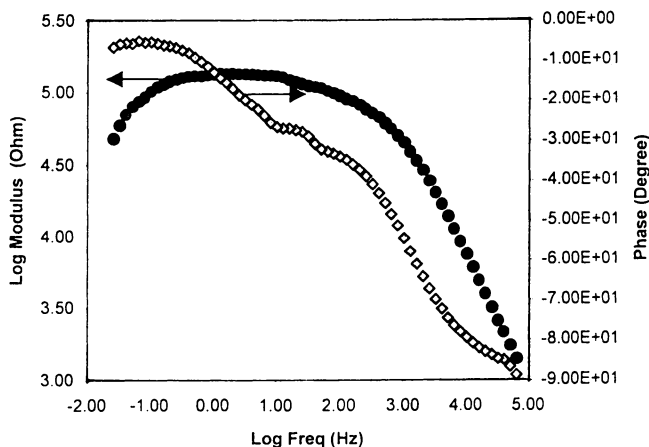


Figure 4. Log Modulus (o) and Phase angle (\diamond) vs. log frequency (Bode) plots of a long oil alkyd coating containing 10% MLO and a PVC of 40% of borosilicate pigment (VOC 6.5-3%; 9% in clear binder; film thickness: 75 μ m).

Only the thickest film showed a slightly protective behavior. Also, we conclude that for this pigment a thick film is not much more protective than a thin one.

Zinc Molybdate Pigments

Zinc molybdate pigments (Moly-White ZNP[®]) were also under investigation. We chose a PVC ranging between 10 and 40% and a MLO content of 40% w/w (corresponding to a VOC of 4-1.5% in paint and of 6% in the clear binder). After drying a relatively high and constant layer thickness around 70 μm was obtained. The coatings were investigated by the aforementioned methods. DC Resistance (for the chosen PVC) was initially high at around $10^8\text{-}10^9\Omega\cdot\text{cm}^2$. For a PVC from 10-30 % it dropped only slightly within the exposure time to values around $10^7\Omega\cdot\text{cm}^2$ while it stayed nearly constant at $10^8\Omega\cdot\text{cm}^2$ over 8 weeks for a PVC of 40% - indicating good protection. Almost the same behaviour was found for Noise Resistance measurements, which ranged in the same order of magnitude as the DC Resistance (Figure 5). Since the layer thickness was nearly constant, a slight increase of the resistance with increasing PVC could be observed. Additionally, the voltage (noise) and the average potential in Electrochemical Noise Measurements decreased only slowly and mostly stayed positive for several weeks of immersion. This indicates that the coating provided good protection. EIS Spectra support the aforementioned results again: Figure 6 shows the observed log impedance vs. log frequency (Bode) plots of a 20% PVC coating after 0 and after 56 days of immersion. The initial plot indicates or predicts a relatively high resistance and a good protection because the Ohmic resistance is relatively high and the breakpoint frequency is low.

Phosphosilicate Pigments

A calcium phosphosilicate pigment (CW-491[®] of Halox) was used in a 10% MLO containing alkyd binder solution. This system showed a slightly faster decay of noise resistance than zinc molybdates within 8 weeks (cf. Figure 5 & 7), namely from $10^8\Omega\cdot\text{cm}^2$ (initial measurement) to around $10^5\Omega\cdot\text{cm}^2$ (after 8 weeks of immersion). Remarkably, no significant influence of the PVC (ranging from 10 to 40%) or layer thickness (55 -95 μm) could be found in this case. Again, the values were confirmed by EIS (Figure 8, for a PVC of 30% at a layer thickness of 65 μm) and by DC Resistance measurements (Figure 7).

Zinc Phosphate Pigments

We also investigated a pure zinc phosphate pigment (Phosguard Hispafos J-0853 of Mineral Pigments). Generally, zinc phosphates are well known as good corrosion inhibitors (12). Therefore, alkyd coatings containing 10% w/w MLO were produced, pigmented by 10 to 30% PVC of the aforementioned pigment (VOC: 6-3.4% in paint). The layer thickness increased strongly with the PVC from 85 (PVC 10%) to 110 μm (PVC 20%) and 160 μm (PVC 30%) using a 7 mils bar-coater. For this system DC Resistance after immersion in 3% NaCl solution was measured. Initially, we found a relatively high and long-lasting resistance around $10^8 - 10^9\Omega\cdot\text{cm}^2$ even for a low PVC. The highest PVC (and highest layer thickness) system showed the

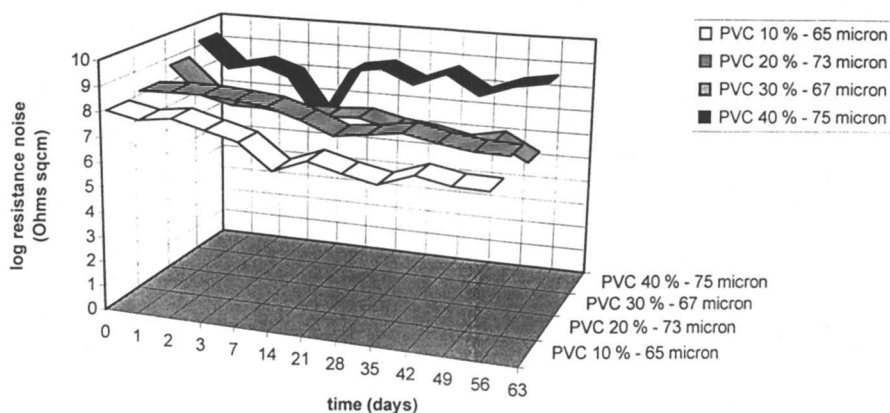


Figure 5. Resistance Noise and DC Resistance of coatings pigmented by 10-40 vol % inhibitive pigment Zinc Molybdate/Phosphate in dependence of immersion time in 3% NaCl solution (VOC: 4 - 1.5% in paint; 6% in clear binder).

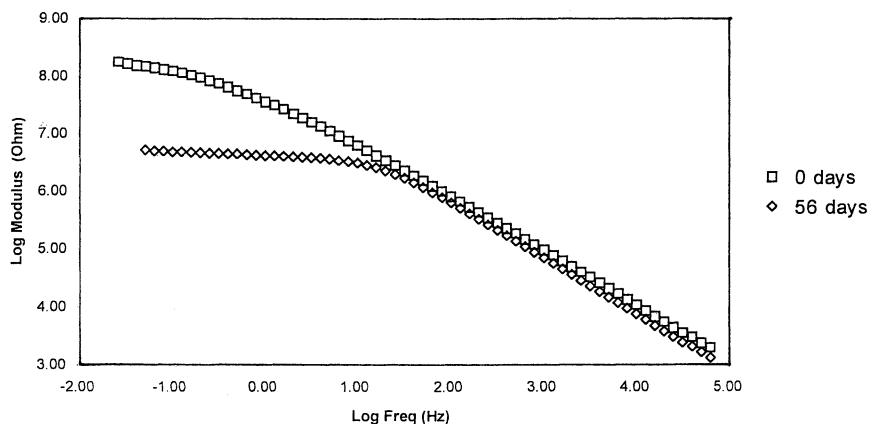


Figure 6: Log impedance vs. frequency plot (Bode plot) of a 73 μm alkyd coating on steel containing 40% w/w MLO and 20% PVC pigment Zinc Molybdate/Phosphate after 0 days and after 56 days of immersion in 3% NaCl solution.

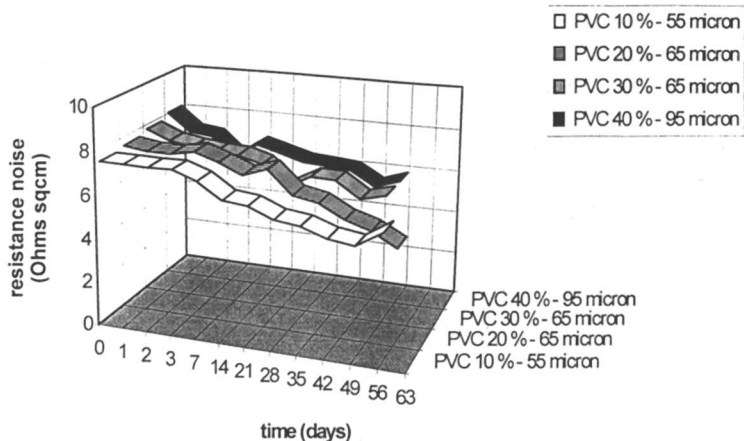


Figure 7: Synopsis of log resistance noise vs. PVC/layer thickness vs. immersion time of alkyd coatings containing 10% MLO and a PVC of 10 - 40% of phosphosilicate pigment.

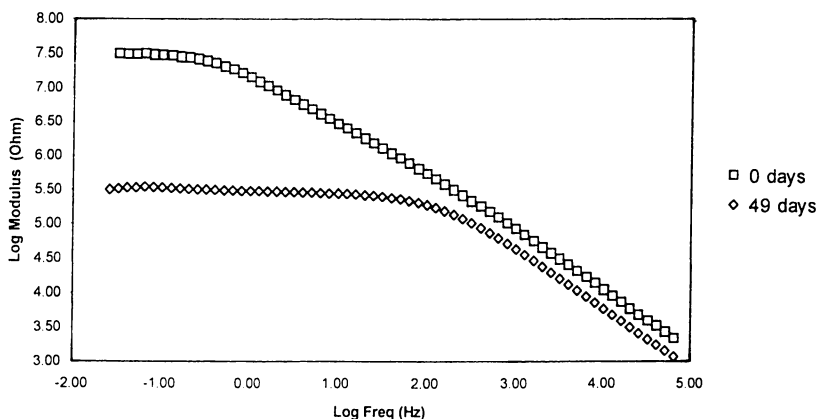


Figure 8: Log Impedance (Modulus) vs. Frequency (Bode) Plot of a 65 μm Alkyd Coating on Steel containing 40% w/w MLO and 30% PVC Calcium Phosphosilicate Pigment after 0 and after 49 days of immersion in 3% NaCl solution.

highest DC Resistance maintaining for at least eight weeks. One series containing a PVC of 10% was additionally dried hot (5 hrs at 80° C in the oven). This series however, showed only slightly higher resistance values than the series cured at ambient. These long lasting, high DC Resistance systems give hope that high resistance noise values combined with excellent EIS spectra and a long service lifetime will be obtained.

CONCLUSIONS

Unpigmented and pigment containing coatings consisting of a long-oil alkyd and a variable amount of a modified linseed oil product were applied onto mild steel substrates. DC Resistance, EIS spectra and ENM spectra were measured and showed a good agreement. A good correlation of electrochemical (resistance) data and the visual appearance was mostly observed (e.g. the slow growth of blisters or rusty spots after some weeks of exposure to the corrosive medium). Thinner films mostly showed a lower resistance and a faster decrease than thicker ones (except in the case of phosphosilicate pigment). No significant differences with changing content of MLO could be observed which makes this product a useful reactive diluent for the studied alkyd system.

The pigments used showed a very different behavior. ENM in combination with the well-known EIS technique and DC Resistance were able to detect these differences in performance and could provide (at least partially) a lifetime prediction. Borosilicate pigments in alkyd binder consistently showed a poor performance, while basic zinc molybdates and zinc phosphates showed much better protective properties with longer lifetime and stable level of resistance especially for thicker films and/or high PVC. Phosphosilicate pigments showed a mediocre performance without significant effects of PVC or layer thickness.

Deviations of noise resistance in the initial phase of immersion can be related to diffusion effects and remaining frequency dependent parts (high frequency fluctuations of noise based on elementary corrosion processes) of resistance/impedance. High frequency fluctuations in noise resistance can be correlated with a low corrosion rate and an excellent protection (11).

In future work we intend to study further alkyd systems and waterborne coatings like alkyds or acrylic copolymers pigmented with the aforementioned corrosion inhibitive pigments. Additionally, further corrosion inhibitive pigments (chromate replacements) in alkyd/linseed oil binders and/or different electrolyte solutions (cf.10) will be under investigation next.

ACKNOWLEDGEMENTS

We thank USDA-CSRS (contract no. 93-COOP-1-9537) for financial support. Further, we thank Halox Pigments Inc., the Sherwin-Williams Co. and Mineral Pigments Corp./Davis Colors for the supply of corrosion inhibitive pigments. We also thank McWhorter Technologies and Cargill, Inc. for the supply of binder materials.

Literature Cited

- 1 Formo, M. In 50th Meeting of the Flax Institute, Fargo, ND, January 26-27, 1989, 14.
- 2 Maty, J. *Am. Paint & Coat. J.* **1994**, Aug. 15, p. 19.
- 3 Lane, K.; Wilhelmi, M. *Am. Paint & Coat. J.* **1994**, Aug. 15, p. 53.
- 4 Holmberg, K. In *High Solids Alkyd Resins*; Dekker M.; New York, NY, 1987; p.182.
- 5 Kodali, D. (Cargill Inc., Central Research, Minneapolis, MN, USA) Western Coatings Society, 22nd Biennial Symposium, San Francisco, CA, February 20-22, 1995.
- 6 Bacon, R. C.; Smith, J. J.; Rugg, F. M. *Ind. Eng. Chem.* **1948**, 40, p. 161.
- 7 Kendig, M.; Scully, J. *Corrosion* **1990**, 46(1), p. 22.
- 8 Scully, J.; Hensley, S. *Corrosion* **1994**, 50(9), p. 705.
- 9 Skerry, B.; Eden, D. *Progr. Org. Coatings* **1987**, 15, p. 269.
- 10 Mills, D. J.; Bierwagen, G. P.; Skerry, B.; Tallman, D. In *12th International Corrosion Congress*, Sept. 1993, Houston, TX, USA, published by NACE, p. 182.
- 11 Moon, M.; Skerry, B. *J. Coat. Techn.* **1995**, 67(843), p. 35.
- 12 Bierwagen, G. P. *Corrosion 95* (The NACE International Annual Conference and Corrosion Show), Research in Progress Symposium, March 27 - 29, 1995 Orlando, FL, USA.
- 13 Penne, R. *J. Coat. Techn.* **1982**, 54(690), p. 51.

Author Index

- Aklian, J. H., 223
Balbyshev, V. N., 292
Barbour, Carleton J., 31
Barinov, V. Yu., 302
Bauman, Albert J., 420
Bellucci, F., 199, 211
Berg, R. L., 292
Bierwagen, Gordon P., 1, 123, 151, 292, 308, 423
Bonora, P. L., 92
Brady, Robert F., Jr., 282
Brandt, C. P., 238
Briggs, G. A. D., 106
Chang, S. S., 211
Connors, K. D., 332
Crossen, J. D., 106
de Wit, J. H. W., 45, 69
Deflorian, E., 92
Ding, Tianzhong, 382
Fangmeier, A. W., 238
Fedrizzi, L., 92
Ferrari, G. M., 45, 69
Ford, T. E., 211
Gilicinski, Andrew G., 396
Gu, J.-D., 211
Han, L. T., 174
Hauser, V. H., 423
Hermann, U. G., 423
Hörnström, S.-E., 335
Jansen, Susan A., 382
Jeffcoate, Carol S., 123, 151
Jennings, G. Kane, 409
Jia, Xinru, 382
Jin, Danliang, 382
Johnson J. B., 270
Kalenda, P., 366
Kalendová, A., 366
Karlsson, J., 335
Kock, E., 238
Laibinis, Paul E., 409
Latanision, R. M., 211
Lee, C. C., 174
Lewis, K. J., 223
Lomas, J. P., 106
Mansfeld, F., 174
McAndrew, T. Page, 396
Miller, Susan A., 396
Mills, D. J., 423
Mitchell, R., 211
Mitton, D. B., 211
Monetta, T., 199
Murray, J. N., 10
Nguyen, T., 137
Nicodemo, L., 199
Panasyuk, V. E., 302
Pommersheim, James M., 137
Prots, S. R., 302
Robeson, Lloyd M., 396
Ruschau, G. R., 259
Shulman, Garson P., 420
Simpson, Charles, 356
Skerry, B. S., 270
Snupárek, J., 366
Sykes, J. M., 106, 161
Tait, W. Stephen, 58
Tallman, Dennis E., 123
Tang, N., 335
Tay, H. K., 161
Thierry, D., 23
Toshima, S., 211
Twite, R. L., 308
van der Weijde, D. H., 45, 69
van Ooij, W. J., 322, 335
van Westing, E. P. M., 45, 69
Vogt, Otto, 249
Vohwinkel, F., 238
Vreijling, M. P. W., 69
Wang, Jianguo, 382
Wei, Gu, 382
Wei, Yen, 382
Xiao, H., 174
Yamabe, H., 345
Yang, Chuncai, 382
Yeh, Jui-Ming, 382
Zlotnick, Joel, 123
Zook, J. D., 223
Zou, F., 23

Subject Index

A

Accelerated test procedures

cyclic indoor corrosion test by Volvo, 336, 338
environmental exposure (GM-scab) test, 325, 333

filiform corrosion, 253, 255–257

influence of surfactants adhering to steel
substrate after dry blast cleaning, 250–251, 252f

performance of coatings on aluminum substrates, 251–253, 254f

Accelerated UV degradation. *See* Photooxidative degradation

Accelerating test factors

adhesion evaluations, 266–267

cold wall effect, 265–266

deionized or distilled water, 266

temperature increase, 264–265

thermal gradient increase, 265–266

Adhesion and disbonding of coatings

accelerating factor for testing, 266–267

adhesion testing procedures, 107

blister volume determination, 114, 115f

exposing water to coatings on metal, 106

four basic stages of blister growth, 114, 116f, 117f, 118f

micro-blister disappearance on drying, 119, 121f

procedures for scanning acoustic microscopy (SAM), 107–108

pull tab test standard in petroleum industry, 260

recovery of adhesion, 119, 120f

SAM and time-of-flight SAM during water exposure, 110, 114

SAM micrographs of coating stainless steel, 111f, 112f

time-of-flight SAM technique, 108

typical SAM scan with three groups of fringes, 110, 113f

wet adhesion testing of stainless and mild steel samples, 108–110

Aerospace industry

aluminum alloys containing copper, 223

chromated and chromate-free primers, 238–240

electrochemical impedance spectroscopy (EIS) and galvanic current quantitative tests, 236

visual evaluation methods, 224

waterborne coatings due to environmental regulations, 224

See also Aluminum; Aluminum corrosion-inhibiting coating predictions; Chromated and chromate-free primers

Aging quantification for coatings

alkyd and epoxy coatings for marine applications, 83, 85–89

alkyd coating weathering in laboratory, 86, 88f

electrochemical impedance spectroscopy (EIS)

measurements and analysis, 70–71

electrolyte composition of artificial rainwater, 71

epoxy-based coating after multiple immersions,

71–77, 78f

epoxy coating weathering in laboratory, 86, 88f

experimental epoxy- and alkyd-based coatings, 70

industrial epoxy-based coating on phosphated mild steel, 77, 79–83

outdoor exposure of alkyd coating for marine application, 86, 87f

Aircraft aluminum. *See* Aluminum

Alkanethiols. *See* Self-assembled monolayers on copper

Alkoxy-silane coatings. *See* Concrete protection

Alkyd coatings. *See* Aging quantification for coatings

Alkyd coatings with modified linseed oil

borosilicate pigments, 427, 429f, 430

DC resistance measurements, 425

electrochemical AC impedance spectroscopy (EIS), 425–426

electrochemical noise measurements (ENM), 426

layer thickness measurement, 425

long oil alkyd resin binder, 424–425

phosphosilicate pigments, 430, 432f

pigments for corrosion inhibition, 425

substrates and treatment, 425

unpigmented films, 426–427, 428f

zinc molybdate pigments, 430, 431f

zinc phosphate pigments, 430, 433

Aluminum

basic corrosion reactions, 224–225, 227f

coating adhesion by accelerated test, 251–253, 254f

protection effects of alloys with copper, 421

See also Anodized aluminum with organic acid sealants

Aluminum corrosion-inhibiting coating

predictions

acid-resistant inhibitors, 229, 230f, 231f

barrier property versus electrochemical inhibition, 235

comparison of primer coatings by electrochemical impedance spectroscopy (EIS) and filiform testing, 235

EIS measurement of formulated coatings and sealants, 226, 228

EIS measurement of solutions, 226, 227f

EIS of nonbonded film, 235–236, 237t

EIS results for coatings and sealants, 232, 234f

EIS results for inhibitor solutions, 232, 233f

EIS results for topcoats or uncoats, 232, 235

galvanic current of formulated coatings and sealants, 226

galvanic current of solutions, 226

galvanic current results, 228–229, 230f

inhibitor-containing solution tests, 225–226

inhibitor passivation of bare, damaged areas next to coating or sealant, 229

low pH current acceleration, 229

matrix effects, 228

methods to compare inhibitors on aircraft alloys, 225

substrate effects, 228

surface transport properties of inhibitors in damp environment, 229

tests on formulated coatings and sealants, 226

Aniline oligomers and epoxy-cured derivatives chromium-based material replacements, 382

coatings preparation, 386

cold-rolled steel (CRS) coupon preparation with coatings, 390

conventional polyaniline emeraldine base (EB), 383–384

corrosion protection comparisons of coated and uncoated CRS, 390–391, 392f

corrosion rate equation, 386

electrochemical measurements, 386

experimental materials and instrumentation, 384–385

infrared spectra of epoxy coatings before and after curing, 388, 389f

oligomer synthesis, 385

solubility and maximum UV absorbance in various solvents, 388

synthesis of aniline trimers, 385, 387

synthetic scheme and yields, 386–387

Tafel plots for uncoated, EB- and oligomer-coated CRS, 391, 393f

trimer-cured epoxy polymer films, 388, 389f

Anodized aluminum with organic acid sealants alloys with copper, 421

carboxylic acid sealants for corrosion protection, 420–421

conventional sealing, 420

electrochemical impedance spectroscopy (EIS) and galvanic corrosion testing, 420–421

paintability, 422

protection of other metals, 422

surface cleaning with solvents and absorbent materials, 421

water-soluble dyes for color, 422

Anti-corrosive latex paint films. *See* Latex paint films

Anti-fouling protection of marine coatings, 152

Artificial versus natural UV radiation. *See* Photo-oxidative degradation

Atlas cell, preferred test for petroleum production industry, 261–263

Automotive coatings, lifetime and cost issues, 5–6

B

Biodegradation of polyimide-coated chromium criterion for failure of coating, 213

electrochemical and microscopic measurement, 212–213

electrochemical cell configuration, 215f

electrochemical data for control and inoculated solutions, 214–220

equivalent circuit model of deteriorating polymer-coated metal, 214, 215f

experimental materials, 212

fungal species, *Aspergillus versicolor* and *Chaetomium* sp., 213

incidence of failure for inoculated and non-inoculated cells, 217, 219f, 220

inoculated sample typical performance, 214, 217, 218f

in situ confocal laser scanning micrograph of fungal growth, 220

in situ stereo micrograph exhibiting fungal growth, 220, 221f

non-inoculated sample typical performance, 214, 216f

Blister predictions

analysis of blister growth, 140–142

concentrated impurity dimensions, 143–144

concentrated spots of impurity, 141f, 142–144

formation and growth in absence of corrosion, 139–140, 141f

growth rate for concentrated impurity, 143

growth rate for uniform impurity distribution, 144

results versus theory, 145–148

uniform distribution of impurity, 141f, 144–145

uniform impurity distribution dimensions, 144–145

volume and mantle surface area calculations, 148–149

volume versus time for concentrated KHSO₄ spots, 146f

volumetric growth constant versus mass of impurity, 146*f*

Blisters

anodic and cathodic region formation, 138
corrosion complications, 138
electrochemical analysis for defect area calculations, 317
growth stages by scanning acoustic microscopy (SAM), 114, 116*f*, 117*f*, 118*f*
initiation and growth, 137–139
micro-blister detection by localized electrochemical impedance spectroscopy (LEIS), 25–27
volume calculations, 313
volume determination, 114, 115*f*

Borosilicate pigments, alkyd resin with modified linseed oil, 427, 429*f*, 430

Break-point frequency (BPF) methods
assumptions, 317
defect area calculations combining capacitance and resistance terms, 310–311

C

Calcium leachability

concrete measurement after exterior exposure, 279
concrete measurement before exterior exposure, 277–278
concrete performance assessment method, 273
See also Concrete protection

Carbonation depth

concrete performance assessment method, 273
measurement after exterior exposure, 280
See also Concrete protection

Censored tests

comparison of estimated and observed failure levels, 66–67
expected failure time equation, 61
experimental descriptions, 59
failure levels estimation, 58–59
failure times for pitted samples, 60
pitting corrosion, 59–61
pitting rate equation, 60
reliability statistics, 61–65
Weibull probability plots, 65

Chromate and lead-based inhibitor replacements

anticorrosive mechanism of molybdates, 358, 359*f*, 361*f*
concerns for chromate and lead-based materials, 357, 359*t*
improved corrosion Prohesion™/QUV test method, 362–365
molybdate-based inhibitors, 358, 360, 361*t*

molybdate inhibitor applications, 360, 361*t*
test method correlation to outdoor exposure, 356–357

Chromate-based pigments and metal pretreatments

environmental regulations pending, 2–3
molybdate pigments, 356
new technologies, 6
See also Aniline oligomers and epoxy-cured derivatives; Spinel-type pigments

Chromated and chromate-free primers
aerospace industry, 238–240
corrosion category definitions, 243, 248*t*
electrochemical measurements, 242
extract preparation and alternate immersion/emersion (A.I.E) tests, 240–241
extract preparation from cured and powdered primer, 241
filiform corrosion test results, 245, 248*f*
results of A.I.E. tests, 241–242
second test cycle procedure, 242–243
second test cycle results, 243–247

Cold-rolled steel (CRS)

environmentally friendly pretreatment, 322–323
materials for plasma polymerization, 323–324
plasma cleaning procedure, 322–323
See also Aniline oligomers and epoxy-cured derivatives; Plasma polymerized hexamethyldisiloxane (HMDS) films

Cold wall effect

accelerating factor for testing, 265–266
negative thermal gradient across coating to steel, 262–263

Concrete protection

alkoxy-silane and polyisocyanate coating systems, 281
calcium leachability after exterior exposure, 279
calcium leachability before exterior exposure, 277–278
carbonation depth after exterior exposure, 280
concrete performance assessment methods, 273
concrete preparation, 271
contaminant salts, 271
corrosion of steel reinforcements, 270–271
critical importance of concrete recipe, 280
exposure test, 272–273
surface coatings, 272
surface contaminations, 271–272
visual observations, 274, 275*f*
water surface capillary rise after exterior exposure, 276–277
water surface capillary rise before exterior exposure, 274, 275*f*, 276

Conductive polymers. *See* Polyaniline

Constant Phase Element (CPE), coating response in impedance measurements, 69–71

- Copper corrosion inhibition
 material in heat transfer applications, 410
 molecular agents containing sulfur or nitrogen
 sites for ligation to surface, 410
See also Self-assembled monolayers on copper
- Corrocell or standard glass atlas cell, preferred
 test for storage tanks and low pressure
 pipelines, 261
- Corrosion failure
 blistering and related defects, 124
 organic coating defects, 123–124
See also Blister prediction; Blisters; Defects and
 heterogeneities in coating films
- Corrosion protective coatings
 control measurement, 5
 design and development needs, 2
 fundamental research support, 2
 lifetime and cost issues of coatings, 5–6
 major areas of use, 4–5
 most successful polymers, 4–5
 new technologies, 6
 roles of coatings, 3–4
- Critical pigment volume concentration (CPVC),
 porosity defects above CPVC, 126, 127f
- D**
- Defect area calculations
 assumptions of electrochemical methods, 315,
 317
 blister analysis, 317
 blister volume equation and assumptions, 313
 break-point frequency methods, 310–311
 digital image analysis (DIA), 314
 electrochemical analysis, 314
 electrochemical noise method (ENM) using
 coupling current, 312–313
 electrolyte test solutions, 313–314
 ENM and EIS analysis of defect areas, 314–315,
 316f
 equivalent circuit (EC) method, 309–310
 experimental coating systems, 313
 pore resistance method, 311–312
 Prohesion™ showing contrast between pores and
 continuous coating, 318, 319f
 Prohesion™ weatherometer conditions, 314
 scanning electron microscopy method, 314
 SEM/DIA analysis for quantitative estimation of
 pore area, 318–319
 surface morphology changes by SEM, 318–319
- Defects and heterogeneities in coating films
 alignment variation for impermeable flake
 pigments, 127–129
 application process, 124–125
 corrosion failure, 123–124
 effect of induced heterogeneities on
 performance, 130–133
 film resistance, 125
 film thickness fluctuations, 125, 126f
 local property fluctuations, 127, 128f
 porosity in films above critical pigment volume
 concentration, 126, 127f
 variations in application quality, 129–130
- Degradation of organic coatings
 detection of micro-blisters by LEIS, 25–27
 LEIS spectra of defected painted steel samples,
 28–30
- Degradation of polymer coatings on steel
 artificial and natural seawater, 174
 calculated versus observed corroding area, 180,
 181f
 comparison of impedance spectra, spectral noise
 plots and R_n , 184, 186f, 187f, 188f
 electrochemical and visual observation methods,
 175, 177f
 environmental scanning electron microscopy,
 175, 179f, 180
 experimental coatings systems, 174–175, 176f
 experimental electrochemical noise data, 180,
 183f, 184
 impedance spectra for series with varying primer,
 190, 194f, 195f, 196f, 197f
 impedance spectra obtained in natural seawater,
 175, 178f
 power spectra density plots, 184, 186f, 187f,
 188f
 primer and topcoat role in corrosion protection,
 190, 198
 relationship between spectral noise plots and
 impedance plots, 190
 result comparison of lab and marine test sites,
 184, 189f, 190, 191f, 192f, 193f
- Digital image analysis (DIA)
 defect area calculations, 314
 SEM/DIA analysis for quantitative estimate of
 pore area, 318–319
See also Defect area calculations
- Disbonding. *See* Adhesion and disbonding of
 coatings
- Downhole tubing, service class in petroleum
 production, 259
- Dry blast cleaning, accelerated test for surfactant
 influence on subsequent coatings, 250–251,
 252f
- E**
- EIS. *See* Electrochemical impedance spectroscopy
 (EIS)

- Electrically conductive polymers. *See* Polyaniline
- Electrochemical evaluation
 defect area calculations, 308–313
 gaining popularity in petroleum industry, 260
- Electrochemical impedance spectroscopy (EIS)
 activity of microorganisms on polymer-coated metal, 212
 latex paint film analysis, 33
 lifetime prediction possibilities, 45–46
 objective predictive method, 3
 modified Randles circuit, 32, 34f
 technique description, 32–33
See also Biodegradation of polyimide-coated chromium; Localized electrochemical impedance spectroscopy (LEIS)
- Electrochemical noise impedance
 supplemental to ENM and EIS, 294–296
 vinyl ester coatings, 297, 299–301
- Electrochemical noise methods (ENM)
 blister volume calculation, 313
 coupling current for defect area calculations, 312–313
 flowing versus stationary electrolyte, 154–157
 non-perturbing technique, 151
 objective predictive method, 3
 variations in coating application quality, 129–130
See also Defect area calculations
- Electrolyte, flowing versus stationary
 comparison of ENM results, 157
 degradation of marine coatings, 151–152
 electrochemical cell design, 152–153
 electrochemical (EIS and ENM) methodology, 153–154
 electrochemical impedance spectroscopy (EIS) results, 158–159
 electrochemical noise method (ENM) results, 154–157
 marine coatings sample preparation, 152
 noise resistance results for flowing electrolyte, 155, 156f
 noise resistance results for stationary electrolyte, 155, 156f
 sample pairing for noise studies, 153
- Electrolytic polymerization stainless steel
 treatment. *See* Stainless steel surface treatment
- ENM. *See* Electrochemical noise methods (ENM)
- Epoxide bisphenol-A diglycidyl ether, polyaniline
 blend for corrosion resistance, 402, 404
- Epoxy coatings
 break-point frequencies, 16, 21
 coating capacitance data, 12, 14–16
 conventional EIS analysis, 13f
 electrochemical impedance data, 12
 experimental procedures for naval coatings, 11–12
 maximum impedance at low frequency, 16, 17f, 18f, 19f, 20f
 physical appearance, 12
 potentials relative to Ag/AgCl reference, 12, 13f
See also Aging quantification for coatings;
 Aniline oligomers and epoxy-cured derivatives
- Equivalent circuit model (ECM)
 cold-rolled steel pretreatment analysis, 325–326, 327f, 330–331
 defect area calculations based on EIS, 309–310
 polyimide-coated chromium, 214, 215f
- ## F
- Failure levels of censored samples, 58–59
- Failure mode prediction of organic coating on metal
 electrochemical impedance spectroscopy technique, 204
 impedance response over film lifetime, 204–207
 mathematical model of salt transport, 200–204
 organic coating preparation, 204
 polymer/aluminum system comparison to model, 207, 209
 polymer/iron system comparison to model, 209–210
 result comparison with mathematical model, 207–210
- Fast Fourier transform (FFT), noisy signal
 analysis at low frequencies, 297, 299
- Fickian water absorption, initial behavior of intact
 organic coatings, 47f, 48
- Fick's Law (modified) for diffusion, blister
 growth analysis, 140–142
- Filiform corrosion, accelerated test, 253, 255–257
- Fluorinated polyurethane coatings
 anticorrosive coatings for ships' bilge, 290
 biuret of hexamethylene diisocyanate curing agent, 284, 286f
 coatings formulations, 284–285, 286f
 collection, holding, and transfer tanks, 290
 fluorinated diols for polyol synthesis, 283f
 fluoropolymer properties, 283–285
 polyol synthesis process, 284, 285f
 poly(tetrafluoroethylene) as extender pigment, 285, 287t, 288t
 ship hulls applications, 286–288
 specialized defense and industrial applications, 282–283
 submarine radome coatings, 290
 tank lining applications, 286, 289f

unique properties suggest future applications, 291

Fluoropolymers. *See* Fluorinated polyurethane coatings

Fouling of marine coatings, 152

Fuel tanks

corrosion products, 292, 296–297

See also Vinyl ester coatings

Fungi, microorganisms in biodegradation, 212

G

Galvalume

nontoxic pretreatment replacements, 335–336

trade name of metal-coated steel strip, 335

See also Plasma polymerized

hexamethyldisiloxane (HMDS) films

GM-scab test, cyclic accelerated environmental exposure test, 325, 333

H

Hack/Scully analysis, break-point frequencies of epoxy coatings, 16, 21

HDPE. *See* High-density polyethylene (HDPE)

Hexamethyldisiloxane (HMDS). *See* Plasma polymerized hexamethyldisiloxane (HMDS) films

High-density polyethylene (HDPE), influence of relaxation on water uptake, 48–49

HMDS. *See* Plasma polymerized hexamethyldisiloxane (HMDS) films

Holidays and holiday detectors, imperfections penetrating to metal surface, 124

Hoogovens Corrosion Test, epoxy-based coating on phosphated mild steel, 77, 80f, 81

I

Immersion test, standard in petroleum industry, 260

Intact organic coatings

alkyd and epoxy coatings for testing, 46

cathodic delamination model, 53–56

degradation phase, 51

initial Fickian water absorption, 47f, 48

intact coatings with defects, 51–53

lifetime predictions with EIS, 45–46

mechanically damaged coatings, 53–56

stationary region, 47f, 50–51

water absorption phase, 48–50

Internal coatings for corrosion control. *See* Petroleum production industry

L

Latex paint films

anti-corrosive latex film exposure, 33, 34f, 35–39

EIS experiment description, 32–33

latex film formation properties, 33, 37f, 39, 41f, 42–43

near infrared spectroscopy procedure, 33, 35

Lead and chromium-based pigment replacements. *See* Spinel-type pigments

Le Chatelier's principle, maintenance of unoxidized carbon steel surface, 406

LEIS. *See* Localized electrochemical impedance spectroscopy (LEIS)

Lifetime prediction of organic coatings

coatings with defects, 46

intact coatings experiments with EIS, 46–47

intact coatings without blisters, 47

possibilities with EIS, 45–46

See also Intact organic coatings

Line pipe, service class in petroleum production, 260

Linseed oil

high cross-linking rate due to high linolenic acid content, 424

replacement for volatile organics in paints, 423

See also Alkyd coatings with modified linseed oil

Localized electrochemical impedance spectroscopy (LEIS)

micro-bliester detection, 25–27

microprobe description, 23–24

novel method description, 23–24

probe and experimental setup, 24

specimen preparation, 24–25

spectra of defected painted steel samples, 28–30

See also Electrochemical impedance spectroscopy (EIS)

M

Marine coatings

anti-fouling protection, 152

corrosion protection performance, 151–152

electrochemical comparison of flowing and stationary electrolyte, 151–152

fluorinated polyurethanes, 282–283

See also Electrolyte, flowing versus stationary;

Epoxy coatings; Fluorinated polyurethane coatings

Maximum entropy spectrum analysis (MESA),

low-frequency noise impedance values for vinyl ester coatings, 297, 299

Metal pretreatments. *See* Plasma polymerized hexamethyldisiloxane (HMDS) films

Microorganisms

biodegradation activity, 211–212
potential detection by EIS, 212
See also Biodegradation of polyimide-coated chromium; Degradation of polymer coatings on steel

Molybdate inhibitors

anticorrosive mechanism, 358, 359*f*, 361*f*
applications, 360, 361*t*
nontoxic inhibitor types, 358, 360, 361
ProhesionTM/QUV corrosion test evaluation, 362–365

Molybdenum disulfide

faults in polyethylene supermolecular structure, 304, 306
internal lubricant in polyethylene films, 304, 305*f*
mechanical properties in polyethylene, 304, 305*f*, 306
See also Polyethylene coatings with molybdenum disulfide

N

Naval coatings. *See* Epoxy coatings; Marine coatings

Near infrared spectroscopy (NIR), latex paint film analysis, 33, 35

Noise impedance. *See* Electrochemical noise impedance

O

Oilfield production. *See* Petroleum production industry

Open time, latex paint films, 39, 42–43

Organic acid sealants for corrosion protection
cleaning acid from surfaces, 421
corrosion protection for anodized aluminum, 420–421

paintability of sealed anodized aluminum, 422
protection of other metals, 422
water-soluble dyes for imparting color, 422

Organic coatings degradation

detection of micro-blisters by localized electrochemical impedance spectroscopy (LEIS), 25–27
LEIS spectra of defected painted steel samples, 28–30
See also Intact organic coatings; Lifetime prediction of organic coatings

P

Petroleum production industry

accelerating factors for test methods, 263–267
cold wall effect, 262–263
internal coatings and classes of service, 259–260
preferred test methods, 261–263
pressured atlas cell for production vessels, 261–262

rocker arm test for tubular coatings, 261, 262*f*
standard glass atlas cell or corrocell, 261
standard industry tests, 260–261

Phosphating/chromating metal pretreatment replacements. *See* Plasma polymerized hexamethyldisiloxane (HMDS) films

Phosphosilicate pigments, alkyd resin with modified linseed oil, 430, 432*f*

Photooxidative degradation

biuret versus urethane functional groups, 94–96, 97*t*

chemical bond modifications, 93
competitive phenomena in complex mechanism, 100

EIS analysis to quantify barrier properties, 96, 98, 99*f*

principle steps of degradation, 96
samples and weathering procedure, 94, 95*t*
solar and artificial UV radiation effects, 94–96, 97*t*

thickness distinction between artificial and natural UV radiation, 96, 97*f*
water barrier versus ionic resistance, 100–102, 103*f*

Pigments active for corrosion control

classifications, 367–368
effect of polymeric binders on inhibitive efficiency, 368–370

See also Spinel-type pigments

Pitting corrosion

mature pit steady state growth, 59–61
pit growth to critical size, 59
pit nucleation, 59
pitting rate equation, 60

Plasma polymerized hexamethyldisiloxane (HMDS) films

accelerated indoor corrosion test by Volvo, 336, 338, 342, 343*f*
analysis and characterization of cold-rolled steel (CRS) samples, 324–326, 327*f*
atomic emission spectroscopy (AES) depth profiles on Galvalume, 338–341
capacitance and resistance changes for CRS in solution exposure test, 331–333
CRS sample analysis by equivalent circuit model, 330–331

- custom-built DC reactor for polymerization on Galvalume panels, 337f
- GM-scab test results for CRS samples, 333
- impedance modulus for CRS samples, 326–330
- materials and procedures for Galvalume pretreatment, 336–338
- materials and sample preparation for CRS, 323–324
- phosphating/chromating system replacement for cold-rolled steel, 322–323
- plasma cleaning and deposition conditions for Galvalume, 336, 338f
- reflection–absorption infrared (RAIR) spectra of films on Galvalume, 336, 341–342, 343f
- Polyaniline**
- applications in coatings, 397
- corrosion performance, 399–400
- dynamic mechanical analysis, 399
- electrically conductive polymers, 396–397
- electrochemical impedance spectroscopy (EIS), 399
- emeraldine base (EB), 383–384
- epoxide blends, 402, 404
- film preparation and protonation on steel panels, 398–399
- immersion and salt fog testing, 399
- mechanism of corrosion resistance, 405–406
- oxidative polymerization of aniline monomers, 383–384
- performance of polyaniline blends, 400–405
- polyimide blends, 400–402, 403f
- solution preparations, 398
- styrene–acrylic acid copolymer blend, 405
- synthesis method, 398
- urethane-linked diisocyanate blend, 404–405
- See also* Aniline oligomers and epoxy-cured derivatives
- Polyethylene coatings with molybdenum disulfide
- adhesion strength measurement, 303
- electrical measurements, 303
- flow temperature determination, 303
- mechanical properties, 304, 305f, 306
- property improvements, 306–307
- protective properties, 303–304, 305f
- sample preparation, 302–303
- tension of films, 303
- Polyimide-coated chromium. *See* Biodegradation of polyimide-coated chromium
- Polyimide pyromellitic dianhydride oxydianiline, blend with polyaniline for corrosion resistance, 400–402, 403f
- Polyisocyanate coatings. *See* Concrete protection
- Polyols, synthetic process for fluorinated polyols, 284, 285
- Poly(tetrafluoroethylene), extender pigment in fluorinated polyurethane coatings, 285, 287f, 288f
- Polyurethane coatings. *See* Fluorinated polyurethane coatings
- Pore resistance method, defect area independent of capacitance, 311–312
- Pressured atlas cell, preferred test for production vessels, 261–262
- Production vessels, service class in petroleum production, 260
- Prohesion™/QUV corrosion test
- contrast between pore and continuous coating, 318, 319f
- evaluation of molybdate and anticorrosive inhibitors, 362–365
- weatherometer conditions, 314
- PTFE. *See* Poly(tetrafluoroethylene)
- R**
- Rainwater (artificial), electrolyte analysis for aging tests, 71
- Randles circuit (modified), EIS data analysis, 32, 34f
- Reflection–absorption Fourier transform infrared spectroscopy (RA–FTIR), triazine thiols polymerized on-stainless steel, 350, 351f
- Reflection–absorption infrared spectroscopy (RAIR), plasma polymerized hexamethyldisiloxane films on Galvalume, 336, 341–342, 343f
- Reliability statistics
- censored sample failure levels, 61–65
- observed versus estimated failure levels, 66–67
- statistical ranking method comparison, 63
- Weibull probability plots, 65
- Renewable natural products. *See* Linseed oil
- Rocker arm test, preferred for tubular coatings, 261, 262f
- S**
- Salt fog test, poor performance predictions, 2–3
- Salt transport in coatings
- mathematical model, 200–204
- pores incorporated into model, 202–203, 205f
- See also* Failure mode prediction of organic coating on metal
- Scanning acoustic microscopy (SAM)
- adhesion testing procedure, 107–108
- blister growth stages by SAM, 114, 116f, 117f, 118f
- See also* Adhesion and disbonding of coatings
- Scanning electron microscopy (SEM)
- degradation of polymer coatings on steel, 175, 179f, 180
- experimental method, 314
- monitoring surface morphology changes for defect area calculations, 318–319

- SEM/DIA analysis for quantitative estimation of pore area, 318–319
- Seawater, natural and artificial. *See* Degradation of polymer coatings on steel
- Self-assembled monolayers on copper assembly of alkanethiols, 411
- corrosion inhibition under oxidizing conditions, 415–416
- monolayer formation schematic, 412*f*
- multilayer strategies, 416–417, 418*f*
- oxidation studies, 411–412
- sample preparation, 411
- wetting experiments, 412
- X-ray photoelectron spectroscopy quantifying extent of oxidation, 412–415
- SEM. *See* Scanning electron microscopy (SEM)
- Ships' hull and bilge, fluorinated polyurethane coatings, 286–288, 290
- SIMS. *See* Static secondary ion mass spectroscopy (SIMS)
- Spinel-type pigments
- accelerated corrosion tests, 372
 - alkyd-based coating formulation, 369*t*
 - anticorrosive action in coatings, 373–375
 - chromium and lead-based replacements, 366–367
 - corrosion-inhibiting properties, 378–379
 - corrosion inhibitive activity determination of coatings, 373
 - corrosion resistance test results, 376–378
 - double metal oxides characterization, 368
 - epoxy-based coating formulation, 369*t*
 - metal soap formation, 375
 - microscopic determination of diffusion into coating films, 372–373
 - polymeric binder characterizations, 368–369
 - preparation of various spinels, 370–371
 - salt spray test results, 377*t*
 - styrene-acrylate coating formulation, 370*t*
 - testing methods for anticorrosive pigments, 371, 372*t*
- Stainless steel surface treatment
- adhesion loss in humid environments, 345
 - adhesion study, 346, 349*f*, 351*f*
 - coating thickness, 346, 349*f*
 - electrolytic polymerization with triazine thiol compounds (TTN), 345
 - interface characterization techniques, 350–353, 354*f*
 - polymerization mechanisms of TTN on metal, 353, 354*f*
 - pretreatment procedure with TTN, 346, 348*f*
 - reflection-absorption Fourier transform infrared spectroscopy (RA-FTIR), 350, 351*f*
 - static secondary ion mass spectroscopy (SIMS), 353, 354*f*
 - triazine thiol compounds, 346, 347*f*
 - X-ray photoelectron spectroscopy (XPS), 350, 352*f*, 353
- Standard glass atlas cell or corrocell, preferred test for storage tanks and low pressure pipelines, 261
- Static secondary ion mass spectroscopy (SIMS), triazine thiols polymerized on stainless steel, 353, 354*f*
- Statistics. *See* Reliability statistics
- Steel. *See* Degradation of polymer coatings on steel; Stainless steel surface treatment
- Storage tanks, service class in petroleum production, 260
- Styrene-acrylic acid copolymer, polyaniline blend for corrosion resistance, 405
- Submarine radome coatings, fluorinated polyurethanes, 290
- ## T
- Tank linings, fluorinated polyurethane coatings, 286, 289*f*, 290
- Time-of-flight scanning acoustic microscopy (TOFSAM)
- adhesion testing procedure, 108
 - See also* Adhesion and disbonding of coatings
- Toxicity characteristics leaching procedure (TCLP), regulatory concerns for chromate and lead-based inhibitors, 357, 359*t*
- Triazine thiol compounds
- electrolytic polymerization on stainless steel, 345–346, 350, 353
 - functionality, 346, 347*f*
 - polymerization mechanisms on metal surfaces, 353, 354*f*
- ## U
- Ultraviolet (UV) radiation. *See* Photooxidative degradation
- Urethane-linked diisocyanate, blend with polyaniline for corrosion resistance, 404–405
- ## V
- Vinyl ester coatings
- advantages over conventional metal and polyester materials, 292–293
 - cell preparation, 293–294
 - chemically resistant structure, 292–293
 - complementary electrochemical methods, 300–301

DC resistance most intrusive method, 299
 electrochemical noise impedance, 297, 299–301
 electrochemical noise method ranking coatings, 297, 298*f*
 electrochemical test methods, 294–296
 fast Fourier transform (FFT) analysis of noisy signals at low frequencies, 297, 299
 impedance spectra, 297, 298*f*
 maximum entropy spectrum analysis (MESA) for low-frequency noise impedance values, 297, 299, 300*f*
 noise impedance calculations, 296
 test electrolytes realistic for fuel tank corrosion products, 296–297

W

Water barrier properties. *See* Photooxidative degradation
 Waterborne polymeric coatings
 activation energies for water transport, 166, 169
 diffusion equation under non-steady state conditions, 162–163
 effect of pH on latex films, 166, 169, 170*f*
 effect of pigment for water uptake at paint pH = 3 and pH = 5, 163–166, 167*f*
 environmental emphasis, 31–32
 link between water uptake and pigment content, 169, 170*f*
 paint preparation with varying pigment content, 163, 164*t*

permeability to water vapor, 161–162
 quantifying water transport, 162–163
 temperature effect on water uptake at paint pH = 3 and pH = 5, 166, 168*f*
 vinyl chloride/vinylidene chloride copolymer latex, 161–162
 water uptake effects for pigment content at pH = 3, 169–171
See also Latex paint films
 Water surface capillary rise measurements
 after exterior exposure, 276
 before exterior exposure, 274, 275*f*, 276
 concrete performance assessment method, 273
See also Concrete protection
 Weibull probability plots, censored samples, 65

X

X-ray photoelectron spectroscopy (XPS)
 self-assembled alkanethiol monolayers on copper, 412–415
 triazine thiols polymerized on stainless steel surfaces, 350, 352*f*, 353

Z

Zinc-based pigments in alkyd resin with modified linseed oil
 zinc molybdate pigments, 430, 431*f*
 zinc phosphate pigments, 430, 433